THE DETECTION AND ANALYSIS OF VLF TRIGGERED EMISSIONS

(A Rocket Borne Very Low Frequency Radio Receiver and The Analysis of Triggered Emissions Received at Medium and High Latitudes)

A Thesis

Presented to the

University of Sheffield

by

D. Morgan

for the degree of

Doctor of Philosophy

April 1974

SKUA LAUNCH

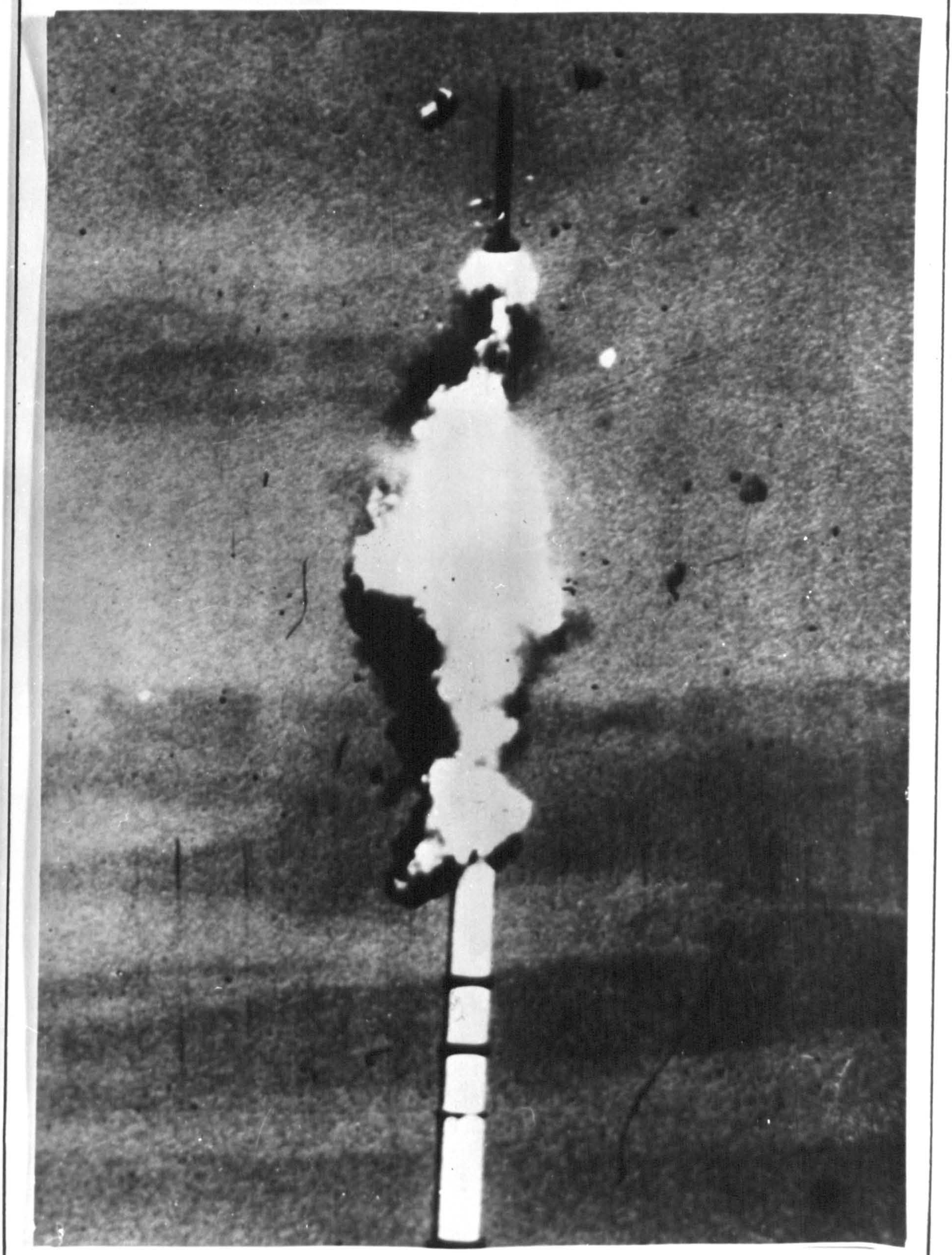

~~A rocket-borne very low frequency radio receiver and the analysis~~

~~of medium and high latitudes~~

The Detection and Analysis of Triggered Emissions

A thesis presented to the University of Sheffield by D. Morgan for the degree of Doctor of Philosophy.

Summary

The work described in this thesis consists essentially of two parts. The first is the design and development of a rocket-borne V.L.F. receiver for the observation of the magnetic field component of electromagnetic waves in the frequency range 100 to 20,000 Hz. The author's particular contribution was the optimisation of the design of a small μ-metal rod aerial. The approach was necessarily partly empirical, partly theoretical. The former involved the systematic adjustment of the number of turns, coil geometry, dimensions and type of wire, etc. for the particular rod length small enough to be flown in the space available in the rocket nose-cone. This was complemented by a theoretical approach involving the rod and equivalent circuits which satisfactorily reproduced the measured frequency response and signal/noise properties of the aerial and preamplifier.

The second part of the thesis is concerned with the analysis and interpretation of discrete V.L.F. emissions using the phenomenological theory of Helliwell. Both medium and high latitude emissions were analysed in detail. Significant advances were made in the computer iteration techniques applied to the analysis of these emissions and limitations in the analytical methods used were investigated in great detail. Particularly interesting were several "slow risers" recorded at Andoya (L = 6.6) in northern Norway. The analysis determined the time varying energy spectrum of the phase-bunched electrons giving rise to the emission in the vicinity of the earth's equator (~ 6.6 earth radii) for a range

of possible equatorial ambient electron densities. It was possible to determine an upper limit to the electron density at the equator which, since it was in excellent agreement with that (2 to 5 electrons/cc) determined by more direct measurements, provided new experimental support for the theory. The limitations in the theory were examined and a small error in the original formula of Helliwell corrected.

ACKNOWLEDGEMENTS

The author would like to thank Professor T.R. Kaiser for making available the facilities of the Department of Physics at the University of Sheffield and for his help and instruction in matters arising out of this work.

Thanks are also due to Dr. K. Bullough, the author's supervisor throughout the period of these researches, for his guidance, help, kindness and forbearance.

The author wishes to acknowledge the help received during many conversations with members of the Department of Physics at the University of Sheffield especially Mr. W. Gibbons and Mr. M. Ashworth.

Thanks are also due to Mr. J. Bradley and to members of the Mechanical Workshop at the University who expertly engineered the flight payload and to several persons in the Photographic and Tracing Department for their help in preparing this thesis.

A considerable debt is owed to Mr. G. Garside for his help in the design of various pieces of electronics and especially for his help in integrating a difficult payload.

In this latter respect thanks are also due to Mr. B. Wynne of the British Aircraft Corporation for his help and wholehearted co-operation.

The author also wishes to thank members of the Special Projects Division of Dunford & Hadfields who worked so well on the production of prototype and flight electronics.

The author is indebted to the Science Research Council for an award covering the greater part of the period of this research.

To my friends.

CONTENTS

CONTENTS (Contd)

CONTENTS (Contd)

NOTATION

D	Whistler dispersion measure
f	Signal frequency
f_h	Gyro frequency
f_p	Plasma frequency
N_e	Electron density
H	Magnetic field intensity
L	McIlwain parameter
n	Particle density
T_e	Electron temperature
T_p	Ion temperature
K	Boltzmans constant
T	Temperature
R	Resistance
ω	Angular frequency
N	Number of turns
S	Coil area
b	Magnetic induction
μ	Permeability of free space
μ_i	Initial permeability
μ_{eff}	Effective permeability
D	Demagnetising factor
m	Ratio of length to diameter
d	Core diameter
ℓ	Core length
e	e.m.f.
L	Self inductance
M	Mutual inductance
e	Electronic charge
m	Electron mass
B	Magnetic induction
$v_\perp$	Perpendicular velocity
$v_{//}$	Paralle velocity
v_p	Wave phase velocity
v_s	Electron streaming velocity
$E_\perp$	Perpendicular electric field

$E_{\parallel}$	Parallel electric field
μ	Permeability of a magneto-ionic plasma
k	Wave number;
ω_h	Angular gyro frequency
C	Velocity of light in vacuo
f_n	Plasma frequency
f_{ho}	Equatorial gyro frequency
f_{no}	Equatorial plasma frequency
v_g	Wave group velocity
α_o	Equatorial pitch plane
S	Distance along field line from equator
R_m	Geocentric distance to field line in the equatorial plane
f_{eq}	Equatorial gyro frequency (880 kHz)
R_o	Radius of the earth
R	Radius of field line in equatorial plane
ϕ	Geomagnetic latitude
ϕ_o	Geomagnetic latitude of a field line entering the earth
T_i	Ionospheric dispersion delay time
$\underline{E}$	Wave electric field vector
$\underline{B}$	Wave magnetic field vector
θ	Phase angle
V_I	Interaction region velocity
n_{eq}	Equatorial electron density
R	Normalised field line radius
R_E	Normalised field line radius in the equatorial plane
E	Resonant electron energy

LIST OF FIGURES

LIST OF FIGURES (Contd)

LIST OF FIGURES (Contd)

LIST OF FIGURES (CONTD)

LIST OF FIGURES (CONTD)

LIST OF FIGURES (CONTD)

LIST OF FIGURES (CONTD)

LIST OF FIGURES (CONTD)

LIST OF FIGURES (CONTD)

LIST OF FIGURES (CONTD)

LIST OF FIGURES (CONTD)

LIST OF FIGURES (CONTD)

CHAPTER 1

NATURALLY OCCURRING V.L.F. EMISSIONS

1.1 INTRODUCTION

At the audio frequency end of the electromagnetic spectrum there are a number of naturally occurring emissions. They can be detected by using a sensitive audio amplifier connected to a large aerial at a quiet site which is free from man made interference.

The variety of spectral characteristics (frequency - time plot) is great. However the emissions can be catalogued as belonging to one of about half a dozen types of emission which are named according to the particular sound which is heard when the emission is played through a loudspeaker. There are emissions known as whistlers, chorus, tweeks, spherics, risers, hiss and a few others. Chorus, for example is so named because it sounds like a flock of birds chirping, a whistler is often heard as a gently falling tone, spherics are sharp and impulsive and the term 'hiss' is self explanatory.

Although the study of these naturally occurring very low frequency emissions is fascinating in its own right, the knowledge gained about the emissions themselves and that gained about the region of space surrounding the earth through their observation, has importance in the field of radio communications and so in our every day lives.

Indeed some of the interest and finance concerned in the study of the propagation and occurrence of very low frequency radiation has been stimulated by the need for longrange military communications and world wide radio navigation.

1.2 HISTORICAL BACKGROUND

Whistlers were probably the first V.L.F. emissions to be heard. The first report on them was published by Preece in 1894 and subsequently by Barkhausen in 1919. Eckersley (1925,1926) reported several observations of whistlers and attempted to explain their frequency-time characteristics. He with others reported observing an emission 'which sounded like the warbling of birds' and which occurred most frequently around dawn (Eckersley et al 1928). For these reasons it was called 'dawn chorus'.

Soon after in 1933 two American workers Burton & Boardman detected a 'frying sound' which appeared to be connected with an auroral display (Burton & Boardman 1933). This appears to be the first recorded observation of 'hiss.'

In England Eckersley (unpublished, quoted by Storey 1953) also observed hiss. The observation was made at a frequency of about 5 KHz on a receiver which was connected to a pair of large direction finding loops. The signals were reported as 'coming from a northerly direction'.

After this there was little work in this field until Storey 1953 made a comprehensive study of whistlers with data recorded at Cambridge. He produced the

first explanation of the known properties of whistlers. He verified Eckersley's law of propagation, that the whistler dispersion $D = t\sqrt{f} = ct$, where f and t are the co-ordinates of points on the whistler's frequency-time profile. Storey showed that for a frequency $f \ll f_h$ and $f \ll f_p^2 / f_h$ the whistler ray direction lies within a cone of half angle 20° centred on the direction of the local magnetic field.

Possibly the most important part of Storey's work was to deduce that the whistler dispersion could yield information about the physical properties of the medium through which the whistler had propagated. He showed that the dispersion of the signal can be expressed by;

$$D \propto \int \sqrt{\frac{N_e}{H}} \, ds \qquad \text{for} \quad f \ll f_h \quad \text{and} \quad f \ll f_p^2 / f_h$$

From the reduction of the Cambridge data he showed that the electron density at L=3 was of the order of $400 el/cm^3$ this being at least 10 times greater than had been supposed up to this date.

Later, at high geomagnetic latitudes, a new type of whistler was observed with a frequency-time characteristic such that at a frequency called the 'nose frequency', the signal travels faster than at lower or higher frequencies. This whistler can be explained in terms of the magnetoionic theory if the maximum frequency of the emission is comparable with the electron gyro-frequency in the medium. (Ellis 1956, Helliwell et al 1956).

The nose frequency provides information about the geomagnetic field line along which the whistler had propagated. The discovery of nose whistlers therefore led to a significant improvement in the use of whistlers as a means of investigating the magnetosphere.

By studying whistlers observed on the ground Smith 1961 showed that they had to be much more strongly guided along the geomagnetic field than would be predicted in Storey's theory. He suggested that field aligned irregularities of electron density would be able to guide V.L.F. waves much like a metallic waveguide. It might be said that by explaining the properties of whistlers Storey opened the way for the study of phenomena which were not explained by his theory. It seemed likely that emissions such as hiss, chorus, hooks, risers etc were propagated and guided along field lines in the same way as whistlers and could therefore have been generated in the magnetosphere.

With the great interest in whistlers being 'boosted' with the IGY many workers began recording them. They automatically recorded other V.L.F. emissions such as those mentioned above. The correlation of hiss and chorus phenomena with magnetic activity was noticed by Storey 1953, Gallet 1959, Allcock 1957.

Crouchley & Brice 1960 and Dinger 1960 found that chorus activity was considerably higher than usual during most of 1958 (sunspot maximum). It was shown by Allcock and Crouchley & Brice, (Allcock 1957, Crouchley & Brice 1960) that the strength or frequency of

occurrence increases with geomagnetic latitude and reaches a peak at about 60°. Similar observations were made by Helliwell & Carpenter 1961.

A noise storm observed by Watts 1957 and Helliwell 1958 showed a band of hiss from 1 to 10 KHz with the peak intensity at about 3 KHz. At times the bandwidth was extended from 100 Hz to 20 KHz.

Helliwell & Carpenter 1961 found that hiss occurred in a broad band, or in one or more narrow bands. The narrow bandwidths being about 1 KHz.

Other emissions such as 'surf' which is intensity modulated hiss were observed by Pope and Campbell 1960 and Gallet 1959 noted 'gliding tones'.

However whistlers were still being observed and Carpenter 1963 confirmed a sharp discontinuity in electron density as a function of radius along the geomagnetic equator which had been observed by Gringauz 1960 using ion traps on board Soviet satellites. This discontinuity, which is a permanent field aligned feature of the magnetosphere, occurs at about L = 4 with a typical electron density variation of 10:1 across it. This discontinuity is now called the Plasmapause and it separates the plasmasphere or dense inner plasma which co-rotates with the earth, from the outer less dense region sometimes called the plasmatrough.

In later analysis of whistler data Carpenter 1966, 1967 was able to study the dependence

of the position of the plasmapause on local time and the magnetic activity in the magnetosphere. More recently some of the best detailed work on the plasmapause was reported by Chapell et al 1970 from ion mass spectrometer measurements made aboard the OGO 5 satellite.

At high latitudes there is evidence of a general downward shift in frequency of observed emissions. After a year's observation at Godhavn, Greenland (G.M. Latitude 80°N) Ungstrup 1959 found that chorus which occurred around 10-12 hr local time was almost exclusively confined to the frequency range 500 Hz to 1 KHz. At medium latitudes as previously mentioned the frequency range is 1 - 5 KHz. If the observed chorus was not a local phenomenon but had been propagated any great distance along the earth-ionosphere waveguide it would have been appreciably attenuated. Curves given by Watt & Maxwell 1957 show the attenuation at these frequencies to be about 6 db/1000 km.

It is difficult to see similar behaviour for hiss because it can cover such a wide frequency range. However there is a form of hiss called 'quiet hiss' which is narrow band, stable in frequency and amplitude, and often occurs at times of weak magnetic activity. At medium geomagnetic latitudes (below 50°) this is observed at around 4 KHz (Dowden 1963). At high latitudes, for example Kiruna, Sweden (G.M. Latitude 65°N) a stable band appears at about 750 Hz $\pm$ 150 Hz (Gustafsson et al 1960, Aarons et al 1960). Egeland 1959 made observations at Tromso, Norway (G.M. Latitude 67°N) and reported a similar

band centred on 800 Hz.

The work described in the later part of this thesis is concerned with the analysis of two types of emission which have not yet been discussed in any detail. These are risers and hooks observed at medium latitudes (S.Ulst Scotland L = 3.4) and high latitudes (Andøya Norway L = 6.2). The medium latitude risers range in frequency between 2 and 6 KHz whereas those recorded at Andøya range between 1 to 1.5 KHz.

Together with the observation of V.L.F. electromagnetic waves the magnetosphere has been studied by many different means which are too numerous to list. However it is important when studying wave-particle interactions to realise that much work has been done to investigate the behaviour of energetic charged particles, particularly electrons, using rocket probes and satellites. Chapter 5 describes a rocket payload which carried a charged particle experiment from the University of Southampton together with a V.L.F. receiver and other equipment.

Several other rocket payloads have been designed to measure V.L.F. signals and the pitch angle and energy distribution of charged particles. Three such payloads are described by Gendrin et al 1968 and one by Ungstrup 1971.

Summarising, it may be said that over the last 20 years a great deal of effort has been put into understanding the nature of the earth's magnetosphere and the processes which occur within it. Some phenomena such as whistlers are now well understood but the origin of discrete V.L.F. emissions and hiss is still being investigated. This work describes the design of a VLF receiver which together with a

charged particle experiment from Southampton University and other experiments from Birmingham and Sussex Universities formed a Skylark rocket payload which was launched from Andøya in December 1973. This payload collected data on wave-particle interactions during a magnetic sub-storm. The latter part of this work is concerned with the analysis of simple risers and hooks, which are thought to be generated by wave-particle interactions in the magnetosphere, using a theory proposed by Helliwell (1967).

1.3 SOME EXAMPLES OF V.L.F. EMISSIONS

Having discussed briefly the discovery of very low frequency emissions and their impact as a means of investigating the magnetosphere, it is appropriate to give some examples of these emissions. A selection of frequency-time profiles has been assembled from several sources and it is hoped to indicate the characteristics of the various emissions and show the wide range of observed profiles.

Frequency-time diagrams are produced usually by moving film slowly past a C.R.T. display which takes the form of an intensity modulated spot scanning through frequency up and down the tube. The 'Rayspan Spectrum Analyser' is an example of this type of equipment. The other most used method is to burn the signal intensity level onto carbon paper which revolves on a metal drum as the emission is scanned repeatedly in frequency, the best known equipment to use this technique is the 'Kay Sonograph'.

Spherics

We firstly consider well understood emissions such as spherics which are short bursts of electromagnetic energy having a very wide

FIG. 1.1

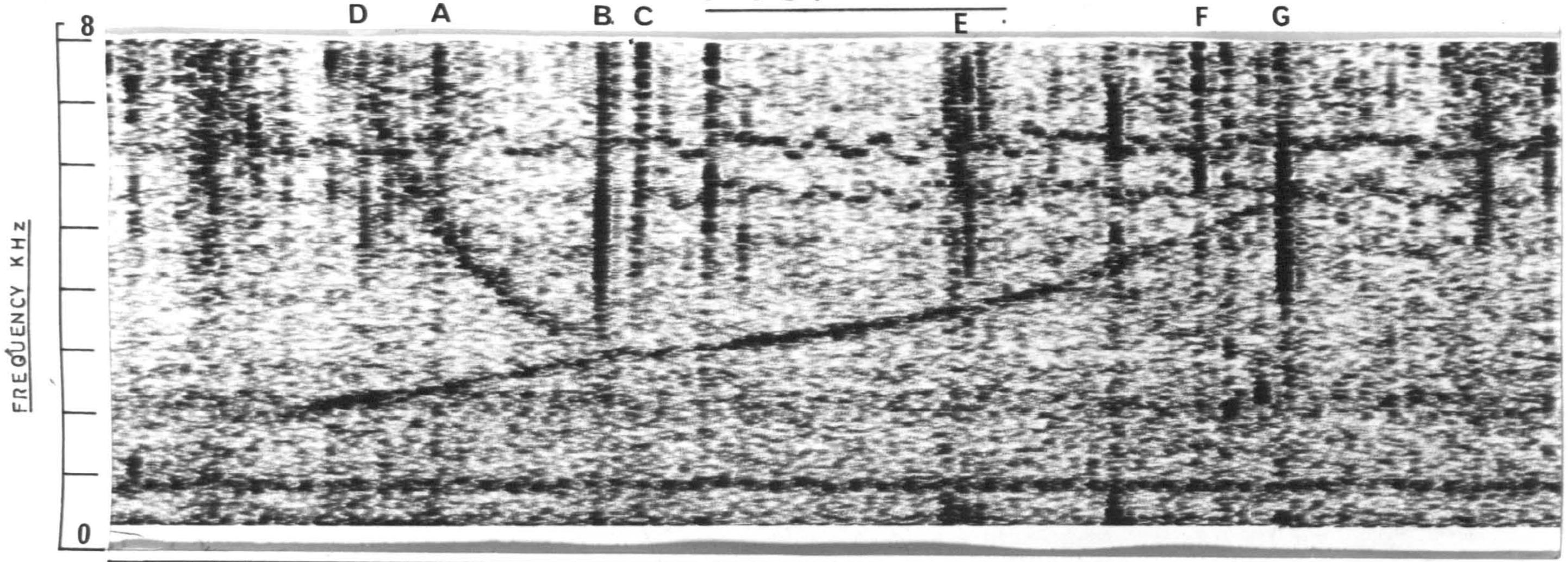

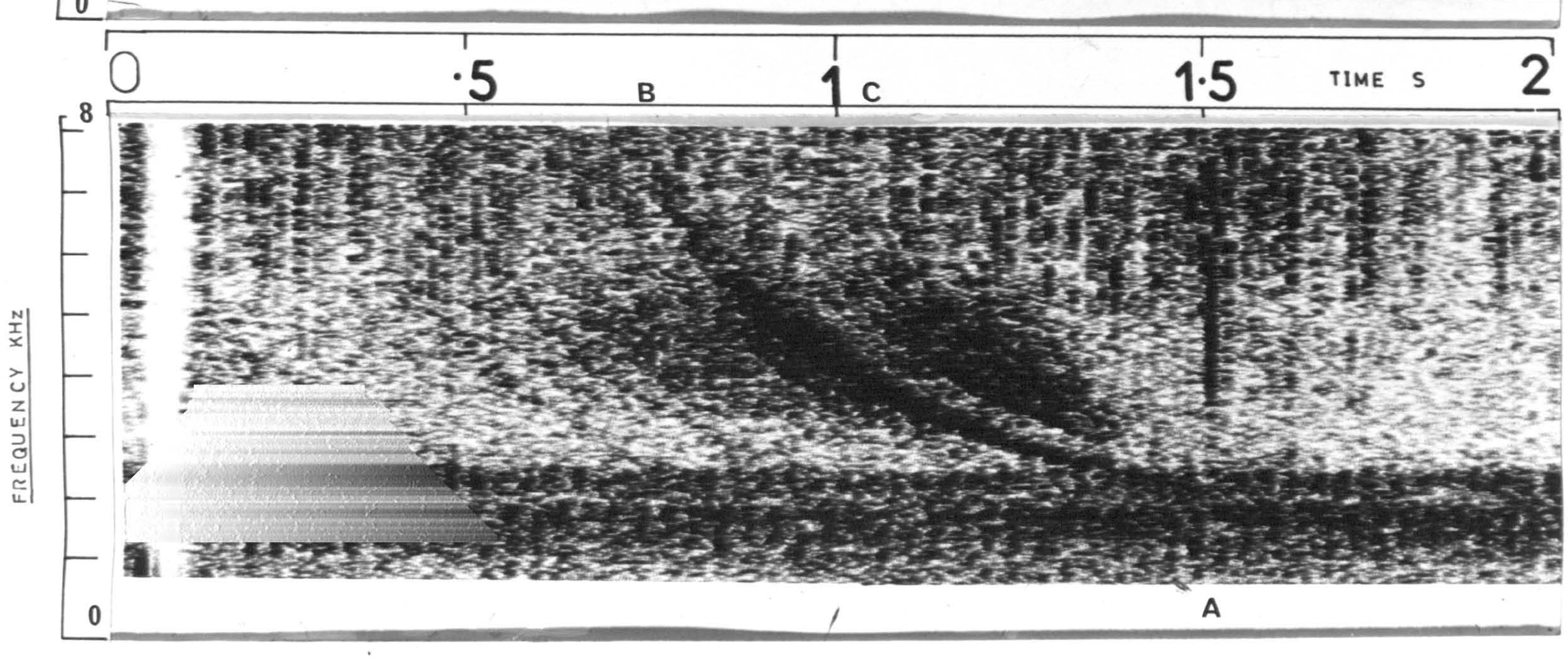

FIG. 1.2

spectrum. This is shown as a thin vertical line on a 'Sonograph' chart. Examples can be seen in Fig. 1.1 marked as A,B,C etc and in Fig. 1.2 marked A. These spherics were recorded at Sheffield University V.L.F. station at Halley Bay, Antarctica (L = 4) in 1972.

Whistlers

A whistler is heard as a falling tone often starting at about 10 KHz and falling to 1 or 2 KHz in a matter of half a second. Examples can be seen in Fig 1.1 marked D and in Fig 1.2, B & C and also in Fig. 1.3,A.

Nose whistlers

Quite a good example of a train of 'nose whistlers' can be seen in Fig. 1.4. The position of the nose is denoted by the letter 'n' and there are at least six clearly defined emissions. These were also recorded at Halley Bay in 1972.

Man made signals

A great number of V.L.F. transmitting stations with powers ranging from ½ to 1 MW exist at many places around the world. They can be used to give information about the magnetosphere and ionosphere as well as providing a fixed signal source which can be used to 'check' the accuracy of apparatus which takes bearings of V.L.F. signals. Examples of such stations can be seen in Fig 1.5. The lower horizontal lines are the OMEGA navigation stations, the upper trace is thought to be NRX. Both stations are being 'keyed' on this record which was taken at Andøya, Norway in November 1972.

Hiss

In Fig.1.5 a dark band of hiss can be seen ranging from about 4 to 8 KHz. It has a fairly stable amplitude

FIG. 1.3

A
8
FREQUENCY KHz
0

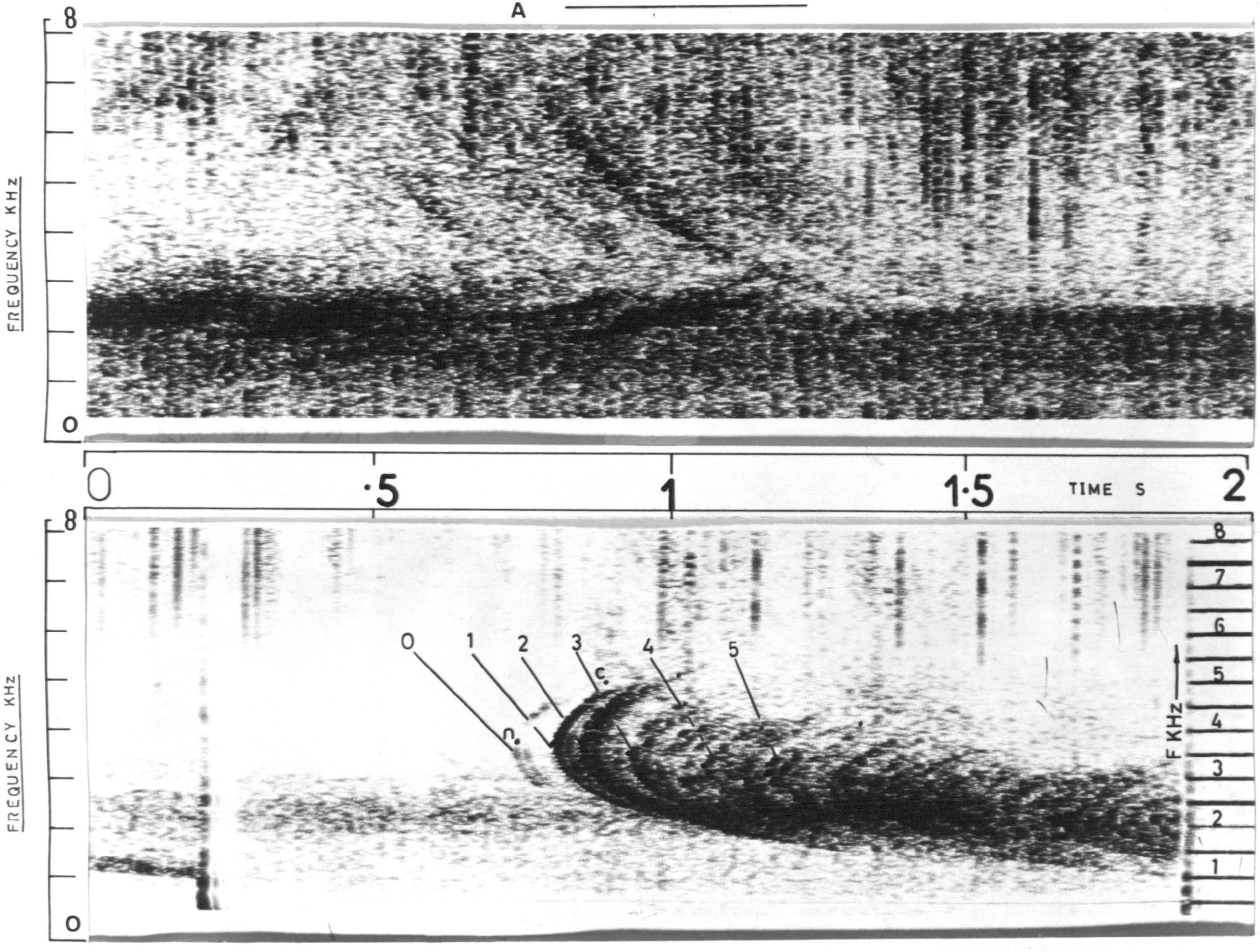
0
·5
1
1·5
TIME S
2
8
FREQUENCY KHz
0
0
1
2
3
c.
4
5
n.
F KHz
8
7
6
5
4
3
2
1

FIG. 1.4

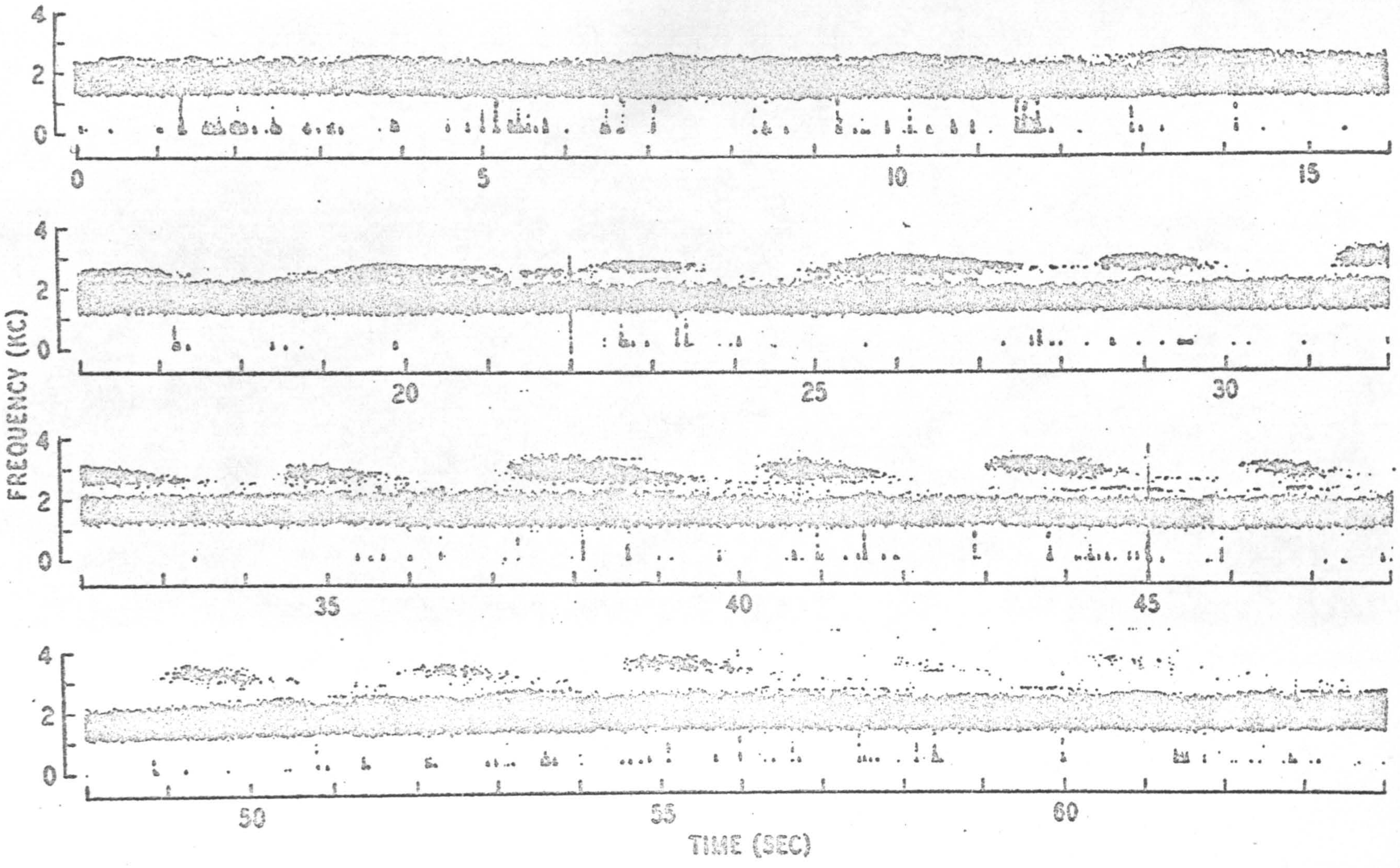

"Surf" recorded at College, Alaska (after Pope and Campbell [13]).

Fig. 1.6

SONAGRAM P47H

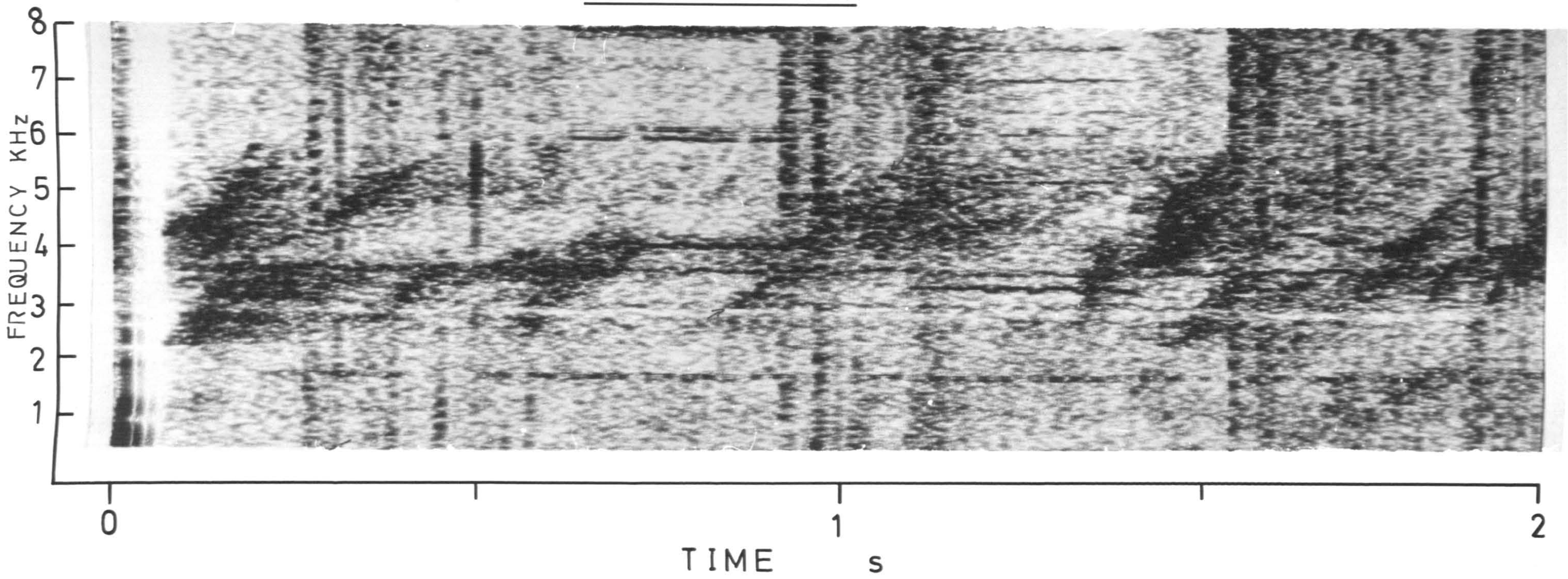

FIG.(1.7)

FIG. 1.5

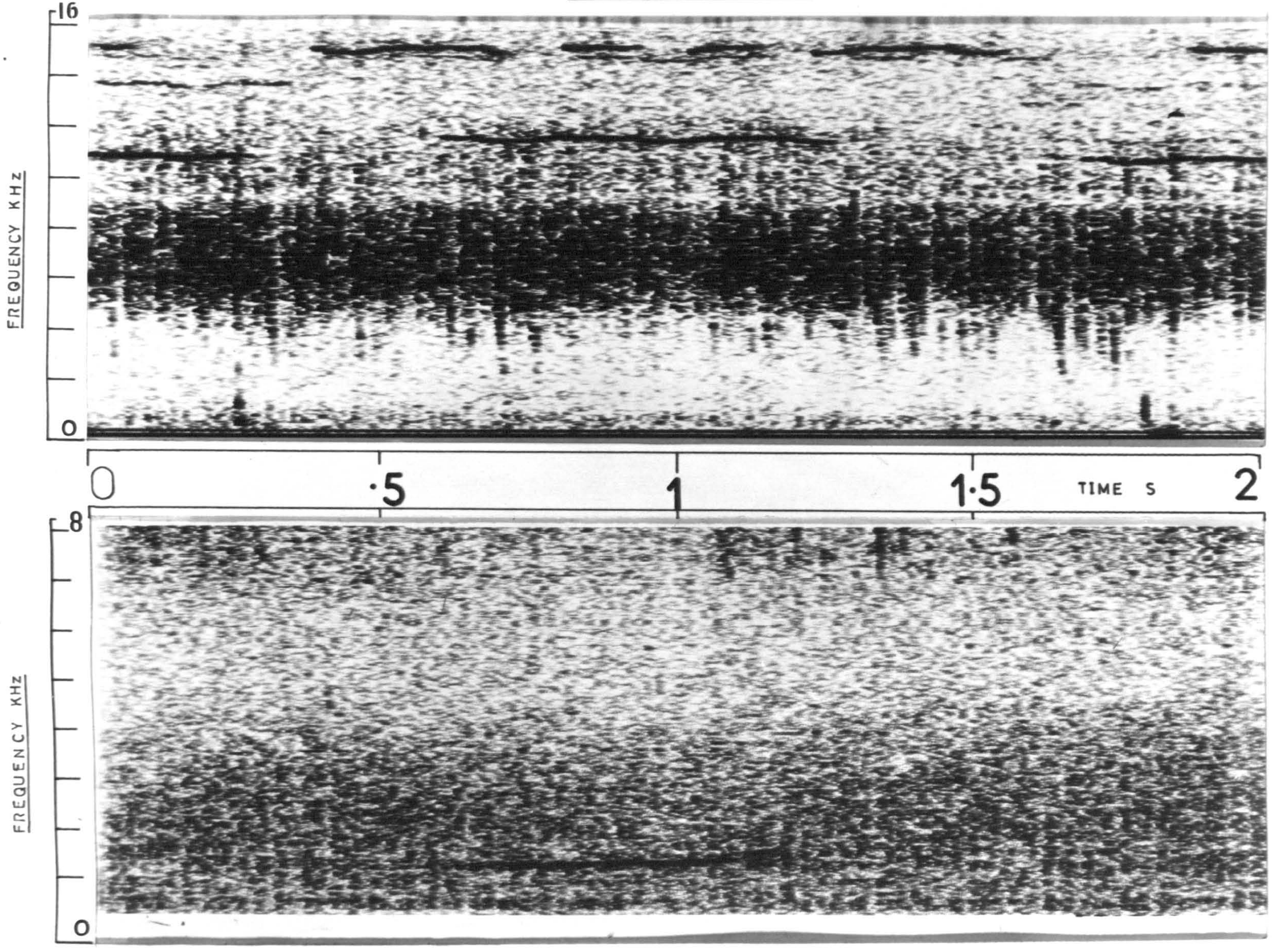

FIG. 1.8

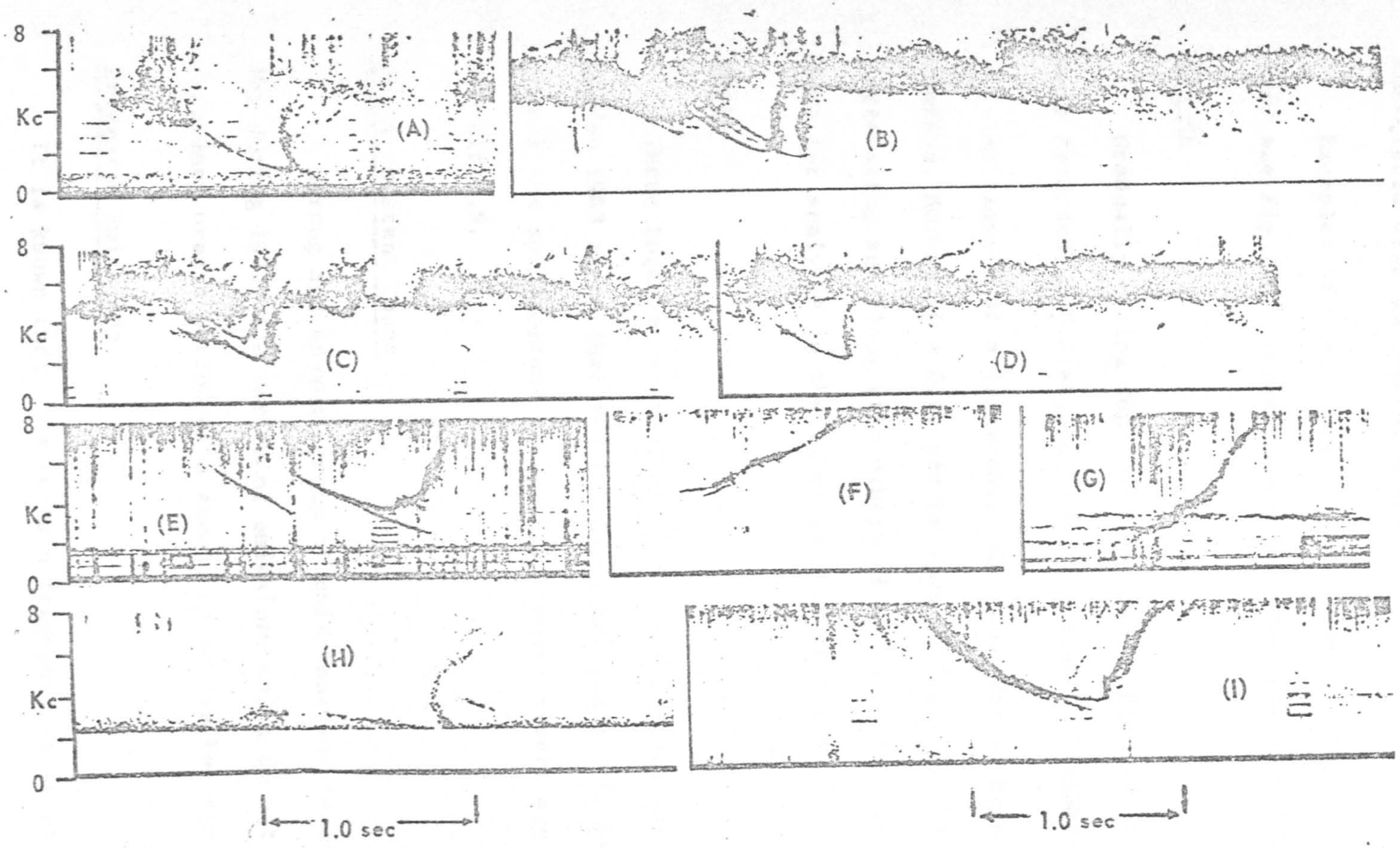

Spectrograms of discrete V.L.F. emissions (after Helliwell and Carpenter, 1961) "Falling tones" appear in *E*, "quasi-constant tones" in *G*, and "risers" in *F* and *G*. The other forms are probably all "hooks".

Fig. 1.9

over the period of this record and the appearance of this hiss was correlated with an auroral display.

Examples of 'surf' are given by Dowden 1963 after Pope & Campbell 1960 see Fig 1.6. These recordings were made at College Alaska.

Risers

Gradually rising tones can be seen in Fig 1.7. These examples were recorded at S.Uist,Scotland (L = 3.4) in November 1970.

An example of a riser which was recorded at high latitudes (Andøya, Norway, L = 6.2) can be seen in Fig 1.8. This emission is interesting and along with others of the same type provide the basic data for analysis in the later part of this work.

Hooks

These together with other discrete emissions are given by Dowden 1963 after (Helliwell & Carpenter 1961). Hooks can be seen on all the spectrograms except F & G where risers are the main feature. See Fig.1.9.

Quasi-constant Tones

A strong and unusual group of emissions was recorded at Halley Bay during 1972. The series of emissions which do not vary greatly in frequency over a period of a second or so can be seen in Fig. 1.10.

Triggered Emissions

It is known that at a certain frequency it is possible for a signal such as a whistler to trigger off a second emission which may persist for some time. An example of this interesting behaviour can be seen in Fig.1.11 where a 'nose whistler' triggers a shallow hook.

FIG. 1.10

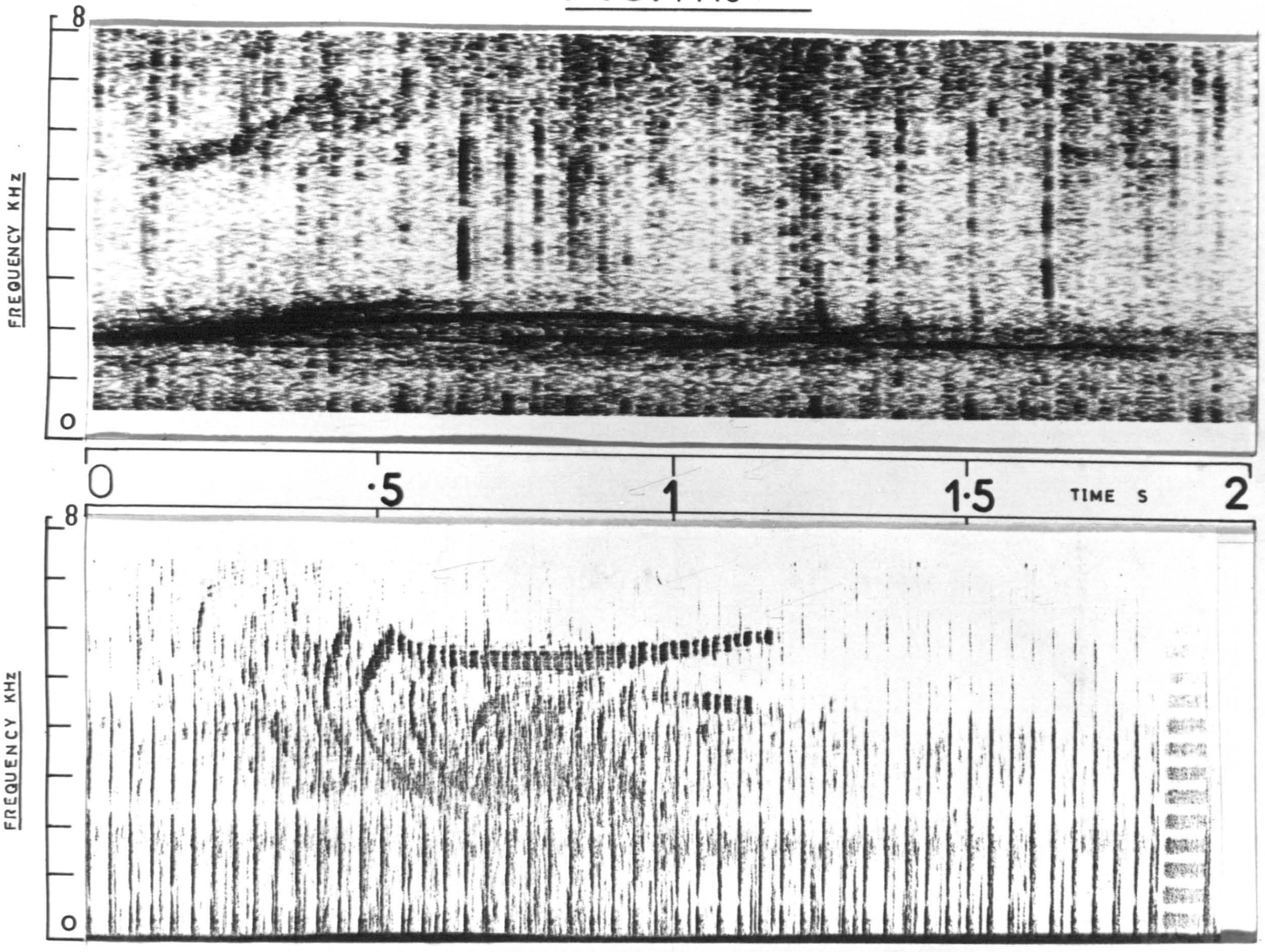

FIG. 1.11

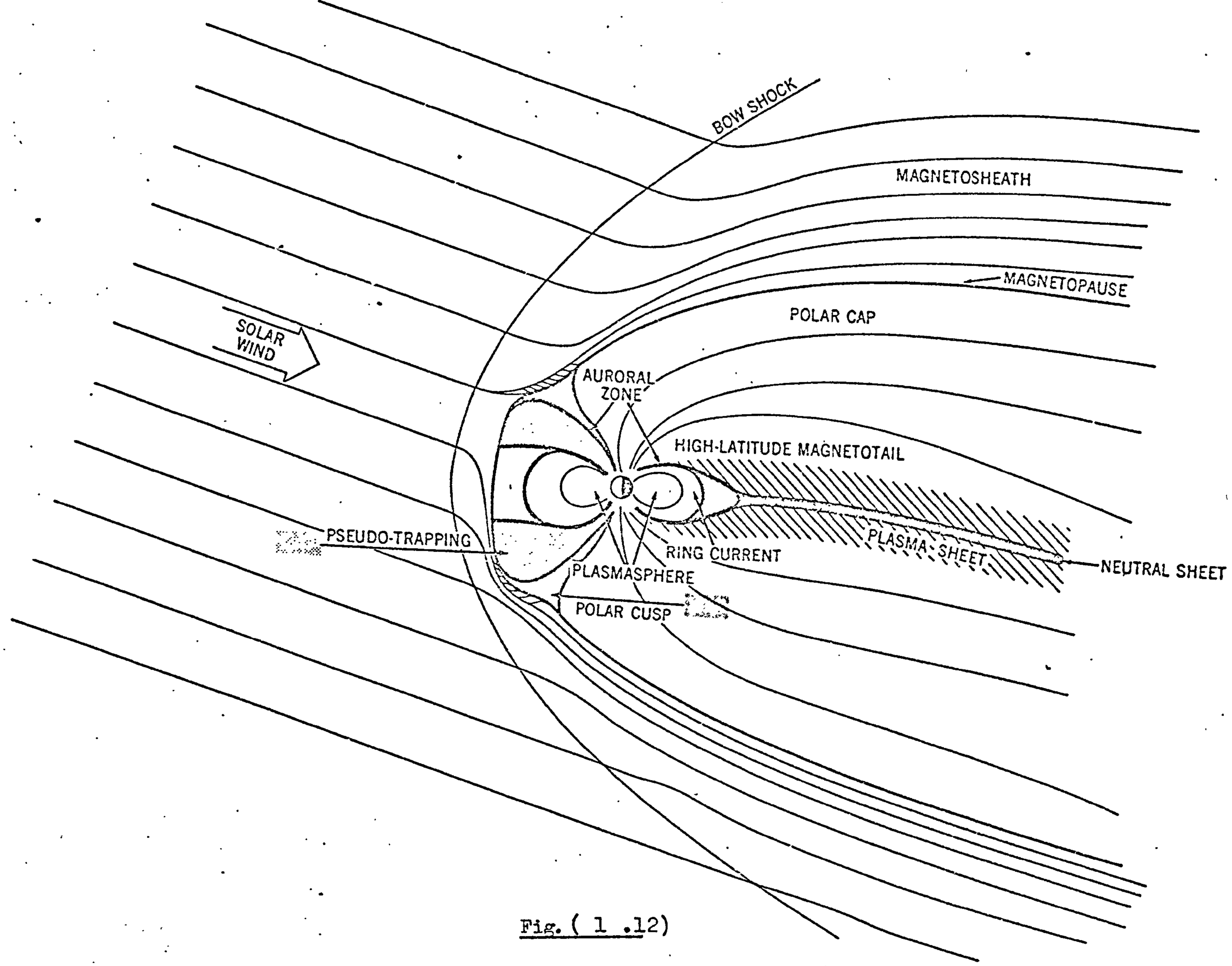
BOW SHOCK
MAGNETOSHEATH
MAGNETOPAUSE
POLAR CAP
SOLAR WIND
AURORAL ZONE
HIGH-LATITUDE MAGNETOTAIL
PSEUDO-TRAPPING
RING CURRENT
PLASMA-SHEET
NEUTRAL SHEET
PLASMASPHERE
POLAR CUSP

Fig. (1 .12)

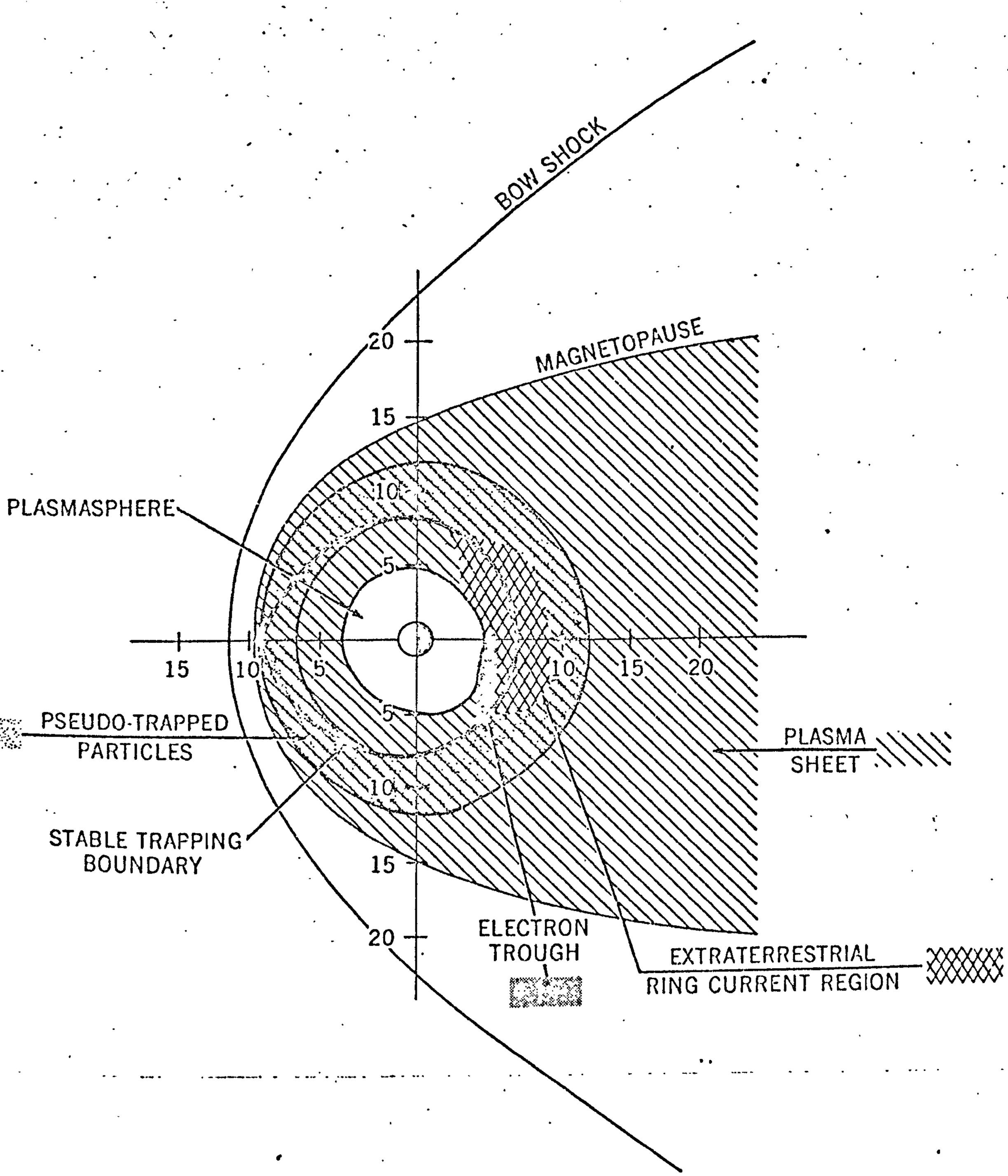
BOW SHOCK
MAGNETOPAUSE
PLASMASPHERE
PSEUDO-TRAPPED
PARTICLES
STABLE TRAPPING
BOUNDARY
PLASMA
SHEET
ELECTRON
TROUGH
EXTRATERRESTRIAL
RING CURRENT REGION
20
15
10
5
5
10
15
20
15
10
5
5
10
15
20

Fig.(1 .13)

This recording was made during September 1970 at Halley Bay.

It can be readily seen that the variety of V.L.F. emissions is great and it is interesting to speculate on a mechanism or mechanisms which would be capable of generating them, It has been shown by Helliwell (1967) and others that the interaction of energetic electrons and R.H. circularly polarised whistler-mode electromagnetic waves in the magnetosphere can give rise to some of the observed forms.

1.4 A BRIEF DESCRIPTION OF THE MAGNETOSPHERE

In understanding how emissions may be generated by wave-particle interactions it is important to know something of the types, locations and flux densities of particles in the magnetosphere.

Since the early discovery of energetic particles within the magnetosphere, one of the first sources postulated was the solar wind. However,'the detailed manner in which the particles could flow into the cavity and subsequently be accelerated has been somewhat obscure,' states Vette (1972). Recent ideas and measurements have clarified the position greatly and particles found in the interplanetary medium seem to be the source for most regions of the magnetosphere.

As shown in Fig 1.12, the solar wind flow is diverted around the magnetopause and.fills the magnetosheath region. Hundhausen (1970) has summarised the plasma parameters under quiet conditions for both the interplanetary medium and for the magnetosheath near the dawn-dusk meridian. The solar wind which consists mainly of protons and electrons with a small alpha particle component of

some 5 - 20%, has a particle density of $n \sim 5$ cm^{-3} and a speed of flow of approximately 320 km sec^{-1} nearly radially from the sun. The random motion of the electrons and protons can be represented by temperatures $T_e \sim 1.5 \times 10^5$ ^oK and $T_p \sim 5 \times 10^4$ ^oK. In the magnetosheath region part of the solar wind streaming energy is converted into a heating of the plasma, and typical parameters are : $n \sim 15$ cm^{-3}, velocity of $\sim$ 250 km sec^{-1} with $T_e \sim 5 \times 10^5$ ^oK & $T_p \sim 10^6$ ^oK. The magnetosheath electron and proton spectra peak at about 150 and 300 eV respectively.

Frank 1970 has sometimes detected interplanetary protons in addition to the normal solar wind, with energies in the region 5 to 50 keV lasting about one day. The maximum density of $n \sim 10^{-2}$ cm^{-3} occurs at energies of around 20 keV.

At first it seemed that the magnetopause acted as an impenetrable barrier to any plasma flow from the magnetosheath into the magnetosphere. However measurements by Heikkila and Winningham 1971 and Frank 1970a have shown that the magnetosheath plasma flows through a region associated with the polar neutral points. This flow of plasma which goes into the dayside auroral oval, is a usual feature of the region and occurs in a broad band (in longitude) across the magnetosphere. This region is called the polar cusp and is marked in Fig. 1.12. As is true for most magnetospheric regions, the location of the polar cusp is variable depending on interplanetary conditions. Russel et al 1971 have reported observing it as low as 43^o (magnetic latitude) with the OGO 5 satellite.

Frank 1970a and Hill & Dessler (1971) have given magnetospheric models in which the particles from the polar cusp flow into the plasma sheet region of the magnetotail.

Within the plasma sheet at 18 R_E, Hones 1970 and Hones et al (1971) have summarised the particle population. Electrons and protons have average energies of $\sim$ 1 and $\sim$6 keV respectively and number densities of $\sim$ 0.5 cm^{-3}. The plasma sheet pressure responds proportionally within minutes of a change in the dynamic pressure of the solar wind and Hones et al (1971a) have shown that there is a thinning of the plasma sheet during substorms which represents a net loss of magnetospheric plasma.

Inside the plasmasphere at about 4 R_E (see Fig.1.13) there is a dramatic rise in the electron number density from about n = 1 - 10 cm^{-3} to n $\sim 10^3$ cm^{-3}, for moderately disturbed conditions Angerami 1966. Typical energetic electron energies inside the plasmasphere are about 1 keV to 1,000 keV with fluxes of 10^6 to 10^8 electrons cm^{-2} sec^{-1} at the equator, (Vette 1972) quoting results from OGO 1 and OGO 3 satellites.

A detailed description of the energetic particle populations of the various magnetospheric regions can be found in the report by Vette 1972 and in the book "The Radiation Belt and Magnetosphere" by W.N. Hess, (Hess[1]).

A great deal of work studying energetic particles is continuing to be done using particle detectors on board rocket probes and satellites.

CHAPTER 2

OBSERVATIONAL TECHNIQUES

2.1 GROUND BASED RECEIVERS

In its elementary form the equipment needed to receive man made and naturally occurring very low frequency radiation is quite simple. It consists basically of an antenna which can be either a long wire suspended above the ground or a loop consisting of a number of turns of wire in which the E.M. wave generates an e.m.f. The antenna is coupled to a low noise preamplifier and the signal is passed through a filter bank to remove unwanted signals such as mains derived interference. Finally the signal is recorded on magnetic tape. As most quiet sites suitable for making V.L.F. observations are remote the ability to make tape recordings allows the collected data to be transported to the laboratory for processing and storage in a most convenient form.

A receiver which uses a long wire antenna, due to Ashok[2] has been used by the author at Andøya to great effect. Its only drawback is that in a high wind the aerial wire tends to vibrate resulting in the production of interfering signals. This also happens with loop antennas but to a lesser degree.

Several receivers which use loop antennas have been used by the author and such receivers are commonly used throughout the world. Dowden (1963) made use of two vertical loops which were triangular measuring 40 ft at the base with the apex 20 ft above ground giving a loop area of 40 m^2. A rectangular loop approximately 3m x 2m acts as the antenna at a V.L.F.

receiving station on S.Ulst Scotland (Rycroft[3]) and was used to record dawn chorus which was present at the time a V. L.F. rocket payload P47H was launched. Evidence of the effectiveness of relatively simple equipment can be seen in Fig.1.7.

More sophisticated equipment utilising a pair of crossed loop aerials which have an area of 100 m^2 has been developed by Bullough (1973). Using the two loops it is possible to electronically synthesize a rotating loop aerial. This allows the bearing of a received signal to be determined and much information can be obtained on the movements of exit points from ducts of enhanced electron density in the magnetosphere by observing the direction of arrival of whistlers Sagredo (1973). Such equipment has been operated at Halley Bay since the mid 1960's by the Sheffield group.

Other, earlier workers have used the crossed loop goniometer technique Watts (1959), Crary(1961) & Ellis and Cartwright (1959) but all used some mechanical device to simulate the rotating loop. Pulley (1935) was probably the first to synthesize a rotating loop electronically.

Until recently one of the problems with ground based receivers was the size of the aerial required to achieve the high sensitivities ($10^{-14}\gamma^2/Hz$) necessary to observe magnetospheric emissions, which are attenuated by the ionosphere and in the earth-ionosphere waveguide. However, advances in transistor and particular F.E.T. technology have made possible the production of extremely low noise wide band audio amplifiers. This has meant a reduction in antenna loop area of about 20 times for the same sensitivity.The design of such a system using a $5m^2$ loop was produced by K.Bullough and the author, but is not reported here.

2.2 ROCKET BORNE RECEIVERS

The characteristics of V.L.F. signals can be studied as a function of altitude by using skilfully designed miniature transistorised receivers which are flown on rocket probes. Ideally with six antennas and receivers the polarisation, wave normal direction and Poynting vector of a signal which is propagating through the ionospheric plasma may be determined as a function of height, Shawhan (L970).

Rycroft (1972) points out that up to that date relatively few such experiments had been carried out. Cartwright (1964 & 1964a) has reported the reception by rocket borne equipment of two-hop whistlers with wave normals at 30^{o} to static magnetic field which were not observed by ground based receivers. He concludes that the emissions were probably not ducted but loosely guided along the earth's magnetic field. It is convenient to describe rocket borne equipment used by workers to date in groups according to the type of receiving antenna employed. There are;single axis open loops,multiple axis open loops, multiple axis'cored' loops, all measuring the strength of the magnetic component of the electromagnetic wave being studied. Rocket borne V.L.F. receivers often have antennas which are sensitive to the electric field component of the wave. Two types of antenna are widely used; the short dipole and the capacitative double spheres.

a) Examples of payloads using a single axis open loop antenna

Ungstrup (1971) presents the results of three rocket borne experiments having a single loop perpendicular to the rocket spin axis in each case.

They were flown on Centaure &

60 turns
Area=0.2 m^2

Loop Aerial

Match. Trans.

Preamplifier

Low Imp.

Filter

Voltage controlled amp.

Narrow band filter 2.35 KHz

Detector & Smoothing.

A.G.C. line

2.9 KHz

3.5 KHz

4.4 KHz

5.4 KHz

9.6 KHz

16 KHz

5,17

2,18,10

4
12
20

6
14
22

11
23

19

9,21

V.L.F.Section of Payload P47H

V.H.F FM-AM TX.

24 way comutator.

Data from Langmuir Probe.

Temp.

Sweep

Current

Nose Cone Deployment

Housekeeping

Low Speed

FIG(2.0)

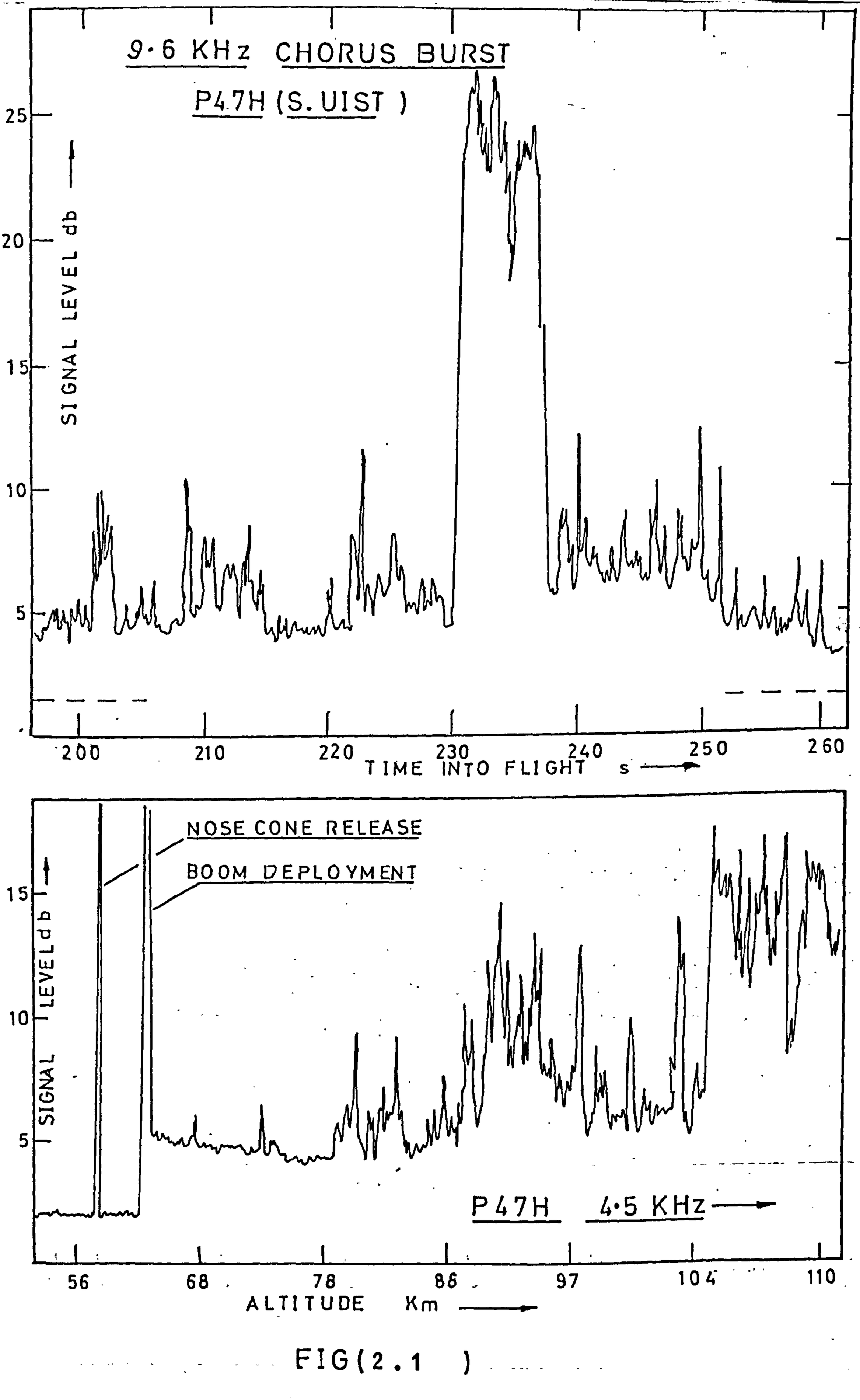
9·6 KHz CHORUS BURST
P47H (S.UIST)
SIGNAL LEVEL db
25
20
15
10
5
200
210
220
230
240
250
260
TIME INTO FLIGHT s
NOSE CONE RELEASE
BOOM DEPLOYMENT
SIGNAL LEVEL db
15
10
5
P47H 4·5 KHz
56
68
78
86
97
104
110
ALTITUDE Km

FIG(2.1)

Nike-Apache vehicles being launched from ES Range, Sweden (L = 5.5) and Andøya (L = 6.3) and reaching altitudes of 126 & 138 km respectively. He concluded that auroral hiss at 7.35 KHz is, in some cases, generated in auroral arcs at altitudes of 105÷110 km and from the occasional observation of spin modulation that the wave normal angle to the magnetic field can be $\sim 80^{o}$.

Rycroft et al (1972) describes the results of observations of dawn chorus made with a single axis loop receiver aboard a Petrel rocket which was launched from S.Ulst (L = 3.4). This payload was the product of a co-operative effort by the Universities of Sheffield and Southampton. The author was involved with the engineering and launching of this payload and it will be described briefly to indicate the composition of such experiments..

The design of the V.L.F. receiver is due to Vavra (1970) and that of the Langmuir Probe electron density package due to Beckingham (1970) and Gibbons, (unpublished). A block diagram of the multi-channel V.L.F receiver is shown in Fig.2.0 and a photograph of the complete experiment showing the deployable loop aerial and Langmuir Probe is numbered Fig.2.2.

The filter bandwidths are nominally 100 Hz and the centre frequencies were chosen to provide coverage from 2 to 6 KHz for the study of chorus emissions and at 16 KHz for the study of the GBR wavefield in the ionosphere. The Langmuir Probe provides a measurement of the refractive index of the magnetoionic plasma which is necessary for the interpretation of the VLF data.The large dynamic range of VLF signals $\sim$ 60 db requires the filtered components to be subject to a logarithmic compression which is achieved by the use of an AGC amplifier.The AC signal is then detected and passed to the telemetry such that is is sampled at regular intervals.

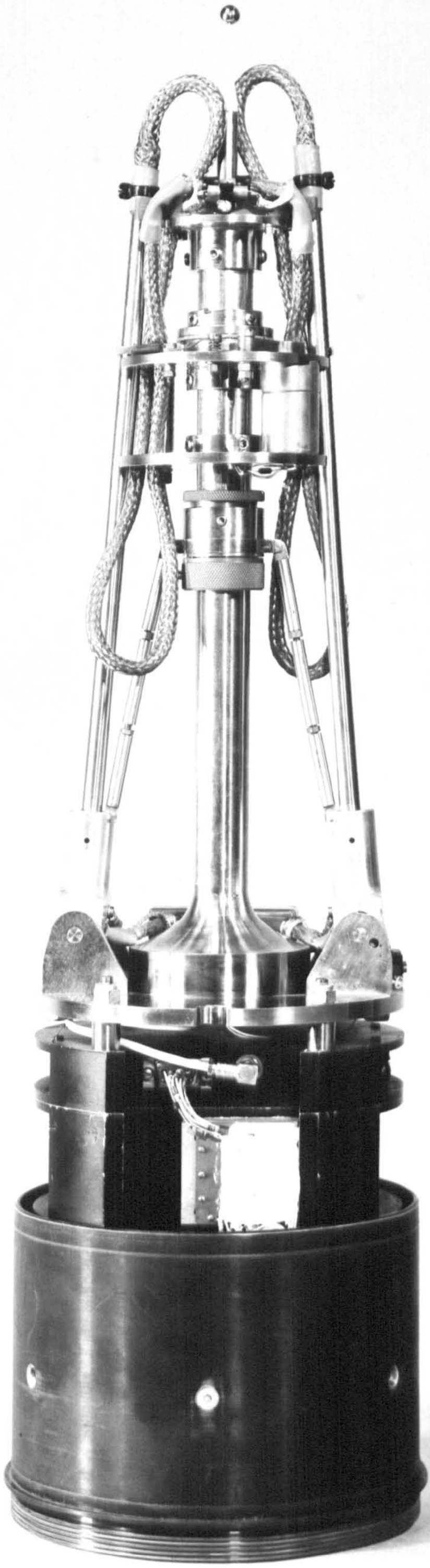

P47H

FIG.2 . 2

Examples of the 9.6 KHz signal level and the 4.5 KHz level as functions of flight time and altitude respectively are given in Fig. 2.1. A general increase in chorus signal strength can be seen as the payload passes through the absorbing D region and single events become more evident showing up as narrow spikes. Single spikes can often be seen in frequency channels at slightly different times indicating the reception of a riser etc. It has been possible to correlate some events with the reception of discrete emissions on the ground. An unusual burst of high frequency chorus was observed for a period of 10 minutes in the 9.6 KHz channel. This feature is discussed by Rycroft et al (1972).

From the observations made with payload P47H it was possible to deduce that the wave normal directions of chorus signals propagating at altitudes between 90 and 130 km at (L = 3.4) were at times consistent with their being a plane wave propagating in the whistler mode along the geomagnetic field lines, Rycroft et al (1972).

A similar payload (P 55A) was launched from Andøya in October 1972 into auroral hiss. This experiment will be discussed later. Using loop antennas with areas of about 0.2 m^2 the experiments achieved a sensitivity of 5 x $10^{-10}\gamma^2$/Hz at 3 KHz rising at 6 db/octave over the frequency range up to 20 KHz. This figure is in line with results published by Shawhan & Gurnett (1968) who achieved a sensitivity of $10^{-11}\gamma^2$/Hz with 1 m^2 loops.

Although single axis loop antenna receivers are useful, especially if the rocket is spinning rapidly, they can provide only limited information and a better description of the characteristics of an EM wave can be achieved by the use of multiple antennas, Shawhan (1969).

b) Examples of payloads using multiple open loop antennas

Shawhan (1969) states that Helliwell (1956) had considered the optimum design of V.L.F. loop aerials. Shawhan & Gurnett (1968) flew experiments consisting of three orthogonal open loop antennas along with several electric field probes on board Javelin rockets. They observed a noise band having both electric and magnetic components in the frequency range 7 to 30 KHz and at 10 KHz the electric and magnetic spectral densities were about $10^{-4}Vm^{-1}\ Hz^{-\frac{1}{2}}$ and 2 x $10^{-4}\gamma Hz^{-\frac{1}{2}}$ respectively. From the simultaneous measurements of electric and magnetic components of

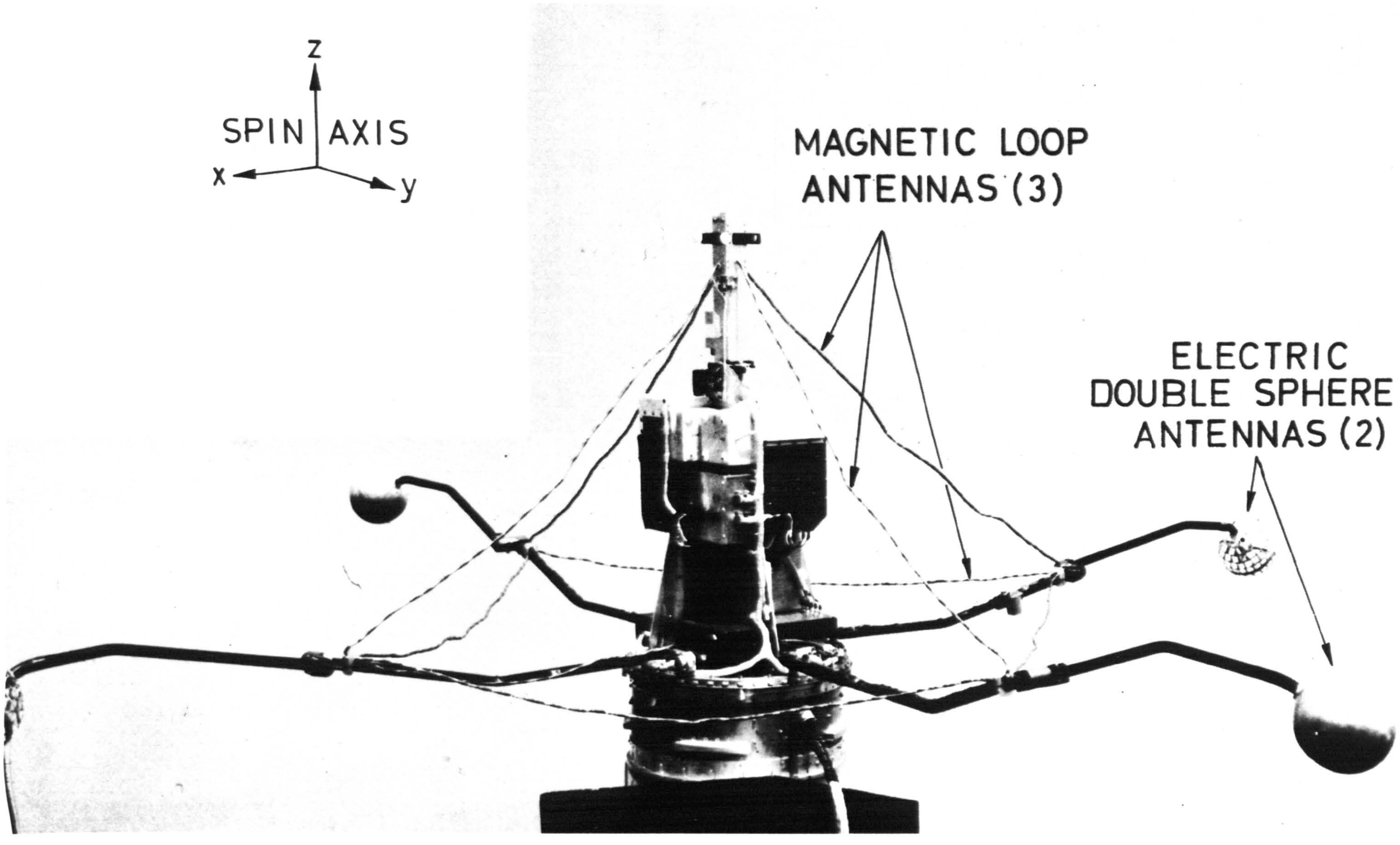

JAVELIN **8.45**

FIG. 2.3

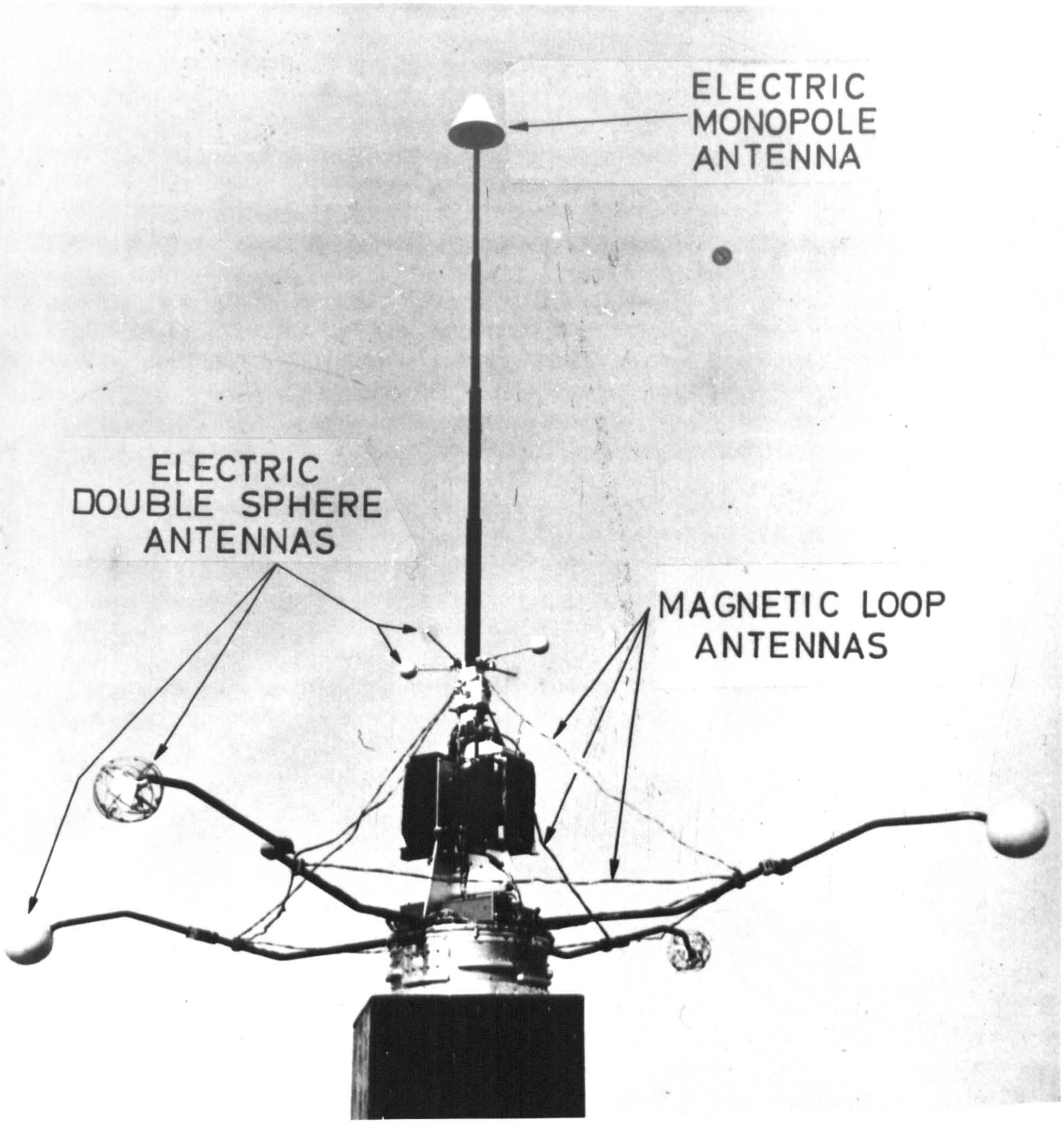
ELECTRIC
MONOPOLE
ANTENNA
ELECTRIC
DOUBLE SPHERE
ANTENNAS
MAGNETIC LOOP
ANTENNAS
JAVELIN. 8.46

FIG. 2.4

the wave it was possible to show that the wave normals were for the greater part nearly 90° to the static magnetic field. These signals were evidently not propagating in the whistler mode where the wave normals are closely aligned to the magnetic field. Photographs of the javelin rocket payloads 8.45 to 8.46 can be seen in Figs. 2.3 and 2.4.

A Petrel rocket experiment P129A which had three orthogonal open loop antennas was launched from Andøya in November 1972. The loops and receivers were essentially those used on P47H and P55A. The signal levels occurring in narrow bands at 1.25KHz, 3.2 KHz & 16 KHz were telemetered to the ground station during the flight which achieved an altitude of 128 km. The payload was launched into high latitude or 'Polar Chorus', an example of which can be seen in Fig. 1.8. A picture of the payload can be seen in Fig 2.5. Although only preliminary analysis of the data has been completed examples of the signal levels at 1.25 KHz, 3.2KHz and 16 KHz as functions of altitude can be seen in Fig 2.6. Using auto-correlation and fourier transform routines it is possible to compute the power spectrum of the narrow band signals. An example of the low frequency end (0 to 24 Hz) of the power spectrum of the 16 KHz channel shows clear evidence of spin modulation at 5.3 Hz. The spin history of P129A can be seen in table 2.1. Although the author was involved with the building testing and launching of this round and also with the preliminary analysis shown here the period of the research work was such as to prevent any deeper analysis, although there is clearly much interesting work to be done. It is hoped that the study of wave normal angle distribution will show that these chorus elements are propagating in the whistler mode which is consistent with their being generated near the equator by particle-wave interactions.

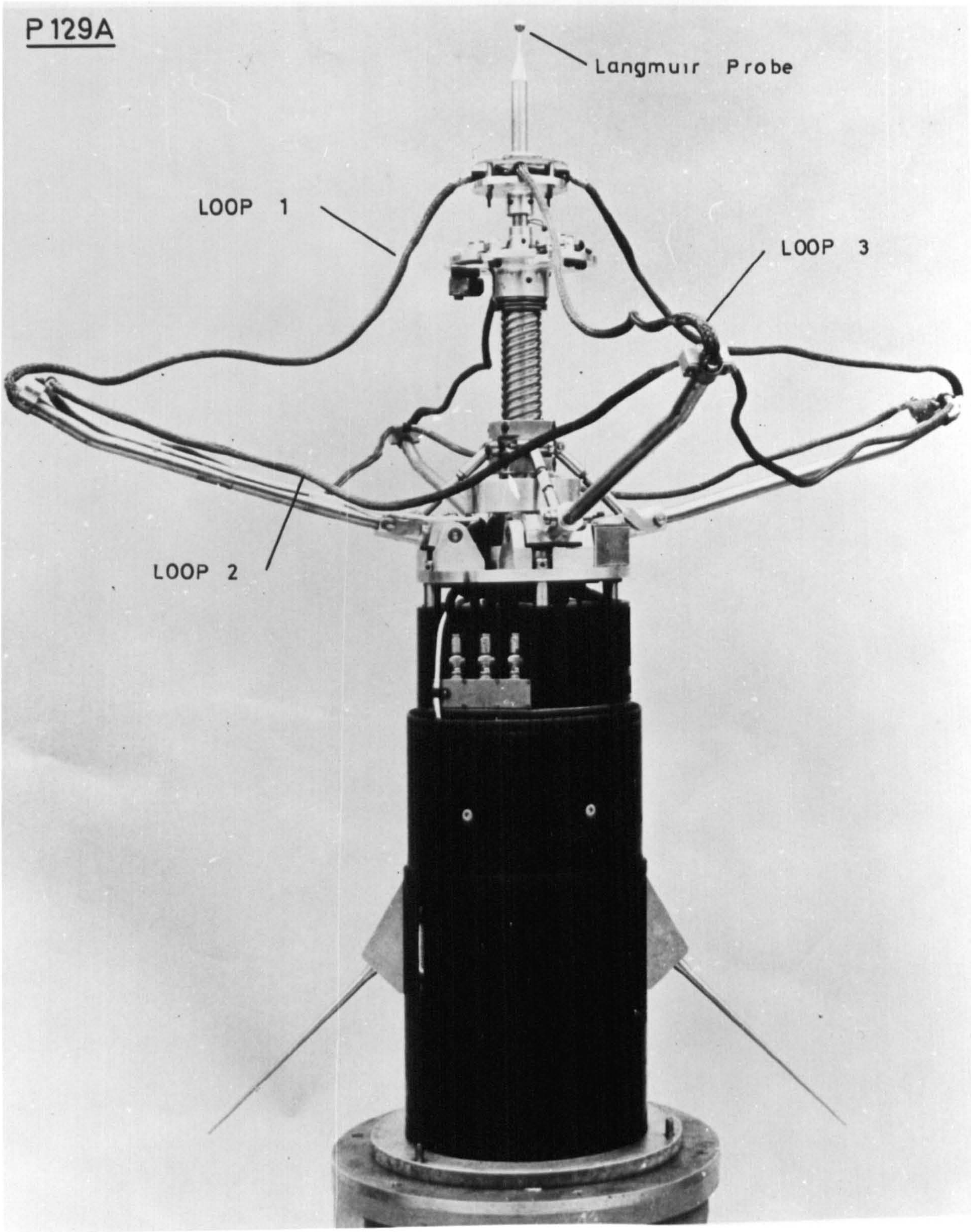

FIG. 2.5

P129A (Spin History)

Time (secs)	Spin Rate (c.p.s.)
11	2.4
12	2.5
13	2.6
14	2.6
15	2.8
16	3.0
17	3.3
18	3.4
19	3.7
20	3.9
21	4.1
22	4.3
23	4.7
24	5.1
25	5.4
26	5.8
27	6.2
28	6.7
29	7.0
30	7.4
31	7.6
32	7.8
33	7.7
34	7.7
35	7.7
36	7.6
37	7.5
38	7.4
39	7.4
40	7.3
50	7.1
60	7.1
70	5.5
80	5.4
90	5.4
100	5.3
110	5.3
120	5.3
130	5.3
140	5.3
150	5.3
160	5.3
170	5.3
180	5.3
190	5.3
200	5.3
210	5.3
220	5.3
230	5.3
240	5.3
250	5.3

TABLE 2.1

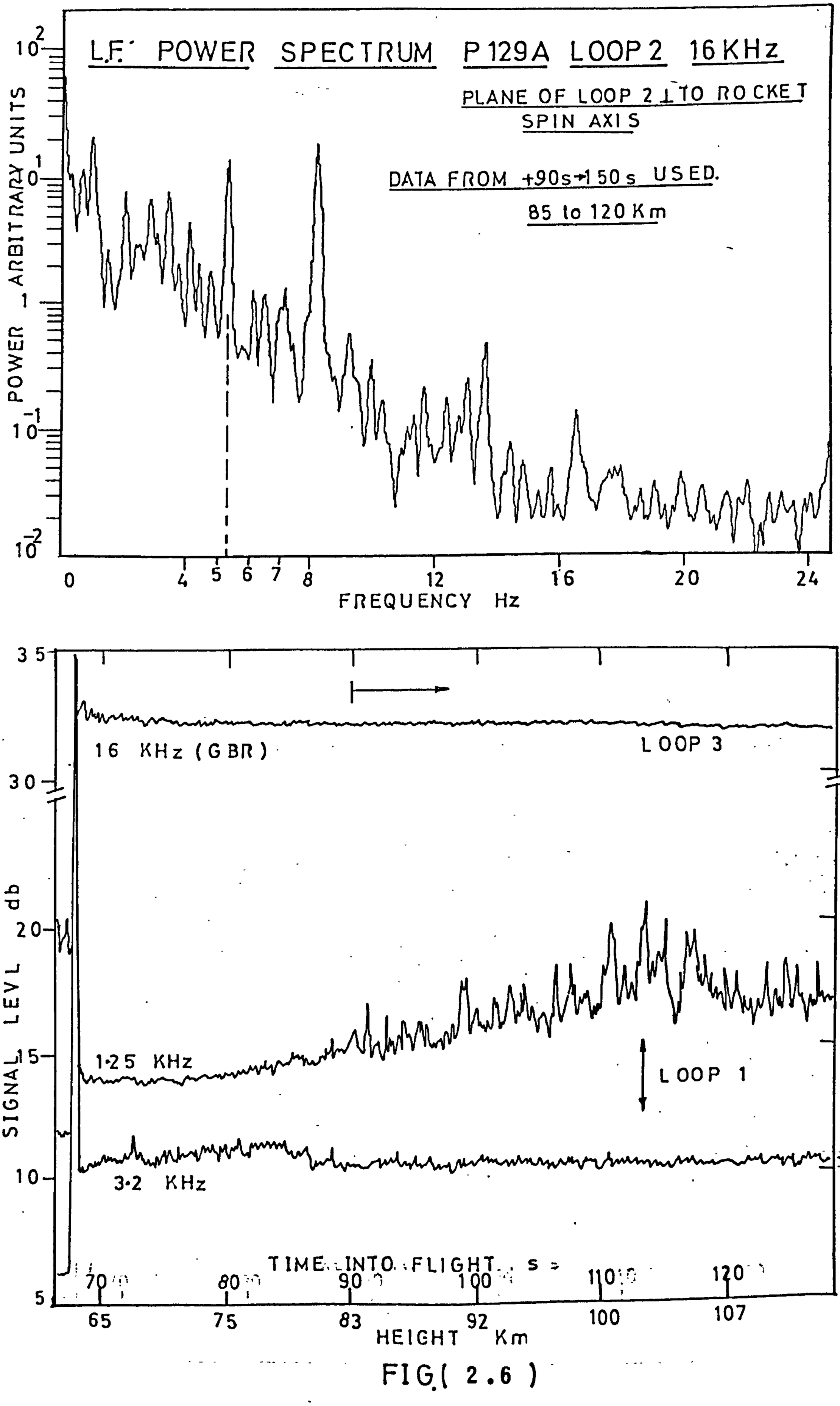
L.F. POWER SPECTRUM P129A LOOP 2 16 KHz
PLANE OF LOOP 2 ⊥ TO ROCKET SPIN AXIS
DATA FROM +90s→150s USED.
85 to 120 Km
POWER → ARBITRARY UNITS
10^{2}
10^{-1}
10^{-1}
10^{-2}
0
4
5
6
7
8
12
16
20
24
FREQUENCY Hz
16 KHz (GBR)
LOOP 3
1·25 KHz
LOOP 1
3·2 KHz
SIGNAL LEVL db
35
30
20
15
10
5
TIME INTO FLIGHT s →
70
80
90
100
110
120
65
75
83
92
100
107
HEIGHT Km

FIG.(2.6)

The design of two multi-antenna (2 vertical loops, 1 horizontal loop and an electric field probe) rocket payloads for use on Aerobee vehicles (4.58 UI & 4.59 UI) is discussed in great detail by Orsak et al (1965). One of the vertical loops acted as the antenna for three receivers operating in the ranges 0.2 - 1.6 KHz, 1.6 -12.5 KHz and 12.5 -100 KHz. The second vertical loop was connected to a receiver operating from 1250 KHz up to 1.6 MHz and the horizontal loop was used to observe the wavefield of NSS V.L.F. transmitter on 22.3 KHz.

The V.L.F. experiment was augmented by an aerial impedance experiment which used a short electric dipole. The rocket flights as well as producing useful data in their own right also acted as a test of the equipment to be flown on NASA's EOGO satellite.

On payload 4.58 the electric antenna was ripped off and there was some interference in the receiver bands, however a hiss band was observed between 1.5 - 12.5 KHz above 85 km. There were no signals above the receiver threshold in the frequency range 0.2 - 1.5 KHz. Many V.L.F. stations and broadcast stations were observed with the high frequency receivers. On payload 4.59 the equipment functioned perfectly and intermittent hiss like signals were observed between 85 and 110 km in the frequency range 5 to 9 KHz. The most interesting observations were those made of 75 whistlers. This night time flight revealed some examples of a new whistler mode phenomenon. Most previously reported whistlers support a propagation model in which the electromagnetic radiation penetrates the ionosphere and propagates in the right hand circularly polarized mode along approximately field-aligned paths to the opposite hemisphere. Travel times from one hemisphere to the other are of the order of 1sec.Aboard this flight however, whistlers with

travel times of the order of 0.1 sec were found. The first example of a 'low dispersion whistler' was reported by Barrington & Belrose (1963) from their observation of Alouette records. Not until this flight was the widespread and frequent occurrence of this phenomenon appreciated. Orsak (1965) suggests that the upgoing E.M. energy from a lighting flash is reflected at an altitude of roughly 1000 km and that it may suffer mutliple reflections back and forth between this altitude and the lower ionosphere or the ground. Carpenter et al (1964) have summarized the results of their detailed measurements on 11 of the Aerobee 4.59 UI whistlers and Smith (1964) proposed a theoretical model for the propagation of short hop whistlers.

It is evident from the brief description of a small selection of V.L.F. rocket payloads which have now been flown that the technique is extremely useful in determining the characteristics of V.L.F. emissions including the mode of propagation. The disadvantage of such rocket borne experiments is the necessity to deploy large loop aerials. This is complicated to do and even the most well engineered systems have been known to fail. It would be a great step forward to have a small V.L.F. magnetic antenna which did not need to be deployed.

(c) Cored Loop Antennas

Increasing the effective area of a loop antenna by means of a high permeability core has been known for many years and small ferrite cored loops are commonly used in portable radio receiveivers. An antenna consisting of 12,000 turns of fine wire wrapped around a ferrite core 254 mm long by 16 mm diameter was constructed Gendrin et al (1968). A detailed description of the sensors and preamplifiers are given by Mayer (1969) and Vilar-Mestre. (1966).

Gendrin et al (1968) give an account of

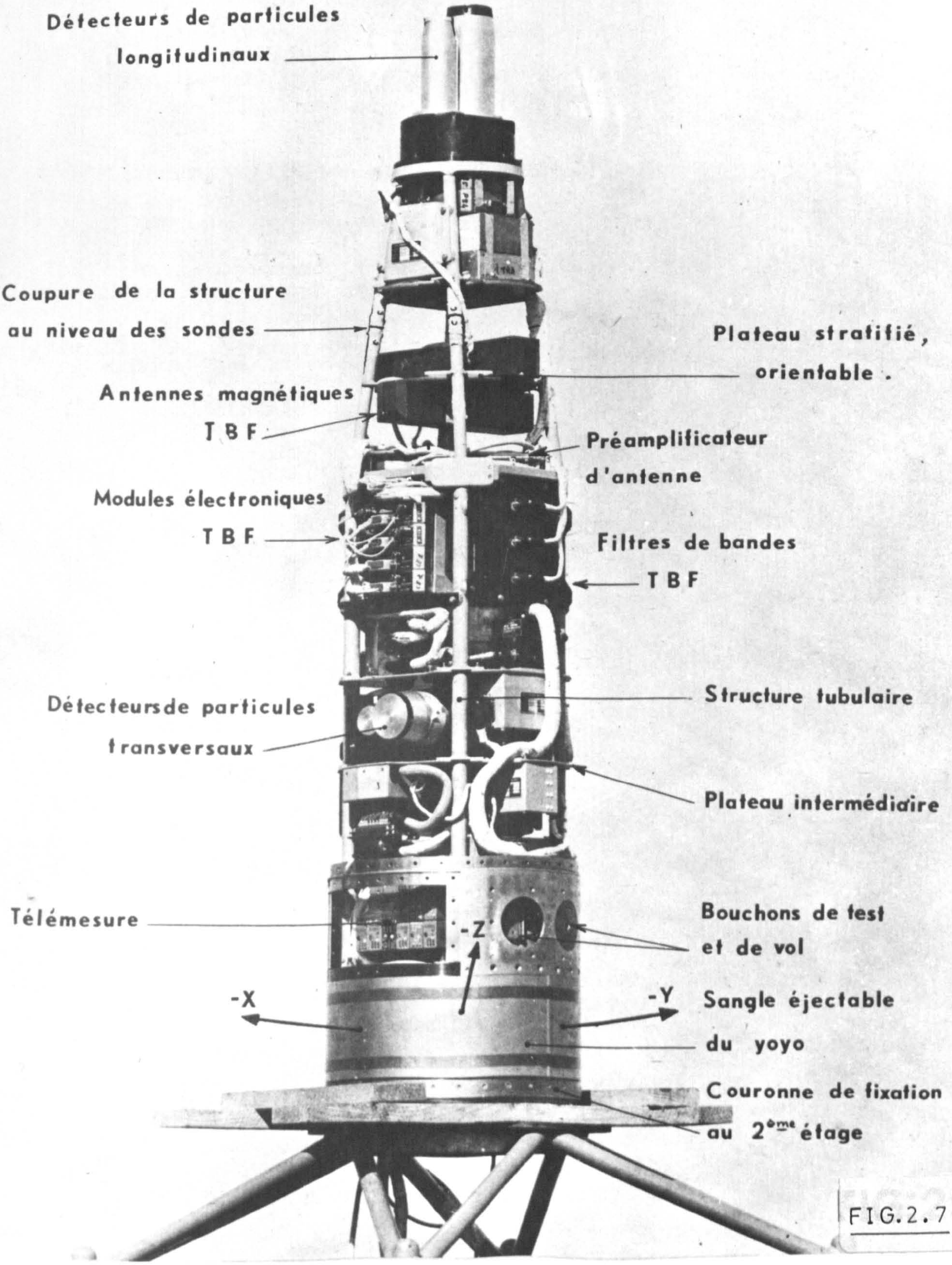
Détecteurs de particules longitudinaux
Coupure de la structure au niveau des sondes
Antennes magnétiques T B F
Modules électroniques T B F
Détecteursde particules transversaux
Télémesure
-X
-Z
-Y
Plateau stratifié, orientable .
Préamplificateur d'antenne
Filtres de bandes T B F
Structure tubulaire
Plateau intermédiaire
Bouchons de test et de vol
Sangle éjectable du yoyo
Couronne de fixation au 2ème étage

FIG.2.7

three rocket experiments having two orthogonal cored antennas on board each payload. The rockets were launched from Kerguelen Islands (50^{o} S,Geographic) into two dawn chorus events and one mainly hiss event. A diagram of the payloads (D251,2,&3) can be seen in Fig 2.7, the V.L.F. antennas are fixed in the main body of the structure as they do not need to be deployed. The receivers operated in the frequency range 0.1 to 6 KHz and the frequency response to incident E.M waves was flat to within 1 db in this range. A sensitivity of 2.5 x $10^{-9}\ \gamma^{2}$/Hz at the centre of the band.was achieved.

A full analysis of the data obtained during these rocket flights has been made by Berthommier (1969). It was found that incident waves were propagating in a right hand circularly polarized mode over the whole frequency range of the experiment. A great deal of reflection of the downward propagating radiation was observed in the ionosphere. Also an 80 second periodicity in the observed electron flux was correlated with a hiss emission seen during the third flight.

A major part of the work to be presented in this thesis is concerned with the development of a V.L.F. rocket payload which uses three orthogonal laminated MU-METAL cored loop antennas.

2.3 V.L.F. Receivers on board Satellites

Satellites have two major advantages as vehicles from which observations of V.L.F. emissions can be made. Firstly, they operate above the ionosphere which reflects, refracts and absorbs V.L.F. radiation and secondly they can cover most of the surface of the globe sending back information on the large scale structure of the magnetosphere and the spacial and temporal variations in the occurrence of V.L.F.emissions.

Many satellites have been launched into a variety of orbits to study V.L.F. emissions. Some have made use of open loop magnetic antennas and others have used short electric dipoles or capacitative double spheres. Satellites which have been launched into near circular polar orbits at altitudes of about 2000 km include Alouette 1,2, Ariel 3,4, Injun 3,5 and OGO's 2,4 & 6. Those put into highly eccentric orbits out to 10 R_E include OGO 1,3 & 5 whilst a few experiments have been placed in geostationary orbit at $L \approx 6.6$ such as ATS 1,3, -F and the proposed new ESRO satellite GEOS which is to be launched in 1976, ESRO[1].

Gurnett (1968) showed from Injun 3 measurements that the regions of most intense V.L.F. emission activity (chorus & hiss) and electron precipitation are nearly coincident, suggesting a close association between the two phenomena. The statistical occurrence of the different types of V.L.F. emissions with changing local time, magnetic latitude, and magnetic activity has been studied with the one component open loop aboard Ariel 3. At medium latitudes V.L.F. emission intensities exhibit two maxima, one in the morning the other on the noonward edge of the evening plasmapause bulge. During magnetic storms the emissions extend over many hours of local time, Bullough et al (196) and Bullough (1971). These emissions are believed to be generated by cyclotron resonance in the vicinity of the geomagnetic equator, Kennel & Petschek (1966). A sketch of Ariel 3 showing the $3m^2$ loop and a block diagram of the receiver can be seen in Fig. 2.8. The receiver achieved a sensitivity of about $10^{-11}\ \gamma^2/Hz$. at 3KHz which was three orders of magnitude better than Injun 3. With this sensitivity Ariel 3 observed a steady background of spherics indicating that there is little point in producing new equipment with even greater sensitivity.

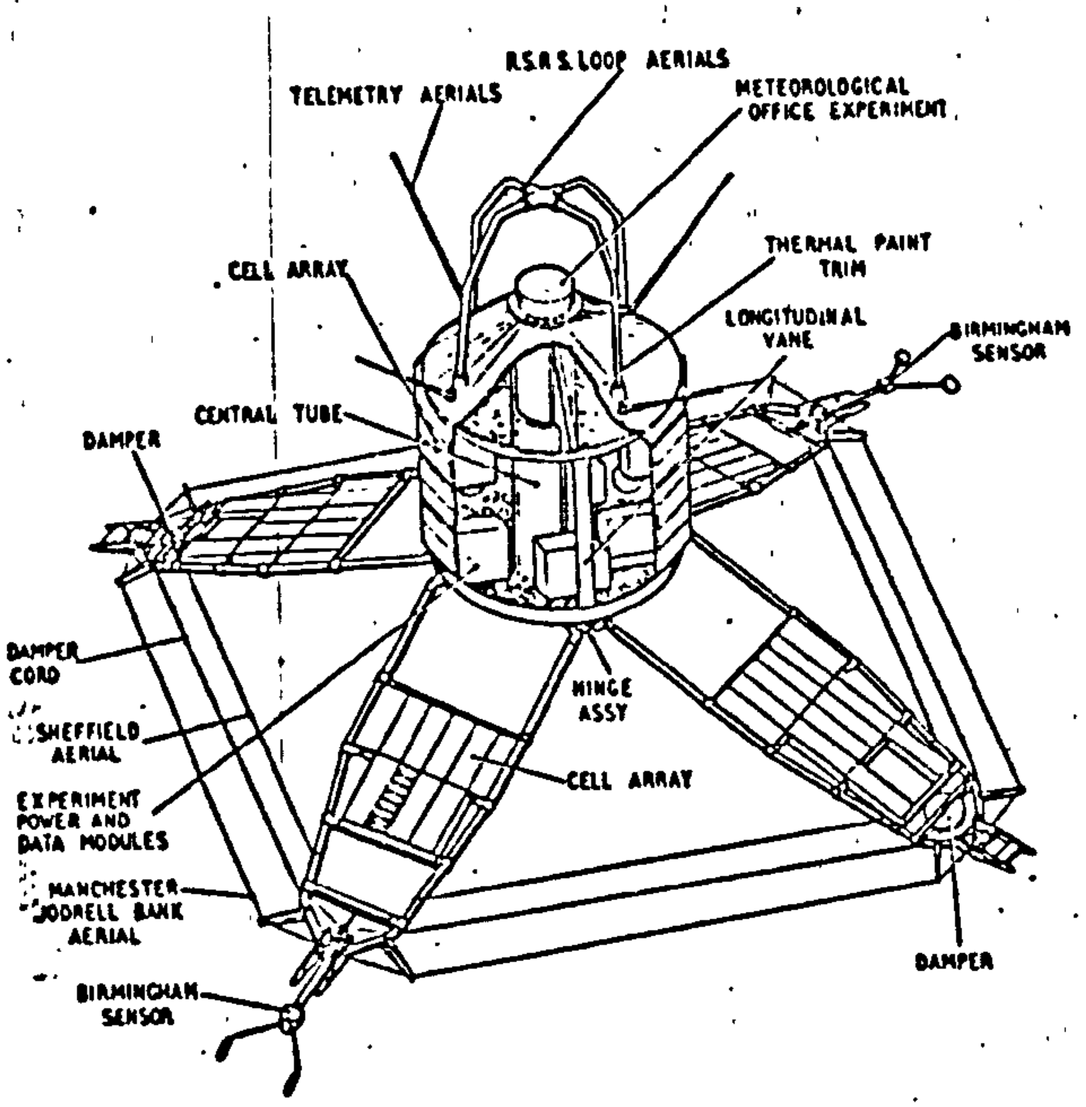

ARIEL 3

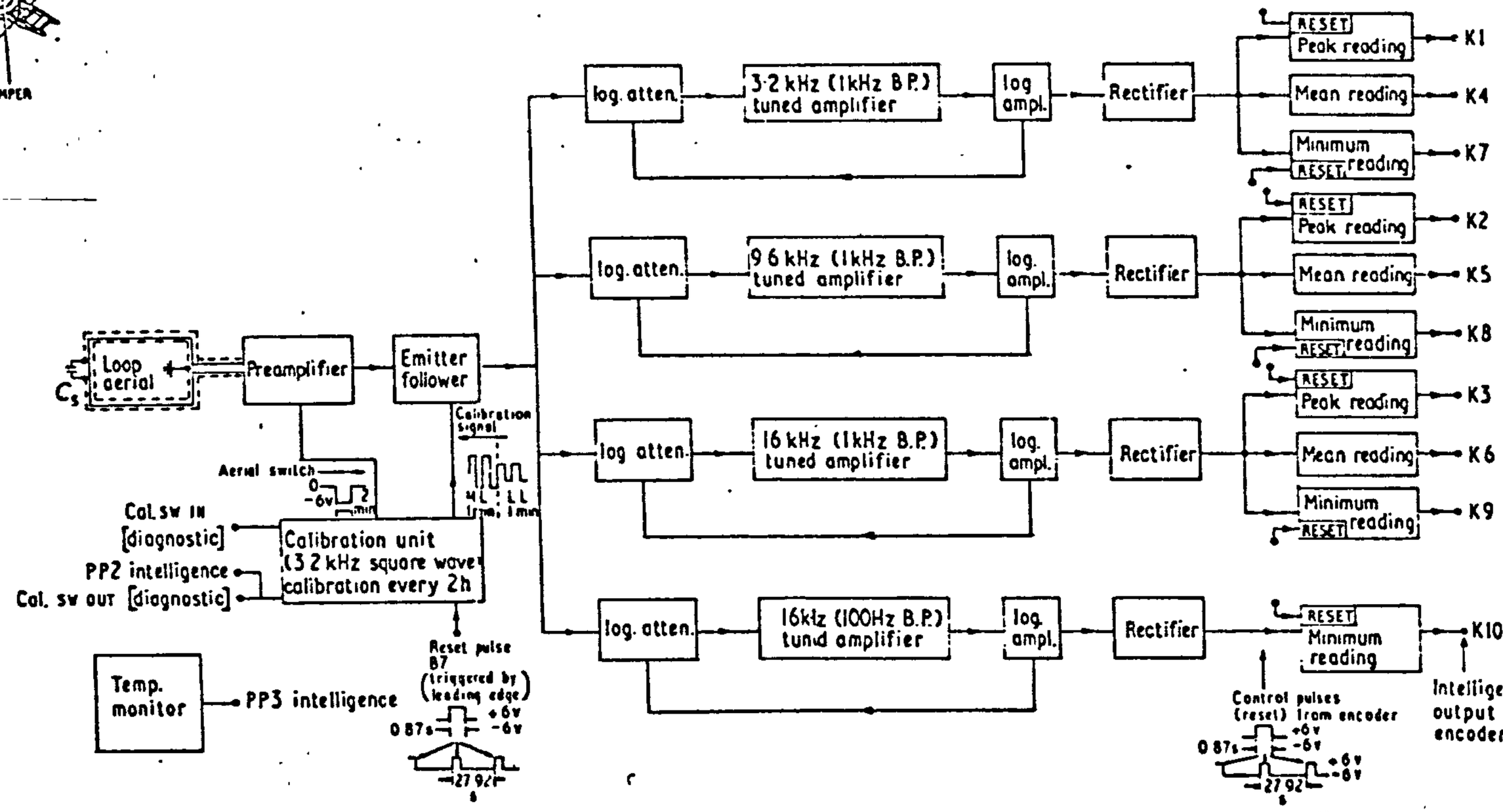

Fig. 2.8

This was taken into account when designing the receiver for the Skylark payload S1124. A detailed description of the V.L.F. experiment on Ariel 3 is given by Bullough et al (1968). Mosier & Gurnett (1969, 1971) have discussed the derivation of V.L.F. Poynting flux from Injun 5 measurements using one electric dipole and one magnetic loop antenna. A description of the V.L.F. electric field experiment on board the Alouette and Isis satellites is given by Franklin (1967) and a study of the rate of reception of whistlers as a functions of invariant latitude near the plasmapause was made by Carpenter (1968) and Laaspere (1971) with data from Alouette 1 & 2 and OGO 6. Belrose and Barrington (1965) also studied V.L.F. emissions observed on Alouette 1 and on occasion observed emissions which were triggered by fractional hop whistlers. They also observed regularly, noise bands located between L ≈ 2.5 and I = 4. Russel & Holzer (1970) have identified two differing types of hiss from OGO 3 data and Russel et al (1972) have comprehensively reviewed the subject of V.L.F. experiments aboard satellites probing the distant magnetosphere. A general review of satellite experiments is also given by Rycroft (1967). Satellites have provided a wealth of information about the nature of the magnetosphere and the occurrence and propagation of V.L.F. emissions and there is every expectation that they will continue to do so,for workers in Europe the launching of GEOS is eagerly awaited.

2.4 Combined measurement of an event

Satellite,rocket and ground based receivers can be used as we have seen to great effect,but the maximum amount of information abouf VLF emissions can best be collected by simultaneous measurements from all three vantage points.Most V.L.F./Particle rocket probes are flown

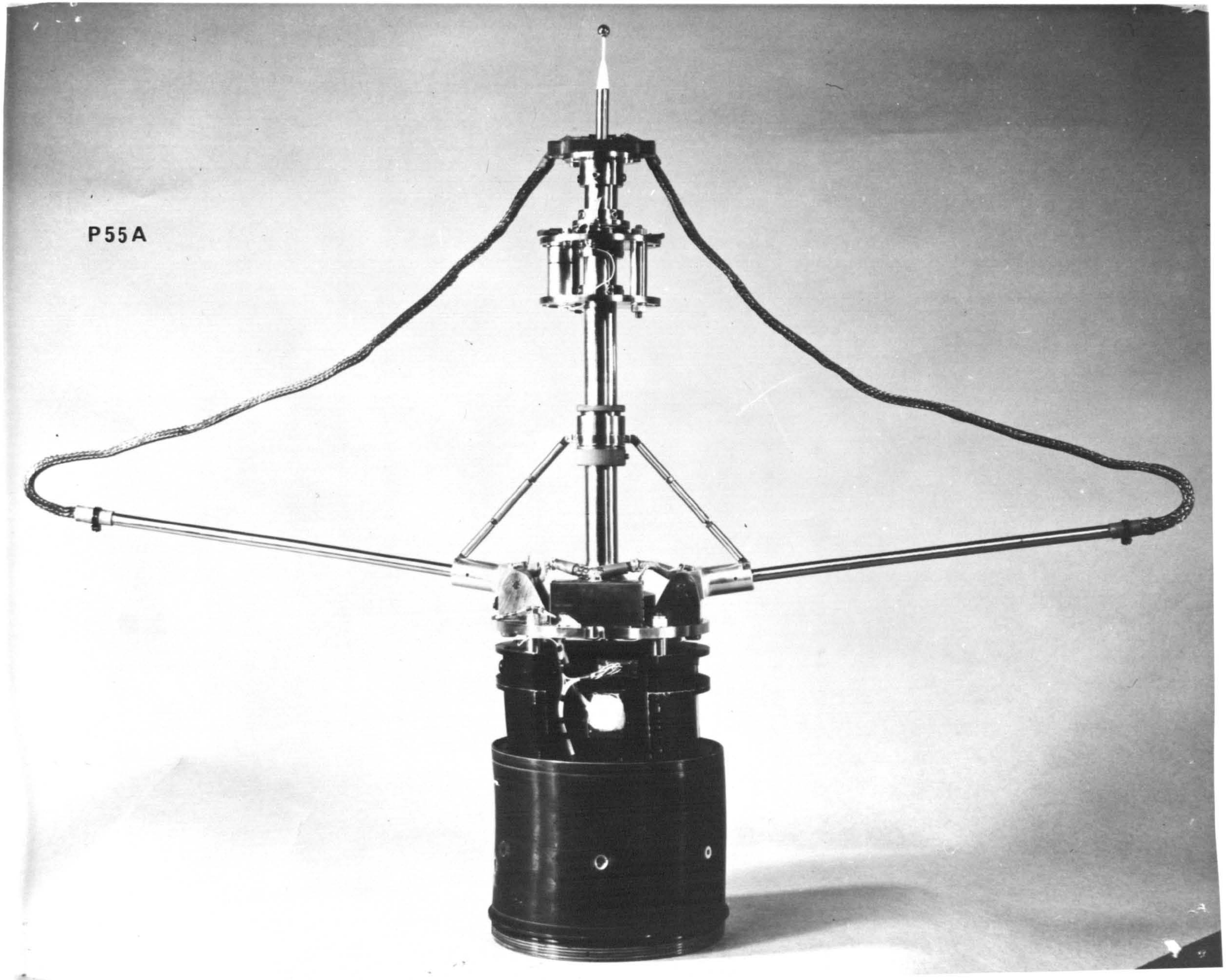

FIG. 2.9

in conjunction with ground based observation of the V.L.F. phenomena and occasionally it is possible to have a satellite suitably positioned such that measurements above, below and in the ionosphere can be made on a single event. The auroral hiss and display observed at Andøya around local magnetic midnight on 10..10..72. was investigated on the ground with a V.L.F. goniometer receiver, in the D region with a Petrel rocket payload P55A see Fig.2.9 and in the topside ionosphere by Ariel 4. Both V.L.F. and energetic particle data were supplied by the satellite and a quick look at the results from the three sources indicate a correlation between the auroral display, the V.L.F. hiss and the precipitation of energetic particles at or near the invariant latitude of Andøya. The hiss spectrum as recorded on the rocket and on the ground can be seen in Fig.2.9a showing an increasing D region attenuation with decreasing frequency below about 4 KHz. Fig. 2.10 indicates the path of UK4 as it passes through a region with the same L value as Andøya but about 20^{o} W. The output from the Iowa University particle experiment as the satellite moves through this region can be seen in Fig 2.11. (An exact determination of the energies observed is difficult without a deal of work due to the energy step monitor malfunction which occurred.) However this example shows the usefulness of simultaneous measurements and further analysis of this particular event should yield interesting results.

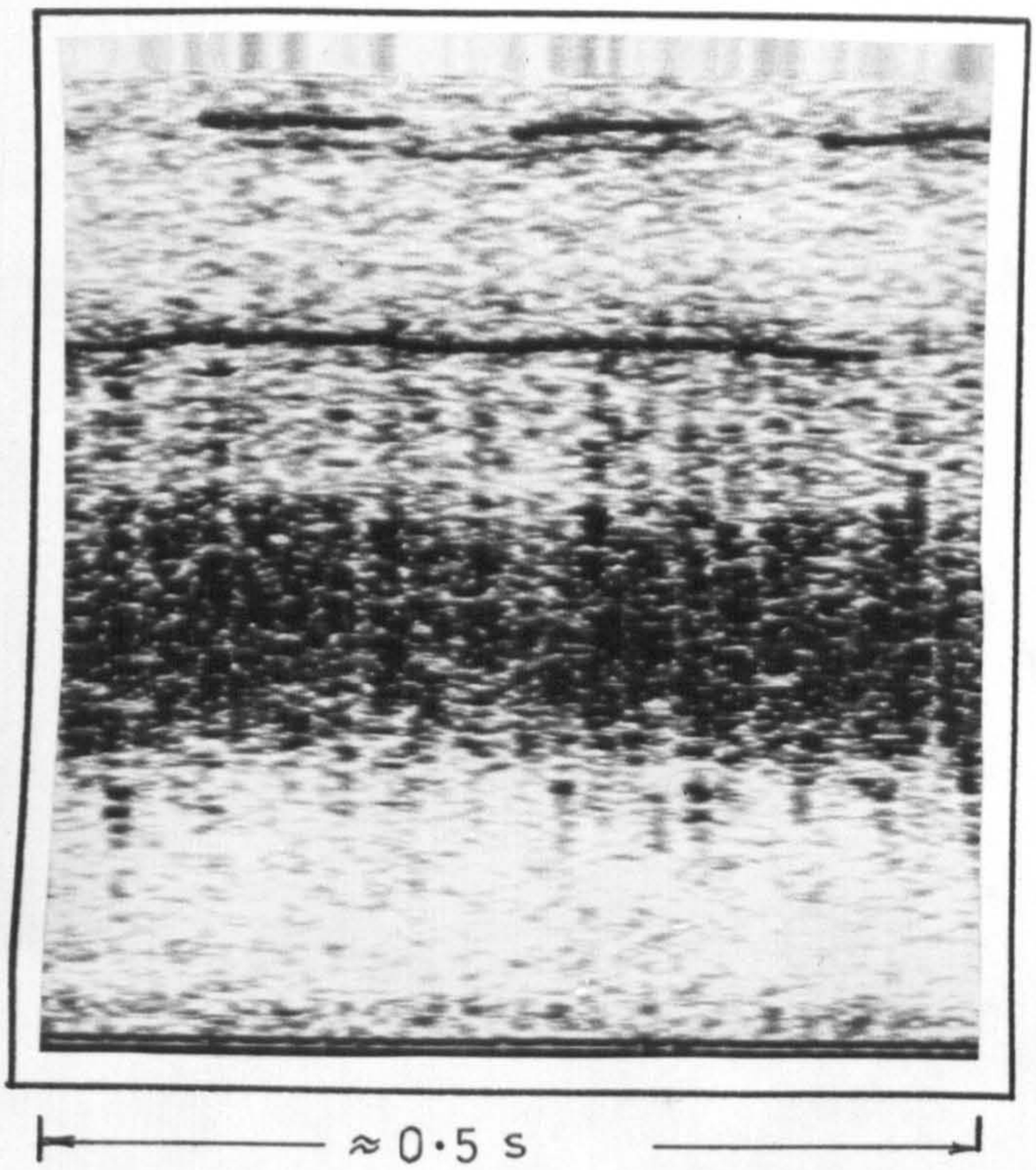
≈0·5 s

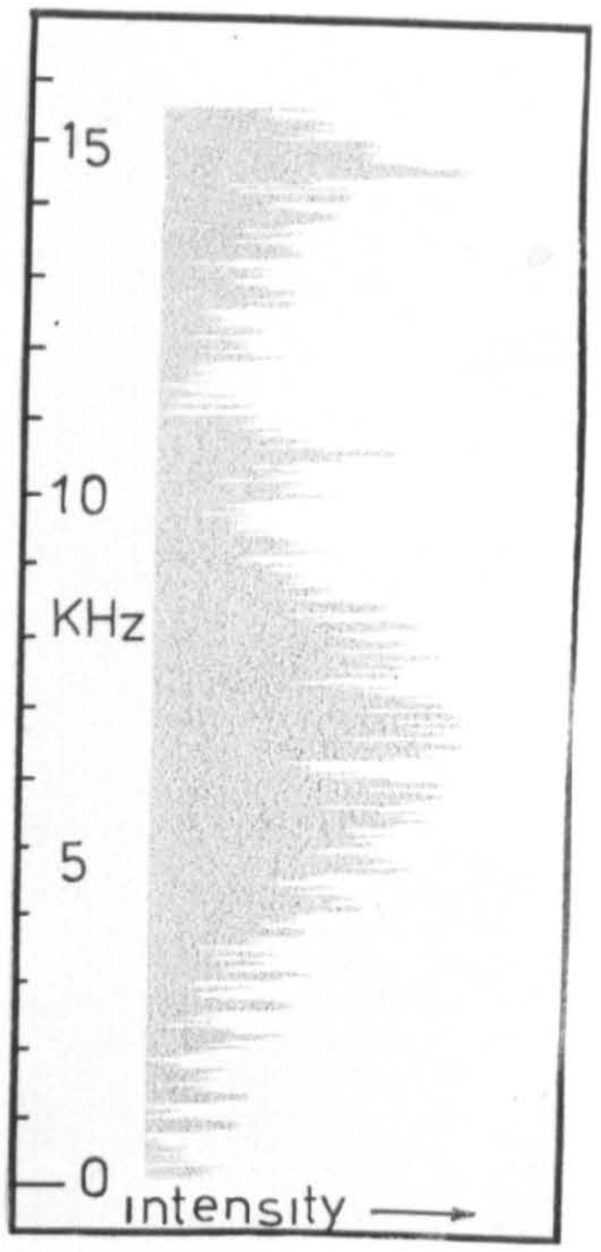
15
10
KHz
5
0
intensity

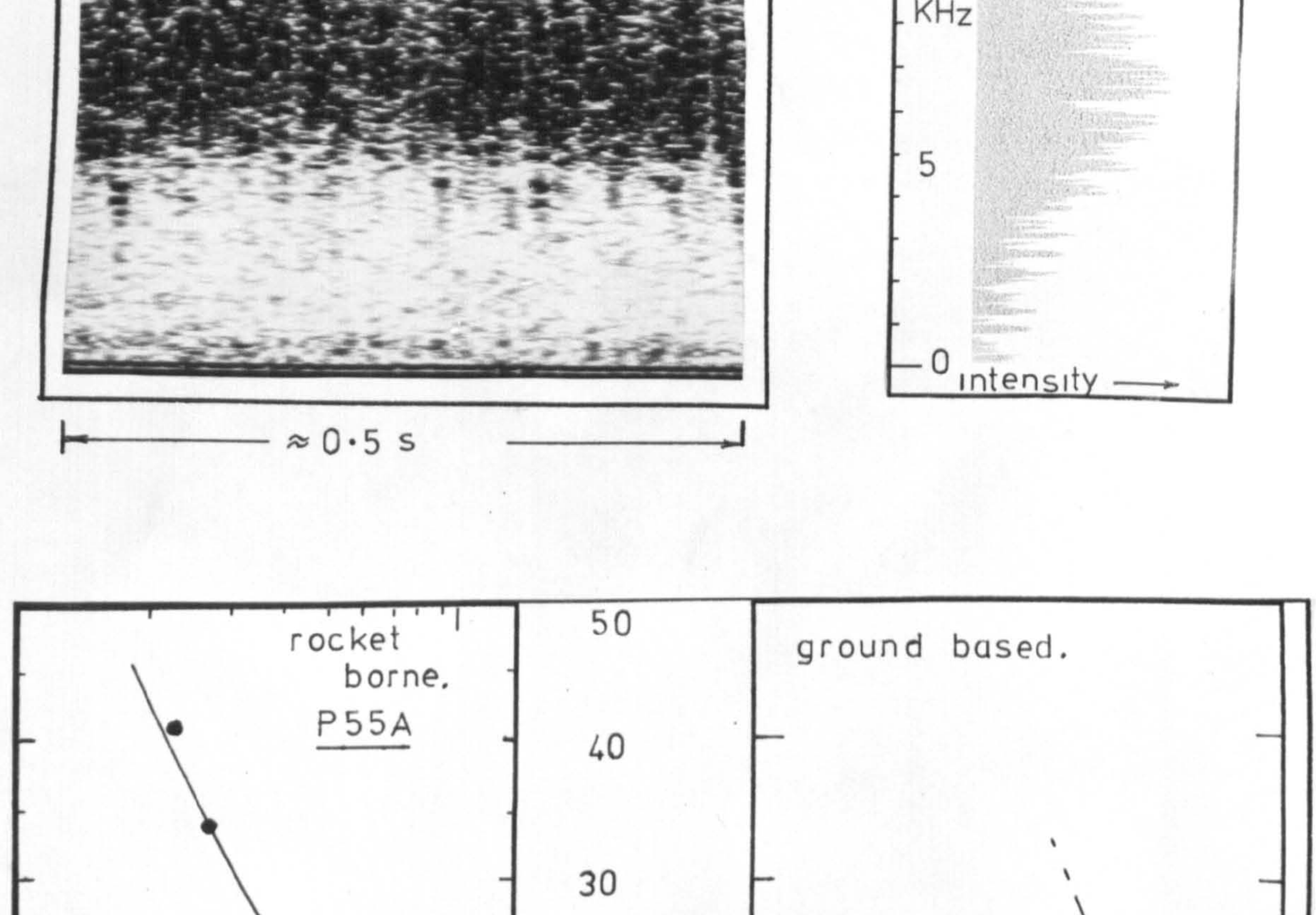
rocket
borne.
P55A
ground based.
50
40
30
db
20
10
0
1
2
3
4
5
6
7
8
9
10
FREQUENCY KHz

FIG. 2.9A

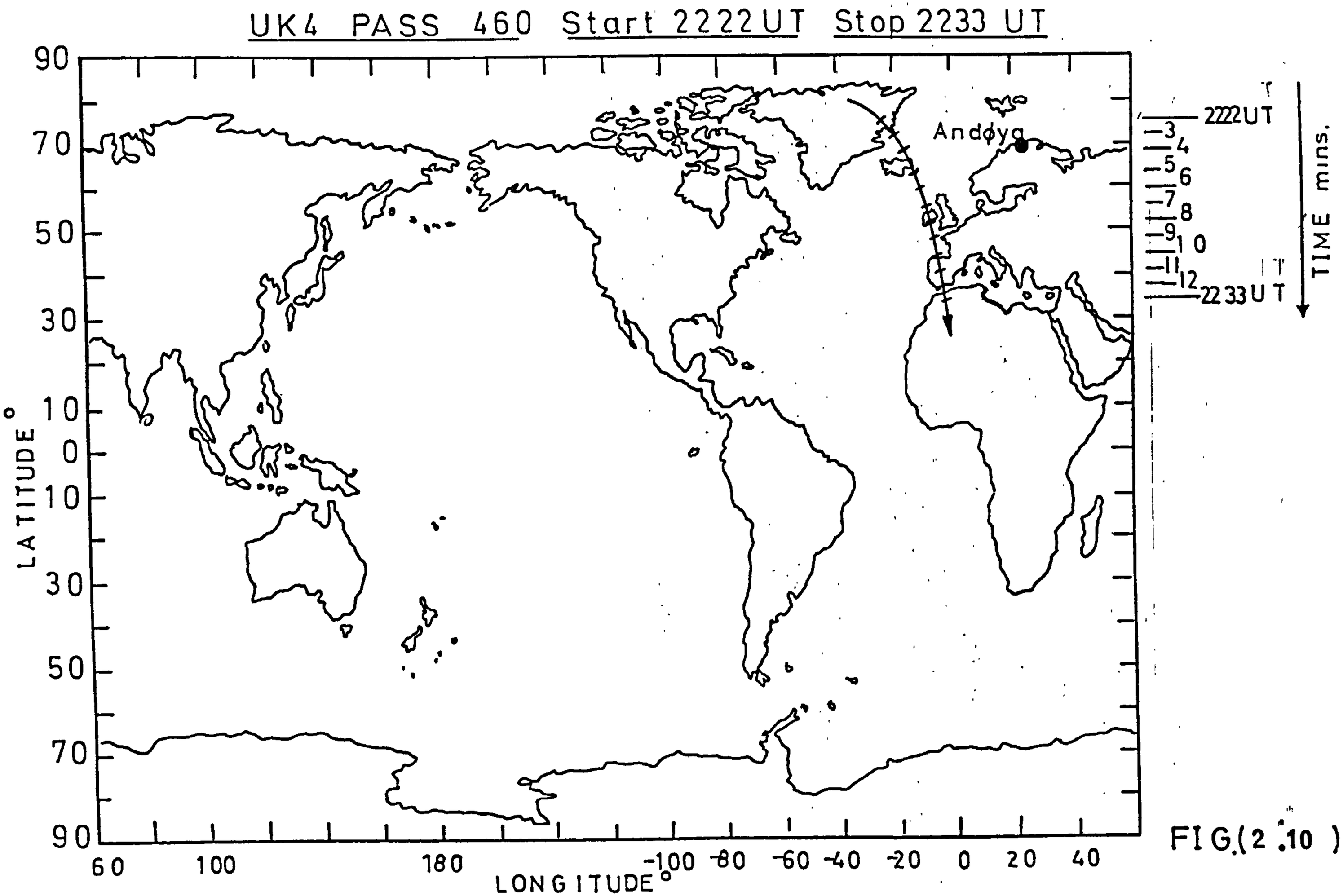
UK4 PASS 460 Start 2222UT Stop 2233 UT
90
70
50
30
10
0
10
30
50
70
90
LATITUDE°
60
100
180
-100
-80
-60
-40
-20
0
20
40
LONGITUDE°
Anddya
2222UT
3
4
5
6
7
8
9
10
11
12
2233UT
TIME mins.

FIG.(2.10)

2222 hr UT

UK4

A

TIME →

B

2223 hr UT

B

C

2224 hr UT

C

D

PARTICLE FLUX (arbitrary units) →

FIG(2.11)

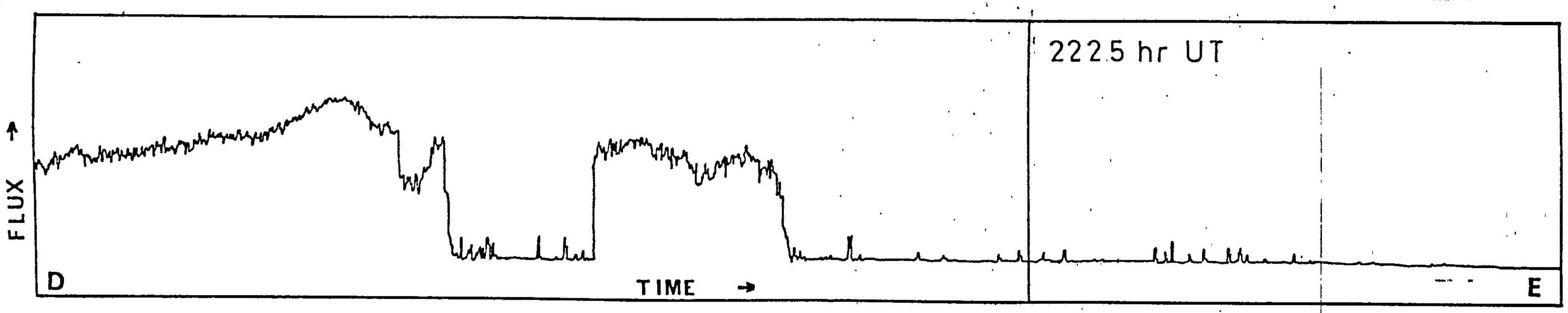

FIG. (2 . 11 Cont'd)

CHAPTER 3

A SMALL V.L.F. ANTENNA USING A HIGH PERMEABILITY CORE

3.1 The feasibility of producing small cored antennas with high sensitivity at very low frequencies.

The UK3 satellite had an open loop antenna consisting of 14 turns of wire encompassing an area of approximately $3m^2$ with a resistance of 11 ohms and an inductance of 1.83 mH Bullough et al (1968). The loop was matched to a conventional low noise transistor (2N930) preamplifier by a transformer. The receiver achieved a threshold of about $10^{-12}\gamma^2/Hz$ at 10KHz which was sufficient to observe the continuous spheric background in orbit. This is the sensitivity which represents a design aim for the new small cored antennas. It is convenient to use the example of UK3 in the comparison of the performance of cored and open loop aerials which follows.

Assume that the Johnson noise generated by the antenna (of either kind) is much greater than the effective input noise of the preamplifier connected to it and that the simplified equivalent circuit shown in Fig 3.1 represents the electrical characteristics of the antenna and preamplifier input.

The spectral density of the coil noise is given by :

$$e_n^2 = 4KTR \quad V^2/Hz \qquad 3.1.1$$

and that of the induced signal is:

$$e_s^2 = \omega^2 N^2 \mu^2 S^2 b^2 \quad V^2/Hz \qquad 3.1.2$$

The minimum detectable signal is therefore given by ;

$$b^2 = \frac{4KTR}{\omega^2 N^2 S^2 \mu^2} \quad T^2/Hz \qquad 3.1.3$$

Let the mean coil radius be a metres, and put $\pi a^2 = \alpha S$, 3.1.4.

where $\alpha = 1$ for an open loop and $\alpha > 1$ for a cored loop.

Sensitivity and size of antenna are important criteria for rocket and satellite mounted receiving systems, weight is also important and it is convenient to discuss the comparison of the two types of antennas in these terms.

If r = resistivity of copper (1.56×10^{-8} ohm m^{-1})

V = volume of copper in the coil (m^3)

ρ = the density of copper (8.96×10^3 Kg m^{-3})

W = the weight of copper used (Kg)

s = the c.s.a. of wire used in the coil (m^2)

Then $R = 2\pi a Nr / s$ 3.1.5

and $V = 2\pi aNs$ 3.1.6

also $W = V\rho$ 3.1.7

Then from (3.1.3, 4, 5 & 6) we have that,

$$\overline{b^2} = \frac{16\pi KTr}{\omega^2 V} \cdot \frac{\alpha}{S\mu R} \qquad 3.1.8$$

Simple Antenna/Preamplifier Equivalent Circuit.

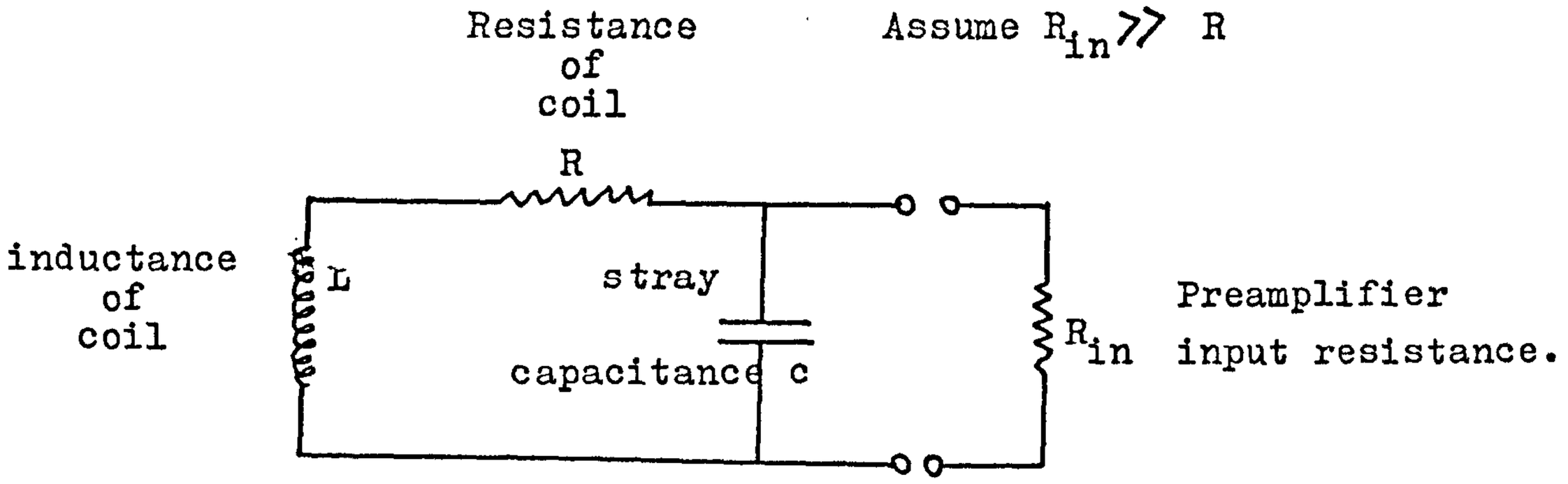

Antenna Preamplifier

Bar of material of permeability μ in a uniform field H_o .

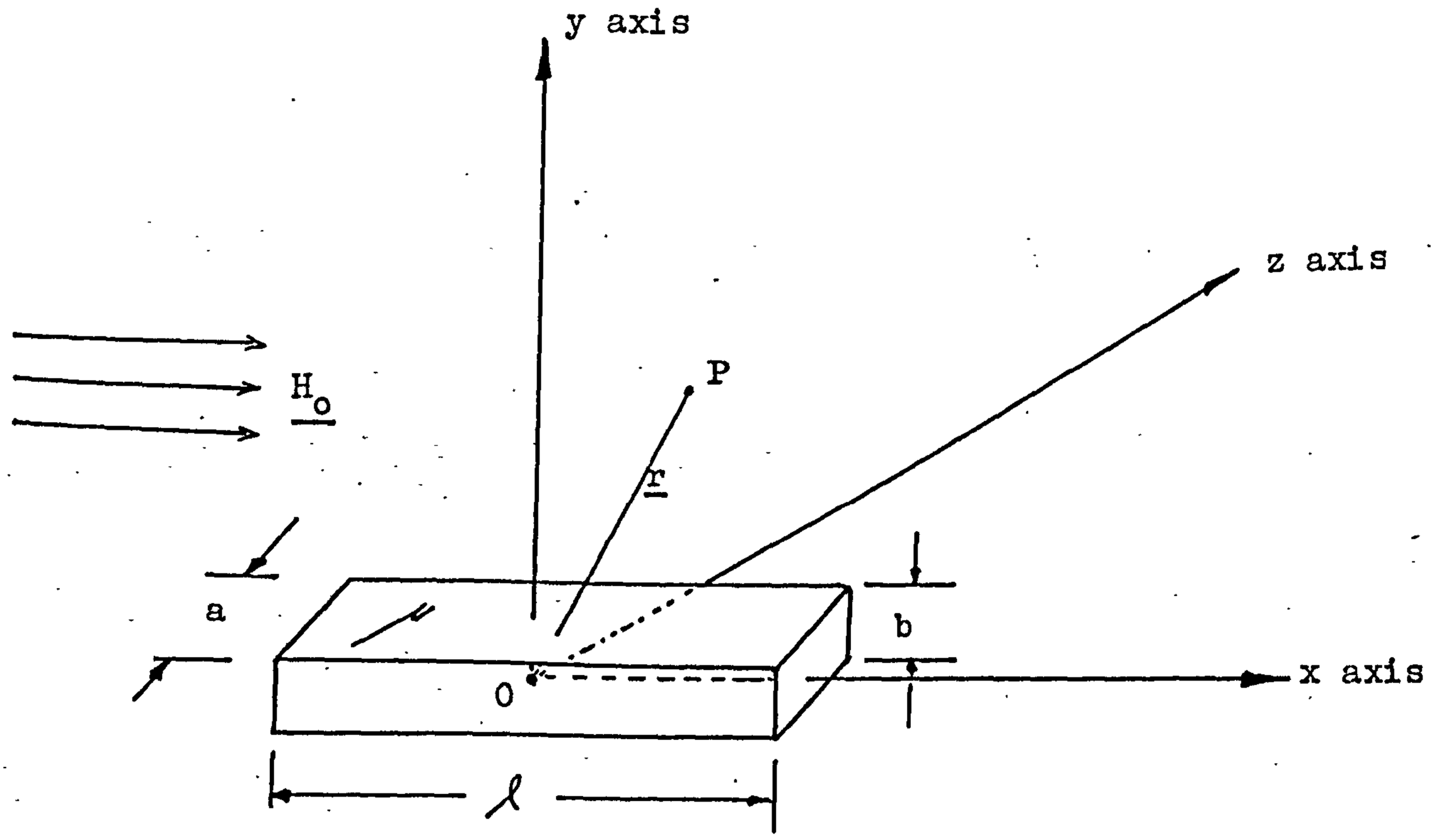

Fig(3.1)

Note that α depends on the geometry of the coil which is wound on the core. Obviously α should be as close as possible to unity but the requirement to minimise lossy stray capacitcance may dictate a compromise.

Define the effective area of the coil ;

$$S_{eff} = \frac{S\mu R}{\alpha} \qquad 3.1.9$$

Now from (3.1.7, 8 & 9) we have that

$$\overline{b^2} = \frac{16\pi KTr}{\omega^2 W S_{eff}} \quad T^2/Hz \qquad 3.1.10$$

Substituting in equation (3.1.10) appropriate values for ρ, r, K, t

$$\overline{b2} = \frac{7.6 \times 10^{-7}}{f^2 W S_{eff}} \quad \gamma^2/Hz \qquad 3.1.11$$

For UK3 W = 0.125Kg and $S_{eff} = S = 3\ m^2$

giving $\overline{b^2} = 2 \times 10^{-15}\ \gamma^2/Hz$ at 10 KHz

the achieved value was some $10^{-13}\ \gamma^2/Hz$ indicating that it was pre-amplifier noise limited.

The effective permeability of a magnetic core is related to the initial permeability of the material from which it is made by the following;

$$\mu_{eff} = \frac{\mu_i}{1 + D\mu_i} \qquad 3.1.12$$

D is the demagnetising factor and is related to the shape of the core.

D has to be measured for each core and it is only possible to calculate it for precise and simple geometries. Stoner (1945) has calculated the demagnetising factor for ellipsoids and shows that the ratio of the semi major and minor axes of the ellipse is an important parameter. If we generalise his work to the case of long thin rods then the length to diameter ratio m is of importance.

A table showing the relationship of m, D and the product m^2D is given below.

Table 3.1

m	D	m^2D	$D.m^{1.5}$
5	0.04	1	.45
10	0.017	1.7	.54
20	0.0053	2.1	.47
30	0.0028	2.5	.46
50	0.0013	3.7	.46
100	0.0004	4	.40
200	0.0001	4	.28

Note that the product m^2D is a slowly varying function of m.

Thus from (3.1.12) & (3.1.9)

$$S_{eff} = \frac{\pi d^2}{4\alpha} : \left[\frac{\mu_i}{1 + \mu_i D}\right]^2$$

Where d is the diameter of the rod, and letting ℓ be the rod length it can be shown that

$$S_{eff} = \frac{\pi \ell^4}{4\alpha (m^2D)^2 d^2}\left[\frac{\mu_{iD}}{1 + \mu_{iD}}\right]^2 \qquad 3.1.13$$

Now for $\mu_i D \gg 1$, that is for $\mu_i = 1000$ and $m = 10$ giving $D = 0.02$ which are all reasonable values, $\frac{\mu_i D}{1 + \mu_i D} \approx 1$ and therefore,

$$S_{eff} = \frac{\pi \ell 4}{4 \propto (m^2 D)^2 \, d^2} \qquad 3.1.14$$

It can be seen from Table 3.1.1 that $m^2 D$ is a slowly varying function of m, (ℓ/d) and so ;

$$S_{eff} \propto \frac{1}{d^2} \qquad 3.1.15$$

This would indicate that d should be as small as possible for the best antenna performance as long as $\mu_i D \gg 1$ for a given ℓ and providing that leakage flux remains small.

To achieve the UK3 sensitivity of $10^{-13}\ \gamma^2/Hz$ from (3.1.11) we need $WS_{eff} = 7.6 \times 10^{-2}$ Kg m^2 (f = 10 KHz) 3.1.16

Now $\rho_{core} = W_{core}$ / Volume of core

and from (3.1.14)

$$S_{eff} = \frac{\pi^2 \ell^5 \, \rho_{core}}{16 \propto (m^2 D)^2 W_{core}} \qquad 3.1.17$$

Multiplying (3.1.17) by W_{copper} we have;

$$W_{copper} \, S_{eff} = \frac{\pi^2 \ell^5 \rho_{core}}{16 \propto (m^2 D^2)^2} \cdot \frac{W_{copper}}{W_{core}} \qquad 3.1.18$$

and if $W_{copper}/W_{core} \approx 1$ and $\rho_{core} \approx \rho_{copper} = 8.9 \times 10^3 Kgm^3$

Then from (3.1.16) & (3.1.18) we have that;

$$7.6 \times 10^{-2} = \frac{8.9 \times 10^{3} \pi^{2} \ell^{5}}{16 \quad (m^{2}D)^{2}}$$

and therefore $\ell^{5} = 5.54 \times 10^{-5} \alpha \quad m^{5}$

if $m^{2}D = 2$, which is a realistic figure attained when m = 25

$$\underline{\ell = 14 \alpha^{\frac{1}{5}} \text{ cm}} \qquad 3.1.19$$

If $m^{2}D = 4$ which occurs when m is very large ($\sim$200)

$$\underline{\ell = 18 \alpha^{\frac{1}{5}} \text{ cm}} \qquad 3.1.20$$

Even if α is $\gg$ 1 say 100 then $\alpha^{\frac{1}{5}}$ will be only 2.5 and the length of core required to equal the desired sensitivity of UK3 will be about 35 cm.

If we take a rod 20 cm long then with m = 25, d = 0.8 cm. With such a rod it should be possible to construct a small V.L.F. aerial for use on rocket borne probes which has a sensitivity of about 10^{-12} γ^{2}/Hz and would represent a significant improvement, of about 20 db on previous receivers which were flown on board the Petrel rockets P47H, P129A and P55A.

Having shown that such a V.L.F. aerial is practical in terms of minimum detectable signal, size and weight it is important to discuss the limitations on the methods available to realise the device. In the following section an attempt is made to show that the theoretical calculation of the performance of an aerial consisting of a many turn coil wound around a high permeability ferromagnetic core is not possible and that in consequence an empirical approach towards optimising the antenna performance is dictated.

3.2 Difficulties in theoretically determining the performance of a cored coil aerial

It will be demonstrated here that it is virtually impossible to evaluate the terms required to solve Maxwell's equations for the quasi-static approximation in the case of a distributed coil wound on a bar of highly permeable ferro magnetic material.

A sketch of the coil and rod can be seen in Fig 3.2. The rod is built up of many laminations of Super Mu-Metal* which are about 1/1000 of an inch thick and coated on both sides with Magnesium Oxide insulation. This construction reduces the eddy current loss in the bar. The coils wound around this bar have typically 10,000 turns of 45 s.w.g. wire and diameters from 1 cm to 5 cm.

Consider a bar of ferro magnetic material with an initial permeability of μ in a uniform magnetic field $\underline{H_o}$ which is slowly varying (See Fig 3.1. The field at the point P will be modified by the induced field in the specimen bar.

In order that the magnetic field $\underline{H}$ at the point P can be related to the scalar magnetic potential ϕ by

$$\underline{H} = \nabla \phi \qquad 3.2.1$$

then $$\text{Curl } \underline{H} = J + \frac{dD}{dt}$$

and as Curl grad $\phi = 0$, then $$J + \frac{dD}{dt} = 0$$

Then if the displacement current term D = 0 (Quasi-static approx). then J = 0. Therefore in this situation no currents are flowing in the region if (3.2.1) is to hold true.

Define the Magnetisation of a material $\underline{M} = \chi \underline{H}$

where χ is the magnetic susceptibility of the material.

and $\mu = 1 + \chi$.

At ordinary temperatures and for most materials χ is small and independent of $\underline{H}$. The exception being ferromagnetics where χ is large and very dependent on $\underline{H}$. ($\underline{M}$ can be finite when $\underline{H} = 0$).

In the case where μ is independent of $\underline{H}$;

if div $\underline{B} = 0$ (No free magnetic poles)

We have that div$\underline{B}$ = div $(\mu\mu_o\underline{H})$ = $-\mu\mu_o$div grad ϕ

and $\therefore$ div$\underline{B}$ = $-\mu\mu_o\nabla^2\phi = 0$

ie $\nabla^2\phi = 0$ 3.2.2

Thus the magnetostatic potential obeys Laplace's equation.

If however χ or μ is a function of $\underline{H}$ and hence of position,

Then $\underline{B} = \mu_o(1 + \quad)\underline{H}$ and $\underline{M} = \chi \underline{H}$

then div$\underline{B}$ = $-\mu_o$div grad ϕ + $\mu_o$div $\underline{M}$ = 0

ie $\nabla^2\phi$ = div $\underline{M}$ 3.2.3

Now for a solution of this equation we must be able to define $\underline{M}$ in the core as a function of position and apply the boundary conditions. Namely that the normal component of $\underline{B}$ is continuous and the tangential component of $\underline{H}$ is continuous across the boundary. Also $\underline{H}$ must be finite in the bar for finite $\underline{H_o}$ and finite μ and that the induced field

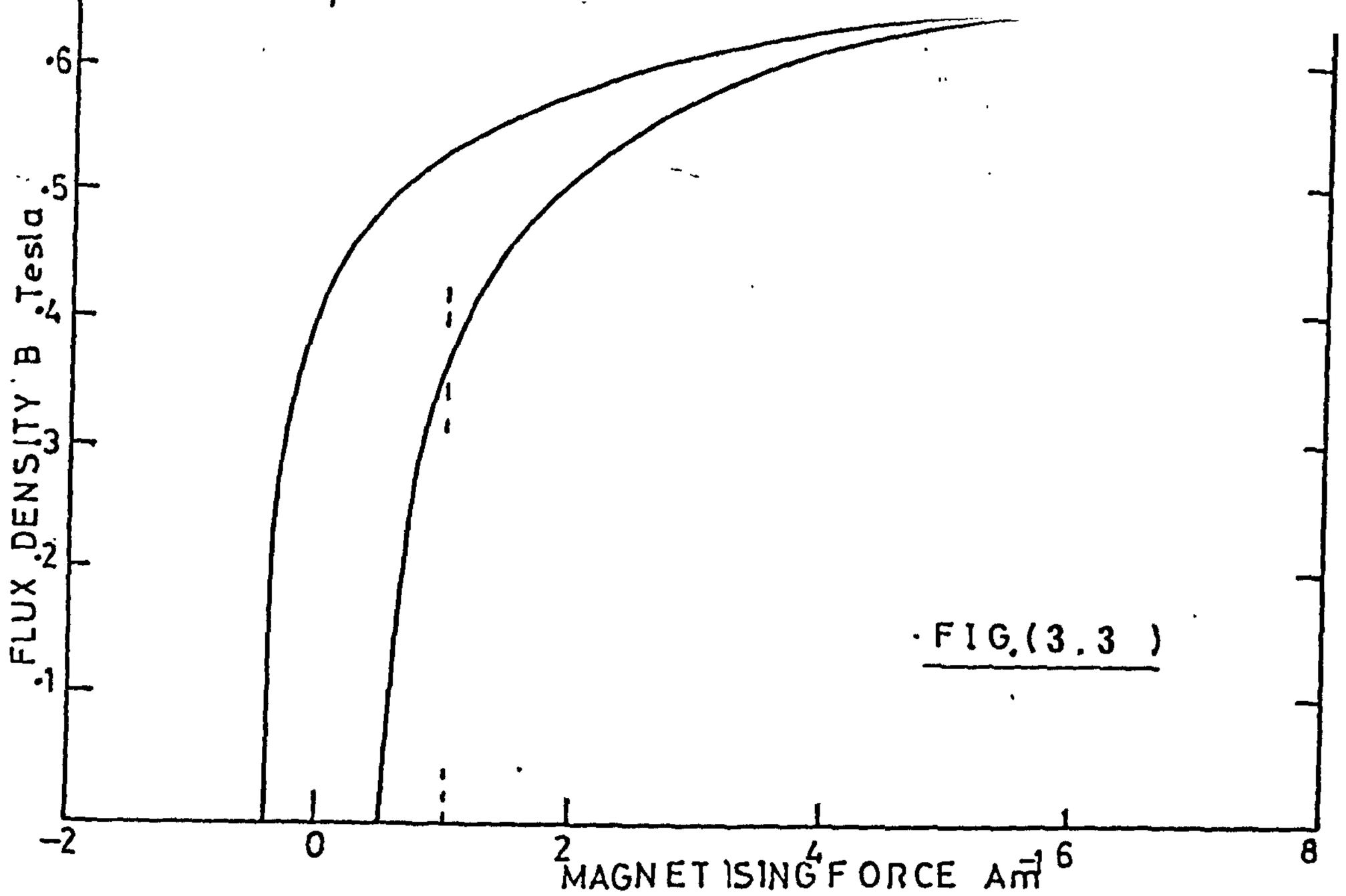
FLUX DENSITY B Tesla
·1
·2
·3
·4
·5
·6
-2
0
2
4
6
8
MAGNETISING FORCE Am⁻¹

FIG.(3.3)

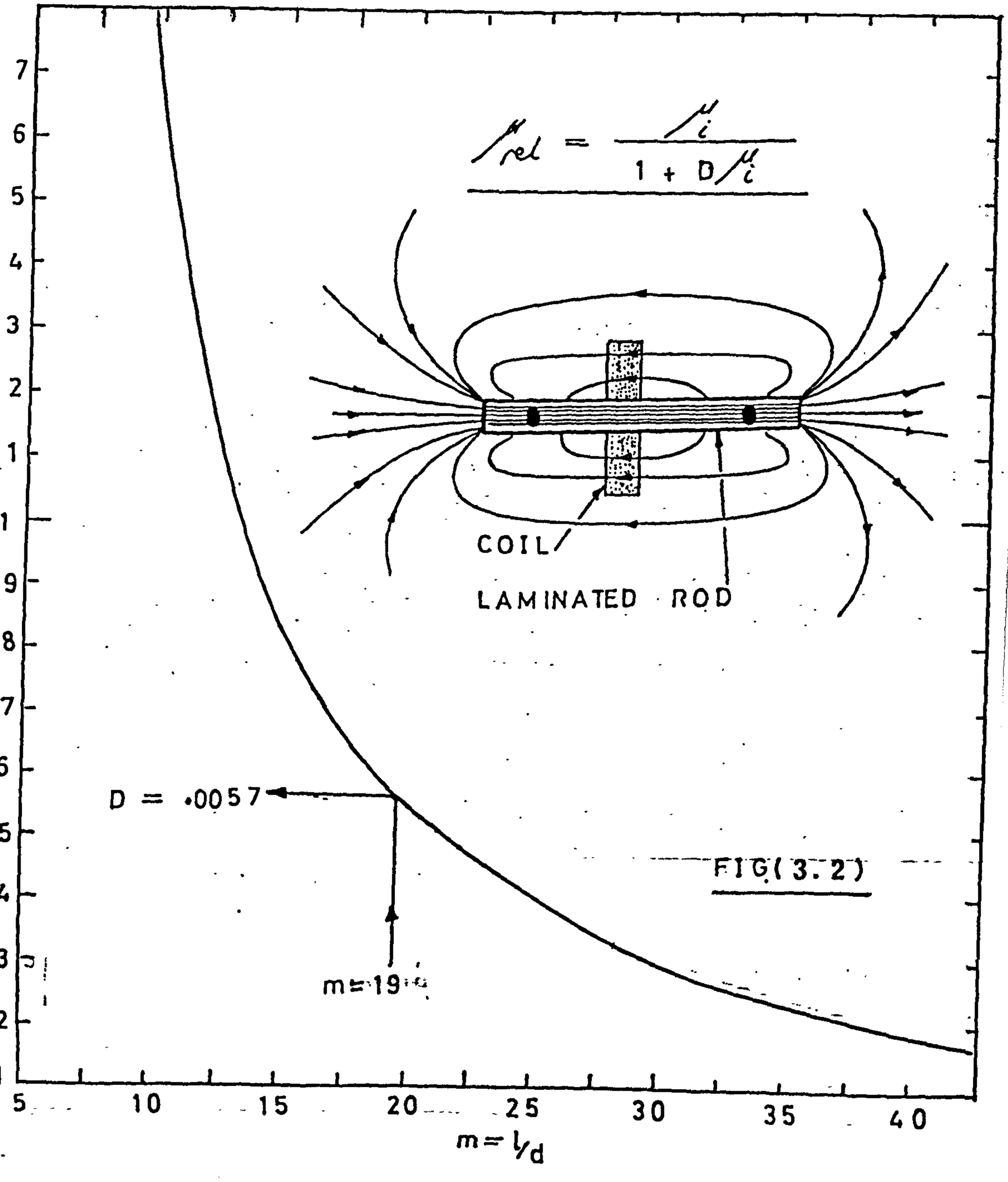
DEMAGNETISING FACTOR D
·001
1
2
3
4
5
6
7
8
9
5
10
15
20
25
30
35
40
m = l/d
D = ·0057
m=19
$\mu_{rel} = \frac{\mu_i}{1 + D\mu_i}$
COIL
LAMINATED ROD

FIG(3.2)

must tend to zero at infinity. Solutions of Laplace's equation have been obtained in terms of spherical harmonics for a uniform magnetised sphere (Bleany & Bleany 1965) but it is not possible to solve the practical case represented by equation (3.2.3). However Maxwell[4] presented the problem of the magnetic induction in an ellipsoid and treated it by following a method due to Poisson. Here the theoretical determination of the magnetic potential due to a uniformally magnetised body is shown to be equivalent to the determination of the gravitational field of a body of the same shape and of uniform density. Consideration of this idea leads Stoner (1945) to the production of a table of values for the demagnetising factor D as a function of shape of ellipsoids for m < 1, oblate and m > 1, prolate. His table is summarised in graphical form in Fig 3.2. In his work Stoner considers a volume element of the speciment having a magnetic moment $\underline{M}\, d\tau$ and then expressing the magnetic potential ϕ in the form;

$$\phi = \int_v \underline{M} \cdot \nabla \left(\frac{1}{r}\right) d\tau$$

which is the form of the expression for the potential due to a simple dipole. Then by applying the divergence theorem ;

$$\int \operatorname{div} \underline{F}.d\tau = \int_s F.dS$$

concludes that; $\phi = \int_s \frac{1}{r}(\underline{M}.dS) - \int_v \frac{1}{r} (\operatorname{div} \underline{M}.d\tau)$

The first term gives the potential ϕ in terms of an equivalent surface magnetic 'charge' of density M cos θ, where θ is the angle $\underline{M}$ makes to the normal to the surface.

For uniform magnetisation the second term vanishes. The great difficulty in predicting the fields due to magnetised materials in forms which are of practical interest such as rods or bars, is that the second term is comparable with the first, Stoner (1945). It is only by very laborious processes that even an approximation to the correct value of the second term can be made.

It appears then that it is almost impossible to calculate $\emptyset$ and hence $\underline{B}$ around a bar of Mu-metal. Even it this were possible it would still be difficult to predict the performance of a cored loop antenna because the pick-up loop or coil is distributed around the rod.

For a single loop or turn of area A m^2 the e.m.f. generated by a time varying $\underline{B}$ is given by;

$$e = -\frac{d\Phi}{dt} \quad \text{where } \Phi \text{ is the flux normal to the loop area.}$$

and $$\Phi = \int_0^A \underline{B}.\ da \quad \text{where da is an element of area}$$

therefore $$e = -\frac{d}{dt}\left[\int_0^A \underline{B}.da\right]$$

So for two concentric loops of areas A_1 & A_2 which are connected together in series the emf produced is;

$$e = -\frac{d}{dt}\left[\int_0^{A_1} \underline{B}.da + \int_0^{A_2} \underline{B}.da\right]$$

For a distributed coil of N turns;

$$e = -\frac{d}{dt}\left[\sum_0^N \int_0^{A_N} \underline{B}.da\right] \qquad 3.2.4$$

Now it is clear that for a distributed coil of some 10,000 turns with diameters from 1 cm to 5 cm it is very difficult to evaluate equation (3.2.4) even if B were known.

These difficulties therefore dictate an empirical approach to developing and optimising the performance of a cored loop antenna. The following sections of this chapter describe the application of this approach with regard to the production of V.L.F. antennas for Petrel and Skylark rocket borne V.L.F. experiments.

3.3 Establishing an Equivalent Circuit for the Antenna

The bar used as the core in the antenna was 156 mm long and 8 mm square cross section built up from 0.05 mm thick strips. The Hysteresis loop for the material used can be seen in Fig.3.3 and it can be seen that the material is driven into saturation with very modest applied fields of the order of 2 A m^{-1}. The initial permeability μ_i of the mu-metal is of the order of 55,000. Its variation as a function of frequency can be seen in Fig.3.4. A number of workers have investigated the performance of various materials formed into a variety of shapes as cores for a loop aerial Wait(1953), Wait (1953a),Belrose(1955) Bozorth & Chapin (1942),Everden(1954),Cawthraw (1954). However most of the work was concerned with Ferrite cores and not with a high permeability material such as Mu-metal. The demagnetising factor of the rod used here is derived from Stoners work and for m = 19,D = 0.0057 See Fig.3.2.

The initial design of the pick up coils was based on several constraints;

a) To minimise the resistance of the coil.
b) To minimise the lossy self capacitcance of the coil.
c) To minimise the lossy stray capacitance to the rod.
d) To keep the coil radius as small as possible to minimise the

0·025 ~ 0·05mm STRIPS USED

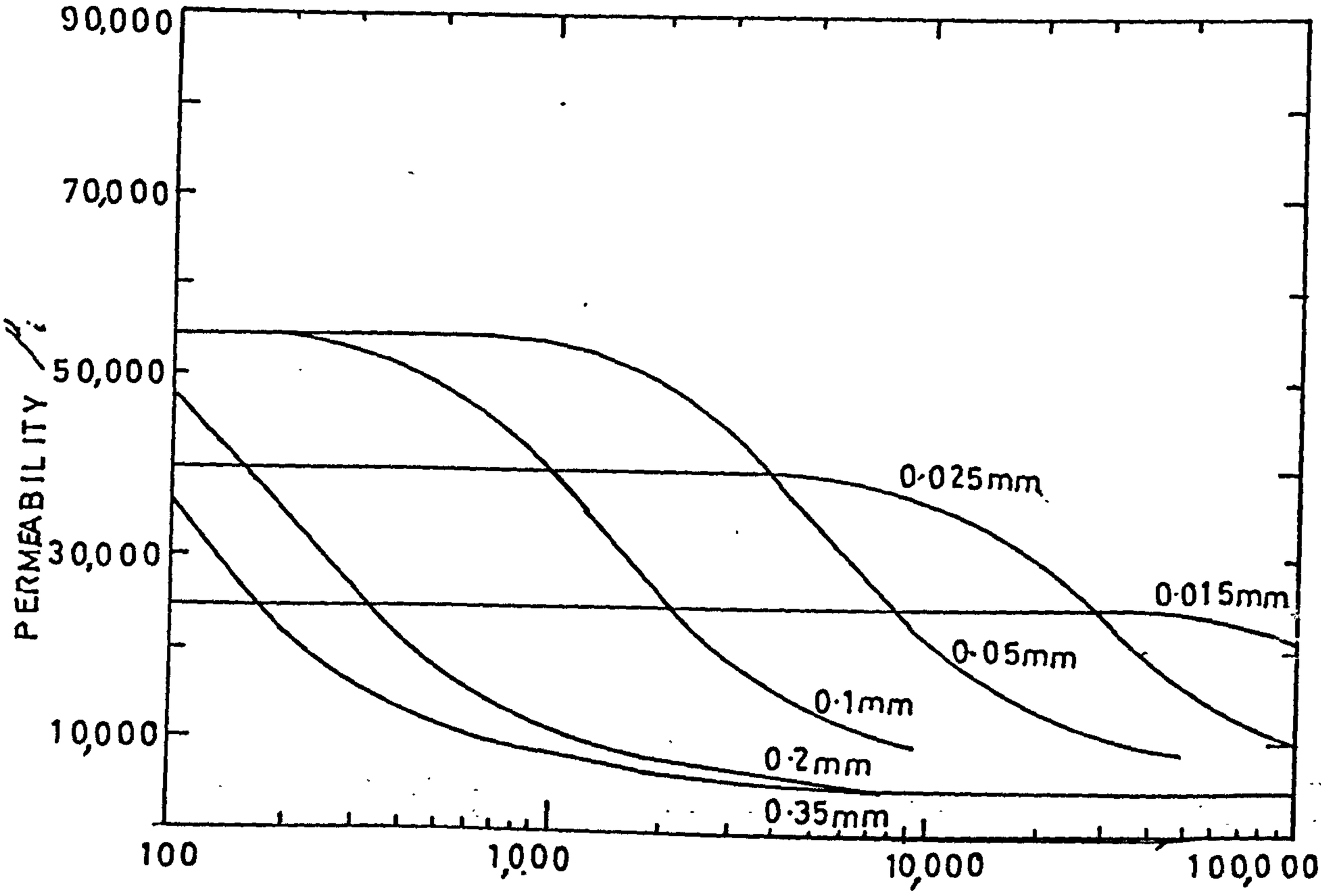

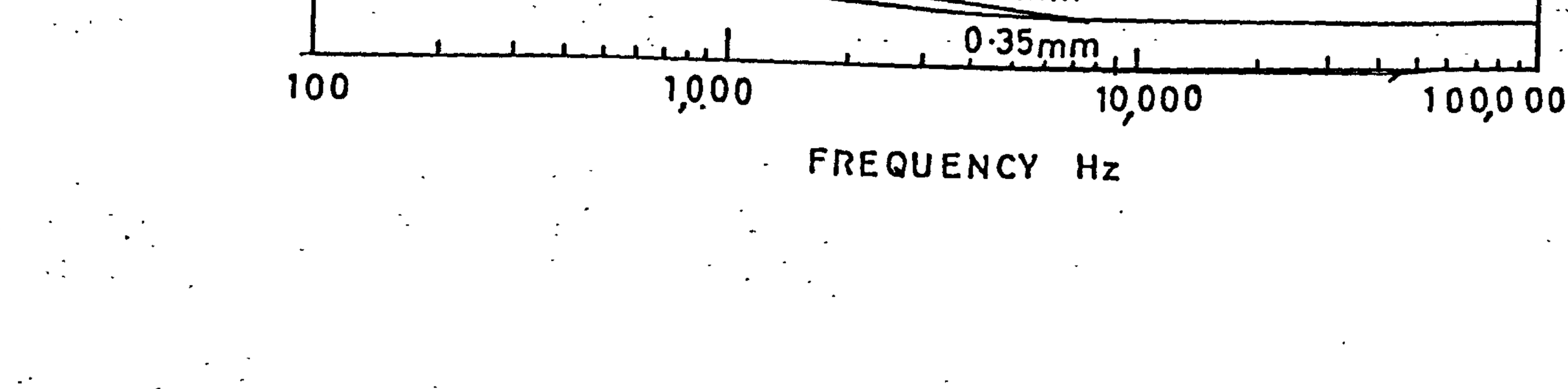

LAMINATED MU-METAL ROD

FIG.(3·4)

effects of flux leakage from the rod.

e) To maximise the signal output from the coil for a given applied field by correct positioning of the coil on the rod.

As a result of these sometimes conflicting requirements a number of compromises had to be made.

f) To meet constraint (a) for a given no. of turns a small wire gauge (large csa) is required. Unfortunately this would conflict with (d) as the coil area would become large. A compromise was arrived at using 45 s.w.g. wire whereby a 10,000 turn coil would have a resistance of less than 4 K ohm with a diameter of less than 4 cm.

g) To meet constraint (b) it is necessary to wave wind the coil but this goes against (d) as a significantly larger volume is required when wave winding rather than lap winding a coil with the same no. of turns. Random winding (some wave winding and some lap winding) is a compromise which was adopted.

h) To meet the requirement (c) it would be preferable to have a narrow coil but for a given number of turns this would result in a large diameter coil which would not satisfy (d). All the coils used were made 1 cm long which enabled the diameter of a 10,000 turn coil to be kept below 4 cm.

i) Condition (e) is met by positioning the coil at the centre of the rod. This maximises the signal output as is shown by Everden (1954).

To summarize then, the coils were placed at the centre of the rod were 1 cm long, up to 6cm dia (for 50,000 turn coil), random wound of 45 s.w.g. enamelled copper wire on nylon formers and were produced with a range of numbers of turns from 1,000 up to 50,000.

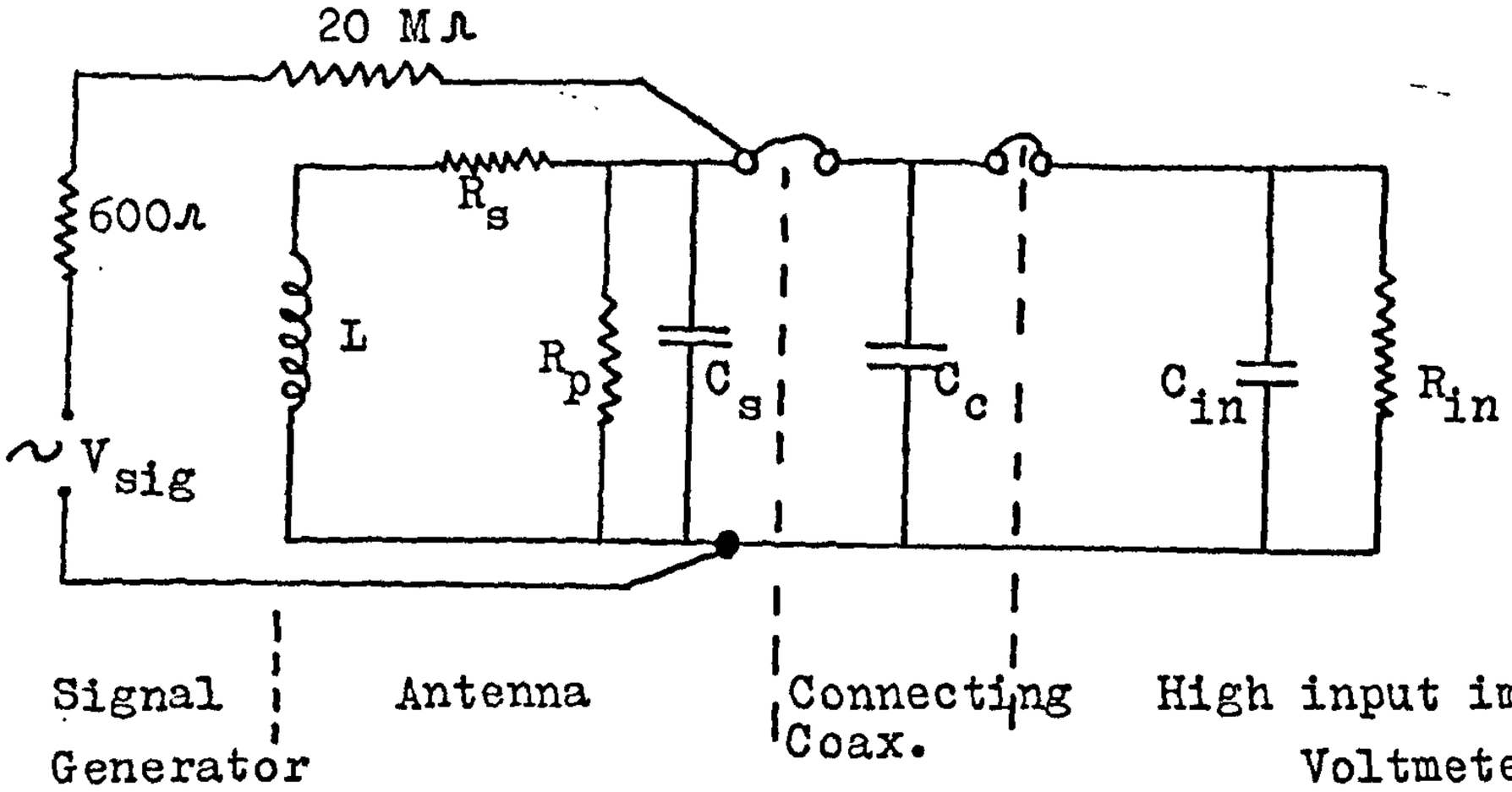

Test Circuit

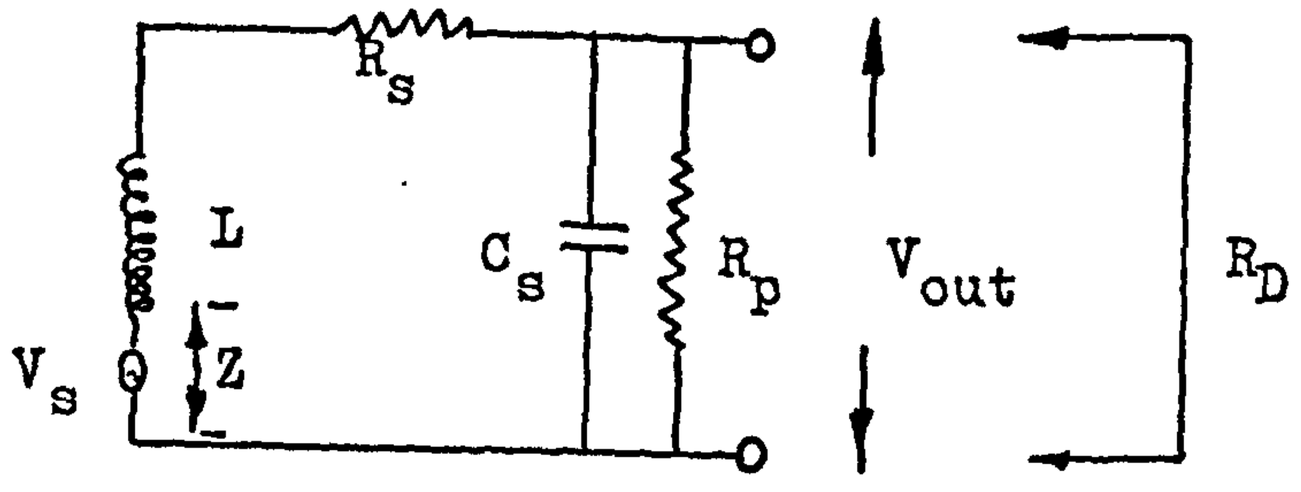

Simplified Equivalent Circuit.

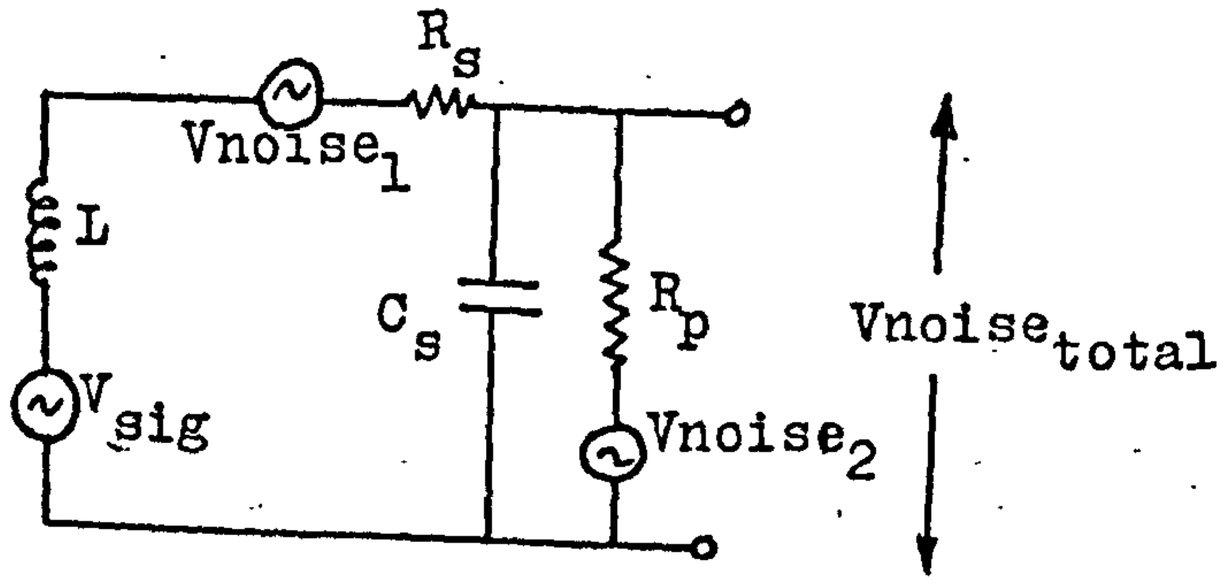

Equivalent Circuit with Noise & Signal Sources.

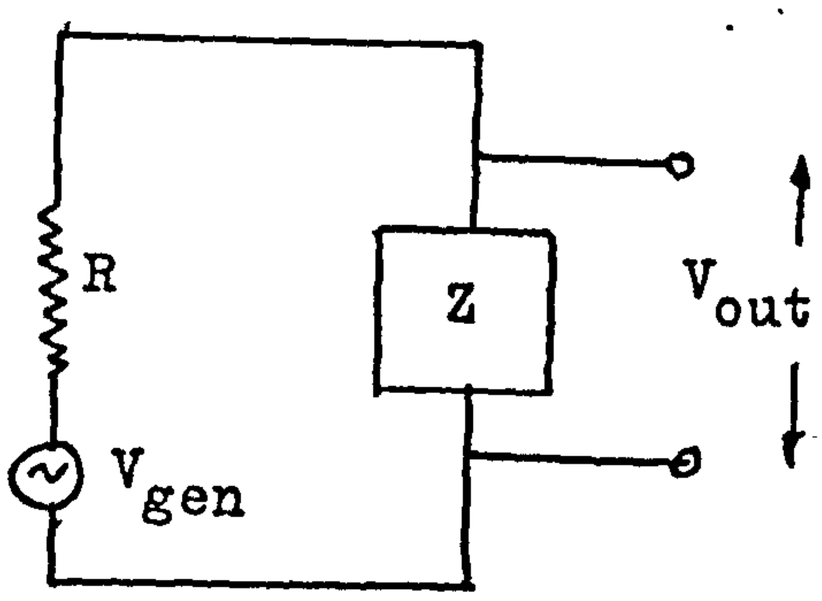

General Circuit.

Fig 3.5.

Details of the seven coils are given in Table 3.2 below.

Table 3.2

Coil No.	1	2	3	4	5	6	7	
No.of turns	1k	2k	4k	10k	16k	30k	50k	
dc.Resistance	0.3k	0.6k	1k	3.7k	7.6k	12.5k	27.3k	ohms

The coils were connected into a test circuit shown in Fig.3.5 and an a.c. signal is applied to the coil. Each coil was found to resonate in the V.L.F. band,the resonant frequencies and Q factors are given in Table 3.3

Table 3.3

No.of turns	Resonant frequency	d.c resistance	Q
50,000	780Hz	27.3kΩ	2.6
30,000	1.41KHz	12.5kΩ	3.2
16,000	2.67KHz	7.5kΩ	5.1
10,000	4.47KHz	3.7kΩ	7.1
4,000	8.99KHz	1.0kΩ	10.7
2,000	20.90KHz	0.6kΩ	11.0
1,000	31.50KHz	0.3kΩ	11.3

The observed resonant property of the antenna can most simply be explained by an equivalant circuit shown in Fig 3.5. The inductor has an associated loss term R_s which is the d.c. resistance of the coil. The coil self capacitance C_s is not purely reactive and has an associated loss term which can be drawn as a parallel resistance R_p.

Consider the simplified equivalent circuit shown in Fig 3.5. Z is the impedance seen by the signal source V_s and R_D is the dynamic impedance seen looking into the antenna output.

$$\text{Now} \quad Z = j\omega L + R_s + R_p \frac{(1 - j\omega C_s R_p)}{1 + \omega^2 C_s{}^2 R_p{}^2}$$

Resonance occurs when;

$$\omega^2 = \frac{1}{L\,C_s} - \frac{1}{C_s^2\,R_p^2} \qquad 3.3.1$$

and at resonance;

$$Z = R_s + \frac{R_p}{1 + \omega^2 C_s{}^2 R_p{}^2} \qquad 3.3.2$$

From (3.3.1 & 2) we have that

$$Z = R_s + \frac{L}{C_s\,R_p} \qquad 3.3.3$$

Now if $\omega^2 C_s{}^2 R_p{}^2 \gg 1$ and $\frac{1}{\omega^2 C_s{}^2 R_p} \gg R_s$

Then $Q = \omega^3 L\, C_s{}^2 R_p = \omega C_s\, R_p = R_p/\omega L \qquad 3.3.4$

Further $\frac{1}{R_D} = \frac{1}{R_p} + \frac{C_s R_s}{L}$

and if $L \gg C_s R_s R_p$ then

$$R_D = R_p \qquad 3.3.5$$

Having briefly covered the properties of the equivalent circuit we are able to derive the component values by making some simple measurements.

a) To determine the Value of R_p we shunt the antenna output by a resistance of approximately the same value as R_p is thought to be. The value of this resistance R_{ext} must be large enough that the condition $\frac{1}{LC_s} >> \frac{1}{C_s^2 R_p^2}$ is still true.

In this case the Q of the circuit will be changed but the resonant frequency will remain the same when R_{ext} is connected.

It can be shown that;

$$R_p = \frac{Q_{old}}{Q_{new}} \cdot R_{ext} \cdot \left[1 - \frac{Q_{new}}{Q_{old}} \right] \qquad 3.3.6$$

The derived values of R_p are given in Table 3.4.

Table 3.4

No of turns in the coil	50,000	30,000	16,000	10,000	4,000	2,000	1,000
R_p mΩ	3:7	3.0	2.5	2.2	1.2	0.85	0.34

b) An estimate of the value of C_s can be made in a similar way.

The circuit is shunted with a capacitor C_{ext} and the change of resonant frequency is measured.

It can be shown ;

$$C_s = \frac{\left[\frac{f_2^2}{f_1^2 - f_2^2} \right] \cdot C_{ext}}{} \qquad 3.3.7$$

The estimated coil self capacitance is given in Table 3.5.

Table 3.5

No of turns in the coil	50,000	30,000	16,000	10,000	4,000	2,000	1,000
C_s pf	86	69	71	36	96	50	147

Having the value of C_s enables the value of L to be determined. See Table 3.6.

Table 3.6

No of turns in the coil	50,000	30,000	16,000	10,000	4,000	2,000	1,000
L H	269.5	91.7	30.0	11.9	1.9	0.51	0.117
Q_{calc}	2.8	3.7	5.4	6.6	10.8	12.9	14
$Q_{meas.}$	2.6	3.2	5.1	7.1	10.7	11.0	11.3
Q_{R_s}	48.2	65.0	64.9	86.8	111	108	78

Also in Table 3.6 can be seen the values of the measured Q factor of the coils at resonance $Q_{meas.}$ and the values calculated assuming $Q = R_p/\omega L$ that is equation (3.3.4).For comparison the Q values which would be observed if the Q was given by $\omega L/R_s$ are also listed in Table 3.6. It can be seen that the loss term R_p defines the Q of the circuit at resonance and that the assumptions made during the derivation of equations (3.3.4,5,6 &7)are justified.

The equivalent circuit with the derived component values represents the actual performance of the antenna rather well but prior to the evaluation of the noise output and minimum detectable signal we must discuss the nature and performance of a very high input impedance low noise preamplifier which is to be connected to

PRINTED CIRCUIT BOARD

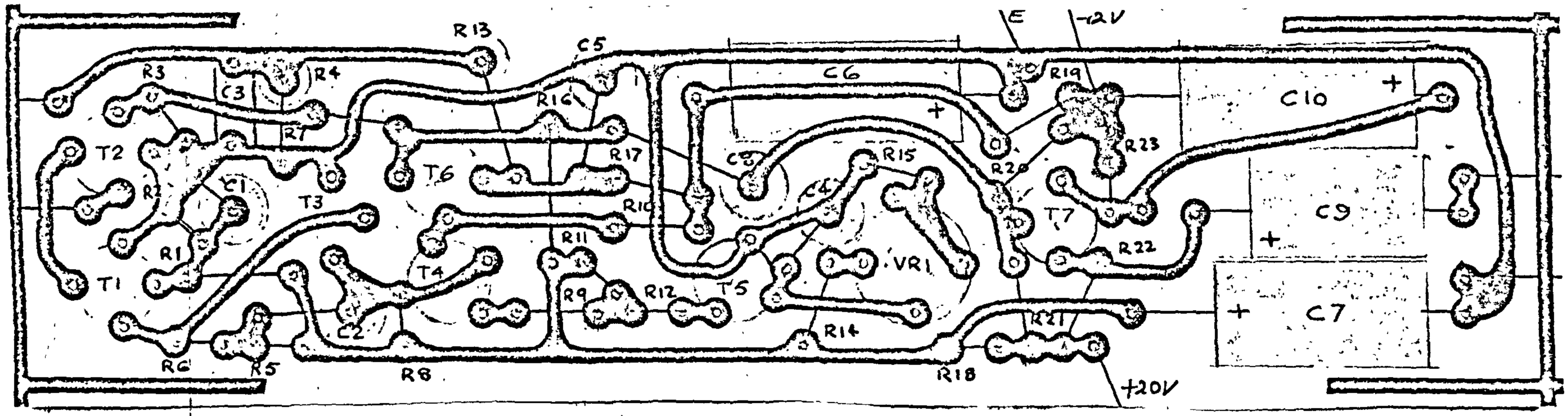

LOW NOISE PREAMPLIFIER

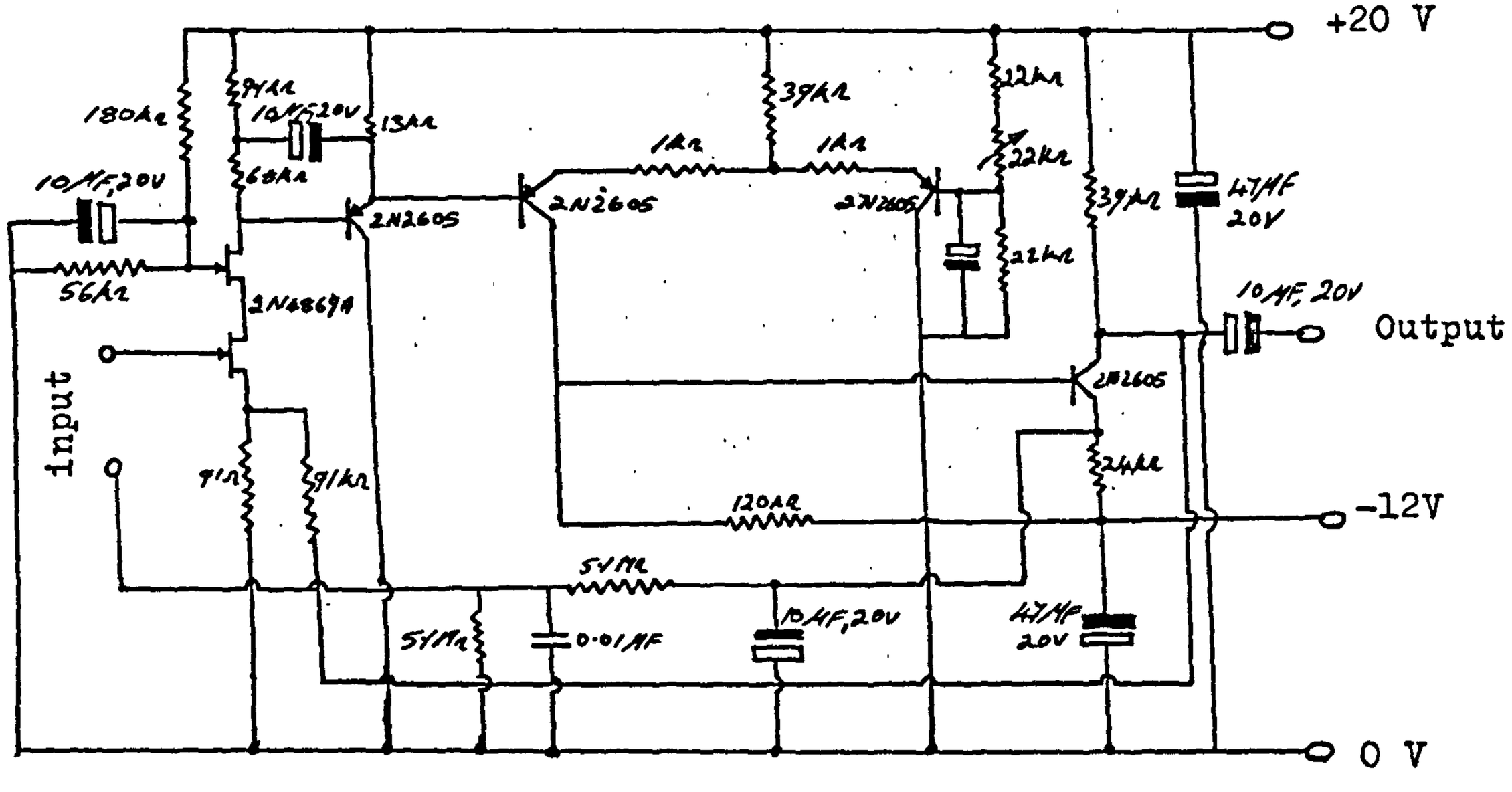

NOISE PERFORMANCE.

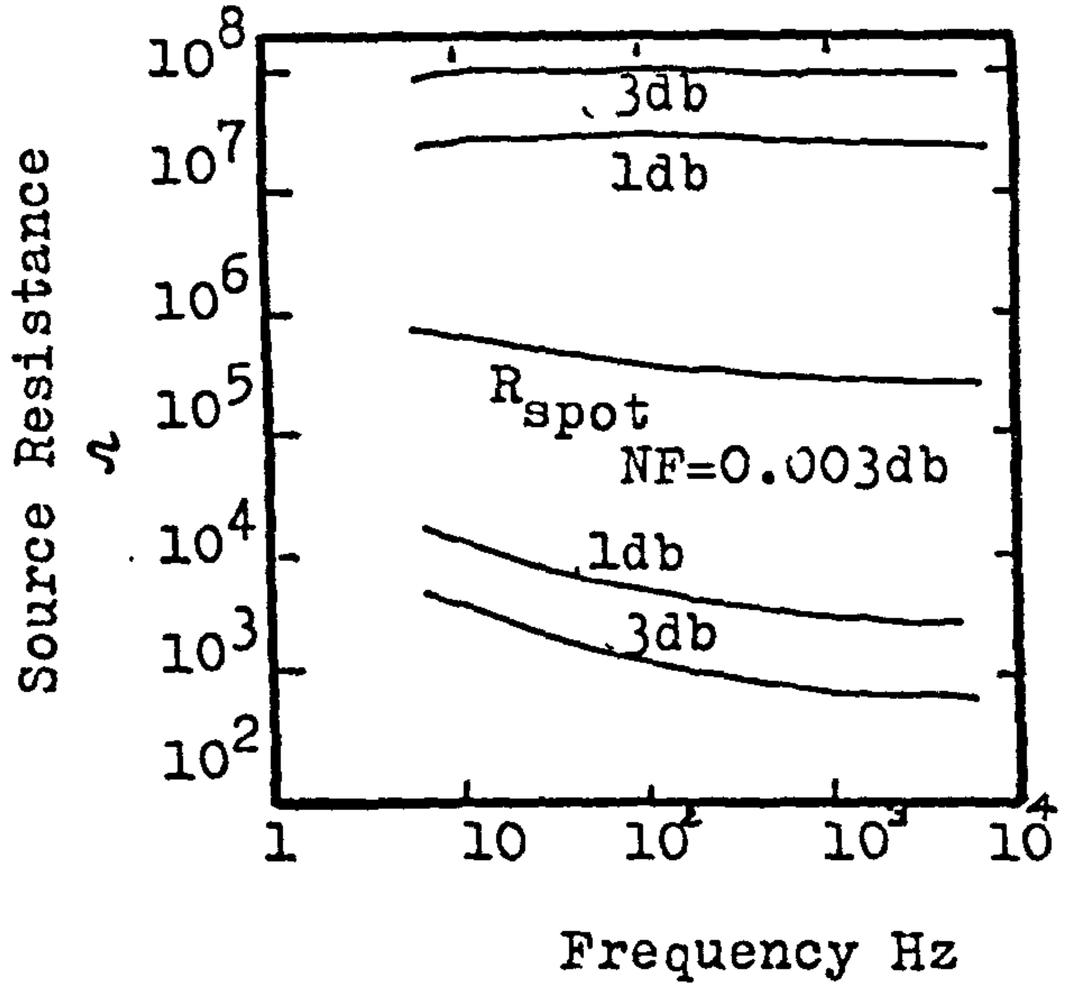

Fig.(3.6)

the antenna.

3.4 A very low noise high input impedance preamplifier

It was realised that a preamplifier which had a very high input impedance (order of 10^8 ohms at 10 KHz) and a low effective input noist voltage would probably have a field effect transistor (FET) as the first stage. The basic design work required to produce an FET input preamplifier with optimum low noise performance is considerable, Holcomb & Sevin (1963), Sevin (1963), Sevin (1963a), Beneteau (1962), Blaser (1962) Benetaeu & Blaser (1963) and Marton (1969). It was decided therefore to conduct a literature search for details of existing high input impedance low noise amplifiers. An excellent design was found due to Cantarano & Pallottino (1970) which used a cascoded Ultra low noise FET from Siliconix[5] (number 2N4867). Time will not be taken up here with a detailed description of the design philosophy and techniques, see Cantarano & Pallotino (1970) but the slightly modified circuit is given in Fig 3.6 along with the noise figure of the amplifier as a function of both frequency and input impedance. The prototype device which was built on a printed circuit board, see Fig 3.6 conformed in every respect with the performance claimed by Cantarano et al. Later preamplifiers were fitted with a variable gain low output impedance integrated circuit output stage but the noise and input impedance characteristics were not changed.

Van Der Ziel (1962) gives a model for the planar junction field effect transistor and calculates the noise output under a variety of bais conditions. Shockly's theory of the FET, Shockly (1952) shows that it operates a true conduction modulation device and that therefore the noise generated by it will be largely thermal noise.

Van Der Ziel (1962) shows that the noise output from an FET varies as a function of gate bias and to a small degree as a function of drain voltage. As well as thermal noise FET's exhibit to a small degree shot noise and 1/f noise in the gate current. For low noise operation the gate current should be a minimum. However this additional noise can be reduced by suitable surface treatment of the semiconductor elements. The FET used in the preamplifier, a Siliconix 2N4869A is a device which has been specially constructed for low noise applications. To a first approximation FET noise generation is independent of the source resistance seen by the gate. This fact enables a simple determination of the effective input noise voltage of the preamplifier to be made.

The preamplifier output noise in a given bandwidth at a given centre frequency is measured with the gate connected to the D.C. bias return, the measured noise level is V_2. If the measurement is repeated with a 10 k ohm resistor in the gate circuit the Johnson noise from the resistor adds to the input noise of the preamplifier and the output level is V_1 where $V_1 > V_2$.

It can be shown that;

$$V_{amp}^2 = \frac{V_{resistor}^2}{\frac{V_1^2}{V_2^2} - 1} \qquad 3.4.1$$

Where V_{amp} is the effective input noise voltage in a given bandwidth of the preamplifier and $V_{resistor}$ is given by;

$$V_{resistor} = \sqrt{4KTBR}$$

For a 10 k ohm resistor at room temperature

$$V_{resistor} = 1.28 \times 10^{-8} \text{ V}/\sqrt{\text{Hz}}$$

With $V_1 = 2.2\text{V}$ and $V_2 = 0.6$ V

we have $\underline{V_{amp} \text{ (for a 10 Hz bandwidth)}} = \underline{1.13 \times 10^{-8} \text{ V}}$

It will be shown later* that this estimate of the effective input noise voltage of the preamplifier is entirely consistent with results derived from calculations of antenna output noise. Having determined the noise performance of the preamplifier which to a first approximation is flat over the frequency range 10 Hz to 20 KHz we are now in a position to discuss the calculation and measurement of antenna coil noise as a function of coil construction and frequency.

3.5 Evaluation of the Antenna Noise

Consider the antenna equivalent circuit shown in Fig 3.5 it has two lossy components R_s and R_p. Each of these resistors has a noise generator associated with it. An equivalent circuit showing the positions of the noise generator and the 'induced signal' generator can be seen in Fig 3.5. It is clear that if there were no noise source associated with R_p then the signal to noise ratio would remain constant as a function of frequency. It can be seen that at frequencies $f > f_{res}$ the noise output from R_p which is present at the network terminals will be falling with frequency at 6 db/octave whereas the signal and noise from the inductor will be falling at 12 db/octave. Thus one might expect the signal to noise ratio S/N to decrease at high frequencies.

If we have a noise generator with an internal resistance R ohms

*Appendix 3

feeding a load of impedance Ż which is assumed to be non-noisy. See Fig 3.5. Then the maximum power which can be dissipated in the load is delivered when R = Z, or more generally when the load impedance it equal to the complex conjugate of the generator impedance. Under these conditions the 'available power' = KTB watts. Therefore the mean square voltage produced by the noise generator is given by;

$$\overline{V_{gen}^2} = 4\,KTBR$$

So for the general case of a noisy resistor R connected to an impedance network Z, the voltage developed across Z is;

$$\overline{V_{out}} = \sqrt{4KTBR} \cdot \frac{Z}{Z + R} \qquad 3.5.1$$

Using equation (3.5.1) and the equivalent circuit shown in Fig 3.5 it is possible to calculate the noise voltage as a function of frequency at the antenna output which is produced by each noise source. Assuming that noise powers are additive ie.

$$Vnoise_{Total} = \sqrt{(Vnoise_1)^2+(Vnoise_2)^2}$$

it is possible, taking account of the effective input noise of the preamplifier to determine the noise output seen at the output of the preamplifier. The circuit calculations can be seen in Appendix 1. and a flow chart of the computer program which performs the calculations can be seen in Appendix 2. Noise performance was determined for each of the seven coils wound but there is space here for only one example. Fig 3.7 shows the noise from each source as a function of frequency between 1 and 20 KHz for the 10,000 turn coil.

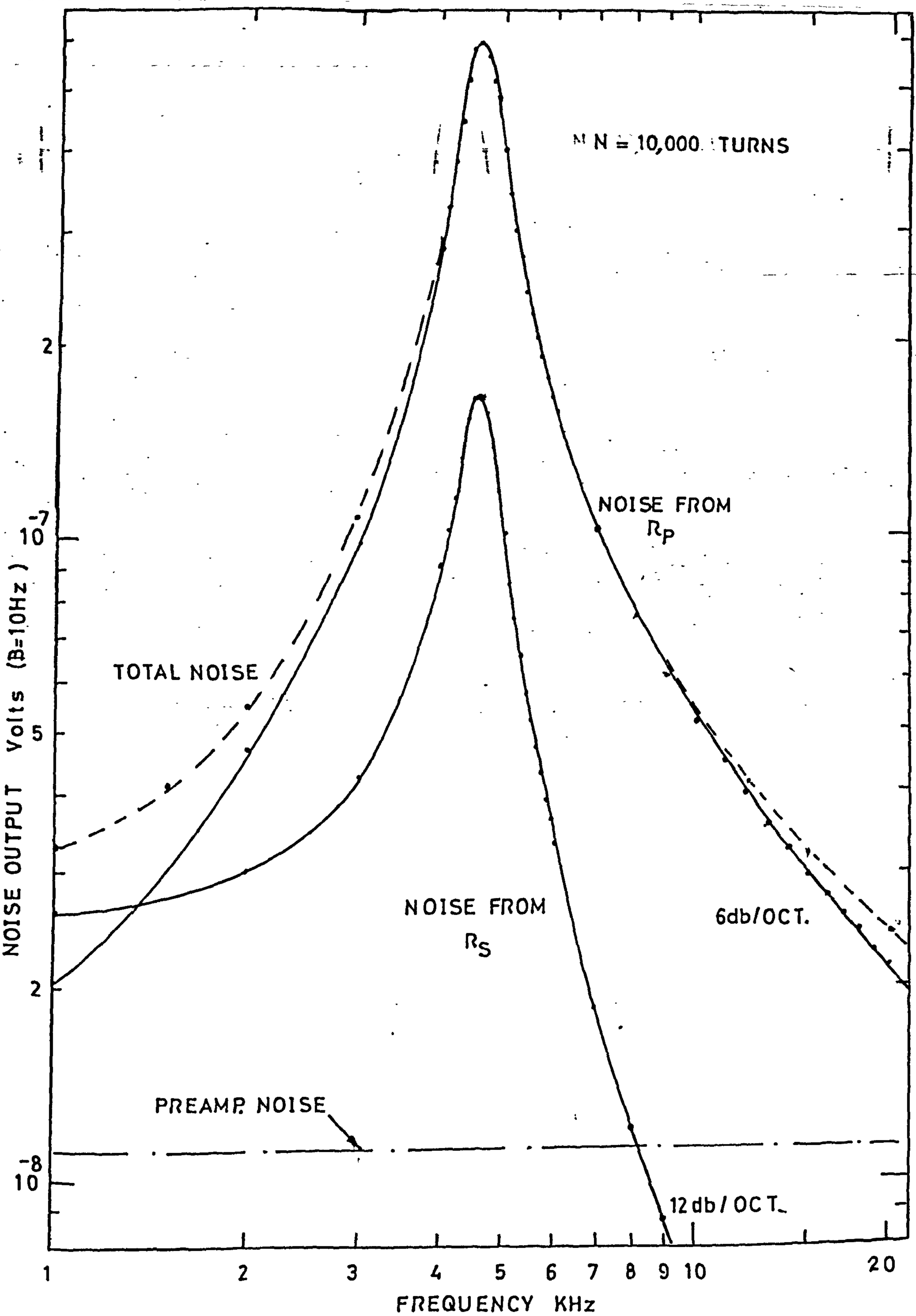
N = 10,000 TURNS
NOISE FROM
R_P
TOTAL NOISE
NOISE FROM
R_S
6db/OCT.
12 db / OCT.
PREAMP. NOISE
NOISE OUTPUT Volts (B=10Hz)
10^{-7}
5
2
10^{-8}
1
2
3
4
5
6
7
8
9
10
20
FREQUENCY KHz

FIG(3.7)

FIG.(3.8)

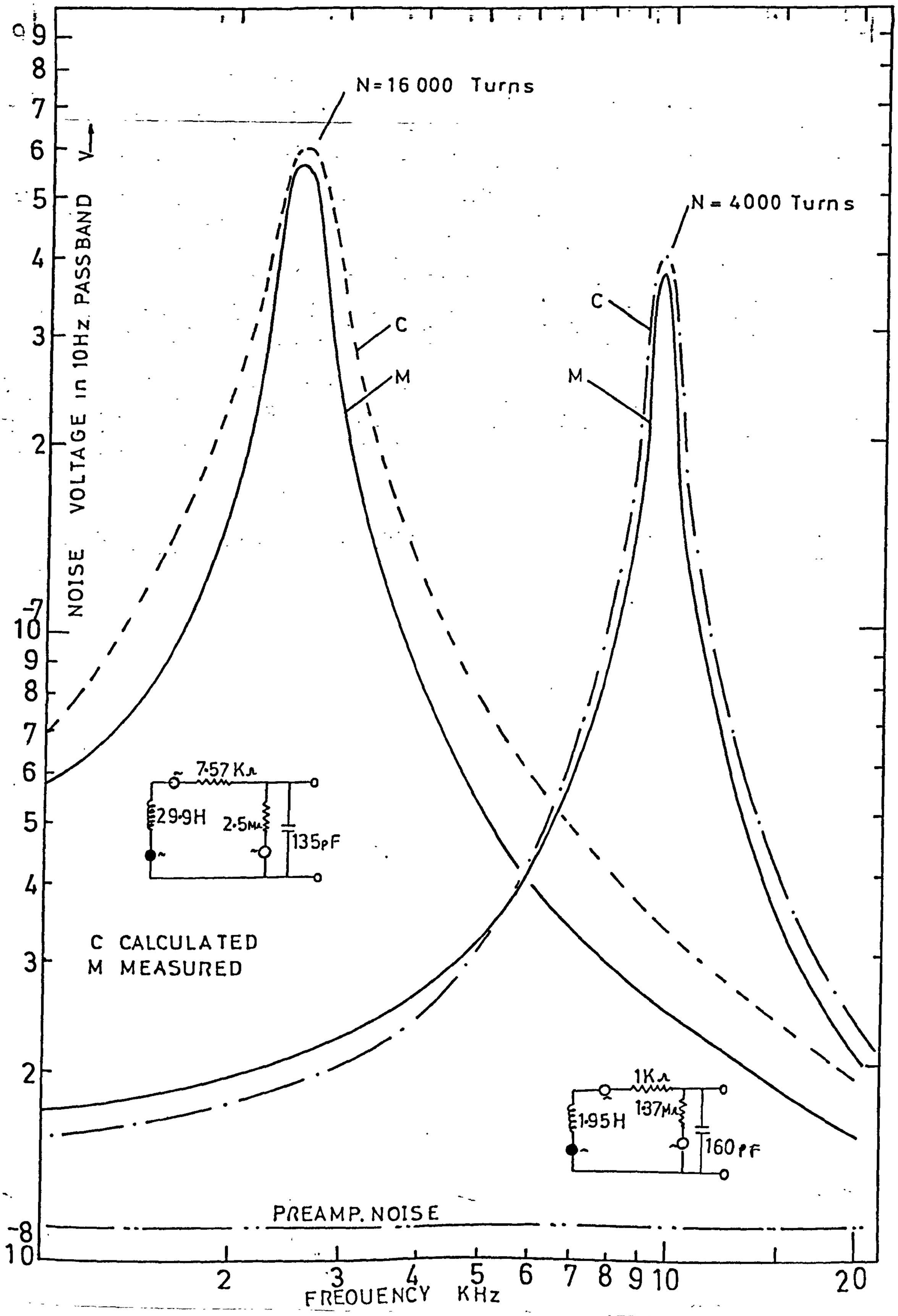
N=16 000 Turns
N = 4000 Turns
C
M
C
M
NOISE VOLTAGE in 10Hz. PASS BAND
7·57 Kλ
29·9H
2·5MΛ
135pF
1Kλ
1·95H
1·37MΛ
160pF
C CALCULATED
M MEASURED
PREAMP. NOISE
FREQUENCY KHz
2
3
4
5
6
7
8
9
10
20

As expected the noise at high frequencies falls off in quite a different manner for the two sources. In general the contribution to the overall noise made by E_{n1} is less than that made by E_{n2}. These together with the preamplifier noise result in the total noise profile which would be observed. The preamplifier noise only starts to become important at the extreme edge of the frequency band of interest and therefore the condition laid down in Chapter 3 section 1 (that the antenna noise must be much greater than the preamp. noise) is fulfilled.

Measurement of antenna noise

The measurement of the noise produced by the antenna under laboratory conditions is rather difficult due to the high ambient electromagnetic noise levels present. In order to reduce this interference the antenna or sensor was placed inside a screened room which was fabricated from large copper sheets. When all orifices are sealed the room acts as a 'shorted turn' and unwanted signals from outside are greatly attenuated. Unfortunately the performance of such enclosures falls off with decreasing frequency and at 50 Hz only a few db attenuation is produced. Antenna noise must be measured therefore in the presence of strong spectral lines at 50,150,250 and 350 Hz, and on occasions even higher mains harmonics. The making of such measurements calls for a narrow band tuneable filter which has very fast roll off outside the analysis band. The two instruments used during the period of this work are manufactured by Wayne Kerr[6] & Bruel & Kjur[7]. They permit the noise voltage in a 10Hz band to be measured over a frequency range 100 Hz to 20 KHz. The results of measurements made using such equipment in a screened enclosure can be seen in Fig3.8 where the noise profiles of the 4,000 and 16,000 turn coils are presented along with the calculated ones.Good agreement between the two was obtained

at most frequencies.

3.6 Determination of Minimum Detectable Signal

a) Calculation of Minimum Detectable Signal

In order to perform the calculation it is necessary to know what e.m.f. is induced in the coil for a given incident magnetic field.

Now $e = -\frac{d\underline{\Phi}}{dt}$ where $\underline{\Phi}$ = the total flux through the coil

and $\underline{\Phi} = \underline{B}\ N\ A$ where B = the magnetic induction

N = the number of turns in the coil

A = the area of the coil

So $\underline{\Phi} = \mu_{rel}\mu_o \underline{H}\ N\ A$

where $\underline{H}$ = the magnetic field

therefore $e = -\mu_{rel}\mu_o\ N\ A\ \frac{dH}{dt}$ 3.6.1

Assuming a sinusoidal variation of H with time so that;

$$H = H_o \sin\omega t$$

which results in $e = -E_o \cos\omega t$

then from (3.6.1) we have that

$$\int_0^{2\pi} E_o \cos\omega t\ dt = \mu_{rel}\mu_o\ N\ A \int_0^{Ho} dH$$

So $E_o = \mu_{rel}\mu_o\ N\ A\ \omega H_o$

or $\bar{E} = \mu_{rel}\mu_o\ N\ A\ \omega \bar{H}$ 3.6.2

---

where the bar denotes r.m.s. values.

It is important to notice that $\bar{E}$ increases with ω for a given $\bar{H}$.

From equation (3.6.2) it can be seen that μ_{rel} must be determined before the calculation can proceed. We know from Table 3.1 and the graph in Fig 3.2 that for an ellipsoid with axes of ratio 19:1 that the demagnetising factor D = 0.0057. From equation (3.1.12) the effective relative permeability of such an object is calculated to be 157. The technique for determining the relative permeability of the rod used is somewhat involved although based on essentially simple principles and for this reason it will not be discussed here. The results of the measurement of relative μ as a function of frequency are shown in Fig 3.12. The fall of μ_{rel} with frequency is small (< factor of 2) and is expected as the initial permeability is seen to fall with frequency from 1 KHz for 0.05mm strips of which the rod was composed. See Fig 3.4 The measured value of μ_{rel} is approximately a factor 2 down on the calculated one. As the calculation was performed for a prolate spheriod and the measurement was made on a bar of square cross section with sharp edges the results are considered to be in reasonable agreement. A value for μ_{rel} of 75 was used throughout the calculations of minimum detectable signal.

As explained in section two of this chapter it is difficult to determine exactly the signal output from the coil for a given applied field due to the extended nature of the coil. However an estimate must be made and therefore we must establish the equivalent area of the coil. For a coil with turns which have radii varying from R_1 to R_2 ($R_2 > R_1$) it might seem reasonable to use the average area ;

$$A = \frac{\pi R_1^2 + \pi R_2^2}{2}$$

and let all N turns have this area.

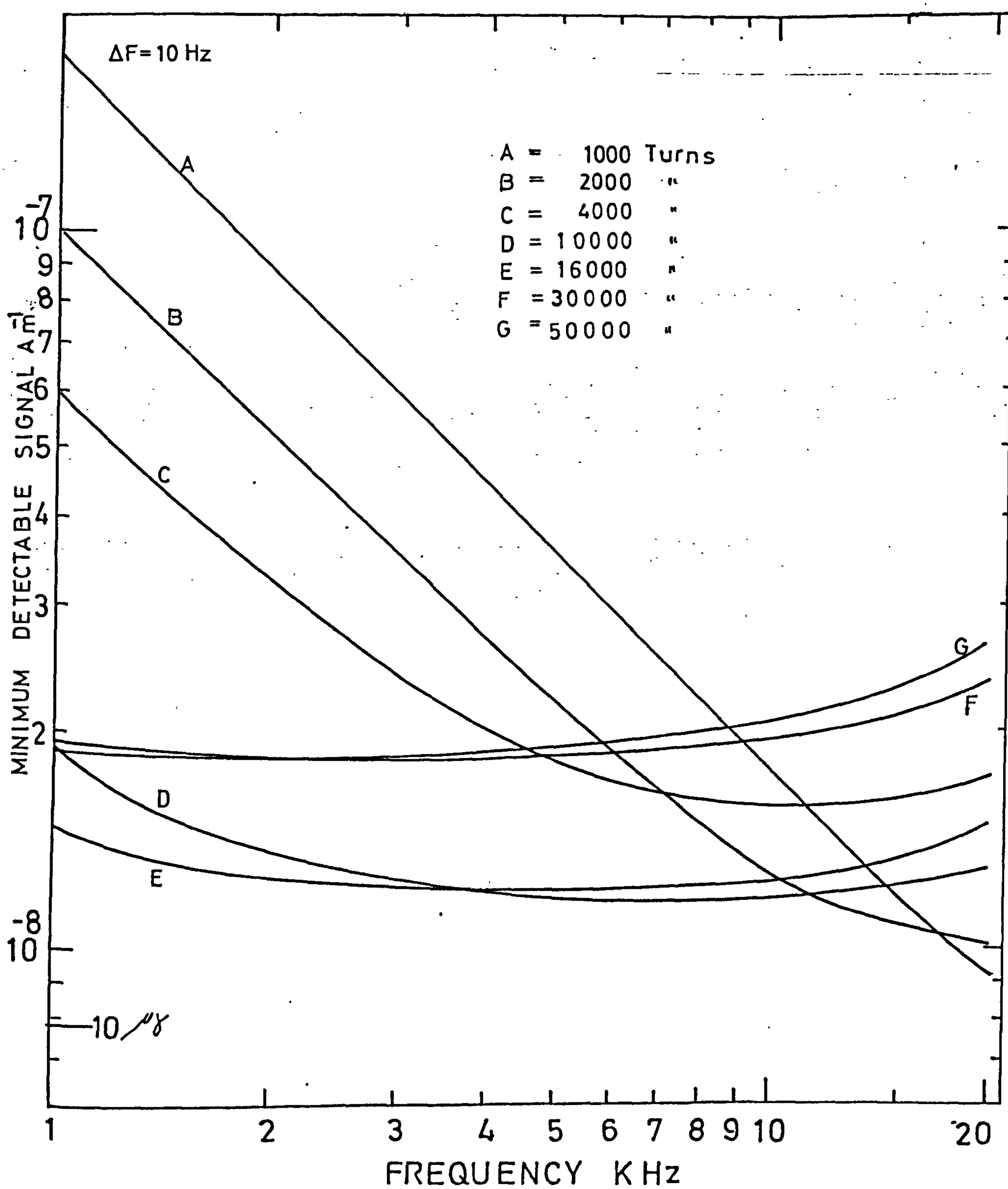
ΔF= 10 Hz
A = 1000 Turns
B = 2000 "
C = 4000 "
D = 10000 "
E = 16000 "
F = 30000 "
G = 50000 "
MINIMUM DETECTABLE SIGNAL Am⁻¹
10⁻⁷
9
8
7
6
5
4
3
2
10⁻⁸
10 μg
A
B
C
D
E
F
G
1
2
3
4
5
6
7
8
9
10
20
FREQUENCY KHz

FIG.(3.9)

Fig. 3.10

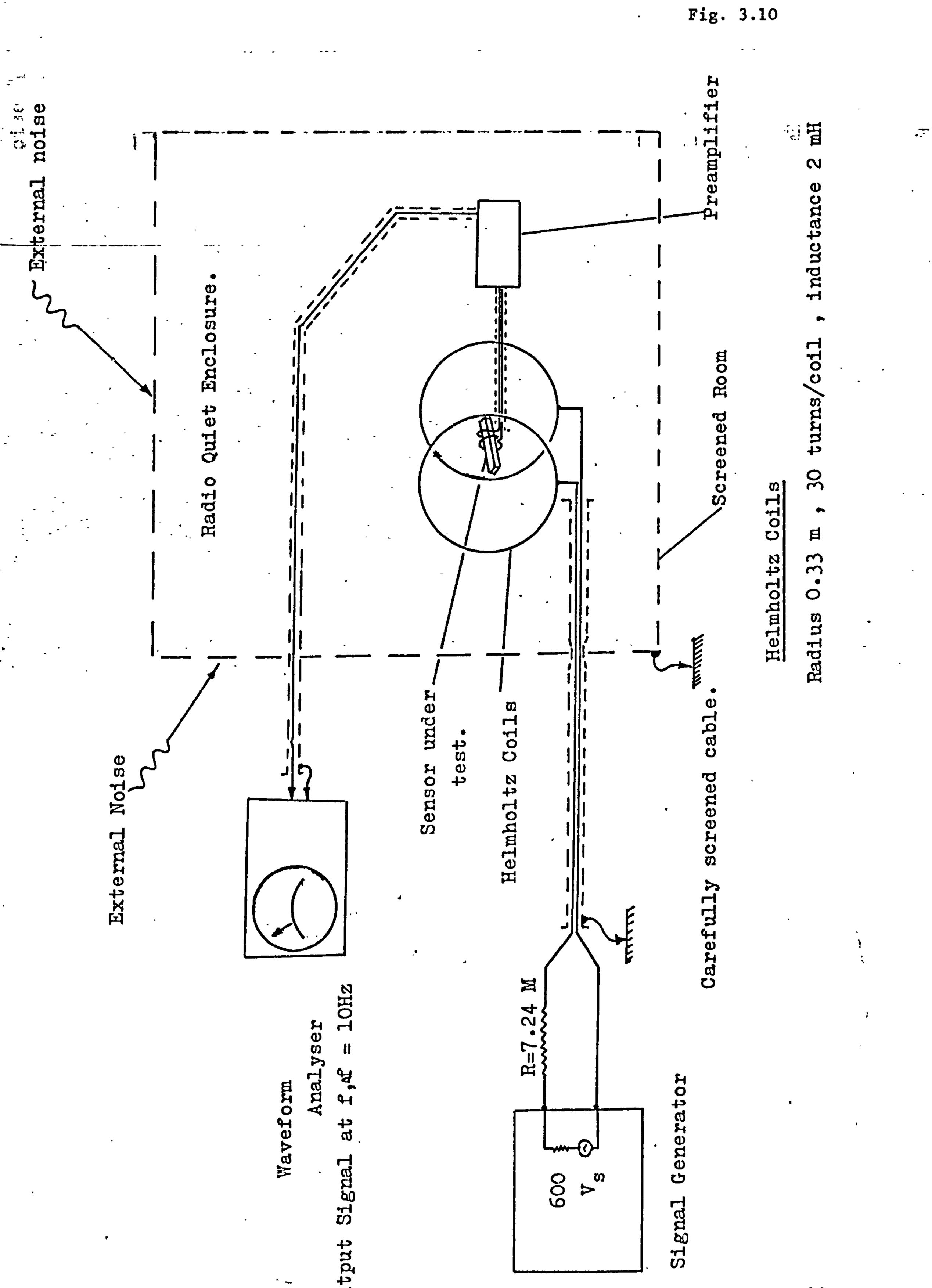

Fig. 3.10

It can be seen From Fig 3.7 that for frequencies is greater than the resonant frequency the noise output from the coil is falling at 6 db/ octave and that the signal output (for a constant input) is falling at 6 dB/octave. However from equation (3.6.2) it can be seen that the signal source output increases at 6 db/octave for a constant applied magnetic field. We may conclude therefore that the minimum detectable signal will be roughly the same at all frequencies above resonance. This is true for coils with $N \gg 10,000$ but for the others it is not so because the coil noise profile is different. The curves of minimum detectable signal as a function of frequency for all seven coils can be seen in Fig 3.9. Here a clear evolution from a steeply falling curve with frequency to a shallow curve which increases with frequency for increasing numbers of turns is evident. The coils become first more sensitive in general over the fréquency range and then less so as N passes through 10,000 or 16,000 turns. Thus it would seem that coils D & E are the optimum.

B) Measurement of Minimum Detectable Signal.

In the previous section is was pointed out that measurements of antenna noise under normal (ie. not electrically quiet) laboratory conditions were difficult but possible. Equally the determination of the minimum detectable signal is difficult and work is best done at quiet times such as evenings or nights. The measurement method and equipment are shown in Fig 3.10. The use of Helmholtz coils as a source is convenient and provides a uniform field around the sensor which is therefore calibrated for a uniform incident field such as exists in a plane wave.

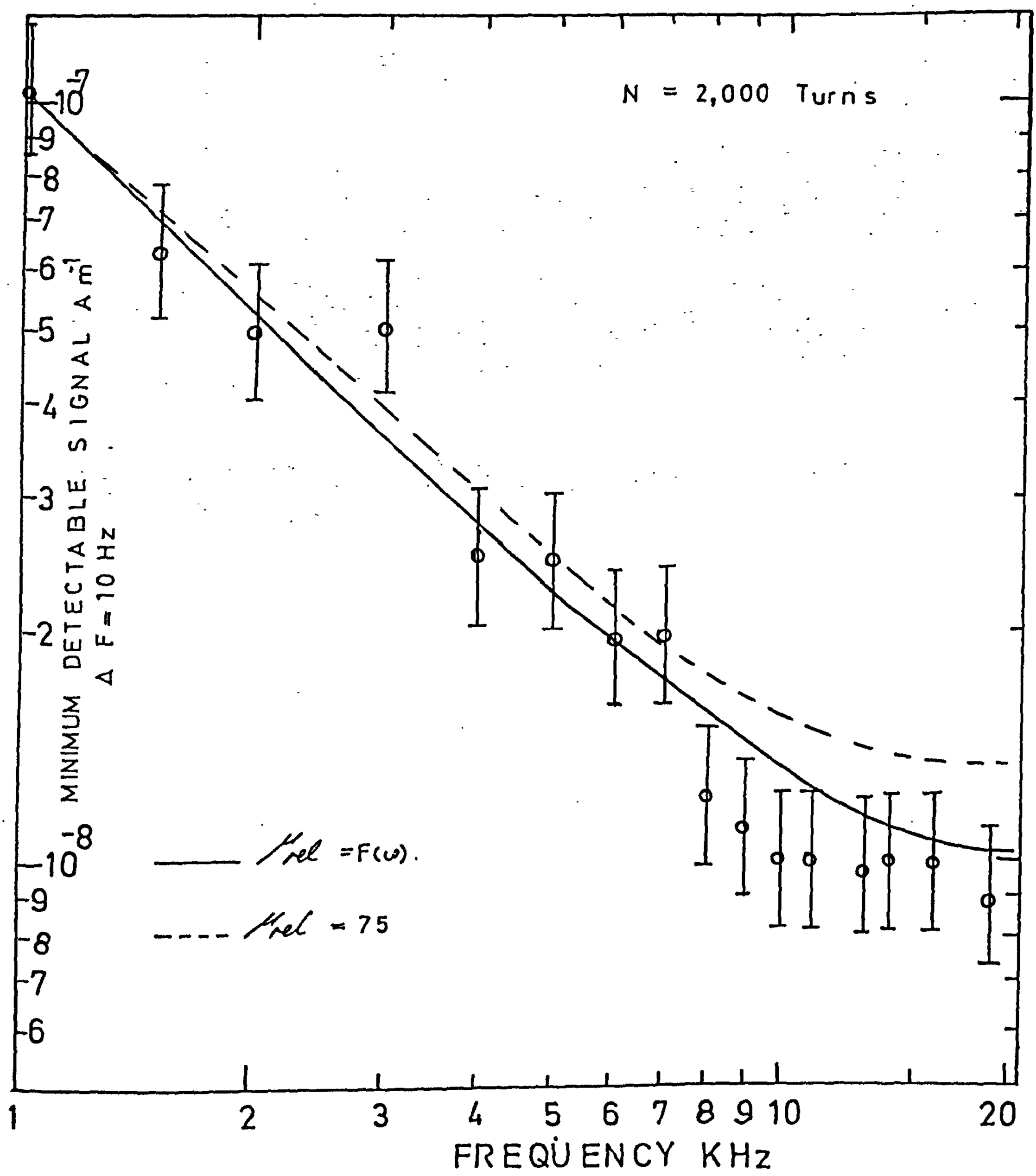
N = 2,000 Turns
SIGNAL A m⁻¹
MINIMUM DETECTABLE
Δ F = 10 Hz
10⁻⁸
10
9
8
7
6
5
4
3
2
10⁻⁸
9
8
7
6
μrel = F(ω).
μrel = 75
1
2
3
4
5
6
7
8
9
10
20
FREQUENCY KHz

FIG.(3.11)

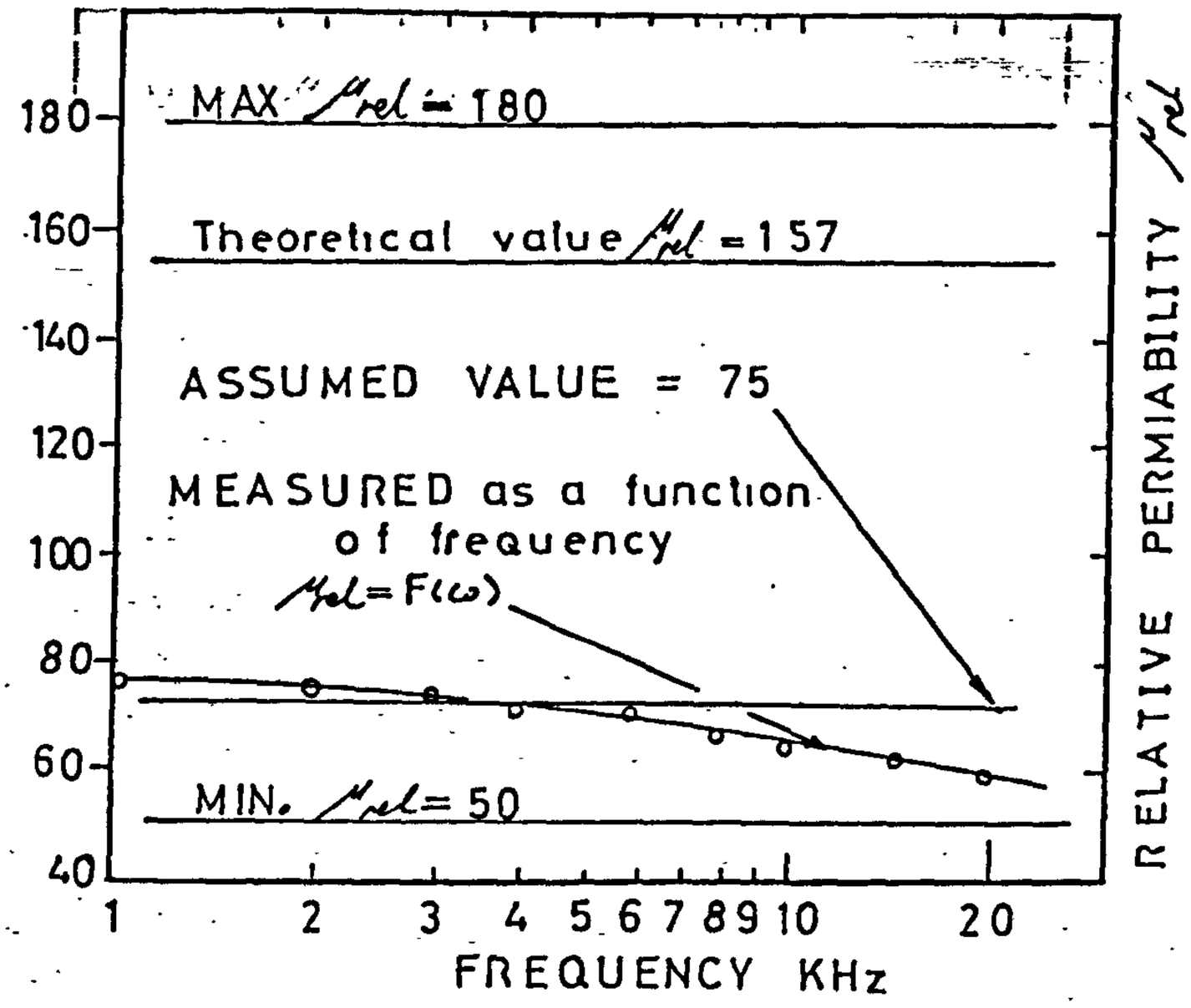

152 mm ROD

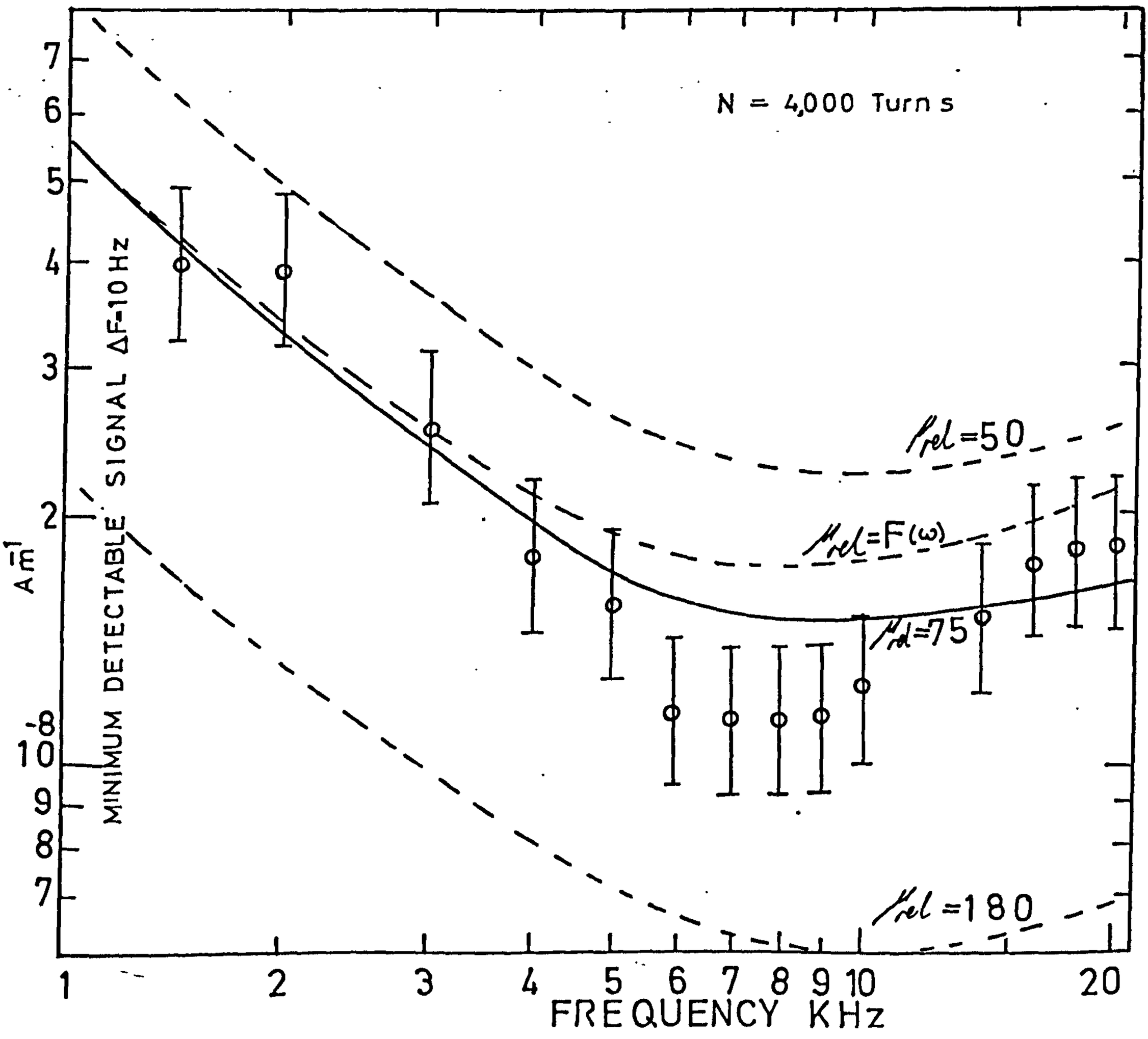

FIG.(3 .12)

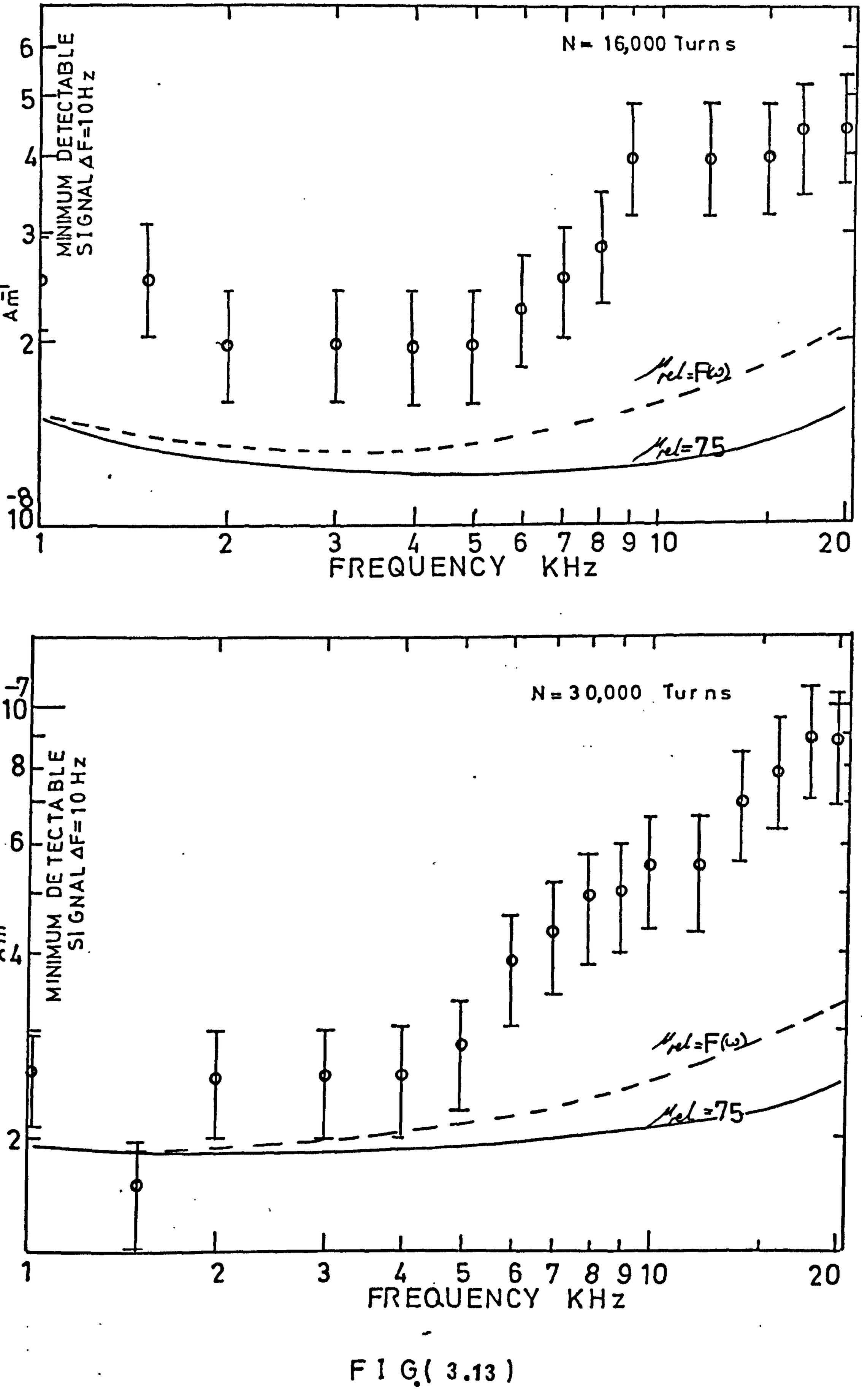
N = 16,000 Turns
MINIMUM DETECTABLE SIGNAL ΔF=10Hz
A m⁻¹
$\mu_{rel}=F(\omega)$
$\mu_{rel}=75$
FREQUENCY KHz
N = 30,000 Turns
MINIMUM DETECTABLE SIGNAL ΔF=10 Hz
A m⁻¹
$\mu_{rel}=F(\omega)$
$\mu_{rel}=75$
FREQUENCY KHz

FIG.(3.13)

The series resistor of 7.24M ohm in the Helmholtz coil circuit has two functions. It determines that for a signal generator setting of 0 db (1mW into 600 ohms) the field produced between the coils is 0.01 γ ($1\gamma = 10^{-9}$T) and ensures that this value remains the same over the frequency range 0 to 20 KHz.

In the series circuit $R \gg \omega L$ such that the current I mA & H Am^{-1} remains constant as ωL changes with frequency. At 10 KHz for the coils used ωL = 20 ohm, thus the condition is well satisfied. If the analyser is used with a long time constant to reduce the signal fluctuations due to the noise and external impulses the output from the signal generator can be adjusted to increase the signal in the bandwidth over which the measurement is being made by 3db. By knowing the current taken from the signal generator the minimum detectable signal (Signal power = noise power in bandwidth B Hz) can be calculated. The computer calculated minimum detectable signal and the measured performance are shown together for the 2,000, 4,000, 16,000, & 30,000 turn coils in Figs. (3.11), (3.12) (3.13) respectively. The error bars shown represent the maximum expected error.

The calculated minimum detectable signal curves have been produced with a value for μ_{rel} = 75 and as a function of frequency $\mu_{rel} = F(\omega)$ which are shown in Fig 3.12. Also in this figure are minimum detectable signal curves for μ_{rel} = 50 & μ_{rel} = 180 showing the variation over these values of μ_{rel}. In general the agreement between measured and calculated curves is excellent especially for coils with low numbers of turns at high frequencies.

CHAPTER 4

A MORE REPRESENTATIVE EQUIVALENT CIRCUIT

4.1 A sensitive determination of coil properties

The equivalent circuit which has been used is one of the simplest which will describe the basic characteristics of the antenna. However it has been shown that it does not very well represent the performance of coils with large numbers of turns at high frequencies. The measurements which were made in order to evaluate the coil parameters such as inductance, self capacitance and series and parallel resistances were, very simple and not capable of great accuracy. In order to determine an equivalent circuit which more closely represents the antenna properties, it is necessary to measure the inductance,capacitance etc of the coil more accurately.

The coil may be connected to an accurate LCR audio frequency bridge which is driven by a stable oscillator of known frequency. The out of balance signal from the bridge is then taken to a very sensitive voltmeter and the bridge is balanced thereby giving values of L,C or conductance. The equipment connection is shown in Fig 4.1. The voltmeter used was a narrow band waveform analyser which measures down to 100 μV signals which appear in the narrow well defined passband producing very useful rejection of unwanted interference.The system is very sensitive and care must be taken to eliminate spurious signals entering the bridge via connecting cables or by induction in the coil itself.

The bridge used will be nulled when sufficient additional capacitance has been added into the inductive circuit such that it resonates at the driving frequency. Thus from the added capacitance and the precise knowledge of the driving frequency the inductance

may be calculated. From two measurements the self capacity may be estimated. The conductance of the component under test can be read directly.

The preliminary work indicates that the 16,000 turn coil is the most sensitive in the frequency range of interest and therefore it was chosen for further analysis. The newly measured values of additional capacitance and conductance are given as a function of frequency in Table 4.1.

Table 4.1

Driving Frequency	Conductance	Capacitance
500 Hz	0.685 mho	2950 pf
1 KHz	0.1835 mho	723 pf
2 KHz	0.0615 mho	164.4 pf
3 KHz	0.0372 mho	60.8 pf
4 KHz	0.0305 mho	24.42 pf
5 KHz	0.02825 mho	7.6 pf
5.79 KHz	0.02820 mho	0.00 pf

If $\omega^2 = \frac{1}{L(C_1 + C_s)}$ (4.1.1) where ω = driving frequency

C_1 = additional capacitance

C_s = self capacitance

L = inductance

Then when $C_1 \gg C_s$ which occurs at low frequencies;

We have $L = 1/\omega^2 C_1$ 4.1.2

Using data for 500Hz L = 34 H

At self resonance, when $C_1 = 0$ (4.1.1) becomes

$$C_s = 1/\omega_o^2 L \qquad 4.1.3$$

Using data obtained at 5.79 KHz, C_s = 22.2 pf

This value was obtained for the 16,000 turn coil with NO electrostatic screen and is less than the previously determined value of 71 pf which was determined with a screen.

The condition that $C_1 \gg C_s$ is clearly fulfilled at 500 Hz.

The soundness of the determined values of L & C_s may be checked by using (4.1.1) to determine ω from $L, C_s \propto C_1$. Using data at 5 KHz the predicted frequency = 4.998 KHz. (Better than 0.05% agreement).

The Q factor of the circuit is given by;

$$Q = \frac{R_e}{\omega L} = \frac{1}{\omega L G}$$ where G = conductance, R_e = effective parallel loss resistance.

As $(R_e = 1/G)$

A comparison of measured Q, and Q if only the series resistance is important in determining coil performance, is given as a function of frequency in Table 4.2.

Table 4.2

Frequency	Measured Q	Q(Due to R_s only)
500 Hz	13.6	14.11
1 KHz	25.5	28.22
2 "	38.05	56.44
3 "	41.94	84.66
4 "	38.36	112.88
5 "	33.14	141.1
5.75 KHz	28.66	163.42

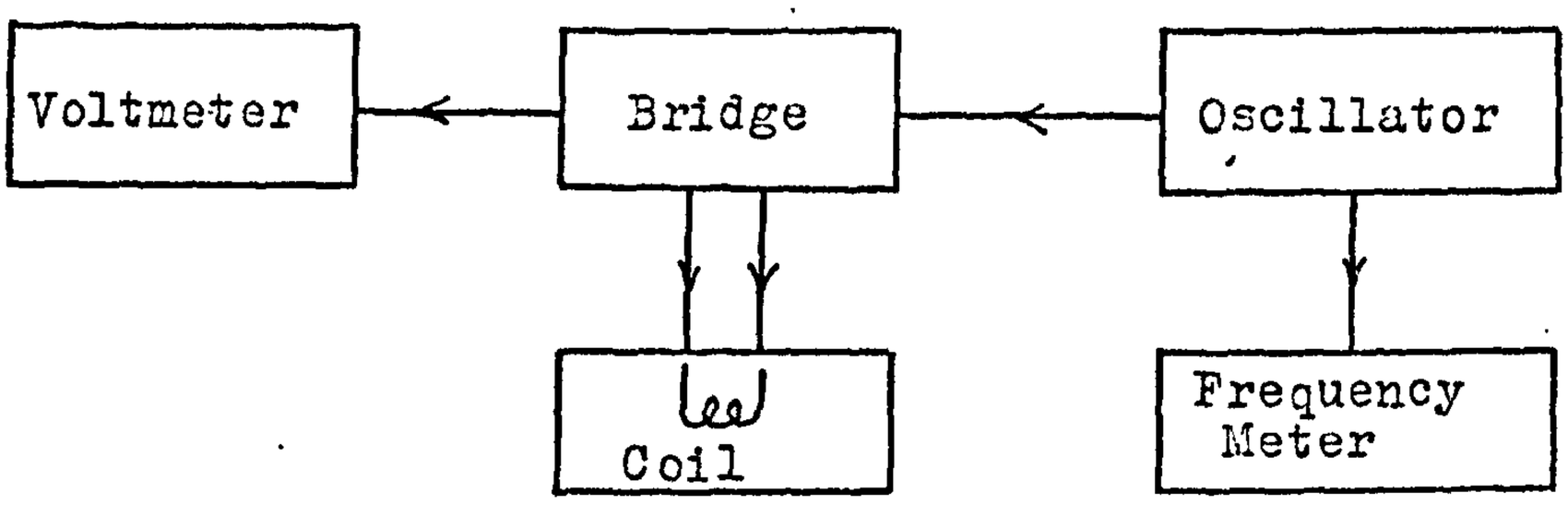

(a)

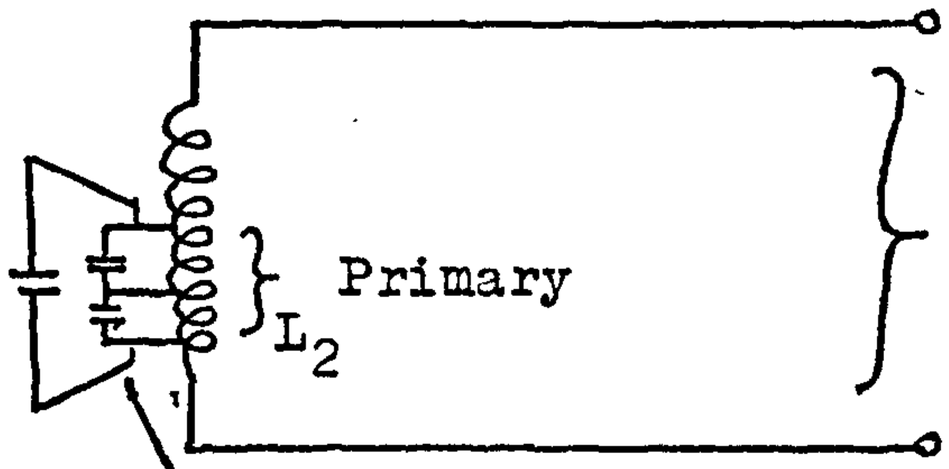

Secondary;
Auto-transformed
lossy self capacitance
appears across output.

(b)

Capacitance between turns = c
Resistance of one turn =

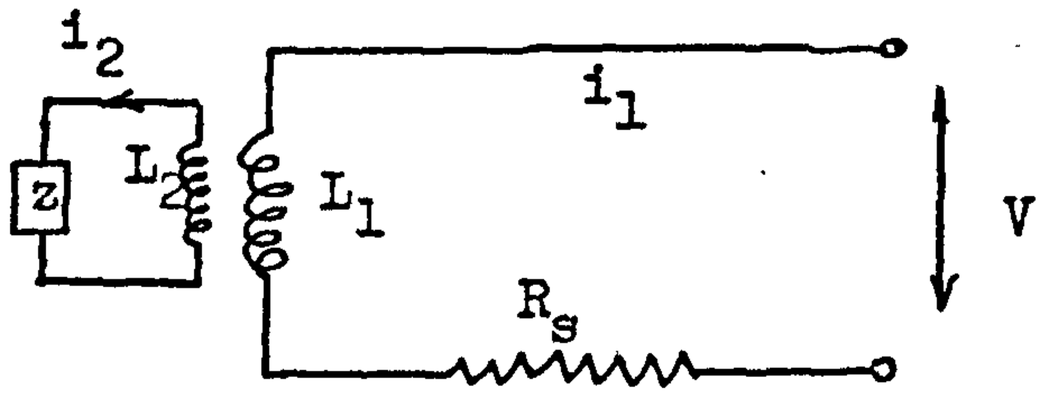

(c)

Primary Secondary

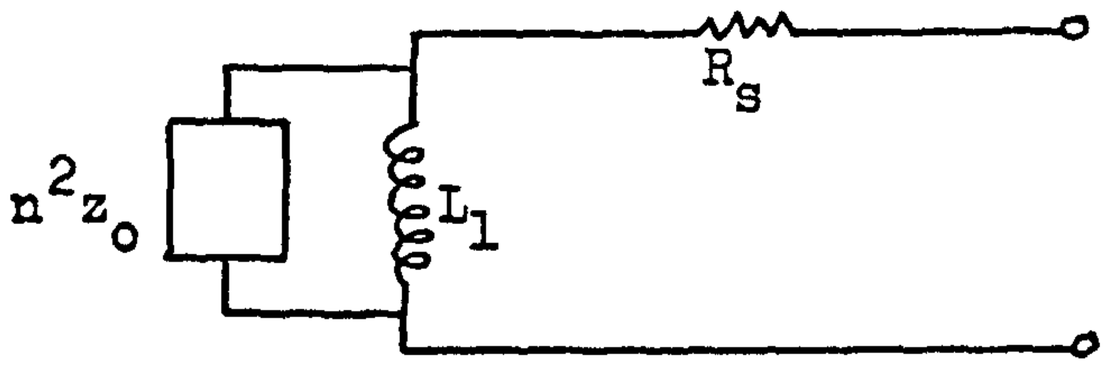

z_o =  The self capacity of one turn. (d)

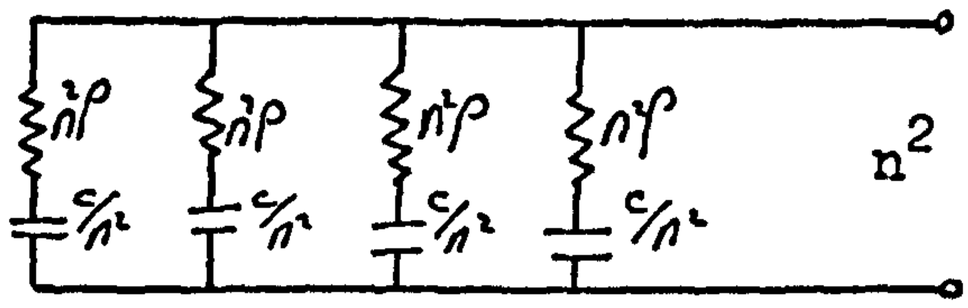

n^2 times =  (e)

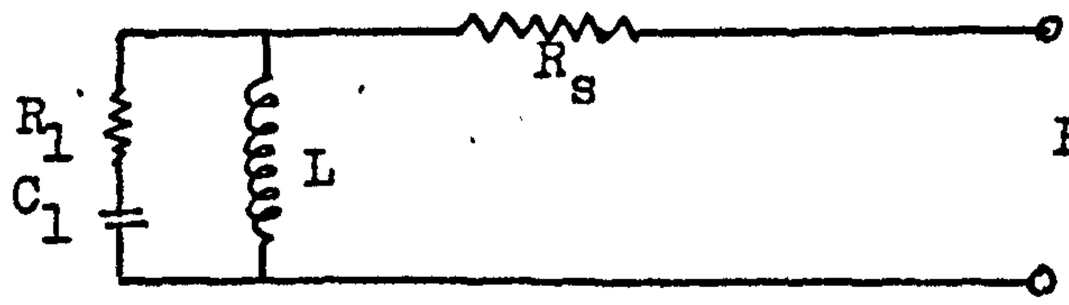

(f)

Final Circuit.

Fig.4.1

The measure Q increases with frequency up to 3 KHz but then falls slowly as self resonance is approached. The Q due to R_s only, simply increases with frequency. Thus it would seem that the series resistance determines the Q at low frequencies but other losses become important above 1 KHz.

4.2 An additional loss term

It appears that another lossy component which only becomes important at frequencies above 1 to 2 KHz is required to explain the antenna performance. It is likely that coil self capacitance would be lossy and would also be frequency dependent.

We here consider the coil as an 'auto transformer' which transforms elements of lossy capacitance due to a single turn and reflects them across the antenna output, See Fig 4.1.

Consider a voltage V driving a current i_1 through the coil. The current in the imaginary transformer primary is i2 flowing into some load Z. Then;

in the secondary, $V = j\omega L_1 i_1 - j\omega M i_2 + R_s i_1$

in the primary $\quad 0 = (J\omega L_2 + Z) i_2 - j\omega M i_1$

$$\text{Now} \qquad \frac{V}{i_1} = j\omega L_1 + \frac{\omega^2 M^2}{j\omega L_2 + Z} + R_s$$

and for tight coupling such that $M = L_1 L_2$ and $L_1 = n^2 L_2$

It can be shown that;

$$\frac{V}{i_1} = Z_{in} = \frac{j\omega L_1 (n^2 Z)}{J\omega L_1 + n^2 Z} + R_s \qquad 4.2.1$$

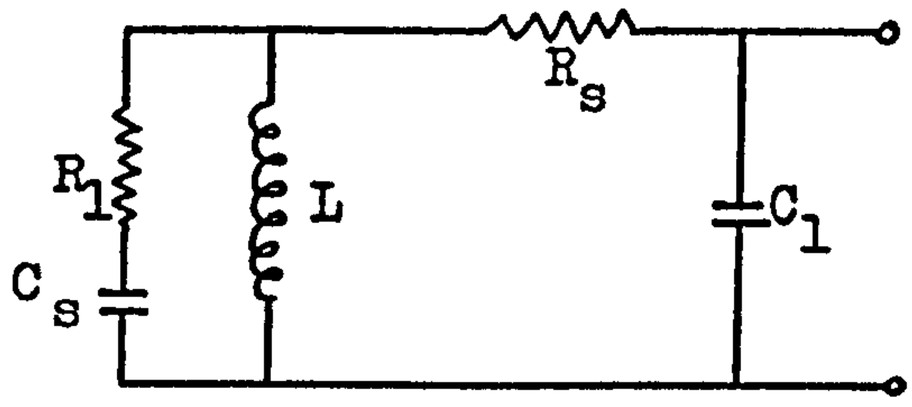

Fig 4.2a

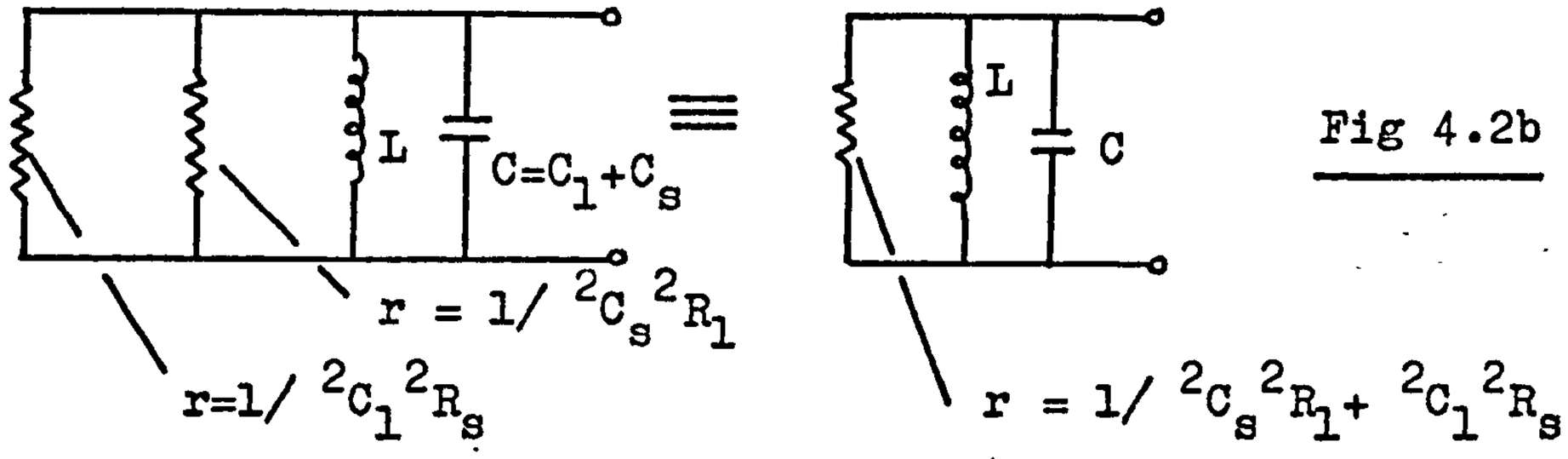

Fig 4.2b

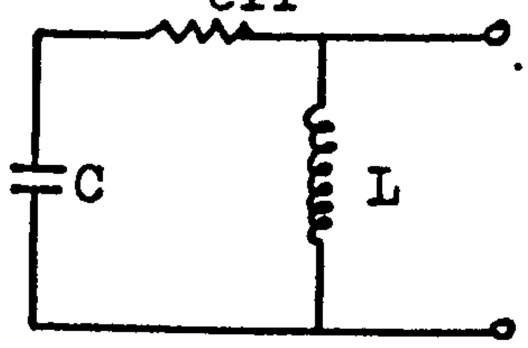

$$R_{eff} = \frac{C_s{}^2R_1 + C_1{}^2R_s}{(C_1 + C_s)^2}$$

Fig 4.2c

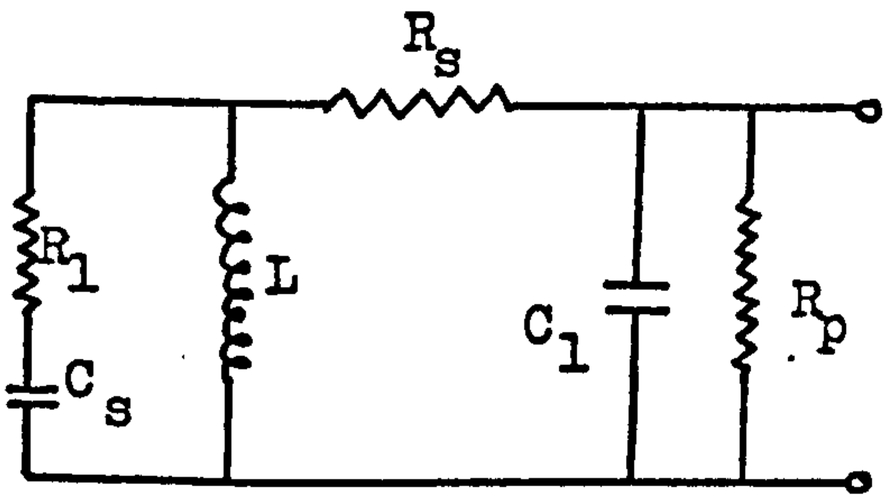

Fig 4.2d

Fig. 4.2

It is clear that Z_{in} is composed of the parallel combination of XL and n^2Z, these being in series with R_s as shown in Fig 4.1. Now each turn in the coil has a capacitance to some other turn and current will flow via this capacitance. As each turn also has a resistance, the current will flow through a combination of R and C, thus the lossy capacitance for one turn is as shown in Fig 4.1 and the total load is n^2 times this single turn impedance. This is shown as a 'ladder' in Fig 4.1. Therefore the equivalent circuit of the auto-transforming coil will be as shown at the bottom of Fig 4.1.

Including the additional capacitance of the LCR bridge, or in operating configuration the capacitance of the connection leads and preamplifier input the circuit is modified as shown in Fig 4.2a. It is then possible by manipulating the positions of equivalent capacitors and resistors to reduce the circuit to that shown in Fig 4.2b and thence to that given in Fig 4.2c where the effective series resistance is given by;

$$R_{eff} = \frac{C_s^2 R_1 + C_1^2 R_s}{(C_1 + C_s)} \qquad 4.1.5$$

As low frequencies well removed from resonance $C_1 >> C_s$ and therefore $R_{eff} \rightarrow R_s$ and the Q is determined by R_s as required. At high frequencies C_1 becomes smaller until at resonance $C_1 = 0$ and $R_{eff} \rightarrow R_1$ and the Q is now determined by R_1 which can quickly be evaluated by measuring the conductance at resonance. The value valculated for R_1 was 43.2 K ohm. Knowing this and the values for C_s, L, R_s and C_1 it is possible to calculate the effective series resistance and hence the Q for the circuit at various frequencies. A comparison of the calculated and measured Q factors can be seen in Table 4.3.

Table 4.3

Frequency	R_{eff}(calc.)	R_{eff}(meas.)	Q(meas.)	Q(calc.)
1 KHz	7.16 K ohm	8.38 K ohm	25.5	29.8
3 "	7.15 "	15.28 "	41.94	89.6
5 "	24.45 "	32.23 "	33.14	43.69
5.79	43.17 "	43.17 "	28.66	28.66

It can be seen that the agreement between the measured and calculated values of R_{eff} and Q is poor at around 3 KHz but good above and below this frequency. We must include the parallel loss term R_p which was present in the simple equivalent circuit as it represents the losses which are external to the coil (such as preamplifier input resistance) and also the core losses which are reflected across the output. The circuit becomes as shown in Fig 4.2d and the effective series loss term is given by;

$$R_{eff} = \frac{\omega^2 L^2}{R_p} + \frac{C_1^2 R_s + C_s^2 R_1}{(C_1 + C_s)^2} \qquad 4.2.2;$$

Or transposing to an effective parallel loss term as :

$$R_{eff(para)} = Q^2 . R_{eff(ser)}$$

we have the value which would be measured by the bridge,

$R_{eff(para)} = 1/G$ where G = circuit conductance,

and the equivalent circuit as shown in Fig 4.3.a.

Using this circuit the effective series resistance can be calculated at a number of frequencies and is shown in Table 4.4 together with the measured values.

Table 4.4

Frequency	$R_{eff(meas.)}$	$R_{eff(calc.)}$
1 KHz	8.38 K ohm	8.275 K ohm
2 "	11.23 "	10.46 "
3 "	15.28 "	14.63 "
4 "	22.28 "	21.43 "
5 "	32.23 "	31.77 "
5.79	43.17 "	43.17

It is clear that good agreement is obtained over the frequency range and that the circuit proposed represents the coil characteristics very well. Of course many refinements to the circuit could be introduced, for example it is obviously a simplification to allocate the whole of the series resistance to its present location as it is distributed throughout the coil and a better description could be obtained with the circuit shown in Fig 4.3b. However the description of coil characteristics obtained with the simpler circuit is sufficiently accurate and further work was not undertaken.

At low frequencies when $C_1 >> C_s$ the loss term R_1 can be ignored and the Q is determined by R_s and R_p. The conductance which is measured by an LCR bridge is then given by ;

$$G = \frac{1}{R_p} + \omega^2 C_1^2 R_s$$

Therefore R_p may be easily calculated and using the values for the

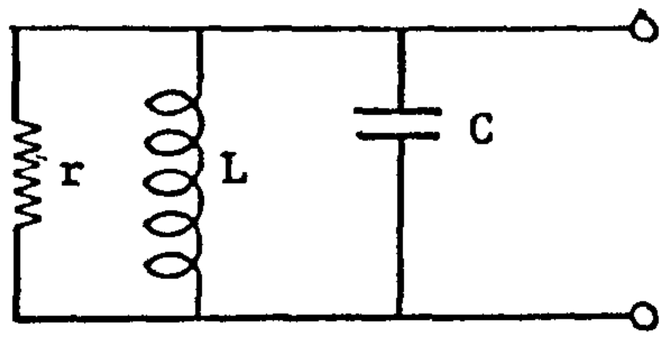

The measured conductance G = 1/r

r = the effective parallel resistance $R_{eff(para)}$

$R_{eff(para)} = Q^2 \times R_{eff(ser)}$

$R_{eff(ser)}$ is given in equation (4.2,2)

(a)

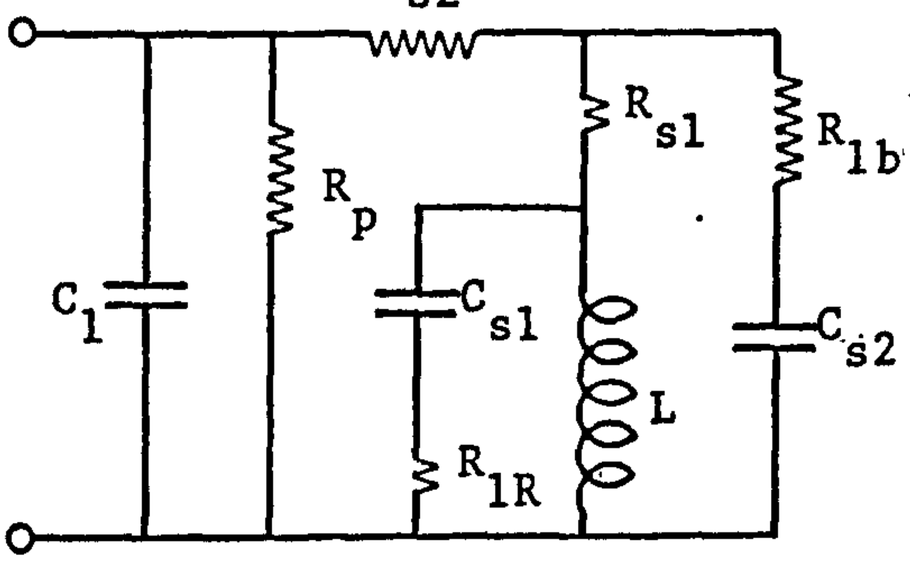

A possible further circuit which would be more representative of the coil characteristics

(b)

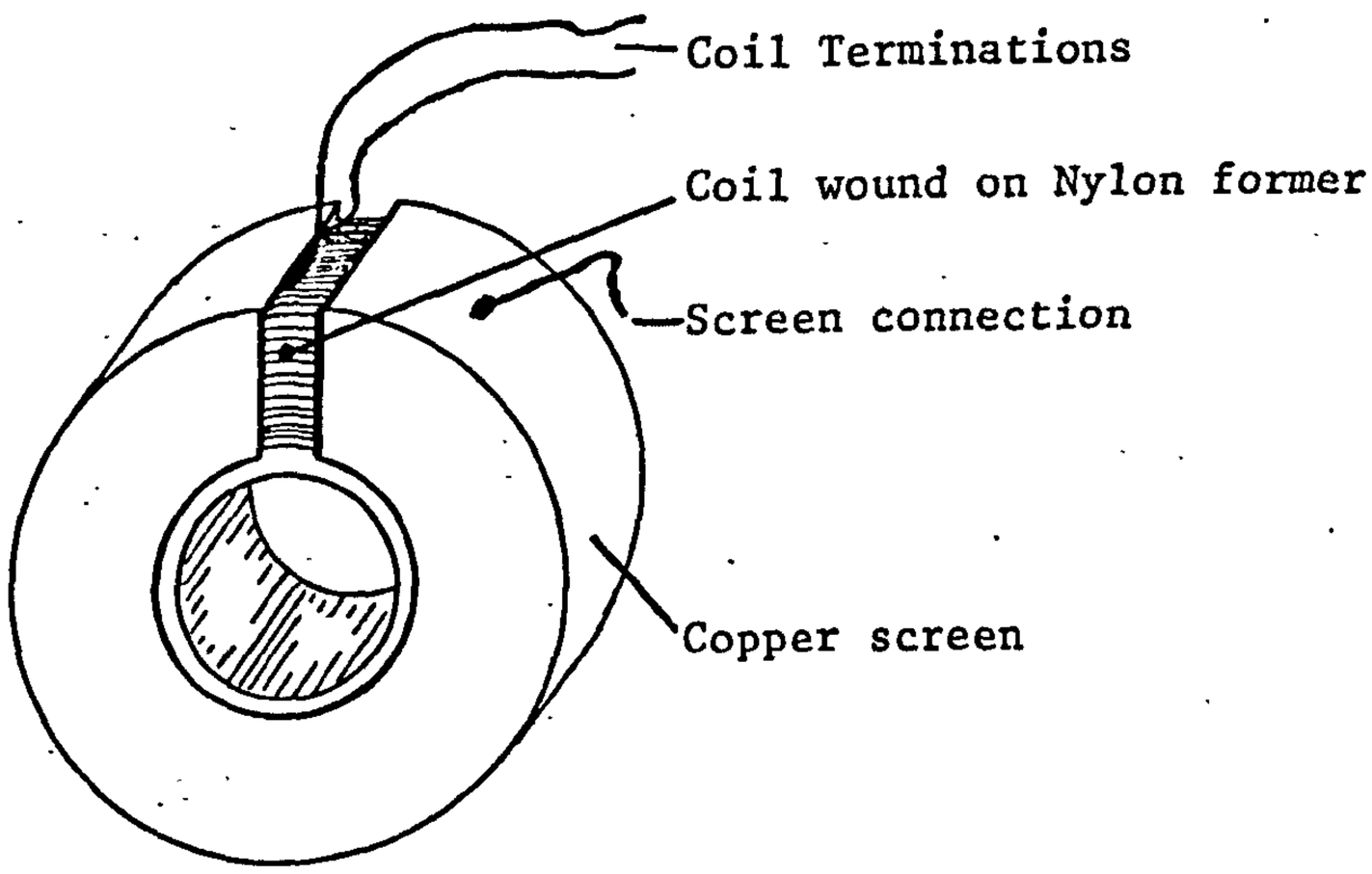

(c)

Fig. 4.3

circuit components and the equations describing the behaviour of the equivalent circuit it is possible to calculate the effective parallel loss term at a number of frequencies and thereafter to compare this with the measured value which is derived from the conductance measurement.

The coil must be covered with a thin sheet of copper which has a slit as shown in Fig 4.3c to eliminate the effects of radio frequency signals (> 100 KHz), which are always present, from entering the sensitive preamplifier and being demodulated resulting in unwanted signals in the VLF band. If the screen is connected to one or the other of the coil leads the lossy self capacitance changes and the equivalent circuit component values must be altered. The value of C_s varies from 22pf to 41pf to 65pf for no screen, screen to outer windings & screen to inner windings respectively. The proposed equivalent circuit can be shown to predict values $R_{eff(para)}$ which are close to the measured ones at a number of frequencies for each of the screen connections considered, see Fig 4.4. It is clear that the screen reduces the performance of the antenna but it is required to reduce RFI and must be tolerated.

4.3 The noise performance of the Equivalent circuit

The output of the noise generators associated with R_s, R_1 & R_p was calculated together with the signal transfer function for the equivalent circuit. See Appendix 1. The calculations were the basis of suit of computer programs which operated with complex functions resulting in a reduction in the amount of mathematics needed prior to programming. The program flow charts can be seen in Appendix 1.

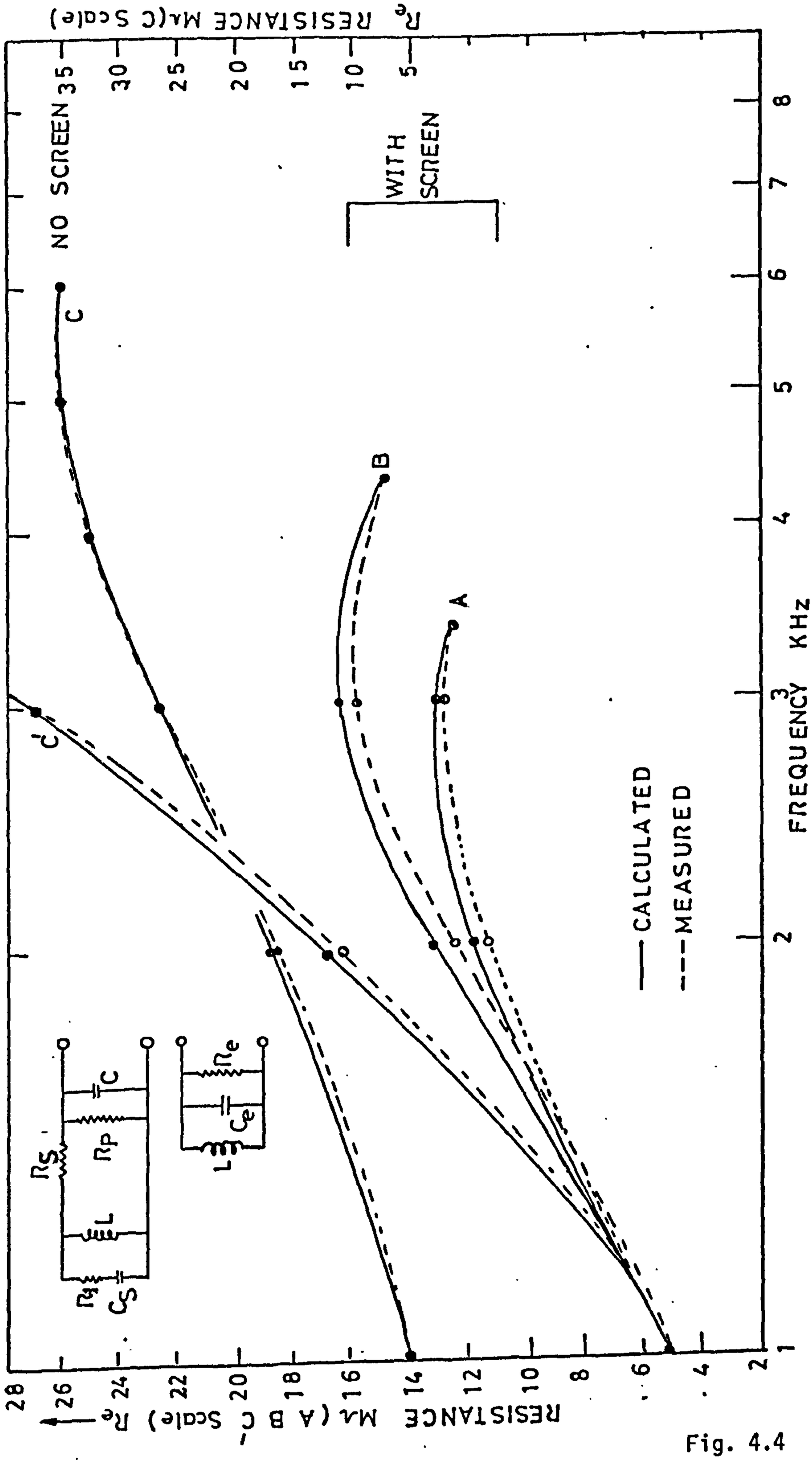
R_e RESISTANCE MA(C Scale)
35
30
25
20
15
10
5
NO SCREEN
WITH SCREEN
8
7
6
5
4
3
2
1
FREQUENCY KHz
C
B
A
C'
CALCULATED
MEASURED
R_S
R_P
C
L
R_e
C_e
L_e
R_e RESISTANCE MA (A B C' Scale)
28
26
24
22
20
18
16
14
12
10
8
6
4
2
1

Fig. 4.4

Taking the 'worst case' connection of the screen for which the self capacity is 65 pf the noise output of each source was calculated as a function of frequency between 1 & 20 KHz. The curves are given in Fig 4.5 together with the equivalent circuit and component values. If R_p = 2.48 M ohm (the value used in the first equivalent circuit and during the antenna performance tests) the noise performance is shown in Fig 4.6. The curve marked TN is the total noise output (R_p = 2.48 MΩ) and the dotted curve marked $NT_{(16.6)}$ is the noise output if R_p = 16.6 MΩ which represents the best possible performance of the 16,000 turn coil with the stated screen connection. A comparison of calculated noise output with R_p = 16.6 M and the measured output is given in Fig 4.7. The agreement is most satisfactory. It can be seen that the noise output of the antenna coil falls off more slowly with frequency at high frequencies with the new circuit than with the one which was first proposed. This slow fall off will reduce the minimum detectable signal at high frequencies and would therefore be closer to the observed antenna performance.

The minimum detectable signal is shown as a function of frequency, with R_p = 2.48 MΩ in the 'new' equivalent circuit in Fig 4.8. It is evident that this is much nearer to the measured performance than the curve derived from the simple circuit. The slight shift below the measured points could be due to a small over estimation of the relative permeability of the rod or of the mean area of the coil, but the forms of the measured and calculated minimum detectable signal curves are in close agreement. The performance indicated by the line (R_p=16.6MΩ) derived from circuit 2 is the best performance which could be expected from a 16,000 turn coil (with the worst screen connection) when mounted on a 152mm long rod. The received signal threshold for the antenna between 1 and 7 KHz is better than

Fig. 4.5

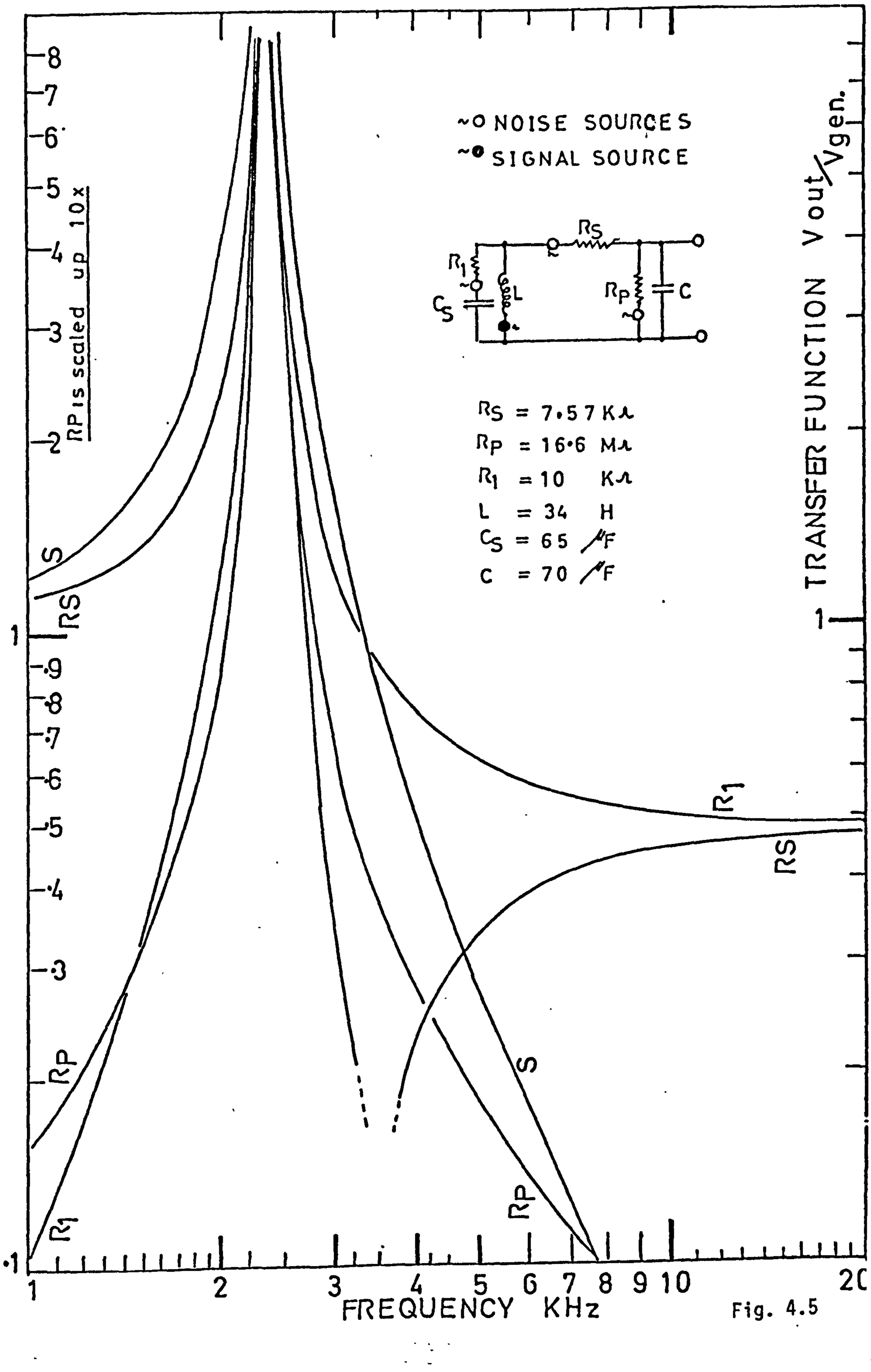
~O NOISE SOURCES
~● SIGNAL SOURCE
Rs
R1
L
Cs
Rp
C
Rs = 7.57 Kλ
Rp = 16.6 Mλ
R1 = 10 Kλ
L = 34 H
Cs = 65 μF
C = 70 μF
RP is scaled up 10x
S
RS
R1
RS
RP
S
RP
R1
TRANSFER FUNCTION Vout/Vgen.
FREQUENCY KHz
1
2
3
4
5
6
7
8
9
10
20

Fig. 4.5

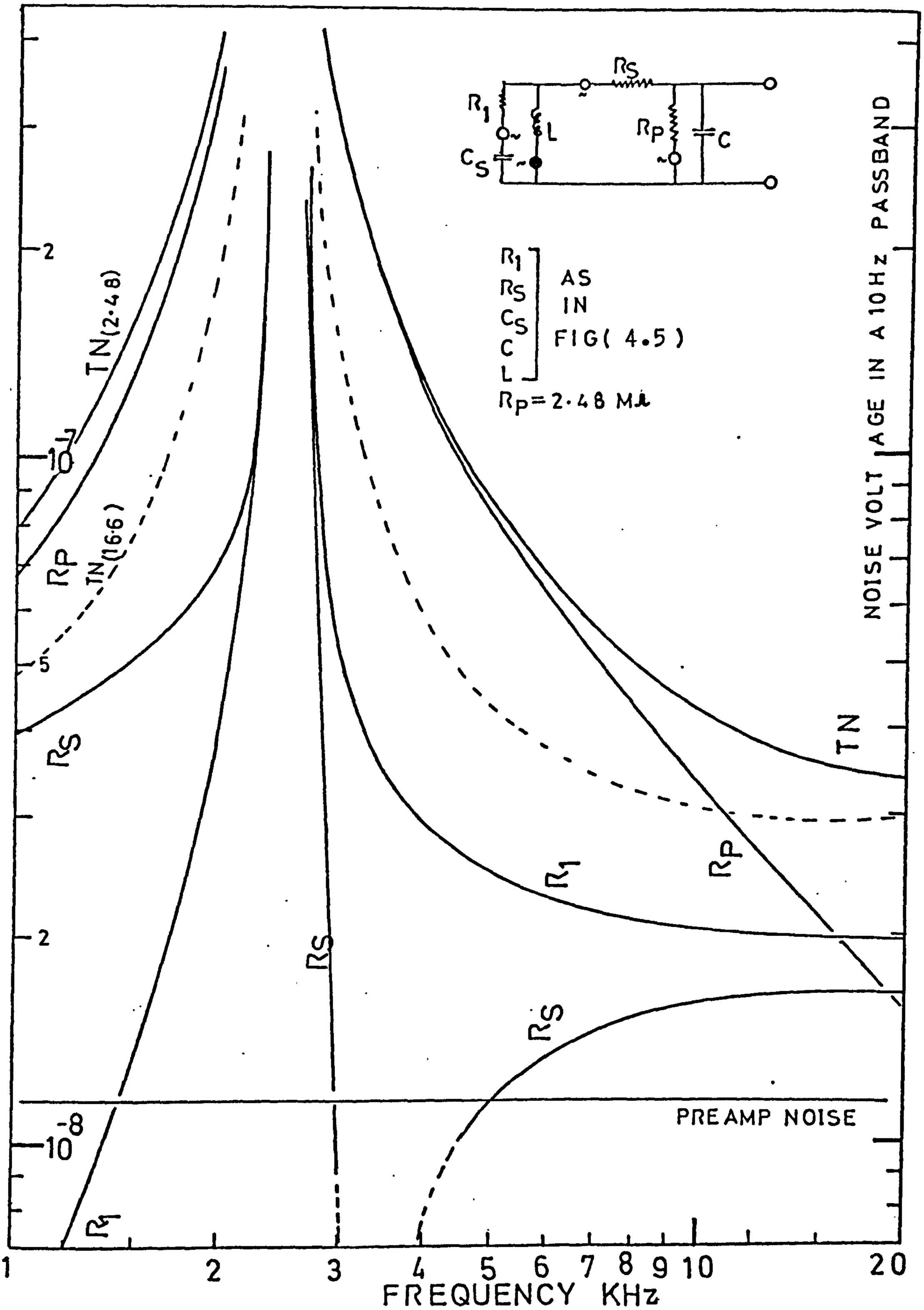
RS
R1
L
RP
C
CS
R1
RS
CS
C
L
AS
IN
FIG(4.5)
RP=2·48 MΩ
NOISE VOLTAGE IN A 10Hz PASSBAND
TN(2·48)
TN(16·6)
RP
RS
TN
R1
RP
RS
RS
RS
PREAMP NOISE
10^-8
1
2
3
4
5
6
7
8
9
10
20
FREQUENCY KHz

Fig.4.6

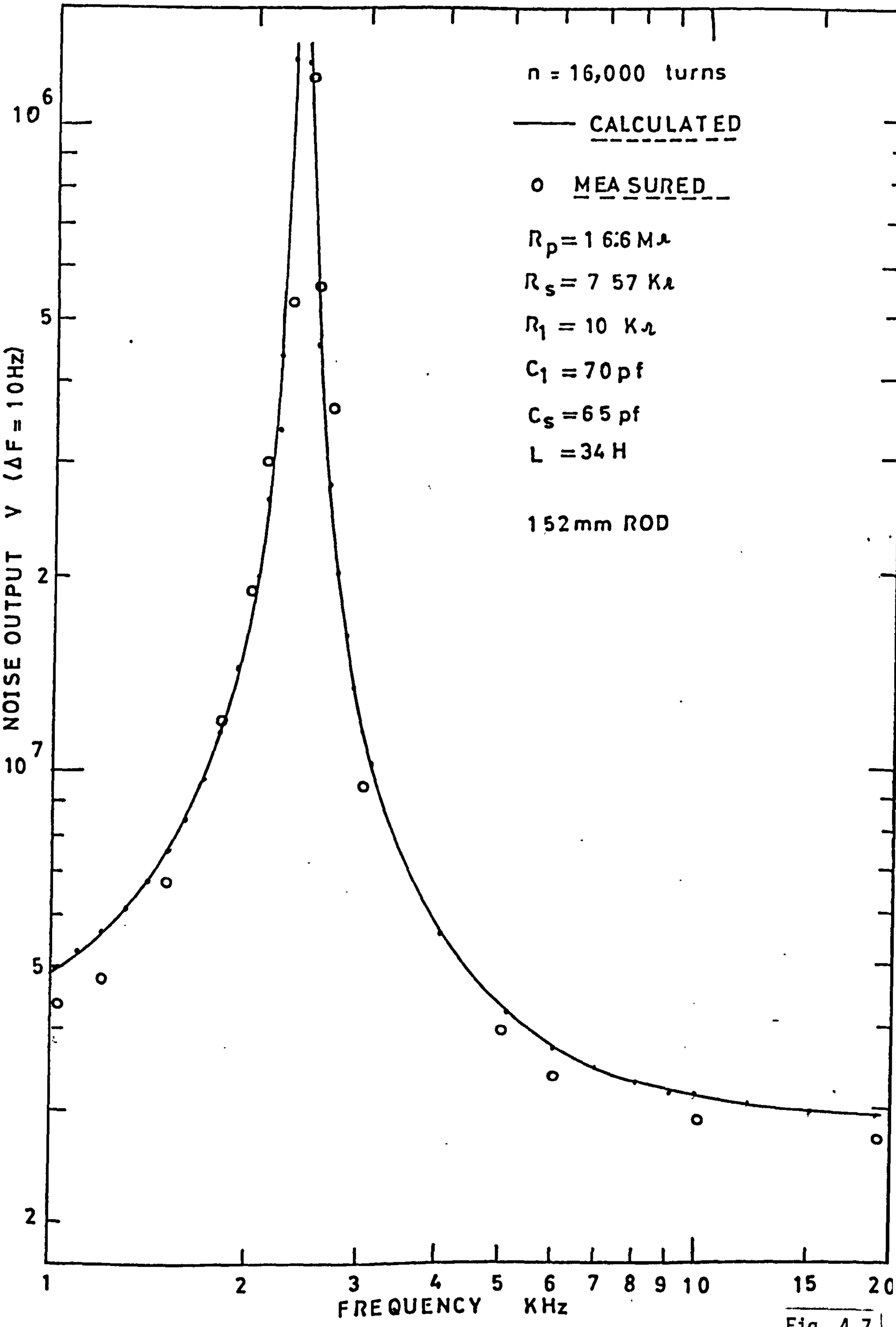
n = 16,000 turns
CALCULATED
MEASURED
R_p = 16.6 MΩ
R_s = 7.57 KΩ
R_1 = 10 KΩ
C_1 = 70 pf
C_s = 65 pf
L = 34 H
152mm ROD
NOISE OUTPUT V (ΔF = 10Hz)
10^6
5
2
10^7
5
2
1
2
3
4
5
6
7
8
9
10
15
20
FREQUENCY KHz

Fig. 4.7

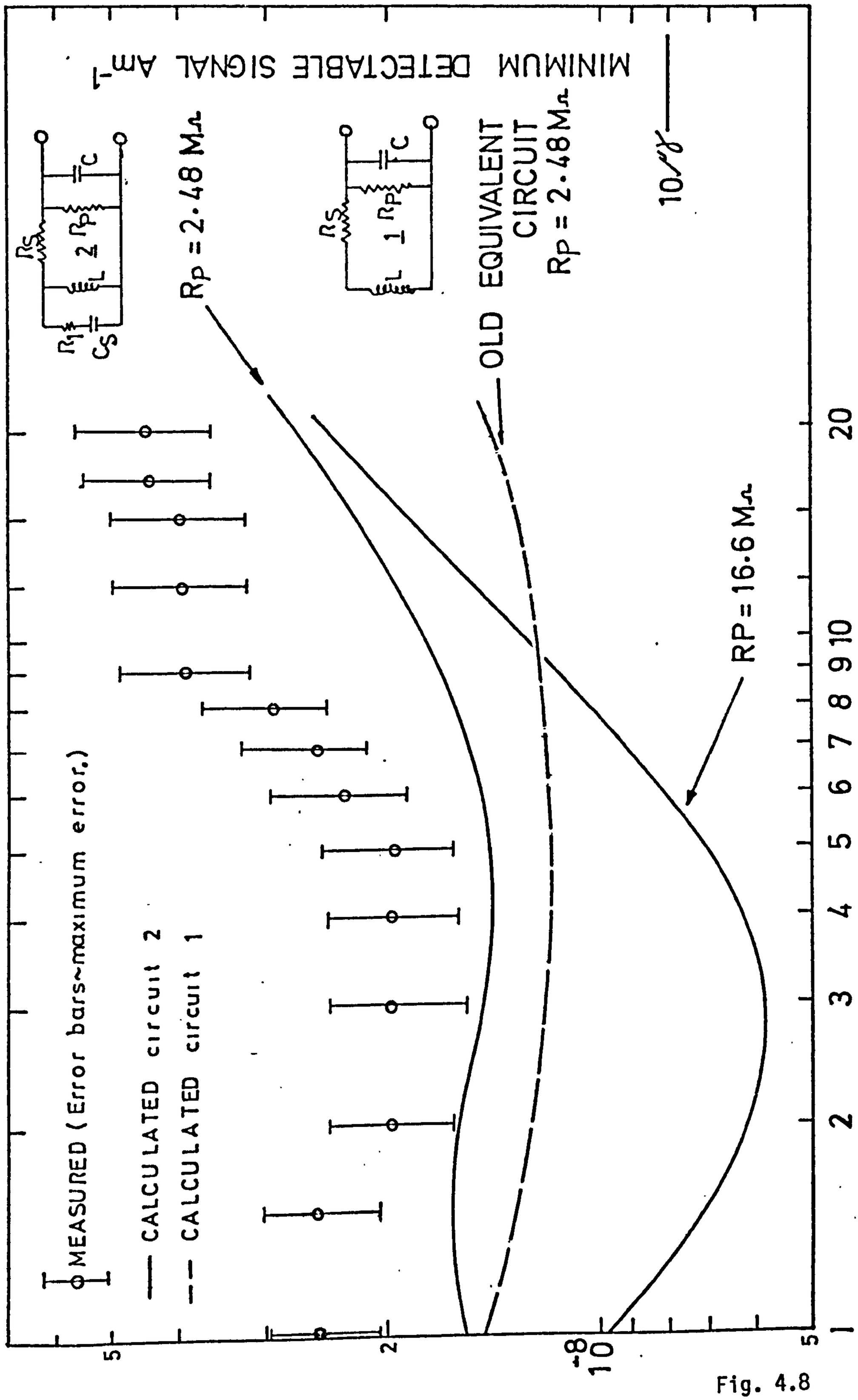
MINIMUM DETECTABLE SIGNAL Am-1
10⁻⁸
EQUIVALENT CIRCUIT
Rp = 2.48 MΩ
Rp = 2.48 MΩ
OLD
RP = 16.6 MΩ
20
9 10
FREQUENCY KHz
3 4 5 6 7 8
2
1
5
2
5
MEASURED (Error bars~maximum error.)
CALCULATED circuit 2
CALCULATED circuit 1
Rs
C
L
R1
CS

Fig. 4.8

$3 \times 10^{-11}\ \gamma^2$/Hz which is an improvement on that achieved with $0.2m^2$ area open loops as used on P47, P55 etc and is comparable with the sensitivity claimed by Shawhan & Gurnett (1968) of $5 \times 10^{-11}\gamma^2$/Hz obtained with $1m^2$ loops.

The performance achieved with a 152mm long rod falls short of the estimate used in the feasibility study of 10^{-12} to $10^{-13}\gamma^2$/Hz but in view of the assumptions made at that stage the achieved performance is considered very satisfactory and the antenna is certainly sensitive enough for use in rocket borne experiments.

CHAPTER 5

A SKYLARK VLF ROCKET EXPERIMENT USING CORED LOOP ANTENNAS

5.1 Experiment purpose and constitution

The skylark rocket SL1124 was prepared for launch along with a number of other Skylark and Petrel rockets which were fired during a High Latitude campaign held at Andøya (Norway) during November and December 1973. The general aim of the campaign was to investigate the nature of auroral substorms. The purpose of the 4 experiments on board SL1124 is given below;

1) Sheffield VLF Experiment

To investigate the intensity, spectral characteristics and polarisation of naturally occurring electromagnetic fields in the range 20 Hz to 11 KHz as a function of altitude during an auroral substorm.

2) Sussex Electric Field Experiment

To investigate the noise modes associated with energetic particles over the frequency range 250KHz to 4MHz by means of an ancillary electric dipole antenna with a swept frequency receiver.

3) Southampton Particle experiment.

To study particle acceleration processes in the negative phase of a polar substorm. The determination of pitch angle distribution of electrons and their energy spectrum.

4) The Birmingham Electron Density Experiment.

To determine the electron density and temperature for evaluation of the VLF refractive index and the identification of ionospheric structure.

ITEM	SECTION	CONTENTS	WEIGHT	LENGTH
			Kg	m.m.
Nose Cone Type 3. B16-01-1748 Modified for spin ejection. Bulkhead B16-01-1006	1	Nose Cone Sheffield Antennae,Pre-amps, batteries Southampton Electrostatic Analysers (4) Southampton Geiger Counters and Electronics Bulkhead	35.5 15 1 2 5.5	1990
Body Parallel 8" Type 5.Bulkhead B16-01-1006	2	Sheffield'465'Telemetry Tx,Antennae and calibration unit Body and Bulkhead	5 11.1	203
Body Parallel 8" Type 5.Bulkhead B16-01-1006	3	Birmingham Electronics Body and Bulkhead	1 11.1	203
Body Parallel 16" Type 3.Bulkhead B16-01-1006	4	Sussex Electronics (Rx) Boom Damping System Body and Bulkhead	2 6 15.3	406
Body Parallel 20" Type 2 Bulkhead B16-01-1006	5	(Batteries & Box (Telemetry Senders Instrumentation (2) (Slant Range System (Timers (2) and (Magnetometer. Body Bulkhead and Structure	6 10 2 1.6 20.5	508
Fwd. Ring Type 3 Sealing ring GW39165	6	Moon Sensor and Accelerometer Assy. Body and Sealing ring	4 6.4	178
Body Parallel 12" Type 4- Sealing Ring GW 35696	7	Body and Sealing Ring	8	305
Body Parallel 20" Type 2 - Sealing Ring GW 35696	8	Sussex Probes and Booms Birmingham Probes and Booms Probe Retaining System Body and Sealing Ring	6 6 5	508
Motor Attachment Ring	9	Raven Ignition Unit	8	184
		Manacle Rings (8) Ballast and Cabling	8 8	
		ESTIMATED TOTALS	223	4485

Fig 5.1

The VLF receiver was situated in the nose cone of the payload along with a separate receiver battery supply. Immediately beneath this was the Southampton particle experiment. It was situated in the nose cone in order that the six Geiger Counters and the four electrostatic analysers should have an unobstructed view of incoming particles. The Sheffield analysis electronics which included narrow band filters, phase comparators, compression amplifiers wide band calibration unit and a broad band telemetry sender was situated in the first 8" high bay below the nose cone.Below this was the electron density set and below that was the Sussex receiver and the boom damping system. The constitution of the total payload can be seen in Fig 5.1. It was expected that it would be lifted to an altitude of about 200 km and that the flight would last for some 12 minutes.

5.2 The Development of a Rocket Borne VLF Receiver

It was decided to use the small mu-metal cored antennas which were described previously. However before a prototype and flight model could be built several experiments had to be performed to determine the layout of the antennas and receiver electronics and its response along with the supporting structure to specified vibration levels which would be encountered during the flight.

Ideally the six components of the incident wave should be measured such that the wave normal angle, polarisation and the Poynting vector can be determined. However Shawhan (1969) ahows that from the measurement of the amplitudes and relative phases of the three magnetic components the wave normal angle and the sense of rotation of the wave can be found. The VLF experiment therefore had three orthogonal antennas with separate preamplifiers

and the necessary electronics in order that the amplitude and relative phases from these antennas at selected frequencies could be determined. It is convenient to discuss the production of the receiver which includes the three antennas, the three preamplifiers and the battery supply separately from the processing or analysis electronics.

Firstly it was considered essential that the receiver should have its own power supply which was in no way linked to the main batteries in the round. This reduces the risk of interference being conducted along power lines from the payload systems such as the magnetometer, moon sensors or telemetry electronics and also from other experiments some of which use TTL logic chips. These are known to draw high peak currents for short times (up to 10 mA for a micro-second) and are liable to cause interference. Using a separate supply also means that only one ground connection is required to the payload 'earth' which is then made by the outer of the coaxial cable which carries the output signals from the preamplifiers. This reduces the possibilities of current loops in the experiment which would radiate interference.

The region of space surrounding a cored antenna in which a uniform field becomes distorted is rather larger than the physical size of the antenna. It is therefore important to determine the minimum spacing necessary between the three antennas if they are to observe the incident wave without it being modified by an adjacent antenna. This can be done by plotting the polar diagram of one antenna repeatedly as it is approached by another.The VLF transmitter at Rugby(GBR) which operates at 16 KHz can be used to provide approximately plane waves at the antenna which are required in order to determine the antenna response pattern.

ALL DIMENSIONS IN MILLIMETRES

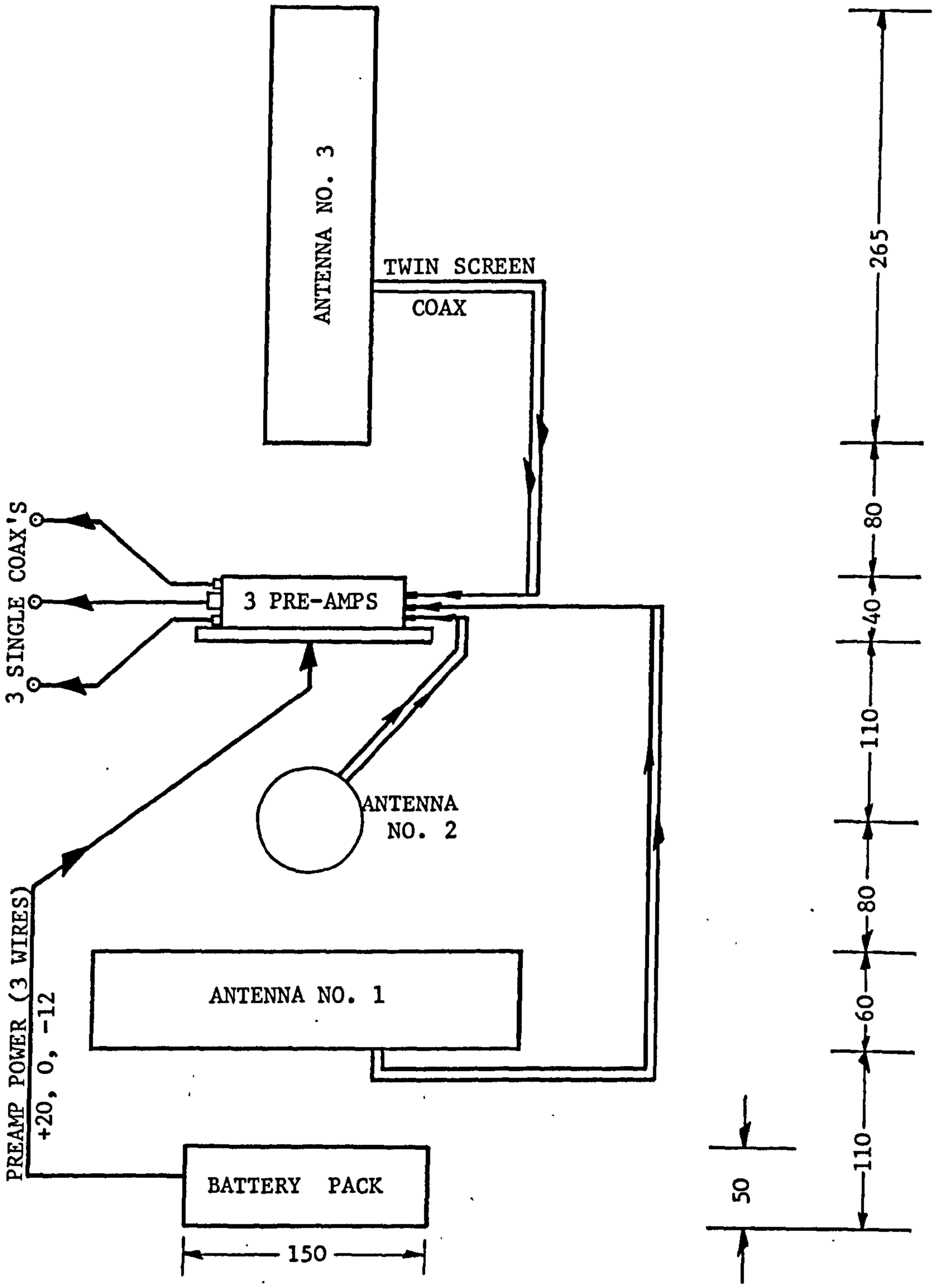

Fig. 5.2

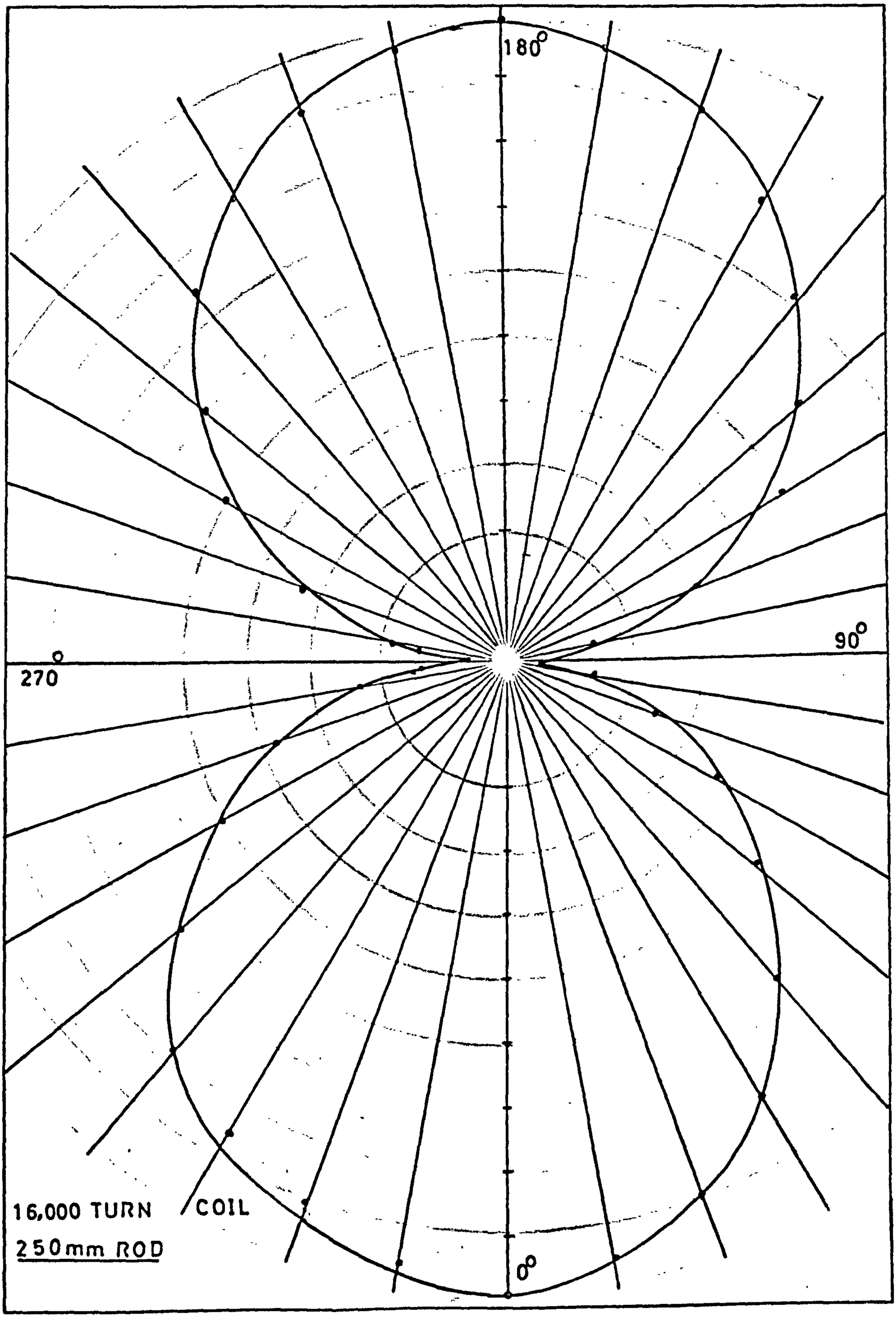

FIG 5.3

It was found that a separation of 10 cm between coil centres was sufficient to eliminate any interaction between antennas. The experiment was performed on a wooden test rig the outer dimensions of which were slightly less than the available space inside the nose cone of the rocket. Using this rig a receiver layout was arrived at which was convenient and workable in terms of separation restrictions and cable runs. This can be seen in Fig 5.2. A typical antenna polar diagram which is that if a dipole, can be seen in Fig 5.3.

It was necessary to design a support structure for the receiver which enabled the Geiger counters and electrostatic analysers to have an unobstructed forward view whilst ensuring that it was stable enough to withstand vibration tests and flight conditions. A further design limit was imposed by having to construct the structure from a non-metallic material in order that eddy current effects should not disturb the incident EM waves. A cruciform construction was envisaged which was manufactured from PVC sheet, the whole assembly being mounted on a stainless steel 'top hat' which would house the Southampton particle experiment. The author undertook the production of some ten engineering drawings which were required for the fabrication of the whole of the support structure. An example of such a drawing is given in Fig 5.4 and photographs of the flight model can be seen in Figures 5.5, 5.6, 5.7, 5.8 and 5.9.

5.3 Flight model Antennas and Receiver Electronics

Prior to the production of the flight model preamplifiers and battery pack there was a prototype system on which various

Fig. 5.4

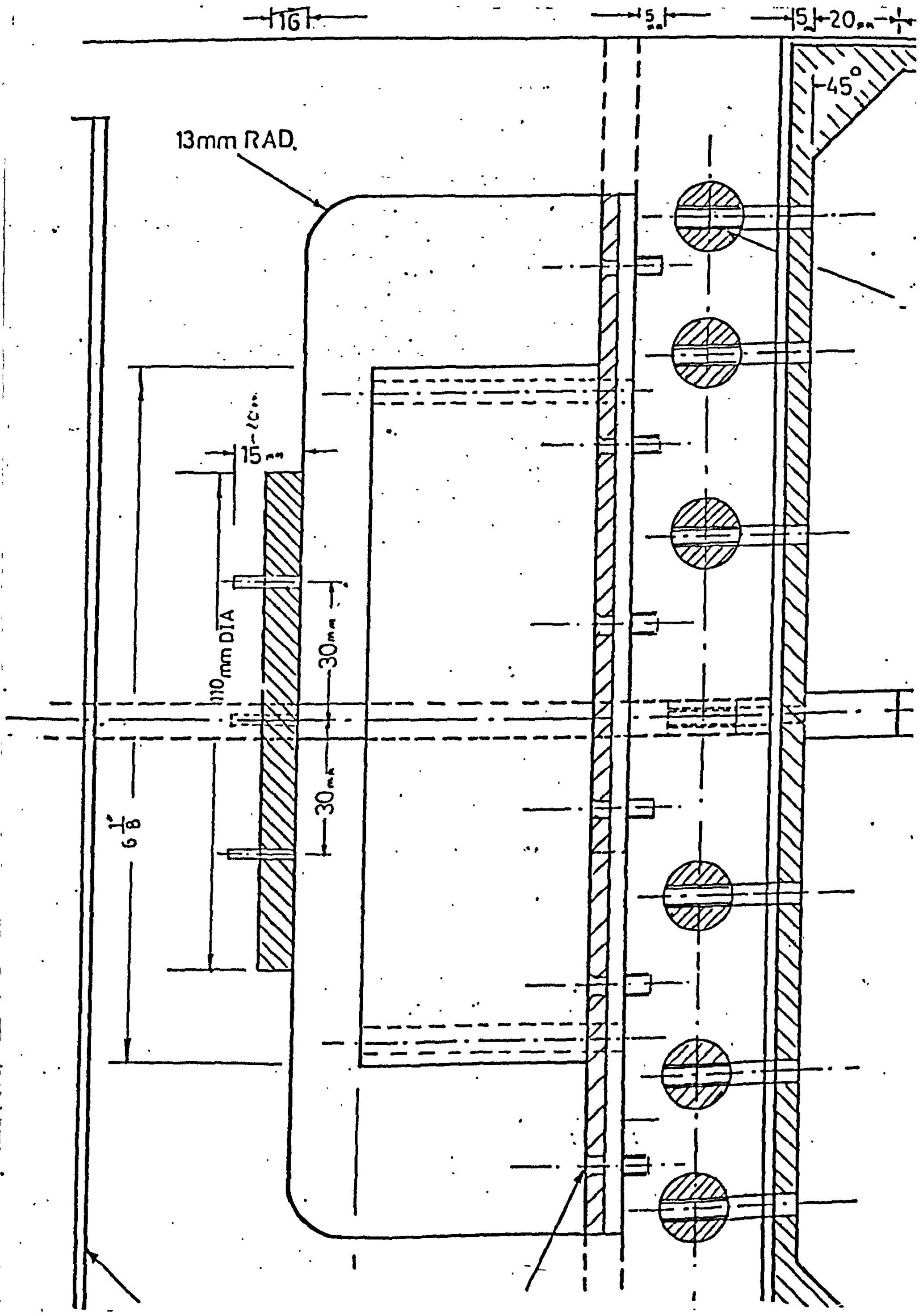

Fig. 5.4

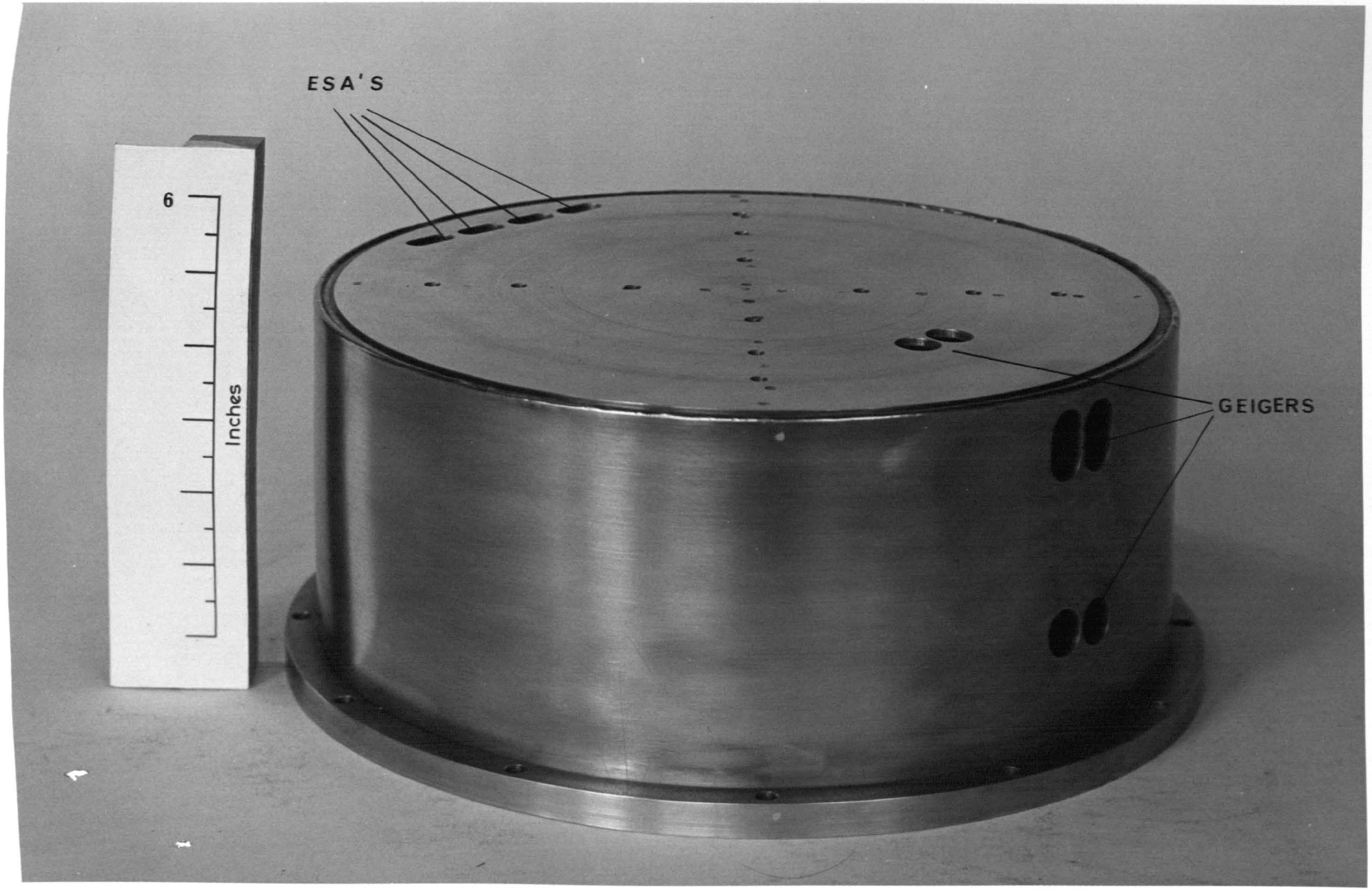

FIG. 5.5

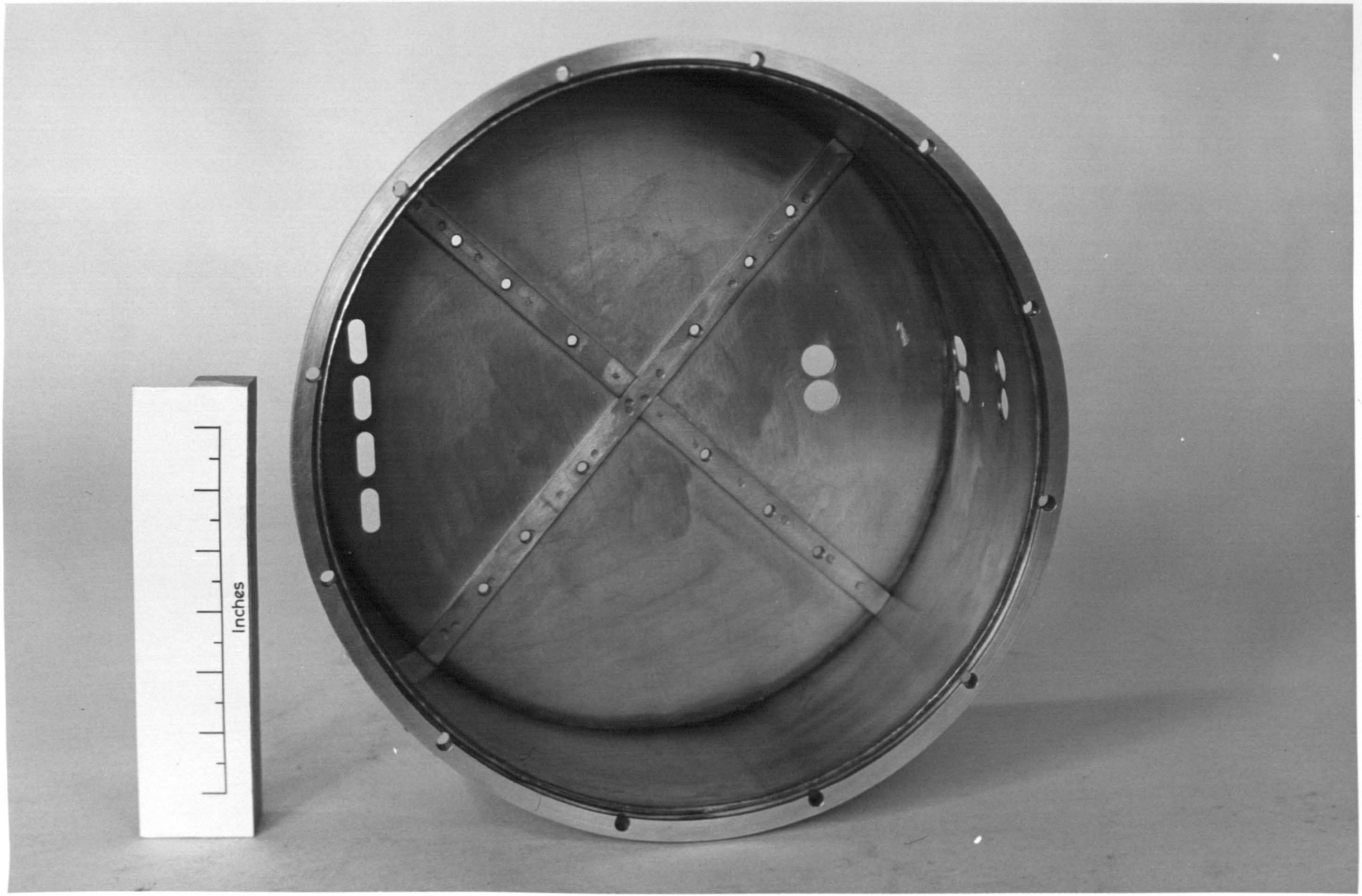

FIG. 5.6

experiments concerning channel crosstalk, conducted interference, physical layout and fabrication,and antenna susceptibility to RFI were performed.

Three preamplifiers were built on fibre-glass PCB's with flight standard components and fitted into a milled aluminium box. The shape of the box was that used on Petrel rockets such that the pre-amplifier unit could be used for both Petrel and Skylark rounds. The incoming battery power lines were passed through small RF filters to reduce conducted interference. The signal from the antenna was conveyed to the preamplifier by two small diameter screened leads with Micro Conhex connectors. The whole preamplifier package was designed to withstand accelerations of 60 g which it would encounter in a Petrel launch by incorporating NASA spec. component separation, stress bends in component leads, platform mounting of PCB's and the use of a milled as opposed to a fabricated aluminium box. A photograph of the prototype unit can be seen in Fig. 5.10 along with a 16,000 turn screened coil mounted on a 250 mm long laminated mu-metal rod. The cross talk between preamplifiers was measured at a number of spot frequencies and found to be at an acceptable level of better than 60 db. The gain of each preamplifier was measured and found to be within 1db over the frequency range 20 Hz to 20 KHz. The measured gain was equal to the design value of 60 db and the amplifier dynamic range was better than 70 db.

A floating rechargeable battery pack was constructed using SAFT NiCad cells of a capacity such that the receiver could be operated for about 24 hours continuously. This large reserve is necessary when the experiment is being tested or being used to monitor signals during the holding phase prior to launch. A photograph of the battery pack,preamplifier unit along with one clad and one unclad antenna can be seen in Fig.5.11.

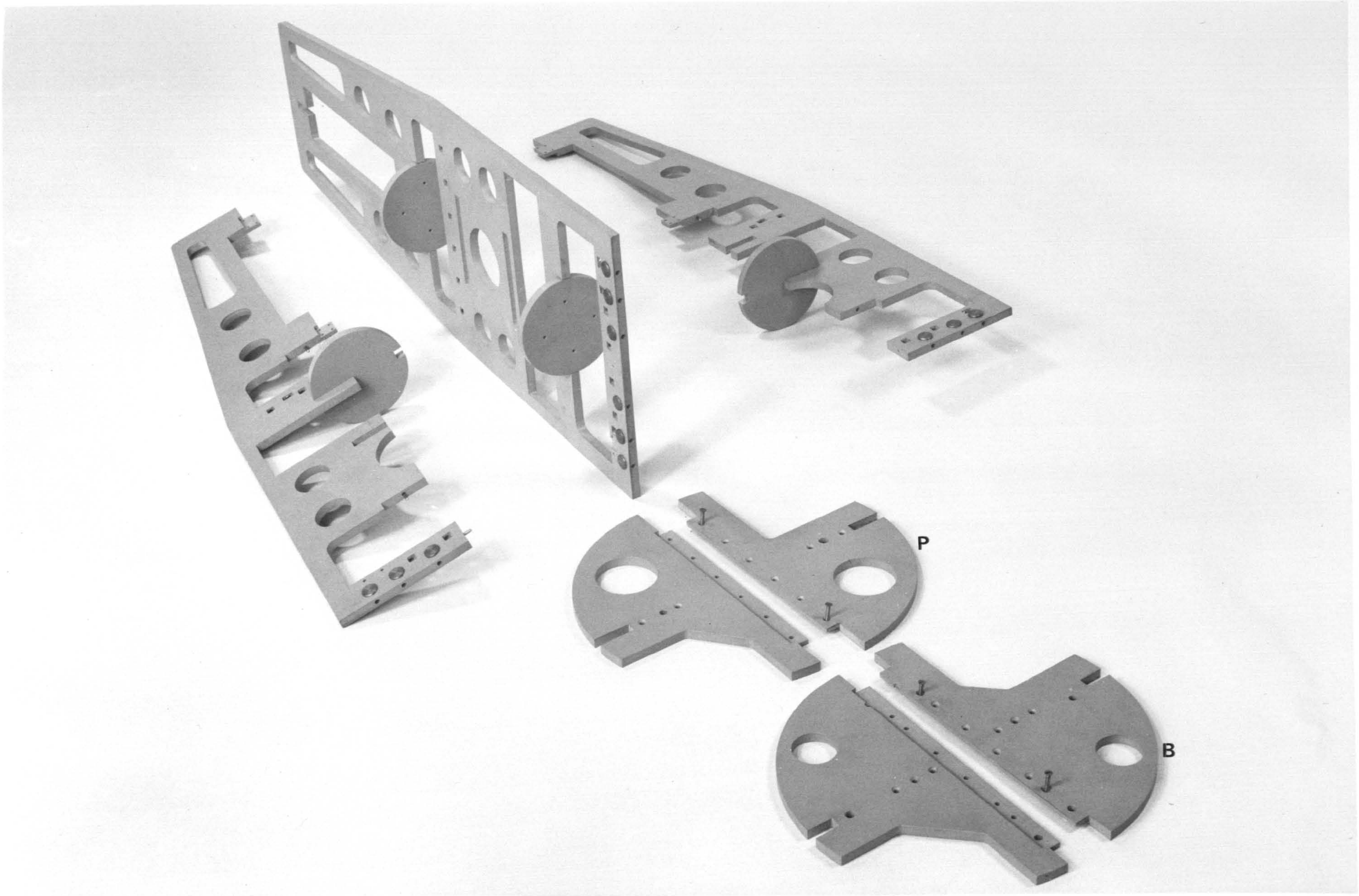

FIG. 5.7

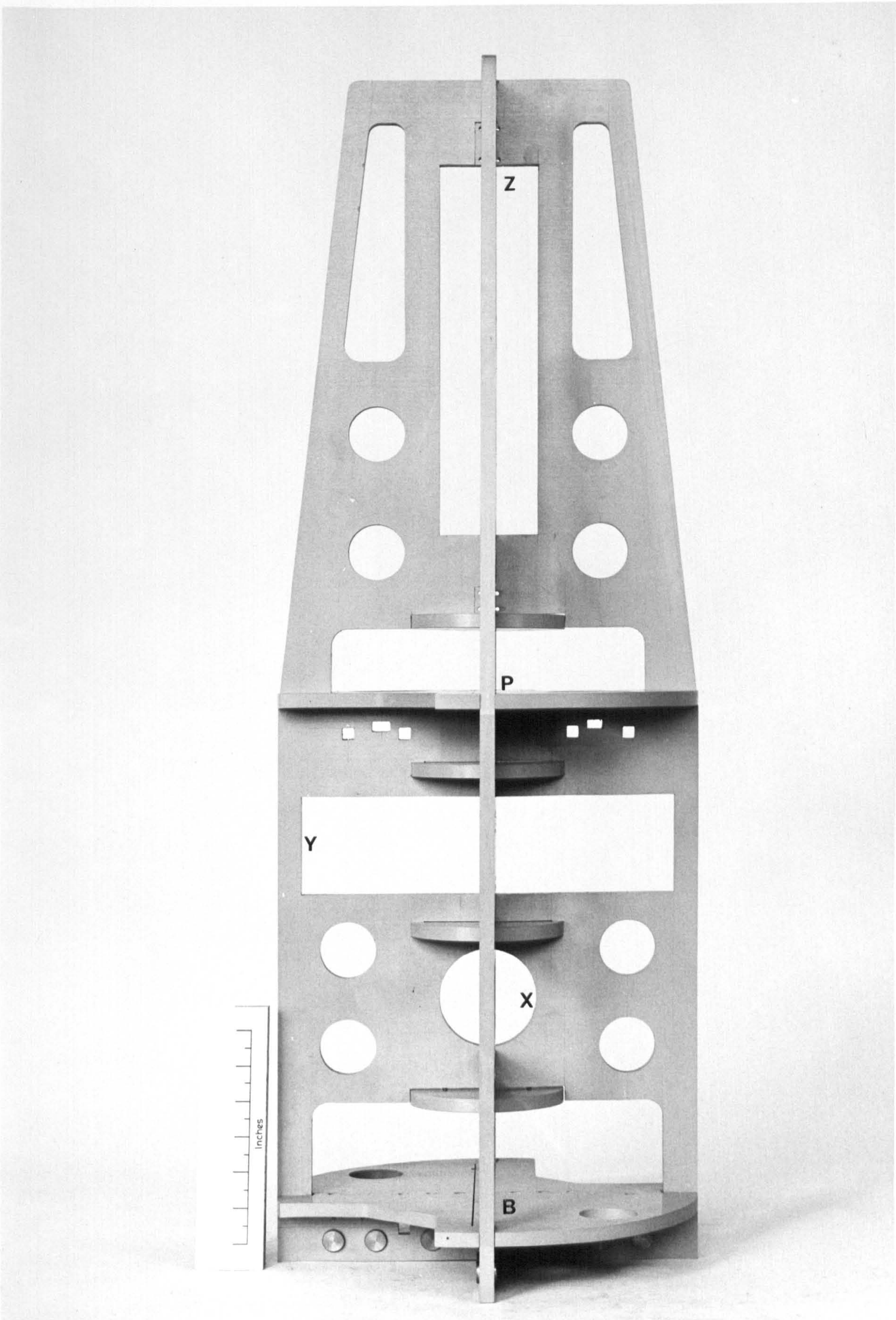

FIG. 5.8

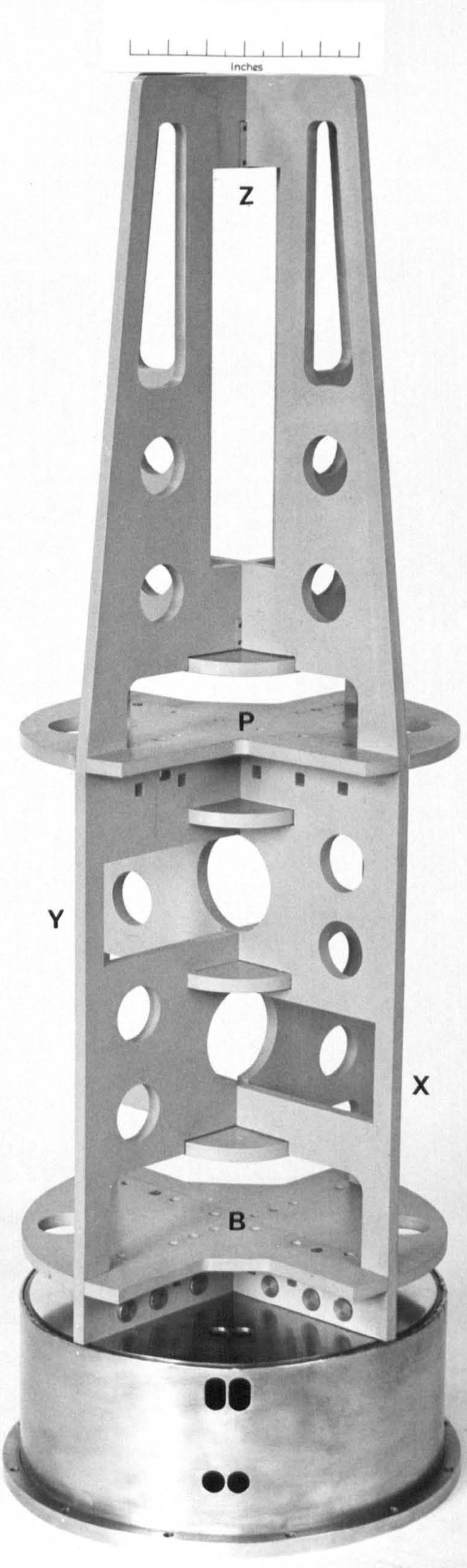

FIG. 5.9

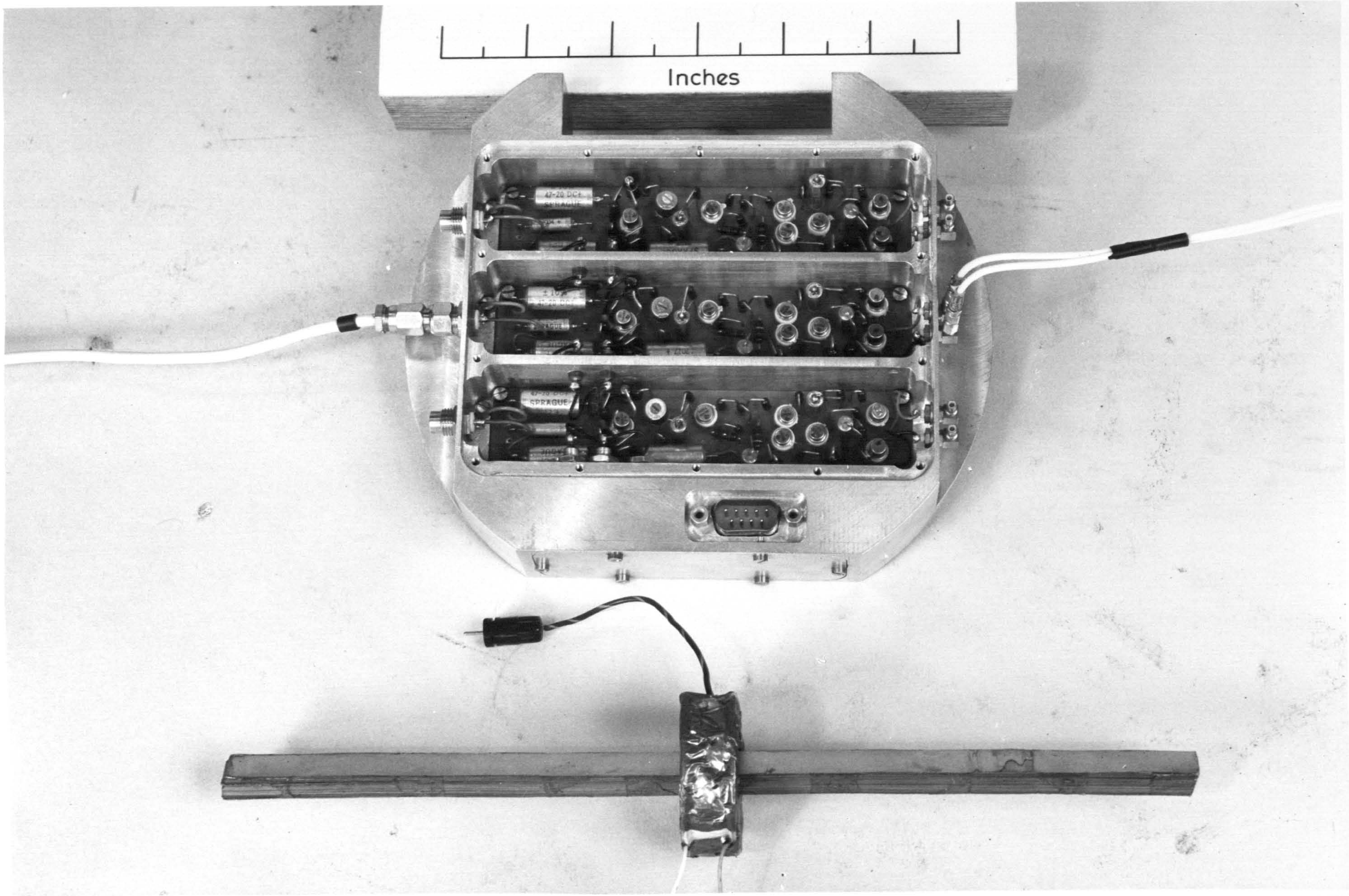

FIG.5.10

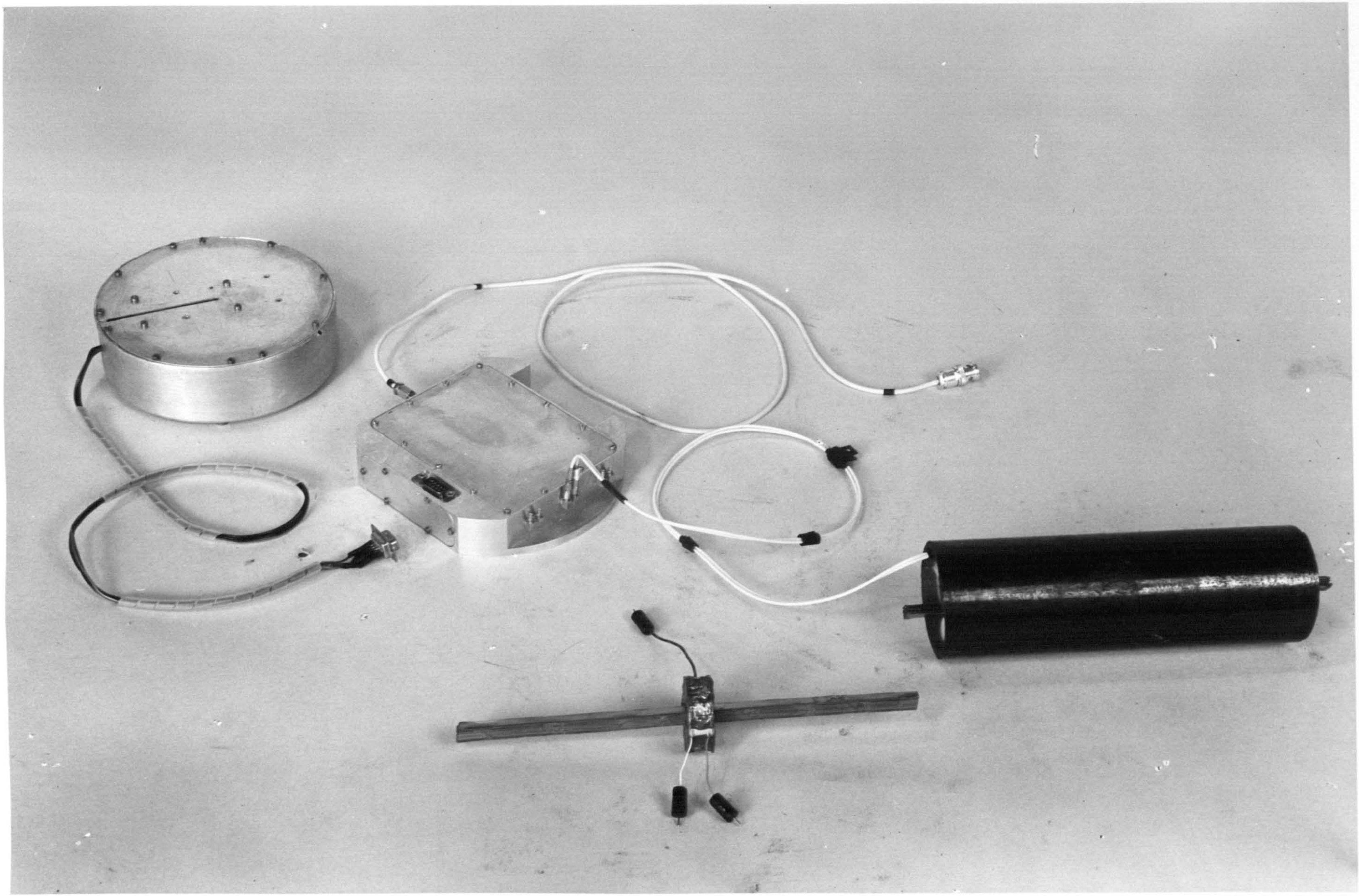

FIG. 5. 11

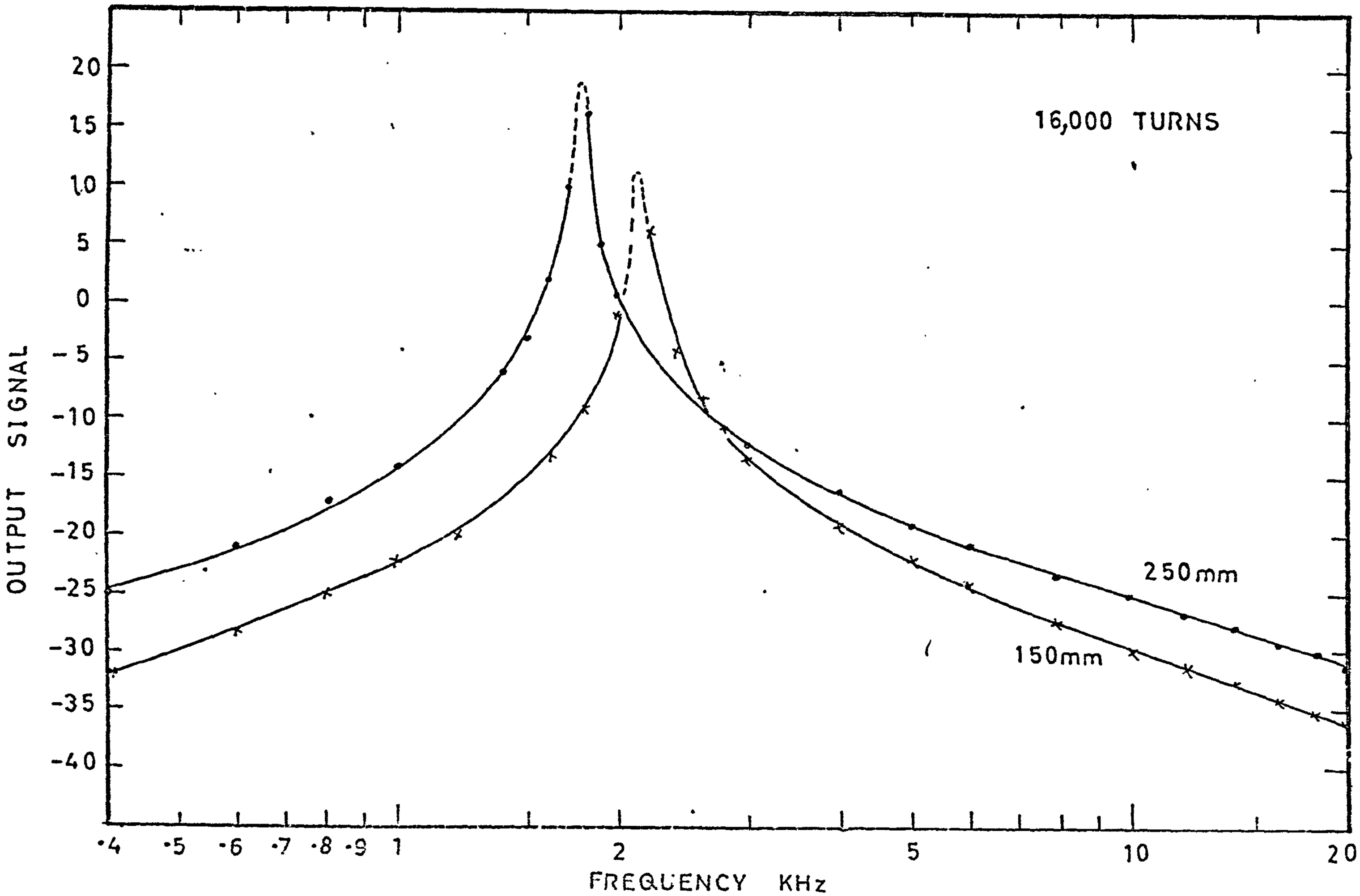
16,000 TURNS
250mm
150mm
OUTPUT SIGNAL
20
15
10
5
0
-5
-10
-15
-20
-25
-30
-35
-40
·4
·5
·6
·7
·8
·9
1
2
5
10
20
FREQUENCY KHz

FIG 5.12

The use of a Skylark sounding rocket which is approximately 18" dia enables the length of the antenna rods to be rather larger than those used previously which were designed for the 7" dia Petrel round. The diameter of the available nosecone space at the height of the Y axis antenna is 300mm and allowing some space for the supporting structure, a rod of 250mm length can conveniently be accommodated. If the same rod cross section is kept then it is clear from Fig 3.2 that the relative permeability of the rod should increase and assuming that the larger rod generates no more noise than the 152mm one, then there should be some improvement in the receiver signal threshold. The effect of a 250mm long rod can be seen in Fig 5.12 and at low frequencies which are well below resonance there is an effective gain of 7db. From Fig 3.2 with m now equal to 31 we see that the demagnetising factor D = 0.0028 which results in μ_{rel} = 370 which is twice that obtained with the smaller rod. The term μ_{rel} appears in equation 3.6.2 and a doubling of its value would yield a 6 db increase in the output level derived from a given field. This is almost exactly what is observed. The expected minimum detectable signal therefore is $10^{-11}\gamma^2/Hz$ between 1KHz and 7 KHz.

With precautions having been taken to reduce the susceptibility of the receiver to interference from the payload electronics it is reasonable to try to reduce the interference which would be generated by acoustic noise in the structure which supports the antennas.Any vibration of the rods in the geomagnetic field will generate spurious signals which will degrade the receiver performance. The rods are supported at each in a cushioning silicon rubber plug which is attached to the Tufnel tube which acts as a cover for the antenna and enables it to be located firmly in the support structure. A light density foam

is injected into the tube and fills the space between it and the aerial. This reduces the mechanical resonance of the rod in the tube and ensures that the coil is located firmly on the rod. These antennas were vibrated at a level of 60 g at frequencies between 1Hz and 5 KHz (Sinewave) and the performance was measured before and after this test showing that no damage or deterioration in performance had taken place.

The only amendments made to the prototype system in constructing the flight equipment were;

1) The output of each preamplifier was buffered with a low output impedance operational amplifier which also provided a gain of 15x.

2) The battery unit was fitted with a latching relay which could be pulsed via the umbilical cable from the control console to effect remote on/off switching of the receiver.

3) The battery unit was fitted inside a milled aluminium box.

Unfortunately there are no photographs of the flight equipment but the location of the preamplifiers and the battery unit for the prototype model can be seen in Fig 5.13.

The analysis electronics which was all located in the bay below the nose cone provided the round telemetry with the following outputs;

1) Narrow band signal levels (B = 200Hz) centred on 750Hz,1.25 KHz and 9.6 KHz for the three antennas. The two lower frequencies cover the range where polar chorus is observed and the 9.6 KHz channel is used to observe hiss.

2) The relative phases of the narrow band signals from each antenna.

3) A calibrated wide band (20Hz - 20KHz) signal output from the X axis antenna. This signal was relayed to the ground receivers by a separate telemetry transmitter which was also housed in the electronics bay.

The design and manufacture of the analysis electronics is due

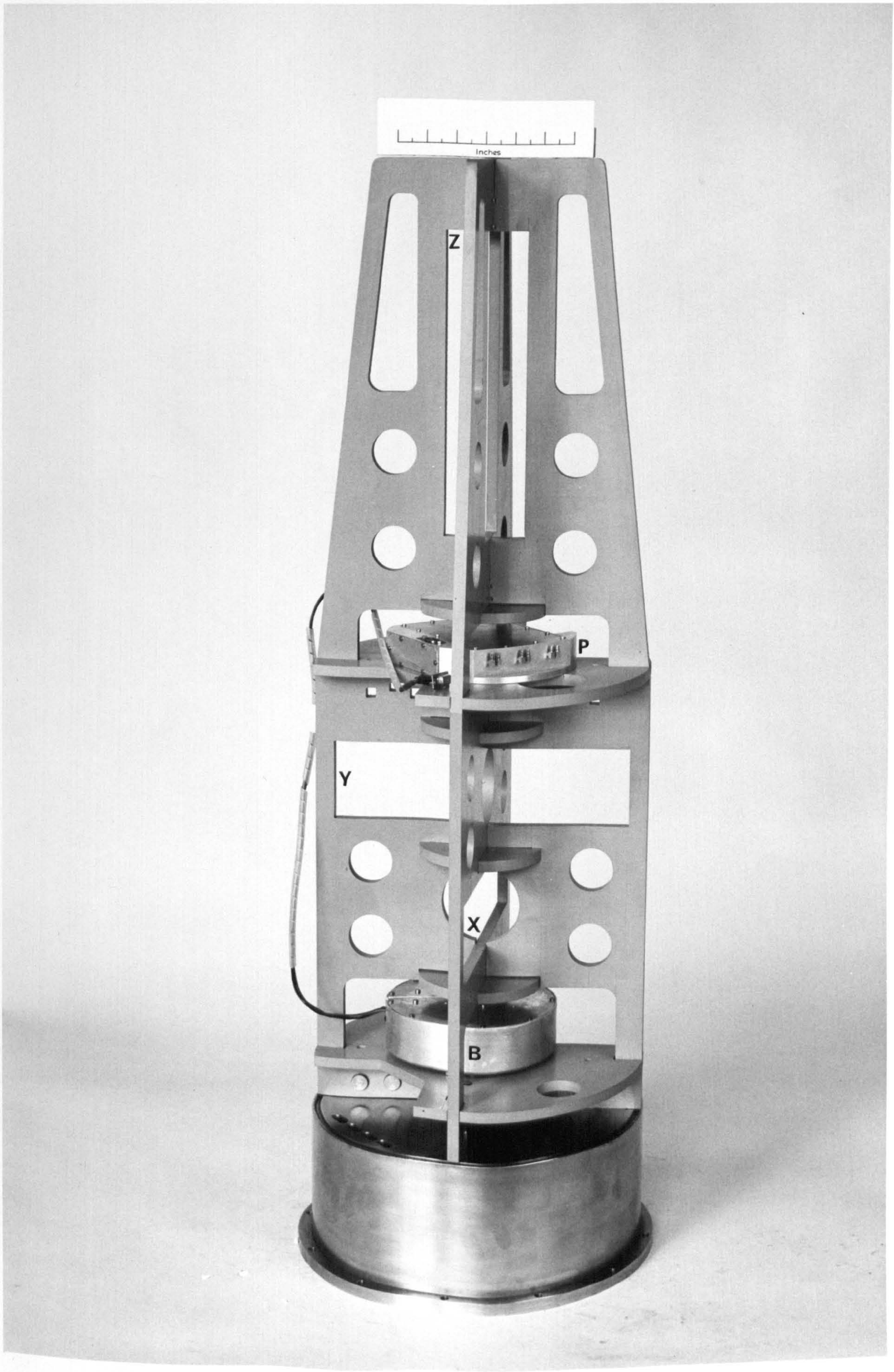

FIG. 5.13

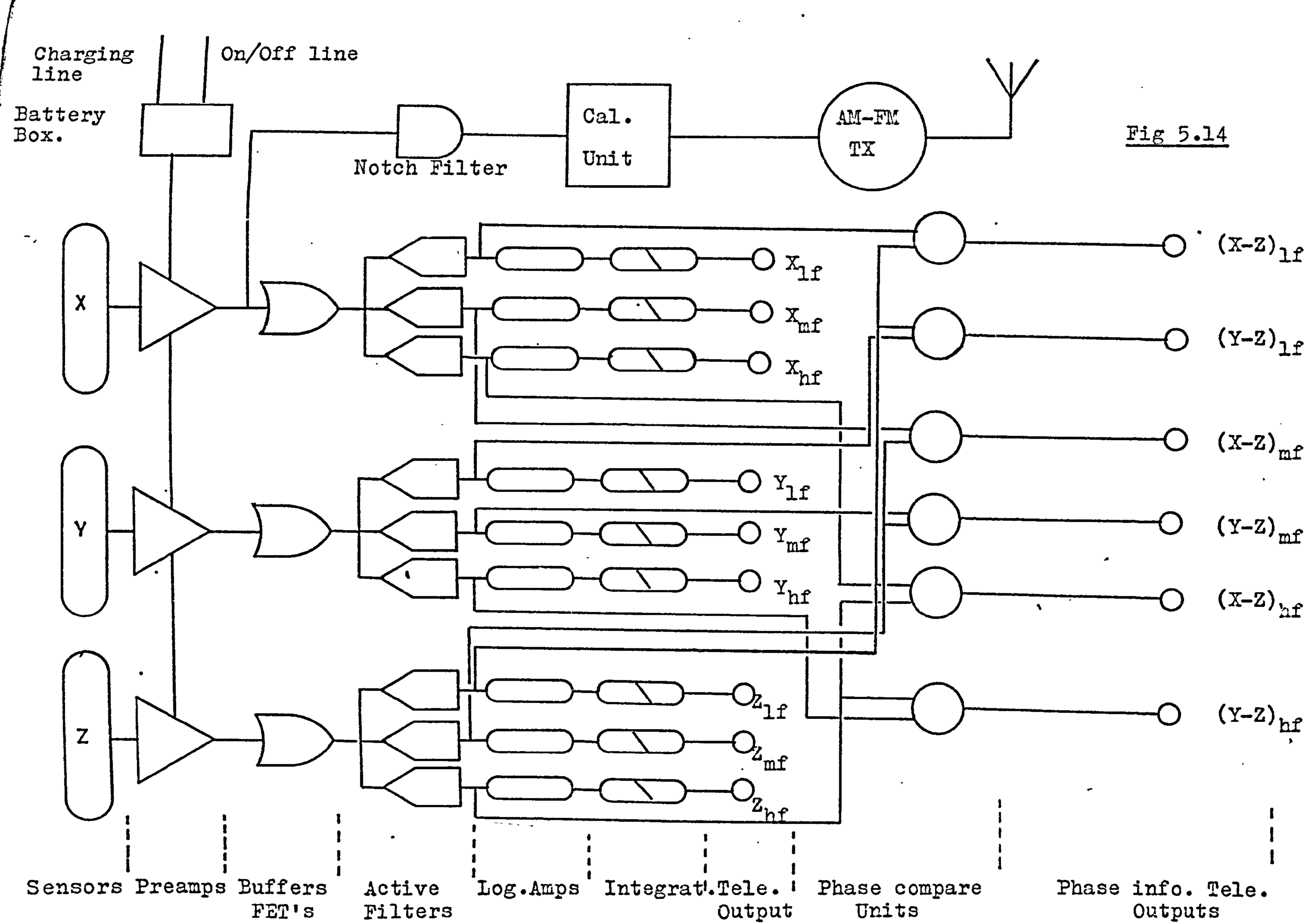
Charging line
On/Off line
Battery Box.
Notch Filter
Cal. Unit
AM-FM TX
X
Y
Z
X_{lf}
X_{mf}
X_{hf}
Y_{lf}
Y_{mf}
Y_{hf}
Z_{lf}
Z_{mf}
Z_{hf}
$(X-Z)_{lf}$
$(Y-Z)_{lf}$
$(X-Z)_{mf}$
$(Y-Z)_{mf}$
$(X-Z)_{hf}$
$(Y-Z)_{hf}$
Sensors
Preamps
Buffers FET's
Active Filters
Log.Amps
Integrat.
Tele. Output
Phase compare Units
Phase info. Tele. Outputs

Fig 5.14

to Mr. G. Garside who is the Senior Experimental Officer with the Space Physics group at Sheffield. A simplified diagram of the VLF experiment on SL1124 is given in Fig 5.14. The use of narrow band channels to sample the incident broad band signals in the frequency domain and the use of many channel time sampled telemetry is common in VLF experiments onboard rockets or satellites. The novel feature of the 1124 V LF experiment is the wide band output which is transmitted unsampled to the ground station. If the signal is recorded on the ground a wealth of information gathered during the flight is available for analysis. The spectral characteristics of incident emissions can be determined with the aid of a Sonograph and accurate noise spectra can be produced with suitable equipment such as the Hewlett Packard 5451B fast Fourier analyser. These two areas of new information can help greatly in the interpretation and understanding of the received emissions, their source locations and generation mechanisms. In view of the importance of the wide band facility a brief description of the main blocks which constitute it will be given.

It can be seen from Fig 5.12 that the antenna has a resonance peak which for the 250 mm long rod with a 16,000 turn coil occurs at 1.7 KHz. In order to return the whole of the broad band signal to the observer with a reasonable signal to noise ratio it is necessary to flatten this peak such that signals at other frequencies can be amplified and transmitted at a high level without signals at the resonant frequency becoming distorted or clipped. A simple parallel tuned LCR notch filter is used to suppress the peak. It was designed to have a notch with a Q which matches the antenna response. A photograph of the notch can be seen in Fig 5.15a. Following the filter is a calibration source which interrupts the flow of broad band

FIG 5·15a

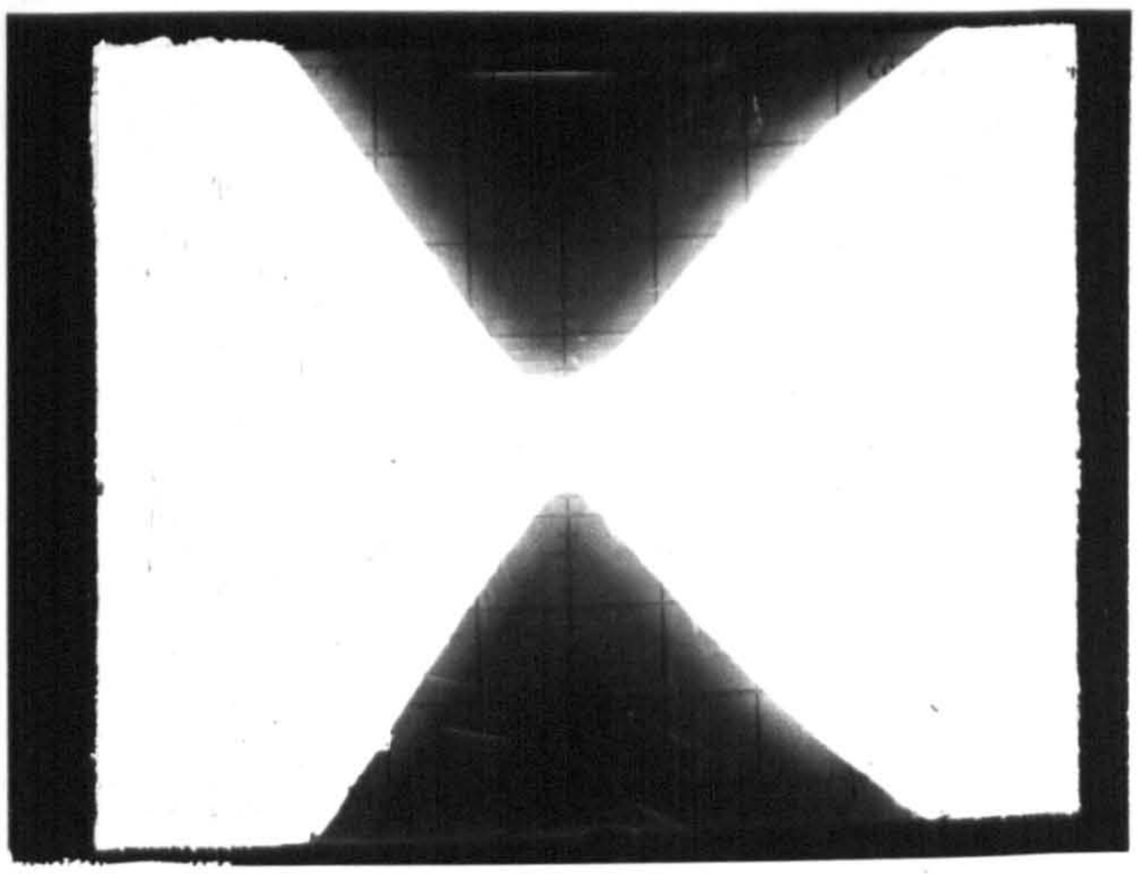

1142Hz 1885Hz 2500 Hz

FIG 5·15b

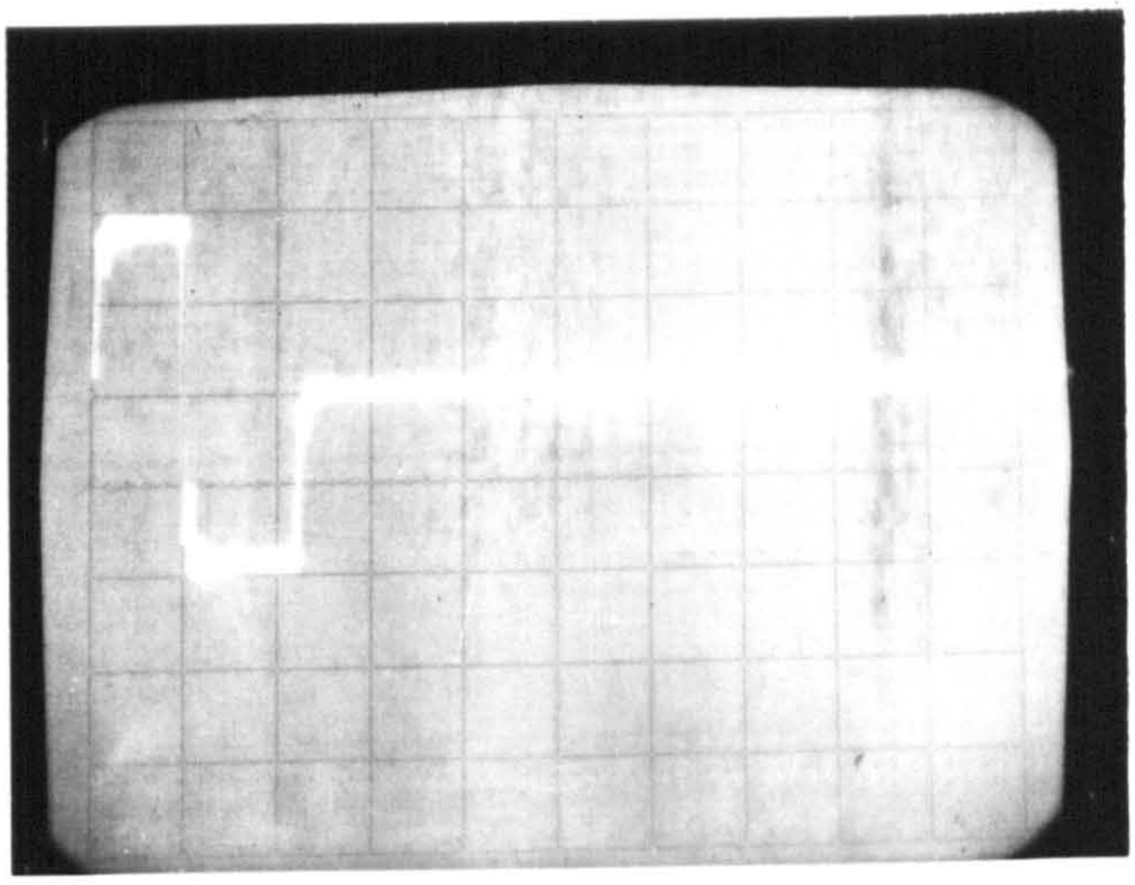

1 ms / div.

FIG 5·15c

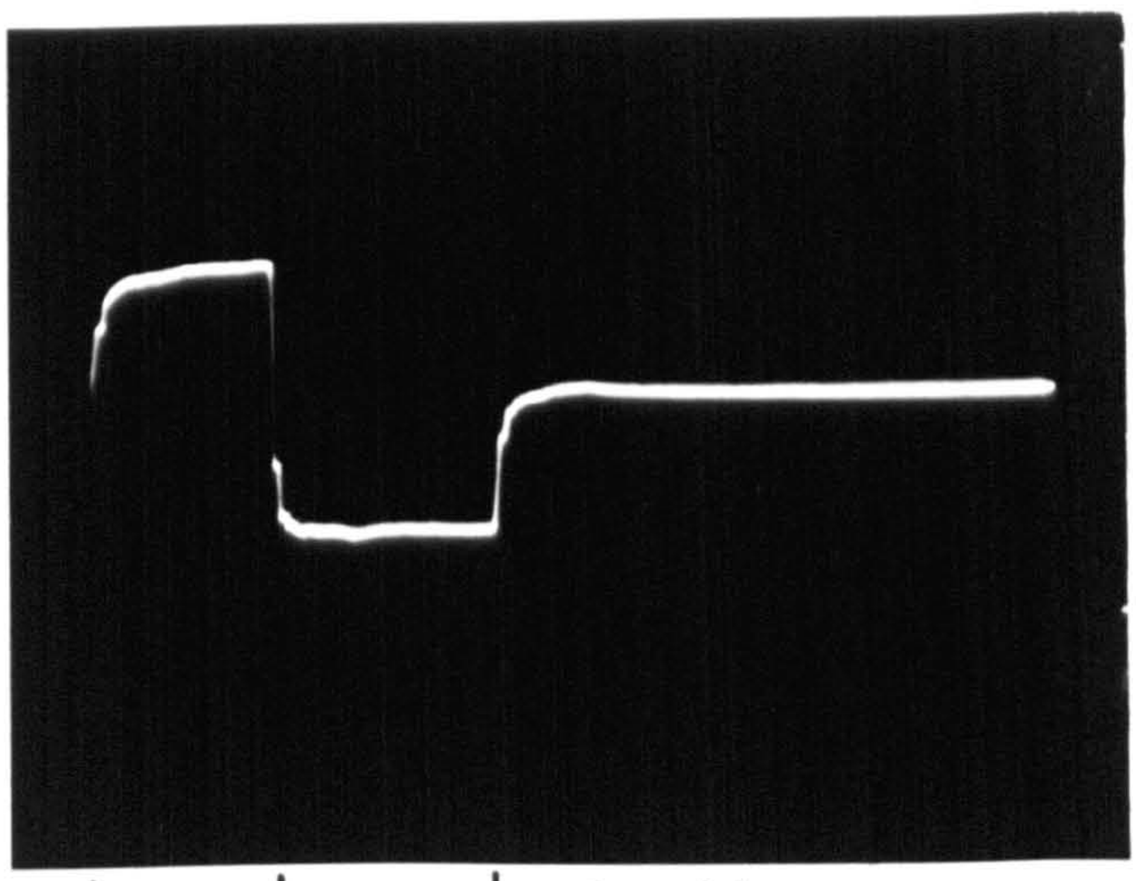

1ms/div.

information for 2 milli-seconds every 2 seconds.During this time the VLF signal is turned off and the output is forced to first +2V for 1 ms then to -2V for 1 ms, see Fig 5.15b.The unit thus provides a check on the gain of the telemetry and the recording equipment and also useful time markers for emission identification.In order that the calibration levels may be recovered,the ground recorder must be an FM machine which will record from DC to the upper frequency limit of the broad band system.An example of a recovered calibration pulse is given in Fig 5.15c. The telemetry transmitter is manufactured by E.M.I. Ltd. type UOM 15 which is normally used with a sampling set in Petrel rounds.It was adapted for use as a broad band sender with great success and performed well beyond its specification of 0-11KHz with the upper -3db point at 18 KHz. This concludes the description of the equipment which makes up the Sheffield University experiment on board SL1124 and we proceed to discuss the integration and test procedure.

5.4 Payload integration

It is not sufficient to merely design and test a VLF experiment which is to be flown on a rocket along with other experiments and equipment if the full potentiallity of the receiver is to be exploited. Such sensitive receivers can be paralysed by interference from the payload systems and other experiments. Thus a detailed evaluation of the payload as a whole must be made from the point of view of the VLF receiver. Of course careful consideration is given at the planning stage to measures which will reduce the risk of interference being generated but usually when the payload is assembled for the first time some problems are experienced.This was true of the UK3 satellite, of P47H and of almost all other payloads which incorporate sensitive VLF experiments.

The problems faced and the manner in which they are met during the integration phase of the payload can make or mar the success of the entire venture.It is intended that the reader should therefore understand some of the problems encountered and the solutions adopted at this critical point in the development of the payload.

The integration of SL1124 was carried out during May and June of 1973 in the Spacecraft Assembly Building at the British Aircraft Corporation's Guided Weapons Division,Filton,Bristol.Prior to electromagnetic cleanliness evaluation of the payload each experiment and payload system was tested to ensure that they were working and in a state that was representative of the flight condition.

The assembly building was found to be much too noisy to make any measurements of interference which might be generated by the payload and all tests had to be performed inside a screened room. An initial check made with the VLF sensors showed that signals were being picked up from a number of devices.

1) The payload magnetometers produced a signal which was 2db above system noise at 20KHz. Later it was discovered that the magnetometers could operate successfully in two modes one of which was quiet (2db above noise) and the other noisy (20db above noise). This behaviour had not previously been observed but repeated tests with other magnetometers of the same type confirmed the existence of two noise modes. The device operated in one or the other mode quite arbitrarily when turned on and it was not possible to predict which mode would be on during the flight.This interference had to be tolerated as replacement types of magnetometer could not be fitted in time for launch.Fortunately there was only one line at 20.2KHz and it would be possible to recognise and disregard it when looking at the signal output.

2) The IRIG FM telemetry senders at 202 and 204 MHz with a power output of 2 W each were turned on but no sensible measurements could be made as the RF energy was confined in the metallic room and almost saturated the receivers. An RFI test had to be made in the open (at a quiet site) or in a large RF anechoic chamber.

3) The electron density experiment produced a signal at 6.291 KHz which was 15 db above system noise. This signal appears on the sensors at the end of the deployed booms and no steps could be taken to eliminate it as it enables the electron density probe to oberate. A further signal which was 15 db above noise was observed at frequencies between 12.5KHz and 13.5KHz. This was identified as a load yariation induced frequency modulation of the DC/DC converter freuqency. This was eliminated by the DC supply being taken from the main round batteries via a stabiliser.

4) The energetic particle experiment consists of three types of electronics.

a) EHT generators using inverters from round batteries.

b) Ramp generating TTL integrated circuit logic for ESA's.

c) TTL counting logic for Geiger tubes and ESA's.

The two EHT converters produced interference which was 68 db above noise at 11756 Hz and 60db above noise at 10750Hz with beats being detected at 22db above noise at 1KHz.Considerable circuit modifications were made,the converter frequency was shifted to 25KHz and the whole device was encased in a mu-metal box.The interference was reduced to 27db above noise at frequencies between 22 & 25.9KHz. This level was tolerable as it was outside the frequency band of interest.

Signals receiver when the ramp generator was running were at levels between 20 and 55db above noise at many closely

spaced frequencies (every 100Hz) from 906 Hz to 5 KHz.
When the ratemeters were counting a much denser spectrum was observed and it became clear that this experiment could not be tolerated in such close proximity to the VLF sensors. Tests showed that if the particle experiment was removed to a distance of 1.5 m from the sensors no interference was seen. Thus the whole experiment was moved to the bottom of the payload, some 2 m away from the VLF experiment. This required major engineering work on the round such as new cable harness and the introduction of another 8" bay and a complete repositioning of the particle detectors such that they had useable viewing angles.

5) The IRIG RFI tests were made in an open field at Filton. No interference was observed due to the two Standard Telemetry Senders.

6) RFI tests with the 440 MHz broad band telemetry also proved negative.

The standard IRIG telemetry checks were performed and the payload was then released for vibration and spin balance test on the return of the VLF package from calibration at Sheffield.
The payload was flown to the rocket range at Andøya in November 1973 and was successfully launched the following month.

CHAPTER 6

THE GENERATION OF VERY LOW FREQUENCY EMISSIONS

6.1 INTRODUCTION

It is well known that the earth has a magnetic field which is similar to that produced by a simple dipole. The effect of the solar wind is to compress the daylight side of the field and to extend the nighttime side as shown in Fig 1.12. For the purpose of what follows we consider the earth's field to be dipolar out to L = 6 or 7. Graphs relating the basic magnetospheric parameters such as Field strength B, gyro-frequency f_h and plasma frequency f_n to position can be found in Helliwell (1965).

Kendall (1970) demonstrates the basic properties of energetic particles moving in a dipole field. He shows that an electron moving in a uniform magnetic induction field B in the absence of an electric field will describe a circular motion about a field line with a frequency which is known as the Larmor or gyro frequency and whichis given by:

$$\omega = -eB/m$$

and the radius of gyration by:

$$r = v_\perp / \omega$$

The dynamics of charged particles in steady fields was investigated by Larmor in the late 19th Century and reported in Larmor (1896).

If an electron which is rotating in the steady field has a velocity component along the z axis see Fig 6.1, then the particle spirals along the field line.

It can be shown that the kinetic energy of such a particle is constant throughout its motion. This property is called the 1st adiabatic invariant. The quantity $m v_\perp^2/2B$ is also constant and is the magnetic moment of the equivalent current loop. This is known as the second adiabatic invariant.

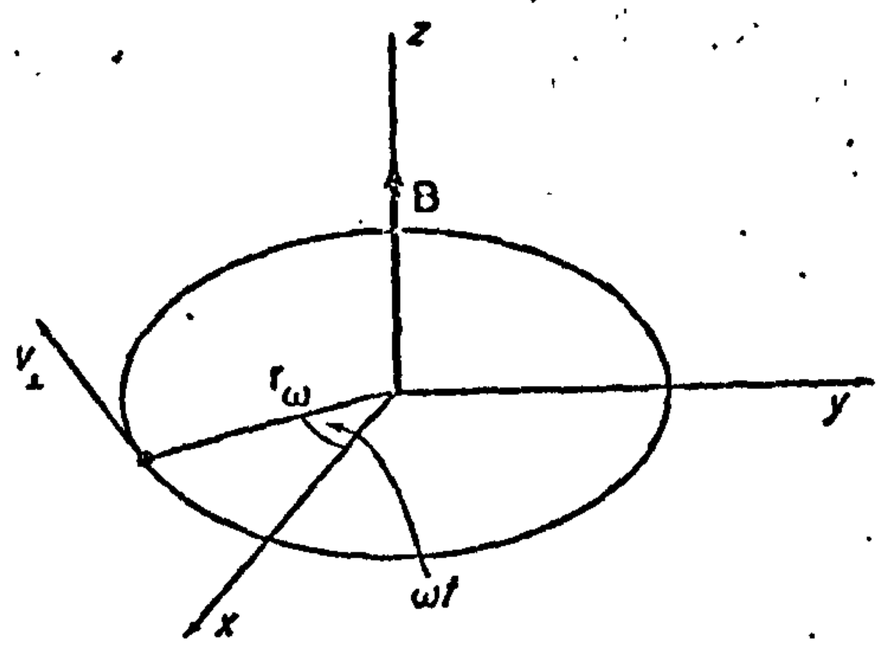

Gyrating electron $V_{11} = 0$

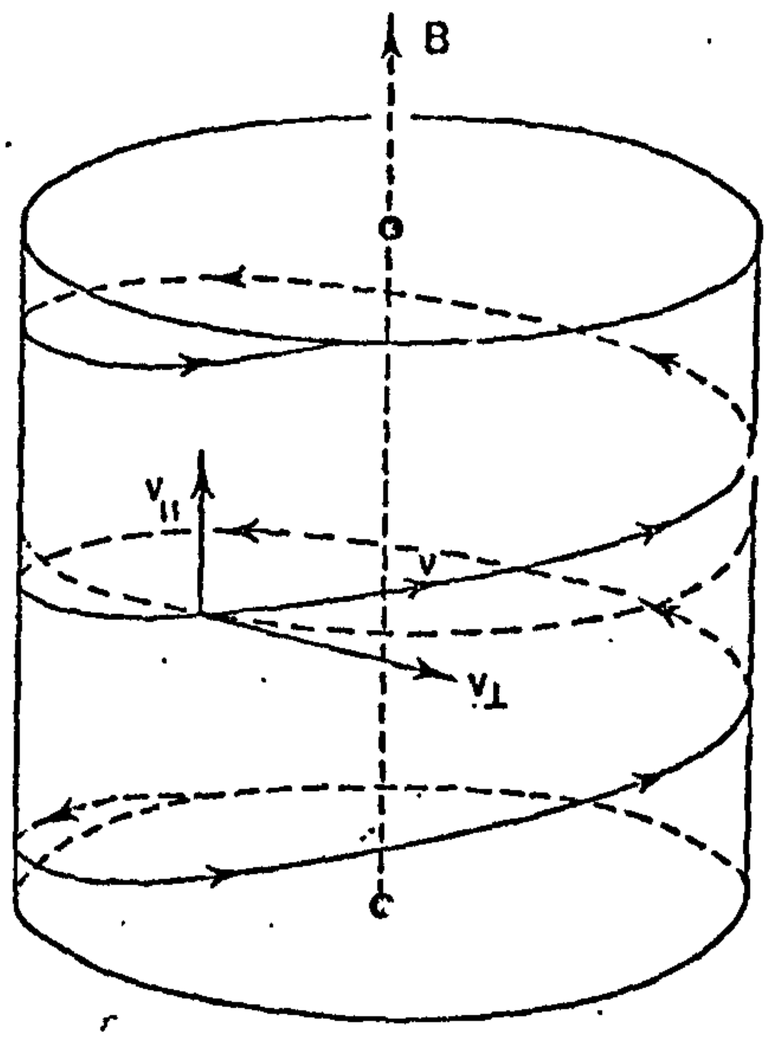

Spiralling electron $V_{11} \neq 0$

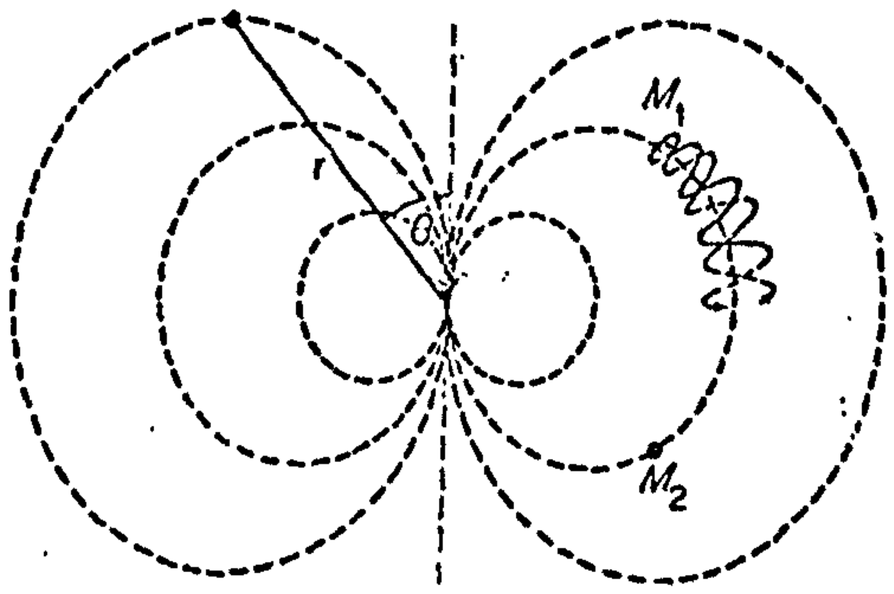

Mirroring electrons.

Fig 6.1

If we inject a particle into a dipole field it will behave in an interesting way. If the field in the equatorial plane at some altitude R is B_e, then using spherical polar co-ordinates with the dipole pointing along the axis $\theta = \pi$ where θ is the co-latitude then the field at any position along that field line is given by:

(6.1.1) -- $B = B_e(1 + 3\text{Cos}^2\theta)^{\frac{1}{2}}/\text{Sin}^6\theta$ (Kendall 1970)

Defining the pitch angle of the spiralling particle as α where:

$v_{//} = v\text{Cos}\,\alpha \qquad v_{\perp} = v\,\text{Sin}\,\alpha$

and applying the two invariants of motion it can be shown that

$\text{Sin}^2\alpha/B = \text{Sin}^2\alpha_e/B_e$

where α_e denotes the pitch angle at the equator.

Using 6.1.1 and the above equation we see that:

$\text{Sin}^2\alpha = ((1+ 3\text{Cos}^2\theta)^{\frac{1}{2}}/(\text{Sin}^6\theta))\text{Sin}^2\alpha_e$ (6.1.2).

Now $\text{Sin}^2\alpha$ increases as $\text{Sin}^2\theta$ decreases. As $\theta \to 0$ the right hand side of (6.1.2) tends to infinity but $\text{Sin}^2\alpha$ cannot exceed 1. Therefore, there will always be points where $\alpha = \pi/2$ corresponding to some value of $\theta = \theta_m$ which will be symmetrically placed about the equator. The particle cannot proceed beyond $\theta = \theta_m$ without violating the invariants. The equatorial pitch angle may be such that the value of θ_m (The mirror points) is very low and the particles are mirrored in the ionosphere where collisions take place. If the particle collides the invariants of motion are violated and the particle is no longer constrained to move back up along the field line to the other mirror point. In this way energetic particles can be 'precipitated' from the magnetosphereinto the ionospher giving rise to phenomena such as auroral displays.

6.2 EARLY THEOREIES OF THE GENERATION OF VLF EMISSIONS

The enormous range of spectral shapes of VLF emissions has been known for some years. As mentioned in Chapter 1 most of the early work was in studying whistlers and their generation and propagation. Disregarding whistlers, tweeks and spherics there are still a great number of emissions such as chorus, hiss, warbling and gliding tones etc which appear to be related to magnetic disturbance and are found most frequently near the auroral zones, Gallet & Helliwell (1959). Whistlers are sometimes followed by one or more rising tones. See Fig 1.11 for a godd example. It appears that the whistler somehow 'triggers off' the emission.

The first attempt to explain the generation of these emissions was made by Gallet & Helliwell (1959). It had been shown by Storey (1953) in connection with the theory of whistlers that the energy of a VLF wave tends to be guided along the earths field lines through the dispersive magneto-ionic medium. However, the wave normal may make some angle to the field and as the polarization of the wave is approximately circular there will be a component of electric field of the wave which is parallel to the magnetic field. The wave velocity in the dispersive medium is a function of frequency and may be up to two orders of magnitude below that in free space.

It is conceivable therefore that streaming electrons which follow the magnetic field lines between mirror points could interact with the longitudinal component of the electric field of the wave if the phase velocity is equal to the streaming velocity of the particles. This longitudinal resonance is similar to that which takes place in a Travelling Wave Amplifier valve Pierce (1950).

The theory of Gallet & Helliwell assumed that whistler mode noise provided the input signal and that amplification would take place at two frequencies for which $v_p = v_s$ for given values of ambient plasma frequency and gyro frequency.

However, the theory required a bunch of electrons with the necessary streaming velocity and the existence of such a bunch was not demonstrated.

The next suggestion also employed bunches of electrons, but assumed that they radiated Doppler shifted, backward travelling whistler mode waves, Dowden (1962). This theory will be explained later, it suffices to say that it could explain rising and falling tones and hooks, but it could not explain long enduring quasi-constant tones. Dowdens explanation of hooks was questioned by Brice (1962) who pointed out that the agreement between an observed series of hooks and the series which would be generated by a mirroring bunch of electrons was poor and could not be accounted for in terms of observational errors.

Helliwell (1963) and Helliwell & Brice (1964) showed that the delay between succesive emissions was equal to the whistler mode echoing period for the path and not the electron bounce time as proposed by Dowden. In addition, it was observed that a periodic emission was often generated in a whistler. These facts led to the idea that each emission in the series was generated by the whistler mode echo of the previous emission, which acted to organize the phases of resonant particles and so cause them to radiate coherently.

It was then discovered that discrete emissions could be triggered repeatedly by man made transmissions from the ground Helliwell et al (1964). This was not compatible with a mechanism based on mirroring particle bunches and suggested that the conditions for generation were omnipresent and that a different mechanism had to be found.

The transverse resonance instability was suggested by Brice (1963) to avoid the problems of particle bunches. Although the mechanism is based on the same resonance condition as Dowden's theory, it differs fundamentally in that it depends on feedback from the backward travelling waves to the forward travelling electrons.

The waves tend to organise the phases of the incoming particles. It was pointed out by Brice that this enabled the interaction region to remain fixed in space and that the mechanism could be viewed as a backward wave oscillator. The importance of phase coherence was also recognised by Hansen (1963), who suggested that a cyclotron emission would tend to be triggered by a strong whistler mode wave in a region where the rate of change of electron gyro-frequency was equal to that of the Doppler shifted wave frequency. A similar idea was proposed by Helliwell (1967) and was developed into a coherent theory which could explain the generation of many spectral forms. This theory forms the basis of the work which is presented in the latter part of this thesis.

A reivew of work concerning particle wave interactions is given in Brice (1964) and more recently by Rycroft (1972). Although we are concerned here with the transverse resonance instability of electrons as defined in Helliwell (1967) it is interesting to mention the possible generation mechanisms which are allowable in terms of longitudinal and transverse resonances with electrons and protons. Either in single particle situations (incoherent) or in the case of coherent radiation from a large number of coherently radiating particles.

6.3 THE TRANSFER OF ENERGY BETWEEN MOVING CHARGED PARTICLES AND WHISTLER MODE WAVES

Detailed descriptions of the effects of waves on the motion of charged particles has been given by Helliwell & Bell (1960) and Dungey (1963). What follows is after Brice (1964).

The force F on a charged particle due to an electric field E and a magnetic field B is given by;

$$F = q\ (E + v \times B) \qquad (6.3.1)$$

where q is the charge on the particle and v is its velocity. The incremental change in energy of the particle ΔW is given by the scalar product of F and the incremental distance Δs.

$$\begin{aligned} \Delta W &= F.\Delta s \\ &= F.\ v\Delta t \\ &= q(E+vXB).v\Delta t \quad \text{(using 6.3.1)} \\ &= qE.v\Delta t \qquad (6.3.2) \end{aligned}$$

To obtain a significant amount of energy transfer, we require E.v to have a constant (zero frequency) component. We have seen that particles spiral back and forth along magnetic field lines in the magnetosphere and that they can be said to have components of velocity parallel and perpendicular to the field of v_{11} and $v_{\perp}$ respectively.

If the longitudinal component of velocity is matched to the wave phase velocity in the medium and the wave has a longitudinal component of electric field (as required in the TWT theory) then we have a longitudinal resonance since;

$$E_{//} \cdot v_{//} = \text{const.}$$

Alternatively, if the particle experience an electric field which rotates about the earth's magnetic field at the same rate and with the same sense as the particle, the transverse resonance condition is satisfied since;

$$E_{\perp} \cdot v_{\perp} = \text{const.}$$

For a whistler mode wave with a wave normal angle of θ^{o} the longitudinal resonance condition is satisfied when;

$$v_{//} \ \text{Cos}\ \theta = v_{p}$$

For transverse resonance the Doppler shifted wave frequency seen by the particle must equal the particle gyro-frequency in magnitude and must have the same polarization. Since whistler mode waves are right circularly polarized the electric and magnetic fields rotate about the static magnetic field in the same sense as the electron. Thus the longitudinal velocity of electrons to satisfy the transverse resonance condition is given by;

$$v_{//} \text{ Cos } \theta = v_p \frac{(f - f_h)}{f} \qquad (6.3.3)$$

and f_h is the electron gyro-frequency
and f is the wave frequency
To obtain whistler mode wave interactions with protons a reversal of polarisation must be effected. This requires an anomalous Doppler shift (Ginzburg 1960) and the parallel component of the proton velocity must exceed the phase velocity of the wave;

$$v_{//} \text{ Cos } \theta = v_p \frac{(f + f_i)}{f} \qquad (6.3.4)$$

$$v_{//} \text{ Cos } \theta \simeq v_p$$

Where f_i is the ion gyro-frequency.

Brice (1964) has computed the particle energies required for longitudinal and transverse resonance with a wave of frequency 5 KHz propagating along a field line at L = 4. The assumed ratio of kinetic energy in the parallel and perpendicular directions for the particles was 1:3. He shows that the lowest proton energies which are capable of resonance (both transverse & longitudinal) occur at the bottom of the field lines close to the ionosphere. This also applies to the longitudinal resonance for electrons. The electron transverse resonance however requires the lowest energies at the geomagnetic equator. Since energetic electrons are generally more plentiful the lower their energy, more electrons are available for

gyro-resonance in the vicinity of the equator than elsewhere, Helliwell (1965).

Rycroft (1972) following the work of Brice (1964) shows that the parallel energy of electrons which are to enter into transverse resonance with whistler mode waves must be $W_{//}$ which is given by;

$$W_{//} = \frac{B^2}{2\mu_o N} \cdot \frac{f_h}{f} \cdot (1 - f/f_h)^3 \qquad (6.3.5)$$

B is the intensity of the magnetic induction
N is the electron density in el. m^{-3}
μ_o is the permeability of free space.

The quantity $B^2/2\mu_o N$ has the dimensions of energy and is the energy density of the magnetic field at a point divided by the density of thermal electrons at that point. It is known as the magnetic energy per electron and is important since for a certain value of f/f_h (usually between 0.1 and 0.5), it determines the energy of resonant particles. When the particle energy exceeds a threshold value proportional to $B^2/2\mu_o N$ an emission can be generated at a frequency f.

Equation (6.3.5) can be written in terms of the Anisotropy A of a population of particles. Rycroft (1972) quotes the work of Kennel & Petschek (1966) who derive the dispersion relation for the magneospheric medium μ^2 (ω, k). This contains in the denominator the term ($kv_{//} - \omega - \omega_h$) and when this is zero the electrons are in gyro-resonance with the wave. The electron resonant velocity is given by:

$$v_{//} = (\omega_h - \omega)/k \qquad (6.3.6)$$

This is a concise statement of the 'first transverse resonance condition'.

For electrons forming the high energy tail of a Gaussian distribution (these are the electrons which have resonant energies) we may define their Anisotropy by;

$$A = \frac{T_\perp}{T_{||}} - 1$$

where $T_{||}$ & $T_\perp$ are the temperature of the electrons parallel and perpendicular to the geomagnetic field.

Kennel & Petschek show that an instability will occur only when

$$A \geqslant \frac{\omega}{\omega_h - \omega}$$

Using the equals condition in the above and substituting into equation (6.3.5) we hae;

$$W_{||} = (B^2/2\mu_o N)(1/(A(A+1)^2)) \qquad (6.3.7)$$

To close this section mention will be made of some other resonances which can lead to the production of VLF emissions although what follows in succeeding chapters is concerned with the transverse resonance instability for electrons only.

Following Brice (1964) in defining L = longitudinal resonance, T = transverse resonance, p = protons, e = electrons, S = single particle effects & I = collective effects leading to instabilities. Thus Cerenkov radiation from electrons may be defined as (L,e,S) and the proton beam amplification of Kumura (1961) as (T,p,I).

Longitudinal resonance mechanisms for protons have not been suggested for VLF emissions as for the same signal output the kinetic energy of protons must be m_p/m_e times greater than that of electrons (where m_p & m_e are the masses of the proton and electron respectively), and the number density of such high energy protons is less than that for electrons, Brice (1964).

Cerenkov radiation from electrons (L,e,S) was considered by Kolomenskii (1956) Ellis (1957) Eidman (1958) Dowden (1960), Ellis (1960) Gendrin (1960), Ondoh (1961,62,63), Gershman & Urgarov (1961), Bendeitkov & Eydman (1961), Clemmow (1962) and McKenzie (1963).

The travelling wave amplification hypothesis (L,e,I) has been examined by Helliwell (1956), Gallet (1959) and Helliwell & Gallet (1959) Bell & Helliwell (1960) Barrington (1960) Kimura (1961) Adachi & Muschiake (1962) and Dowden (1962a).

Doppler shifted cyclotron radiation from protons (T,p,S) has been studied by Aarons (1960), MacArthur (1959), Murcray & Pope (1960a,b), Santirocco (1960) and Knox & Rycroft (1964).

The corresponding radiation from electrons (T,e,S) has been postulated by Dowden (1962, 63a) and considered by Brice (1963) and Hansen (1963).

The transverse resonance for protons (T,p,I) was found by Kimura (1961) and Maeda & Kimura (1962,63) and the transverse resonance for electrons (T,e,I) was suggested by Brice (1963) and was investigated by Bell & Buneman (1964). In the following chapter the basis of Dowden's Doppler shifted backward radiating electron transverse resonance (T,e,I) theory is given. This is followed by the introduction of Helliwell's second' transverse resonance, or 'consistent wave' condition. The application of this theory to actual emissions observed at both medium and high latitudes constitutes the closing sections of this work.

CHAPTER 7

ELECTRON CYCLOTRON RADIATION

7.1 BACKWARD RADIATED DOPPLER SHIFTED CYCLOTRON RADIATION FROM ELECTRONS.

We consider now in more detail the idea put forward by Dowden (1962) of a localised electron oscillator moving along a geomagnetic field line. See Fig. 7.1.

Consider an electron, or small bunch of electrons travelling in a helix about a line of force in the geomagnetic field. Suppose that it is travelling away from the fixed observer on the ground with a component velocity parallel to the field of $v_{//}$. The spiralling electron bunch is equivalent to an oscillator of frequency f_h (the local gyrofrequency) which is moving away from the observer at $v_{//}$ m s^{-1}. The oscillator is thus seen doppler shifted down to frequency f. The velocity of propagation of the electromagnetic wave is C/n, where n is the refractive index of the medium. The observed Doppler shifted wave frequency f is given by ;

$$f = f_h \frac{v_p}{v_p + v_{//}} \qquad (7.1.1)$$

or as $v_p = C/n$ we may write (7.1.1) in the form used by Dowden (1962)

$$f = f_h/(1 + v_{//} .n/C) \qquad (7.1.2)$$

where $n^2 \approx f_n^2/(f(f_h-f))$

for $n^2 >> 1$

and rewriting (7.1.2);

Backward Radiated Doppler Shifted Cyclotron Radiation.

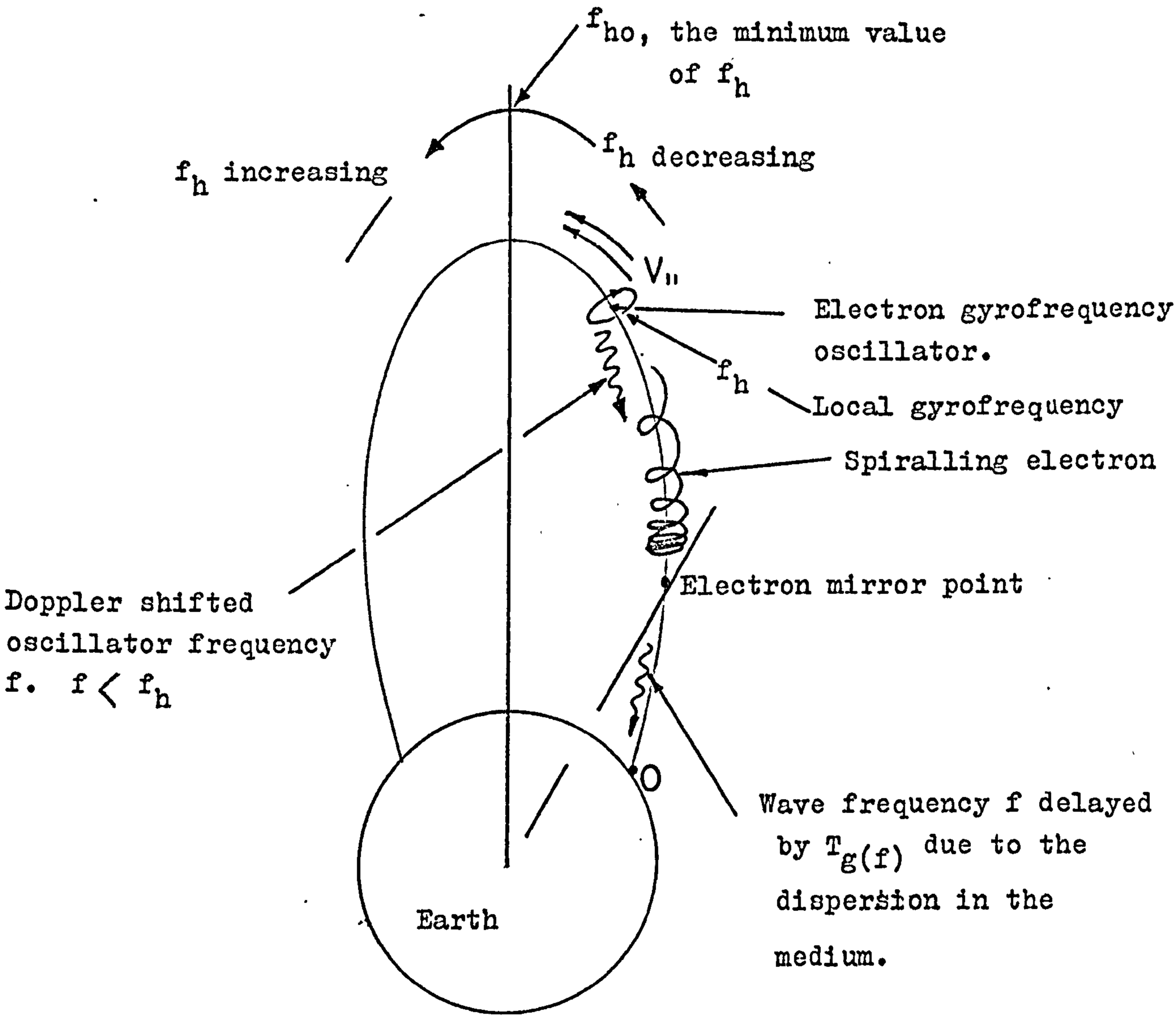

O. is the location of the Observer.

Fig.(7.1)

7.1
(Contd)

$$\frac{f.v_{//}^{2}.f_n^{2}}{c^2} = (f_h-f)^3 \qquad (7.1.3)$$

Smith (1960) has shown that a model for magnetospheric electron density which is proportional to the electron gyro-frequency fits nose whistler dispersion data quite well. His gyro-frequency model may be expressed in terms of :

$$f_n^{2} = kf_h \quad \text{where } k \simeq 1 \text{ MHz}$$

we may therefore in this case rewrite (7.1.3) as;

$$(f_h-f)^3 = k.\frac{v_{//}^{2}}{c^2} f_h.f$$

or as;

$$\frac{(1-\lambda)^3}{\lambda} = \left[\frac{v_{//} \cdot f_n}{c.f_h}\right]^2 \qquad (7.1.4)$$

---

where $\lambda = f/f_h$

Now $v_{//}$ can be calculated for invariance of the particle magnetic moment;

$$\frac{\sin^2\alpha}{f_h} = \text{const.}$$

So $$v_{//} = v(1-(f_h/f_{ho}).\sin^2\alpha_o)^{\frac{1}{2}} \qquad (7.1.5)$$

It should be possible then after specifying the particle energy E and hence $v_{//}$ along with α_o and a particular field line, to calculate the Doppler shifted emitted frequency as the electron bunch moves from the observer's hemi-sphere across the geomagnetic equator and into the other hemi-sphere.

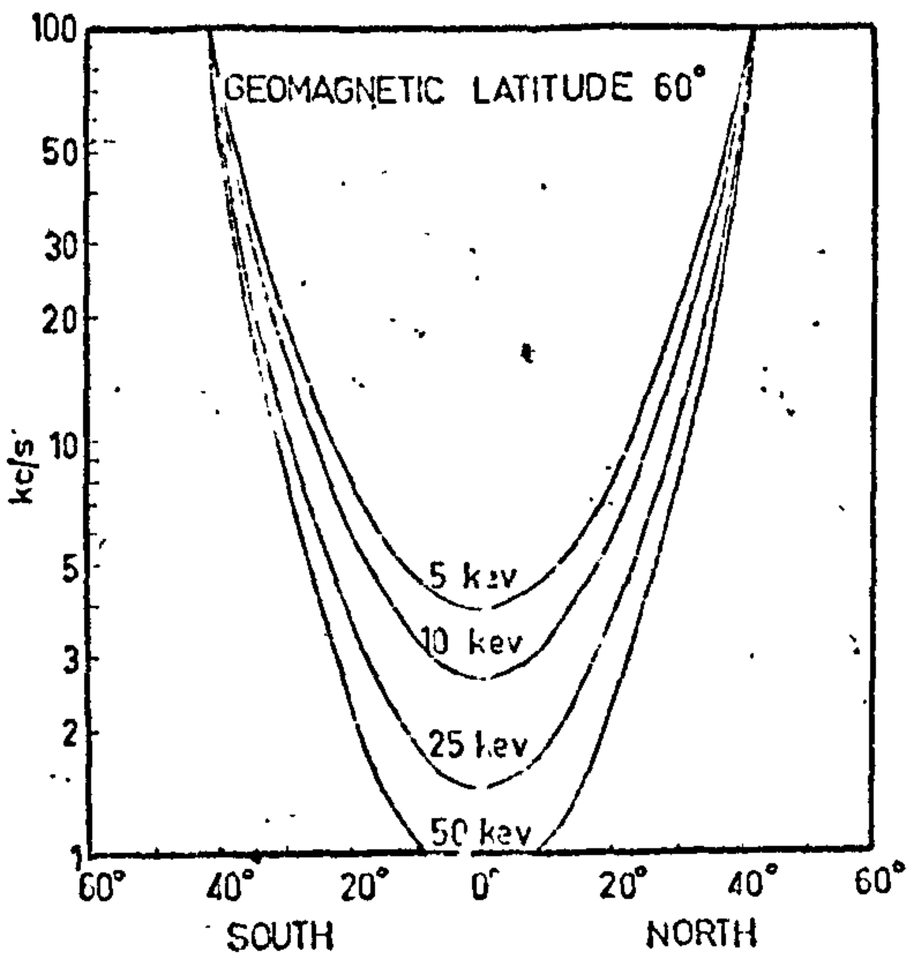

Fig 7.2a

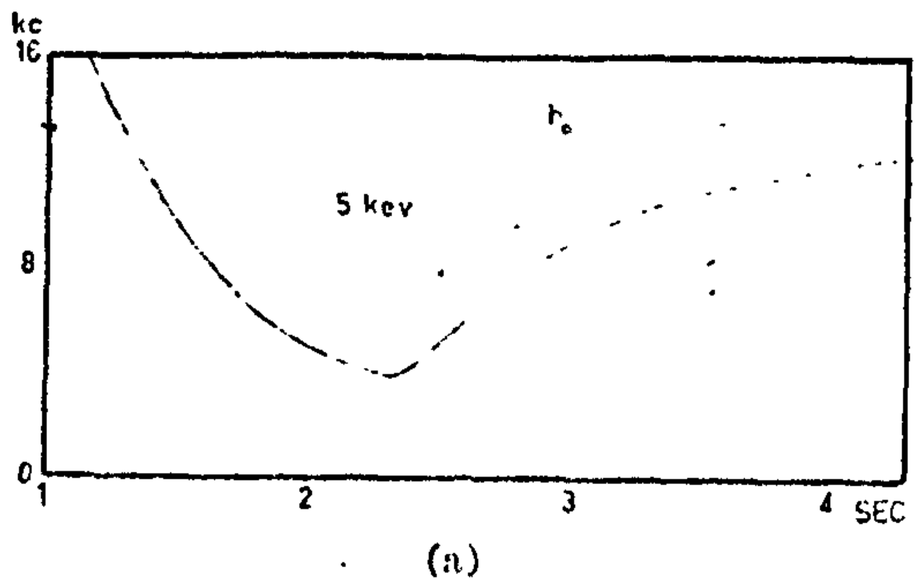

Fig 7.2b

L = 4

$\alpha_o = 20^o$

Gyro-frequency model

f_{ho}= 13.7 KHz

f_{no}= 120KHz

7.1 (Contd) The magnetosphere is a dispersive medium for VLF waves and the form of the frequency - time profile which has been generated will become distorted as the signal travels to the observer on the ground. The time delay at a given frequency $T_{(f)}$ is the sum of the wave group time delay from the point of generation to the ground and the delay introduced due to the velocity of the electron bunch as it travels from the starting position when observations begin.

$$T_{(f)} = T_{e(f_h)} + T_{g(f)}$$

Where the electron delay T_e and the wave group delay T_g are given by;

$$T_e = \int_{obs.}^{gen.point} \frac{ds}{v_{//}} \qquad T_g = \int_{obs.}^{gen.point} \frac{ds}{v_g} \qquad ds=\text{path segment}$$

Dowden (1962) solved the cubic equation (7.1.4) for f partly by the use of graphical methods which are prone to subjective errors. Here a digital computer was used to achieve a solution and the various numerical integrations required to calculate the observed emission profile were also performed in the machine.

Although the theory as described is not recognised as being the likely generation mechanism for VLF emissions it does demonstrate the principles which are required in the later and more sophisticated theory due to Helliwell. Moreover most of the integration and itterative calculation routines used in the later work were proved in the calculation of emissions based on Dowden's theory.

From Fig. 7.2a it can be seen that the frequencies generated by the gyration electrons are symmetrically placed about the equator where there is a minimum. When the time delays at the various frequencies are added the profiles become those shown in Fig. 7.2b and as Dowden points out these are very like observed hooks or if taken in part, like risers.

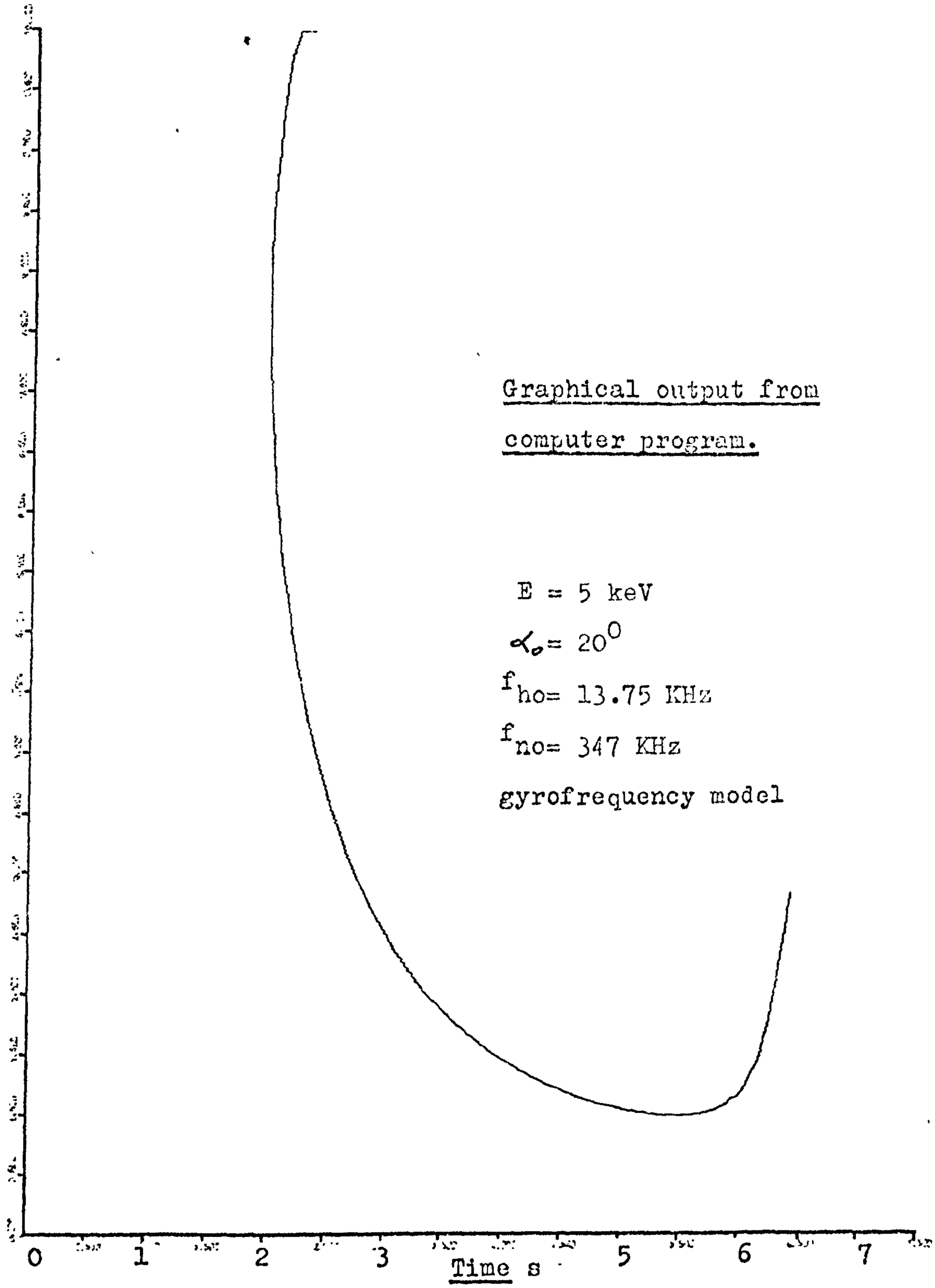

Graphical output from computer program.

E = 5 keV

$\alpha_o = 20^0$

$f_{ho} = 13.75$ KHz

$f_{no} = 347$ KHz

gyrofrequency model

Fig 7.3

7.2 THE SYNTHESIS OF 'HOOKS' USING DOWDEN'S CYCLOTRON THEORY

An attempt to solve (7.1.4) and to calculate the time delay $T_{(f)}$ as a function of position along a given field line was made using a relatively simple computer program (P9ODOWDEN). The calculations were based on a simplification of the dependence of f_h on distance from the equator along a field line, Helliwell (1967).

$$f_h = f_{ho} \left(\frac{1 + 4.5\ S^2}{Rm^2} \right) \qquad (7.2.1)$$

This approximation is good only close to the equator, S=5 x10^6m at L=4. (ϕ -10^o).

The delay time T_g was approximated to by the use of the dispersion relation $(t\sqrt{f})^{-1} = P.f + T$ for whistlers (Quoted in Dowden & Allcock 1970), where P & T are constants and t is the half hop whistler time which is taken to equal T_g at frequency f.

Equation (7.1.4) was solved by a successive approximation method using the differential of the equation to provide corrections which were repeatedly applied to the first guess at the solution. The method worked but had limitations regarding permissible values of solutions and was considered rather unsatisfactory.

Even with all the approximations the program was able to produce results which resembled those produced by Dowden, see Fig. 7.3 but which were not good enough for comparison. The approximations to the gyrofrequency at distance S from the equator and to the time delay $T_{(f)}$ were removed along with the iterative method for solving the basic cubic equation.

From Helliwell (1965) we have the following relations ;

$$f_h = f_{eq} \left[\frac{R_o}{R} \right]^3 (1+3\sin^2\phi)^{\frac{1}{2}} \qquad (7.2.2)$$

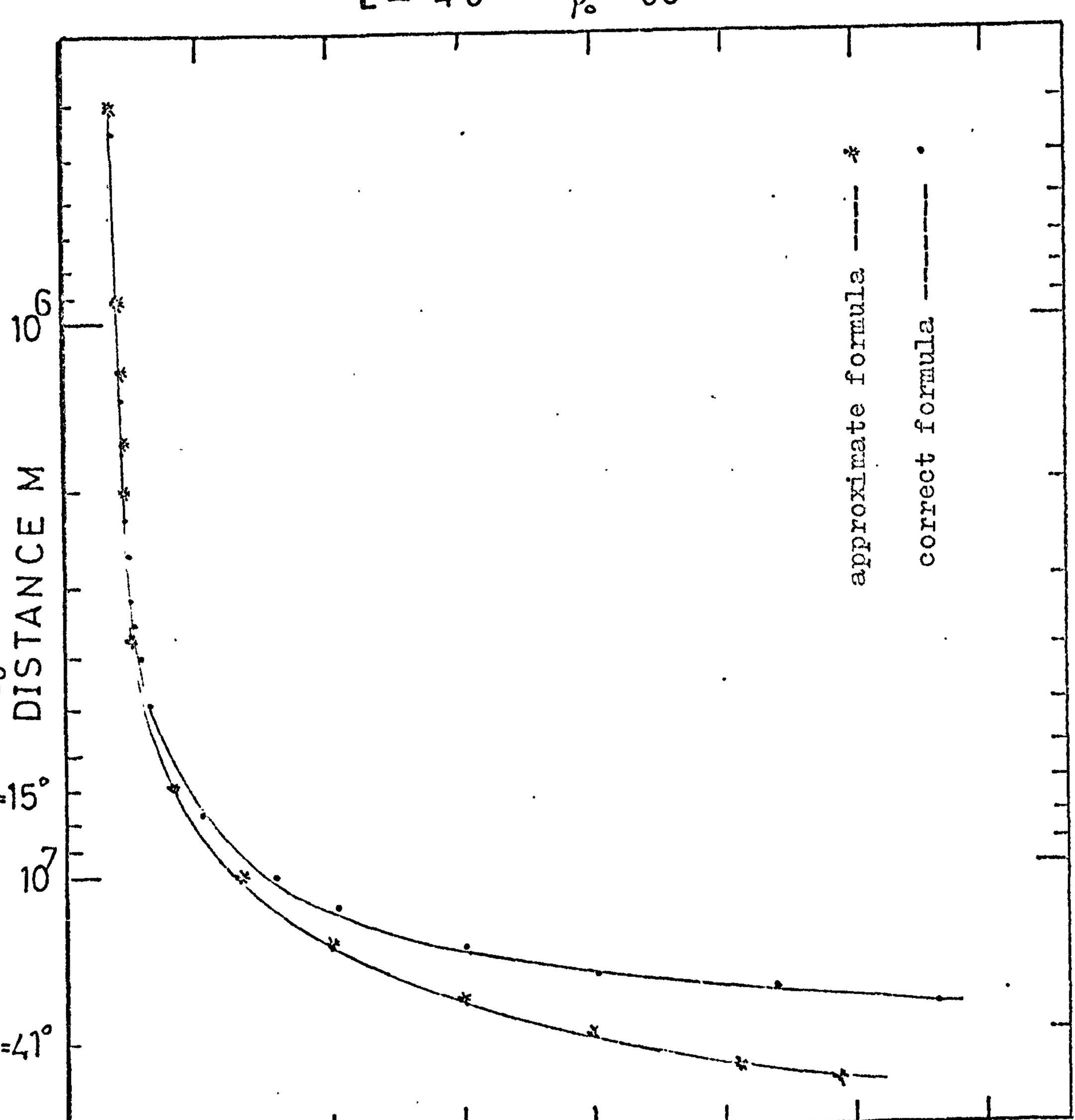
L = 4·0 ϕ_0 = 60°
—— Geomagnetic Latitude.
approximate formula ---- *
correct formula ——— •
DISTANCE M
10⁶
ϕ=10°
ϕ=15°
10⁷
ϕ=41°
1 x 10⁴
2
3
4
5
6
7
8
F_h. Hz

FIG(7.4)

7.2 (Contd)

$$R = R_o \cdot \frac{\cos^2\phi}{\cos^2\phi_o} \qquad (7.2.3)$$

$$S = \frac{R_o}{\sqrt{3}\ .2\cos^2\phi_o} \cdot (x + \sinh(x).\cosh(x)) \qquad (7.2.4)$$

$$\text{and } \sinh(x) = \sqrt{3}\sin\phi \qquad (7.2.5)$$

Now from (7.2.2) & (7.2.4) and with f_{eq} = 880KHz and as $f_{ho}=f_{eq}/L^3$ together with $L = 1/\cos^2\phi_o$, we have;

$$f_h = f_{ho}(1+3\sin^2\phi)^{\frac{1}{2}}/\cos^6\phi. \qquad (7.2.6)$$

A computer program was written to calculate the electron gyro-frequency as a function of geomagnetic latitude ϕ or distance from the equator S for both the approximate formula (7.2.1) and the accurate formula (7.2.6). The result can be seen in Fig.7.4 and shows agreement out to about $\phi \approx 10^o$ and thereafter a progressive discrepancy between the accurate and approximate values of f_h exists.

The cubic equation (7.1.4) was solved by using a routine which is available in the Scientific Subroutine Library in ICL 1900 series FORTRAN. The package called F4CUBIC provides the real and complex parts of three roots of the equation when given coefficients of the terms. Being extremely fast the routine can be used many times in a program without incurring long run times.

It remains then to calculate the electron travel time delay and the wave group delay in order that accurate calculations of observed emission profiles may be made.

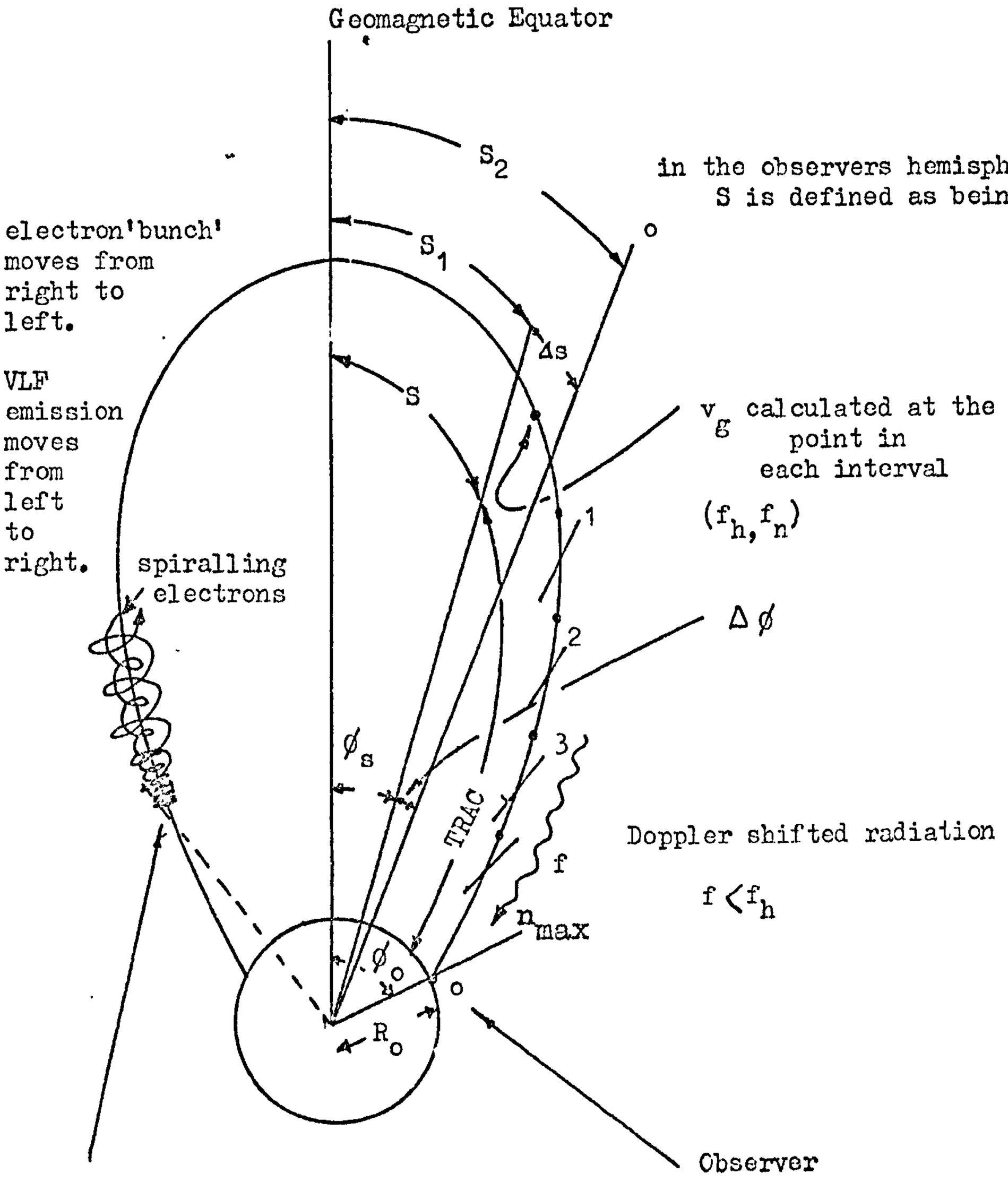

The path length 'TRAC' is split up into n_{max} sgments each As long.

Fig (7.5)

7.2 (Contd)

Consider Fig. 7.5 with the electron bunch of energy E keV starting from a position on the field line S m from the geomagnetic equator which is defined by the latitude ϕ_s. The electrons move towards the equator with a parallel component of velocity $v_{//}$ m s^{-1} and the Doppler shifted radiation travels down the field line a distance TRAC m to the observer at position 'o'. The path denoted TRAC is divided into n_{max} segments which are spaced $\Delta\phi^o$ apart, and $n_{max} \prec$ TRAC. Therefore $n_{max}\Delta\phi = \phi_o - \phi_s$. The group velocity of the emitted wave is v_g and is given by Helliwell (1967) as ;

$$v_g = 2Cf^{\frac{1}{2}} \cdot \frac{(f_h - f)^{\frac{3}{2}}}{(f_n \cdot f_h)} \qquad (7.2.7)$$

It is clear that v_g changes as a function of position along the field line and that to establish the group time delay $T_{g(f)}$ v_g must be integrated along the field line from the observer to the point of emission i.e. along the path 'TRAC'. The value of $\Delta\phi$ used was 2 milli radian giving some 500 segments along TRAC from the observer to the equator for an L value of 4.

The group velocity v_g is calculated at a point half way through the segment ie. at $S_n + \Delta s/2$ and is assumed constant along Δ s. The elemental time delay at frequency f is then;

$$\Delta t = \Delta s / v_g$$

and Δs is calculated from S_1 & S_2 as;

$\Delta s = S_1 - S_2$ s is +ve as v_g is +ve and Δt must be +ve
S is -ve and $|S_2| > |S_1|$

S_1 and S_2 are calculated using equations (7.2.4) & (7.2.5) from values of ϕ, and $\Delta\phi$.

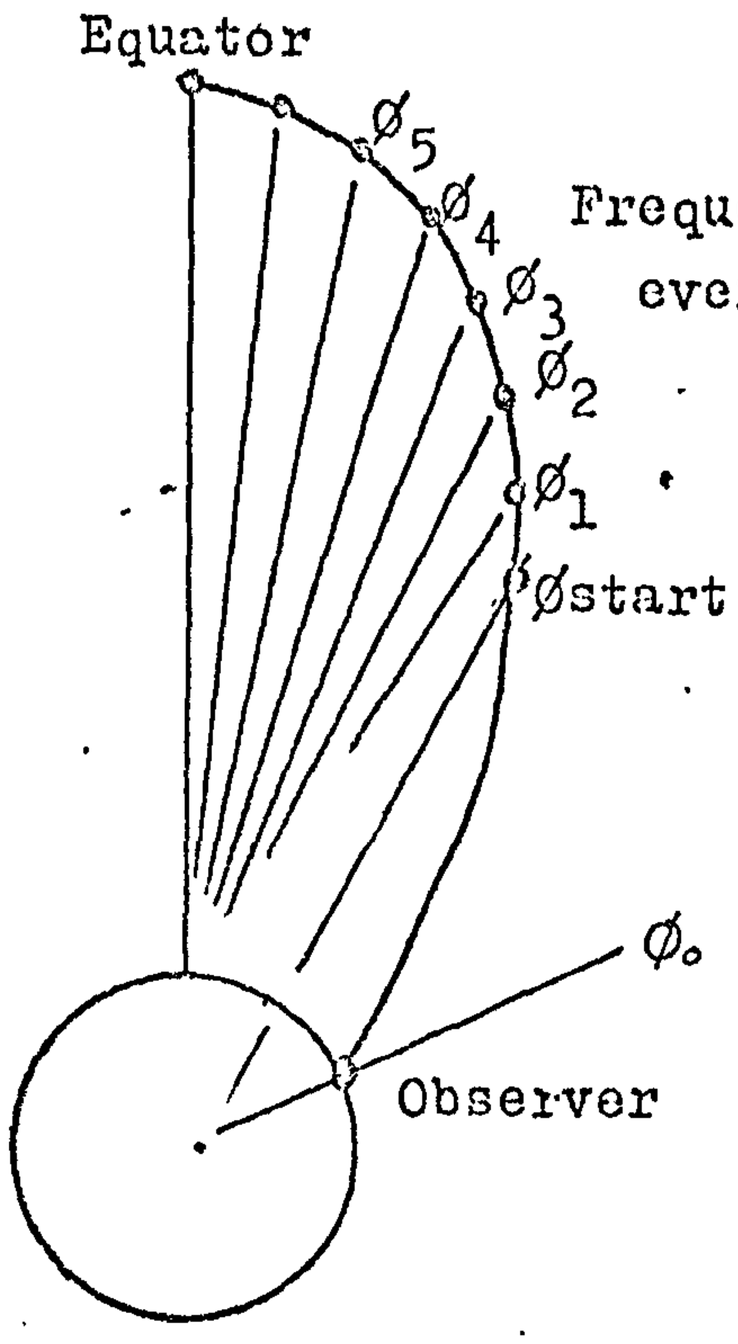

Frequencies calculated every 1^o

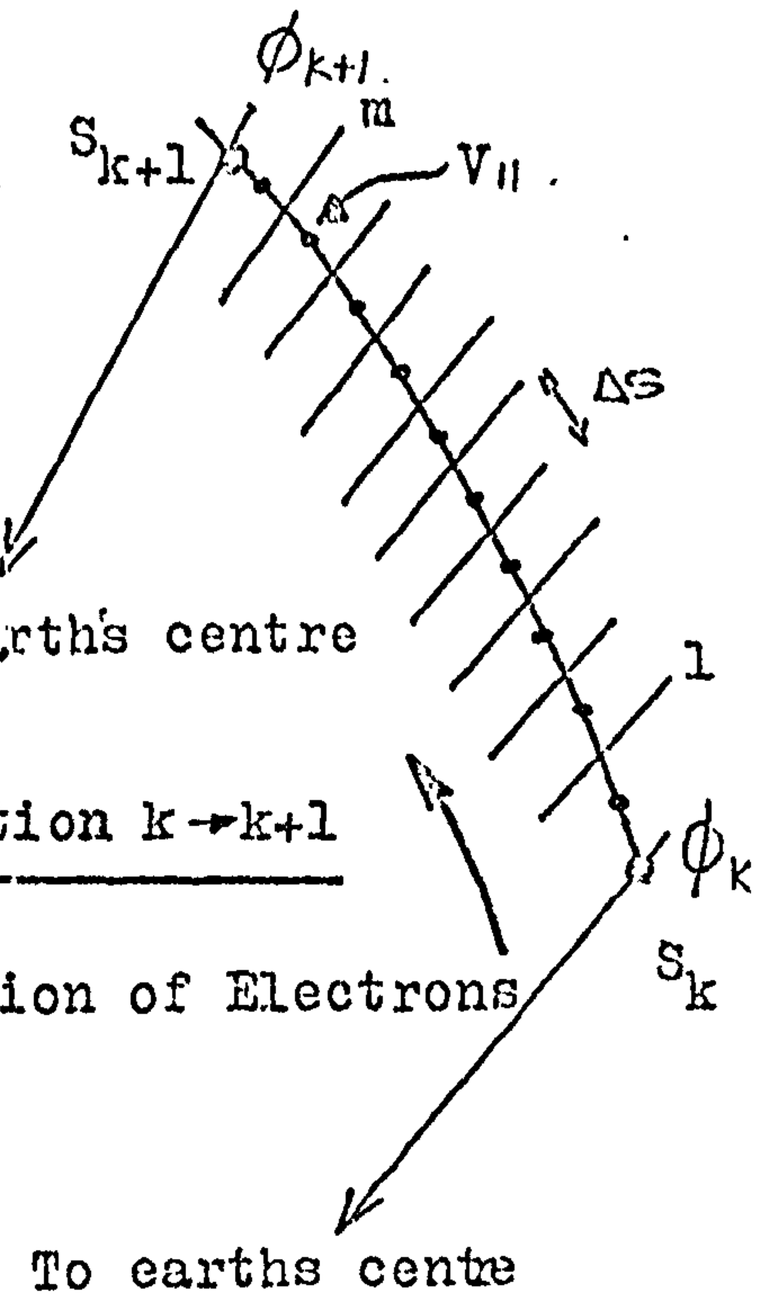

Section k → k+1

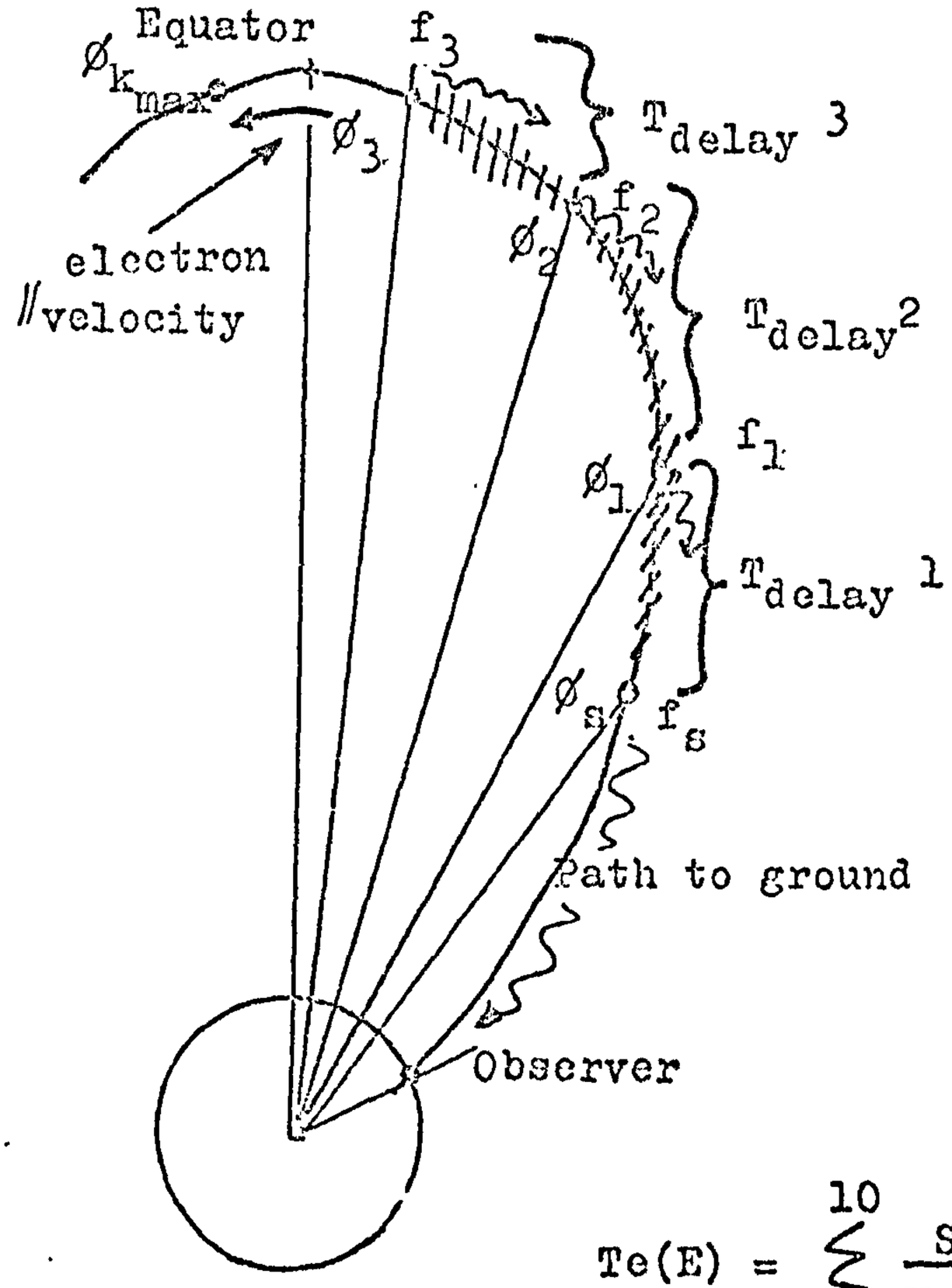

$$Te(E) = \sum_{1}^{10} \frac{S}{V_{||}} \qquad \text{for each section}$$

$$Te(E,\phi_k) = \sum_{1}^{k} \left[\sum_{1}^{10} \frac{S}{V_{||}} \right] \text{ to the k th point.}$$

Fig (7.6)

7.2 (Contd)

Thus
$$T_{g(f)} = \sum_{n=1}^{n_{max}} \Delta s/v_g \qquad (7.2.8)$$

As $n_{max} \to \infty$, $\Delta s \to ds$ and $T_{g(f)} \to \int_{TRAC} \frac{1}{v_g} .ds$

The accuracy of the numerical integration may be checked by observing the difference between $T_{g(f)}$ with ϕ = 2 milli radian and with say ϕ = 1/10 milli radian. The difference tends to zero and the summed value of $T_{g(f)}$ tends to the integral value as n_{max} is increased. Thus a stated accuracy for $T_{g(f)}$ results in a particular n_{max}. For an accuracy of better than 0.1% n_{max}=500 when TRAC covers the path from the equator to the ground. In similar integrations Sagredo (1971) used an interval of 1 milli radian.

ϕ_s is the starting angle and defines S_1, the cubic equation must be solved for the conditions at this point giving rise to an emission at frequency f and then the delay to the ground is calculated as indicated. Thus several thousand calculations are performed for each value of ϕ and by taking pains not to introduce unnecessary delays into the computer program it was found possible to calculate the emitted frequency every 1^o along the field line without incurring long run times of greater than 100 sec CPU time.

As each new point ϕ_k is considered the electrons have taken a time $T_{e(E)}$ (as $v_{//} \propto E$) to get there from ϕ_s. Now $v_{//}$ also depends upon the pitch angle of the electron which of course varies with position along the field line. Therefore in order to establish $T_{e(E)}$ to ϕ_k from ϕ_s we must perform another numerical integration, see Fig. 7.6. Using the same interval criterion as for the group velocity integration we see that it is possible to split up each 1^o interval into m parts where m=10.

HALLEY BAY $\phi_o = 60 \cdot 15$ $L \approx 4$ $f_{h_o} = 12 \cdot 2$ KHz

$f_{n_o} = 212$ KHz

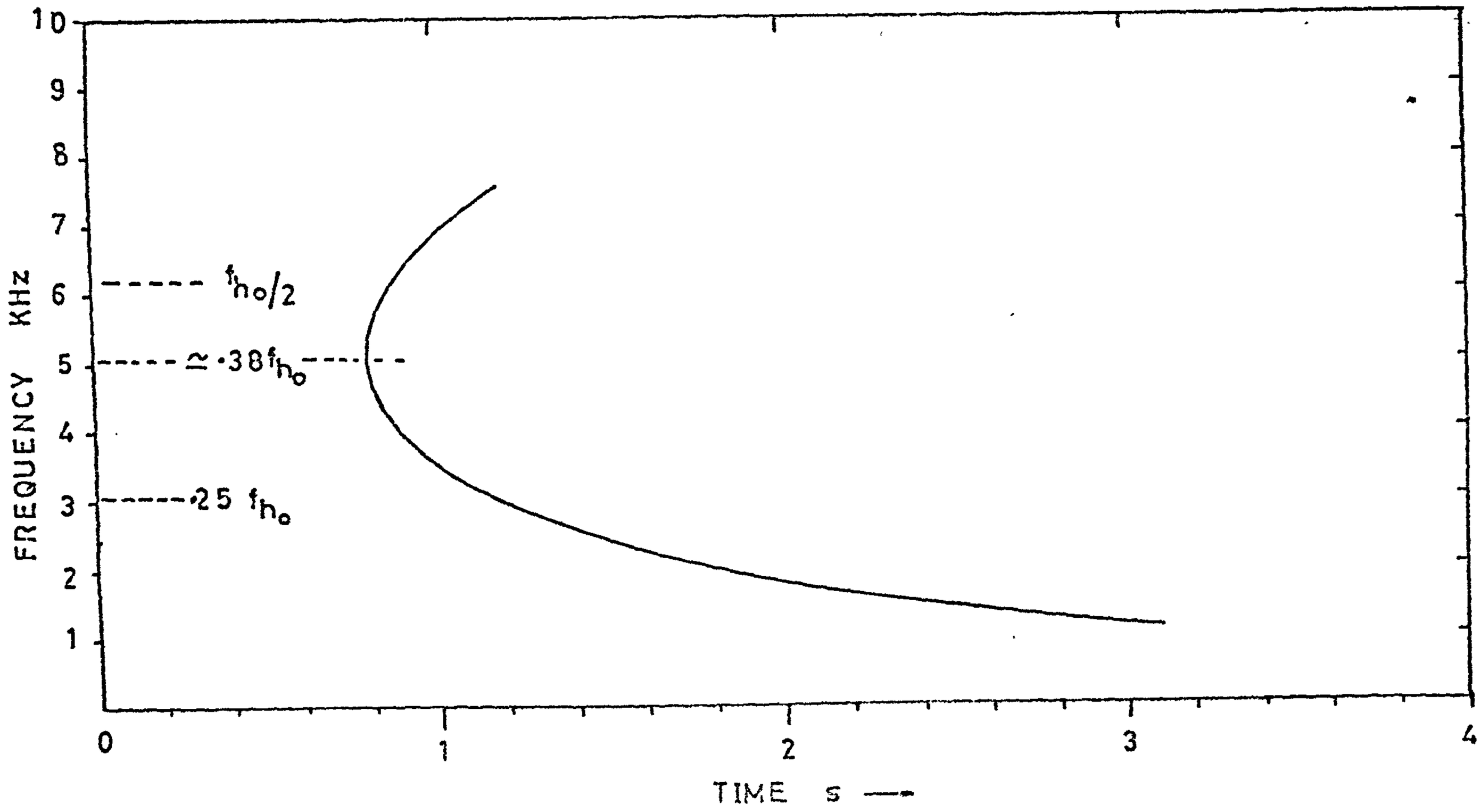

FIG(7.7)

7.2 (Contd)

Now $v_{\parallel}$ is given by equation (7.1.5) and the expression for $T_e(E,\phi_k)$ is given in Fig. 7.6. Again it is clear that several thousand calculations of position, electron parallel velocity, gyro-frequency and plasma frequency have to be made as the emission generation region travels into the other hemisphere. However the computing is minimised by accumulating electron travel time delays $T_{delay\ 1}$ T_{delay2} etc as the generation region moves from ϕ_1 to ϕ_2 etc so that only the additional delay is calculated each time. Program P90SUPERDOWDEN incorporated the features which have been discussed and a logic flow chart is given in appendix A2.3.

As the generation region crosses the geomagnetic equator frequencies from f_{min} up to some value $f_{k_{max}}$ will be produced. The group delay from the equator to the ground must be calculated for each frequency as part of the observed delay $T_{g(f)}$. The values of the time delays from the equator $T_{eq(f)}$ are the half hop whistler times and it is possible to construct a theoretical whistler which could be generated by dispersion of an impulse along the field line concerned. This is useful as whistlers are sometimes observed with hooks and other emissions and indicate the presence of a duct along which the hooks etc may have been guided to the observer. As different magnetospheric electron density models may be included in the program it is possible to study the effect of their variation on whistler or electron cyclotron emission profiles . The gyro-frequency model due to Smith (1960) and the $N_e \alpha R^{-4}$ approximation to the collisionless model, Eviatar et al (1964), quoted by Angerami (1966) were used to generate hooks and whistlers which would be observed on the ground at S.Uist L =3.4 and Halley Bay L = 4 as VLF data was available from these sites for comparison.

7.3 RESULTS CALCULATED USING THE CYCLOTRON THEORY

As stated $T_{eq(f)}$ is calculated as part of the overall group delay $T_{g(f)}$ and if it is plotted against frequency f we have a whistler profile. An example is given in Fig. 7.7 of a whistler that would be received at Halley Bay (Antarctica) if a duct exit existed immediately above the receiver. No attempt has been made to include corrections for dispersion below 1000 km level which would be incurred during the emergence of the emission from the duct. For completeness it is given as $T_i = \frac{D(\text{ionosphere})}{f^{\frac{1}{2}}}$, Dowden (1962)

or from Angerami (1966) $T_i = 6 / f^{\frac{1}{2}}$ for a typical medium latitude ionosphere.

In Fig. 7.7 the familiar shape of a nose whistler can be seen and the effect of the numerical integration of the group velocity $v_{g(f)}$ along the field line is clear. Taking equation (7.2.7) for group velocity as a function of f with parameters f_h and f_n, and putting it in the form;

$$v_g = K f^{\frac{1}{2}}(f_h - f)^{3/2} \qquad (7.3.1)$$

then differentiating the above equation we have ;

$$\frac{dv_g}{df} = k f^{\frac{1}{2}}(f_h - f)^{\frac{1}{2}} \left[\frac{(f_h - f)}{2f} - \frac{3}{2}\right] \qquad (7.3.2)$$

and setting (7.3.2) equal to 0 we have ; $f_h = 0$, $f = 0$ & $f_h - f = 3f$ giving the equality when $f = 0.25\ f_h$. Setting the second differential to zero shows that v_g is a maximum when $f = f_h/4$. The time delay due to dispersion is a minimum for $f = f_h/4$. The effect of integrating the minima along a field line is to push the value up to about $0.38 f_{ho}$ for a gyro-frequency model and to $0.4 f_{ho}$ for a collisionless model,

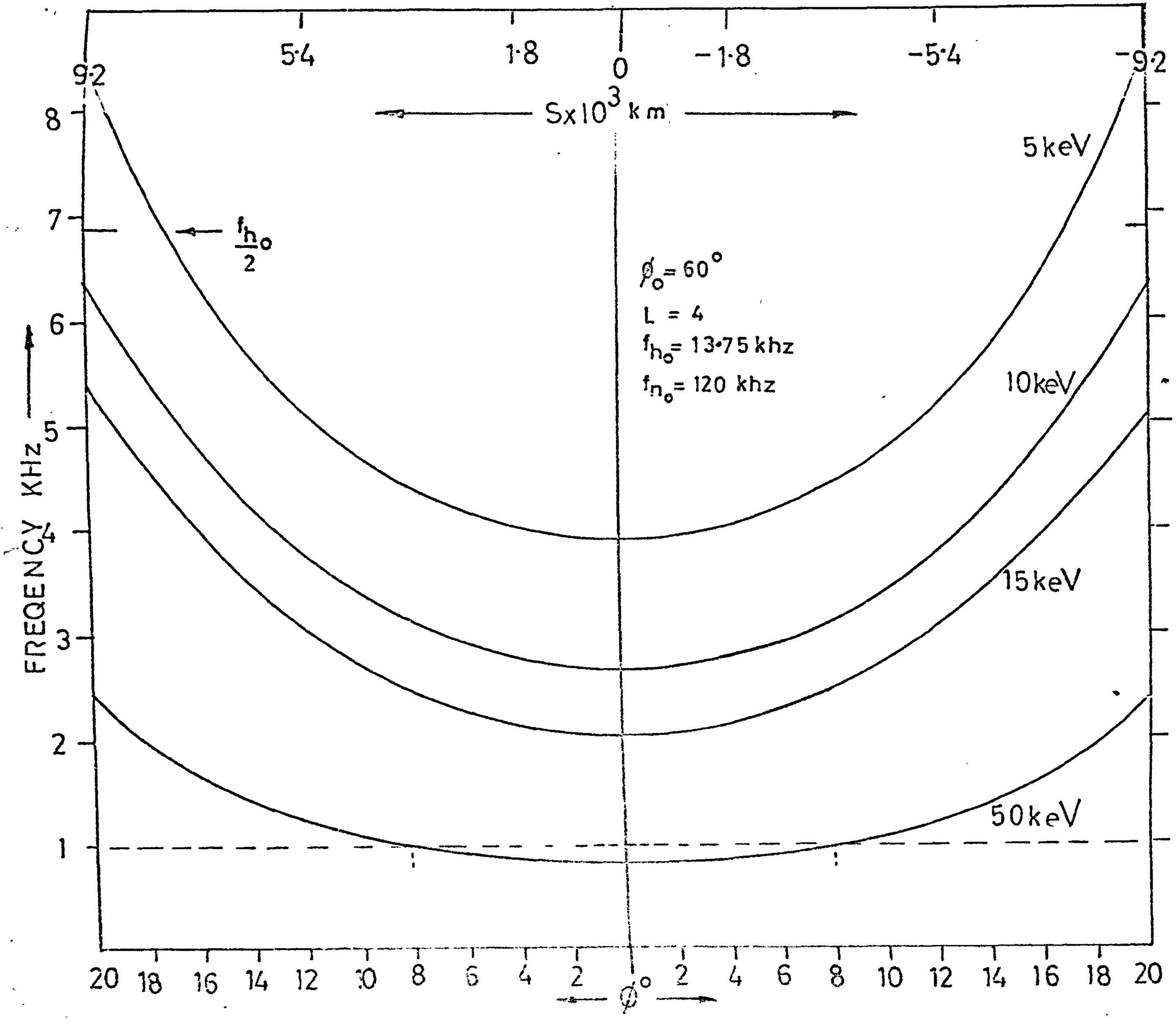
9·2
5·4
1·8
0
−1·8
−5·4
−9·2
S x 10³ km
8
7
6
5
4
3
2
1
FREQENCY KHz
$\frac{f_{h_o}}{2}$
$\phi_o = 60°$
L = 4
f_{h_o} = 13·75 khz
f_{n_o} = 120 khz
5 keV
10 keV
15 keV
50 keV
20 18 16 14 12 10 8 6 4 2 $\phi°$ 2 4 6 8 10 12 14 16 18 20

FIG(7·8)

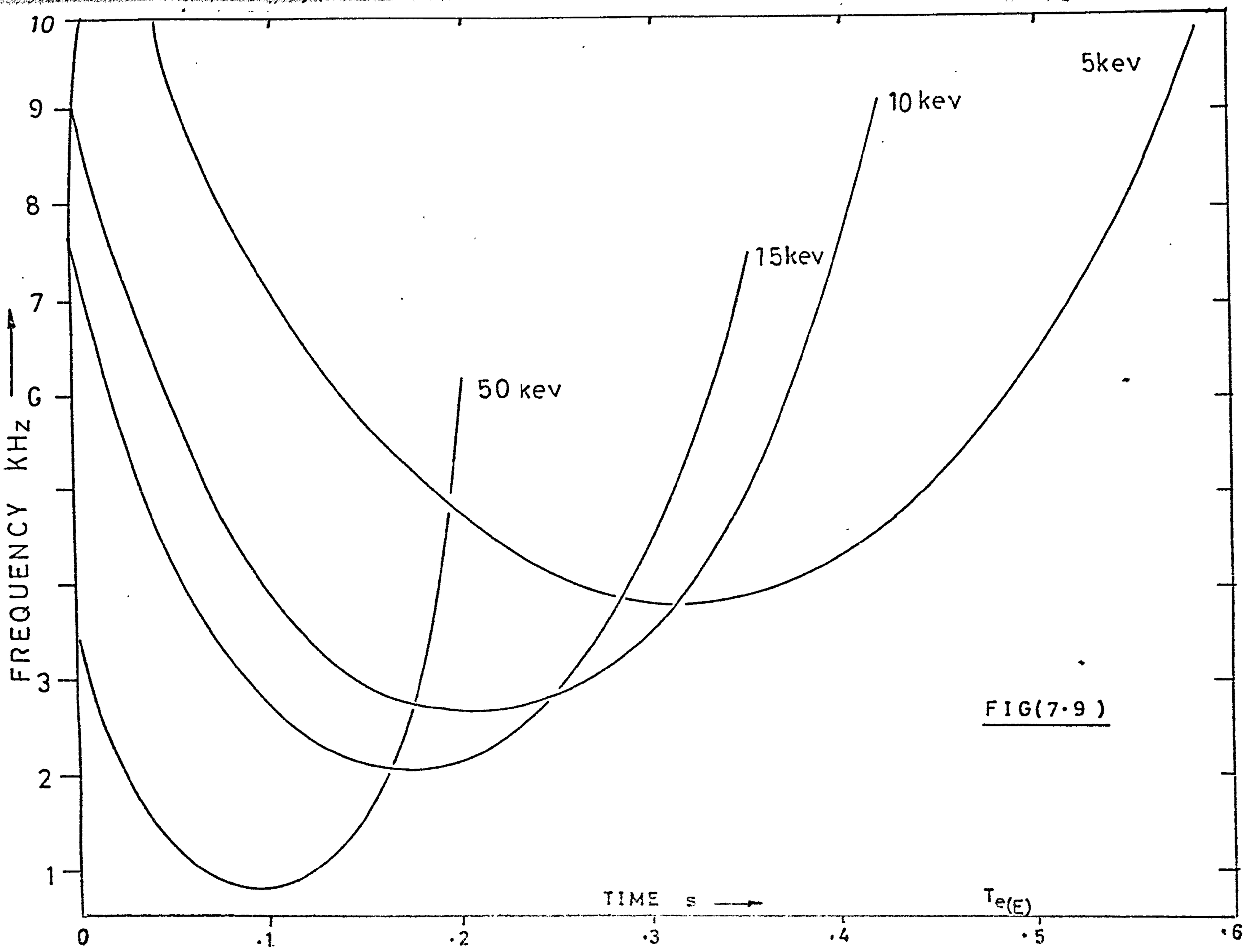
10
9
8
7
6
3
2
1
FREQUENCY KHz
5kev
10 kev
15kev
50 kev
TIME s
$T_{e(E)}$
0
.1
.2
.3
.4
.5
.6

FIG(7·9)

7.3 (Contd)

Helliwell (1965). A detailed discussion is to be found in Sagredo (1971) where graphs of f_{nose}/f_{ho} are given as a function of L value for a variety of electron density models. It is sufficient here to point out that the ratio lies between .35 and .45 for most models over L =2 to 5. The value of $f_{ho}/2$ is shown in Fig. 7.7 and given as a guide to the highest frequencies which would normally be observed in a real whistler. The effectiveness of a duct is reduced as the wave frequency f exceeds $\frac{1}{2}$.local gyro-frequency f_h and some of the energy is lost resulting a weak emission. Whistlers and other emissions are observed to 'cut off' at $f_{ho/2}$ as this represents the minimum gyro-frequency which is encountered during propagation to the ground. The figure may be compared with whistlers received at Halley Bay shown in Fig. 1.4. Here the nose frequencies are rather less than 5 KHz and the cut off frequencies are less than 6 KHz indicating that these whistlers propagated along field lines at higher geomagnetic latitudes than Halley Bay. The similarity between the calculated and observed emissions is good and as stated the availability of a theoretical whistler along with a hook or other emission can help in the interpretation of calculated results.

Turning now to the calculation of the frequency-time profiles of hooks etc in Fig. 7.8 we see the observed Doppler shifted emitted frequency as a function of geomagnetic latitude along a field line at L=4 for various electron energies. It is obvious that the curve is symmetrical about the equator and that the higher energy particles produce lower frequency signals. The agreement between the curves in Fig. 7.8 and those in Fig. 7.2a which were produced by Dowden is good. If we plot the emitted frequency against the electron travel time delay (ignoring the dispersion delay) Fig. 7.9 we have the emission profile which would be seen by a succession of stationary observers as the electron bunch passes. It is clear that the delays $T_{e(E)}$ are almost an order of magnitude less than $T_{g(f)}$ and that the observed profiles which are given in Fig. 7.10 are produced almost exclusively by distortion of the curves in Fig. 7.8 due to dispersion in the magnetospheric medium. The emissions in Fig. 7.10 compare well with those produced by Dowden in Figs 7.2b (a) through (e).

FIG (7.10)

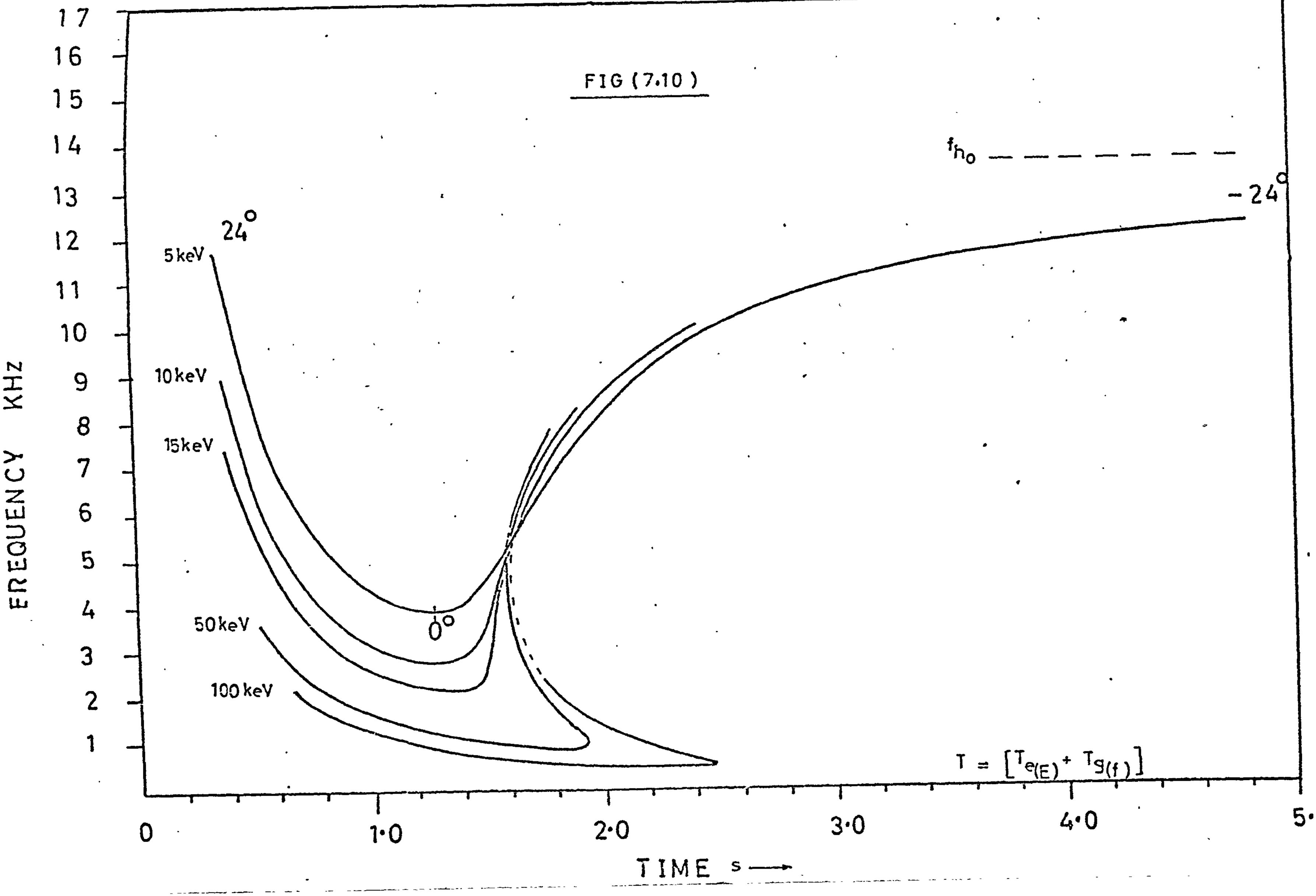
FREQUENCY KHz
17
16
15
14
13
12
11
10
9
8
7
6
5
4
3
2
1
f_{h_o}
24°
-24°
5keV
10keV
15keV
50keV
100keV
0°
$T = [T_{e(E)} + T_{s(f)}]$
0
1·0
2·0
3·0
4·0
5·0
TIME s ⟶

7.3 (cont'd)

Hooks which would be received at S. Uist, Halley Bay and Andøya from electron bunches with energies from 1 keV to 50 keV were calculated for gyro-frequency and R^{-4} models. Some examples of results are given in Fig. 7.11. The equatorial electron density data for the different locations was taken from Sagredo (1971) and the emissions were tacked usually from $+10^{o}$ to -20^{o}, that is from 10^{o} inside the observer's hemisphere to 20^{o} into the other hemisphere.

It is interesting to compare some of the calculated forms with actual profiles, Helliwell & Carpenter (1961), cited by Dowden (1962) which are given in Fig. 1.9. Fig. 7.11a is similar to events (B) & (C) in Fig. 1.9. Fig. 7.11b is similar to event (A) whilst Fig. 7.11c is like event (E) or (I) in Fig. 1.9. If a section of Fig. 7.11c is taken from the equator to about -10^{o} the result is not unlike risers recorded at S.Uist in Fig. 1.7. The profile in Fig. 7.11d is comparable with events (D) or (H). It is not the purpose here to draw accurate comparisons between emissions generated by Dowdens backward radiated Cyclotron oscillator model and real emissions but rather to demonstrate that the theory does produce profiles which have some of the characteristics of observed emissions. In fact the theory was recognised by Helliwell (1967) as being the limiting case of the second order transverse resonance mechanism which he suggested.

It is interesting to compare the calculated emissions shown in Fig. 7.11(e) and (f) for Andøya with an observed profile which is given in Fig. 1.8. If we confine our interest to the frequencies generated from the equator to about -10^{o} (where $f \simeq f_{ho}/2$) we see that the forms are quite similar, starting at about 1 KHz and rising to $\frac{f_{ho}}{2}$ in about 1 sec.

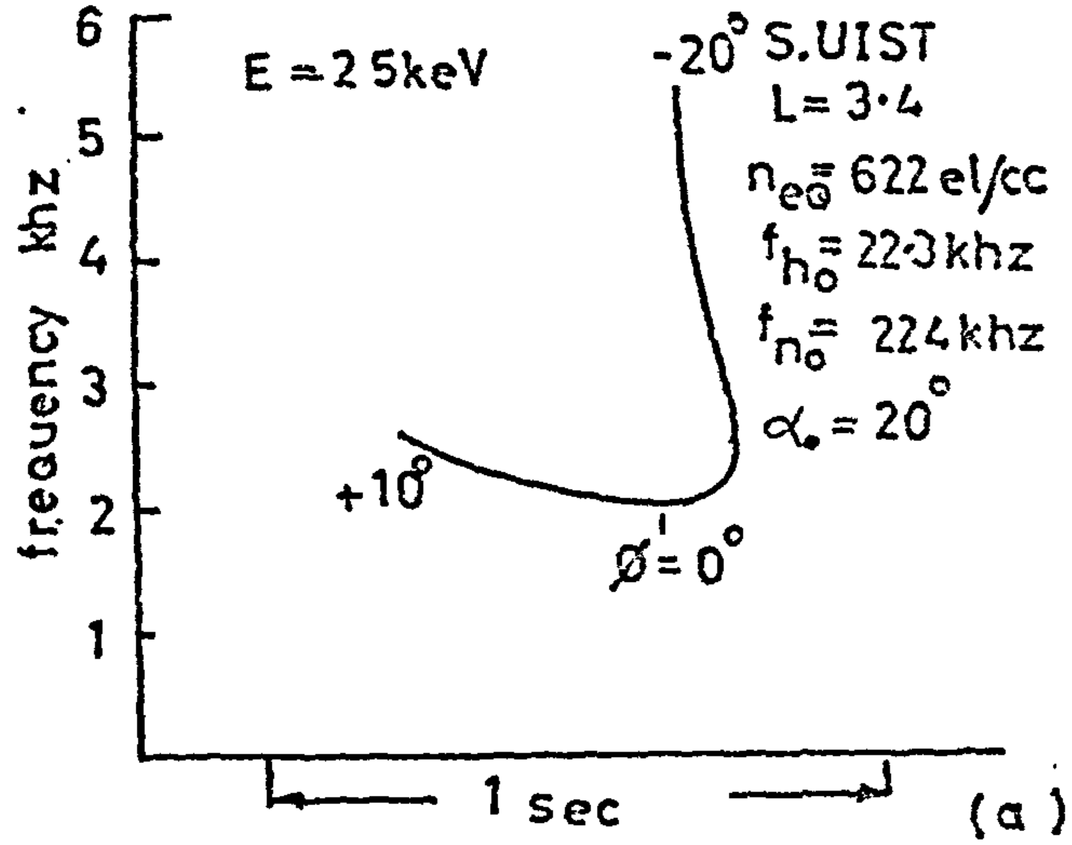

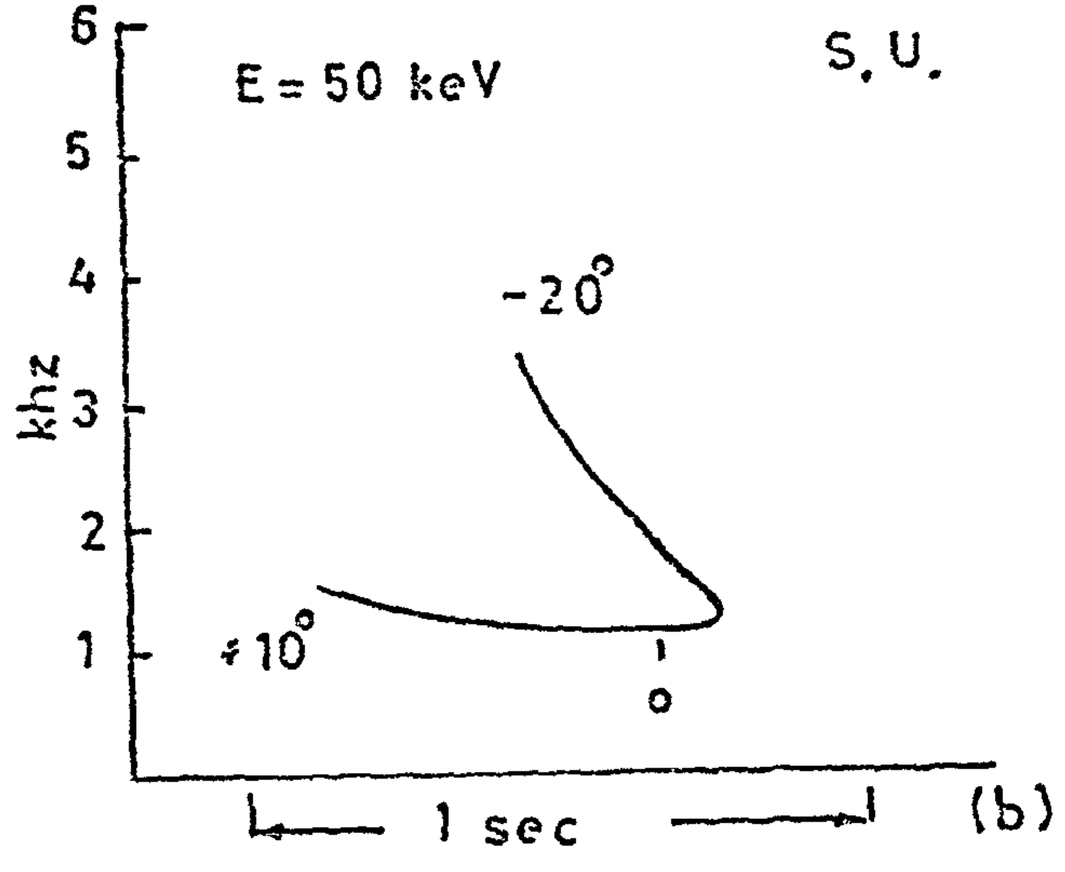

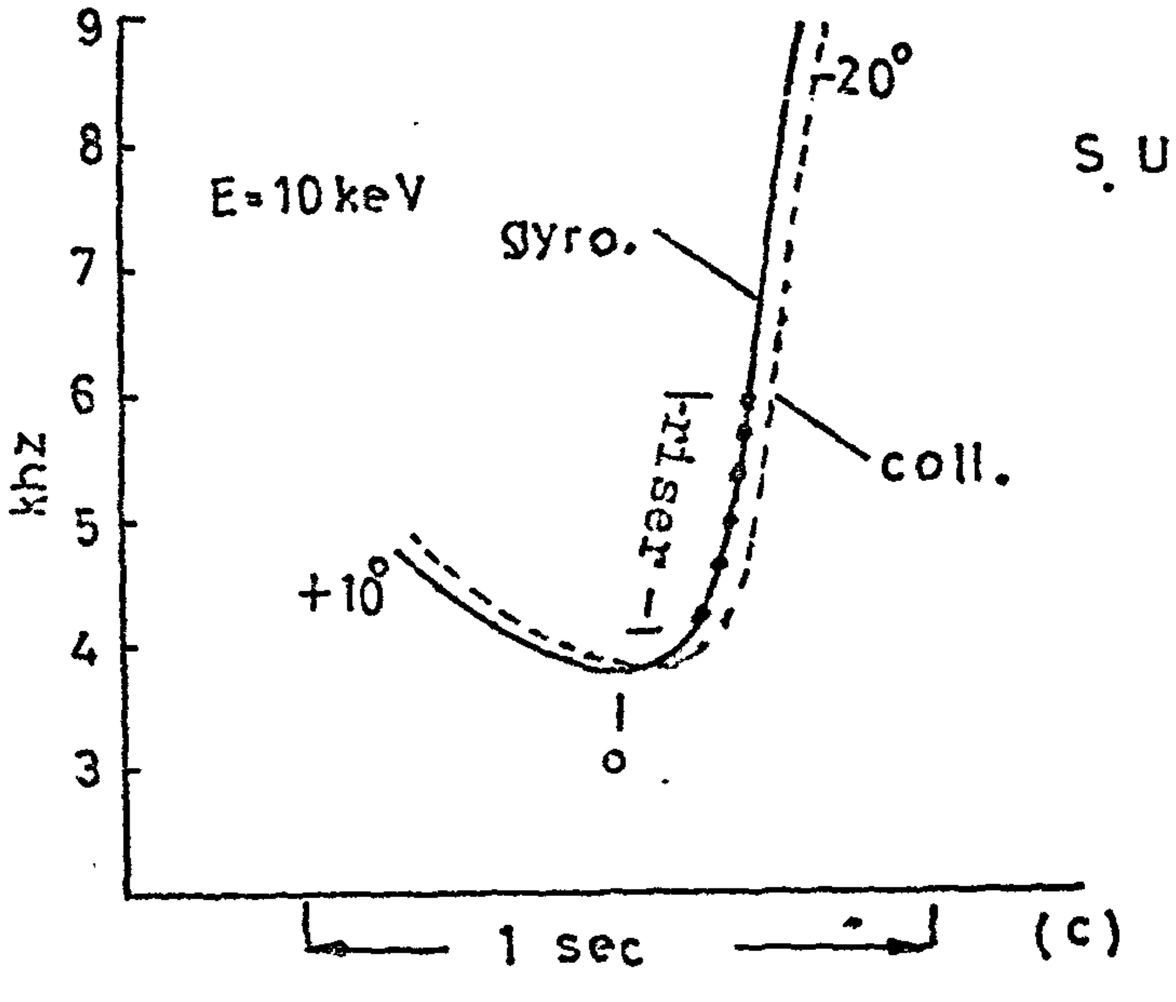

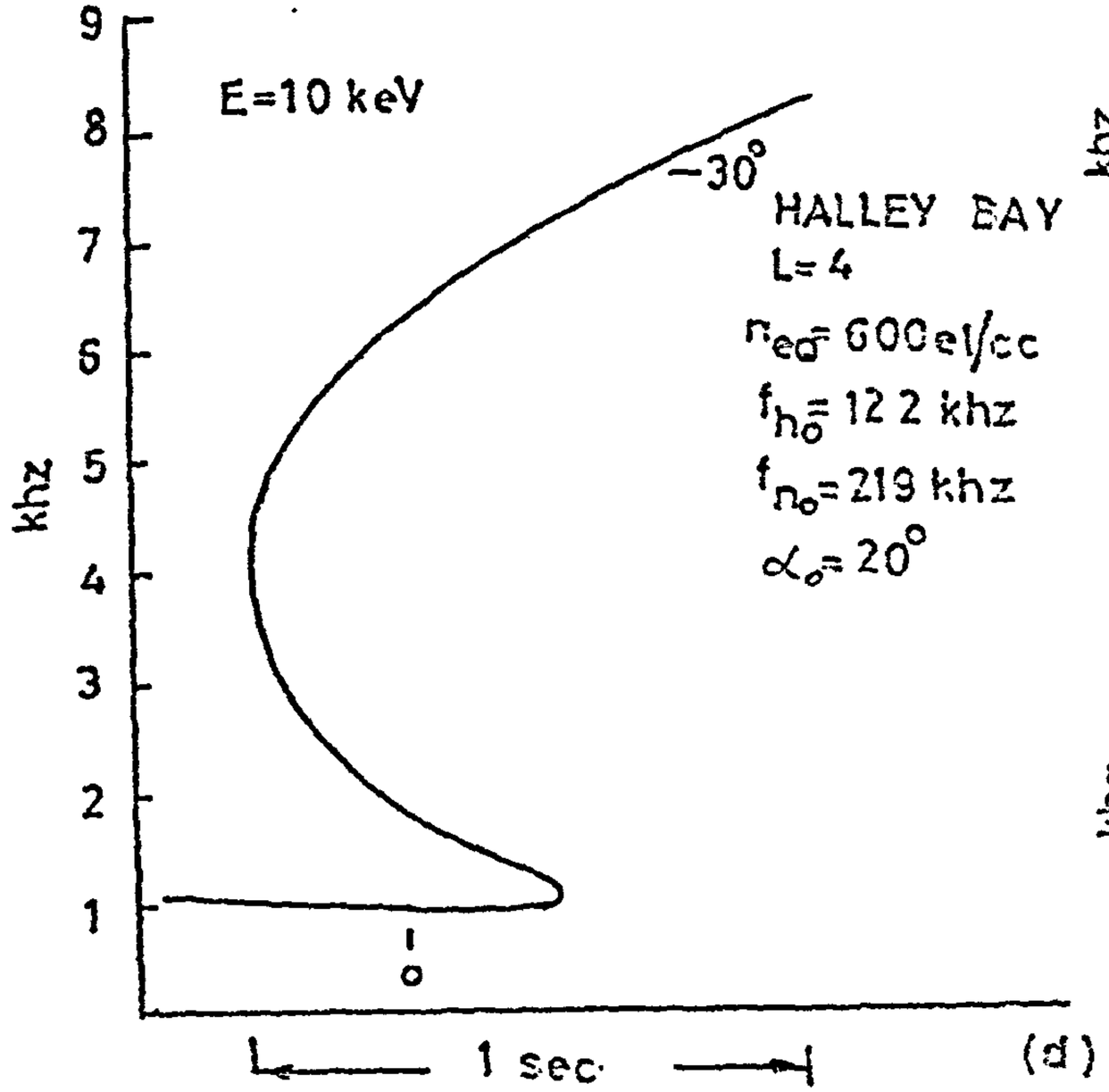

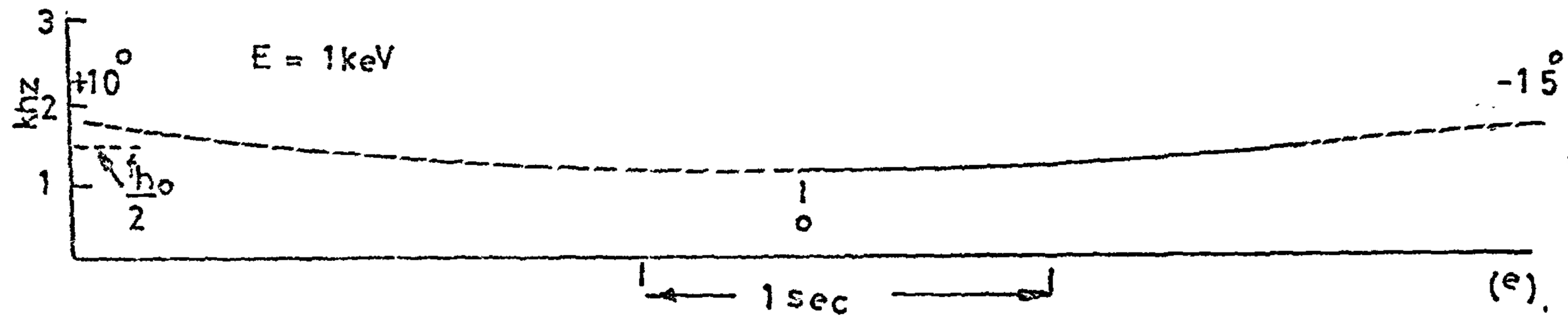

ANDØYA L = 6·4
f_{h_o} = 2·8 khz
f_{n_o} = 40 khz

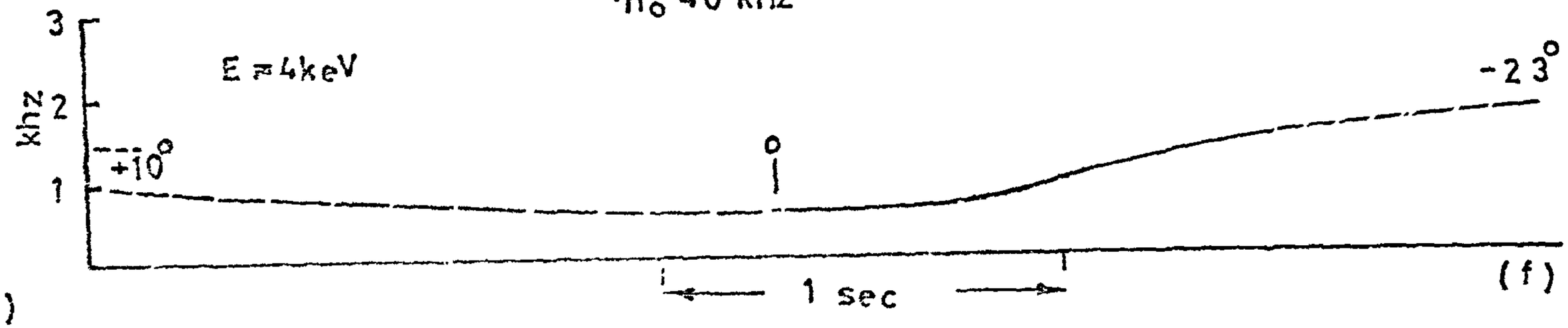

FIG (7·11)

7.3 (Contd) It is clear however from the inability of the thoery to explain man made triggering of emissions and the time lapses between successive triggering of emissions by reflected whistler mode signals that it is not a satisfactory generation mechanism. The theory proposed by Helliwell (1967) which was referred to in section 6.8 involved a generation mechanism that does not require particle bunches and can explain emission characteristics such as those mentioned above. Before proceeding to report the application of this theory to actual emissions it is necessary to discuss it in some detail.

CHAPTER 8

THE GENERATION OF VLF EMISSIONS BY THE TRANSVERSE RESONANCE INSTABILITY

8.1 THE TRANSVERSE RESONANCE INSTABILITY

Brice (1963) suggested that VLF narrow band emissions could be generated by energetic electrons and whistler mode waves by transverse resonance when the Doppler shifted wave frequency equals the electron gyrofrequency. Although similar to the theory advanced earlier by Dowden it differs in that it depends on feedback between the backward travelling waves and the forward travelling electrons. It does not require the existence of electron bunches and enables emissions to be generated at a fixed point along a field line giving rise to a constant tone.

Consider a plane circularly polarized wave propogating along a magnetic field line in a uniform plasma. Assume that energetic electrons are spiralling towards the wave with parallel and perpendicular velocity components $v_{\parallel}$ and $v_{\perp}$. The quantitative effects of the electric and magnetic fields of the wave on the electrons are complex Nunn (1971) however, a simplified physical picture can be given. Hansen (1963) considered the action of the waves electric field on the transverse velocity of the electrons and concluded that they would become 'phase bunched'. Brice (1963) quotes Stix (1963) as demonstrating that the phase change of $v_{\parallel}$ with respect to $\underline{E}$ or $\underline{B}$ of the wave due to effects of $\underline{E}$ are second order whilst that due to $\underline{B}$, if the particles have significant $v_{\perp}$ is first order.

Static Frame

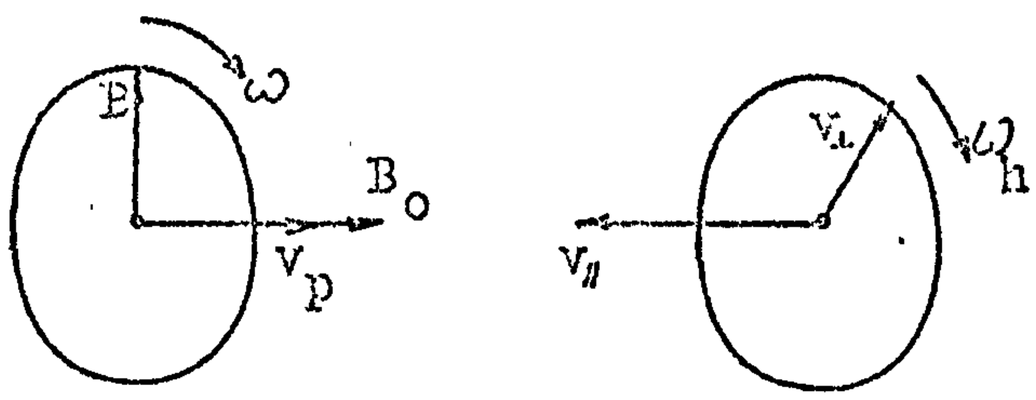

Moving Frame

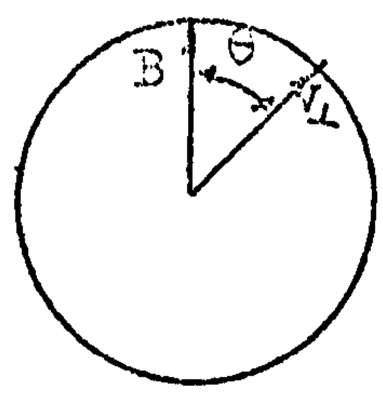

(a)

Wave ——→ ←—— electron $V_{\parallel} = (\omega_h - \omega)/k$

moving frame

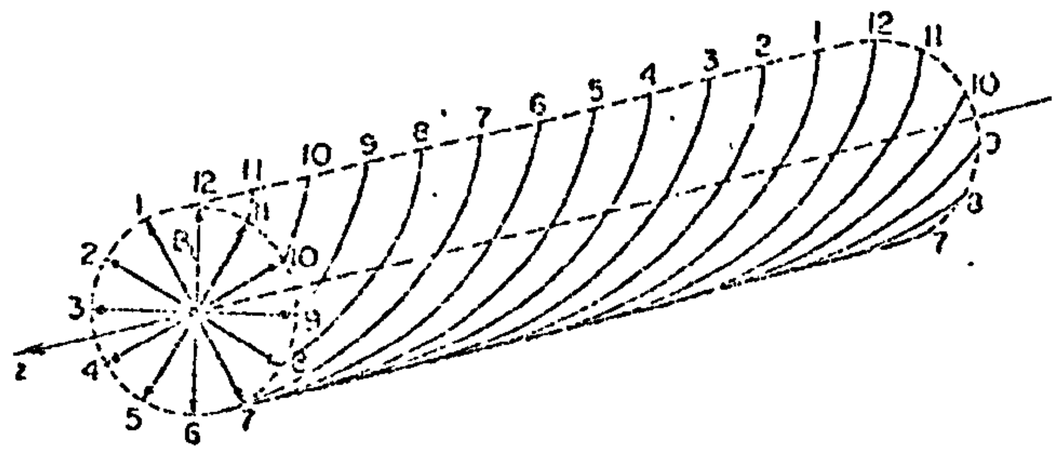

(b)

moving frame

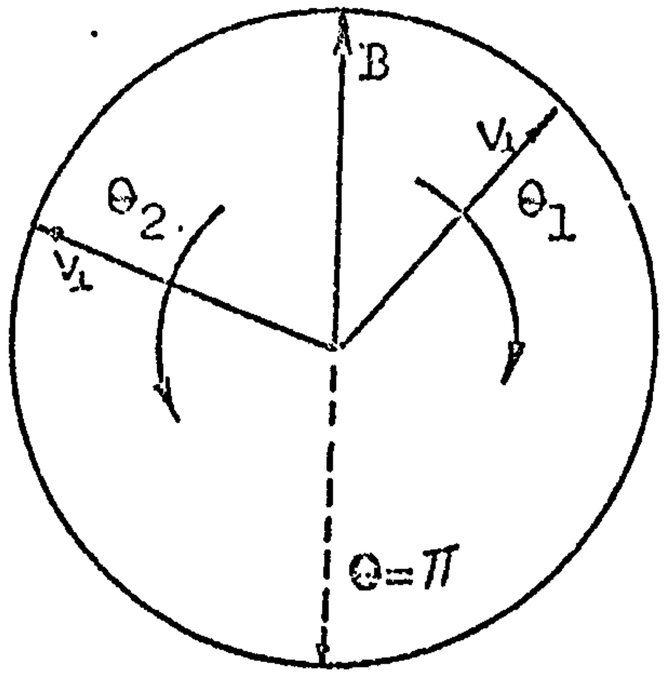

(c)

moving frame

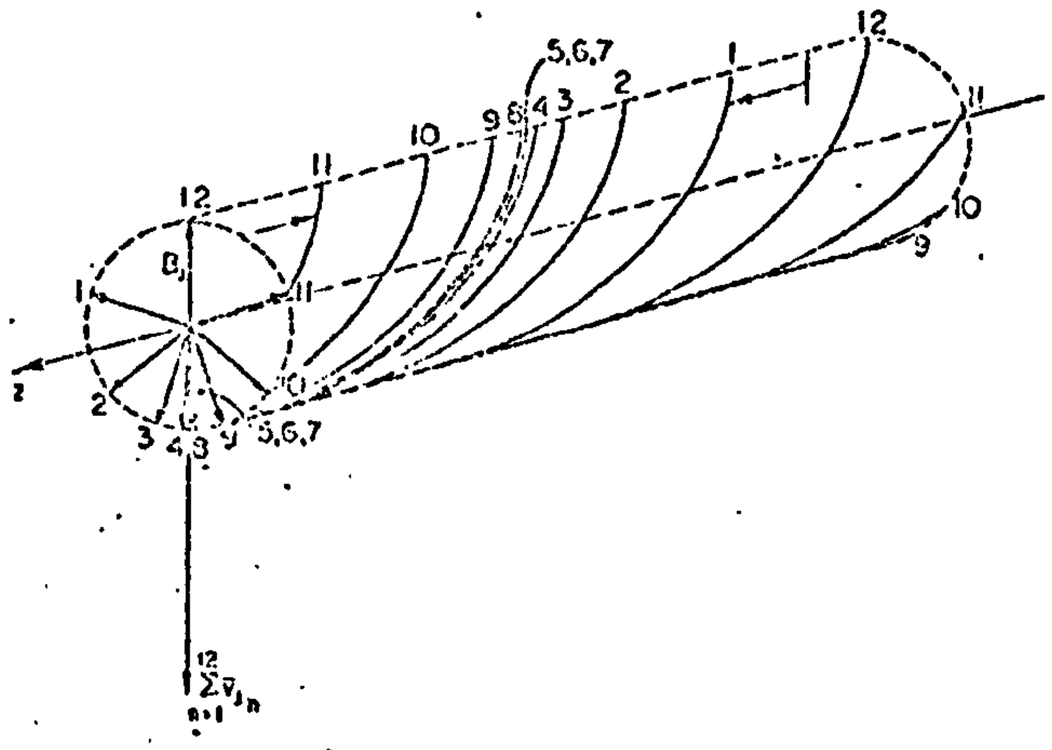

(d)

Fig 8.1

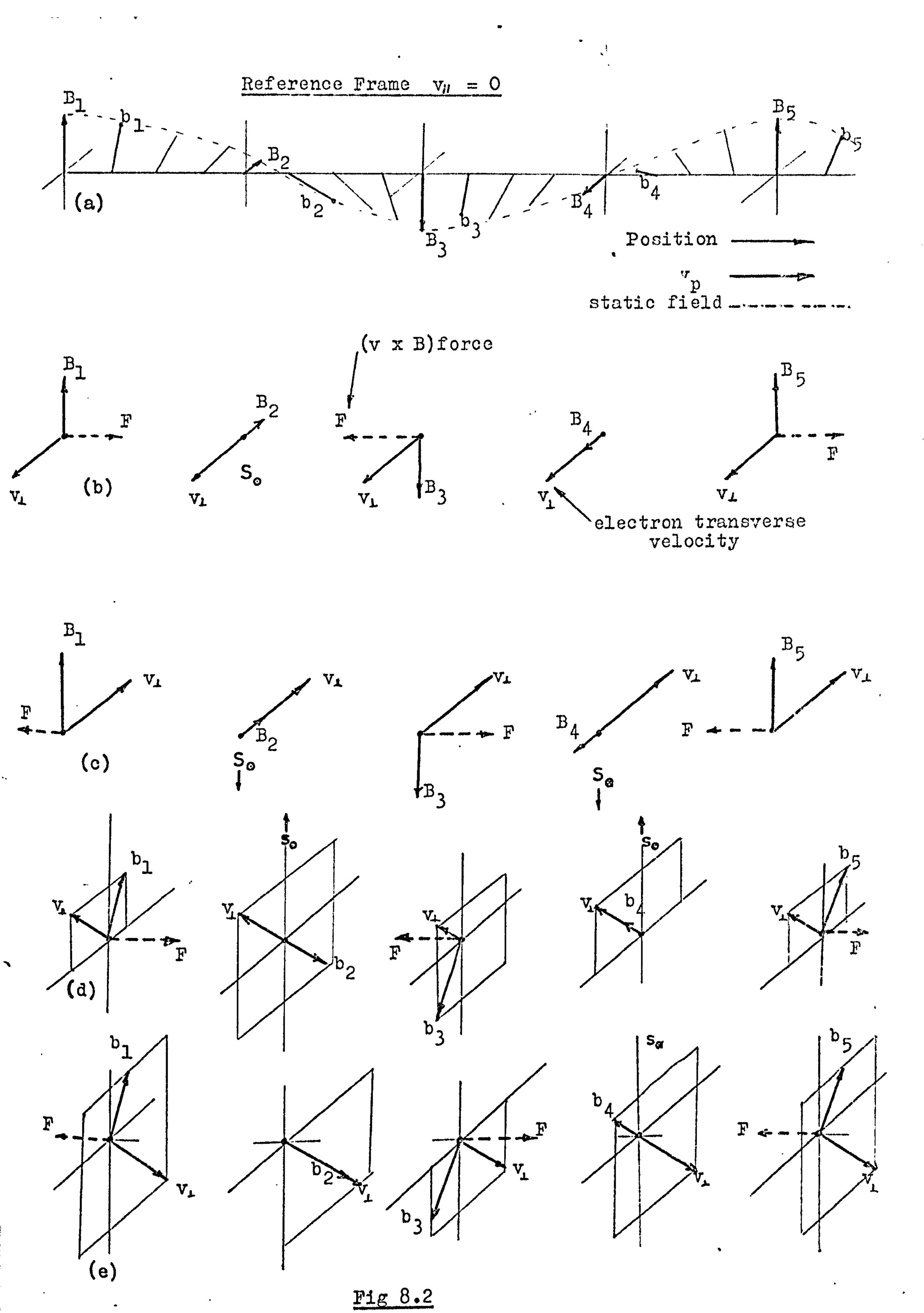
Reference Frame $v_{\parallel} = 0$
B_1
b_1
B_2
b_2
B_3
b_3
B_4
b_4
B_5
b_5
(a)
Position
v_p
static field
(v x B) force
F
$v_\perp$
S_o
(b)
(c)
(d)
(e)
electron transverse velocity

Fig 8.2

8.1 (cont'd) The situation may be viewed as in Fig. 8.1a for an electron which is in gyro-resonance with the wave. We see that in the frame of reference of the gyrating electron $v_\perp$ is at some fixed angle Θ with respect to $\underline{B}$. For a random distribution of phase angles of electrons the net transverse velocity is small, the transverse current is small, the intensity of the radiated wave is small, and the process is said to be incoherent. If we take a symmetrical distribution of phase angles about $\underline{B}$ after Helliwell & Crystal (1973) the situation is shown in Fig. 8.1b. What follows is an attempt to show how this distribution of phase angles may be changed by the action of the wave magnetic vector $\underline{B}$ in order that it becomes assymmetrical with a resulting net transverse velocity and current as shown in Fig. 8.1d.

Consider a frame of reference in which $v_\parallel = 0$. The vectors $\underline{B}$ and $v_\perp$ rotate at the same rate and in the same sense. Fig. 8.2a shows the vector $\underline{B}$ as a function of distance in the moving frame for selected points. Consider points at which the magnetic vector is denoted by B_1 to B_5 (each 90^o) apart. If we assume that the electron transverse velocity is parallel to B_4 as shown in Fig. 8.2b, which is possible in a random distribution, then we see that the electron experiences a longitudinal ($\underline{v_\perp} \times \underline{B}$) force resulting in a shift of the spiralling electron such that $v_\perp$ is anti-parallel to $\underline{B}$. The vector $v_\perp$ drifts in the moving frame to a stable position S. Fig. 8.2c shows the same phase organisation taking place at a different point (when the direction of $v_\perp$ is reversed) this being $S_\oplus$ rather than $S_\odot$.

In the moving frame the phase bunching is seen as the confining of transverse velocities with phase angles Θ to $\overline{B}$ to $\Theta = \Pi$,

8.1 (cont'd) see Fig. 8.1c, or after a limited time T secs the redistribution of phase angles as in Fig. 8.1d. The net transverse current due to the phase bunching produces radiation which can organise the phases of new incoming electrons and the process can be continued.

The radiation is self sustaining and the 'backward wave oscillator' can be located at a point on a field line. The triggering of narrow band emissions by man made signals is also explained by this generation mechanism.

In the simple treatment of transverse resonance instability the effect of the stimulated radiation on the particles is not considered as only a very small part of the kinetic energy of each electron is exchanged with the wave during the interaction. Helliwell & Crystal (1973) show that for a representative electron with an initial energy of 2.9keV and pitch angle of 30^{o} which is exposed to a wave electric field of 30μV/m the energy change is 14 eV. Accordingly the electron gains or loses no more than 5×10^{-3} of its available energy.

This energy change does however have a significant effect on the pitch angle distribution of the electrons and for the above case the pitch angle is modified by 2.4^{o}. It is then possible for transverse resonance interactions to preceipitate particles near the loss cone into the ionsphere at the opposite end of the field line to that at which the emission is observed.

8.2 THE 'SECOND ORDER' TRANSVERSE RESONANCE CONDITION

It was Hansen (1963) who pointed out that given a random distribution of electron velocities then only those whose rate of change of gyro-frequency was matched to that of the input whistler mode wave would be steadily affected such that phase bunching could occur to a significant degree. However, it was Helliwell (1967) who developed the idea into a formalised theory.

Helliwell states the 'consistent wave condition' or 'second order' resonance condition as being that the spacial variation of electron gyro-frequency and Doppler shifted wave frequency must be matched to ensure that the electrons and wave are resonating for the greatest possible time resulting in the maximum transfer of energy to the wave.

Assume that:

1) The propogation of generated waves is controlled by the ambient cold plasma.

2) The direction of propogation is along the static magnetic field.

3) Collissions are neglected.

4) The lateral extent of the interaction is large such that waves can be taken as being plane.

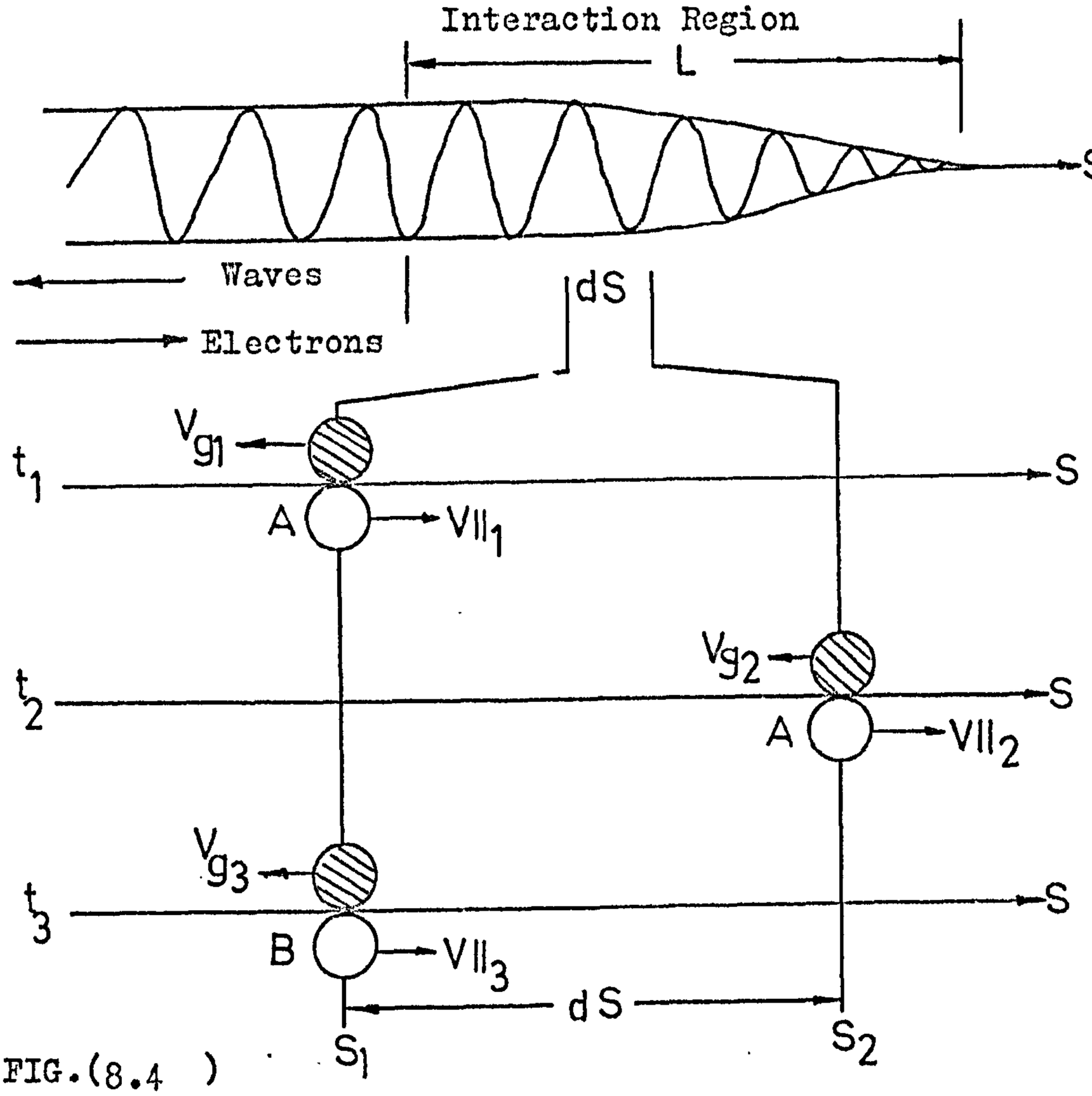
Interaction Region
L
S
Waves
Electrons
dS
V_{g1}
t_1
S
A
VII_1
V_{g2}
t_2
S
A
VII_2
V_{g3}
t_3
S
B
VII_3
dS
S_1
S_2

FIG.(8.4)

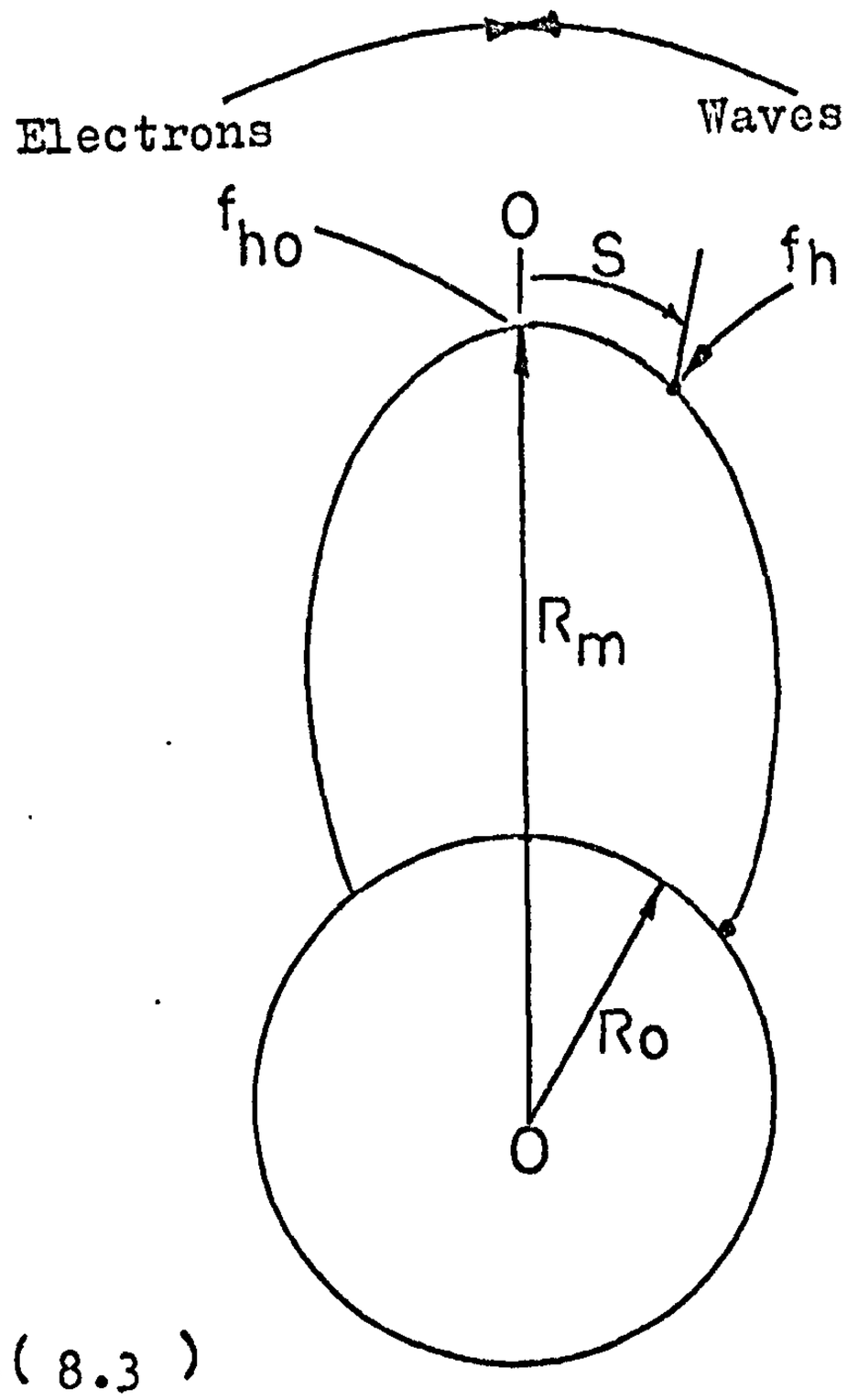
Electrons
Waves
f_{ho}
O
S
f_h
R_m
R_o
O

FIG.(8.3)

8.2 (cont'd) Consider a region surrounding a field line near the equatorial plane. Let S be the distance from the equator to the point of interaction in the direction of the steaming electrons. See Fig. 8.3.

For gyro-resonance the wave frequency is given by:

$$f = f_h \frac{v_p}{v_p + v_{//}} \qquad (8.2,1)$$

and its variation by:

$$df = f \frac{df_h}{f_h} + \frac{dv_p}{v_p} - \frac{f^2(dv_p + dv_{//})}{f_h v_p} \qquad (8.2,2)$$

If the path of propogation is assumed to be aligned with the earth's magnetic field and the refractive index of the medium is assumed to be much greater than unity then it can be shown Helliwell (1965) that the phase and group velocities of a wave are given by:

$$v_p = C f^{\frac{1}{2}} \frac{(f_h - f)^{\frac{1}{2}}}{f_n} \qquad (8.2,3)$$

$$v_g = 2C f^{\frac{1}{2}} \frac{(f_h - f)^{3/2}}{f_h \quad f_n} \qquad (8.2,4)$$

The variation of the phase velocity is:

$$dv_p = \frac{C}{2f_n} \cdot \frac{(f_h - 2f)df + f.df_h}{f^{\frac{1}{2}}(f_h - f)^{\frac{1}{2}}} \qquad (8.2,5)$$

8.2 (cont'd) From equations (8.3,1) & (8.3,3) it can be shown that:

$$v_{//} = \frac{c\ (f_h - f)^{3/2}}{f_n \cdot f^{\frac{1}{2}}} \qquad (8.2,6)$$

which is the gyroresonance condition used in the Dowden cyclotron theory, se equation (7.1,3).

Using (8.2,4) & (8.2,6) we have that:

$$v_g/v_{//} = 2f/f_h \qquad (8.2,7)$$

We have seen that there is an approximation for f_h in terms of S;

$$f_h = f_{ho}\left(1 + \frac{4.5\ S^2}{R_m^{\ 2}}\right) \qquad 8,2,8)$$

and its variation by;

$$df_h = \frac{9\ f_{ho}}{R_m^{\ 2}}\ SdS \qquad (8.2,9)$$

Also that

$$v_{//} = v\left[1 - \frac{f_h\ \sin^2\alpha_o}{f_{ho}}\right]^{\frac{1}{2}} \qquad (8.2,10)$$

and its variation is given by;

$$dv_{//} = -\frac{v_{//}}{2\ f_n}\ (\tan^2\alpha)\ df_h \qquad (8.2,11)$$

8.2 (cont'd) It is assumed that the interaction region is many wavelengths long and that within it the wave amplitude decreases from its maximum value to zero in the direction of the streaming electrons as shown in the upper part of Fig. 8.4. Below this an element of the interaction region has been shown at three instants of time t_1, t_2, and t_3.

At time t_1 and position S_1, a wave packet at frequency f_1 resonates with a group of electrons labelled (A) travelling to the right with velocity $v_{//\,1}$. When they reach position S2 they have a different gyrofrequency and a different streaming velocity $v_{//\,2}$ and therefore resonate with a <u>different wave packet of frequency f_2</u>. This wave packet travels back to S_1 where it resonates with a new group of electrons labelled (B) which is travelling to the right with velocity $v_{//\,3}$. An observer stationed at S_1 sees a frequency change f_2-f_1 in a time t_3-t_1. The frequency change df can be found in terms of the wave frequency and the parameters of the medium by substituting equations (8.2,5), (8.2,3), (8.2,6) and (8.2,11) into (8.2,2) giving;

$$df = \frac{3\lambda}{1+2\lambda}\left(1 + \frac{(1-\lambda)}{3}\tan^2\alpha\right) df_h \qquad (8.2,12)$$

and the elapsed time is given by;

$$dt = dS\left(\frac{1}{v_{//}} + \frac{1}{v_g}\right) \qquad (8.2,13)$$

$v_{//}$ and v_g are the average velocities between S_1 and S_2.

The rate of change of frequency is then;

Helliwell Results

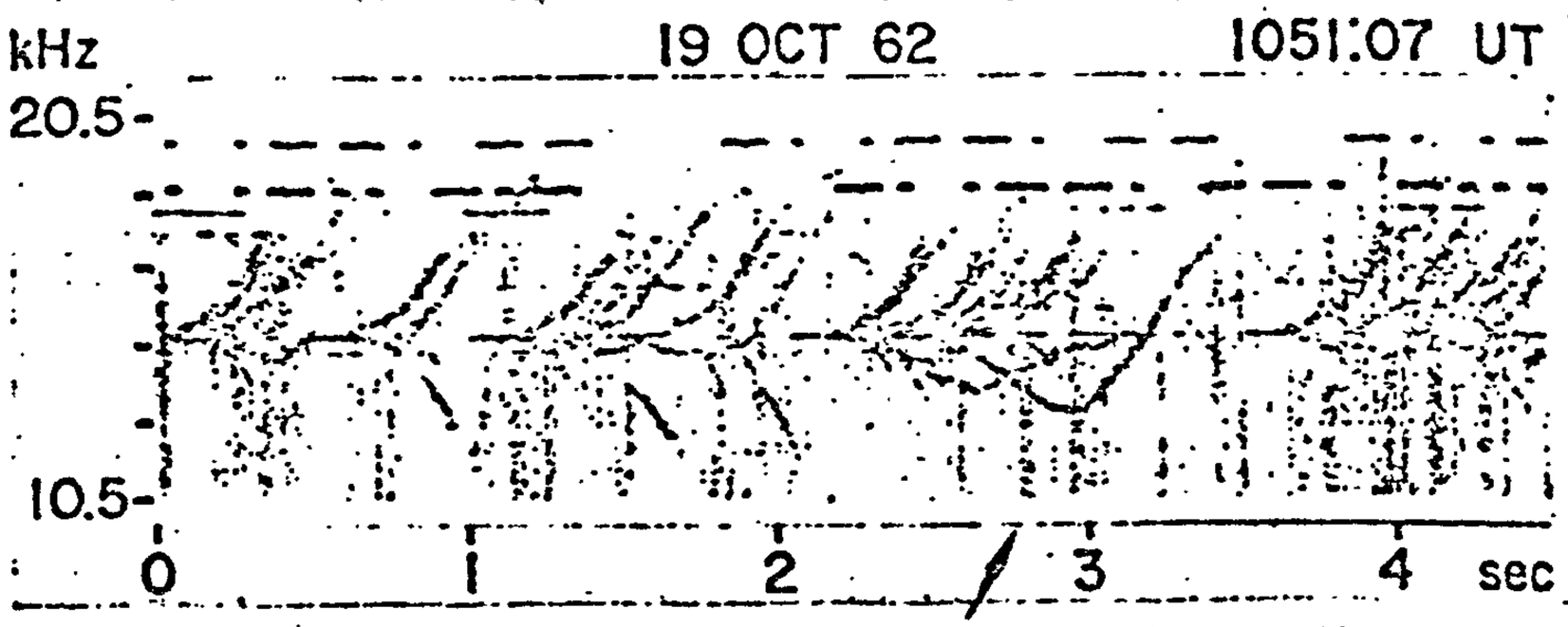

(a)

Spectrogram showing hook at 2.5 sec triggered by NAA on 14.7 khz and recorded on Oct. 19, 1962, at 10h 51m 07s UT (taken from Fig. 7-66c, *Helliwell* [1965].

(b)

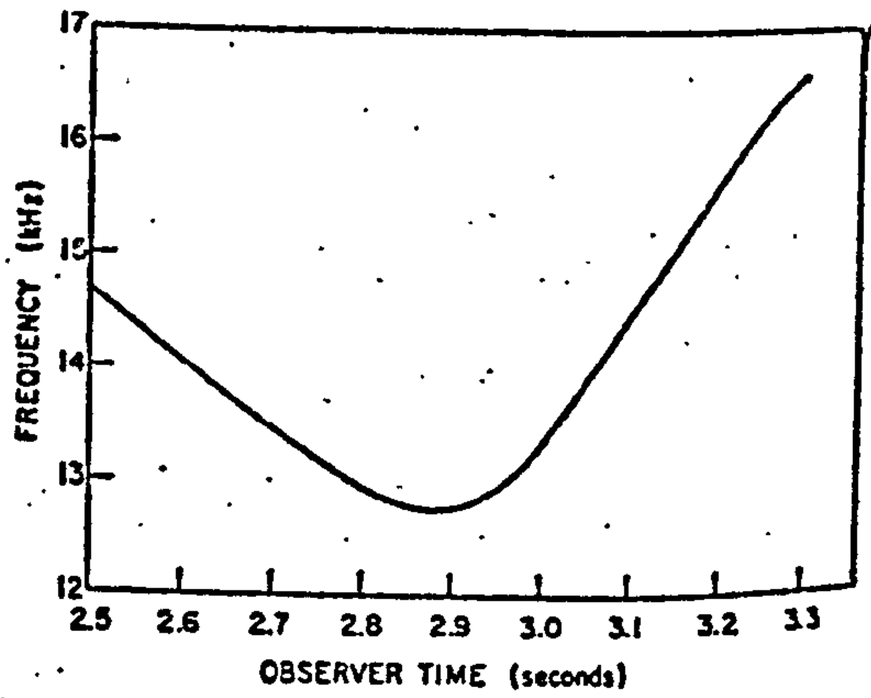

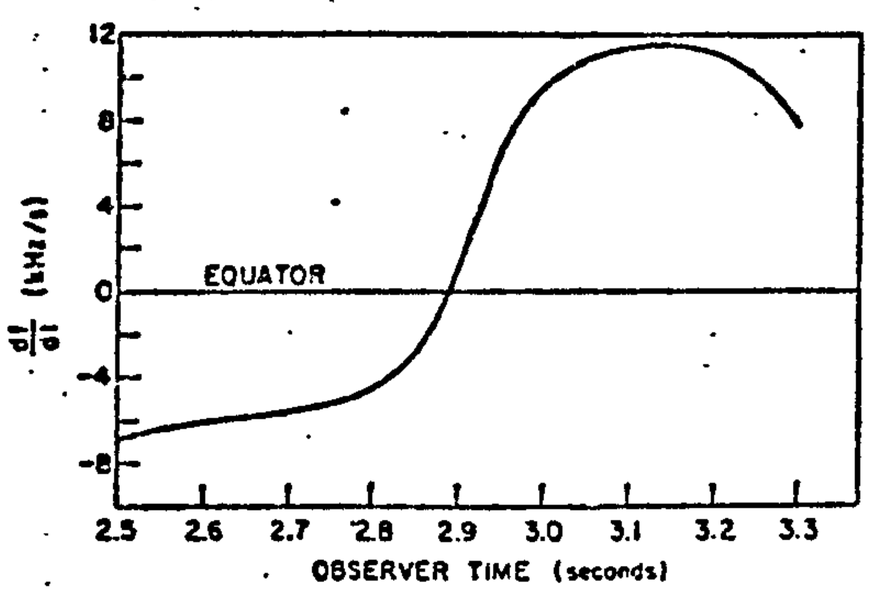

(c)

Slope of hook plotted in Figure b

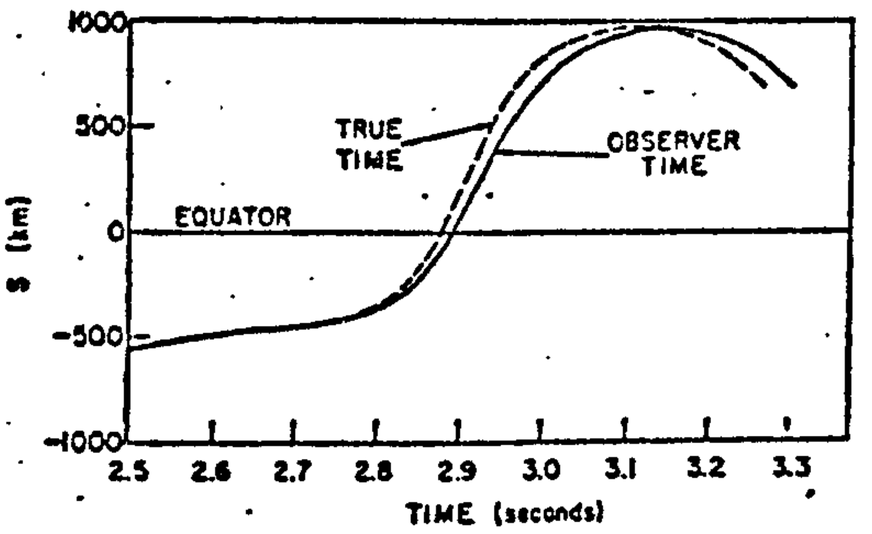

(d)

Position of interaction region as a function of observer time and of true time.

Hook Parameters	
Whistler nose frequency, f_n	14 khz
Minimum gyrofrequency, $f_{Hm} = f_n/0.4$	35 khz
Geocentric distance to top of path, R_m	18,600 km
Plasma frequency, f_N	180 khz
Bandwidth of hook estimated where $df/dt = 0$	100 hz

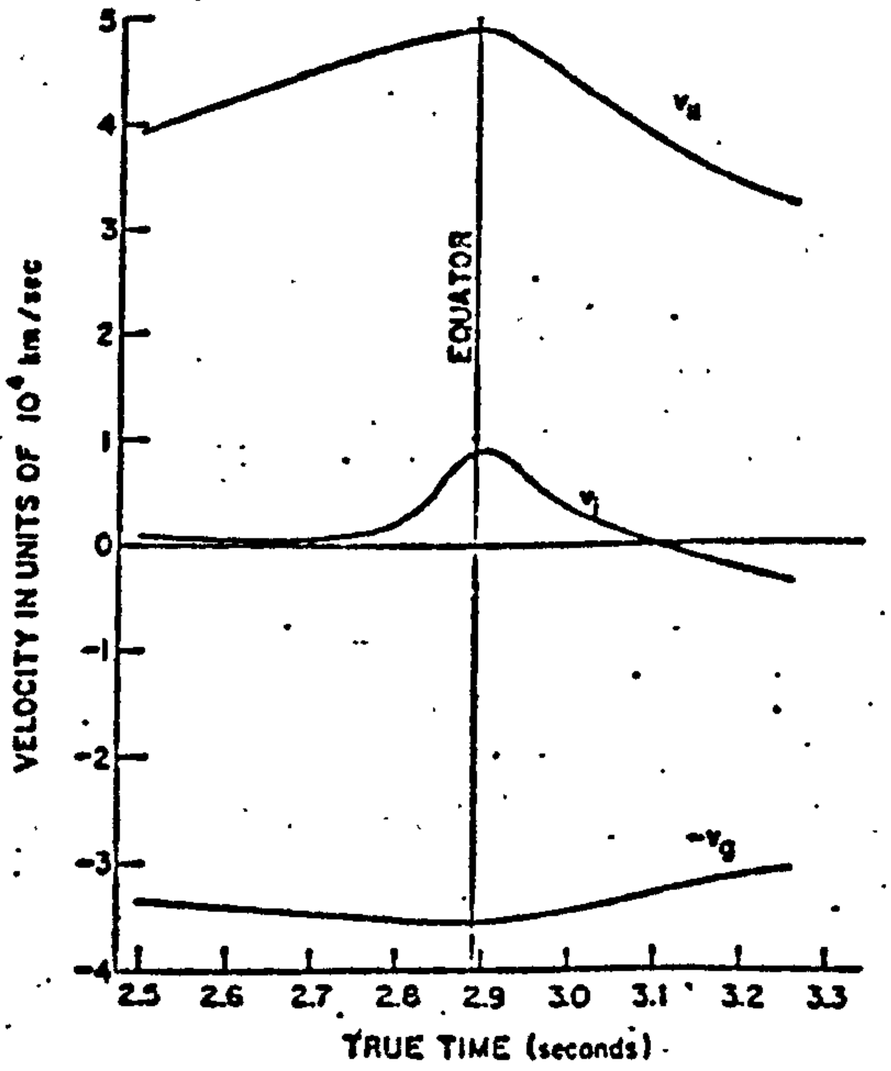

(e)

Parallel, group, and drift velocities versus true time.

Fig 8.5

Observed Frequency - time Profile

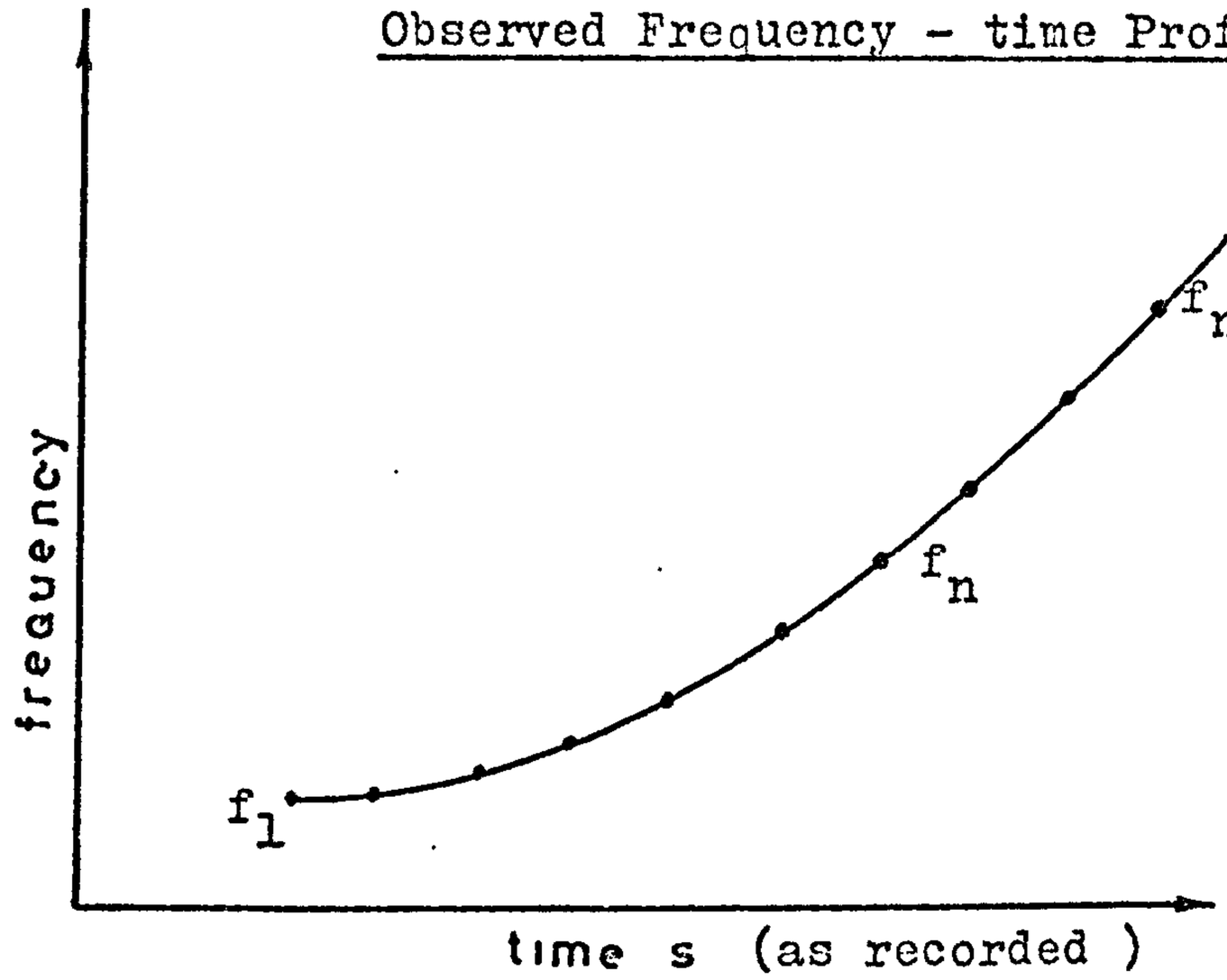

(a)

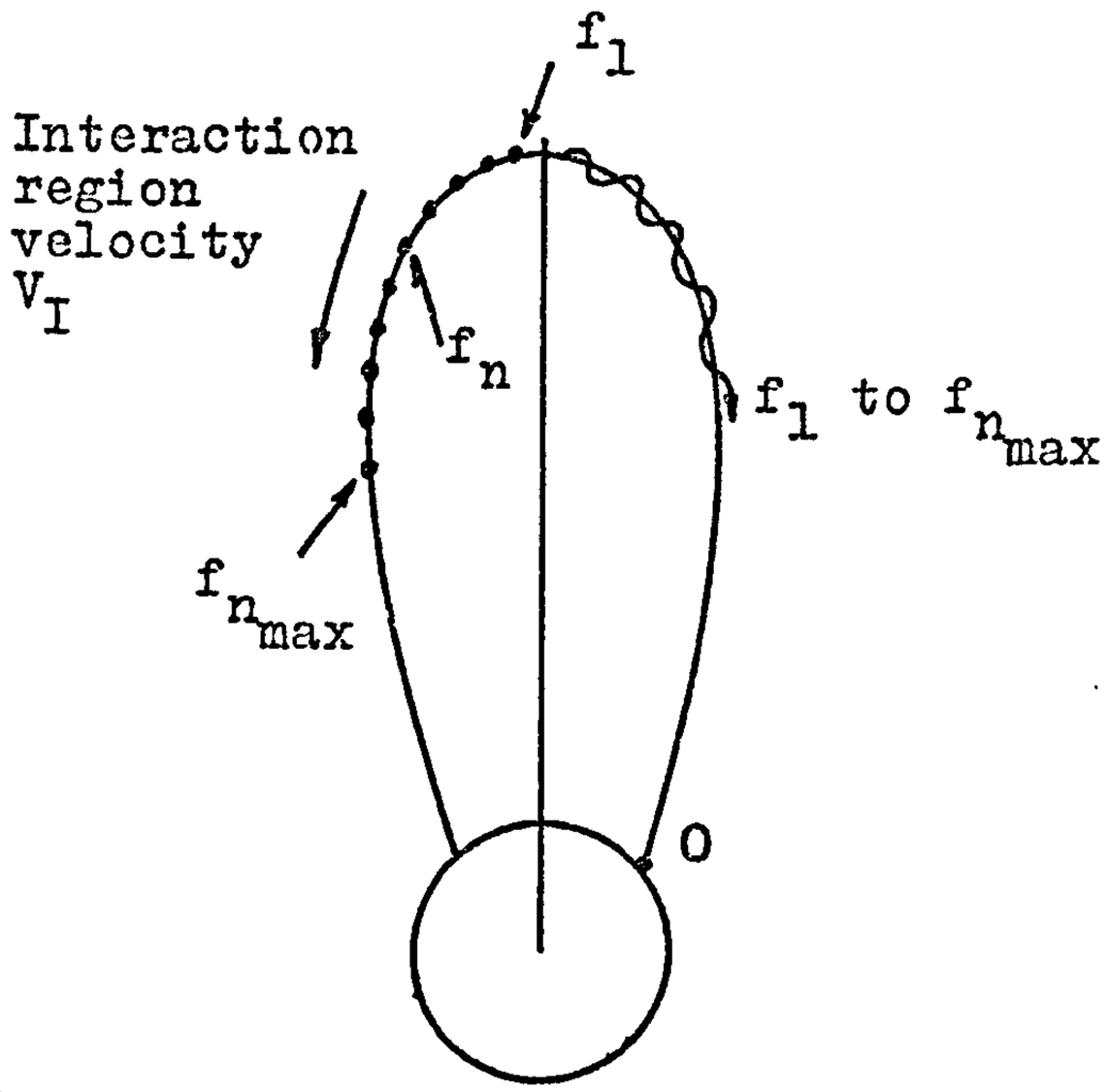

(b)

Fig 8.6

Equatorial Emission Profile

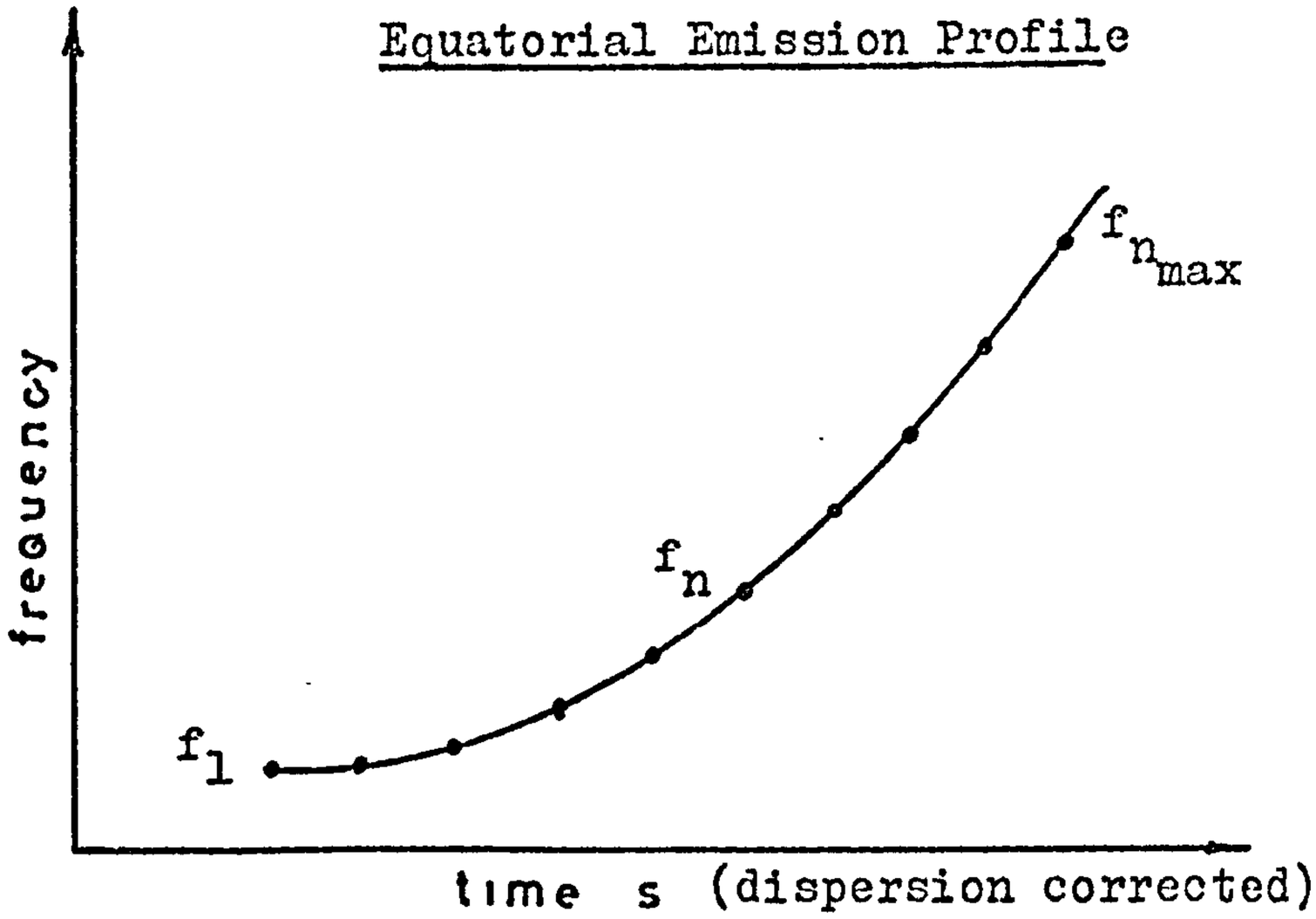

(c)

8.2 (cont'd)

$$\frac{df}{dt} = \frac{df_h}{dS} \cdot \left[\frac{v_g}{1+v_g/v_{//}}\right] \cdot \left[\frac{3\lambda}{1+2\lambda}\right] \cdot \left[1 + \frac{(1-\lambda)}{3}\tan^2\alpha\right] \quad (8.2,14)$$

Using the approximation of (8.2,9) and equations (8.2,4) & (8.2,7) it can be shown that;

$$\frac{df}{dt} = K_1 S^{3/2} \frac{(1-\lambda)}{(1-2\lambda)^2}^{3/2} \cdot \left[1 + \frac{(1-\lambda)}{3}\tan^2\alpha\right] \quad (8.2,15)$$

where

$$K_1 = \frac{54C}{R_m^2 f_n} f_{ho}^2 \quad m^{-1}s^{-2} \quad (8.2,15a)$$

In equation (8.2,15) the term in the square brackets is ignored by Helliwell having shown that the correction is less than 0.1 for a working value of $\alpha = 30^o$. He calculated the location of the interaction region as a function of observed time, and the group velocity of the wave, the parallel velocity of the resonant electrons and the velocity of the interaction region as a function of time for a typical hook which is shown in Fig. 8.5b. The slope, distance and velocities are shown in Figs. 8.5(c), (d) and (e) respectively.

Equatorial Emission Profile

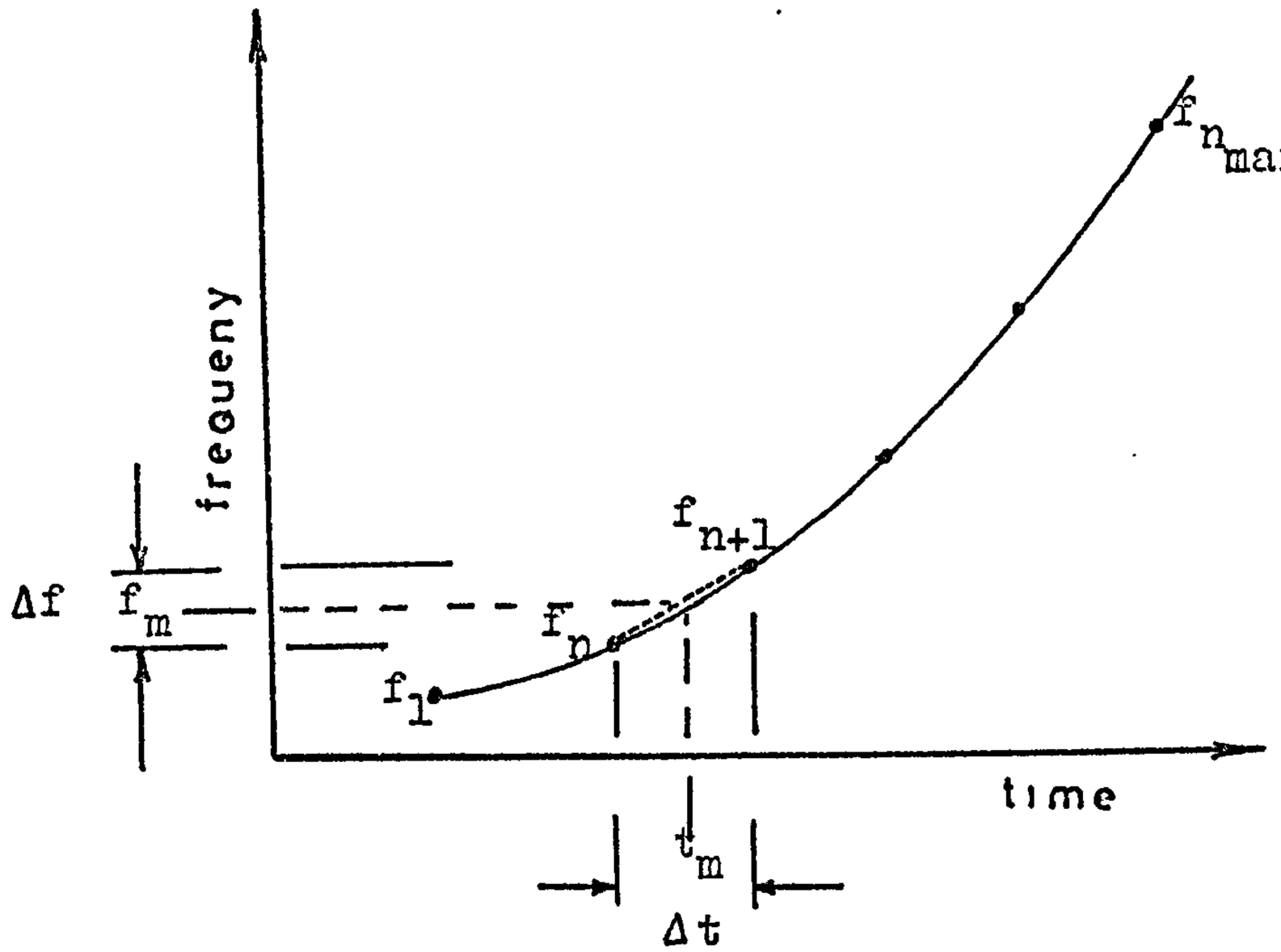

(a)

Distance - time Curve.

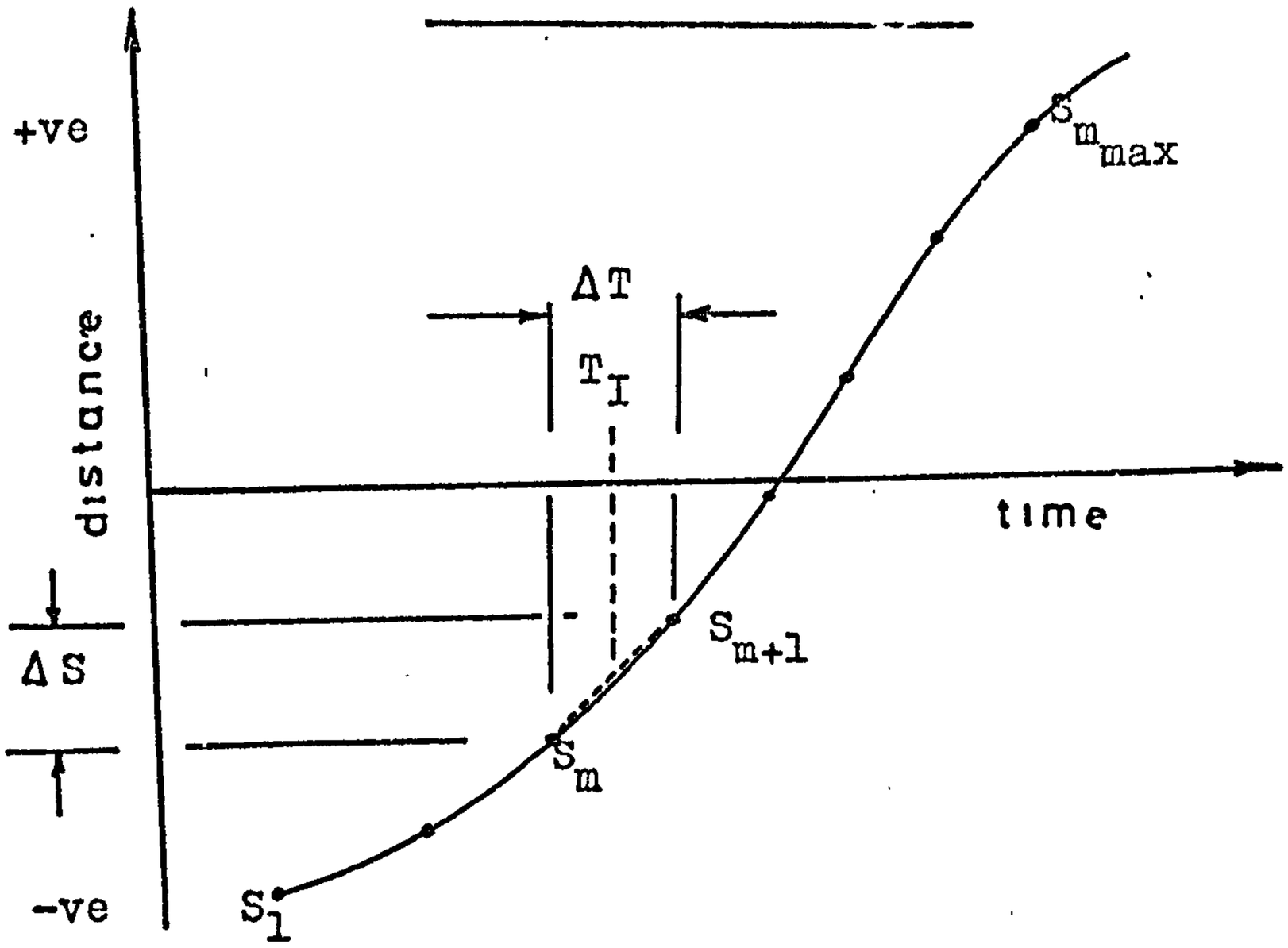

(b)

Fig 8.7

8.3 COMPUTATIONAL METHOD FOR ANALYSING DISCRETE VLF EMISSIONS BASED ON HELLIWELLS THEORY

Consider a simple rising tone recorded by an observer at O in Fig. 8.6b.

Let the interaction region start at the geomagnetic equator and proceed away from the observer.

Discrete emissions can be long, lasting for several seconds, or may be very short, such as chorus elements. Normally they endure for about 1 second. In order to investigate the movement of the interaction region as a function of time, it is necessary to calculate its position at about twenty points which are equally spaced in time. This means that the Helliwell calculations must be performed on the rates of change of frequency at twenty points along the received emission profile, see Fig. 8.6a.

In equation (8.2,14) df/dt is that observed at the interaction region and in order to proceed with the calculation the received emission profile must be resotred to its original shape by removing the effects of dispersion delays incurred during the journey from the point of generation to the ground. It is obviously impossible to do this as the point of generation is the unknown which is being sought. In most cases the best estimate of df/dt which can be made is taken from the equatorial emission profile and is reasonable as emissions are generated near the equator Brice (1964). The time delay incurred from the equator to the observer for a frequency f is calculated by a numerical integration of the group velocity v_g along the field line.

8.3 (cont'd) The integration is performed for n_{max} points with frequencies from f_1 to $f_{n_{max}}$. Then the time for frequency f_n at the equator is given by;

$$T_{eq} = t_n - t_{delay}$$

where $t_{delay} = \sum_p 1/v_g . \Delta S$ where p indicates integration along the propogation path.

The resulting equatorial profile is seen in Fig. 8.6c. The rate of change of frequency of the equatorial profile must then be calculated at each point f_n, t_n.

$$\text{slope}_{(m)} = \frac{\Delta f_n}{\Delta t_n} = \frac{f_{(n+1)} - f_n}{t_{(n+1)} - t_n} = \text{df/dt at point m}$$

The frequency and time co-ordinates for m are arrived at by linear interpolation between point n and n+1 and are designated f_m and t_m. See Fig. 8.7a.

A computer program P90BILBO[++] which takes values of $\text{slope}_{(m)}$, t_m and f_m uses equation (8.2,15) to calculate the distance S_m from the equator to the generation region. S_m is arrived at by a successive approximation in the values f_h and f_n in (8.2,15) & (8.2,15a) the starting values being f_{ho} and f_{no}. The final value of S_m is printed out when the difference between it and the preceding value is less than 1% of Sm. The program cycles the calculation m_{max} times printing out m_{max} values of S_m.

8.3 (cont'd) The group delay for a frequency f_m is calculated from the equator to the position S_m and the time co-ordinate of the point on the equatorial profile is modified to give the time at the interaction region or the 'true time' (using Helliwell's terminology).

After m_{max} calculation the distance S_m as a function of true time t_m is obtained and the differentiation of this curve yields the interaction region velocity V_I. From Fig. 8.7b we have that;

$$\Delta S_m = S_{m+1} - S_m \quad \text{and} \quad \Delta t_m = t_{m+1} - t_m$$

$$\text{and} \quad V_I = \Delta S_m / \Delta t_m \quad \text{with} \quad T_I = t_m + \Delta t_m / 2$$

The interaction region velocity is effectively the second differential of the equatorial frequency - time profile and any random errors in the f,t co-ordinates become greatly magnified during the differentiating process, resulting in large errors in the interaction region velocity as a funciton of time. The errors are best removed at source by very careful preparation of the original frequency - time profile and by accurately digitising it. However, it is possible to reduce random errors by some form of smoothing during the calculations. Before discussing this point it is useful to estimate the typical error in the position of a point on a frequency time profile in its 'raw' state.

Recordings of VLF emissions are played back through a spectrum analysis device such as the 'Sonograph' and pictures similar to those in Fig. 1.10 are obtained. The actual size of a record is about 10 cm by 30 cm and when it is digitised using a DMAC table (which has a

Errors in Slope of an Emission.

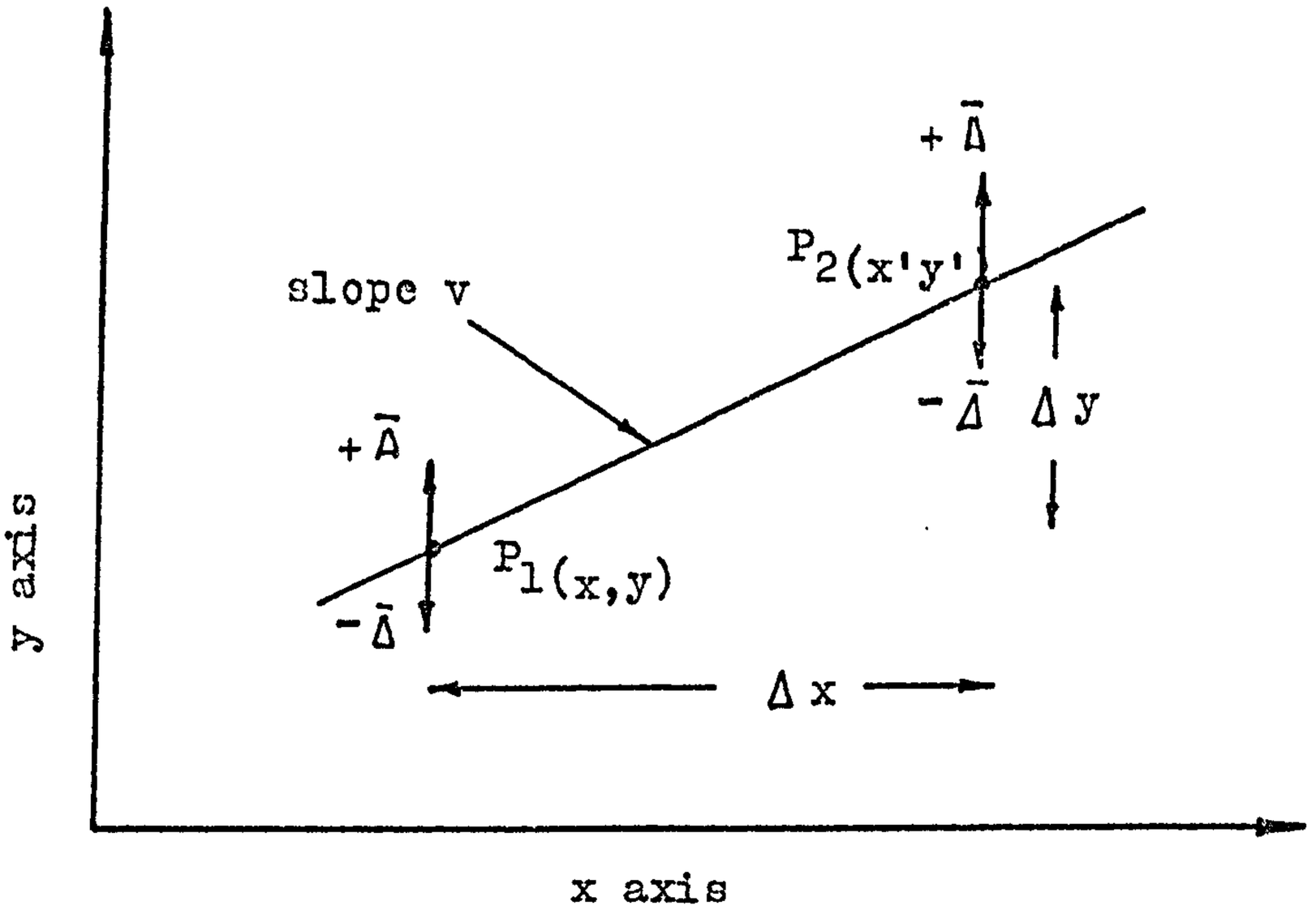

(a)

Running mean Smoothing.

$$S_{j(\text{smoothed})} = \frac{S_i + S_{i+1} + S_{i+2}}{3}$$

$t_j = t_{i+1}$ (for point equally spaced in time.)

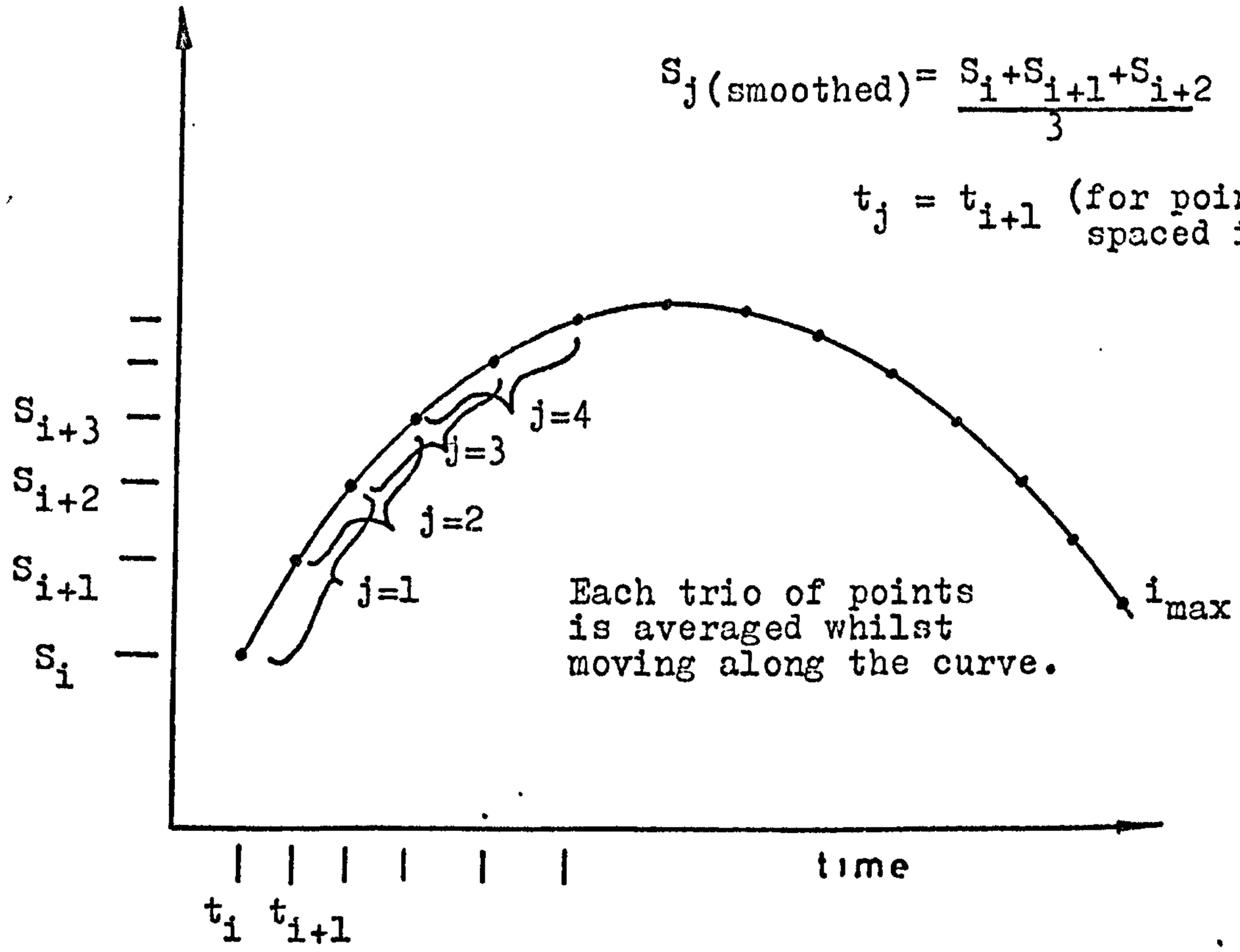

(b)

Fig 8.8

8.3 (cont'd) claimed resolution of 0.1mm) it is difficult to obtain better than ±.5mm accuracy which corresponds to ± 50 Hz.

Consider two points x,y and x',y' on a frequency - time display as in Fig. 8.8a. Let there be an error ascribed to the y co-ordinates of $\pm\overline{\Delta}$ and assume that there is no error in the x co-ordinates. The gradient of a line passing through the two points is;

$$v = \Delta y/\Delta x \qquad \text{(no error)}$$

and $v_{(e)} = v \pm \sqrt{2\overline{\Delta}}/\Delta x$ (for uncorrelated errors)

giving a fractional error in $v_{(e)} = \sqrt{2\overline{\Delta}}/(y - y)$

Typically, frequency - time profiles have slopes of 2 KHz/sec and for points spaced 0.1 seconds apart (y'-y) = 200Hz. The percentage error in the slope is then ($\sqrt{2}$ x 50 /200) x 100 = 35%. This is far too large for sensible values of interaction region velocity to be obtained. A process will be described later which reduces the error to about 1 or 2 percent.

With this level of error it is possible to offset the increase due to differentiation by a running mean smoothing of the distance - time and velocity - time curves. This is carried out as shown in Fig. 8.8b. With between 20 and 30 points representing the curves it was found that averaging over three points gave a degree of smoothing without significantly altering the curve shape.

8.4 TESTING THE ANALYSIS PROGRAM

The computer calculations based on equation (8.2,14) were tested by using the hook in Fig. 8.5b which Helliwell chose for the demonstration of his theory. The curve was digitised with the aid of a DMAC table and then processed to minimise random errors. The observed frequency - time profile was represented by 28 points spaced approximately 30 ms apart. These data were fed into the computer program resulting in the output shown in Figures 8.9 to 8.13.

It was not possible to obtain the original Sonogram used by Helliwell and the frequency - time data had to be obtained from the small scale diagram in Fig. 8.5b which was subject to distortions due to printing and photocopying. Exact correspondence with Helliwell's results was therefore not expected but the exercise was considered useful in indicating the performance of the programmed calculations.

The results are generally in good agreement with those given by Helliwell, the emission slope and distance as functions of time agree to better than 10% at all points. The interaction region velocity curve is drawn by 'eye' through a scatter of points (created by the double differentiation of poor original data) and is again within 10% of that produced by Helliwell. It may be concluded that the program functions correctly on the medium latitude hook (L = 2.9) given in Fig. 8.5b.

The reduced deviation of points from the fitted distance - time curve due to smoothing can be seen in Fig. 8.11 and Fig. 8.10.

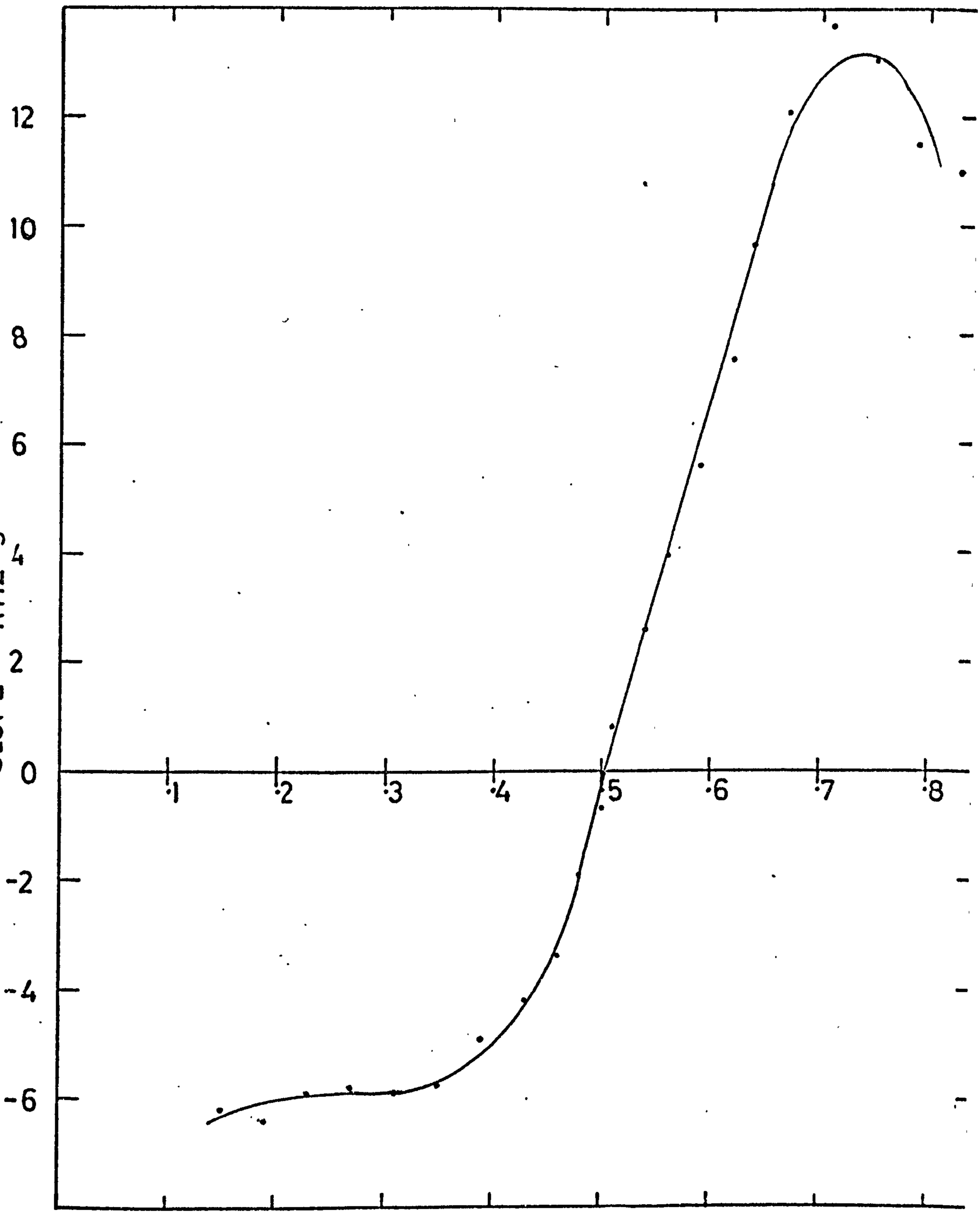

FIG(8.9)

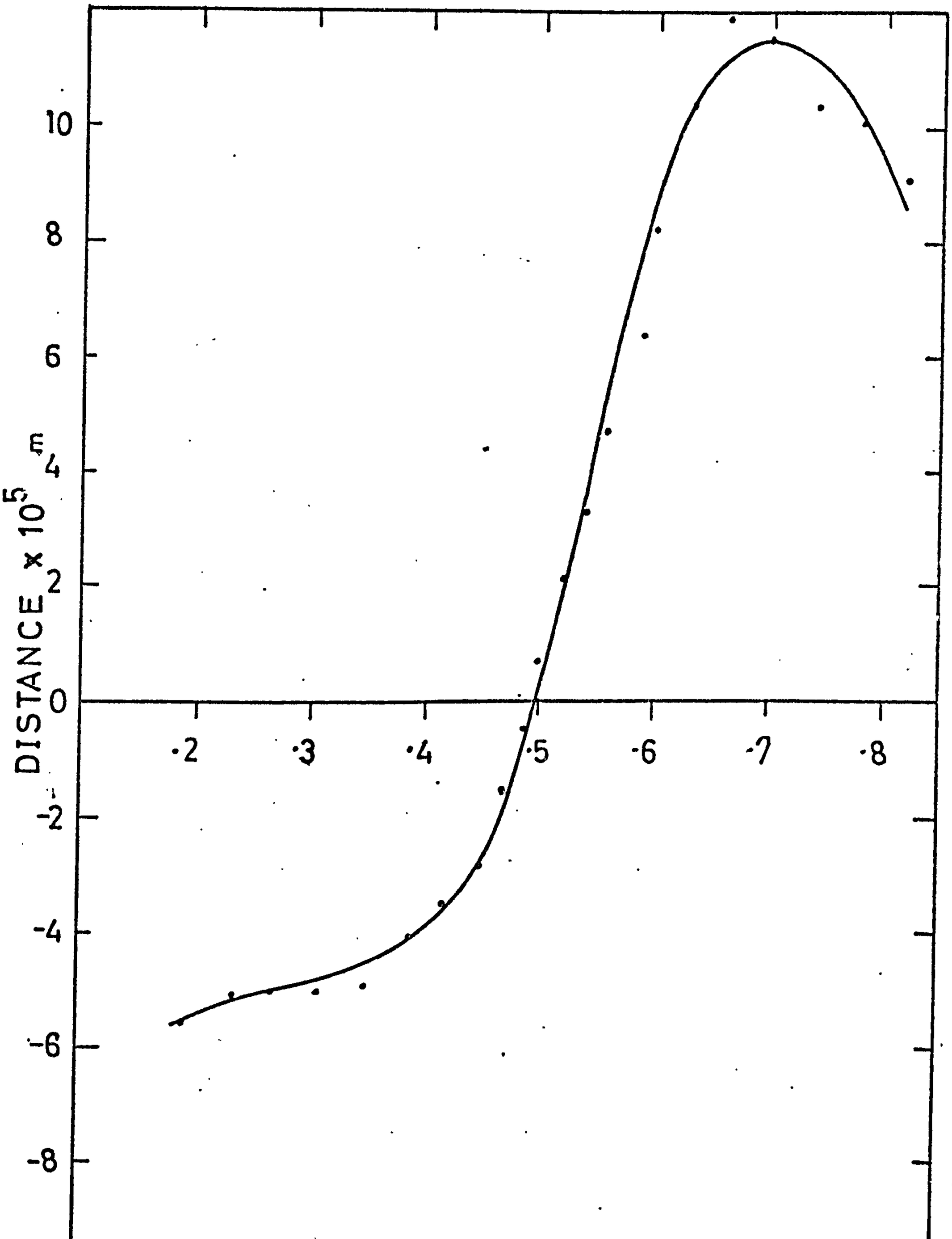

FIG(8.10)

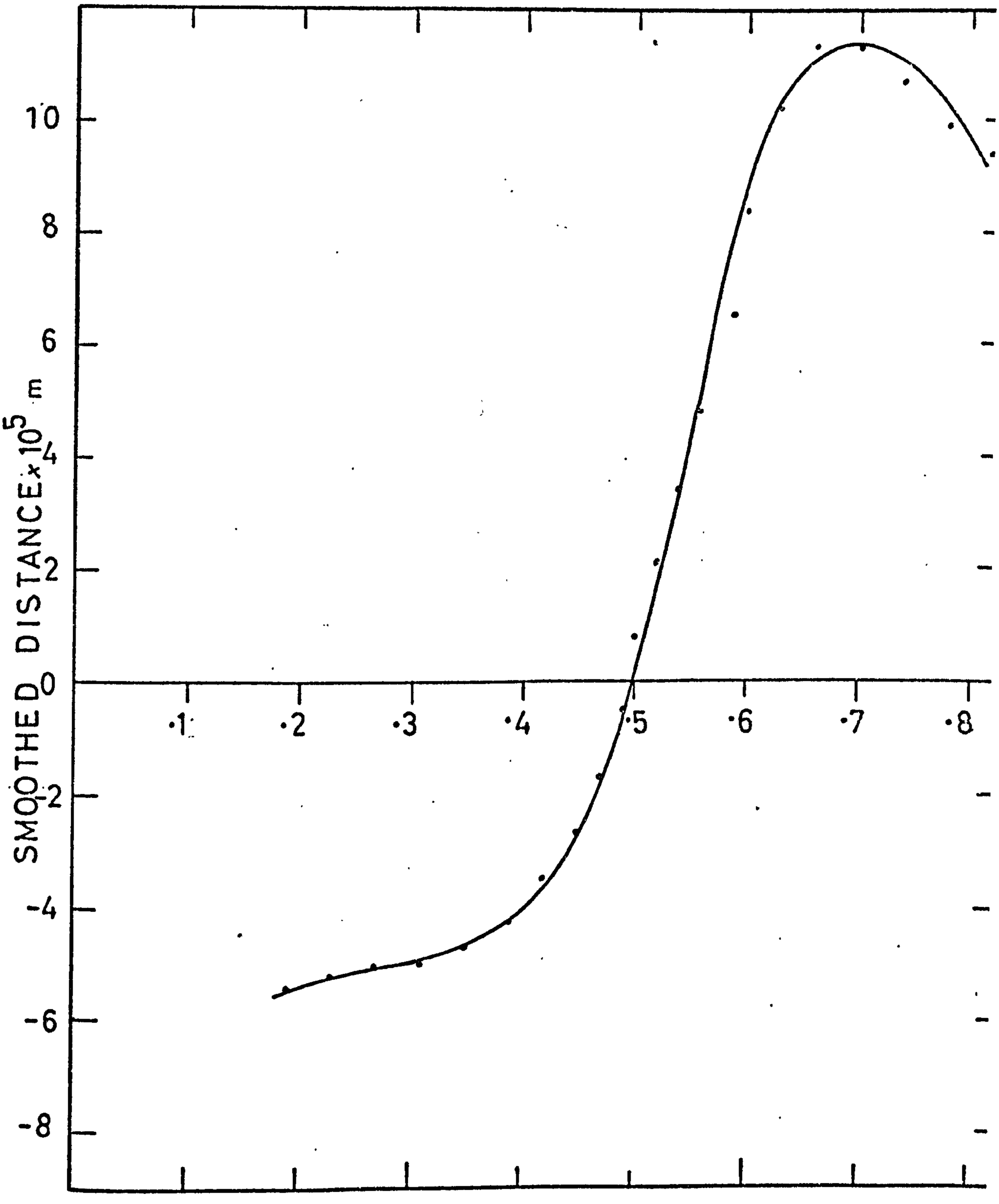

FIG(8.11)

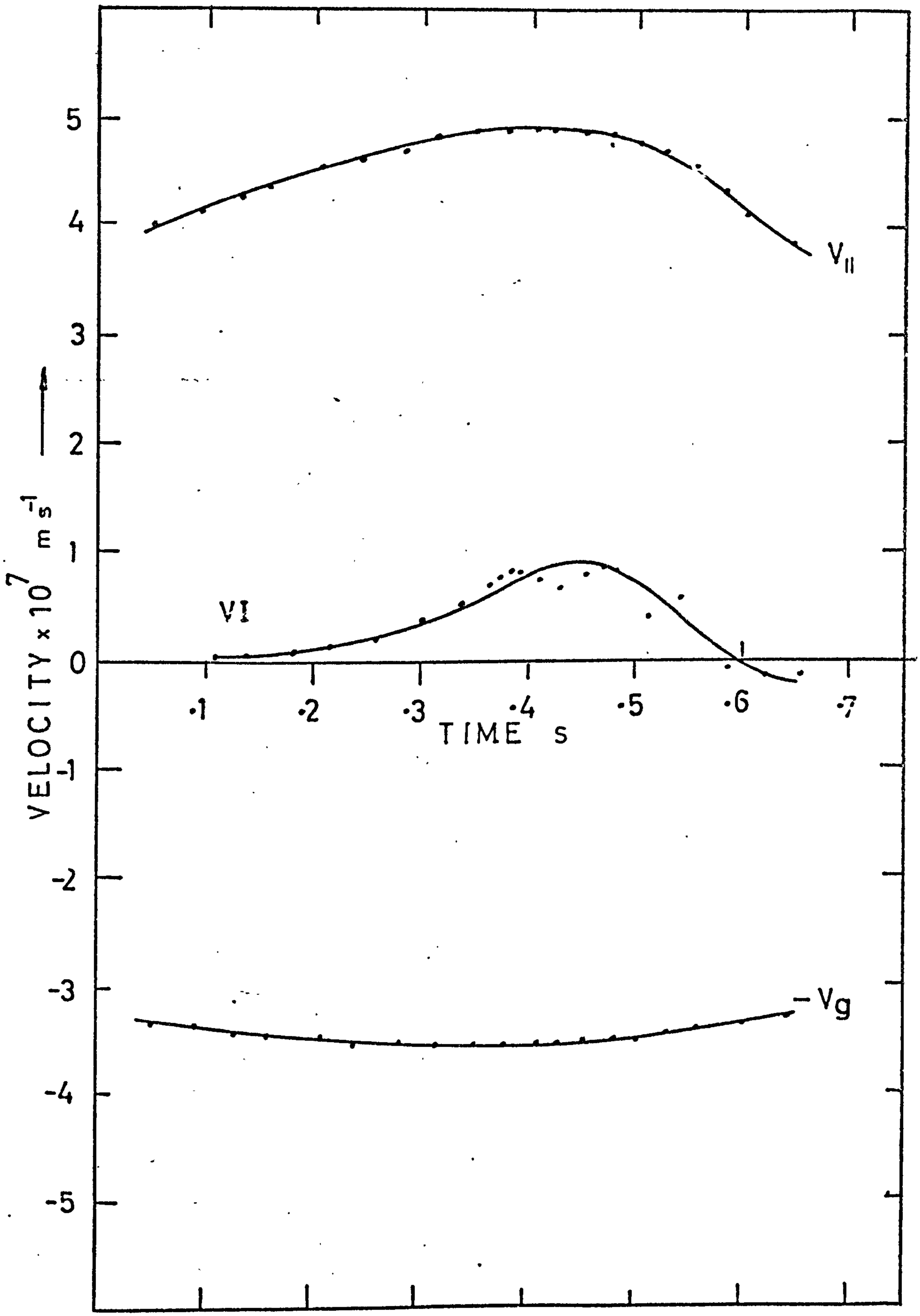

FIG(8.12)

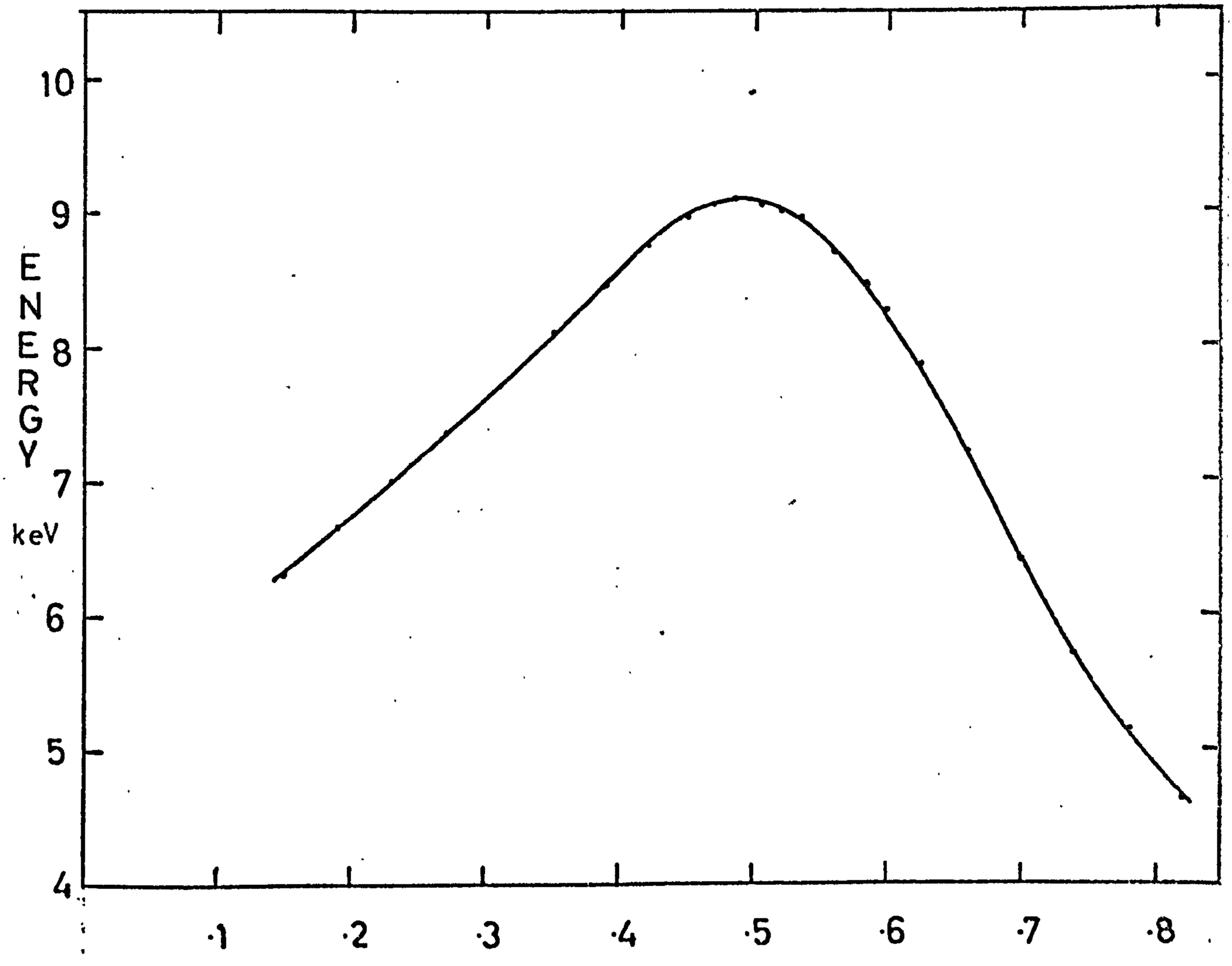

FIG(8·13)

8.4 (cont'd) The energy of resonant electrons has been computed and can be seen in Fig. 8.13. The values between 4 and 10 keV are consistent with curves of $E_{\parallel}$.n against L for a variety of gyroresonant frequencies given by Rycroft (1972).

The possibility of a further check on the analysis program is made possible by the existence of the 'Dowden Cyclotron model' program P90S. Helliwell 1967 states that in the limit when the interaction region velocity equals the parallel velocity of the resonant electrons in his model (see Fig. 8.4) then the situation is exactly that described by Dowden 1962. Therefore it should be possible to specify the energy of resonant electrons in the Dowden model and produce an emission which would be observed on the ground and then analyse it using the Helliwell model and recover the electron energies. This would be a sever test of the numerical integrations in particular and of the calculations in general for both programs.

A Dowden Cyclotron emission was generated by assuming a bunch of 50 keV electrons with an equatorial pitch angle of 20^{o} was spiralling along a field line at L = 4 from + 8^{o} from the equator to - 8^{o}. The Helliwell analysis was performed with P90B and the results can be seen in Figs. 8.14, 8.15, 8.16. There is a slight discrepancy in the actual and recovered positions of the interaction region and although the interaction region velocity is high and is approach $v_{\parallel}$, there is again a discrepancy. The recovered electron energy is very close to the actual value at the equator but differs slightly at $\pm$ 8^{o}.

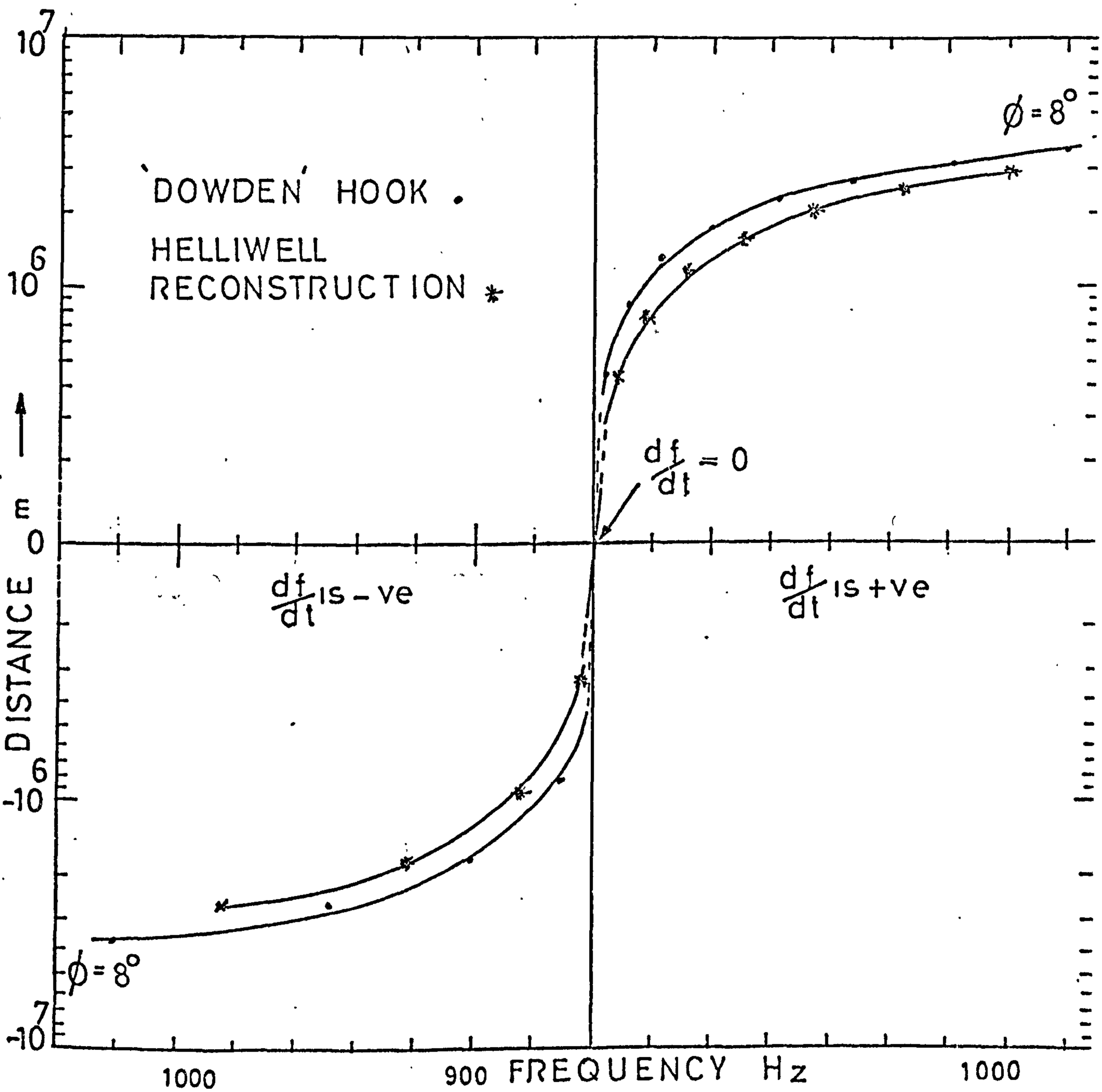
10^7
10^6
0
-10^6
-10^7
DISTANCE m
'DOWDEN' HOOK .
HELLIWELL RECONSTRUCTION *
ϕ = 8°
df/dt = 0
df/dt is - ve
df/dt is + ve
ϕ = 8°
1000
900
FREQUENCY Hz
1000

FIG(8.14)

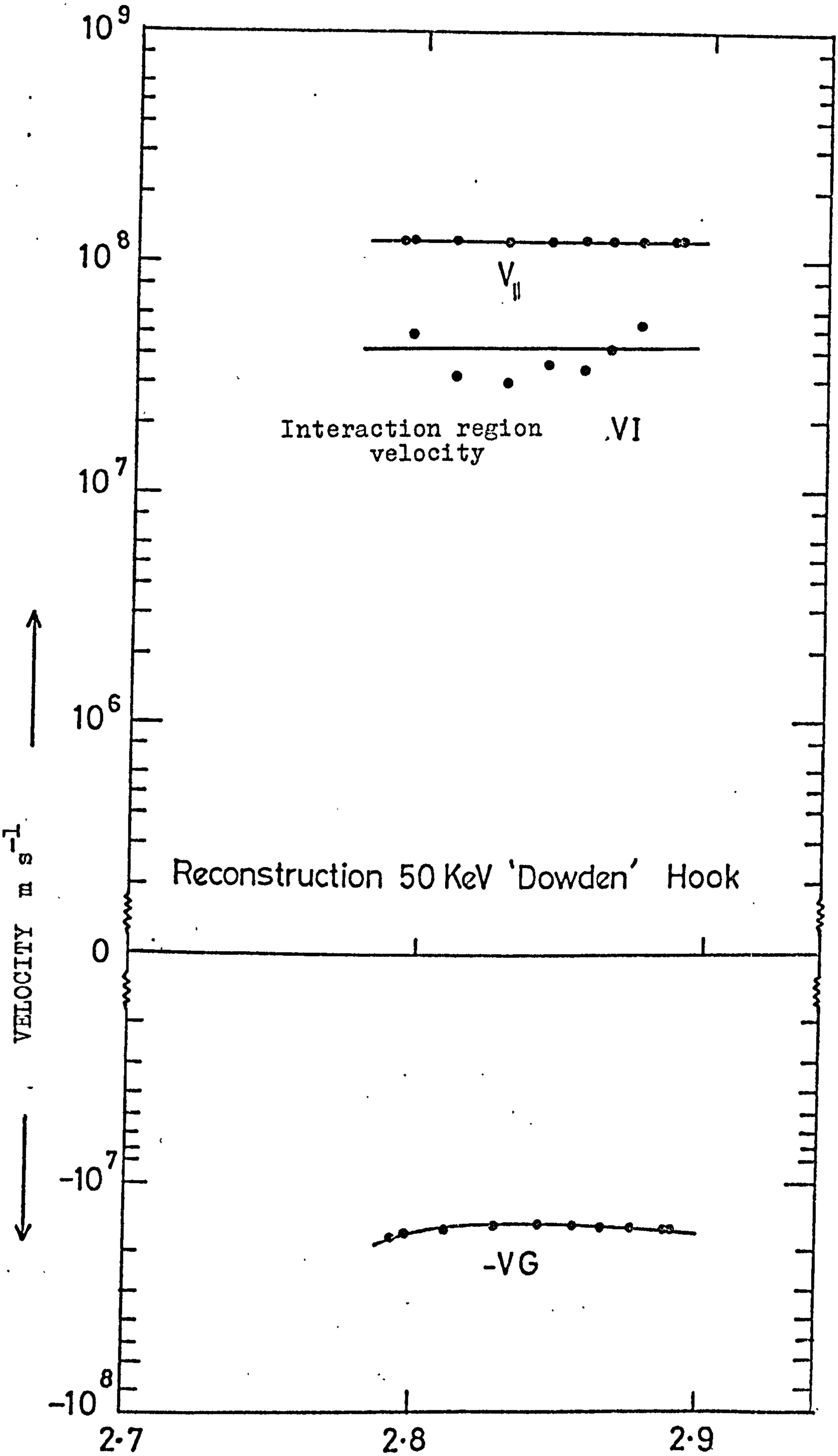
10^9
10^8
10^7
10^6
V_{II}
Interaction region velocity
VI
Reconstruction 50 KeV 'Dowden' Hook
VELOCITY m s^{-1}
0
-10^7
-10^8
-VG
2·7
2·8
2·9
TIME s

Fig.(8.15)

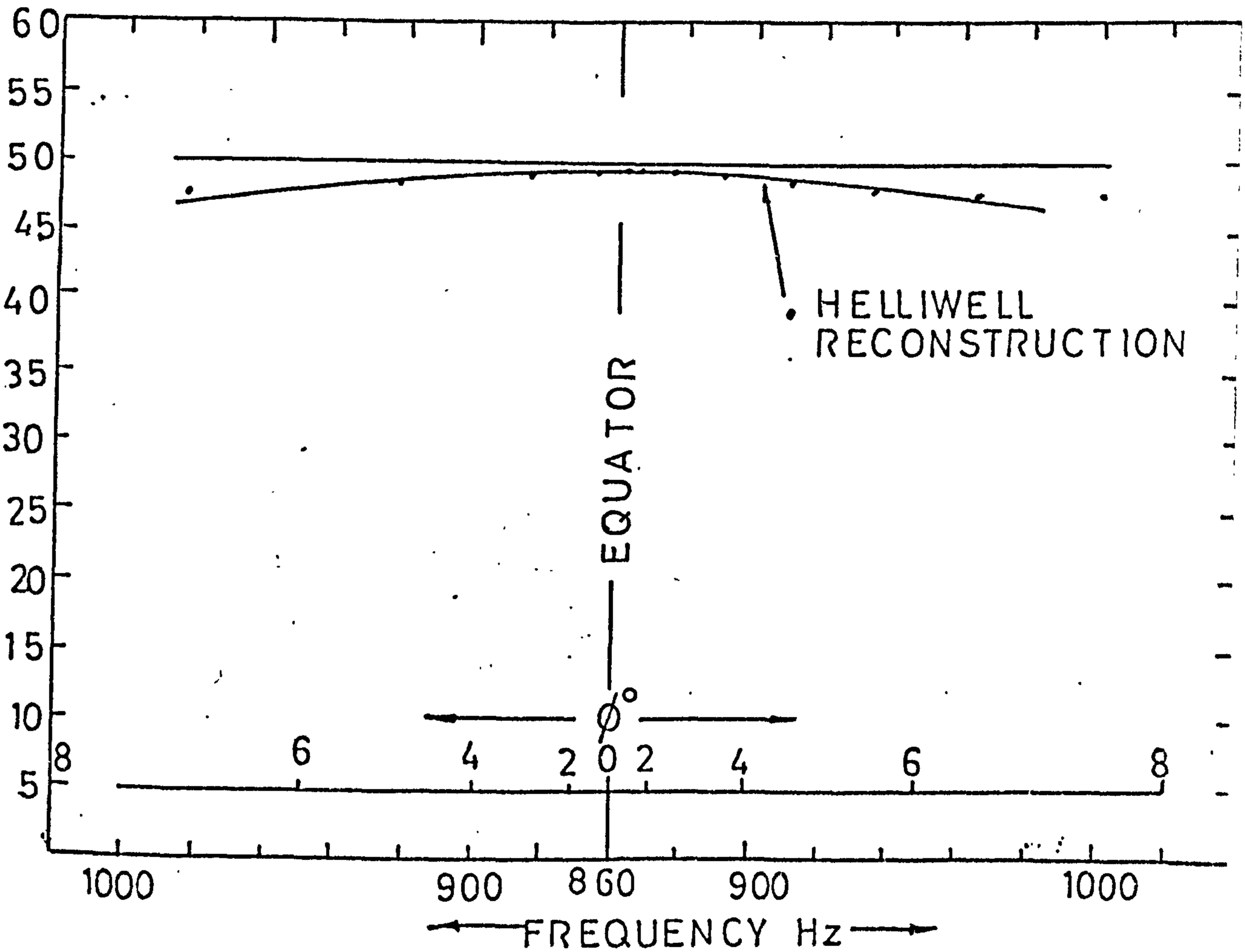
60
55
50
45
40
35
30
25
20
15
10
8
6
5
ENERGY keV
HELLIWELL
RECONSTRUCTION
EQUATOR
0°
8
6
4
2
0
2
4
6
8
1000
900
860
900
1000
FREQUENCY Hz

FIG(8.16)

8.4 (cont'd) This smoothly increases with distance and is not what would be expected due to calculation errors in the numerical integrations, which would be substantially the same from the equator to the ground or from $\pm$ 8° to the ground. A closer investigation of the calculations performed by the two programs reveals that the Helliwell theory in the limiting case does not quite correspond to the Dowden Cyclotron model.

Consider Fig. 8.17b where the detailed interaction region construction proposed by Helliwell (see Fig. 8.4) is shown at two positions of the interaction region S_1 and S_2 at times T_1 and T_2, where $S_2 > S_1$ and $T_2 > T_1$. The observer at 'o' first measures a characteristic rate of change of frequency $\frac{df}{dt}(1)$ at S_1 and later $\frac{df}{dt}(2)$ at S_2. The observed rates of change of frequency are related to the distances by equation (8.2,15) which is based on (8.2,14) and which in turn is dependent on equations (8.2,12) & (8.2,13). Consider the latter equation:

$$dt = dS \left(1/v_{\perp} + 1/ v_g \right) \quad \text{being the limit of;}$$

$$\Delta t = \Delta S \left(1/v_{//} + 1/ v_g \right) \qquad (8.2,16)$$

The velocity of the interaction region in Fig. 8.17b is given by;

$$V_I = \frac{S_2 - S_1}{T_2 - T_1}$$

Consider the limiting case when $V_I = v_{//}$. This situation is shown in Fig. 8.17c where it is clear that $S_2 - S_1 = \Delta S$ and that the same electrons stay in the interaction region.

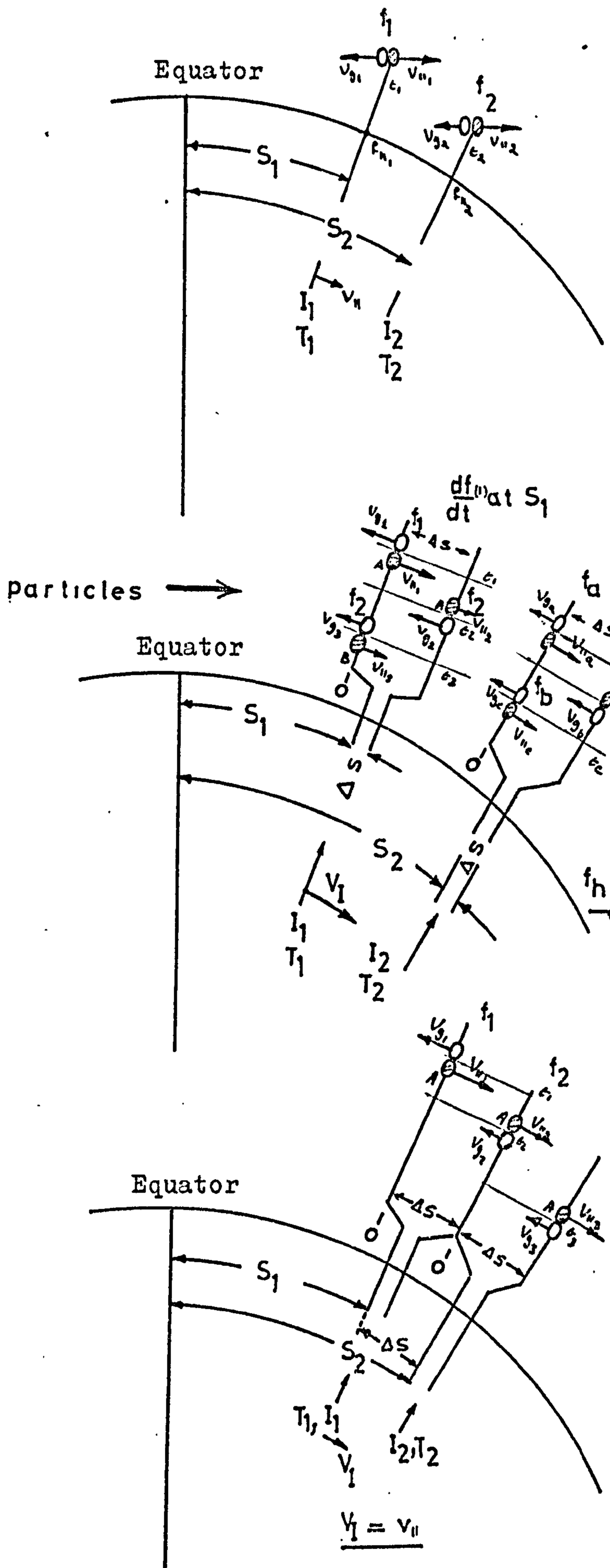

(a)

DOWDEN

(b)

HELLIWELL

(c)

HELLIWELL LIMIT
(DOWDEN)

Fig. 8.17

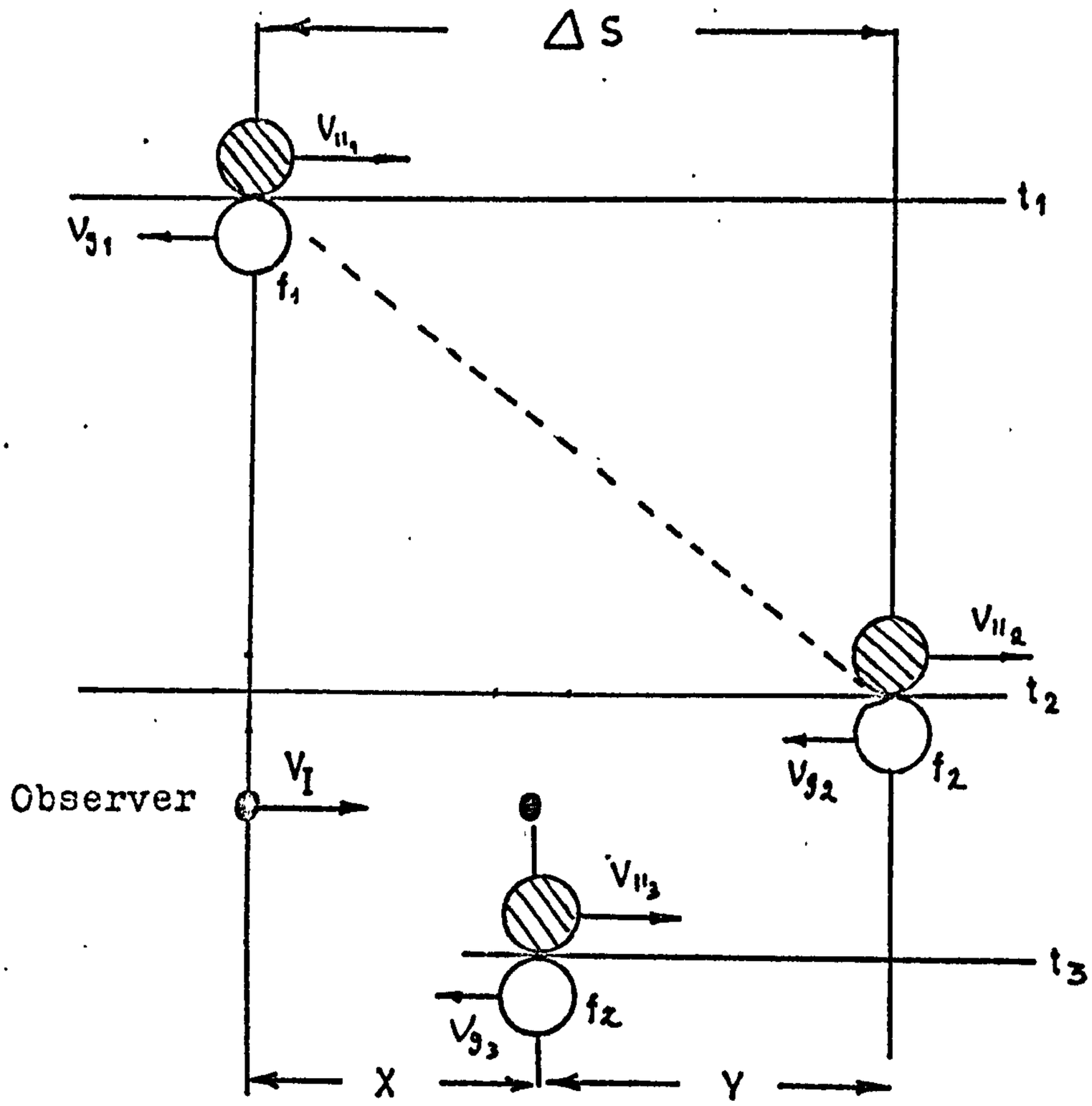

(a)

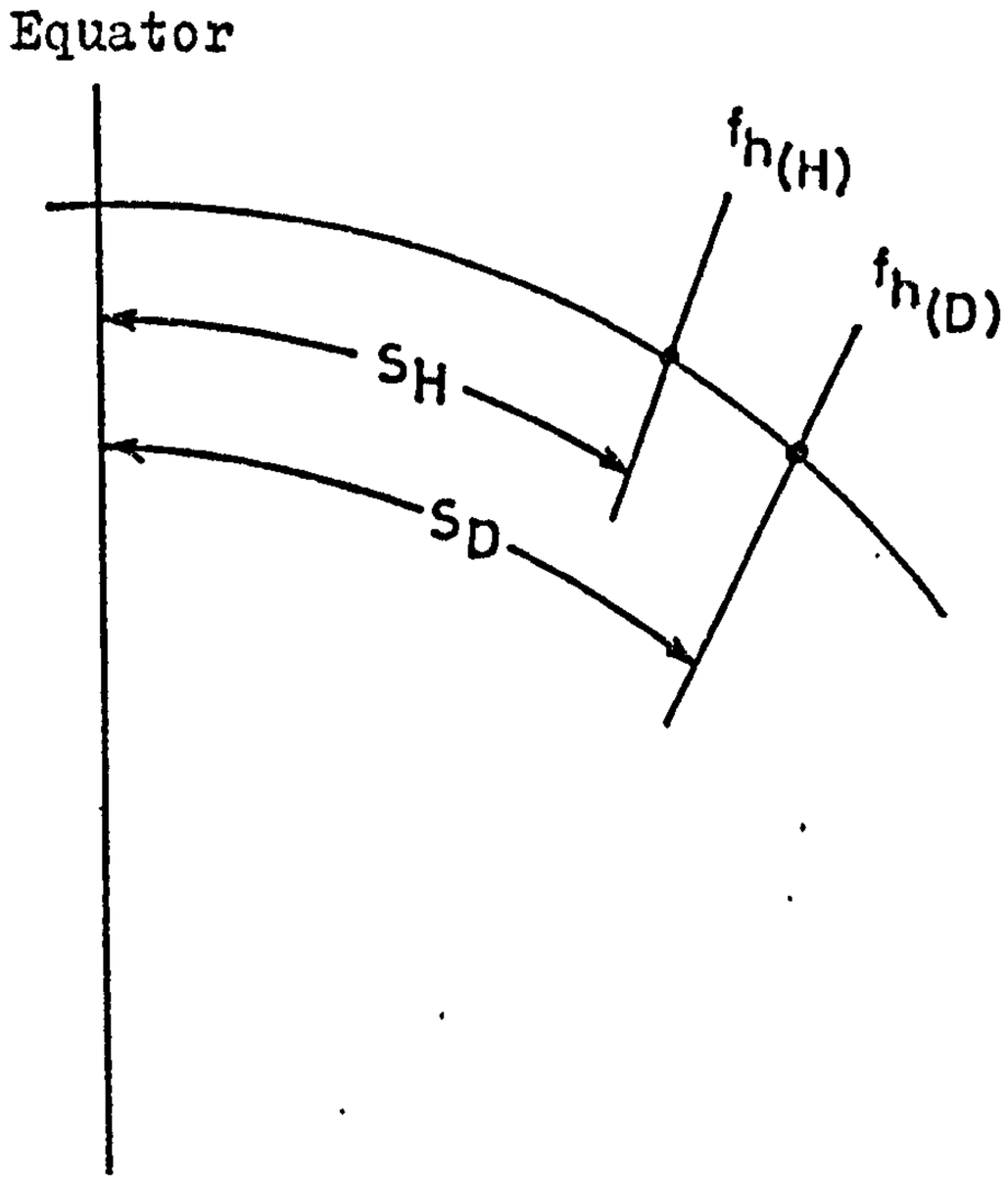

(b)

$f_{h(H)} < f_{h(D)}$

Fig. 8.18

8.4 (cont'd) The idea of the interaction region being extended in space collapses and the observer sees a frequency change f_2-f_1 as he travels a distance ΔS. He does not wait for the wave packet at frequency f_2 to travel back to him because he has moved with the electrons. Thus

$$\Delta t = \Delta S \left(1/v_{//} \right) \qquad (8.2,17)$$

This is the time delay due soley to the electrons and is the same as that derived from the Dowden Cyclotron model in Fig. 8.17a. It is clear that equations (8.2,16) and (8.2,17) are different and that the normal Helliwell equation (8.2,14) which may be rearranged as shown below, is not applicable to the limiting situation which is correctly described by equation (8.2,18).

$$\frac{df}{dt} = \frac{df_h}{dS} \quad \frac{1}{(1/v_g+1/v_{//})} \frac{3\lambda}{(1+2\lambda)} \left[1 + \frac{(1-\lambda)}{3} \tan^2\alpha \right]$$

$$\frac{df}{dt} = \frac{df_h}{dS} \quad \frac{1}{(1/v_{//})} \quad \frac{3\lambda}{(1+2\lambda)} \left[1 + \frac{(1-\lambda)}{3} \tan^2\alpha \right] \qquad (8.2,18)$$

These two formulae represent the cases where $V_I = 0$ and $V_I = v_{//}$. They may be united by considering Fig. 8.18a where the basic interaction region construction is that used by Helliwell but the observer is allowed to move with the interaction region. At time t_1 the electron group resonates with a wave group at frequency f_1, the electrons then move a distance ΔS in a time

$$t_2 - t_1 \text{ where } t_2-t_1 = \Delta S \, (1/v_{//}) \qquad (8.2,19)$$

8.4 (cont'd) During this time the observer and the interaction region has moved a distance X where $X = \frac{V_I \cdot \Delta S}{v_{//}}$

the wave packet then has to travel a distance Y to the observer

$$Y = \Delta S - X = \Delta S \ (1 - V_{I/v_{//}})$$

The time taken for the wave packet to reach the observer is;

$$t_3 - t_2 = \Delta S(1 - V_I/v_{//}) \cdot \frac{1}{v_g} \qquad (8.2,20)$$

Thus the total time elapsed between the observer seeing f_1 and f_2 is;

$$t_3 - t_1 = \Delta t = \Delta S \ \frac{1}{v_{//}} + \frac{(1 - V_I/v_{//})}{V_g} \qquad (8.2,21)$$

Which can be rearranged in the form;

$$\Delta t = \Delta S \ \frac{v_g + v_{//} - V_I}{v_{//} v_g} \qquad (8.2,22)$$

If $V_I = 0$ then (8.2,22) becomes;

$$\Delta t = \Delta S \ \frac{v_g + v_{//}}{v_{//} v_g}$$ which is equation (8.2,13)

or if $V_I = v_{//}$ (8.2,22) becomes;

8.4 (cont'd) $\Delta t = \Delta S \cdot \frac{1}{v_{//}}$ which is what is calculated for the Heliwell limit(Fig. 8.17c) and the Dowden Model (Fig. 8.17a)

Then equation (8.2,14) is modified to;

$$\frac{df}{dt} = \frac{df_h}{dS} \quad \frac{v_g v_{//}}{v_g + v_{//} - V_I} \cdot \frac{3\lambda}{(1+2\lambda)} \cdot \left[1 + \frac{(1-\lambda)}{3} \tan^2\alpha\right] \qquad (8.2,23)$$

Thus for $V_I = 0$ or more generally for $V_I \ll v_{//}$ the above equation reduces to that given by Helliwell, (8.2,14).

For $V_I = v_{//}$ it reduces to (8.2,18) which was calcualted for the Helliwell limit.

It should be noted that in general the interaction region velocity V_I is less than $v_{//}$ and (8.2,14) is operative.

THE CONSEQUENCES OF THE DIFFERENCE BETWEEN (8.2,14) and (8.2,18)

Equation (8.2,14) may be written;

$$\frac{df}{dt} = \frac{df_h}{dt} \cdot \frac{dt}{dS} \quad \frac{v_g v_{//}}{v_g + v_{//}} \cdot \frac{3\lambda}{(1+2\lambda)} \cdot \left[1 + \frac{(1-\lambda)}{3} \tan^2\alpha\right] \qquad (8.2,24)$$

Now considering the limit when $V_I = v_{//}$ and the Helliwell theory becomes the Dowden Cyclotron mode, df_h/dt is the rate of change of frequency emitted by the particle bunch moving at $v_{//}$. From (8.2,17) (for the Dowden model & Helliwell limit) it can be seen that

8.4 (cont'd) $\frac{dt}{dS} = \frac{1}{v_{//}}$ (for the electrons or the interaction region as $v_{//} = V_I$)

and using equation (8.2,1) and (8.2,12) which is its differntial and defining the emitted frequency in this case (the Dowden limit) as $f_{(D)}$ we have;

$$\frac{df}{dt}(D) = \frac{df}{dt}_h \cdot \frac{3\lambda}{(1+2\lambda)} \cdot 1 + \frac{(1-\lambda)}{3} \tan^2\alpha$$

Thus (8.2,24) may be written after defining the rate of change of frequency in the Helliwell equation (8.2,14) as $\frac{df}{dt}(H)$ in the form;

$$\frac{df}{dt}(H) = \frac{df}{dt}(D) \frac{1}{v_g} \frac{v_{//} v_g}{(v_{//} + v_g)} \qquad (8.2,25)$$

and as $v_g / (v_{//} + v_g) < 1$

$$\frac{df}{dt}(H) < \frac{df}{dt}(D) \qquad (8.2,26)$$

From equation (8.2,15) we see that $df/dt \prec S$ (for a given λ & α)

Thus defining the distance from the equator to the generation point of frequency f (in the Dowden case) as being S_D and (in the Helliwell case) as being S_H then from (8.2,26) we see that;

$$S_H < S_D \qquad (8.2,27)$$

However, (8.2,26)does not follow from (8.2,25) if $\frac{df}{dt}(D) = 0$

and $\frac{df}{dt}(H) = \frac{df}{dt}(D) = 0$

8.4 (cont'd) Thus at the equator $S_H = S_D = 0$.

If an emission was generated on the Dowden model and was analysed using the Helliwell theory (as given in Helliwell 1967) the predicted distance of the interaction region from the equator would be less than the actual distance at all points except the equator where it would of course be zero. This is observed int he case of the 50keV hook which was used, see Fig. 8.16. The discrepancy between the two curves is thus accounted for and is not due to calculation errors.

As the duration of the emission is the same, (Helliwell reconstruction) or (Dowden generated) the reconstructed interaction region velocity must be less than the actual velocity $v_{//}$. This is observed in Fig. 8.15.

For the same emitted frequency f the Helliwell calculations place the interaction region which should be at S_D at position S_H see Fig. 8.18b. Therefore the electron gyrofrequency calculated for the interaction region is $f_{h(H)}$ and not $f_{h(D)}$ where $f_{h(H)} < f_{h(D)}$ except at the equator where $f_{h(H)} = f_{h(D)} = f_{ho}$.

The parallel velocity of the resonant electrons is calculated using; equation (8.2,6)

$$v_{//} = \frac{c}{f_n} \frac{(f_h - f)^{3/2}}{f^{\frac{1}{2}}}$$

8.4 (cont'd) For a given f and relating f_n to f_h by the gyrofrequency model for electron density we see that;

$$v_{//} = \text{const.} \frac{(f_h - f)^{3/2}}{f^{\frac{1}{2}}}$$

Then $v_{//} \propto f_h$

therefore as $f_{h(H)} < f_{h(D)}$, for $f_{h(D)} \neq 0$

$$v_{//\,(H)} < v_{//(D)}$$ except at the equator.

Now $v_{//}$ is related to the instantaneous electron velocity v by equation (8.2,10) and we see that;

$v_{(H)} < v_{(D)}$ and therefore the electron energy

obeys the same condition;

$E_{(H)} < E_{(D)}$ except at the equator.

This behaviour is observed in Fig. 8.16.

To conclude, we see that the discrepancies in Figs. 8.14 to 8.16 result from forcing the basic model of the interaction region to deal with sitations where the interaction region length has no meaning. A better description of the situation is given by equation (8.2,23) but its operation requires the previous knowledge of the interaction

8.4 (cont'd) region velocity. It would be possible to construct a computer program which assumed a starting value for V_I and modified it after each solving of the equation. This would result in a better estimate of the interaction region velocity for emissions which were generated by high velocity ($V_I \simeq v_{\parallel}$) interaction regions. Such a program was not attempted in these researches. Taking values of recovered energy close to the equator, the values are within 1% of the actual values. This figure is taken as a guide to the calculation accuracy of the energies of actual emissions. The determination of the overall accuracy is dependent on the reliability of the L value of propagation and the equatorial electron density.

CHAPTER 9

ADVANCED CALCULATIONS BASED ON THE SECOND ORDER TRANSVERSE RESONANCE CONDITION

9.1 AN ACCURATE DISTANCE CALCULATION

The failure of the computer program to produce unconditionally accurate solutions of equation (8.2,15) which contains the approximation inherent in (8.2,9) leads to a closer examination of the methods of solving (8.2,14) for S. The equation may be written simply as;

$$g_{1(f,\phi)} = g_{2(\phi)} . g_{3(f,\phi)} \qquad (9.1,1)$$

Where $g_{2(\phi)} = \frac{df_h}{dS}$ and $g_{3(f,\phi)}$ is the remaining part of the RHS of the equation, excluding the term in α.

Consider the term $g_{2(\phi)}$, we may write equation (7.2,4) in the form;

$$S = K\ (x + \tfrac{1}{2} \sinh 2x) \text{ where } K = \frac{R_o}{2\sqrt{3}\cos^2\phi_o}$$

$$\text{thus } \frac{dS}{dx} = K\ (1 + \cosh 2x)$$

$$\text{now } \frac{dS}{d\phi} = \frac{dS}{dx} . \frac{dx}{d\phi}$$

$$\text{and from (7.2,5) } \frac{dx}{d\phi} = \sqrt{3}\ \frac{\cos\phi}{\cosh x}$$

9.1 (cont'd) therefore $\frac{dS}{d\phi} = \sqrt{3}\ K \cos(\phi).\ (1+\cosh 2x) \cdot \frac{1}{\cosh x}$

and if $\cosh 2x = 1 + 2\sinh^2 x$

and $\sinh x = \sqrt{3} \sin \phi$

then $\frac{dS}{d\phi} = 2\sqrt{3}\ K \cos\phi \cdot (1+3\sin^2\phi)^{\frac{1}{2}}$ (9.1,2)

Now differentiating equation (7.2,6) we have;

$$\frac{df_h}{d\phi} = f_{ho} \frac{(\cos^6\phi \cdot \frac{1}{2}(1+3\sin^2\phi)^{-\frac{1}{2}} \cdot 6\sin\phi \cdot \cos\phi)}{\cos^{12}\phi} +$$

$$\frac{((1+3\sin^2\phi)^{\frac{1}{2}} \cdot 6\cos^5\phi \cdot \sin\phi)}{\cos^{12}\phi}$$

$$\frac{df_h}{d\phi} = \frac{3f_{ho}}{\cos^7\phi} \frac{\cos^2\phi \cdot \sin\phi + (2\sin\phi \cdot (1+3\sin^2\phi))}{(1+3\sin^2\phi)^{\frac{1}{2}}}$$

$$\frac{df_h}{d\phi} = 3f_{ho} \frac{\sin\phi}{\cos^7\phi} \frac{\cos^2\phi + 6\sin^2\phi + 2}{(1+3\sin^2\phi)^{\frac{1}{2}}}$$

finally

$$\frac{df_h}{d\phi} = \frac{3f_{ho}}{} \frac{\sin\phi}{\cos^7\phi} \frac{(3+5\sin^2\phi)}{(1+3\sin^2\phi)^{\frac{1}{2}}} \qquad (9.1,3)$$

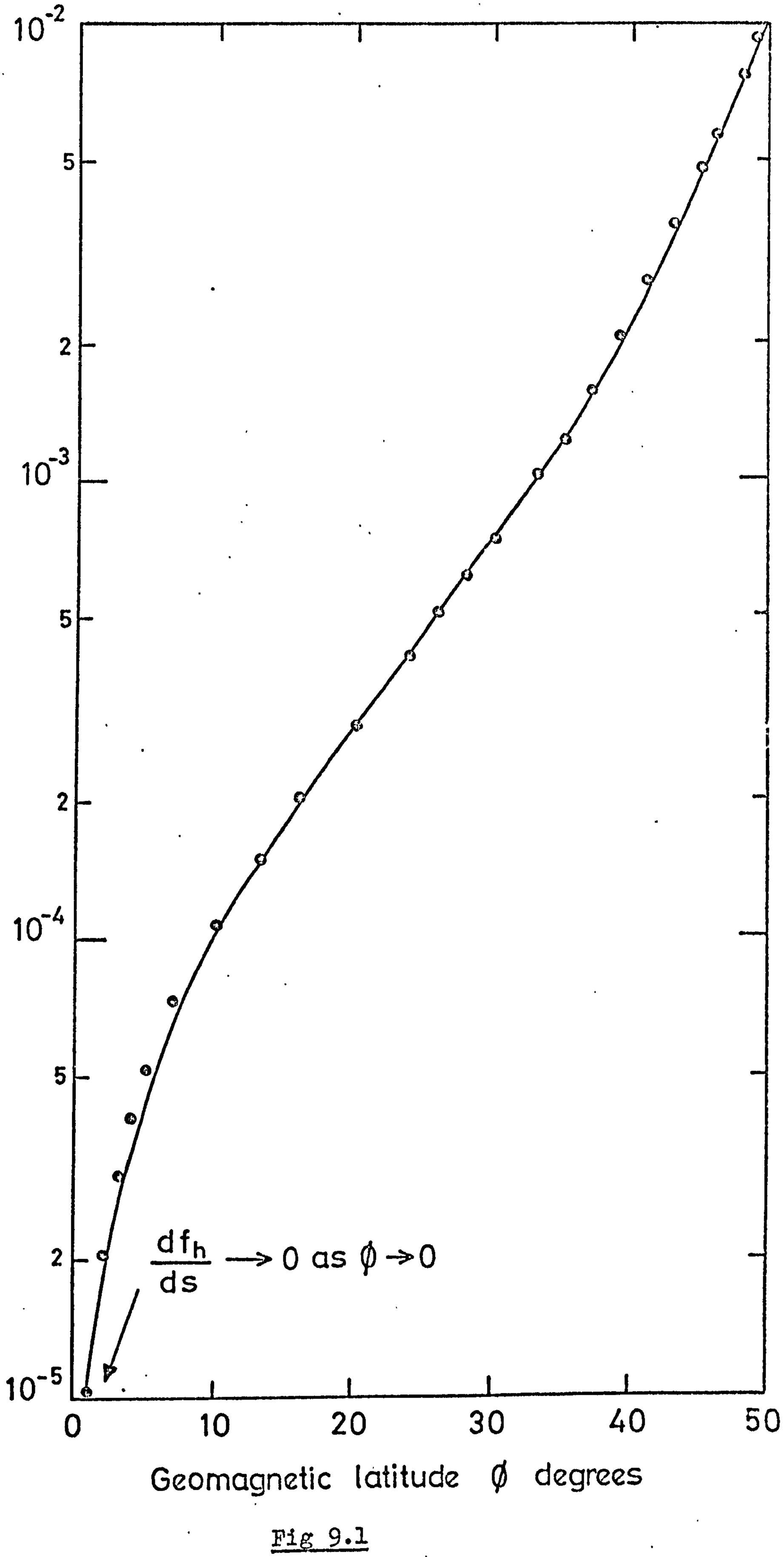
10^{-2}
5
2
10^{-3}
5
2
10^{-4}
5
2
10^{-5}
$\frac{df_h}{ds}$ for ϕ_o = 67·43 i.e. at Andoya
$\frac{df_h}{ds} \longrightarrow 0$ as $\phi \rightarrow 0$
0
10
20
30
40
50
Geomagnetic latitude ϕ degrees

Fig 9.1

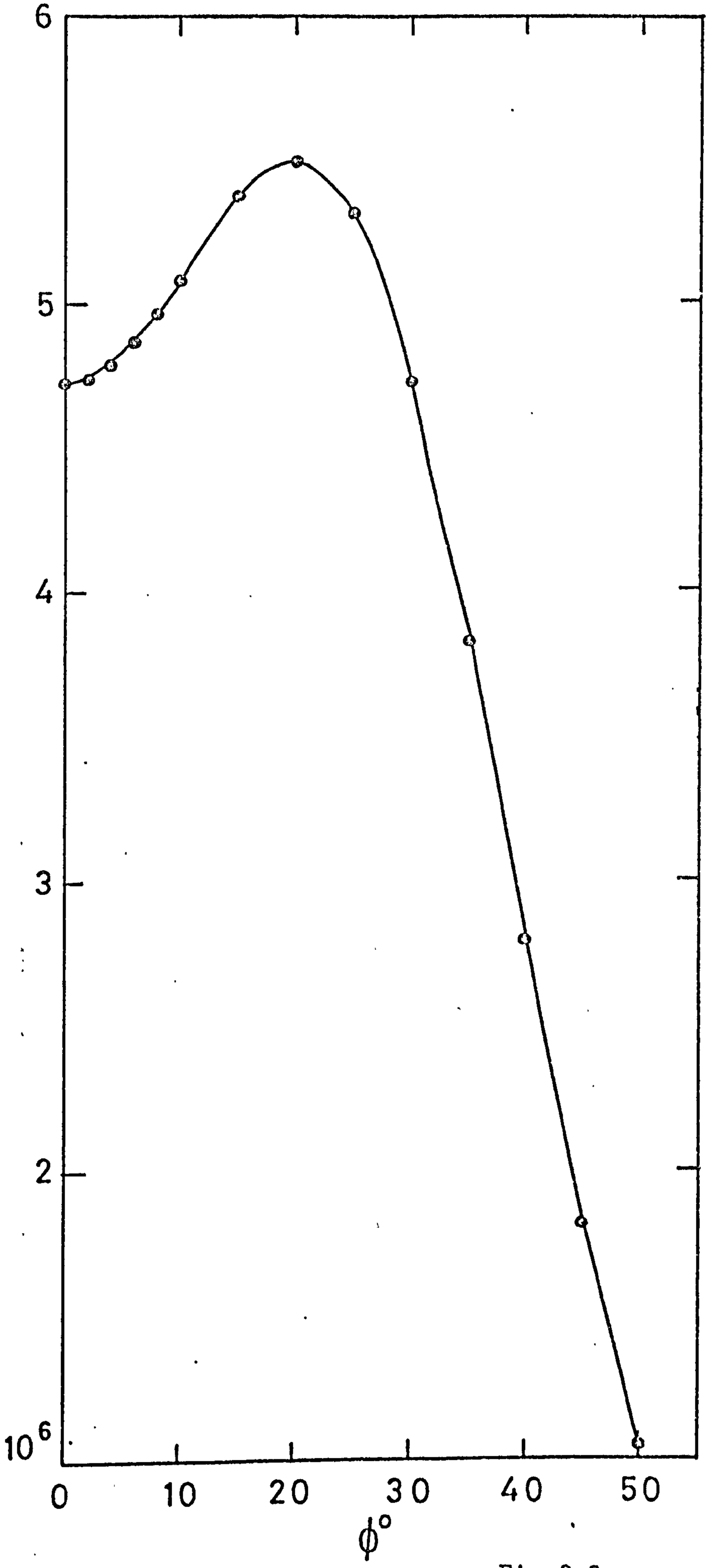
6
5
4
3
2
10^6
0
10
20
30
40
50
ϕ°
$g_3(\phi, f)$ f = 1 KHz and $\phi_o = 67.43$, $f_{n_o} = 20$ elec/cc

Fig 9.2

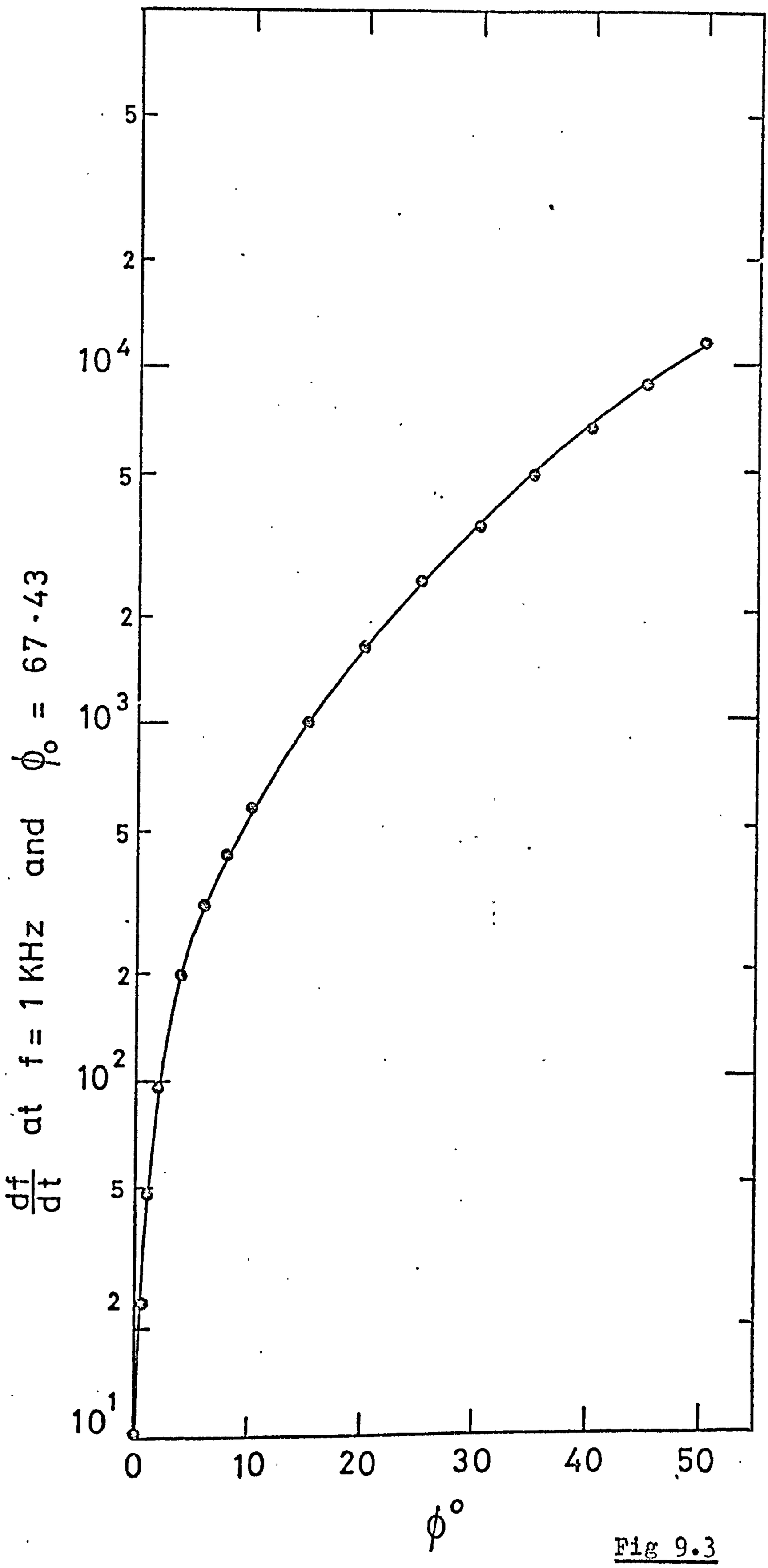
10^4
10^3
10^2
10^1
5
2
5
2
5
2
$\frac{\phi_o}{\phi_{45}}$ at f = 1 KHz and ϕ_o = 67·43
0
10
20
30
40
50
ϕ°

Fig 9.3

9.1 (cont'd) Thus $g_{2(\emptyset)}$ may be determined by evaluating the product $\frac{df_h}{d\emptyset} \cdot \frac{d\emptyset}{dS}$ from equations (9.1,2) and (9.1,3).

A computer program (P90CANT) was written to calculate $g_{2(\emptyset)}$ for $0 < \emptyset < 50^o$ (see appendix 2) at $\emptyset_o = 67.43^o$ (Andøya). A graph of the function inside the bounds can be seen in Fig. 9.1. $g_{2(\emptyset)}$ is a single valued, continuous, monotonically increasing function of $\emptyset$ which tends to 0 at the equator (S=0).

A computer program (P90TIRED) was written to evaluate $g_{3(f,\emptyset)}$ for f = 1 KHz (a typical chorus frequency at high latitudes) for $\emptyset_o = 67.43^o$ over the range $0 < \emptyset < 50^o$. A graph of $g_{3(f,\emptyset)}$ can be seen in Fig. 9.2. It is a single valued, continuous function but it is not monotonically increasing with $\emptyset$.P90TIRED (see appendix 2) also calculated the function $g_{1(f,\emptyset)}$ which is the slope of the emission at frequency f at position $\emptyset$ for the parameters associated with $\emptyset_o$. The function is shown in Fig. 9.3 and it is interesting that the product of $g_{2(\emptyset)}$ and $g_{3(f,\emptyset)}$ results in a single valued, continuous, monotonically increasing function of $\emptyset$ as it enables the full second order resonance condition to be solved by a successive approximation method which will unconditionally produce a solution in S.

Consider a point f_m, t_m on the equatorial emission profile as shown in Fig. 8.7a. The slope df/dt at this point is known together with the location of the field line along which the emission is though to have propagated.

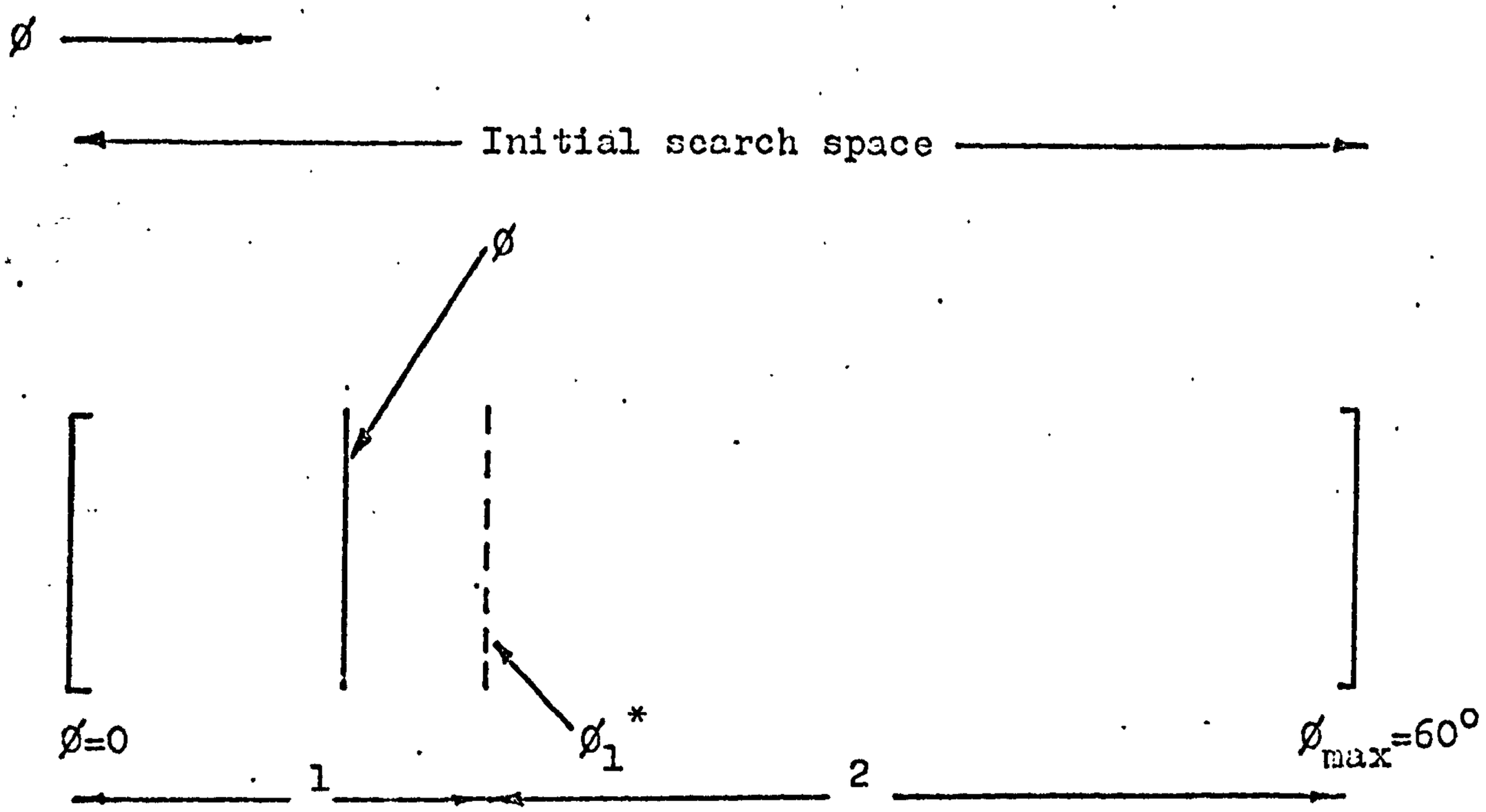

The position of ϕ_1^* is given by;

$$\phi_1^* = T\,(60-0) \quad \text{where } T = \frac{1+\sqrt{5}}{3+\sqrt{5}} \approx 1/3$$

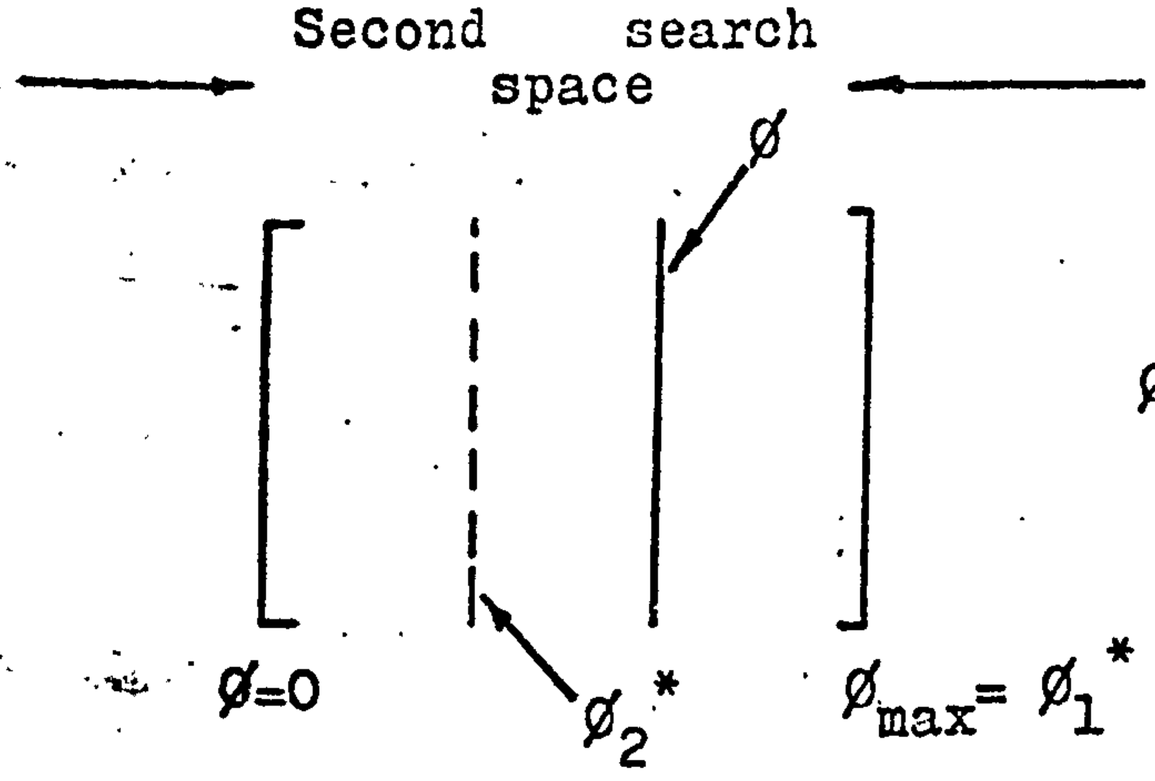

$g_1^* > g_1$ so $\phi_1^* > \phi$ and the search range is reduced to ϕ_1^*.

$$\phi_2^* = T\,(\phi_1^* - 0)$$

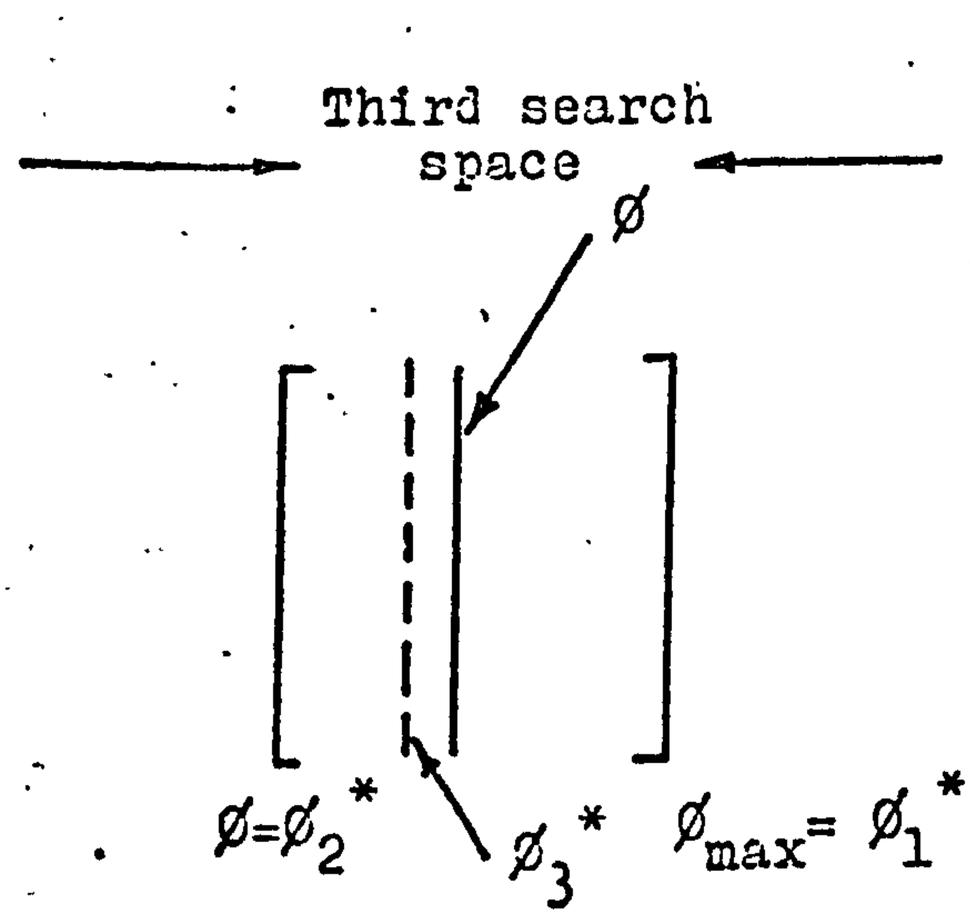

g_1 g_1 so ϕ ϕ_2^* and the search range is further reduced.

$$\phi_3^* = \phi_2^* + T(\phi_1^* - \phi_2^*)$$

Fig 9.4

9.1 (cont'd) If we assume that the interaction region was at a position S_m corresponding to $\emptyset$ then $g_{2(\emptyset)}$, $g_{3(f,\emptyset)}$ and $g_{1(f,\emptyset)}$ may be calculated and compared with df/dt in order that a better estimate of $\emptyset$ may be made.

Let the successively approximated values be denoted by *.

Then with $\emptyset^*$ and f_m we calculate g_2^* and g_3^* and the produce g_1^* which is rate of change of frequency which would be observed if the interaction region was at $\emptyset^*$. Since we know the behaviour of g_1 with $\emptyset$ is well behaved we can draw the following conclusions about the estimated location $\emptyset^*$ and the actual location which is being sought ($\emptyset$) after comparing g_1^* with g_1.

If $g_1^* > g_1$ then $\emptyset^* > \emptyset$ and

if $g_1^* < g_1$ then $\emptyset^* < \emptyset$ but

if $g_1^* = g_1$ then $\emptyset^* = \emptyset$.

If after making the comparison we revise our estimate $\emptyset^*$ in the appropriate manner it is possible to successively reduce the difference $|g_1 - g_1^*|$ and 'home in' on $\emptyset$ and then to finally calculate the corresponding value of S.

In general an upper limit of 60^o may be placed on the range of $\emptyset^*$ as resonant electrons will have been mirrored at angles less than this. A fast convergence routine for the successive approximation is based on the use of the Golden Section Ratio of reduction of the search bounds. A diagramatic explanation is given in Fig. 9.4.

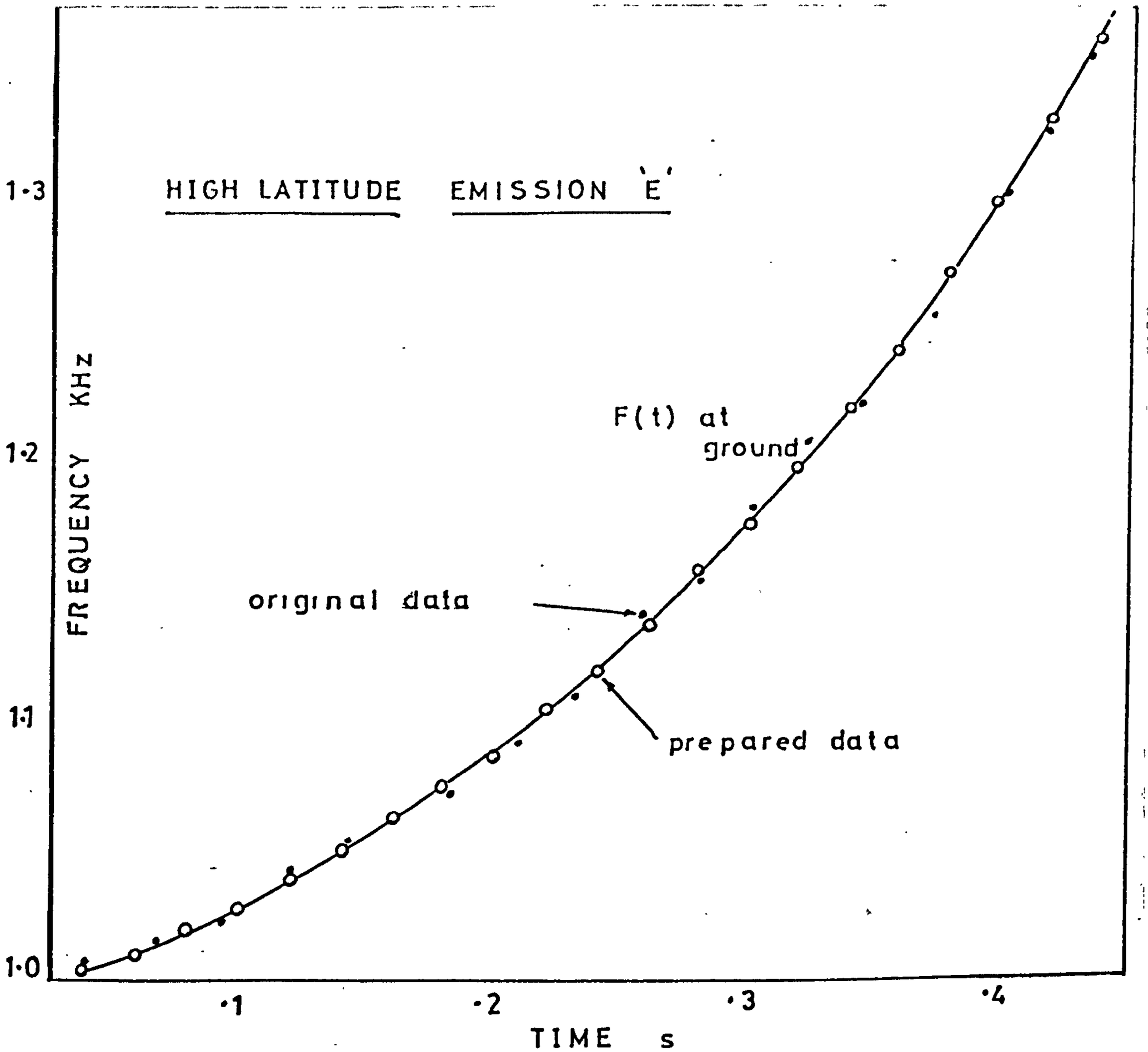
HIGH LATITUDE EMISSION 'E'
FREQUENCY KHz
1·3
1·2
1·1
1·0
F(t) at ground
original data
prepared data
·1
·2
·3
·4
TIME s

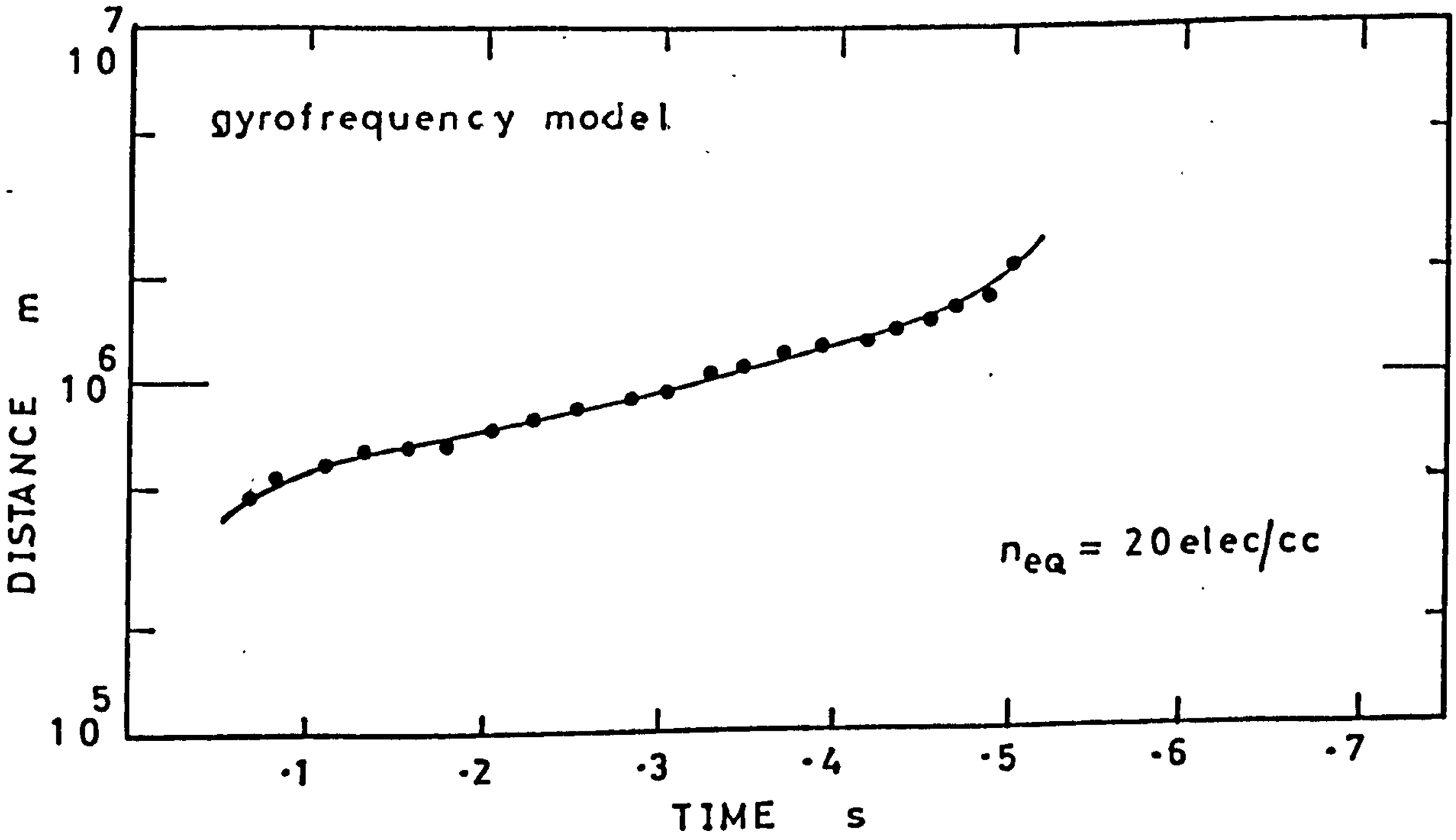
gyrofrequency model
E
DISTANCE m
10^7
10^6
10^5
n_{eq} = 20 elec/cc
·1
·2
·3
·4
·5
·6
·7
TIME s

FIG. 9·5

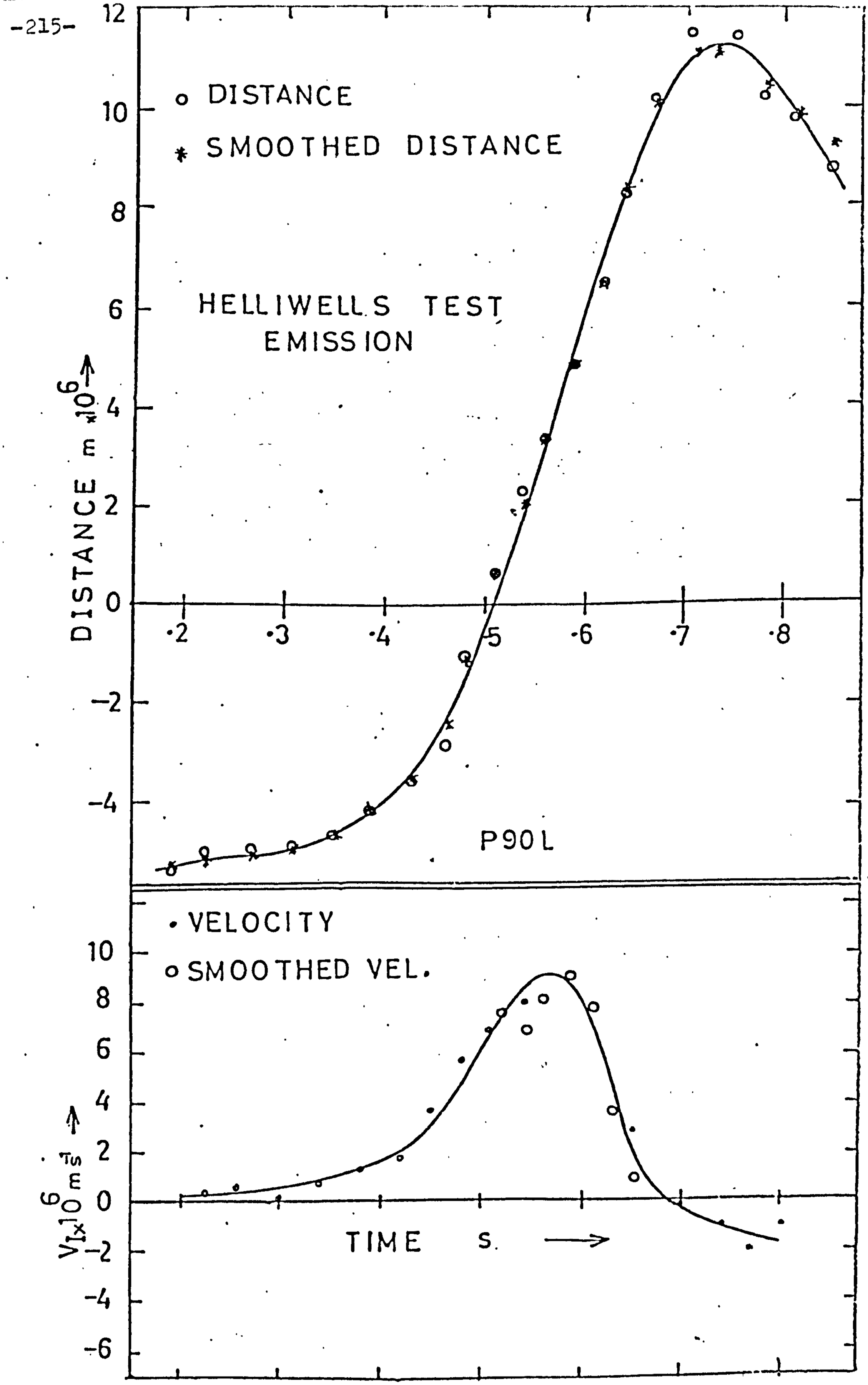
o DISTANCE
* SMOOTHED DISTANCE
HELLIWELLS TEST
EMISSION
DISTANCE m x10^6 →
12
10
8
6
4
2
0
-2
-4
·2
·3
·4
·5
·6
·7
·8
P90L
• VELOCITY
o SMOOTHED VEL.
V_Tx10^6 m/s →
10
8
6
4
2
0
-2
-4
-6
TIME S. →

FIG (9.6)

9.1 (cont'd) The method of determining S which has been described was programmed into P9OLORAINE^{++} and the routine can be seen in appendix 2. It was found possible to match slopes g_1 and g_1^* to 1 part in 10,000 for 30 separate values of g_1 (at frequency f_m) and retain reasonable computing times of up to 500 sec (CPU time).

The program was tested using emission 'E' on which the first program failed to give satisfactory results. This high latitude emission which was recorded at Andøya ($\emptyset = 67.4^{o}$) and can be seen in Fig. 9.5, was prepared for analysis and represented by twenty two frequency - time points, see Fig. 9.5a. The result of the calculation can be seen in the distance - time graph in Fig. 9.5b. The advanced distance calculating routine performed correctly and formed the basis of the work carried out on the analysis of high latitude risers.

The 'Helliwell Test Emission' shown in Fig. 9.5b was analysed using P9OL. The distance - time and velocity - time results of the calculations can be seen in Fig. 9.6. It was concluded that the new distance calculation method was satisfactory for both medium and high latitude emission analysis.

9.2 FITTING POLYNOMIALS TO EMISSION PROFILES

In section 8.3 it was pointed out that even with careful preparation of the original emission profile data it was only possible by 'difference differentiation' to obtain slopes which were accurate to about 1%. This results in a spread of values for inter-action region velocity against time through which a best fit line has to be drawn.

If all the calculated distances are in error by only 5 km (approx. 0.25%) as the results correspond to time intervals of 20 to 30 ms an error in the calculated velocity of about $4 \times 10^5 ms^{-1}$ can be achieved. As normal interaction region velocities are of the order of $5 \times 10^6 ms^{-1}$ this represents an error of 10%.

A method of reducing this error is to fit a polynomial of some degree to the points representing the original frequency - time profile of the emission. The differential of the polyomial is easily calculated and is an exact function. A convenient I.C.L. computer library sub-routine was found, which given a set of data points:

(x_k, y_k, w_k) k=1, m (m points in the set.)

where x_k is the independent variable

y_k is the dependent variable

w_k is the weighting factor (if any) associated with each point.

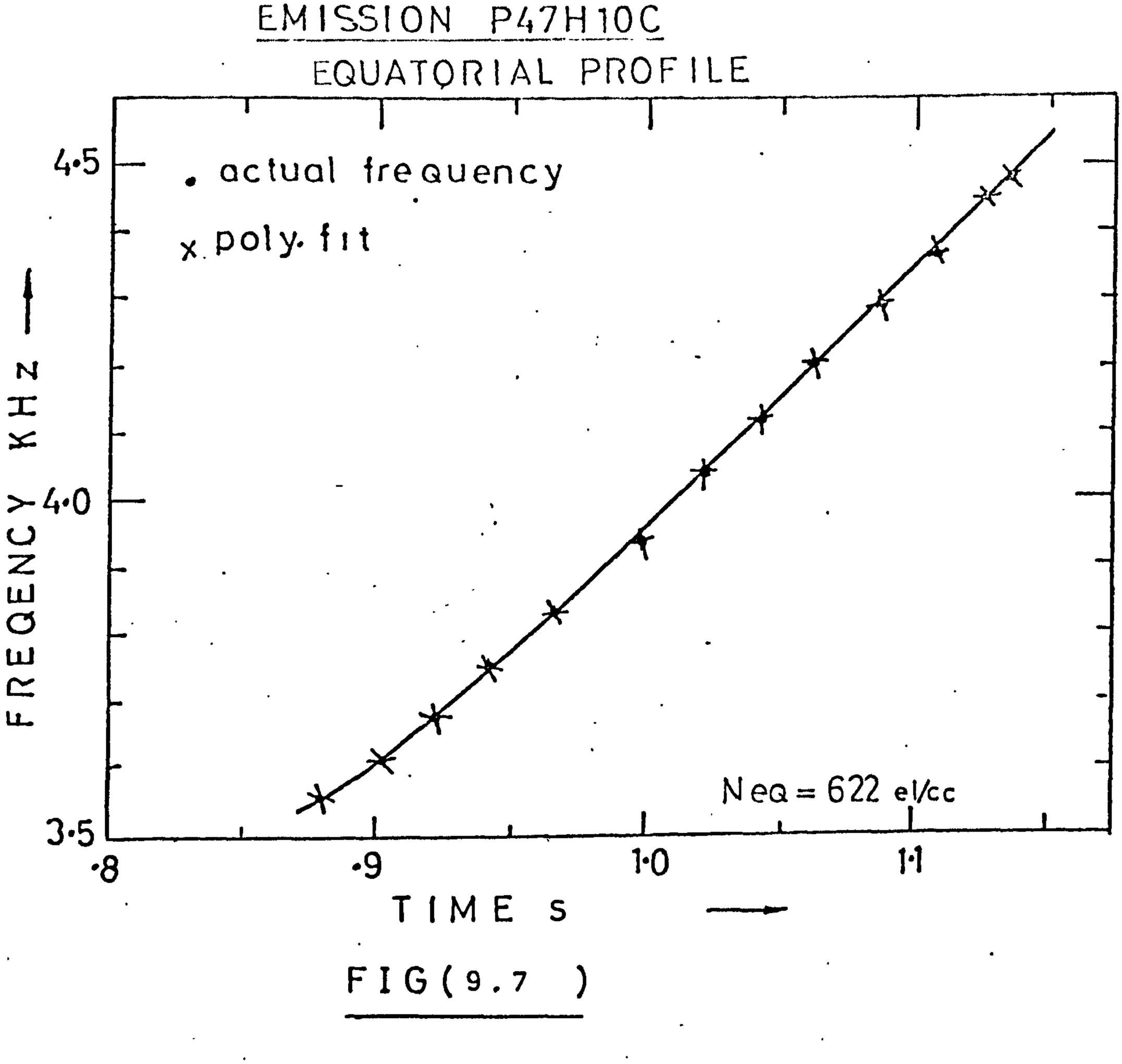
EMISSION P47H10C
EQUATORIAL PROFILE
actual frequency
poly. fit
FREQENCY KHz
4·5
4·0
3·5
·8
·9
1·0
1·1
TIME s
Neq = 622 el/cc

FIG(9.7)

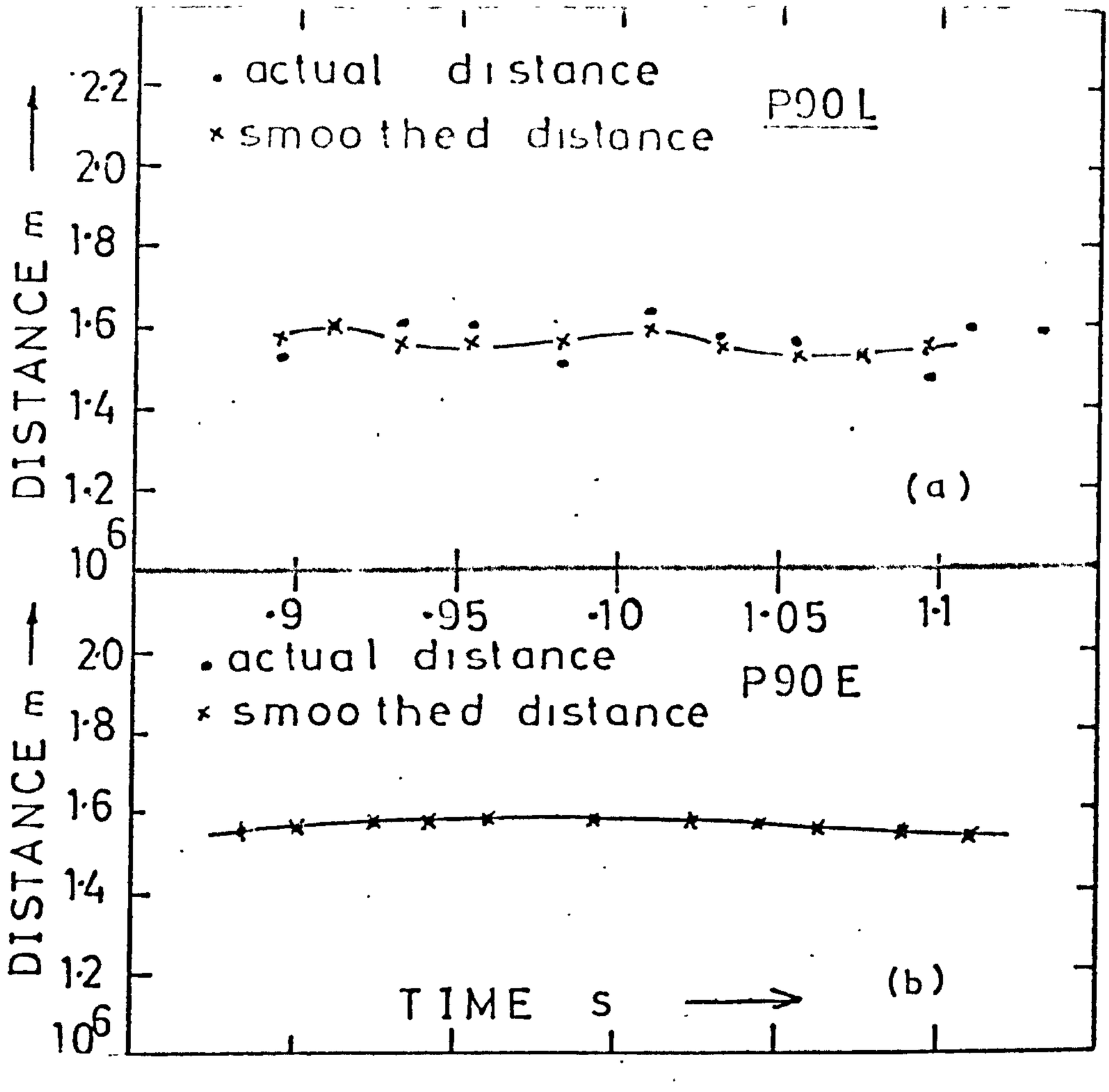

EMISSION P47H10C

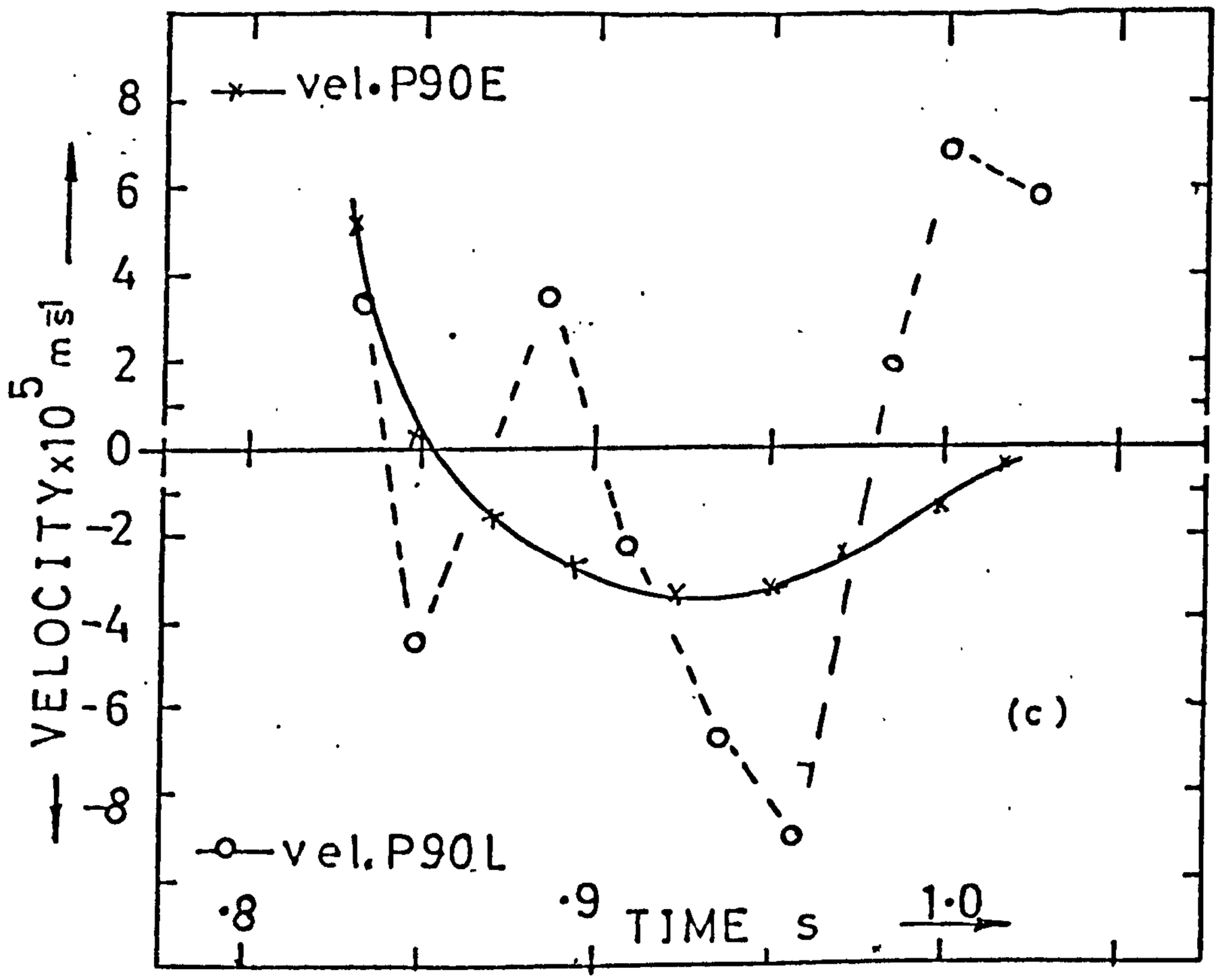

FIG.(9·8)

9.2 (cont'd) will then successively produce approximating polynomials $Q_n(x)$ n = 0,1,2 etc. up to N (the highest order required).

such that the 'error' expression:

$$s_n = \sum_{k=1}^{m} w_k(y_k - Q_n(x_k))^2$$

is minimised.

The algorithm uses orthogonal polynomials and a recursion due to Steiffel (1958), see also Haig (1970).

It was found after some experimentation that a 4th order polynomial was sufficient to give a good fit to most VLF triggered emission forms. After fitting the polynomial we have;

$$f = a_o + a_1 t + a_2 t^2 + a_3 t^3 + a_4 t^4$$

and the slop is given by;

$$df/dt = a_1 + 2a_2 t + 3a_3 t^2 + 4a_4 t^3 \quad \text{at f.}$$

Thus the slope can be accurately calculated at each frequency concerned leading to a distance - time relation which has a low random error on each point. The polynomial fitting replaced the difference differentiation of the frequency - time profile and of the distance - time curve in program P90L resulting in a new program called P90E.

HELLIWELLS TEST EMISSION

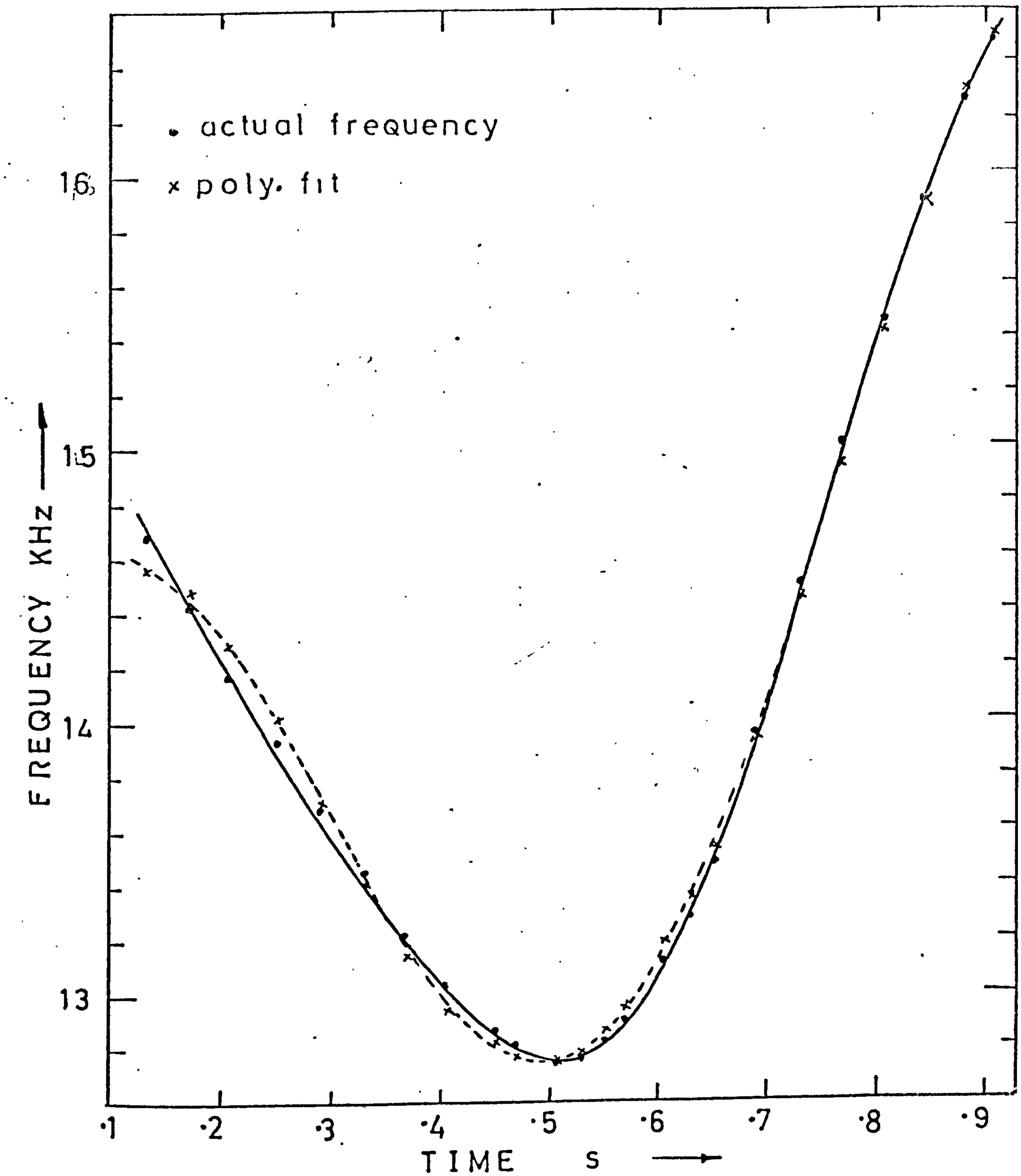

FIG.(9.9)

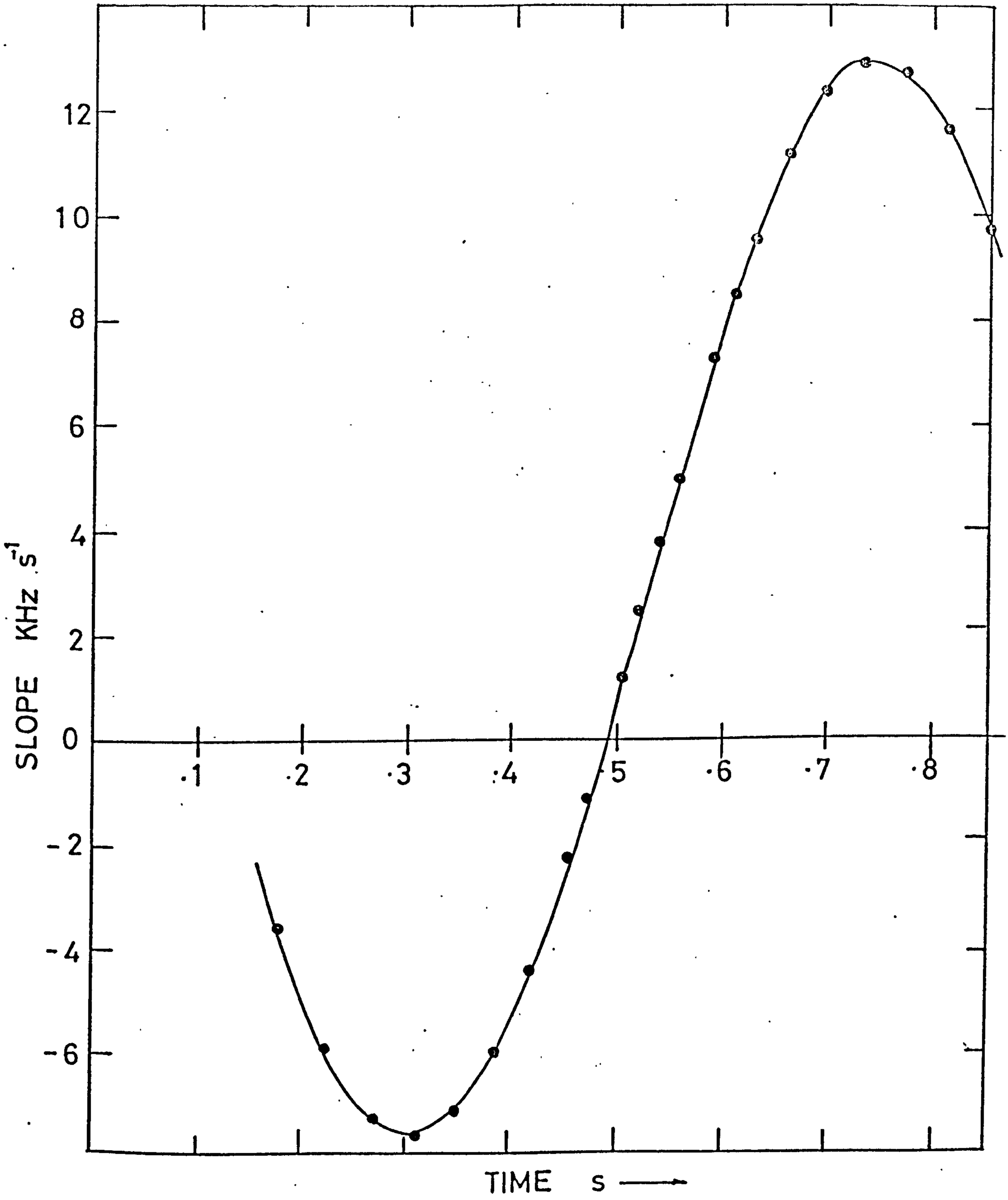

FIG.(9.10)

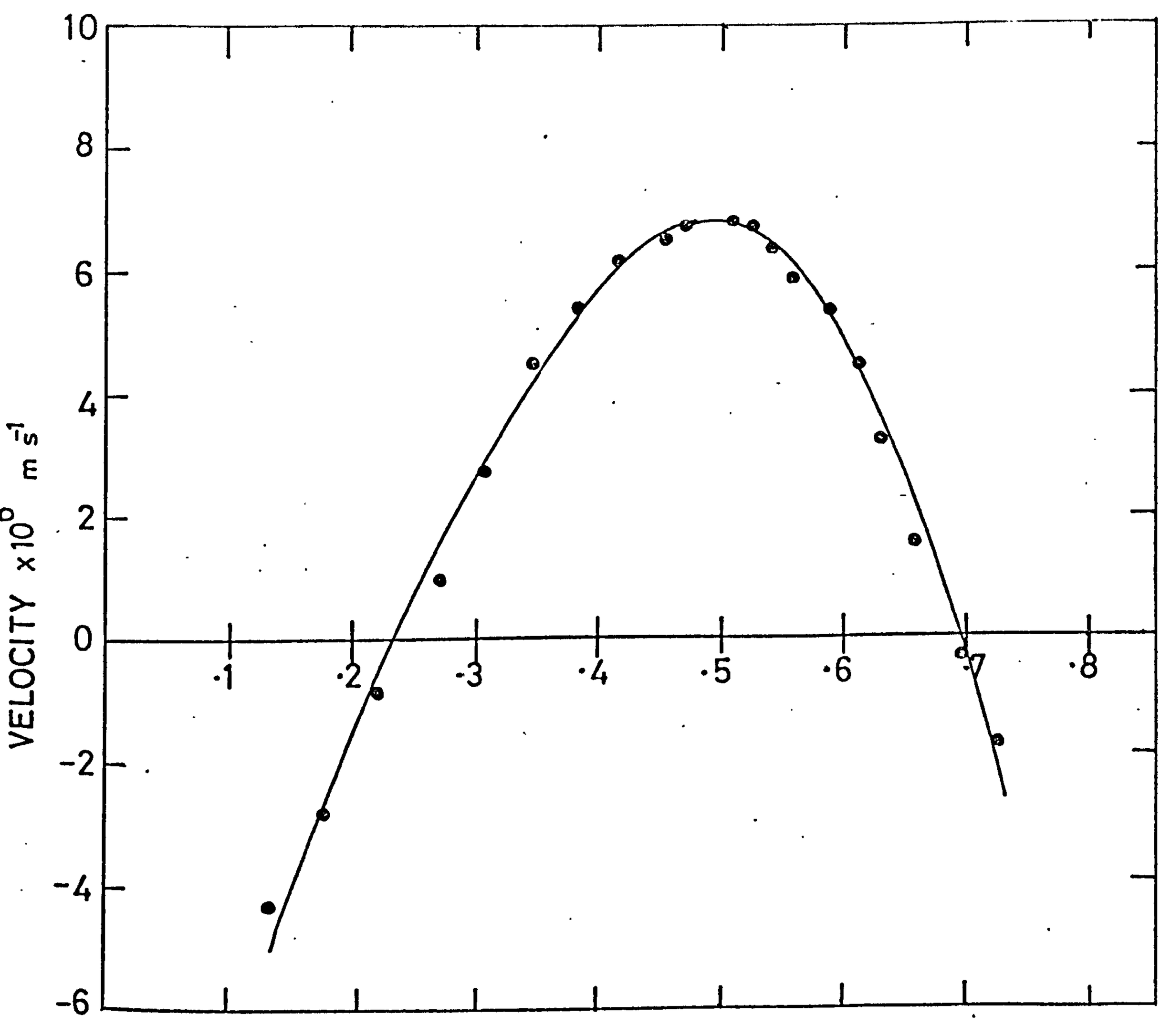

FIG(9.11)

9.2 (cont'd) A single medium latitude chorus element recorded at S.Uist (P47H10C) is shown in Fig. 9.7. A fourth order polynomial was fitted to the frequency - time points representing the equatorial profile of the emission. The resulting distance time curve can be seen in Fig. 9.8b. It may be compared with that which is produced by the earlier program which used 'difference differentiation', see Fig. 9.8a. It is clear that the random error on each point has been dramatically reduced whilst the polynomial fitting has had no gross disturbing effect on the general form or level of the result. The velocity - time relations derived with and without the polynomial fitting can be seen in Fig. 9.8c and it is clear that without it the result is confused, whereas a reliable curve is obtained if polynomials are fitted to the original data and to the distance - time data.

Fitting polynomials in order to obtain differentials without incurring large random errors is a powerful aid to the analysis of discrete VLF emissions but it has a limited application. Polynomials of order 4 to 10 were fitted to the profile in Fig. 8.5b and it was not possible to produce the correct form of the velocity - time curve as shown in Fig. 8.5e. The problem can be illustrated by considering fitting a fourth order polynomial to the data. In Fig. 9.9 it can be seen that at the low frequency end of the emission the fit is rather poor and that a change in the direction of the slope occurs at about 0.3 seconds. This produces a distortion of the slope - time curve, see Fig. 9.10. However, comparison with Fig. 8.9 shows a large decrease in the scatter of the slope values which were calculated using the polynomial. The distortion of the df/dt curve is carried

9.2 (cont'd) over into the velocity - time result and an incorrect profile is produced. Again the scatter of points is much less than with 'difference differentiation', see Fig. 9.11.

Accurate polynomial fitting, especially at the edges of the function, is only possible if the function is relatively simple. Those which are not monotonically increasing or decreasing, present difficulties and the greater the number of changes of sign of the slope then the greater is the difficulty in successfully fitting a polynomial.

Therefore program P90L is used for the analysis of emissions with complicated forms, whilst P90E, which contains the polynomial fitting routine, may be used for simple forms. In the analysis of risers at both medium and high latitudes the forms were simple enough to permit the use of P90E. It is only when hooks or other such forms are to be analysed that P90L is required.

9.3 THE APPLICATION OF THE SECOND RESONANCE CONDITION TO MEDIUM LATITUDE VLF EMISSIONS

Prior to describing the results obtained by analysing a number of emissions which were recorded at S.Uist during the firing of a Petrel Rocket P47H in November 1970 it is necessary to indicate the manner in which data is prepared for analysis and the accuracy which is obtainable. Consider the calibration chart produced by a Sonograph spectrum analyser which is shown in Fig. 9.12. The analyser produces internal frequency calibration every 500Hz and a further external signal from a stable source at a frequency of 1 KHz $\pm$ 1 Hz is also displayed.

The centre of the 1 KHz internally generated line is estimated and digitised at 7 points along its length and plotted on a large sheet of graph paper approximately 40 cm x 60 cm. The top and bottom edges of the external frequency stable line are digitised and also plotted on the same graph. A smaller scale representation of the graph is shown in Fig. 9.13 which shows a typical systematic error of 40 Hz in 2 seconds. The random errors due to the estimation of the centre of edges of a line can also be seen. It is possible to draw a best fit line through the top and bottom edges of a recording and then to draw a new line midway between which is taken to represent the test signal. By this means the random error in digitising a signal may be reduced to 1% which is necessary as mentioned in section 8.3 in order that the interaction region velocity may be determined. All emissions were prepared for analysis in this way and a small scale example is given in Fig. 9.14 of emission 'A' which may be seen as the original Sonogram in Fig. 10.3.

TYPE B/63 SONAGRAM® KAY ELEMETRICS CO. PINE BROOK, N. J.

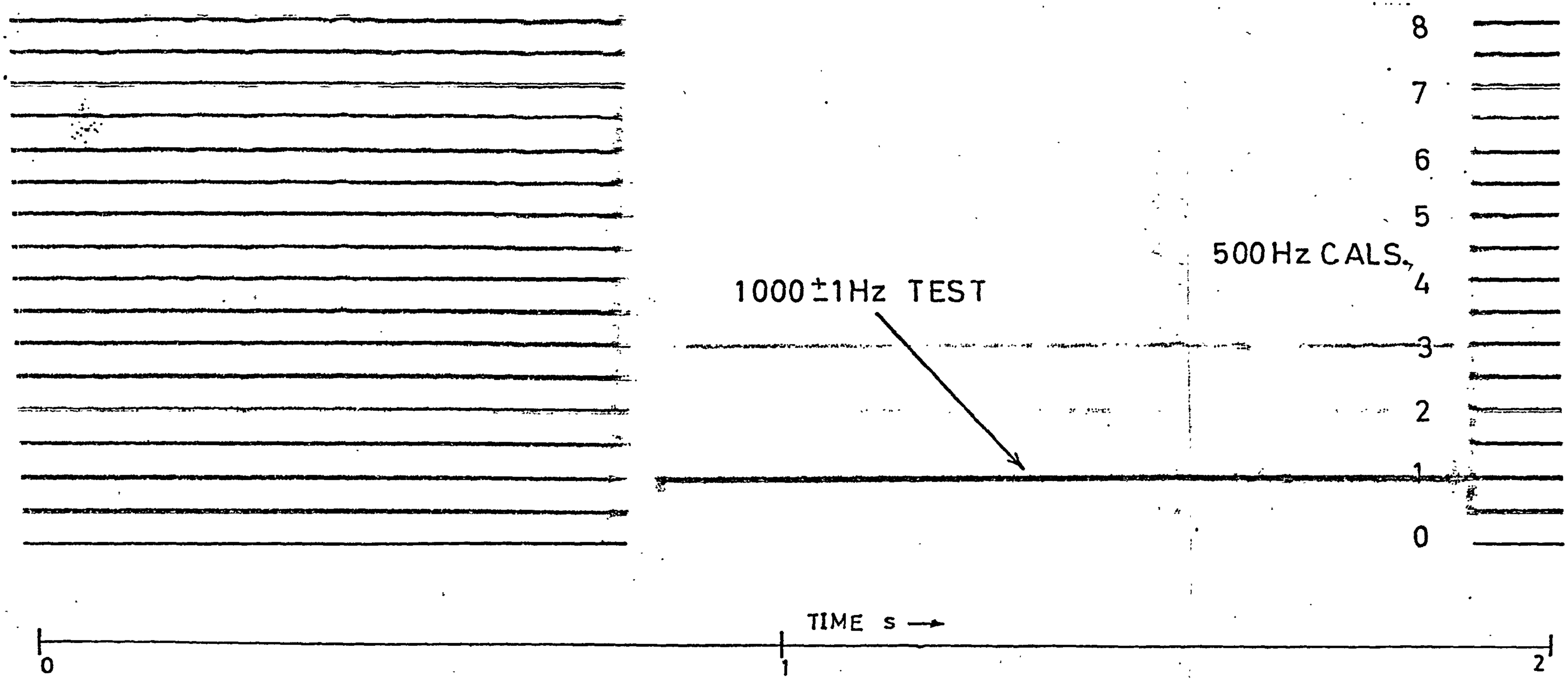

FIG. 9·12

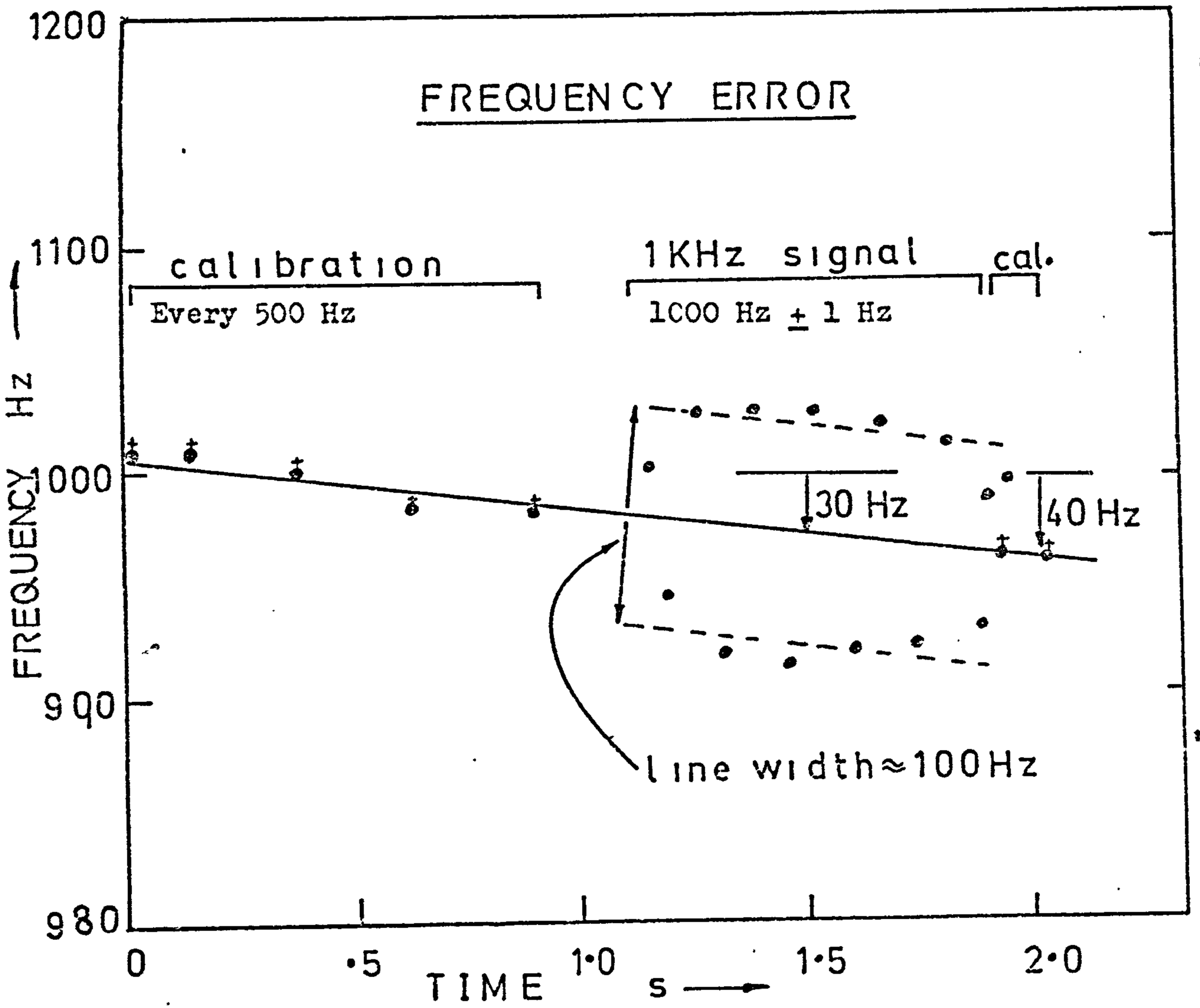

FIG(9.13)

Typical systematic error of 30 Hz in 1000 Hz. 3%.

Error in cal.and test frequencies 0.5%

Error in estimating the centre of a cal.line is aprox. 0.5%

Single frequency test tone is broadened to a bandwidth of aprox. 100 Hz. Bandwidth is dependent on 'mark level' setting on the Sonograph.

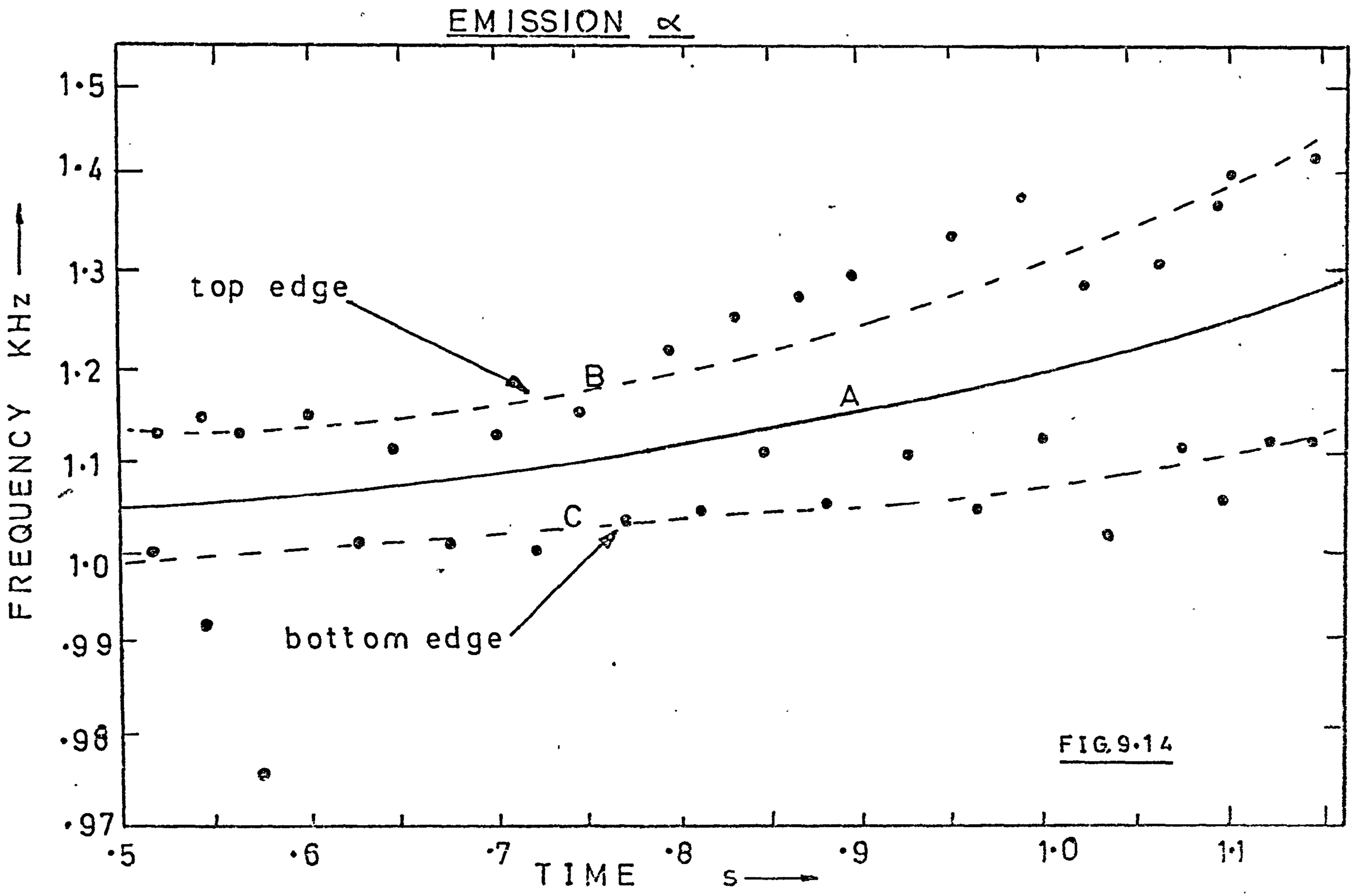
EMISSION ∝
FREQUENCY KHz ⟶
1·5
1·4
1·3
1·2
1·1
1·0
·99
·98
·97
top edge
bottom edge
A
B
C
·5
·6
·7
·8
·9
1·0
1·1
TIME s ⟶

FIG. 9·14

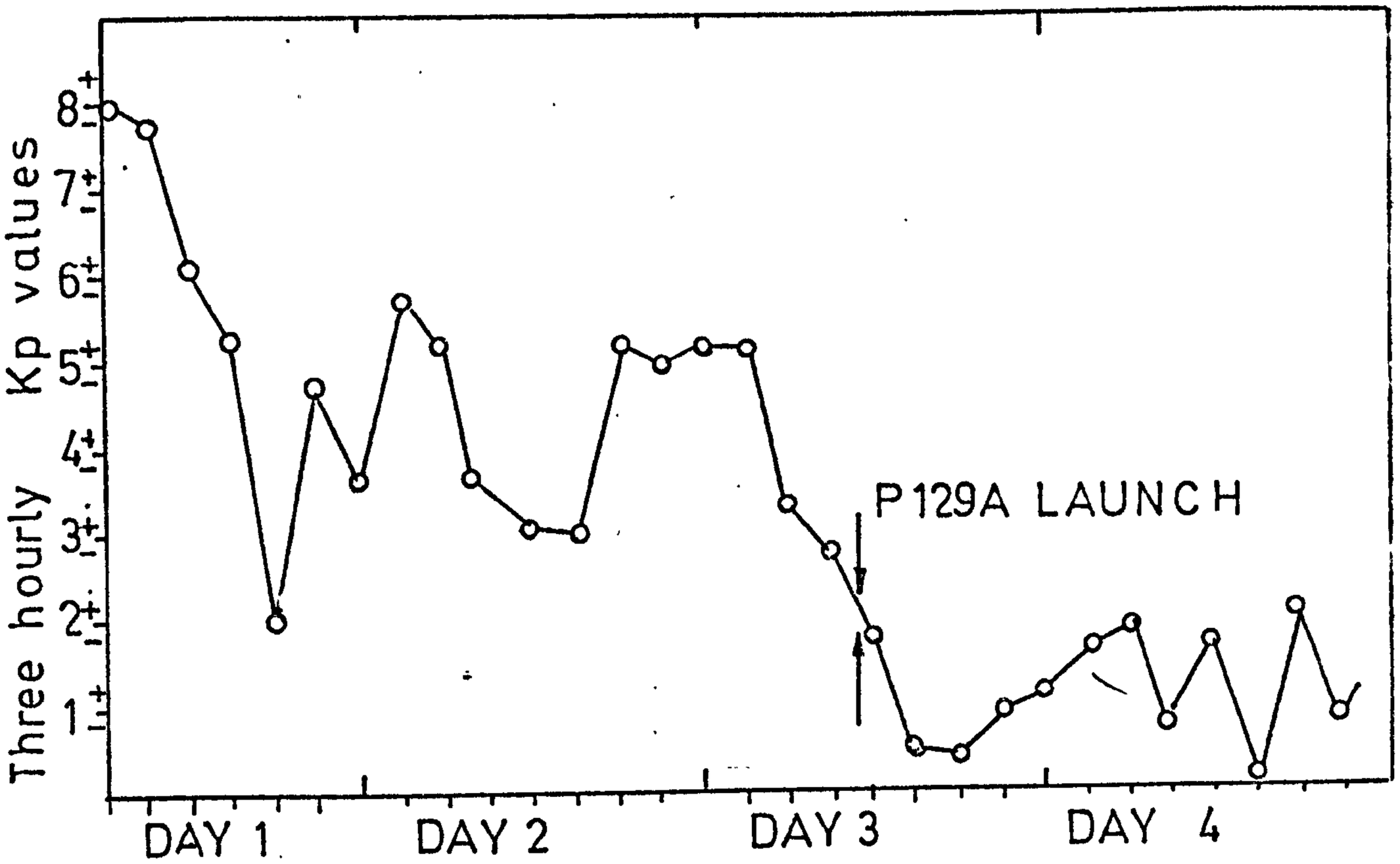
Three hourly Kp values
8+
7+
6+
5+
4+
3+
2+
1+
P129A LAUNCH
DAY 1
DAY 2
DAY 3
DAY 4

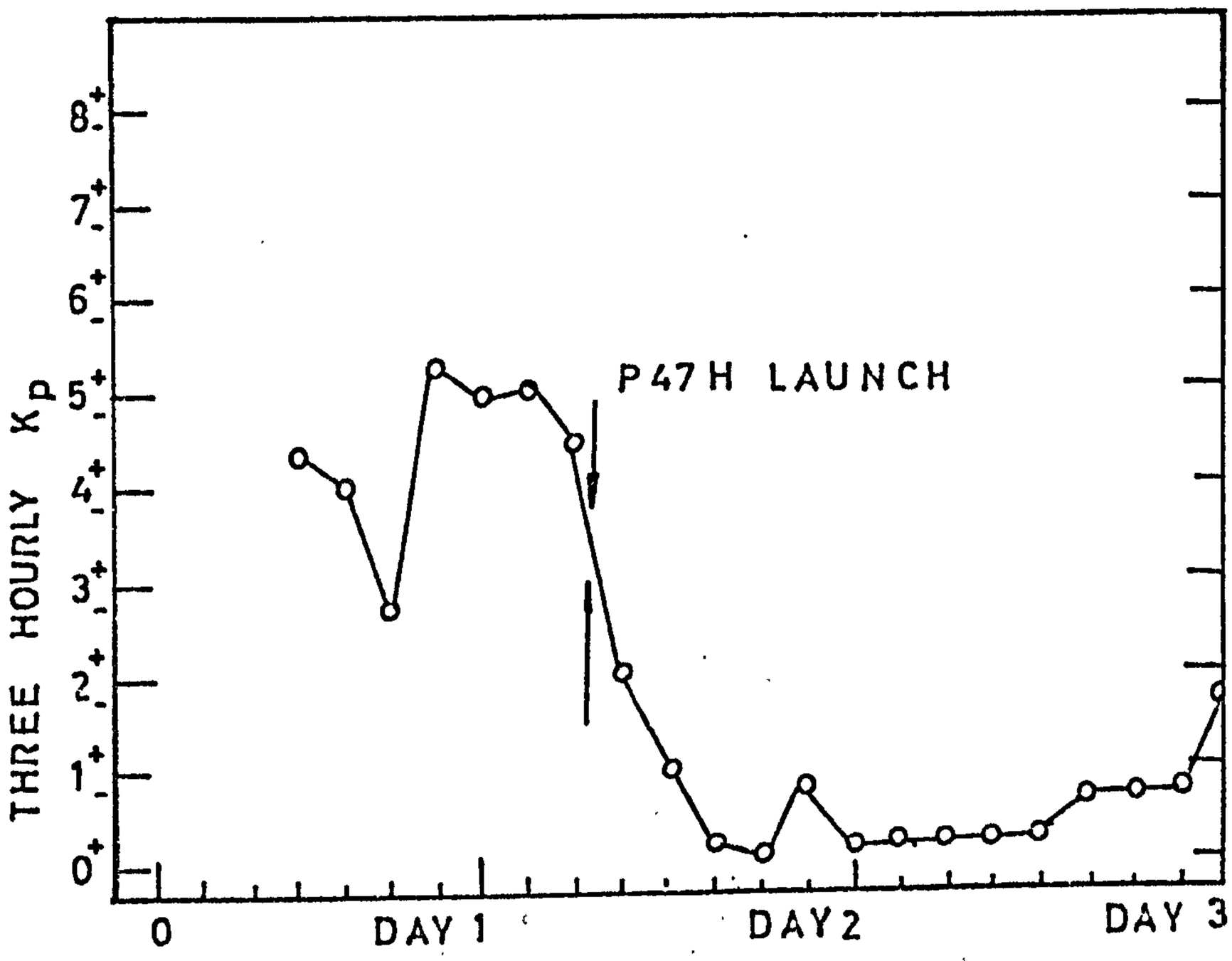
THREE HOURLY Kp
8+
7+
6+
5+
4+
3+
2+
1+
0+
P47H LAUNCH
0
DAY 1
DAY2
DAY 3

FIG.(9.15)

9.3 (cont'd) The thickness of a test line or the bandwidth of an emission is dependent on the 'Mark Level' setting on the Sonograph and usually it is not possible to determine bandwidths of less than 100 Hz. Six emissions recorded on the ground at S.Uist with a large loop antenna VLF receiver operated by the University of Southampton were chosen from a number similar to those shown in Fig. 1.7. The emissions were chosen if they were of high intensity and narrow bandwidth such as the one marked with small arrows in Fig. 1.7.

The chorus, which consisted of many overlapping rising frequency elements between 2 KHz and 6 KHz, was of average intensity (Rycroft et al 1972) and was recorded 2 hours before sunrise at 100 km above the Uist range, at 05 15 U T on the 19th of November 1970. The emissions were received after a day of high magnetic activity as the magnetic index was falling, see Fig. 9.15.

The six chosen emissions were analysed with program P90E and the results of the computations are given in Figs. 9.16 to 9.38. Consider the observed frequency time profile of emission P47H10D in Fig. 9.16 it is a gently curving rising tone covering frequencies from 3.25KHz to 5.8 KHz in about 0.2 seconds. The dispersion effects incurred in the observer's hemisphere are removed, the time delays at 3.3KHz and 5.7 KHz being 1.129 s and 0.932 s respectively. (The higher frequencies travel faster as they approach the nose frequency of 8.5 KHz). The effect of removing the dispersion delay is to 'stretch out' the emission profile to about 0.4 s. The distances to the interaction region are calculated from the slopes of the extended equatorial emission profile.

EMISSION P47H10D

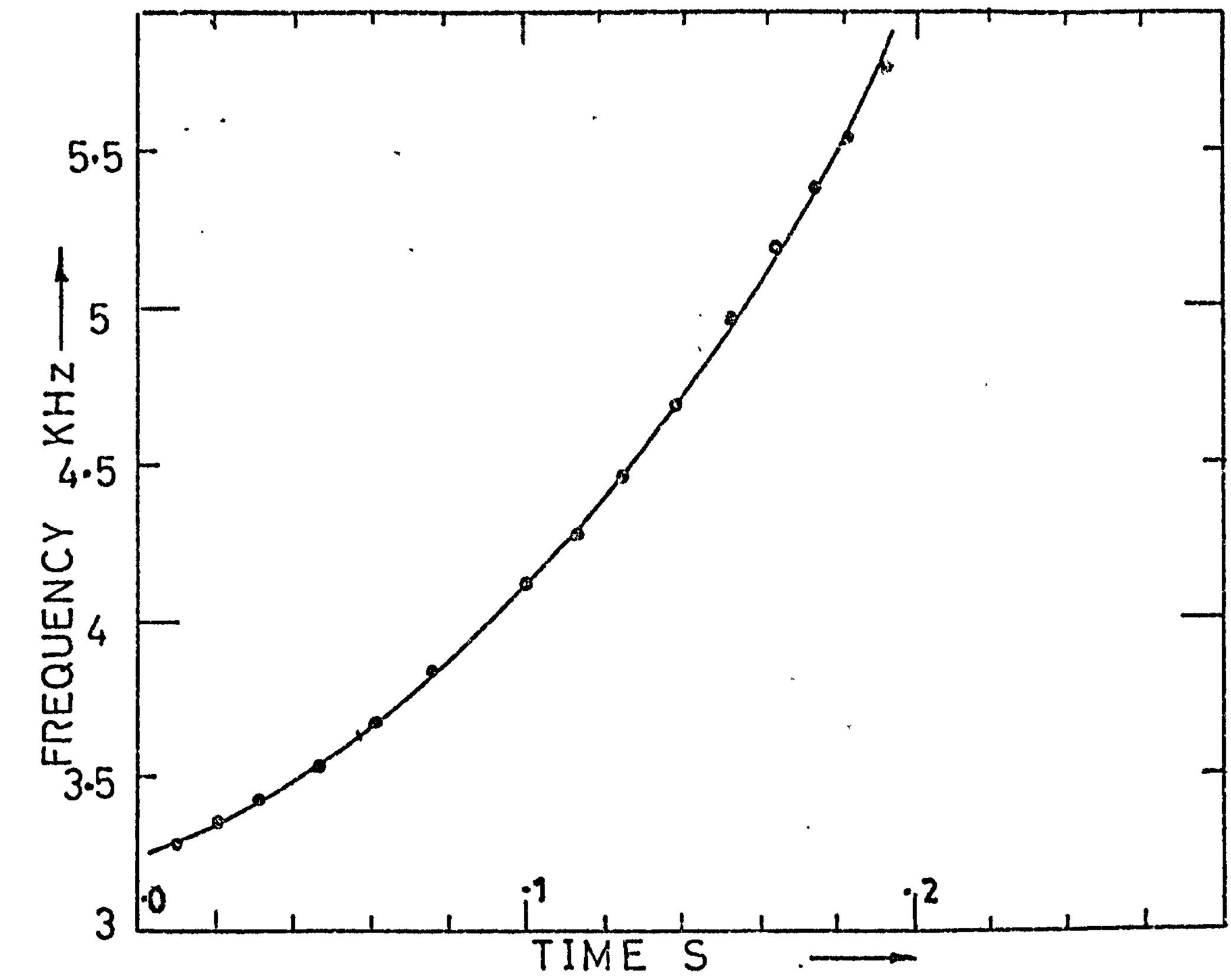

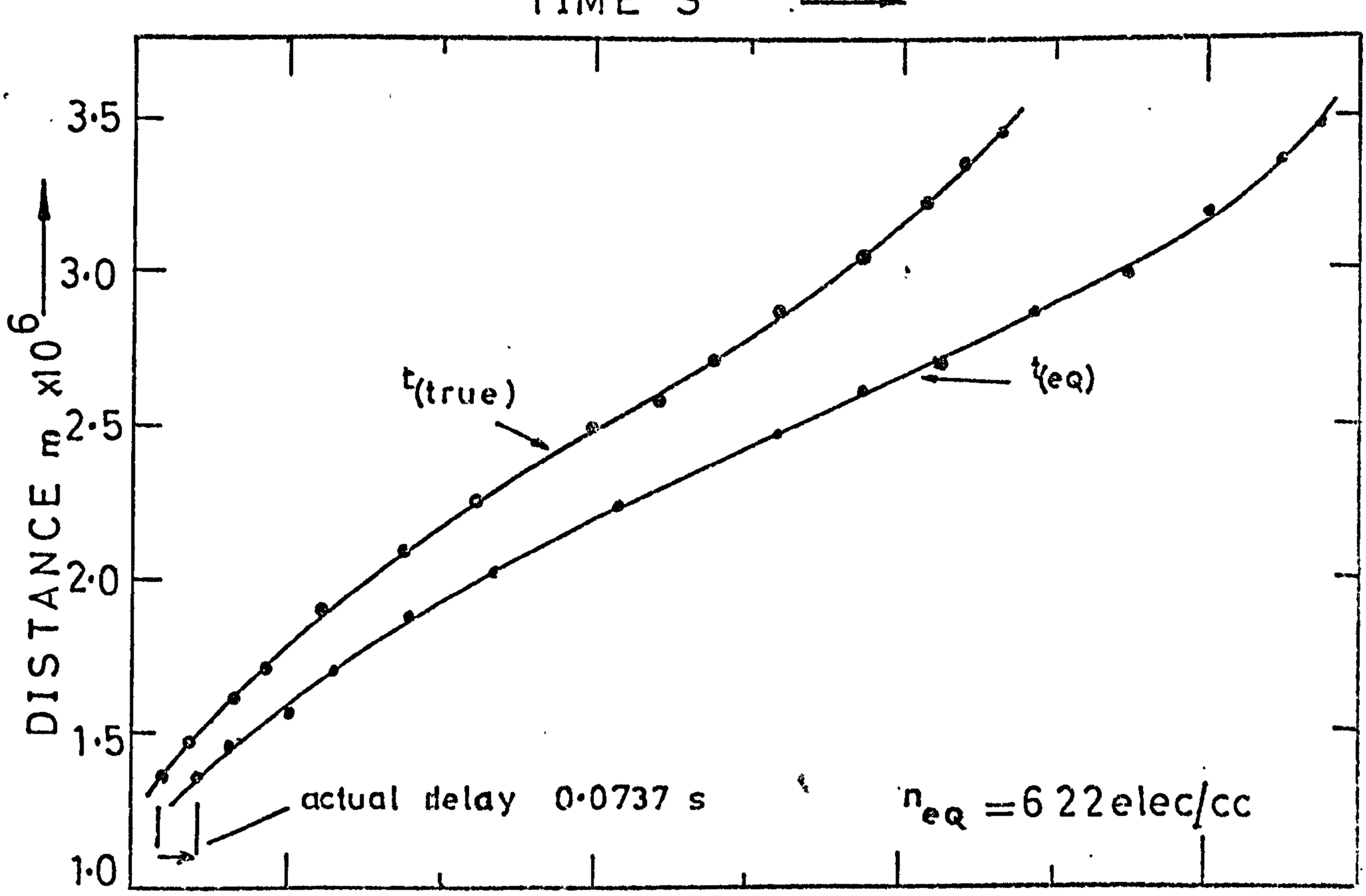

FIG(9.16)

EMISSION P47H10D

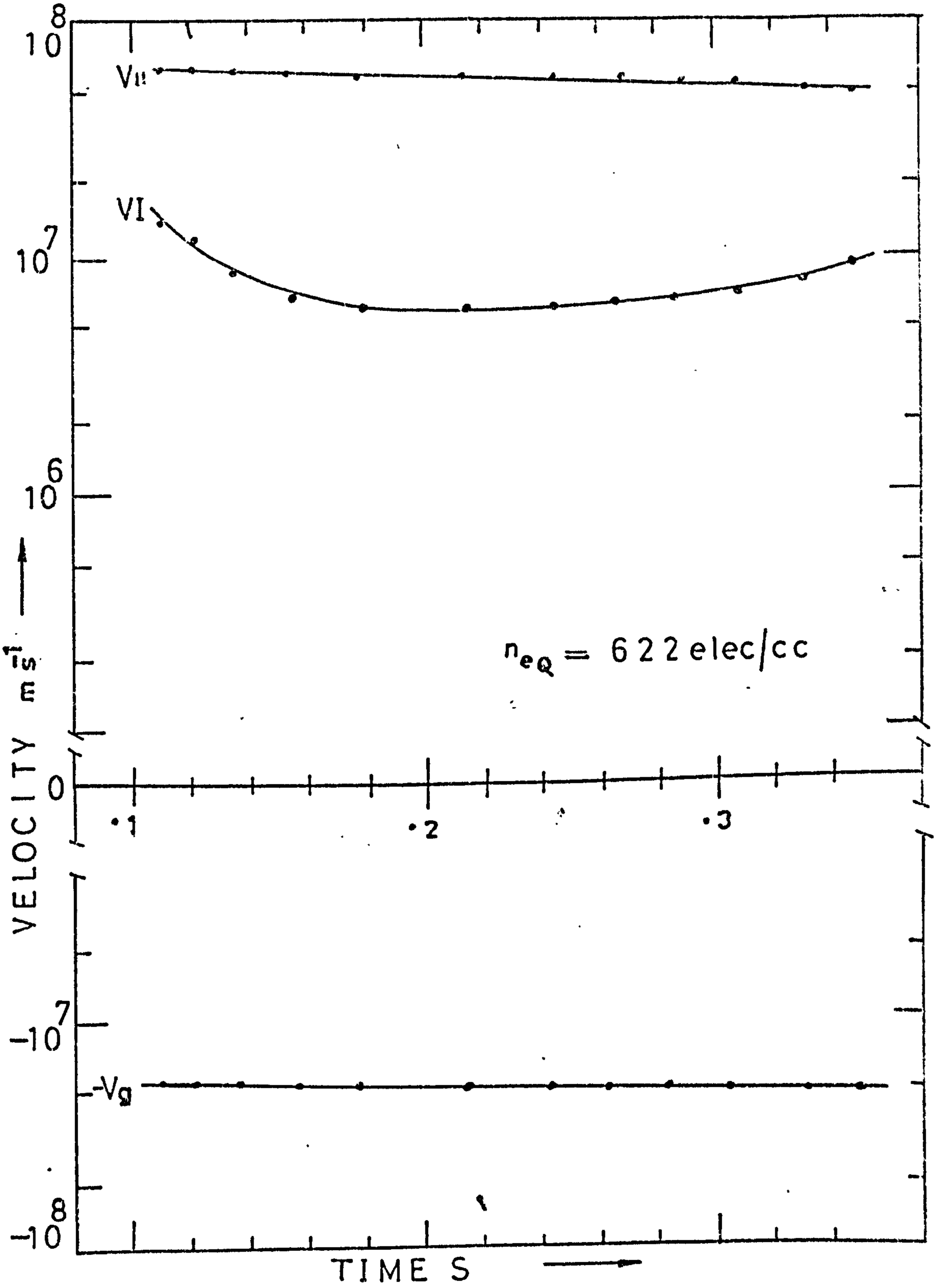

FIG(9 .17)

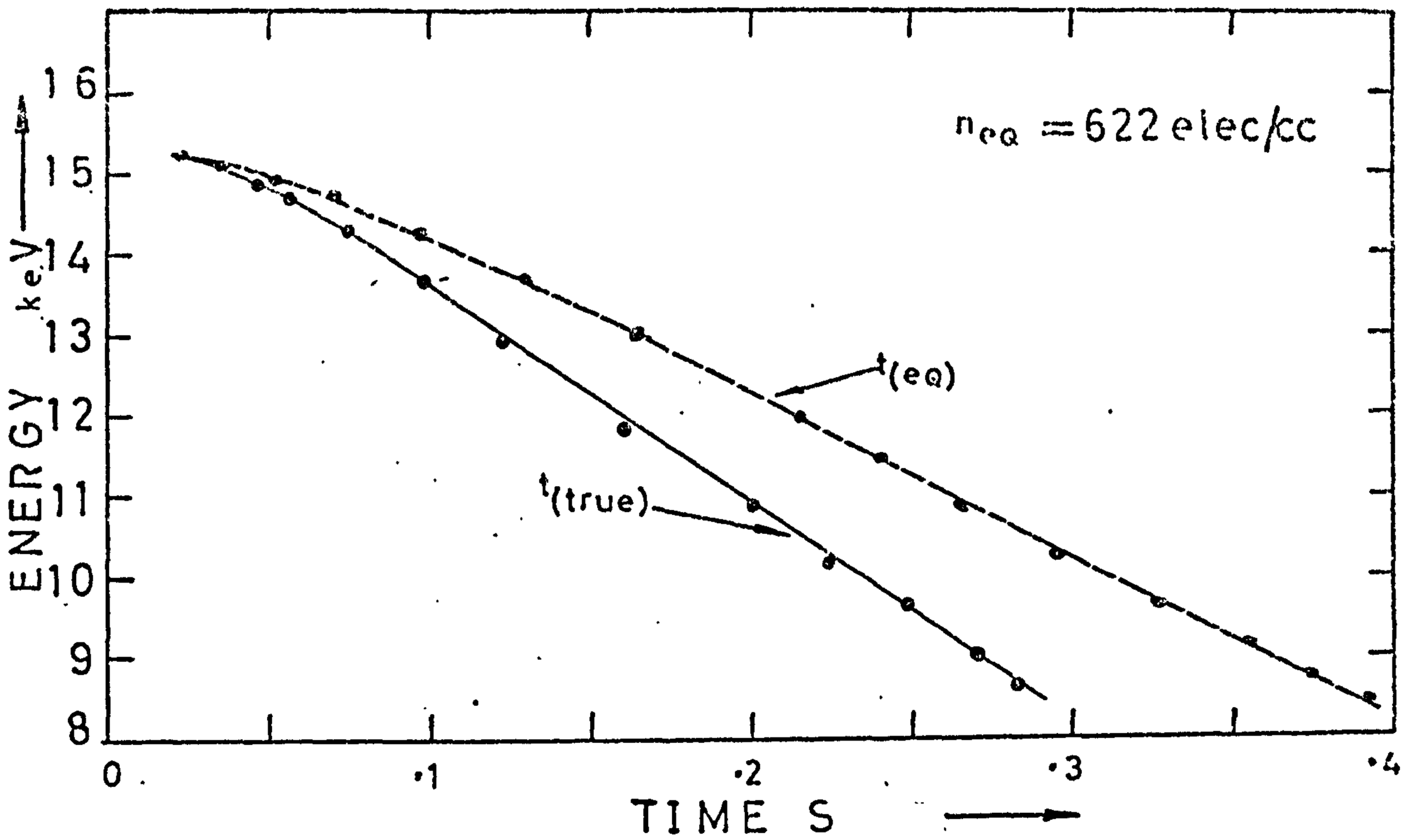

EMISSION P47H10D

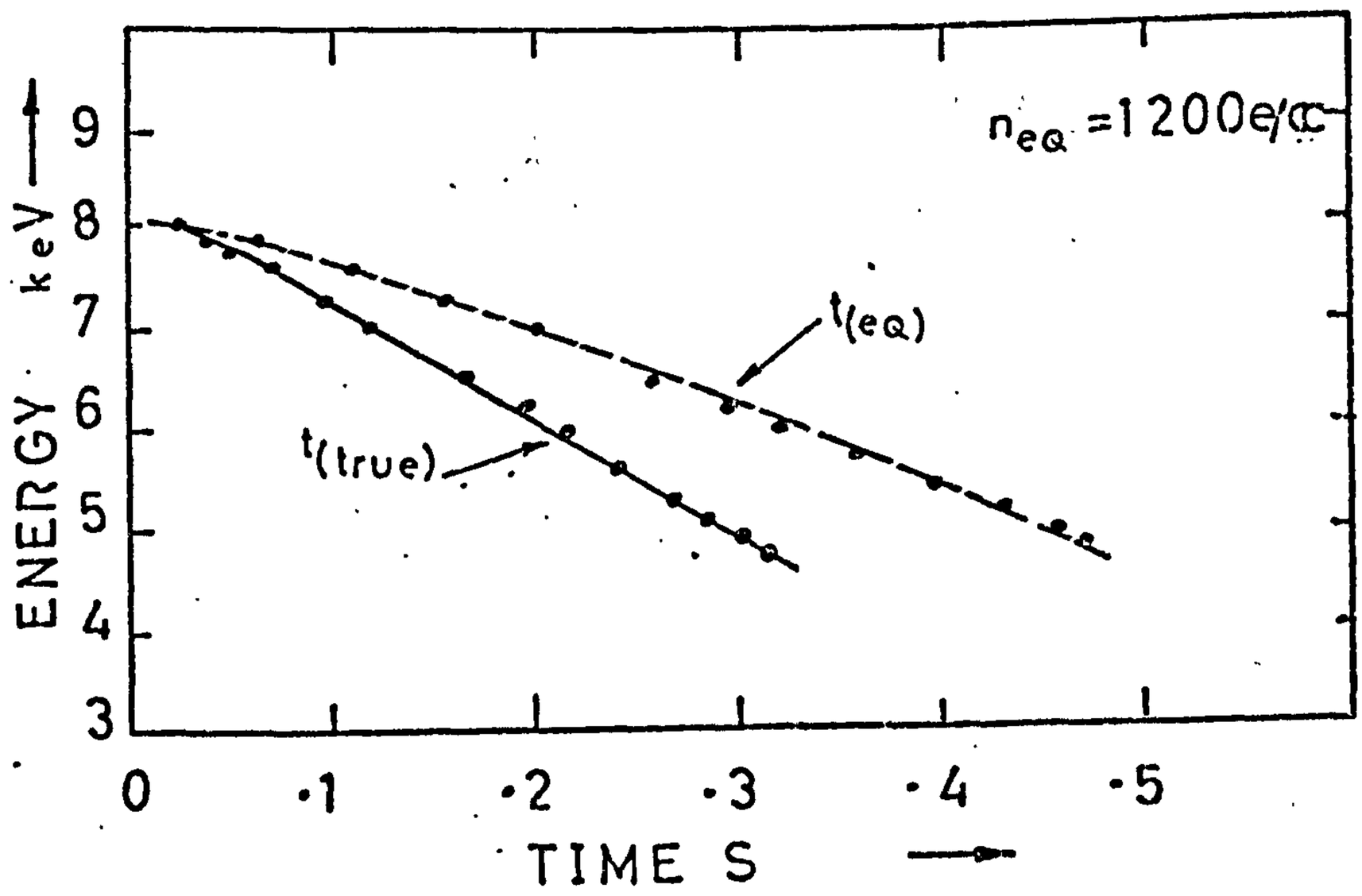

FIG(9 .18)

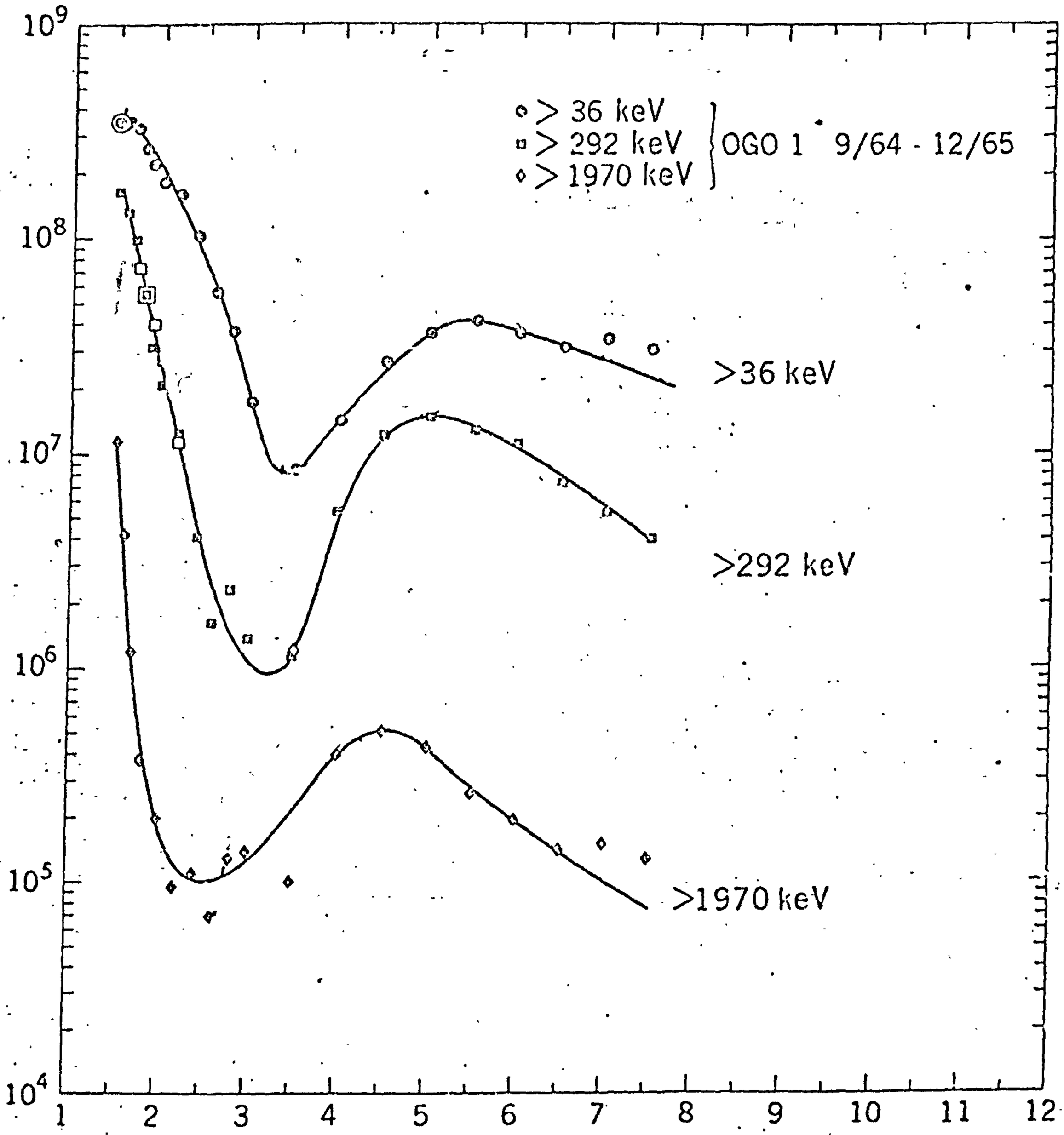
10^9
10^8
10^7
10^6
10^5
10^4
EQUATORIAL OMNIDIRECTIONAL FLUX (electrons cm^{-2} sec^{-1})
> 36 keV
> 292 keV
> 1970 keV
OGO 1 9/64 - 12/65
>36 keV
>292 keV
>1970 keV
1 2 3 4 5 6 7 8 9 10 11 12
L (earth radii)

FIG(9.18A)

9.3 (cont'd) The distance as a function of 'equatorial time' can be seen in Fig. 9.16. When the dispersion delay from the generation point to the equator has been included the curve is compressed as greater delays occur when the generation region is far from the equator. Thus the distance as a function of 'true time' or 'interaction time' is obtained.

The interaction region velocity is calculated using 'true time' and can be seen in Fig. 9.17 with the parallel component of velocity of resonant electrons and the wave group velocity. The interaction region velocity is well behaved and fulfills the necessary energy conservation condition for the interaction, $-v_g < V_I < v_{II}$, see Helliwell 1967. The energy of the resonant electrons is calculated assuming a pitch angle of 30^o which is a likely value as the maximum transverse current density is produced by electrons with this pitch angle (Helliwell 1967). The graphs of resonant energy as a function true and equatorial time are given for two values of equatorial electron densities in Fig. 9.18. Values of 600 and 1200 electrons/cc are used as limiting values of equatorial electron density for the S.Uist field line. These are taken from Sagredo 1971 and correspond to the summer day and winter night conditions using a diffusive equilibrium model of magnetospheric electron density. Thus the resonant energies calculated in the two cases are limiting values and the actual energies of the resonant electrons may be assume to lie within this range. Unfortunately the equatorial electron density was not measured during the chorus burst and the rocket payload which was fired into the event did not carry electron spectrometers and pitch angle measuring equipment.

EMISSION P47H 11C

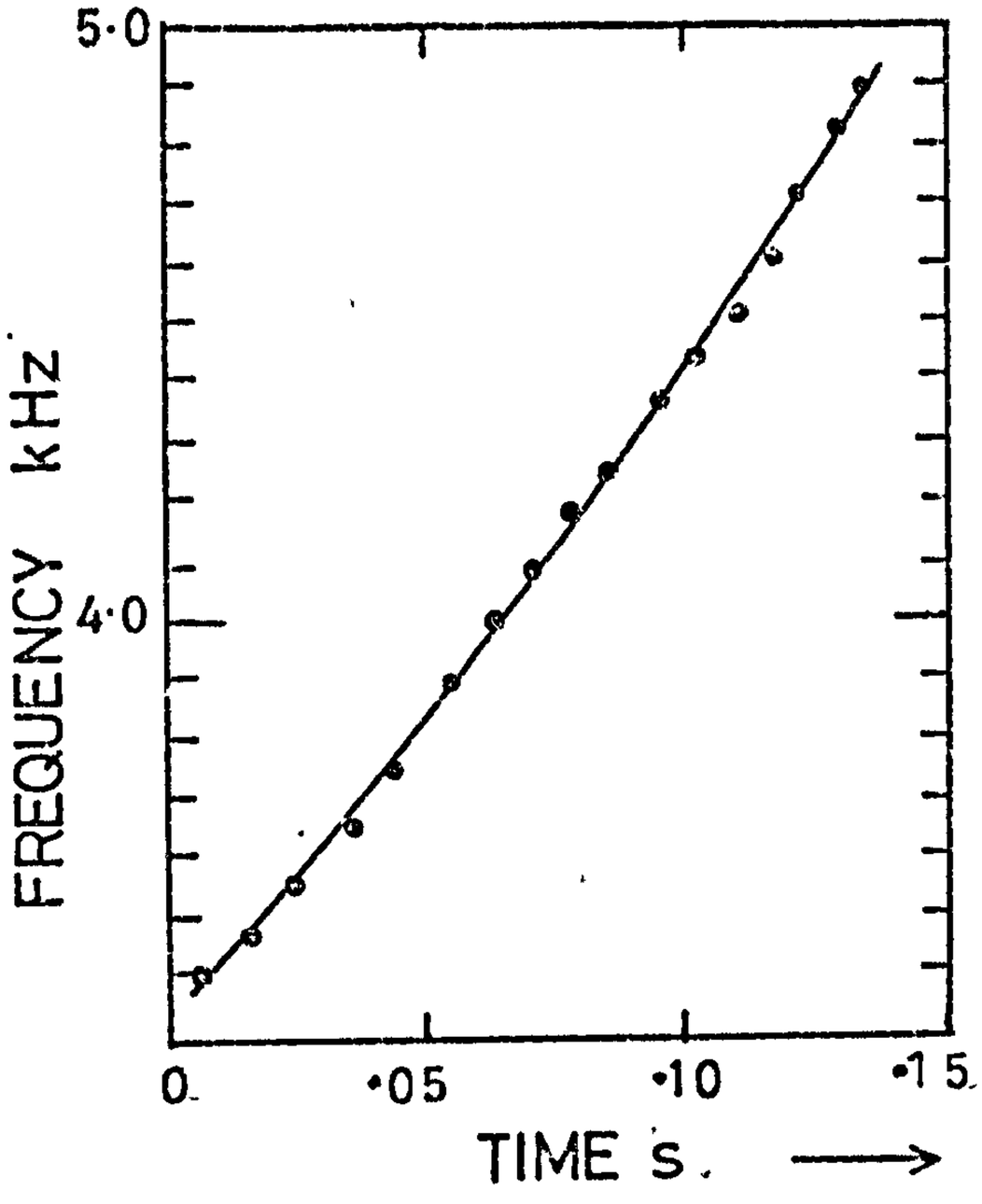

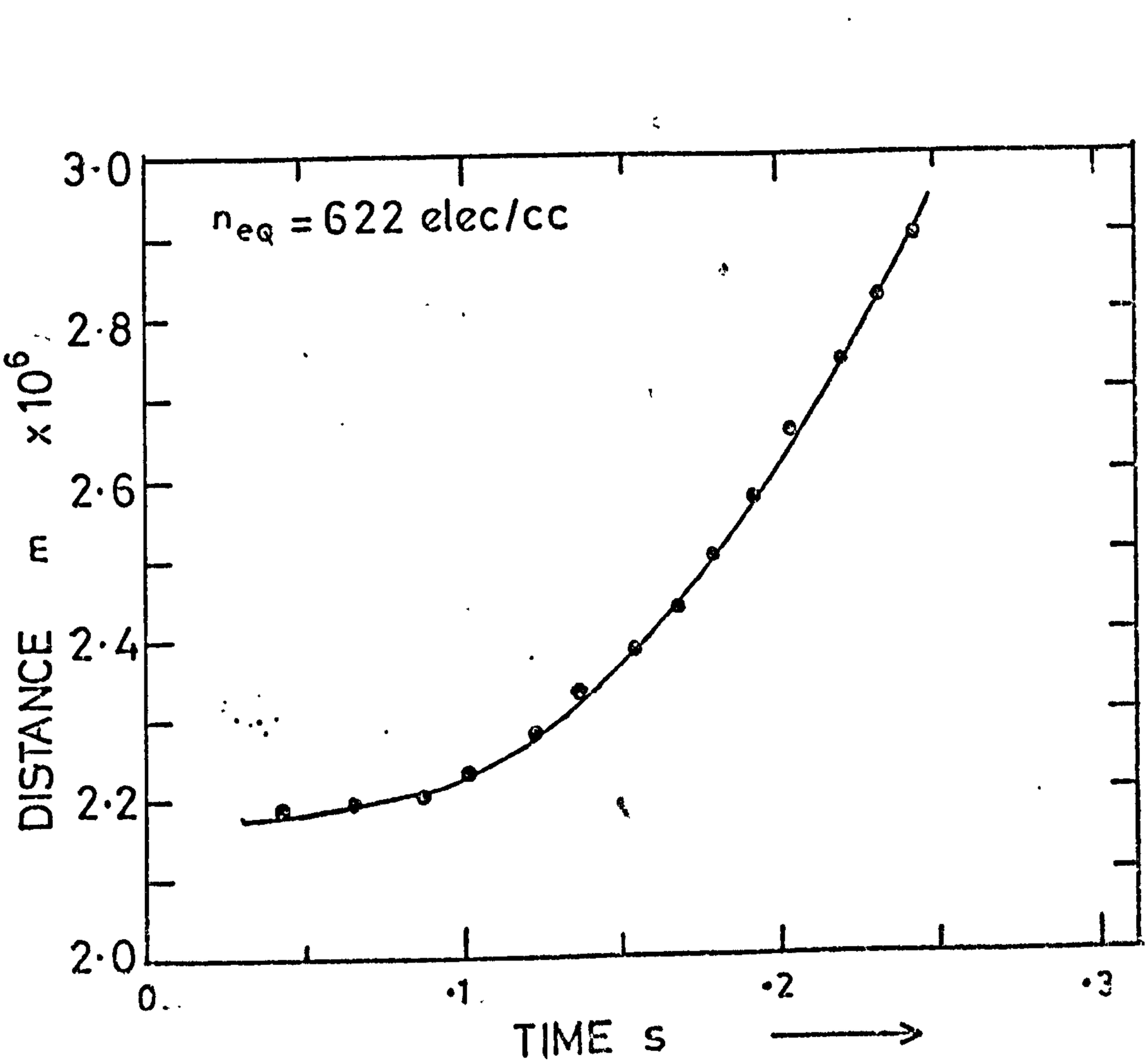

FIG.(9 .19)

EMISSION P47H11C

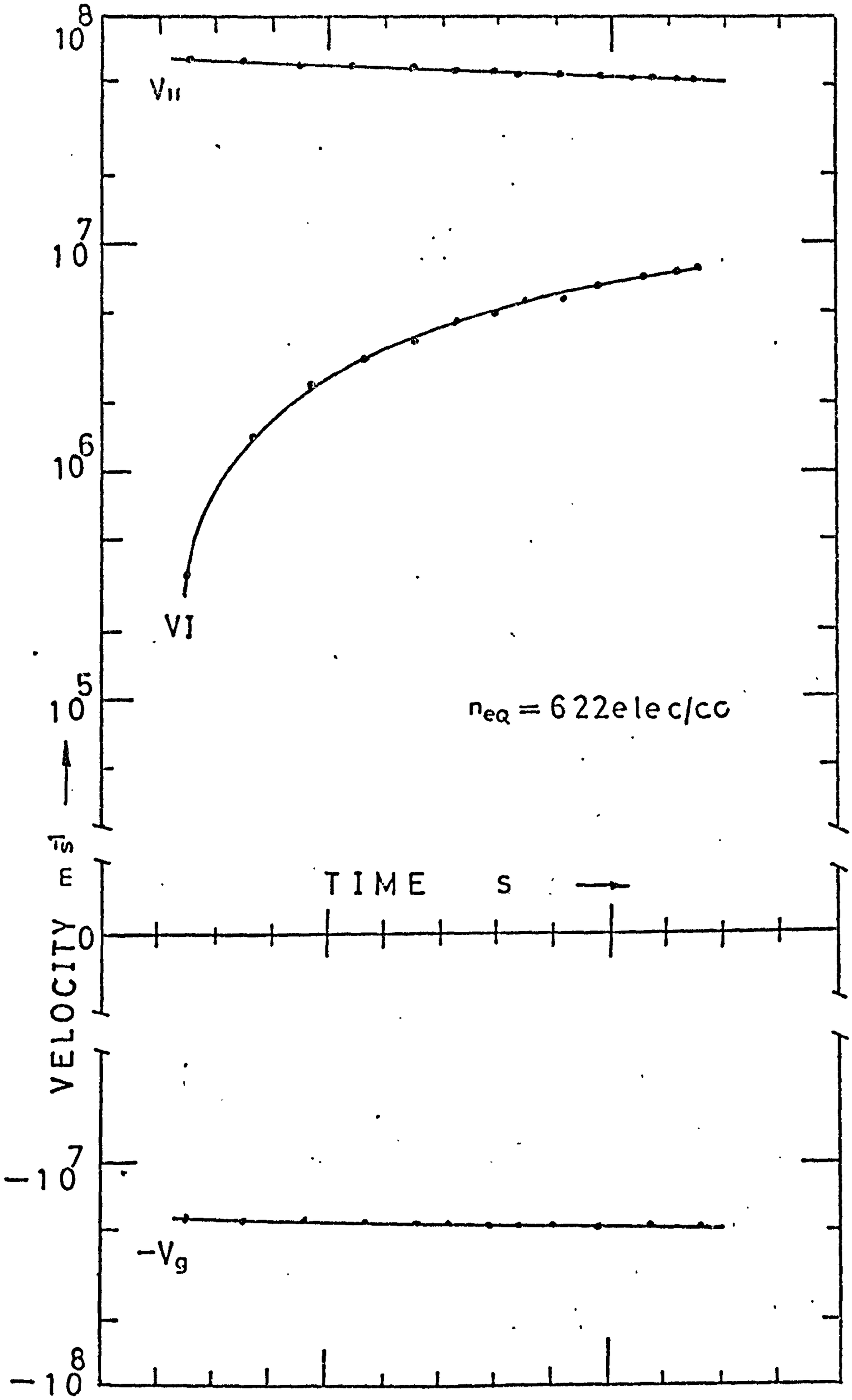

FIG(9 .20)

EMISSION P47H11C

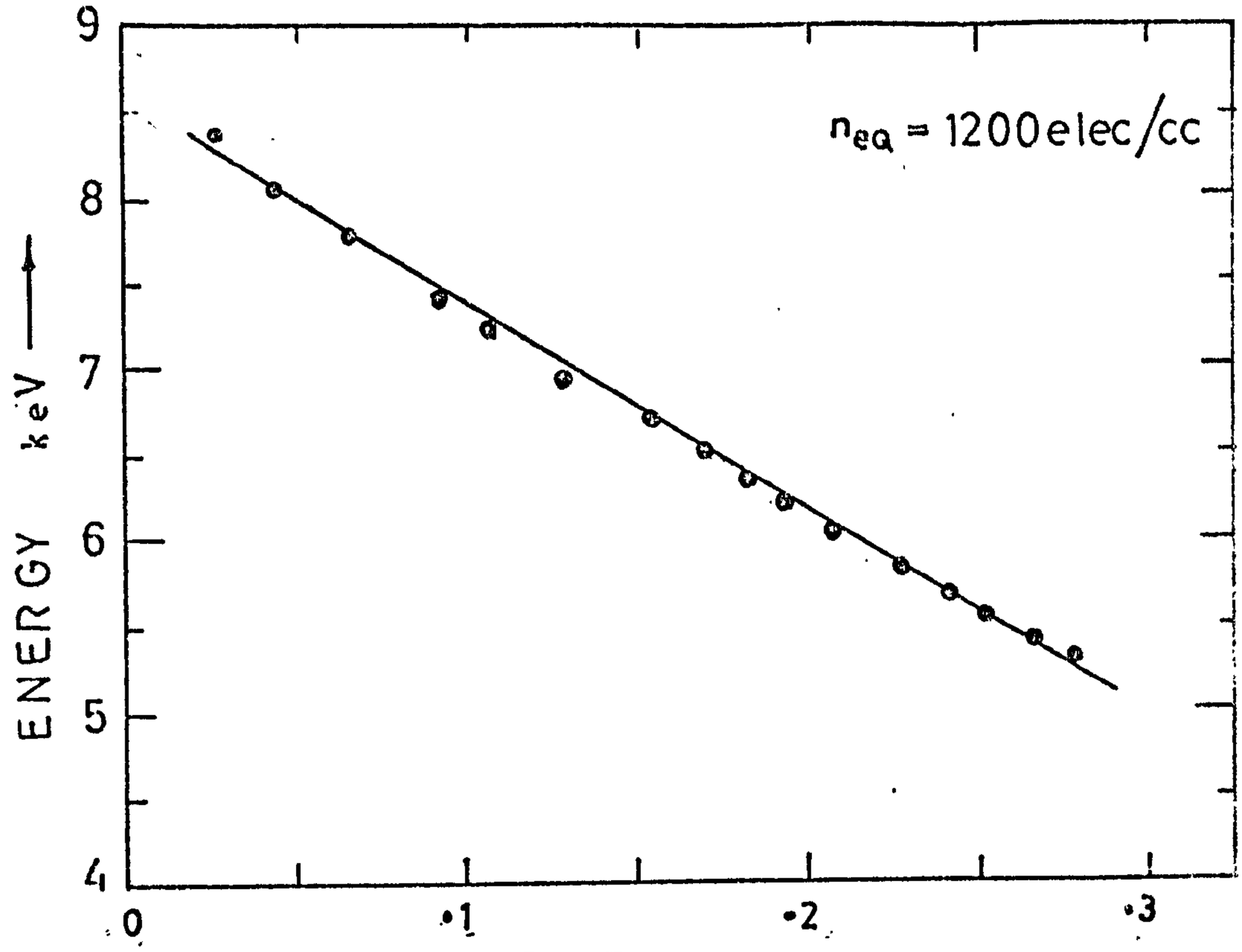

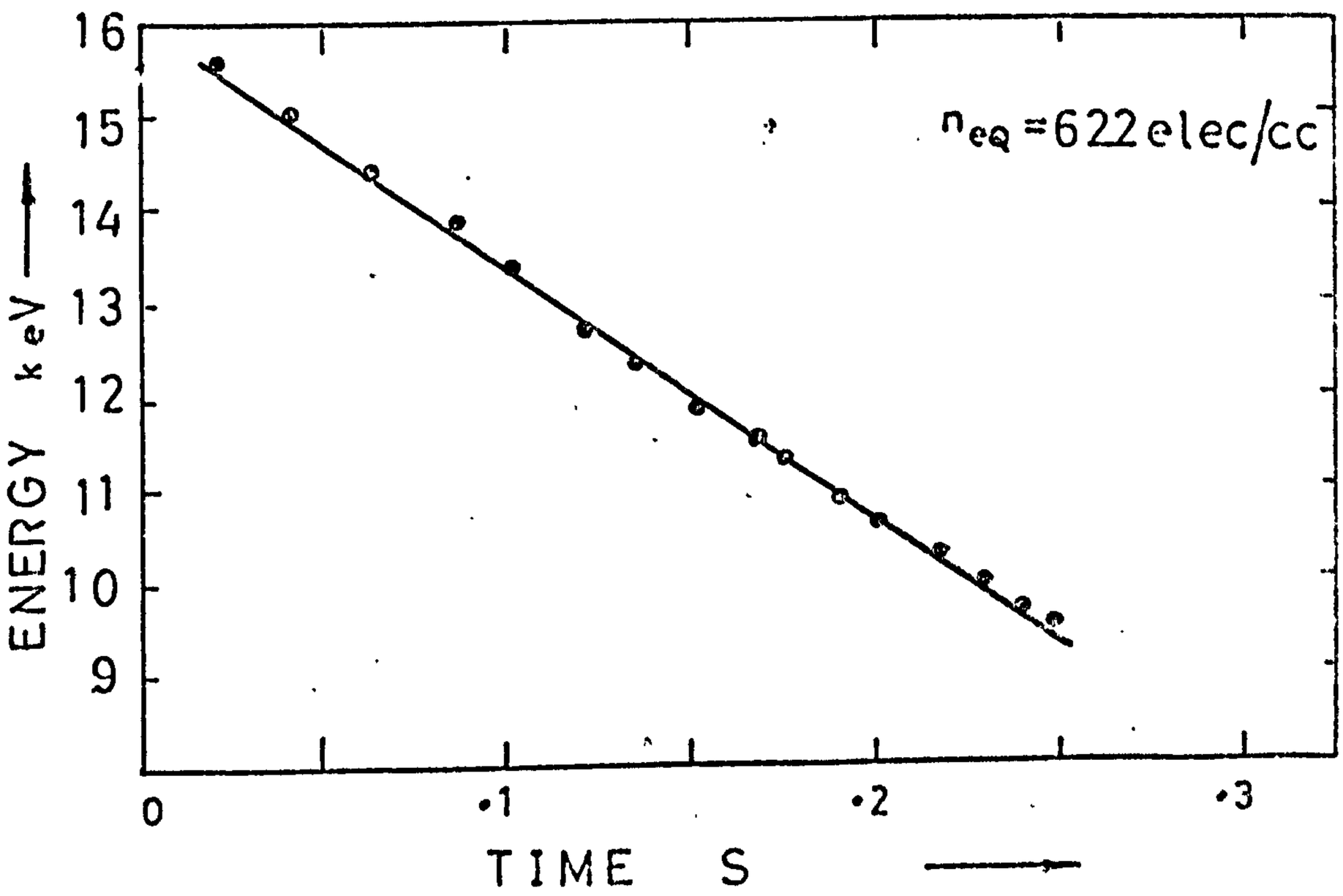

FIG(9 .21)

EMISSION P47H11D

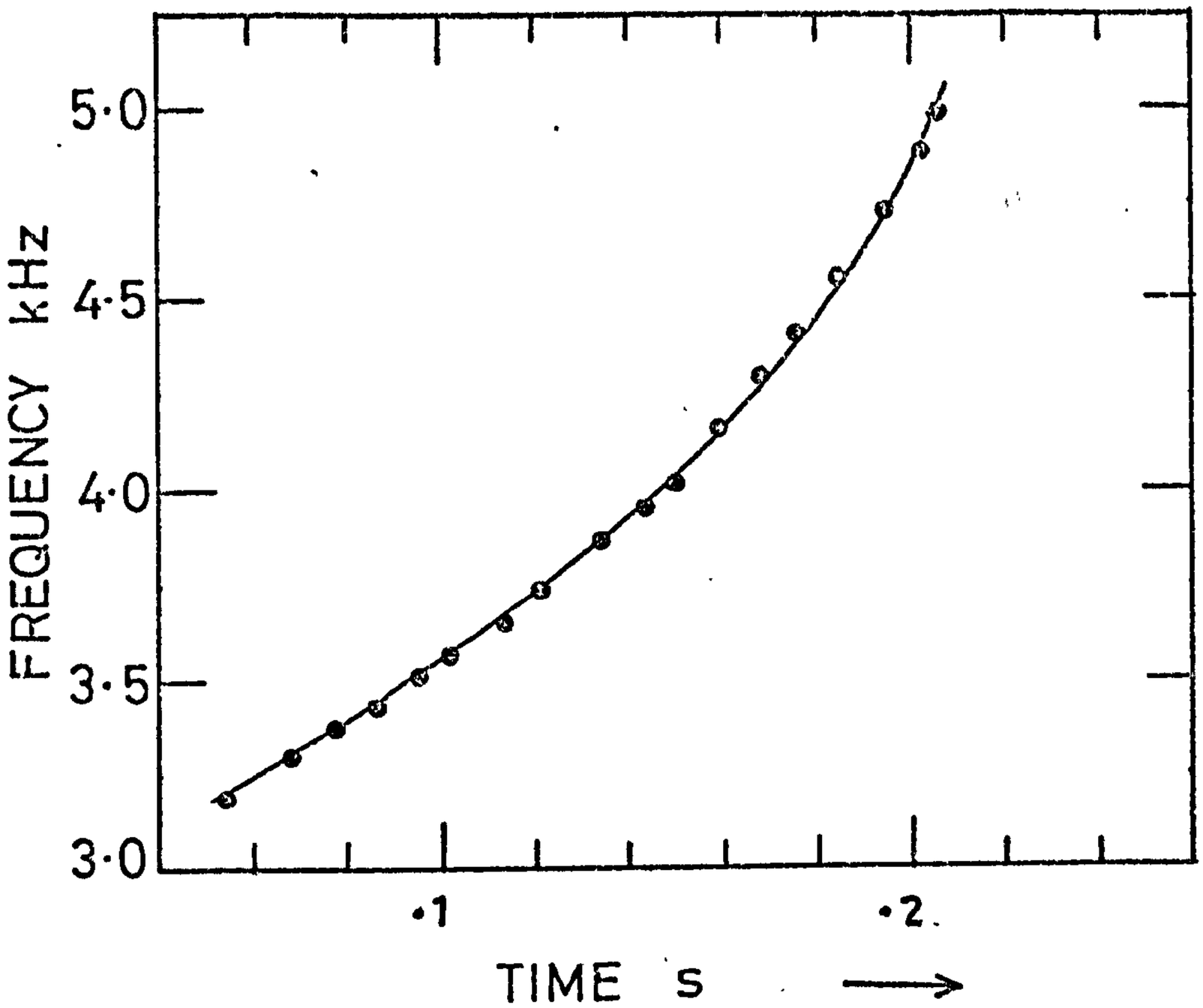

n_{eo} = 622 elec./cc

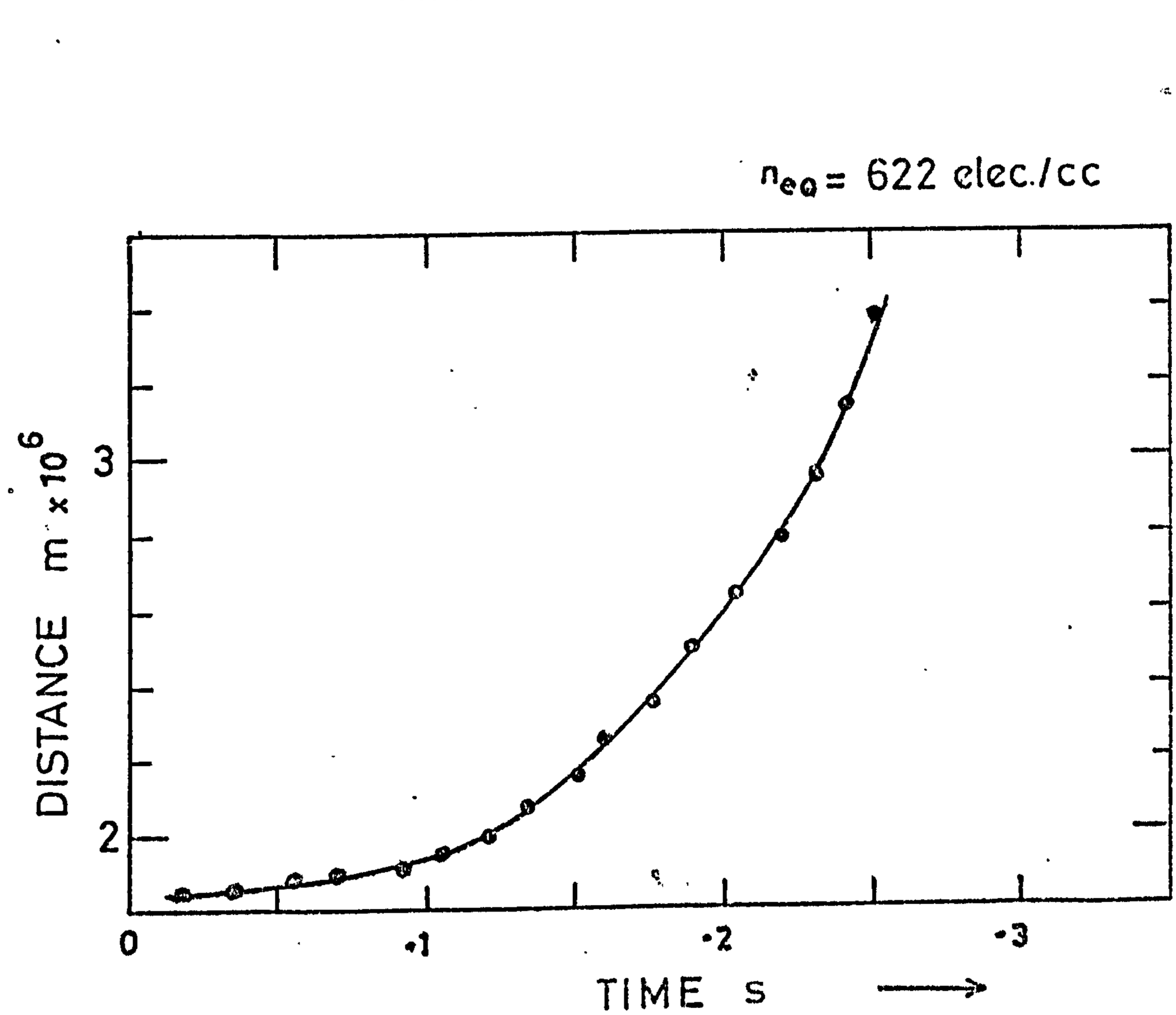

FIG. (9 .22)

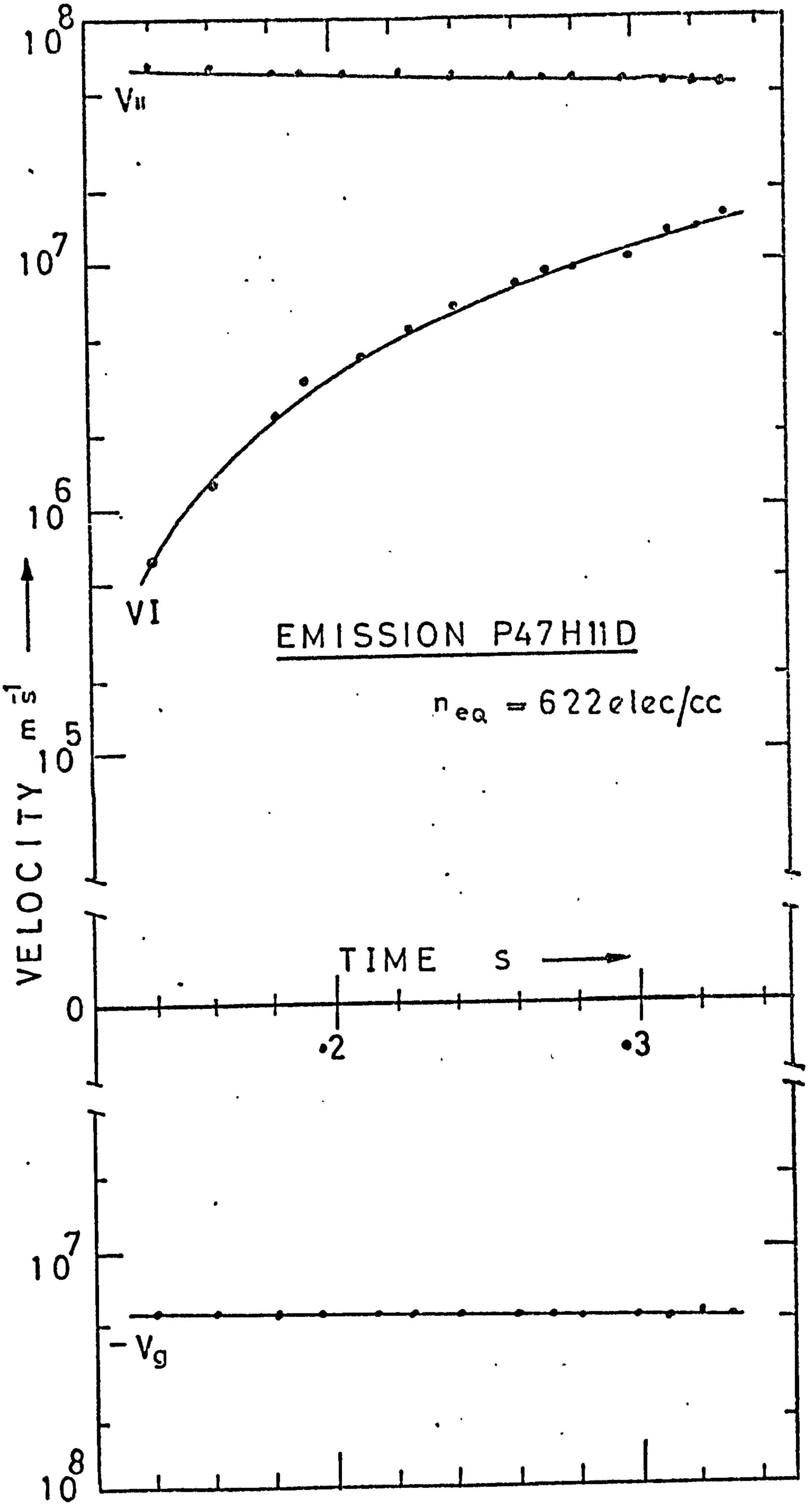
10^8
V_{II}
10^7
10^6
VI
10^5
VELOCITY E^{TS}
EMISSION P47H11D
n_{eq} = 622 elec/cc
0
TIME S
•2
•3
10^7
$-V_g$
10^8

FIG(9.•23)

EMISSION P47 H11D

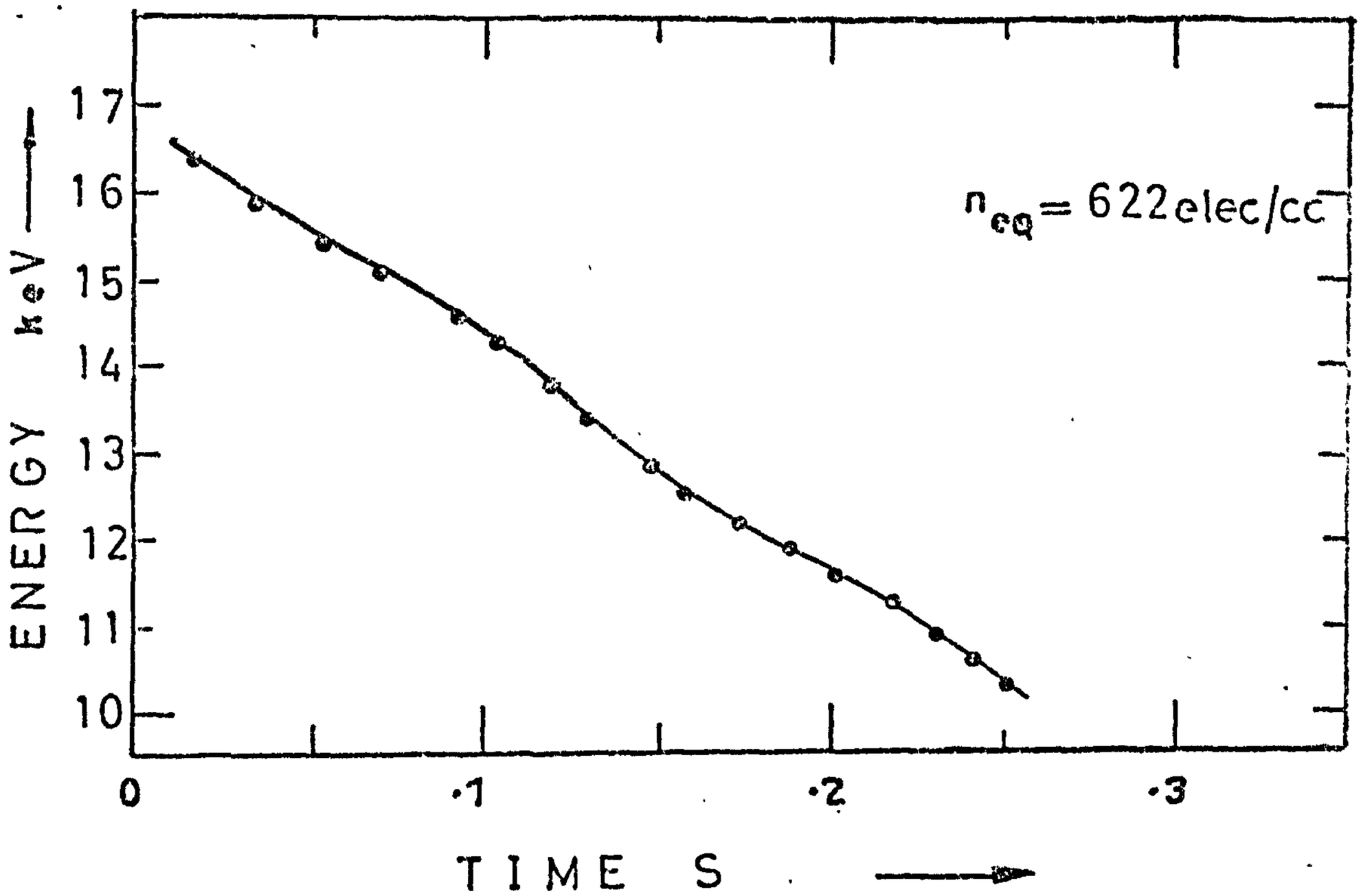

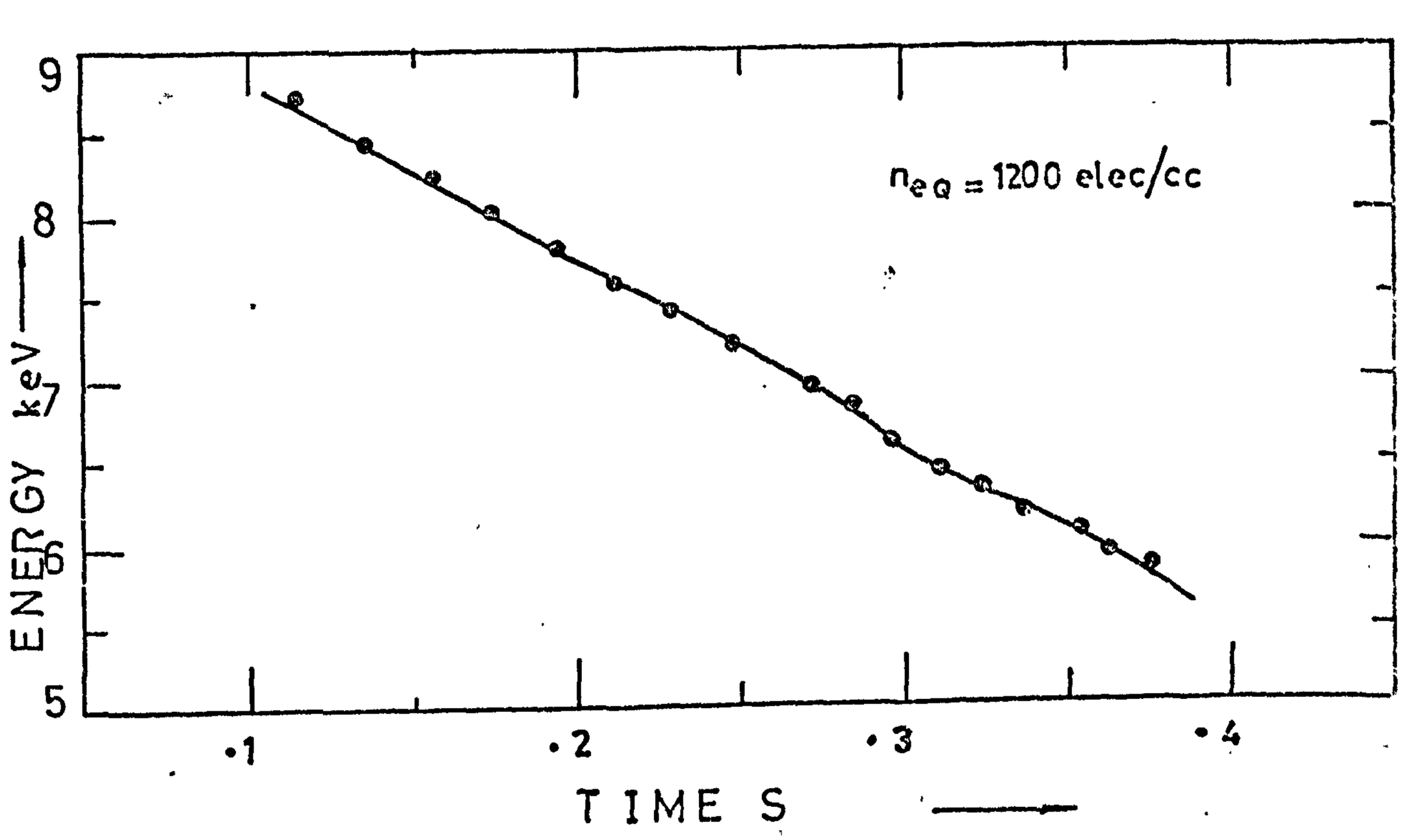

FIG(9. 24)

9.3 (cont'd) However, energetic electrons are most plentiful at this L value with energies between 0.1 and 1 keV falling rapidly at higher energies. Vette 1972 shows the falling energy spectrum by plotting the equatorial omnidirectional electron flux in three energy bands of greater than 36 keV, greater than 292 keV and greater than 1970 keV, see Fig. 9.18a. This diagram also shows the variation of electron flux with L value. The data was gathered by the OGO 1 satellite during 1964 and 1965 as part of a study concerning solar cycle effects on the distribution of energetic particles.

Emission P47H11C is shorter than the previous one and its profile is closer to a straight line which has a slope of about 10 KHz s^{-1}. The distance of the interaction region from the equator during the life of the emission varies between 2000 km and 3000 km see Fig. 9.19, and is of the same order as for the previous emission. The interaction region velocity is given in Fig. 9.20 and it satisfies the necessary condition $-v_g < V_I < v_{II}$. The resonant electron energies for the two limiting equatorial electron densities can be seen in Fig. 9.21. The range of values agrees well with those calculated for P47H10D. The rate of change of resonant energy is almost constant throughout the duration of the emission.

Emission P47H11D has similar characteristics to the previous ones and can be seen in Figs. 9.22 through 9.24. From the energy - time curves for 622 and 1200 electrons/cc for the three emissions it appears that the resonant energy is inversely proportional to the ambient thermal electron density.

EMISSION P47 H11 D

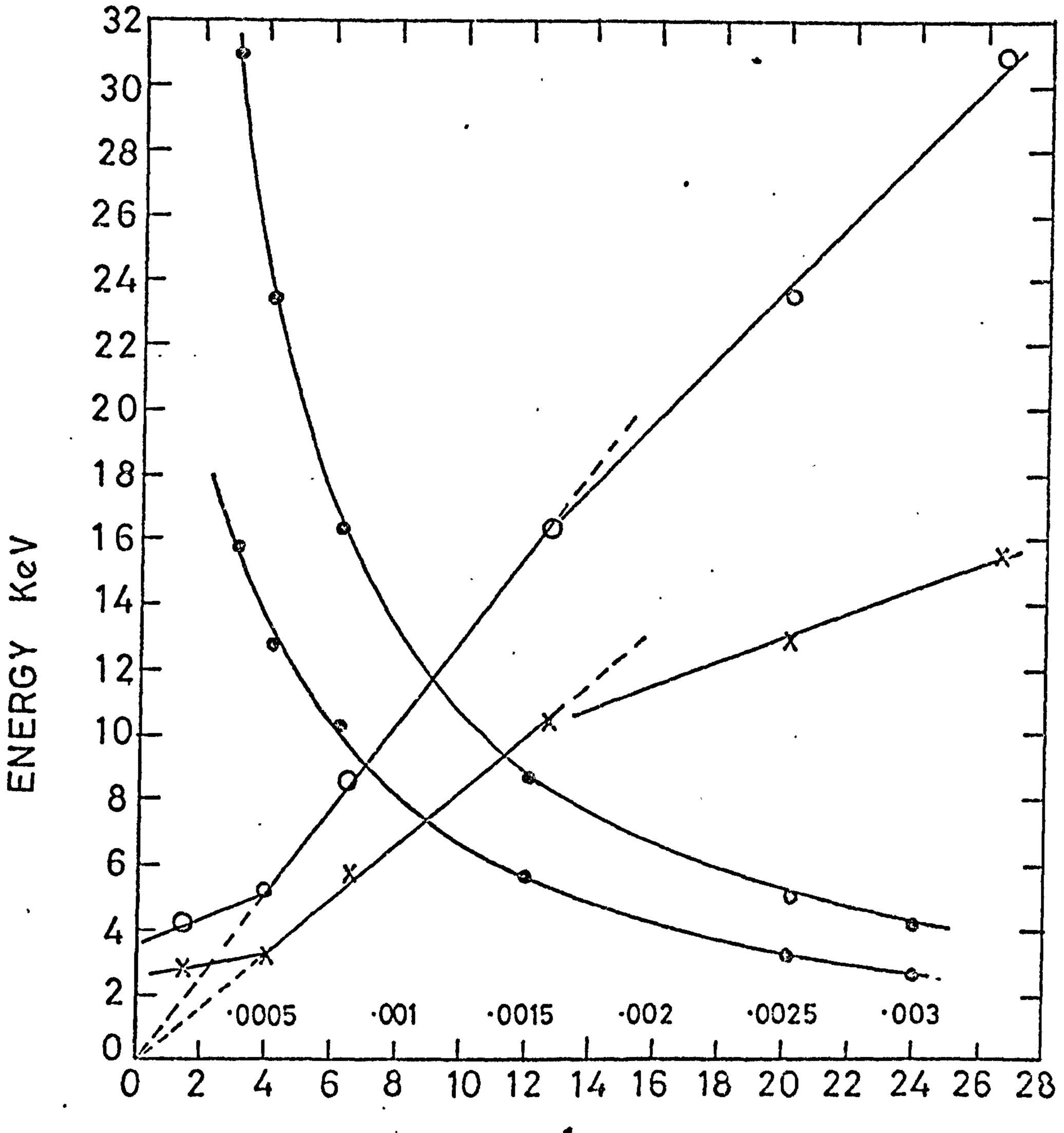

Fig.(9.25)

9.3 (cont'd) This relationship is investigated over a wide range of electron density values using emission P47H11D, the result being shown in Fig. 9.25. The energies corresponding the the lowest and highest observed frequencies in the riser are plotted as a function of electron density from 150 electrons/cc to 2700 electrons/cc. These values more than cover the range of equatorial electron density normally found inside the plasmapause. The hyperbola which is produced indicates that the inverse proportionality holds over this wide range of n_{eq}. Plotting energy against $1/n_{eq}$ reveals that the relationship holds extremely well over the density range 600 electrons/cc to 2000 electrons/cc and less well above and below these values.

This inverse relationship is explained by examining equation (8.2,6)

$$v_{//} = \frac{C}{f_n} \cdot \frac{(f_h - f)^{3/2}}{f^{\frac{1}{2}}}$$

Given that the value of $\frac{(f_h - f)^{3/2}}{f^{\frac{1}{2}}}$ does not change significantly with n_{eq}, (for any value of f the value of f_h is determined by equation (8.2,14) which involves f_n only indirectly.)

then;

$$v_{//} \propto 1/f_n$$

The electron energy E is proportional to $v_{//}^2$ therefore;

$$E \propto 1/f_n^2$$

But $f_n \propto \sqrt{n}_{eq}$

So $E \propto 1/n_{eq}$

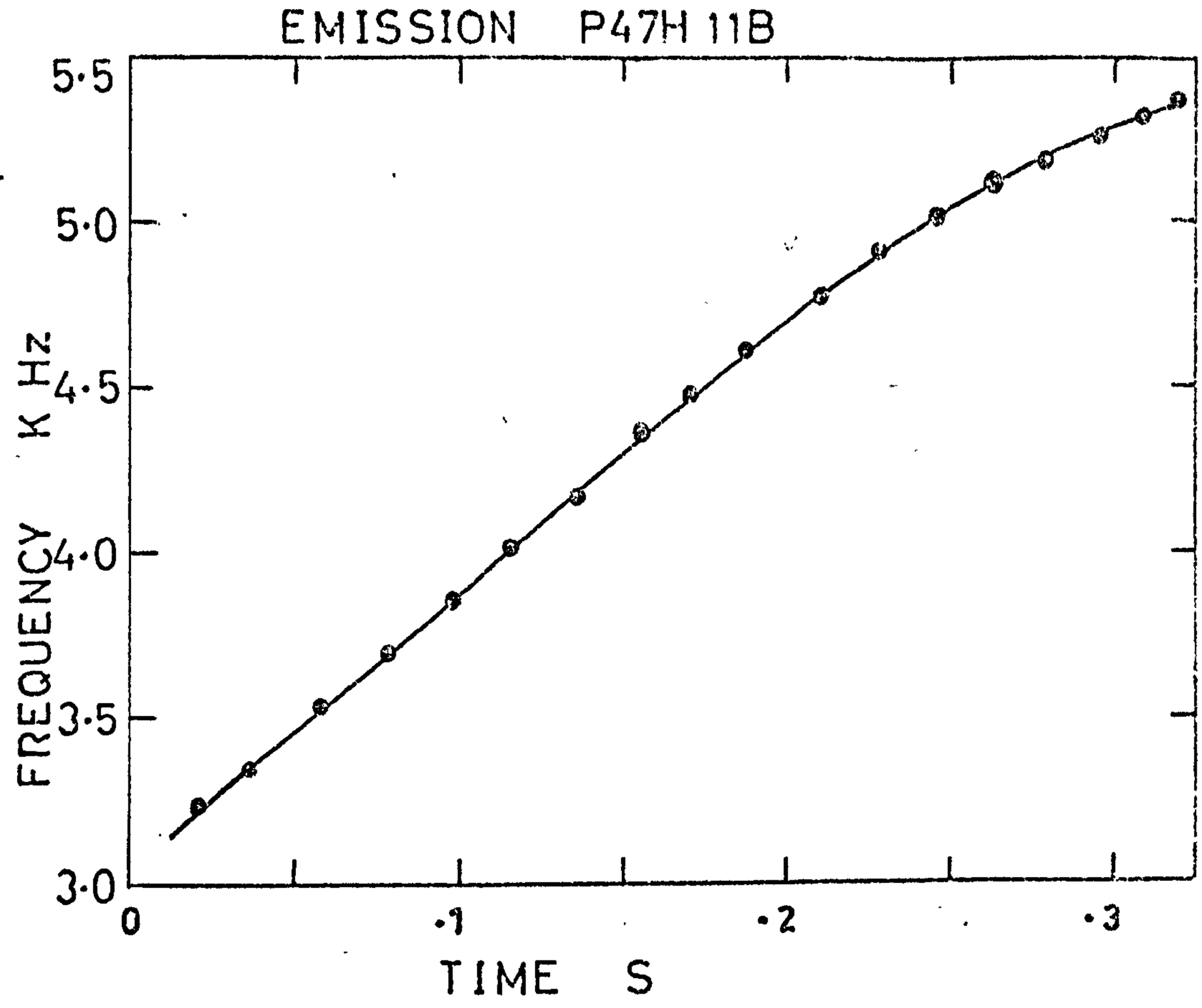
EMISSION P47H 11B
5·5
5·0
4·5
4·0
3·5
3·0
FREQUENCY K Hz
0
·1
·2
·3
TIME S

FIG(9.26)

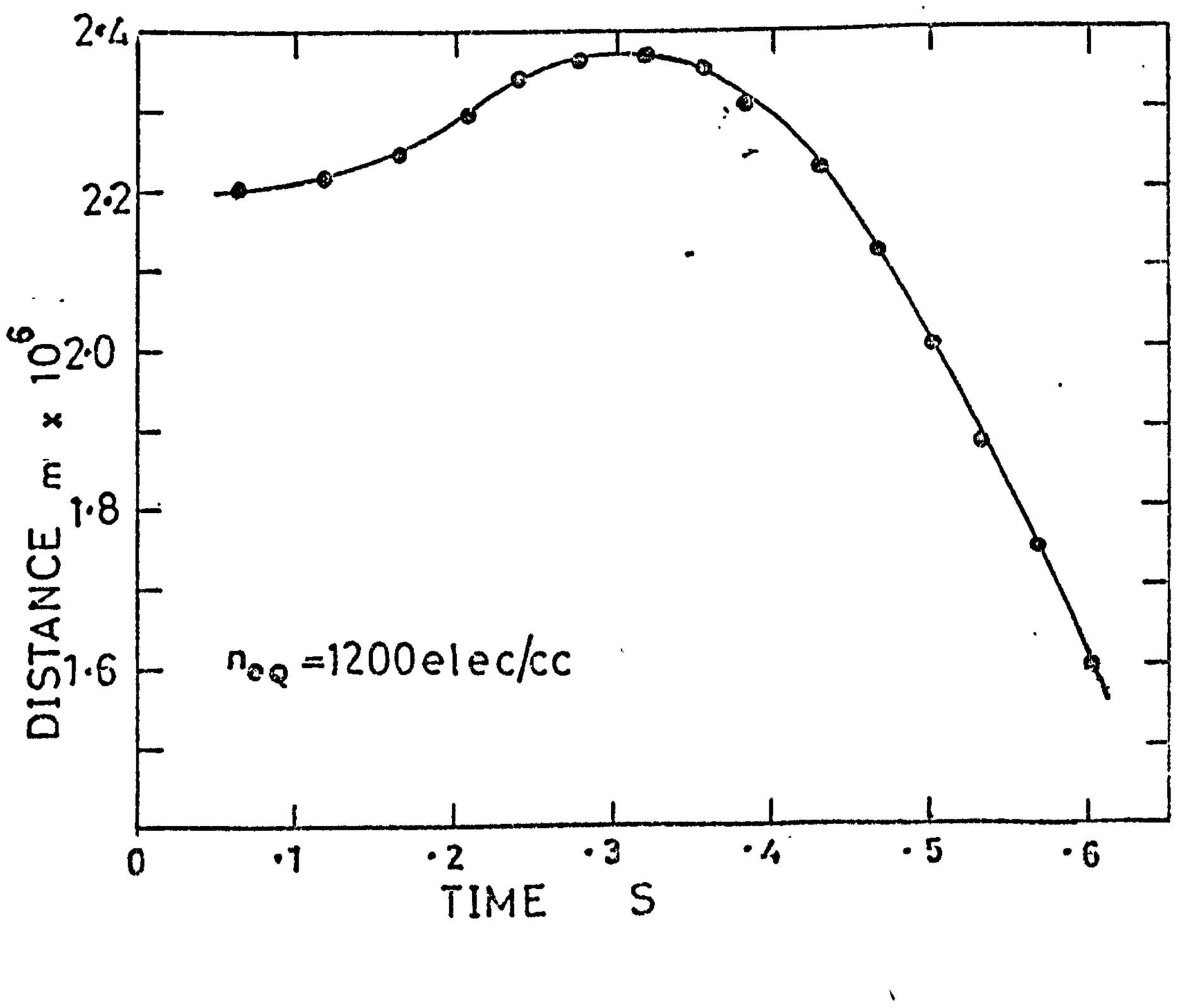
2·4
2·2
2·0
1·8
1·6
DISTANCE m x 10⁶
n_{eQ} =1200elec/cc
0
·1
·2
·3
·4
·5
·6
TIME S

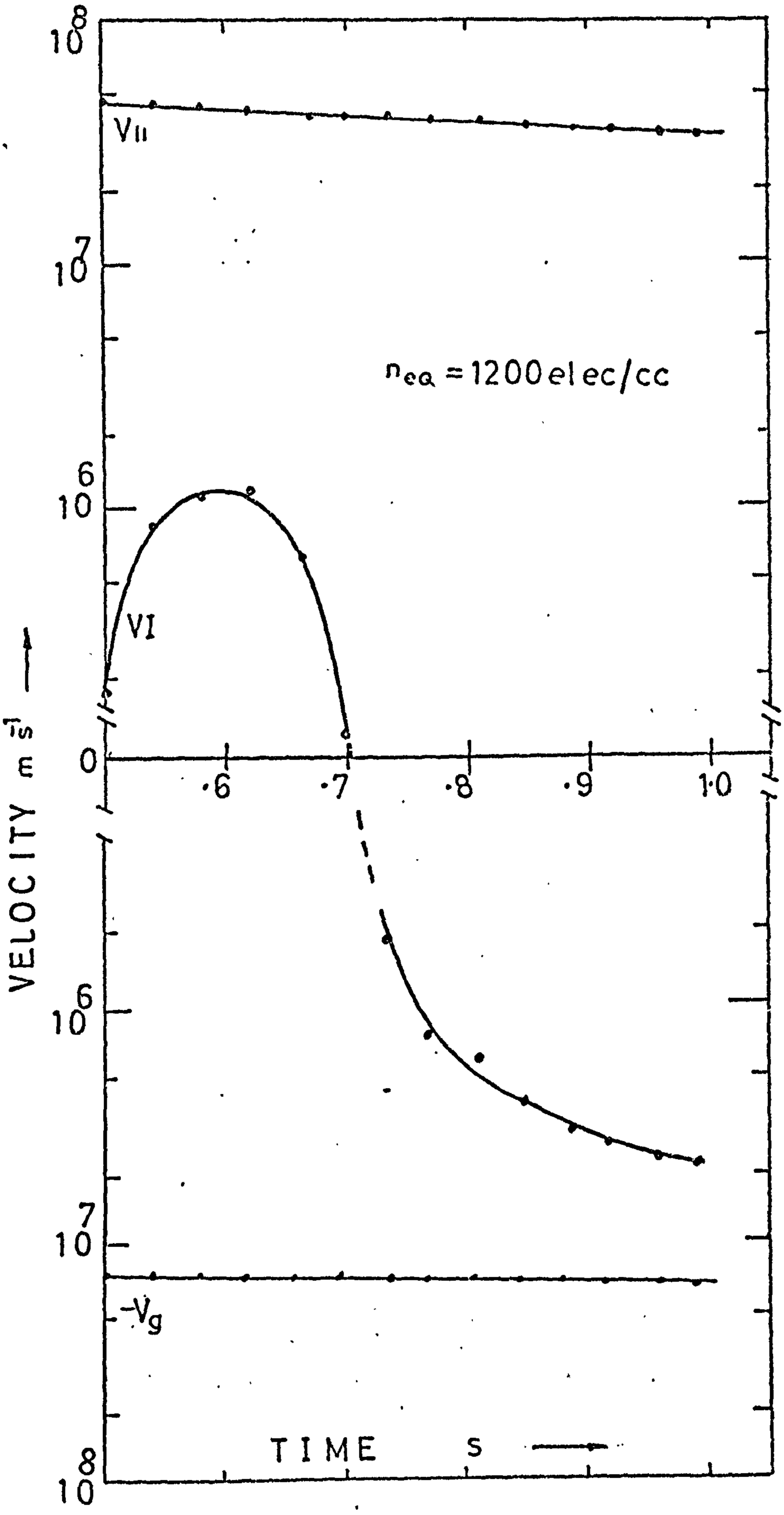
EMISSION P47H11B
10^8
10^7
10^6
10^5
10^6
10^7
10^8
V_{II}
VI
$n_{eq} = 1200$ elec/cc
0
·6
·7
·8
·9
1·0
VELOCITY
$-V_g$
TIME
S

FIG(9 .27)

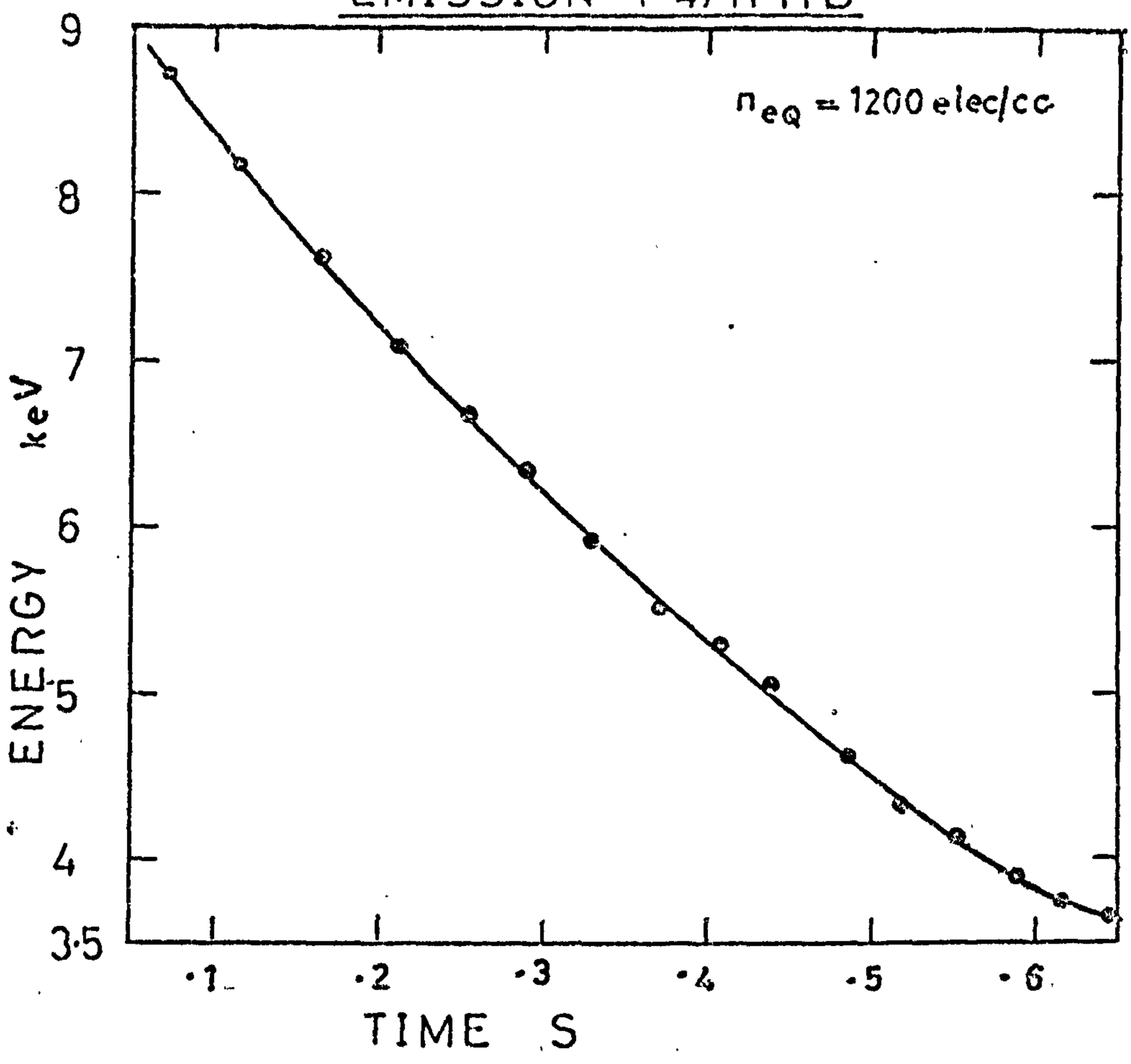
EMISSION P47H11B
n_{eQ} = 1200 elec/cc
9
8
7
6
5
4
3·5
keV
ENERGY
·1
·2
·3
·4
·5
·6
TIME S

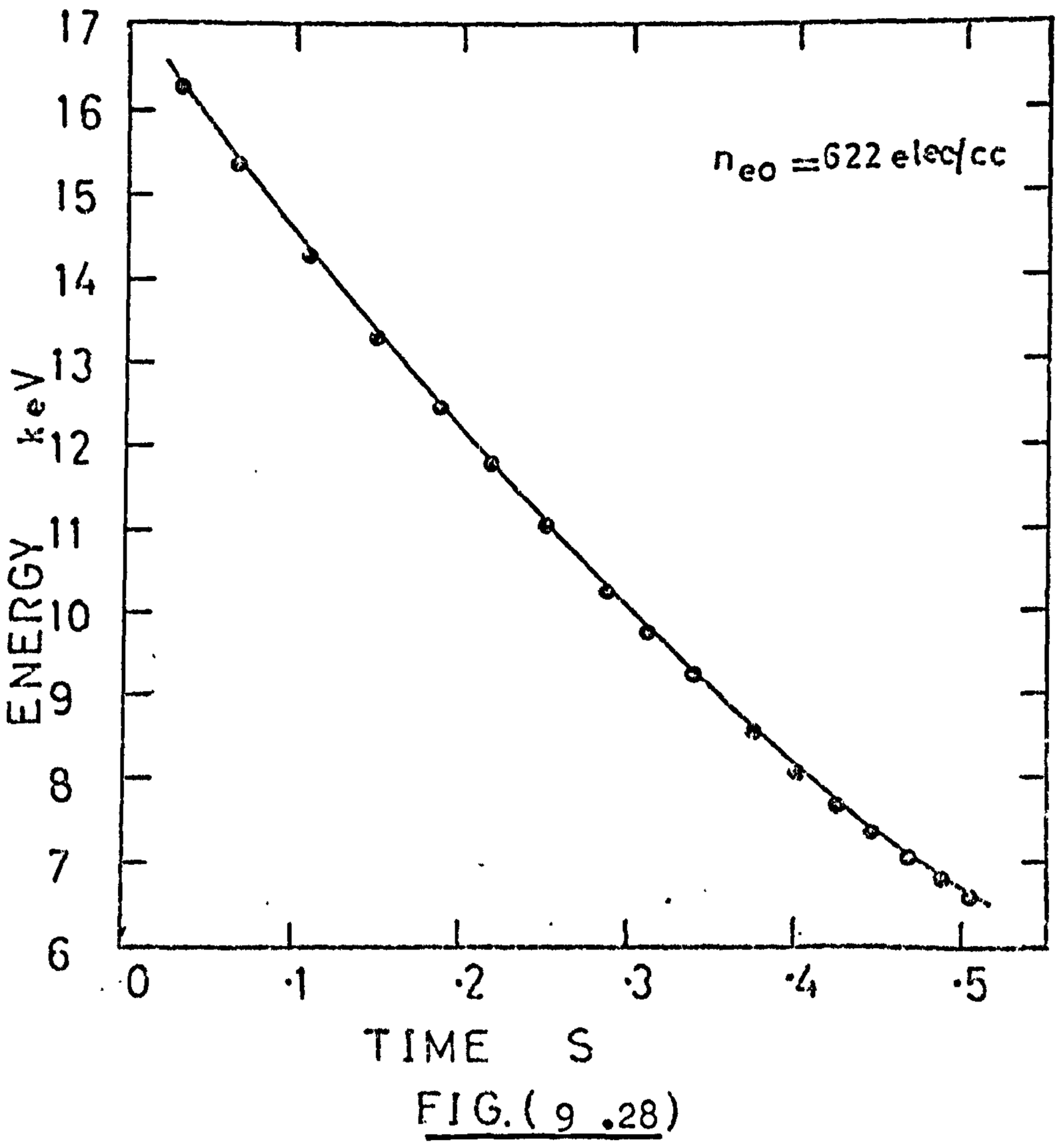
n_{eo} = 622 elec/cc
17
16
15
14
13
12
11
10
9
8
7
6
keV
ENERGY
0
·1
·2
·3
·4
·5
TIME S

FIG.(9 .28)

EMISSION P47H10C

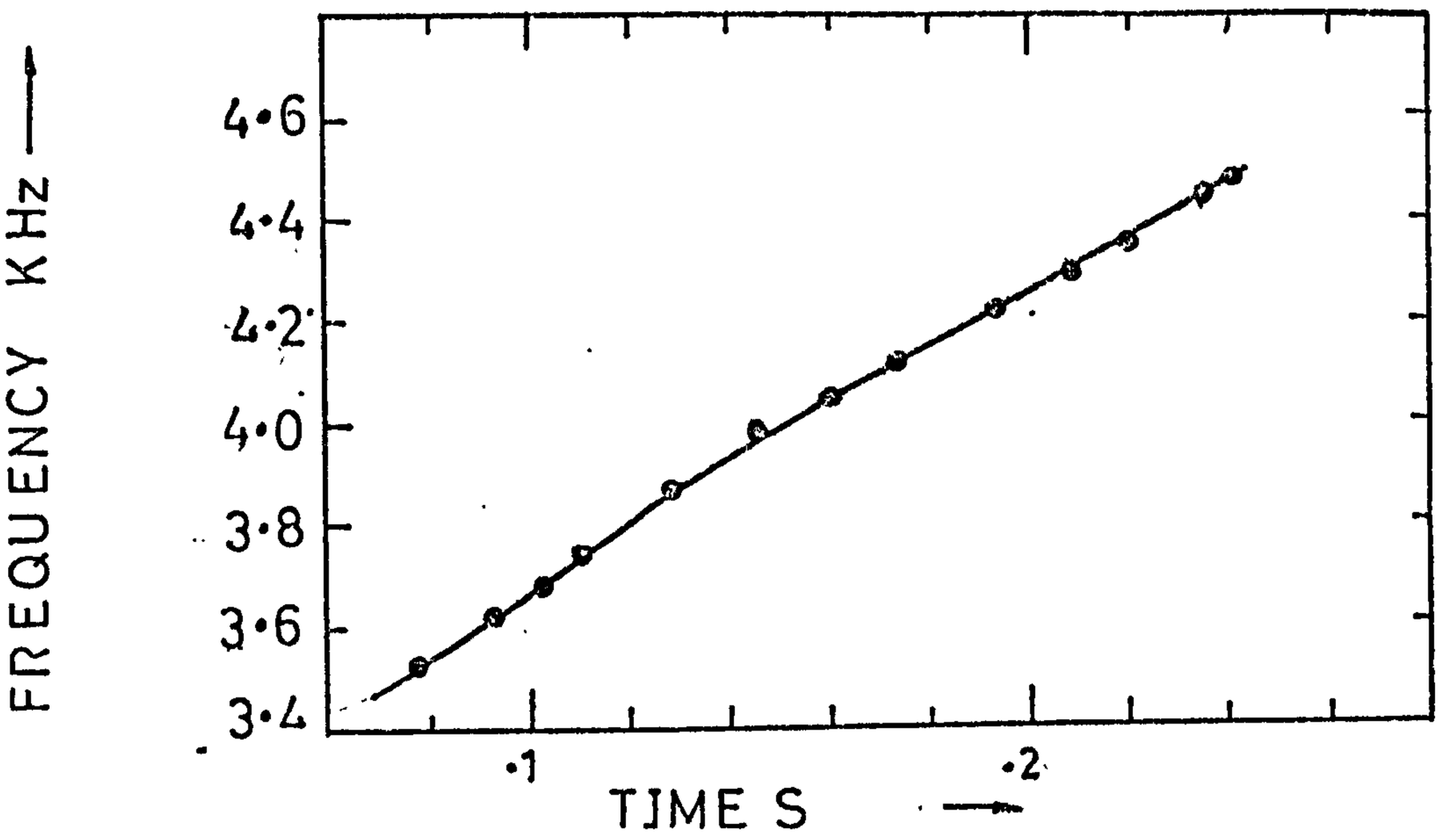

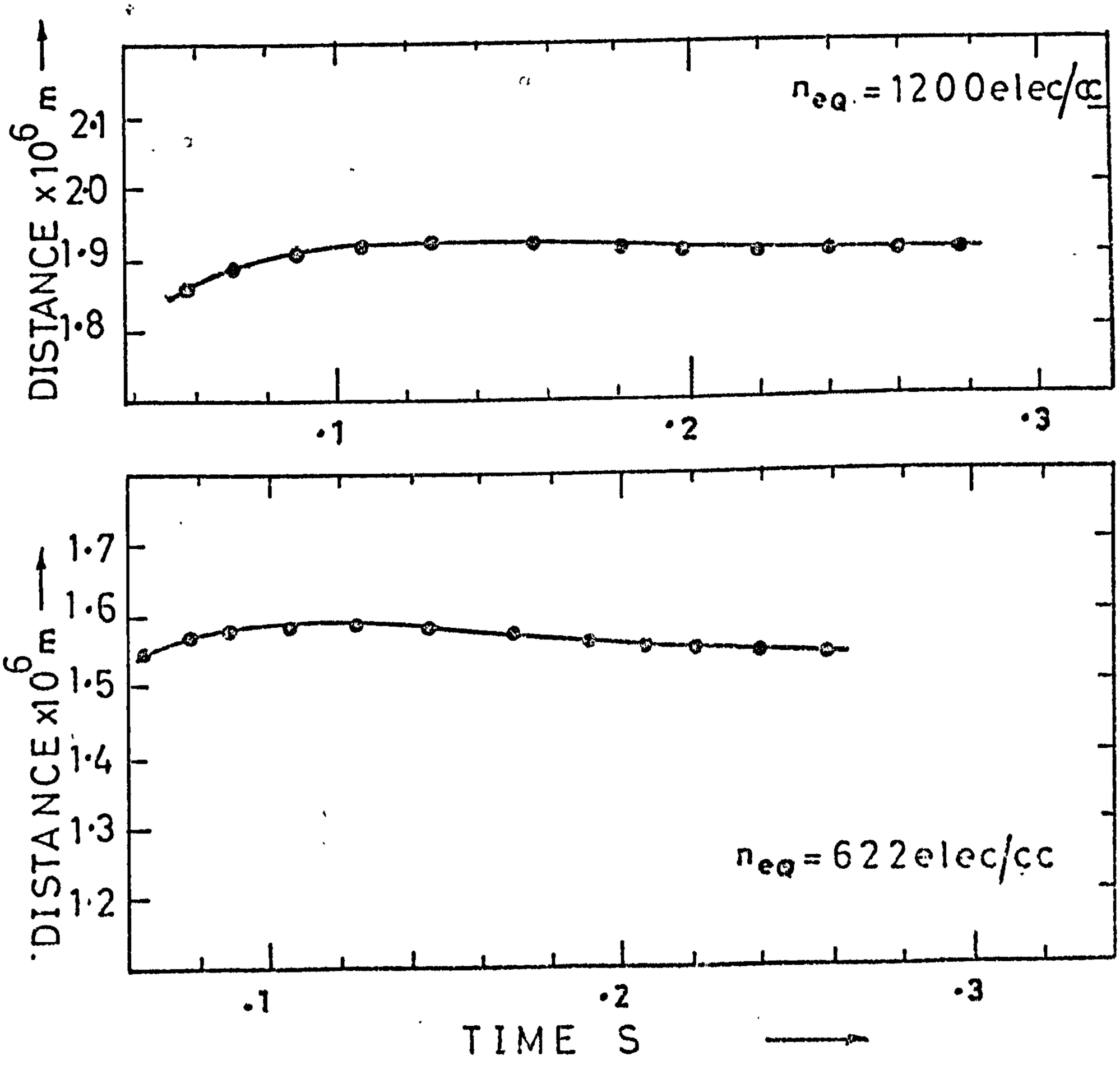

FIG(9·29)

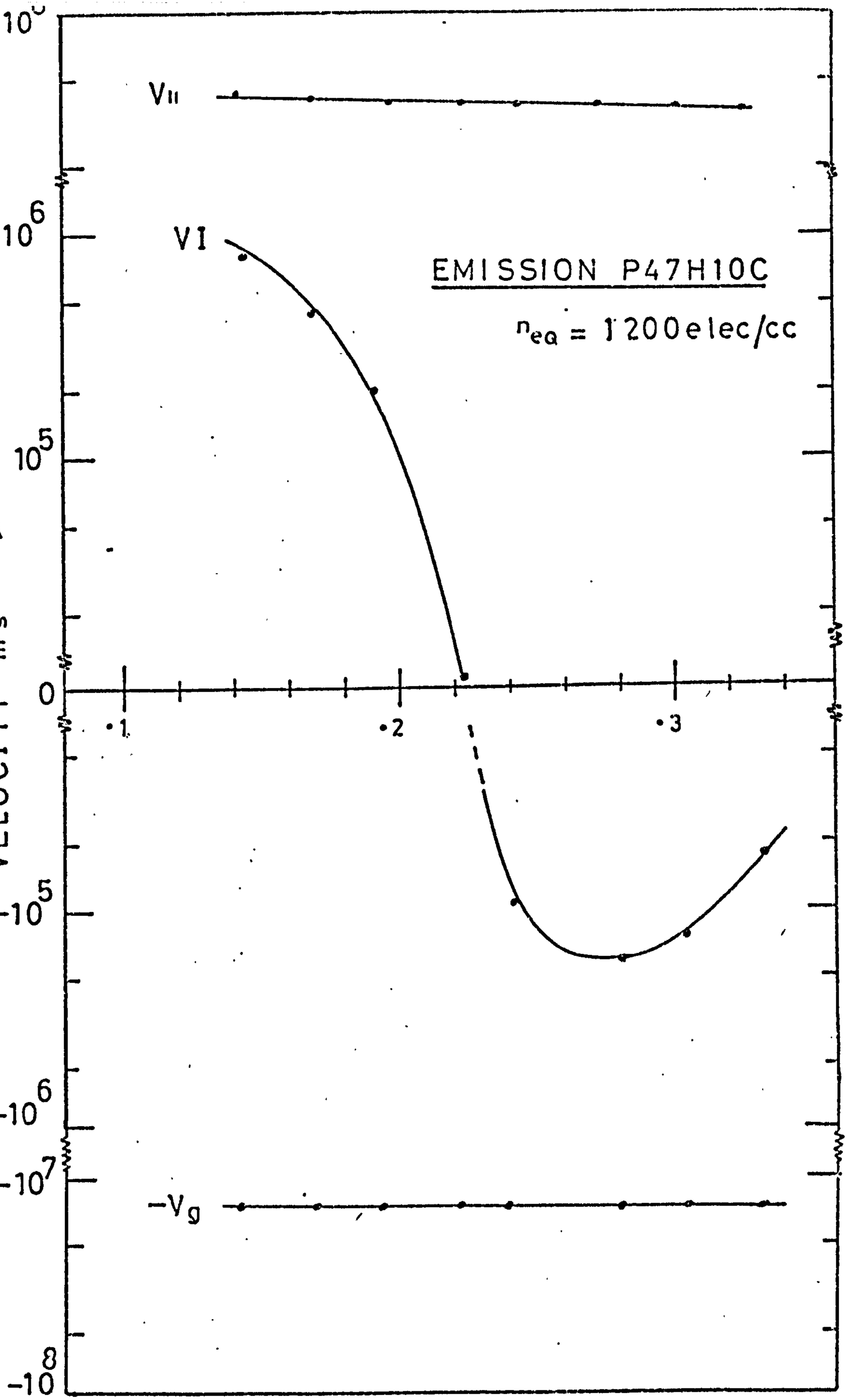
10^{6}
V_{II}
VI
EMISSION P47H10C
n_{eq} = 1·200 elec/cc
10^{5}
VELOCITY m s^{-1} ⟶
0
·1
·2
·3
-10^{5}
-10^{6}
-10^{7}
$-V_g$
-10^{8}
TIME S ⟶

FIG(9 ·30)

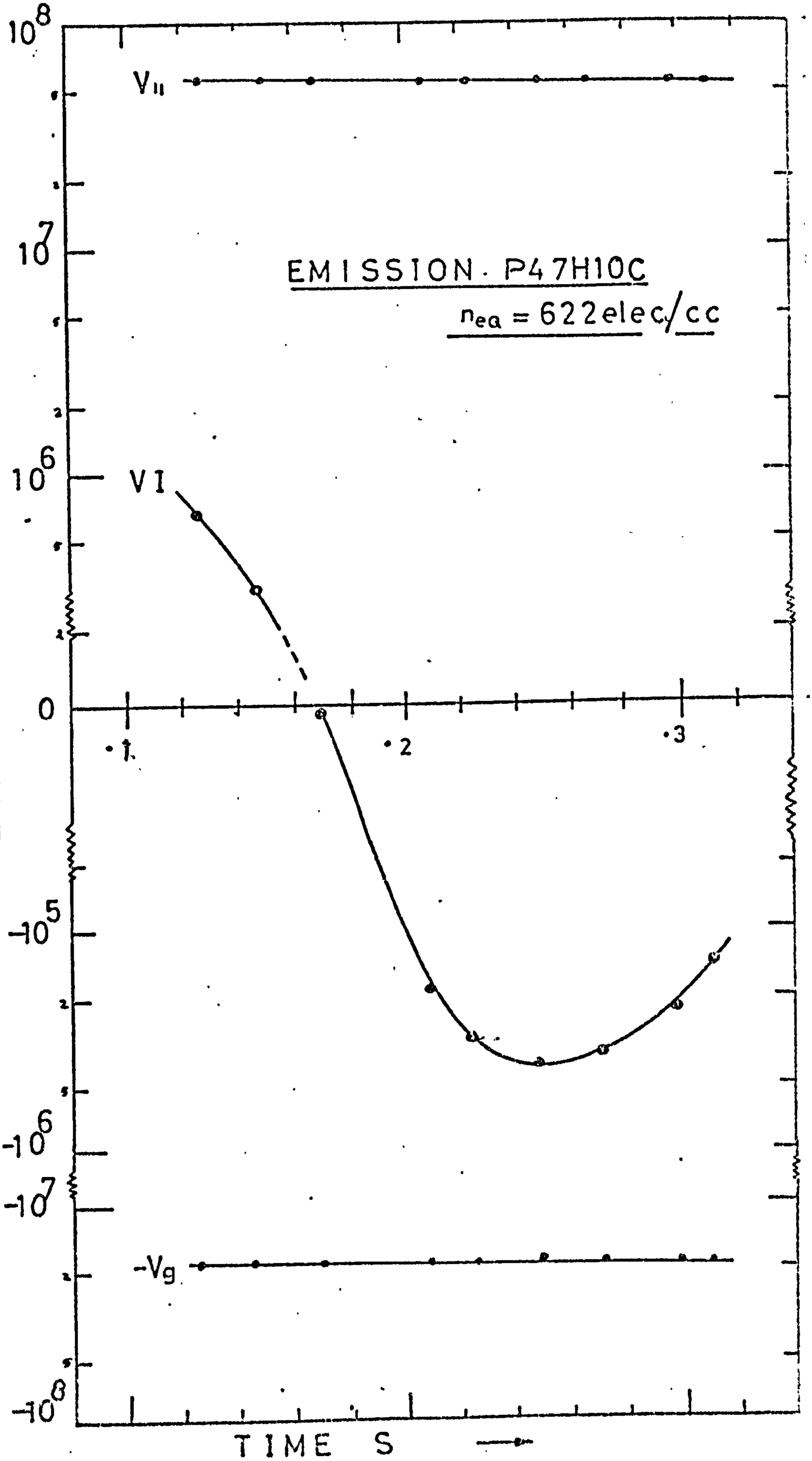
EMISSION. P47H10C
n_{eq} = 622 elec/cc
V_{11}
VI
$-V_g$
VELOCITY m s^{-1}
TIME S
10^8
10^7
10^6
10^5
-10^5
-10^6
-10^7
-10^8
0
·1
·2
·3

FIG(9.31)

EMISSION P47 H10C

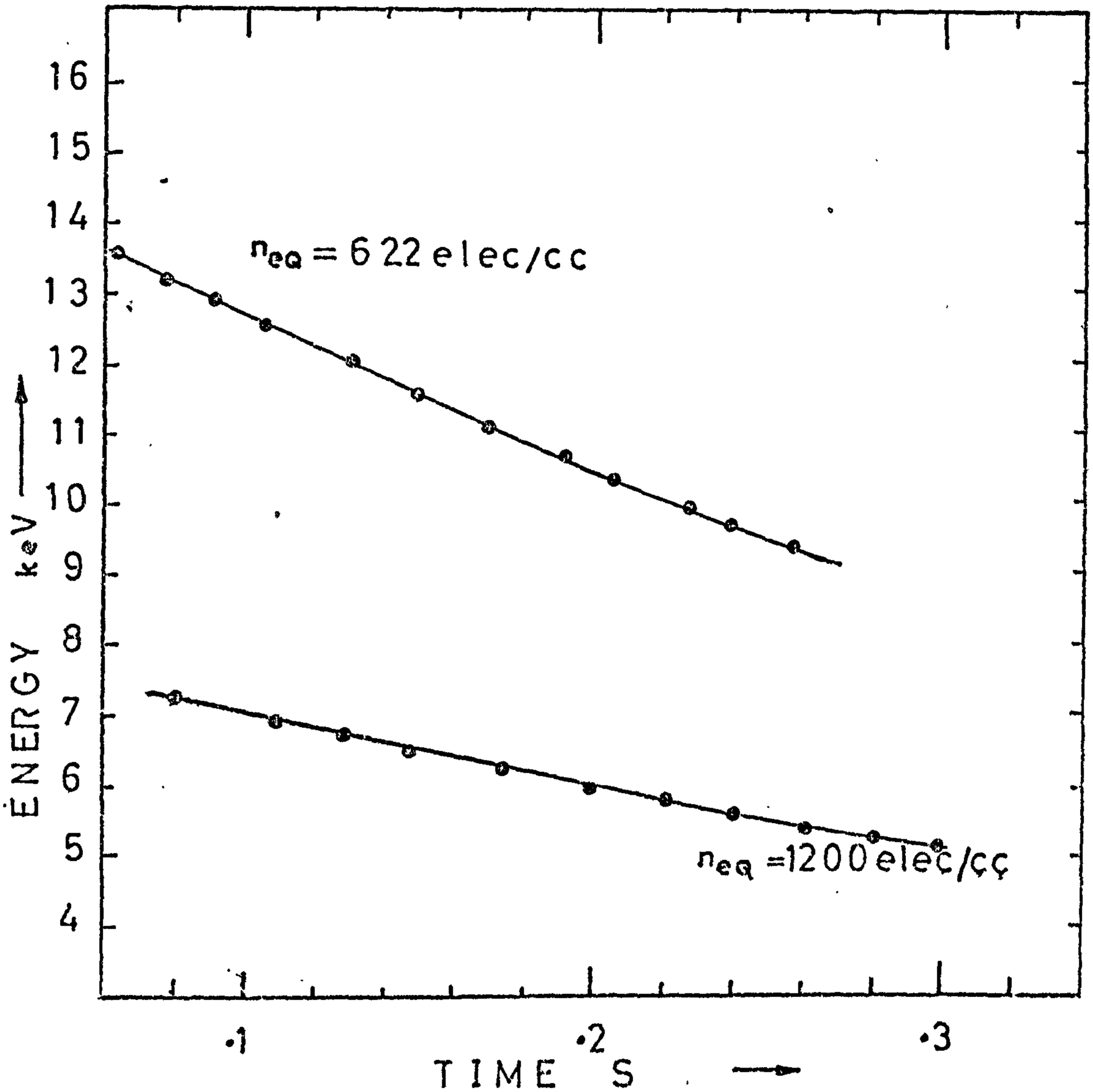

FIG(9 .32)

9.3 (cont'd) Evidence to support the assumption that f_h in (8.2,6) does not change greatly with n_{eq} may be seen in Fig. 9.2 where only a 15% change in the calculated distance results from a 100% change in n_{eq} and we see from Fig. 7.4 that for $S<5x10^6$ m that f_h remains almost constant.

The reciprocal relationship of E with n_{eq} is useful as it enables the analysis to be performed on an emission using a guessed value for the equatorial electron density if no measurements are available and the calculated resonant energies may then simply be scaled between upper and lower practical limits. The resulting range of energies may be compared with likely energetic electron spectra to establish that such an emission of a given intensity could have been produced.

The energy of electrons which are precipitated due to wave particle interaction resulting in a VLF emission may be measured by a rocket probe or satellite. After analysis of the received emission the calculated and measured energies may be equalised by varying n_{eq} in the computions resulting in a measurement of the equatorial electron density which existed at the time the emission was generated. With the reception of a small number of emissions a value of n_{eq} could be produced which would have an associated error measurement.

As it is difficult to determine the magnetospheric equatorial electron density from a few ground based measurements and rocket probe measurements, this technique may be considered.useful and worthy of a practical trial. If measurements were made in conjunction with electron

9.3 (cont'd) density measurements on board a satellite, or discrete emissions were received with whistlers, a comparision of the values of n_{eq} derived by the various methods could be made. Electron density determination from whistler studies has been carried out by Carpenter 1963, 66,67 and from satellite measurements by Gringauz 1960 and Chapell et al 1970.

Emission P4711B in Fig. 9.26 is unlike the preceding three in that towards the end of the emission its slope becomes slightly less than in the earlier parts. This is interpreted as the interaction region moving first away from the starting point at about 2200 km from the equator and later doubling back to finish at a distance of 1600 km from the equator. The interaction region velocity is seen in Fig. 9.27 to be first +ve reaching a maximum value of 10^6 m s^{-1} passing through zero and then becoming -ve as the interaction region travels back toward the equator. The interaction region velocity criterion $-v_g < V_I < v_{II}$ is obeyed throughout the motion. In Fig. 9.28 wee see that in spite of the complicated motion of the interaction region the energy time curves are similar to the preceding ones. The rate of change of resonant energy with true time is almost constant.

In Fig. 9.29 we see emission P47H10C which shows a slight decrease in slope during its lifetime. The interaction region first travels away from the equator and later slowly drifts back twoards its starting point. The values of -ve interaction region velocity are about 10 times smaller than for P47H11B whilst the +ve values are of the same order. The distances and the interaction region velocities are very similar for the two values of equatorial electron density used.

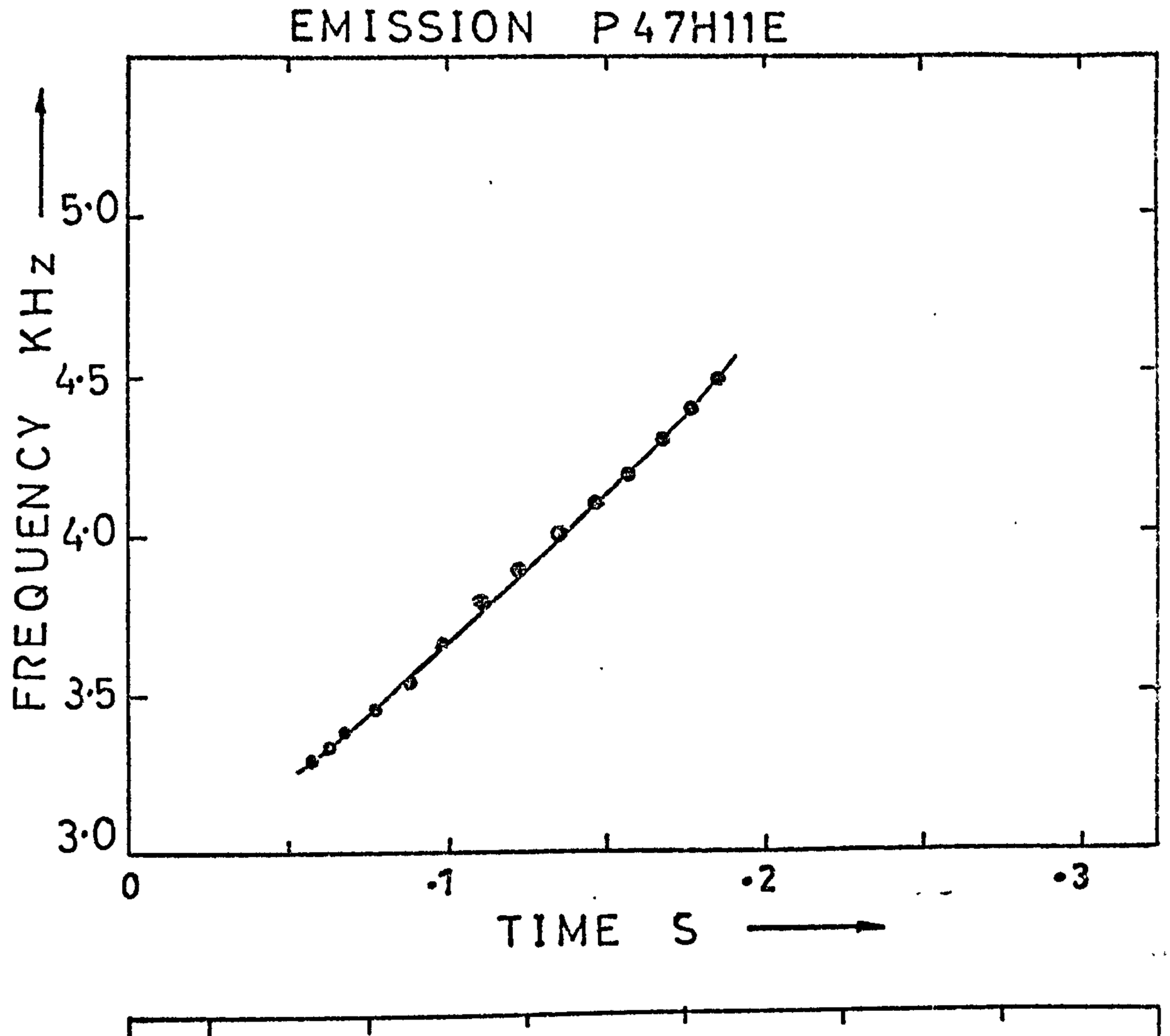
EMISSION P47H11E
FREQUENCY KHz
5·0
4·5
4·0
3·5
3·0
0
·1
·2
·3
TIME S
n_{eq} = 1200 elec/cc
DISTANCE 10^6 m
2·6
2·5
2·4
2·3
2·2
2·1
2·0
0
·1
·2
·3

FIG (9 .33)

EMISSION P47H11E

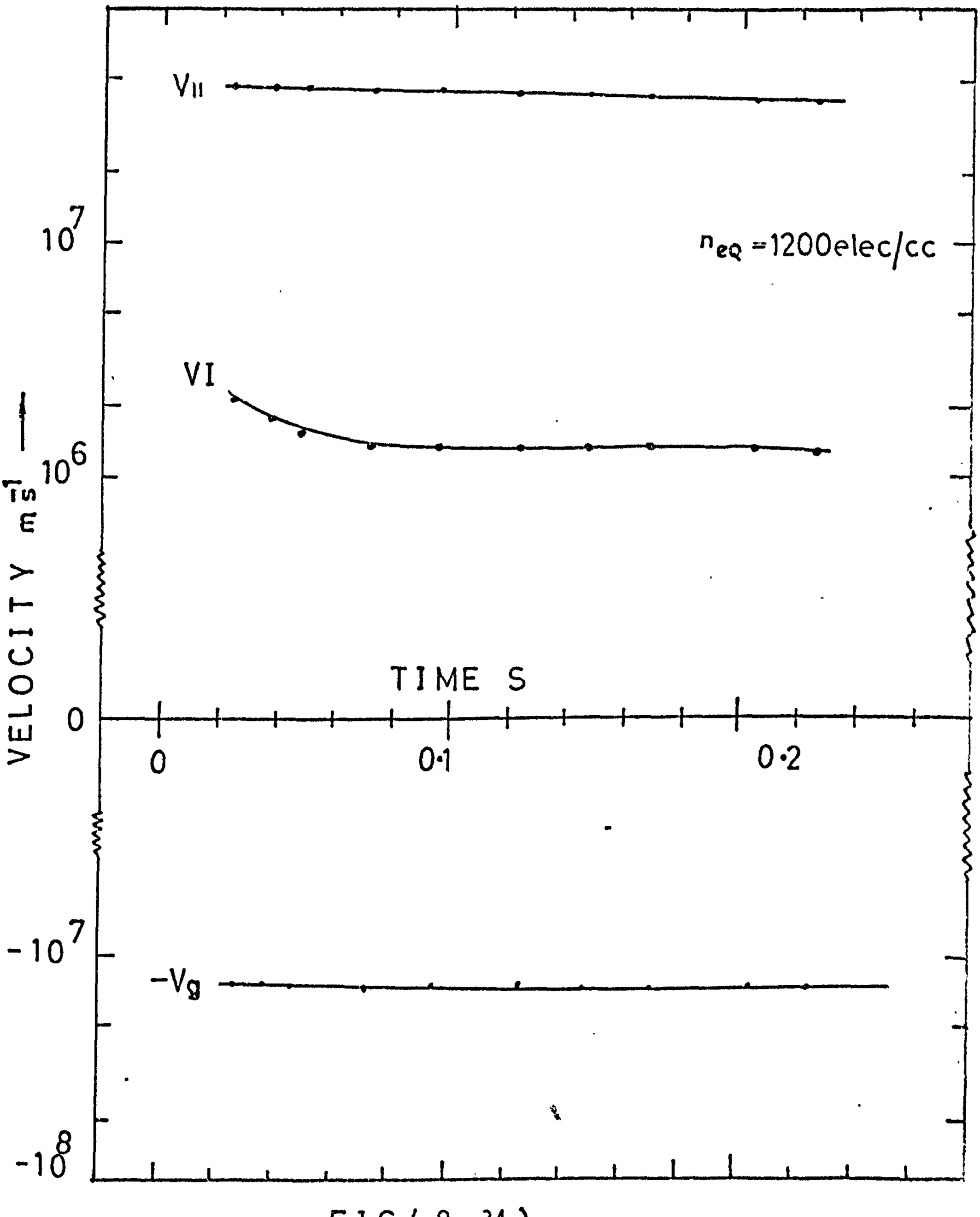

FIG(9 ·34)

EMISSION P47H11E

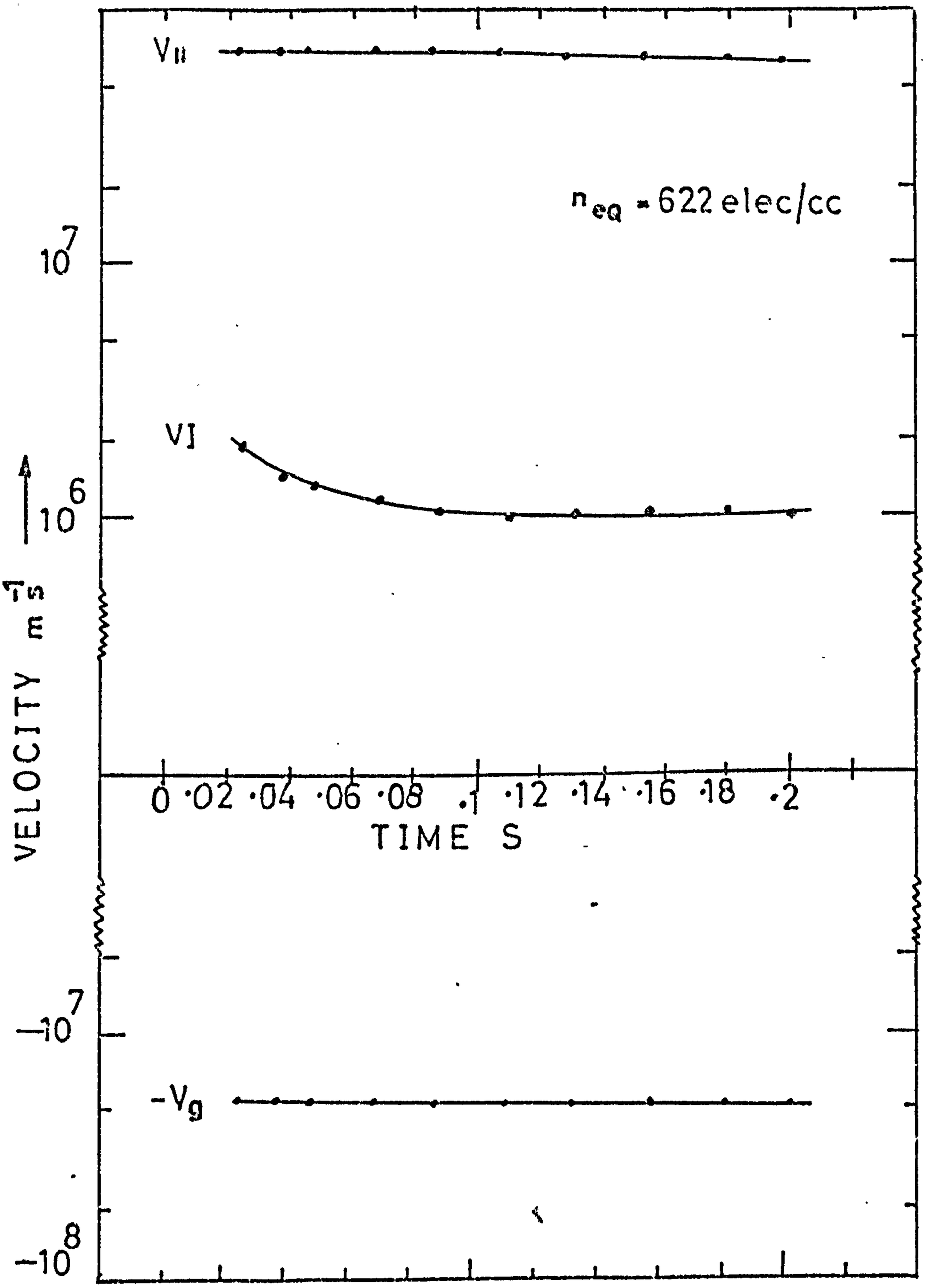

FIG(9 .35)

EMISSION P47H11E

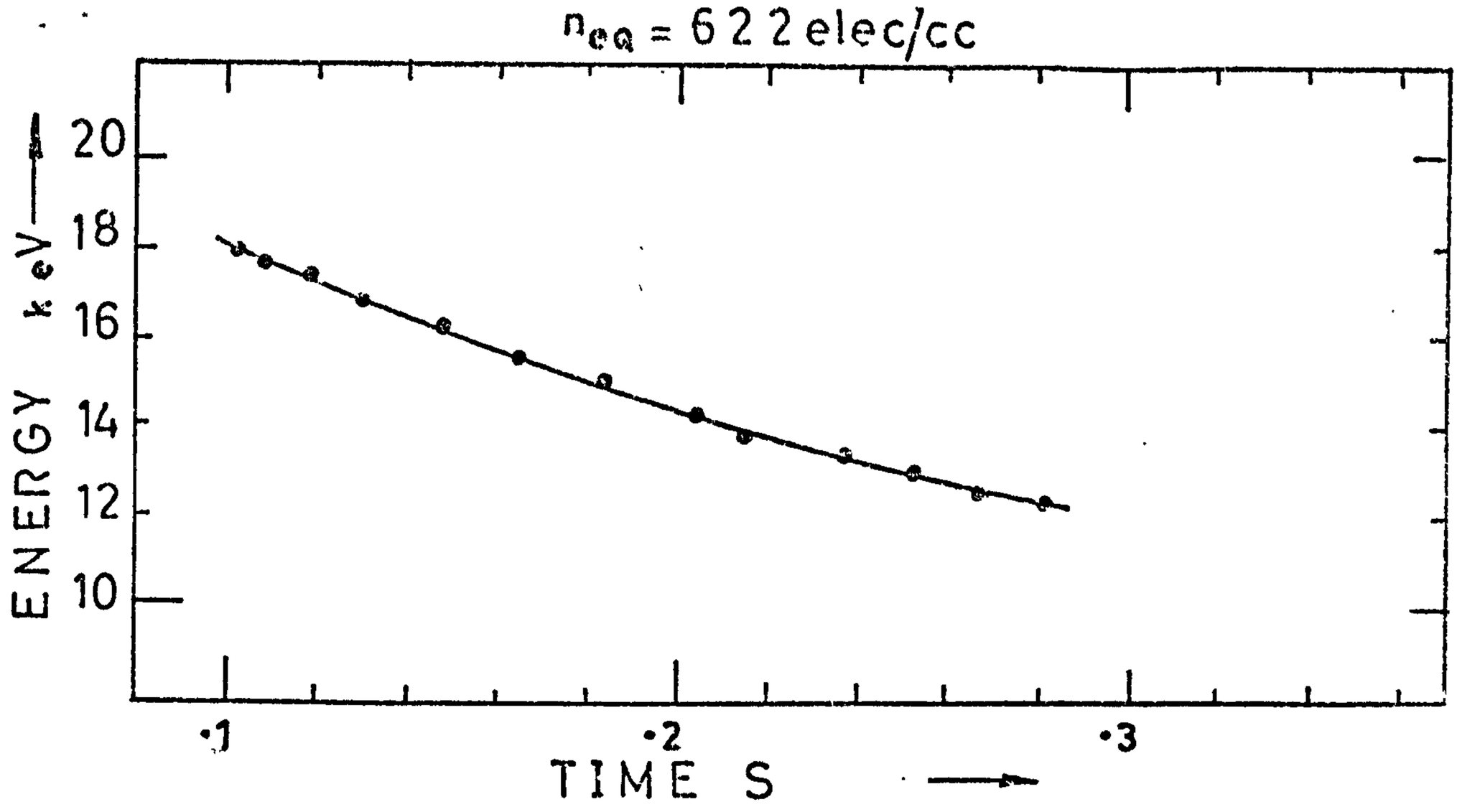

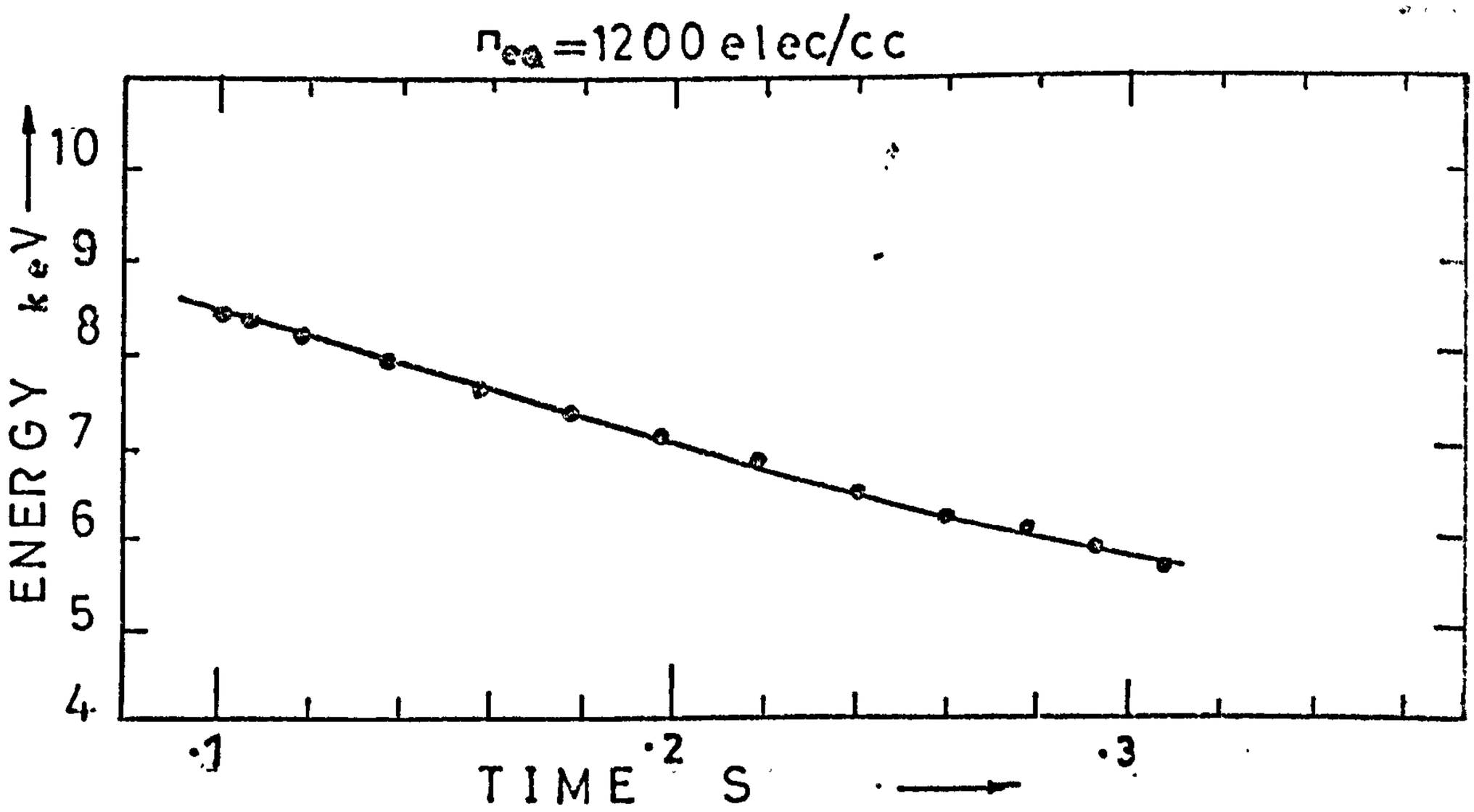

FIG(9.36)

EMISSION P47H11C

COLLISIONLESS MODEL

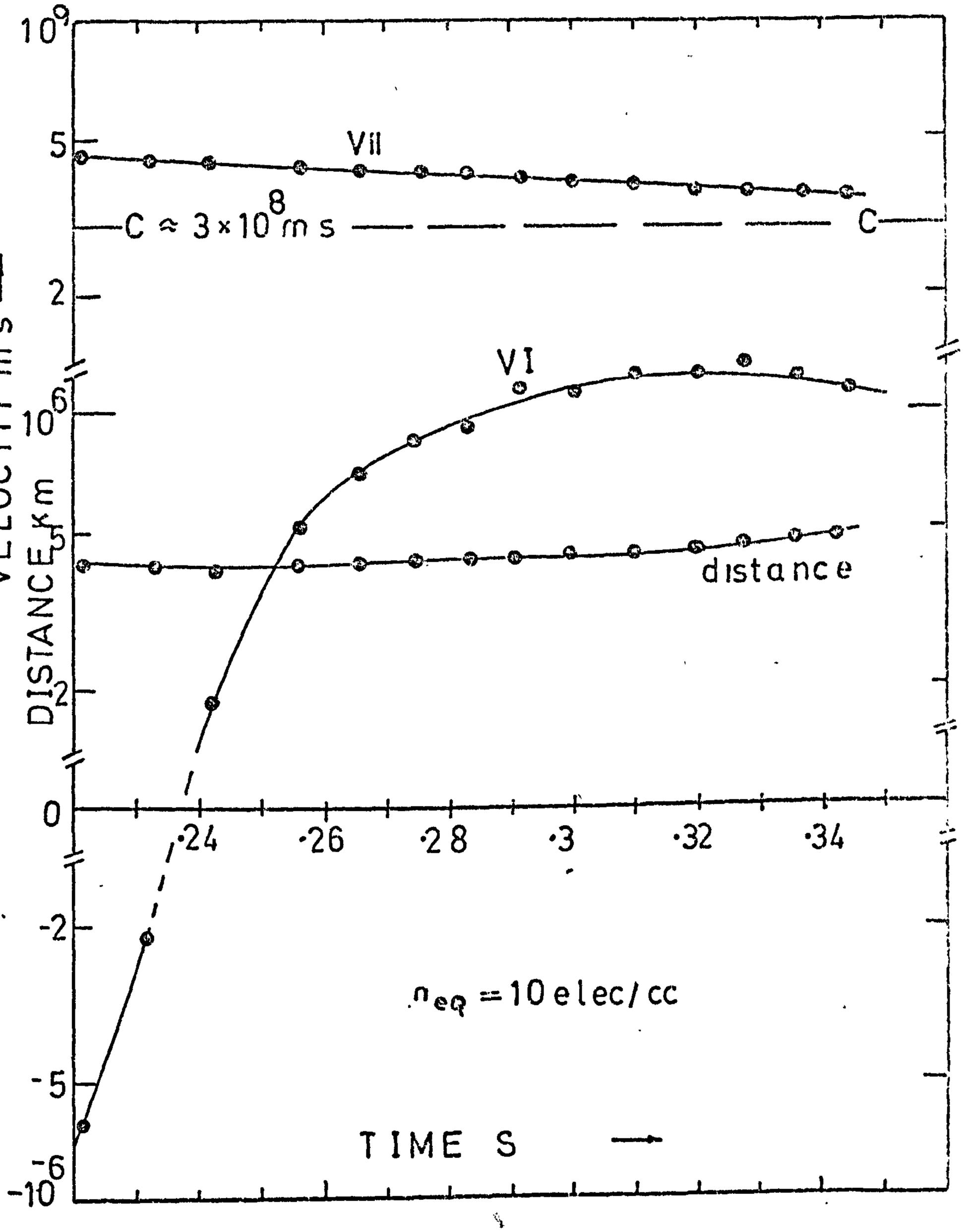

FIG (9.37)

9.3 (cont'd) Again the energy of resonant electrons is the same as for previous emissions and the rate of change of energy is almost constant.

Finally emission P47H11E can be seen in Fig. 9.33. The observed rate of change of frequency is almost constant with a slight tendency to increase as the emission develops. The interaction region in this case moves steadily away from the equator with an almost constant velocity of between 1 and 2×10^6 m s^{-1} for both values of n_{eq}.

Unfortunately it has not been possible to acquire satellite data on the position of the plasmapause with respect to the S.Uist field line (which is the assumed path or propagation for the emissions) at the time of the chorus event. However if we assume that the emissions were generated inside the plasmasphere towards the outer edge and use a gyro-frequency electron density model with values of n_{eq} of the order of 10^3 electrons/cc it is clear that the emissions fulfill the necessary condition ($-v_g < V_I < v$) if they are to be generated by the second order transverse resonance mechanism suggested by Helliwell. The values of resonant electron energies are also realistic and consistent even though individual interaction region motions may be quite different.

If the L = 3.4 field line is taken to be outside the plasmapause and a collisionless electron density distribution with n_{eq} = 10 electrons /cc is used the calculated values of resonant electron energies are meaningless see Fig. 9.37, as $v_{//}$ exceeds the speed of light. This would of course not occur if the relativistic calculations were performed, but extremely high electron energies would still be required.

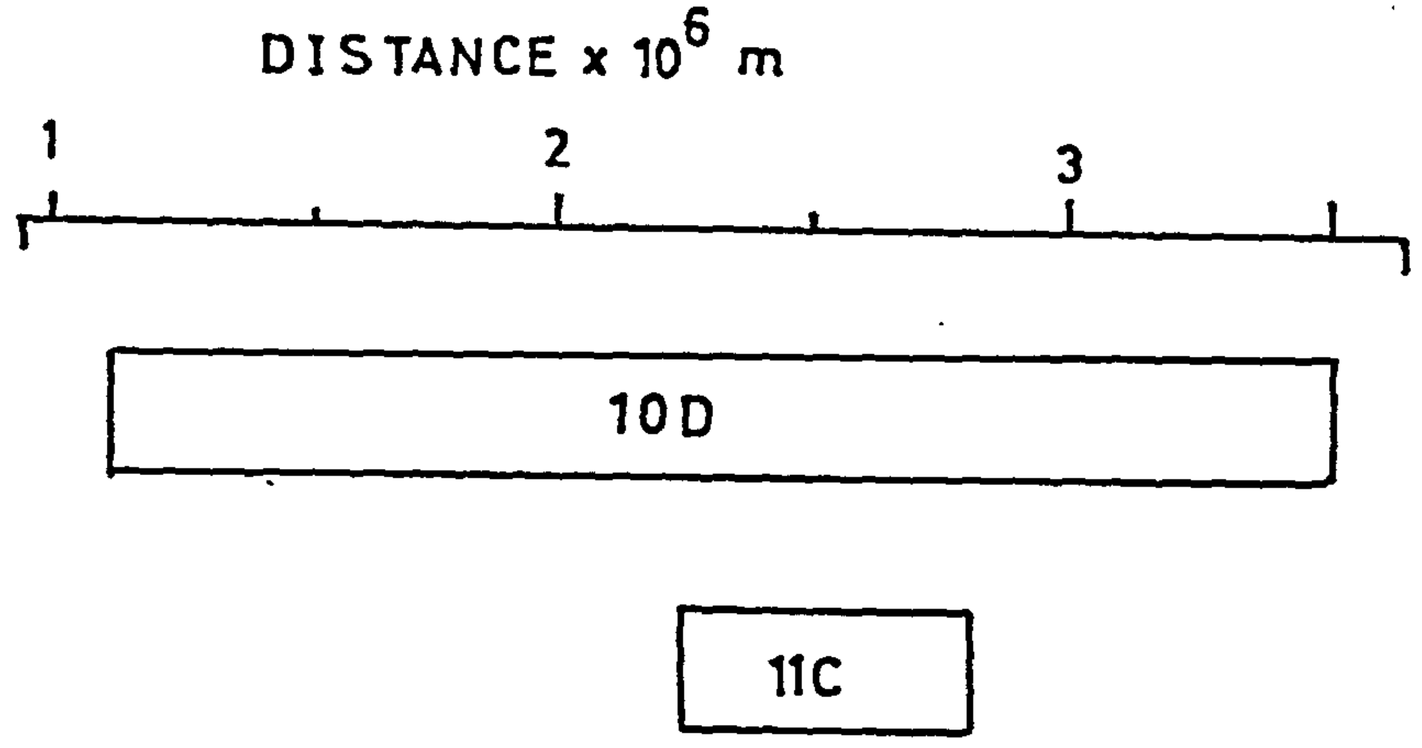
DISTANCE x 10^6 m
1
2
3
10D
11C
11D
11B
10C
11E

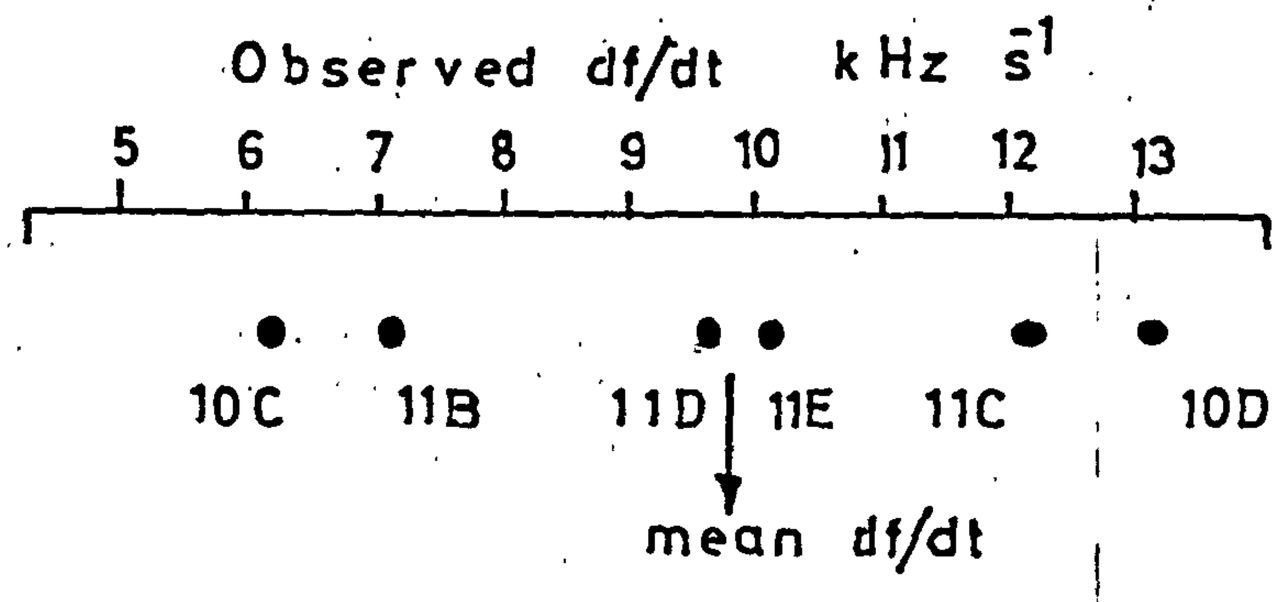
Observed df/dt kHz s^-1
5
6
7
8
9
10
11
12
13
10C
11B
11D
11E
11C
10D
mean df/dt

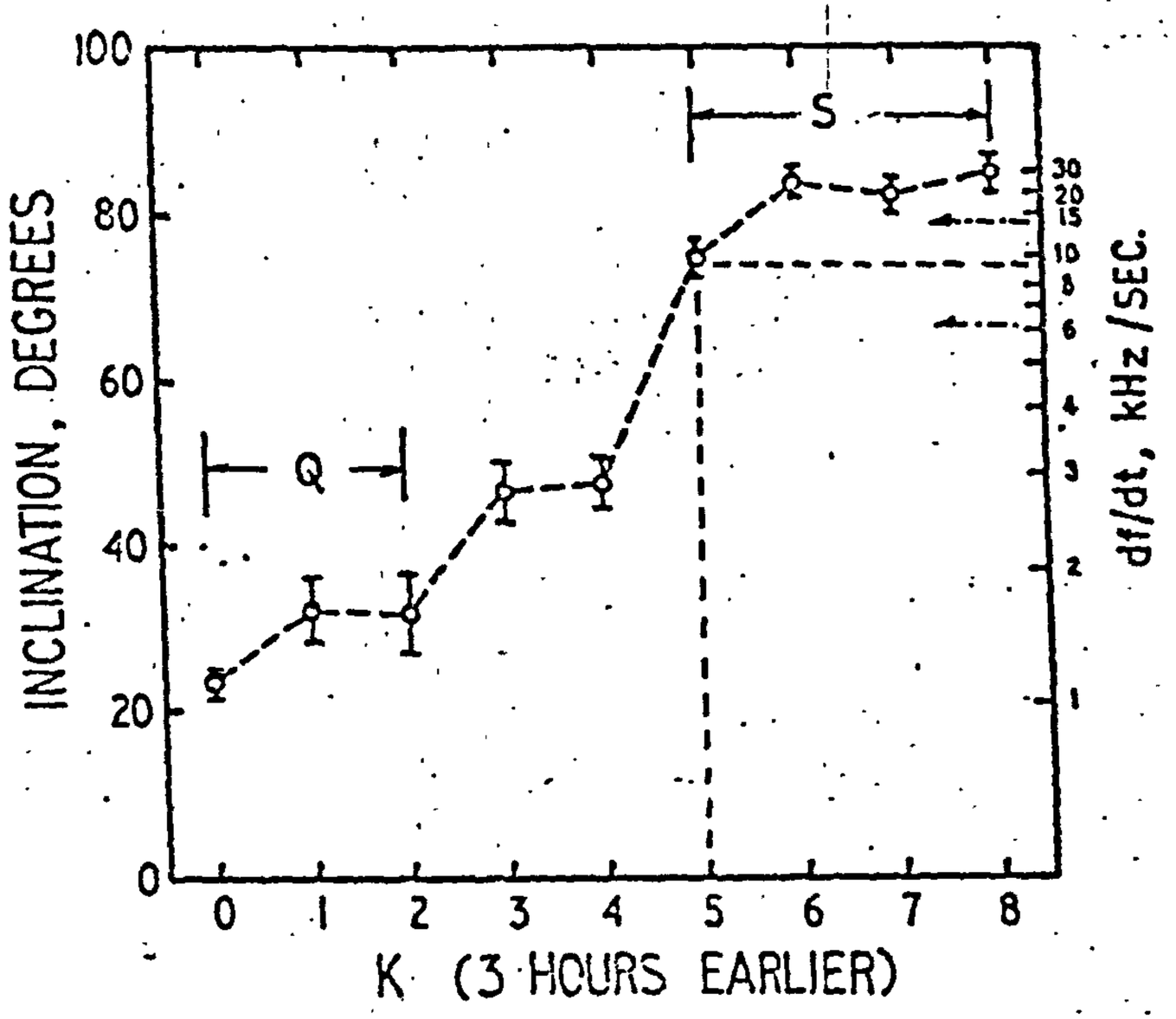
INCLINATION, DEGREES
df/dt, kHz/SEC.
K (3 HOURS EARLIER)
Q
S

FIG (9.38)

MEDIUM LATITUDE (L= 3·4)

EMISSIONS

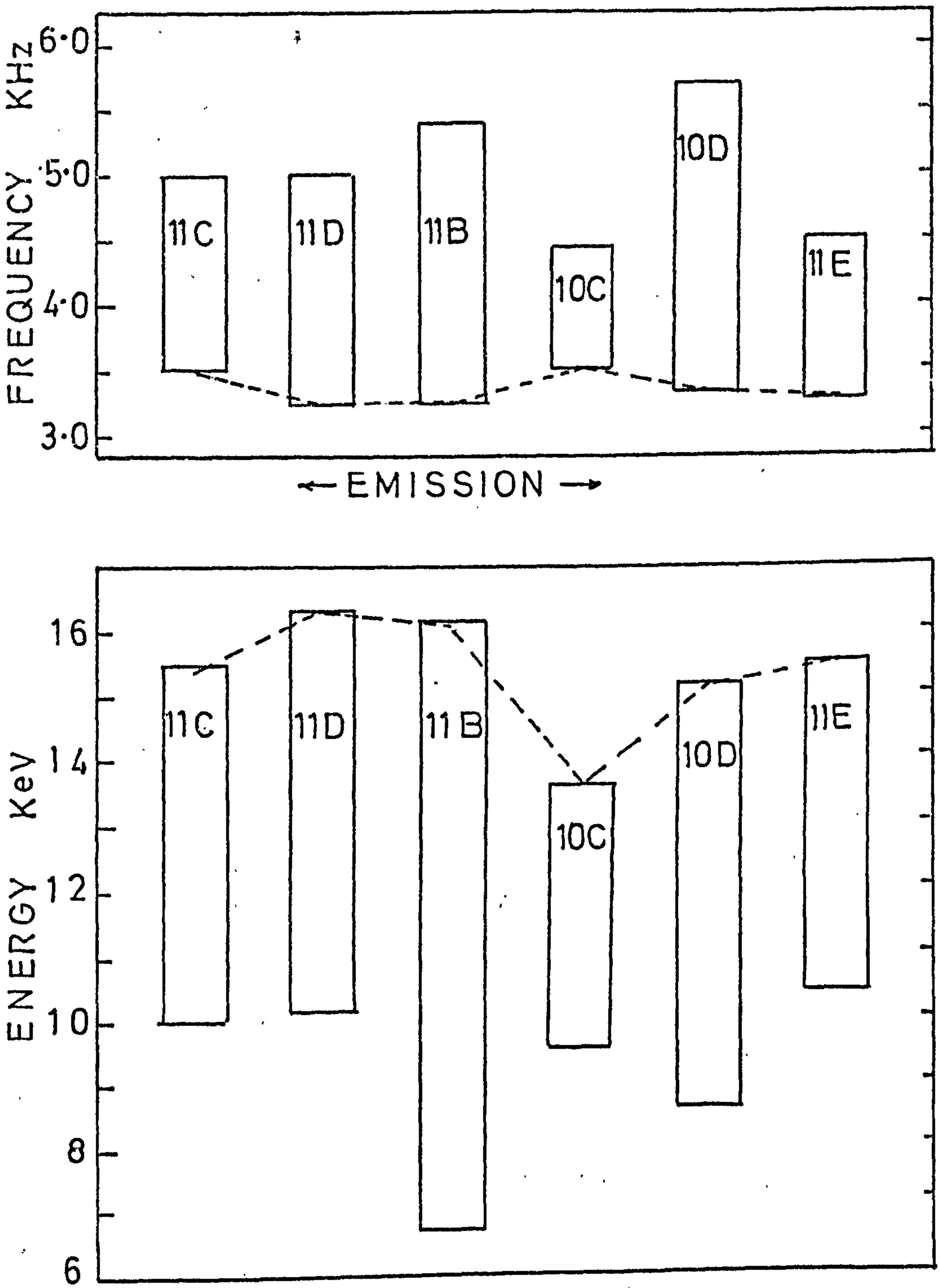

FIG.(9 .39)

9.3 (cont'd) This suggests that the emissions were generated and propagated inside the plasmapause. This is supported by Allcock & Mountjoy 1970 who characterise this type of rapidly rising 1 to 4 KHz chorus as medium latitude S type which is normally associated with magnetically disturbed periods and which is quite distinct from the lower frequency polar chorus such as that shown in Fig. 10.3 which occur at high geomagnetic latitudes and is generated outside the plasmapause.

Allcock & Mountjoy 1970 show a relationship between the observed rate of change of frequency of chorus elements (both quite and storm types) and the local magnetic activity index 3 hours earlier. The data was collected over several months at a station located at 50^{o} S geomagnetic latitude between 0400 and 0700 magnetic local time. Fig. 9.38 shows the values of the average rate of change of frequency as observed on the ground for each of the six emissions. It varies from 6 KHz s^{-1} to 13 KHz s^{-1} and has a mean value of 9.8 KHz s^{-1}. If this mean value is taken in conjunction with Allcock & Mountjoys figure we see that the local K index should have been between 4+ and 6- and centred on 5o. Allcock & Mountjoy point out that the relationship between df/dt and magnetic index is valid if the planetary K index is used as well as K_{local}. The correlation is somewhat better if the local magnetic index is used. From Fig.9.15 we see that the actual value of K_p 3 hours before the chorus event at S.Uist is in excellent agreement with that given by Allcock & Mountjoy.

The variation of distance of the interaction region from the equator for the six emissions is summarised in Fig. 9.38, the extent of the emissions in frequency is shown in Fig. 9.39 along with the range of

9.3 (cont'd) resonant electron energies. There is a clear inverse relationship between the lowest frequency in the emission and the highest electron energies required to produce it. This is simply a consequence of the first resonance condition as stated in equation (7.1,4).

Finally in this section it is appropriate to discuss the form of the energy - time curves and the relationship between the movement of the interaction region and the energetic electron energy distribution. As Brice 1964 points out, the equator is the most likely starting point for an emission because the electron streaming velocity is a minimum there and hence the available resonant particle flux is a maximum.

Consider Fig. 8.3 the power radiated from the drifting interaction region is given by;

$$P_{out} = P_m (v_g + v_I)/v_g \qquad (9.3,1)$$

Quoted by Dowden 1971, from Helliwell 1967.

and the input power from the resonant electrons is given by;

$$P_{in} = E.(v_{//} - v_I)\ dN(E) \qquad (9.3,2)$$

which is given in Dowden 1971, where E = the energy of the resonant electron

dN(E) = the density of resonant electrons within dE of E.

P_m = the limiting radiated power (see Helliwell 1967)

9.3 (cont'd) Helliwell 1967 states that the interaction region moves such that the input power equals the output power. Thus for a falling electron energy spectrum (which is most commonly observed) $E_{\downarrow}$ and $dN(E)$ will increase as the emission moves away from the equator and the generated frequency increases, see equation (7.1,4). If we consider the radiated power to remain constant (for $v_I << v_g$, P_{out} is constant for changes in v_I), then as the emission proceeds from the equator the input power exceeds the output power. Under these circumstances the interaction region velocity increases such that the term $(v_{//} - v_I)$ in equation (9.3,2) is reduced which tends to equalise the input and output powers. A 'simple' riser generated in the presence of a falling electron energy spectrum which may be of the form;

$$N(E) = A\,E^{-n} \qquad (9.3,3)$$

with n typically between 2 and 4 for trapped outer zone electrons in the energy range $40 \lesssim E < 250$ keV (Hess 1968), results in a positive interaction region velocity and a progressive movement away from the equator. The common occurrence of a falling electron energy spectrum leads to the common occurrence of risers over other spectral shapes. Examples of this straightforward interaction region behaviour can be seen in Figs. 9.19 and 20 for emission 11C and in Figs. 9.22 & 23 for 11D. As both Helliwell 1967 and Dowden 1971 point out, if changes, either spatial or temporal, occur in the electron spectrum during the lifetime of an emission the interactionregion velocity will 'respond' to equalise the input and output powers resulting in complicated velocity - time profiles where interaction regions may double back on themselves as for emissions 11B and 10C. It is possible for a later,

9.3 (cont'd) higher frequency to be generated closer to the equator than a preceding lower one if the emission is generated by the mechanism suggested by Helliwell. Examples can be seen for emissions 11B, 10C and for the test emission used by Helliwell which is shown in Fig. 8.5

The relationship between energetic electron spectra, emission profiles and interaction region dynamics has been studied by Dowden 1971 based on Helliwell's theory. He shows that for a variety of emissions received on the ground at L = 3.3 an electron spectrum of the form

$$N(E) \propto E^{-2.2}$$

accounts for their generation if variations in the stream density ranging from 0.5x normal to 10 x normal are allowed over short times (order of 0.01 seconds). Dowden suggests that such density changes resemble electron microbursts as studied by Oliven et al 1968 and Oliven & Gurnett 1968. They show that microbursts are always accompanied by VLF emissions but that emissions are not always accompanied by microbursts. It would appear that microbursts may give rise to some of the more exotic spectral forms of VLF emissions such as hooks with branching risers, but in the case of the six emissions analysed here which are not of this type, it may be assumed that short period variations in the electron stream density do not occur. There is clearly a great deal of interesting work to be undertaken in this field, and as Dowden 1971 points out the verification of Helliwell's theory would "clear up" the long standing problem of the generation of VLF emissions and would provide a useful tool for

9.3 (cont'd) studying the magnetosphere. The essential component which is required to undertake such a study, an accurate, well behaved, fast computer program which does not contain approximations has here been developed and tested. The results from its application to a range of VLF emissions may prove useful in the future study of the Earth's magnetosphere.

In the following pages the development of the computer model based on Helliwell's theory to a more sophisticated level is reported. The program is then used to analyse four Polar Chorus elements which were recorded at Andøya (L = 6.2).

CHAPTER 10

The Analysis of High Latitude Discrete VLF Emissions based on Helliwell's Theory

10.1 A more Sophisticated Computer Model

Having solved a number of problems to produce program P90E the main outstanding one is that of the uncertainty in the results which is introduced by being forced to consider the slope of the first point on the equatorial profile as being that which would have been observed on the interaction region at the start of the emission. The validity of the assumption about the slope decreases as the group delay experienced by the emission increases.

In the new computer modél the aim is to firstly establish accurately the point at which the emission started and then to successively recalculate the form of the emission by removing dispersion effects incurred between the equator and the starting point and between successive points along the path of the drifting interaction region. An extremely accurate picture of the exact movement of the interaction region can be built up and it will be shown that emissions can be reconstituted from interaction region data with great accuracy.

The various routines for integration,dispersion calcualtion & distance calculation used in P90E are again used in this program but the manner in which they are used is quite different, such that the successive recalculation of the emission profile can be carried out. The operation of the program becomes clear if its basic steps are examined one at a time and in the order in which they are called.

Consider Fig.10.1, the emission profile received on the ground is prepared as before as a series of points f,t from 1 to n_{max}. For a typical riser such as emission E, n_{max} = 25. The profile is corrected for dispersion effects back to the equator and profile No.2 is obtained.

First guess. This position calculated from the slope of the equatorial profile at point 1.

Slope at 1 from No.3 profile gives second and better estimate of distance.

Equatorial profile corrected for dispersion to $S_1/2$. To give better estimate of slope at 1.

Equatorial emission profile. Point 1 used to give distance S_1.

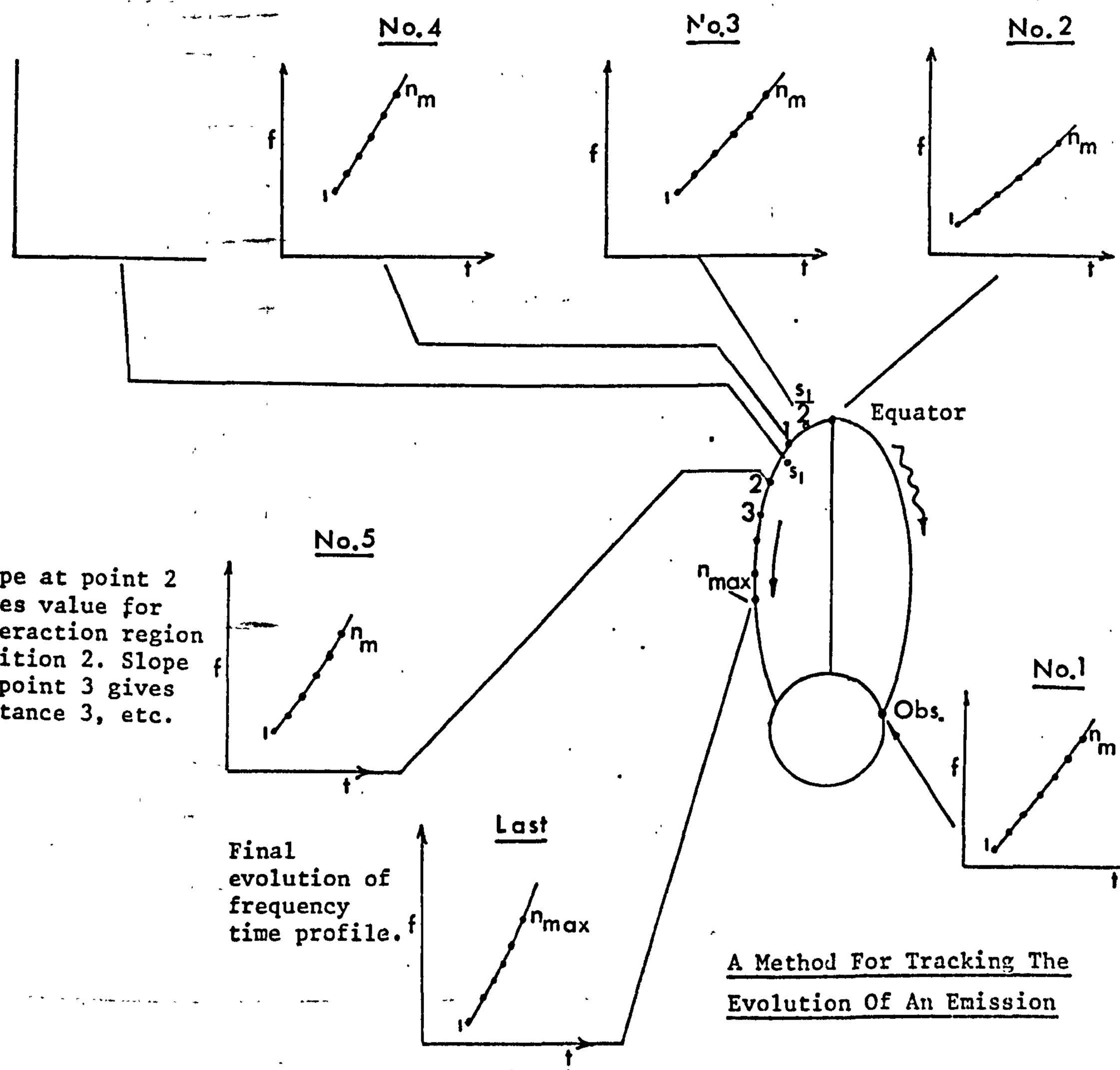

A Method For Tracking The Evolution Of An Emission

FIG.(10.1)

A polynomial is fitted to this equatorial profile and the slope at point 1 is calculated.The distance calculation is performed and this yields a first estimate at S_1. For a simple riser with a starting frequency which is less than the nose frequency S_1 will be too large because dispersion modifies the slope of the emission such that df/dt at the equator is greater than df/dt at the point of generation. A better estimate of the point of generation can be obtained by updating the equatorial profile to that which would have been observed at position $S_1/2$ and using the slope of this profile at point 1 to calculate the distance. As the slope at point 1 in profile 3 is less than that in the equatorial profile the distance will be less than S_1.The difference between S_1 and the distance to position 1(see Fig.10.1)is printed out and an estimate of the accuracy of the position of the first generation point can be obtained. For example using emission E with n_{eq} = 1 electorn/cc and a collisionless electron density model the difference in the distance estimates is 2.3km in 450km which is a discrepancy of approximately ½%.The change in the values of slopes at point 1 is 1.259Hz s^{-1} in 300 Hz s^{-1}. The position of the first generation point(1) is thus obtained with some idea of its validity.

The equatorial profile is corrected for dispersion to position 1 and after fitting a polynomial to profile 4 the second generation point is established by using the emission slope at point 2. The equatorial profile is then corrected for dispersion to position 2 which results in profile 5. Using a polynomial the slope at point 3 is established and position 3 is calculated. The process is repeated until the distance corresponding to point n_{max} has been calculated.In this manner the development of an emission is tracked or retraced from the received signal. All the interesting parameters such as $v_{//}$,v_I,v_g,and resonant particle energy are calculated for each position of the generation region as in P90E.

EMISSION E

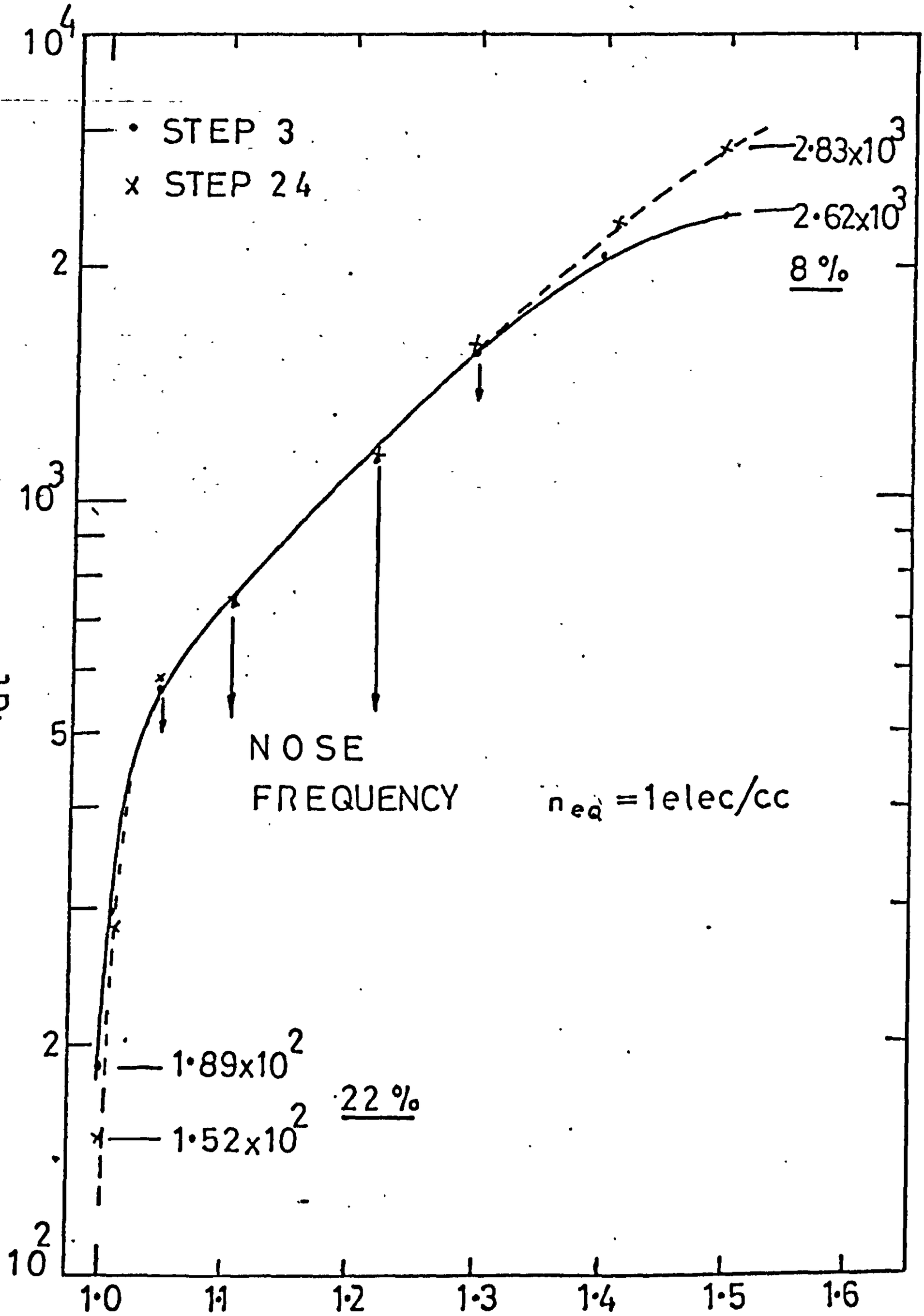

FIG (10.2)

The effect of recalculating the emission profile as the generation region moves along the field line away from the equator can be seen in Fig. 10.2. Here the slope of emission E as a function of frequency is plotted for the equatorial profile and the profile at the last generation position. Frequencies close to the nose frequency show little change of slope, but above the nose frequency the slope is increased and below.it it is decreased.The change in slope at the low frequency end of the emission is not important as the slopes at these frequencies are taken from profiles generated close to the equator but as the frequency of interest moves up the emission and the generation region moves away from the equator, the change in slope becomes important. An 8% change in a slope of 2 KHz s^{-1} at 1.5 KHz for emission E is achieved by successively recalculating emission profiles, this is reflected in the position of the interaction region along the field line and a more accurate estimate of interaction region velocity,parallel velocity and hence resonant electron energy is obtained. The organisation of the computations is involved, but a simplified logic flow chart for the program P90T can be seen in Appendix 2.

10.2 Discrete VLF Emissions Received at Andøya.

A number of narrow bandwidth risers were recorded at Andøya,N.Norway (69.3°N,16.016°E) during the launching of a 3 axis VLF receiver on board P129A which was mentioned earlier.The launching took place on the 3rd of November 1972 at 11.45hr GMT. A VLF goniometer (Bullough & Sagredo 1973) was used to receive the polar chorus.The instrument was situated about 2 Km W of the range at a 'quiet' site.

The chorus emissions were received following a magnetically disturbed period lasting some 3 days during which the planetary magnetic index K_p reached values of 8_o and was commonly 5-,see Fig.9.15. As with P47H the emissions were received when the K_p had fallen below 3,their rec-

EMISSION A

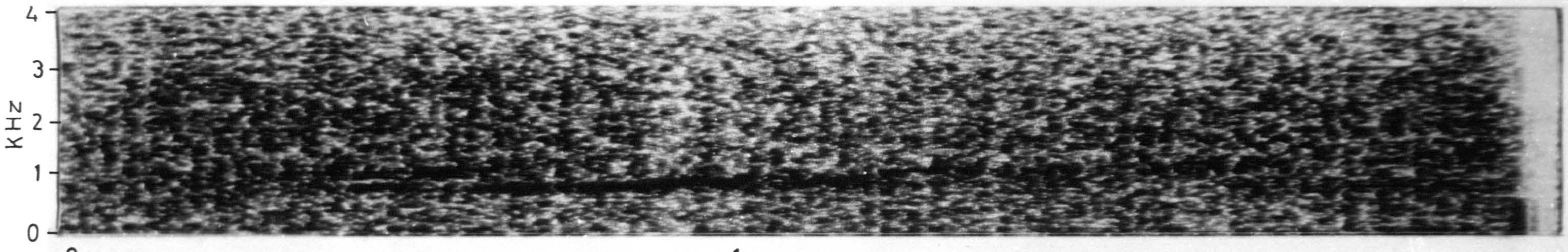

EMISSION E

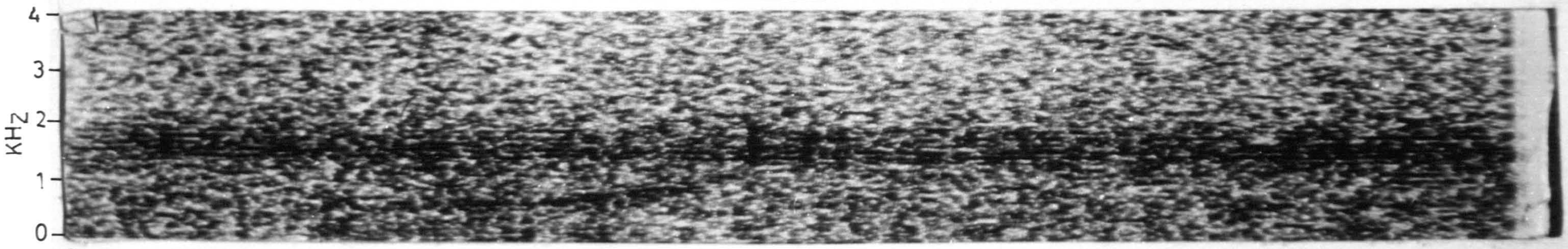

FIG.(10. 3)

EMISSION J

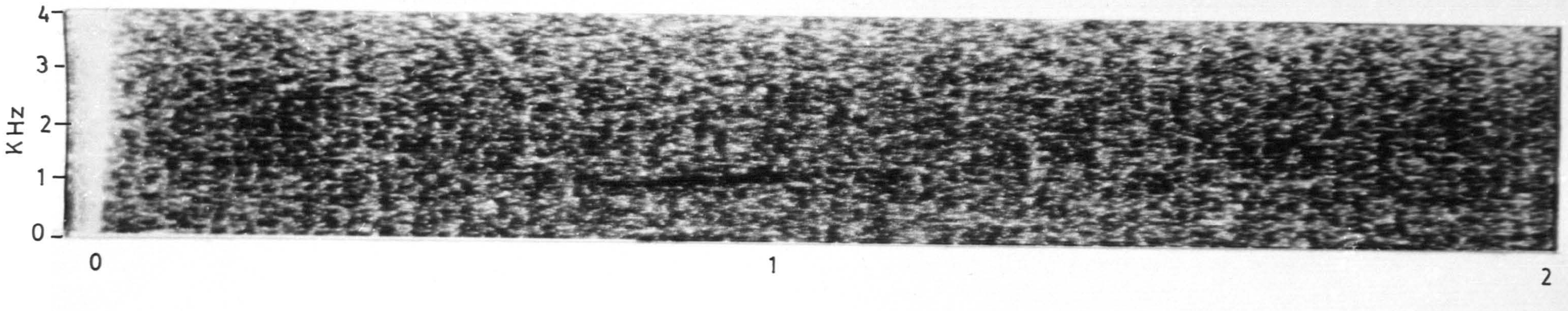

EMISSION B

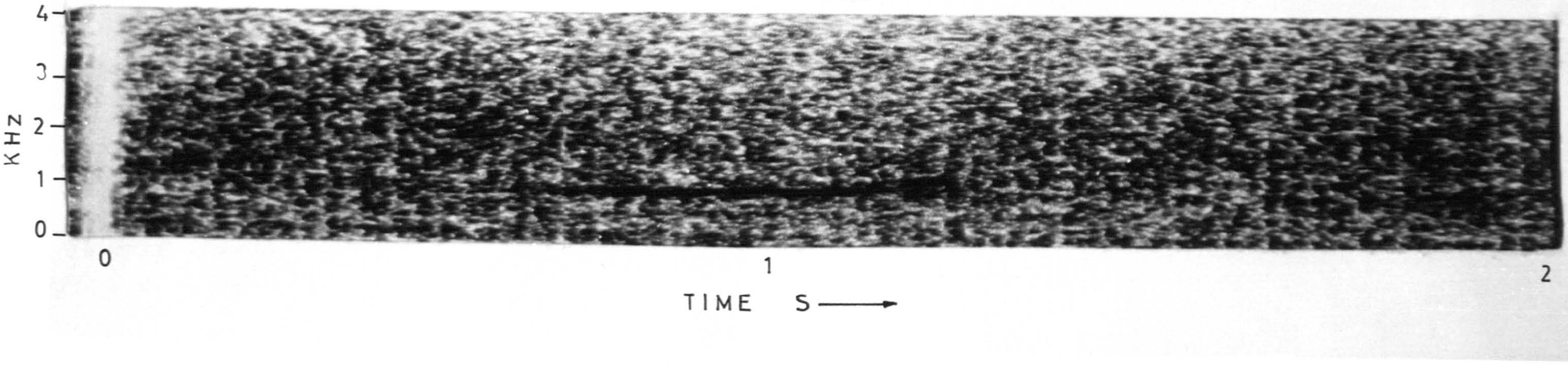

FIG.(10.4)

ception possibly being prevented by ionospheric absorption during the storm event itself. About 20 to 30 emissions were reproduced on a Sonograph these being the most audible ones selected from the 1 hour of recording.From these 4 were chosen for detailed analysis these being of high intensity,narrow bandwidth and with a clear spectral form. The signal strength of these emissions was not great(estimated to be about 10^{-5}gamma) and in consequence the background noise is noticeable on the Sonograms. However the emissions can easily be seen at between 1 KHz and 1.5 KHz, see Figs. 10.3 and 10.4. It is clear that they are much longer lasting than the medium latitude emissions presented earlier and may continue for up to 1 second. They are also confined to a much smaller range of frequencies and most of these emissions cut off at $f_{ho}/2$ for the field lines in the region of Andøya. This is an obvious upper frequency limit for ducted emissions which are generated on the far side of the equator as the guiding of VLF energy along a field line ceases at $f_h/2$ see Helliwell 1965. This simple explanation for the cessation of the emissions is in contrast to the medium latitude ones given earlier where there is no obvious reason for the cut off.

Before considering these high latitude emissions for analysis on the basis of Helliwell's theory using P9OT we must establish both the path of propagation of the emission and which magnetospheric electron density model to use. Unfortunately the VLF goniometer was not able to establish the assumed duct exit point due to interference. The goniometer technique worked extremely well at Halley Bay, Antarctica Sagredo & Bullough 1973 and in a recent campaign in Canada during a solar eclipse Rycroft (private communication).However it is possible to estimate the location of the field line lying at the centre of the assumed duct by using the emission cut off frequencies. In Fig.1.4 we see a number of whistlers with nose frequenies around 3 KHz. The nose frequencies and

cut off frequencies are estimated by eye and marked with a small dot. Using the well known relation;

$$f_{nose} = 0.38\ f_{ho}$$

it is possible to calculate $f_{ho}/2$ and compare it with the cut off frequency. This has been done in Table 10.1.

Table 10.1

Whistler No.	f_n	f_{ho}	$f_{ho/2}$	$f_{cut\ off}$
0	4.2KHz	11.05KHz	5.53KHz	5.5KHz
1	4.2 "	11.05 "	5.53 "	5.3 "
2	4.3 "	11.32 "	5.65 "	5.7 "
3	4.0 "	10.53 "	5.26 "	5.1 "
4	3.75"	9.86 "	4.93 "	4.6 "
5	3.7 "	9.74 "	4.86 "	4.7 "

The average error in $f_{ho/2}$ with respect to $f_{cut\ off}$ is 4% at 5KHz and it would seem reasonable that using the emission cut off frequency it is possible to calculate f_{ho} to within 10%. In the absence of better data relating to the propagation path of the four emissions shown, the cut off frequency at 1.5 KHz gives f_{ho}= 3 KHz. The invariant coordinates of the exit point must be calculated using this value. The calculation is a graphical one, see Fig. 10.5. Firstly the geographic positions of the four points at the corners of the invariant coordinate grid ($\Lambda = 65^\circ, \phi = 100^\circ$), ($\Lambda = 70^\circ, \phi = 100^\circ$), ($\Lambda = 65^\circ, \phi = 110^\circ$) are determined. The 'box' formed by joining these points together contains the position of Andøya which may be placed by knowing its geographic coordinates (69.3°N, 16.016°E). Its magnetic co-ordinates are found by a linear interpolation inside the 'box', they are given as ($\Lambda = 66.75^\circ, \phi = 105.8^\circ$).

Barish & Roederer 1969 have produced tables of calculated mangetic field strength at the geomagnetic equator for a field line referred to the 100 km level for the region around Andøya. The value of the equatorial magnetic field strength for the "Roederer field line" shown in

CALCULATION OF THE INVARIANT COORDINATES

Ø and Λ of ANDØYA (69.30N,16.016E)

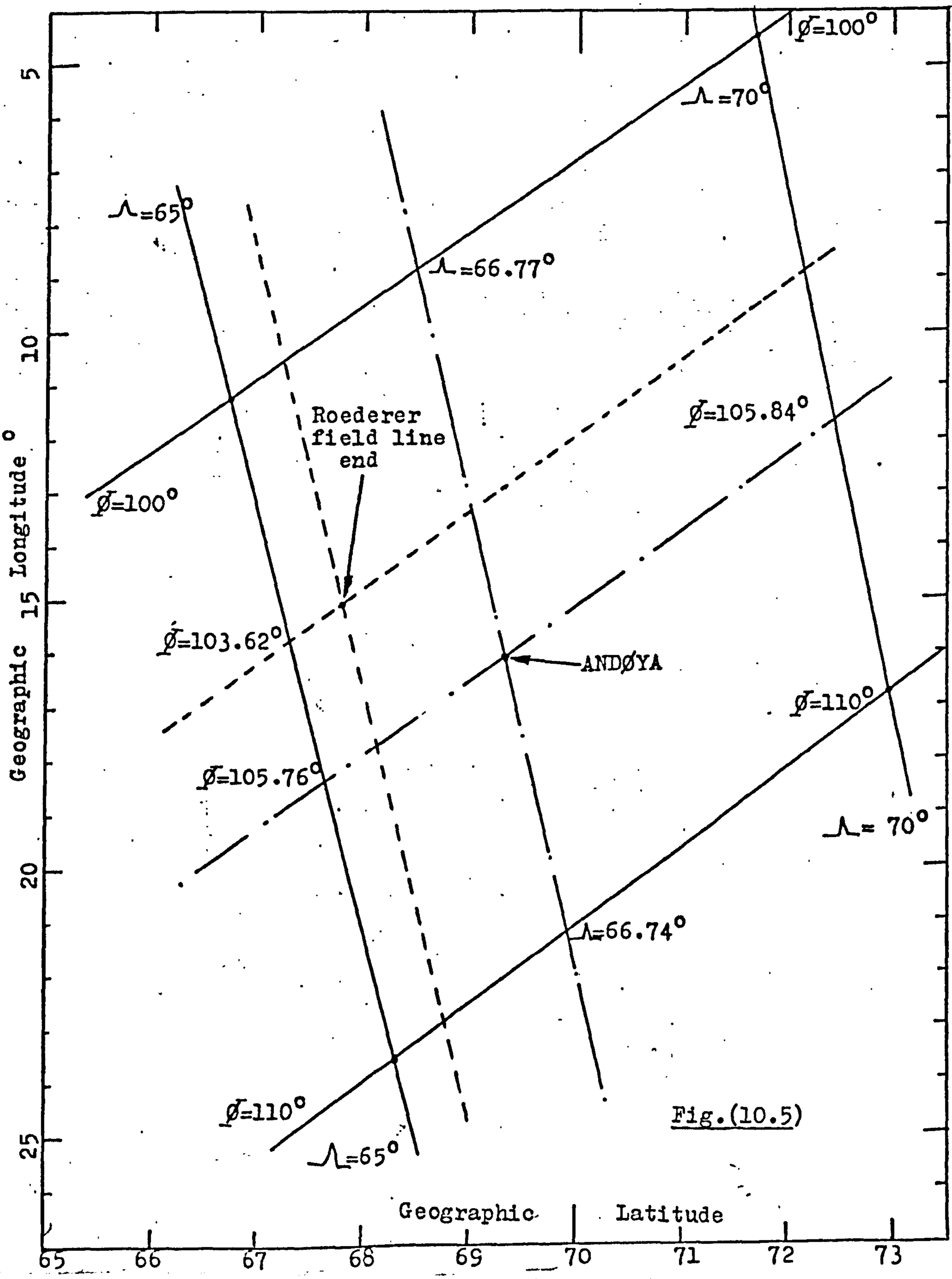

Fig.(10.5)

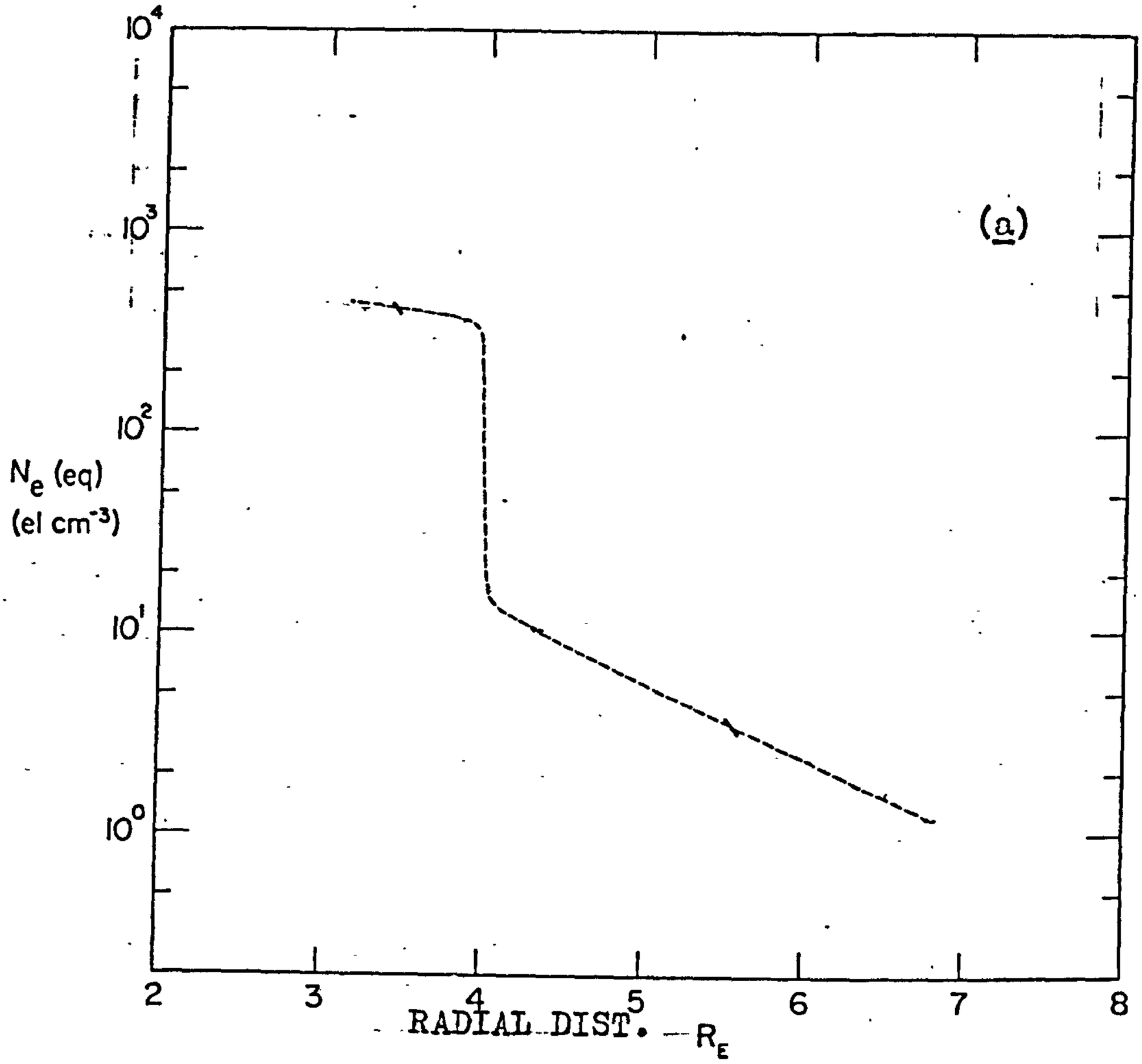
(a)
10^4
10^3
10^2
10^1
10^0
N_e (eq)
(el cm^{-3})
2
3
4
5
6
7
8
RADIAL DIST. — R_E

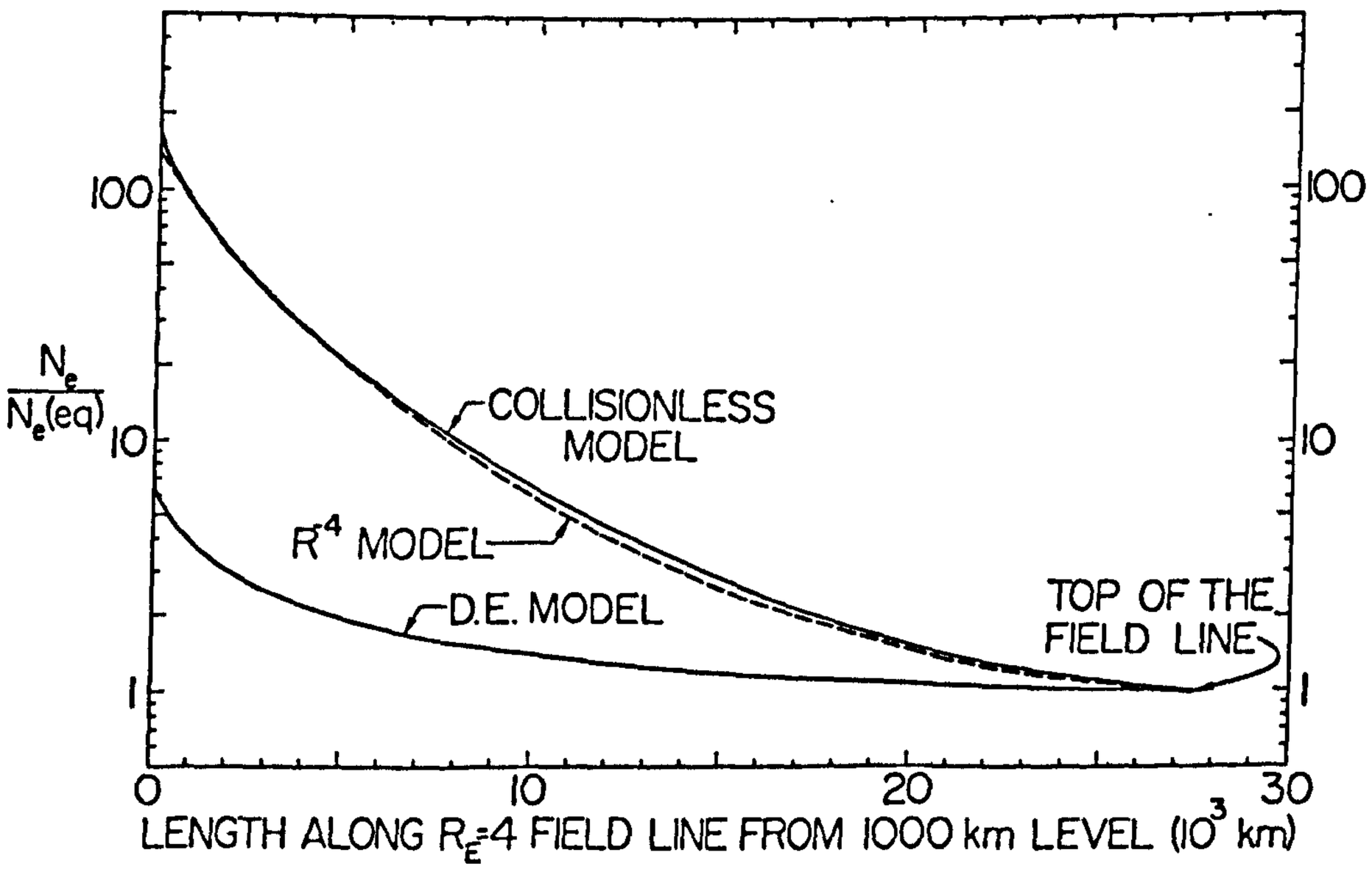
100
10
1
100
10
$\frac{N_e}{N_e(eq)}$
COLLISIONLESS MODEL
R^4 MODEL
D.E. MODEL
TOP OF THE FIELD LINE
0
10
20
30
LENGTH ALONG R_E=4 FIELD LINE FROM 1000 km LEVEL (10^3 km)

Fig.(10.6)

Fig. 10.5 is given as;

129 ɣ predicted for 21..9..75

130 ɣ predicted for 21.11..75

The location of the bottom of the field line is given as 67.69°N, 15°E and in magnetic coordinates $\Lambda = 65.51^{\circ}$, L = 5.819.

If we assume that the magnetic field strength varies as $1/L^3$ at the equator then the field strength for Andøya, B_A is given by;

$$\frac{B_A}{B_R} = \frac{L_R^3}{L_A}$$ where B_R the field strength at the equator for the Roederer field line.

A value of 129.5 ɣ is used to give $B_A = 96.56$ ɣ

The minimum gyrofrequency along the Andøya field line is given by;

$$f_{ho\,(Andøya)} = 27.9938 \times B_A \text{(in gamma)}$$

$$f_{ho} = 2.703 \text{ KHz}$$

Thus for an observed cut off frequency of 1.5 KHz, taking this to be $f_{ho/2}$ and $\frac{L}{L_A} = \sqrt[3]{\frac{2.703}{3.0}}$

we see that the McIlwain parameter for the field line of propagation L is 6.196 and $\Lambda = 66.313^{\circ}$. Assuming that 1° of latitude is equivalent to a distance of 111 km on the earth's surface we see that the emissions may have travelled only 50 km in the earth-ionosphere waveguide. No attempt was made in the analysis which follows to allow for dispersion in the cavity.

The existence of the plasma pause at approximately L=4 during undisturbed conditions is well known. It has been studied over a number of years by many workers employing a variety of research techniques. Fig. 10.6 due to Angerami 1966 shows the equatorial electron density as a function of radial distance from the earth's surface measured in earth radii. At L = 3.4 (S Uist) electron densitites at the equator in the region of 500 electrons/cc are indicated. At the field line

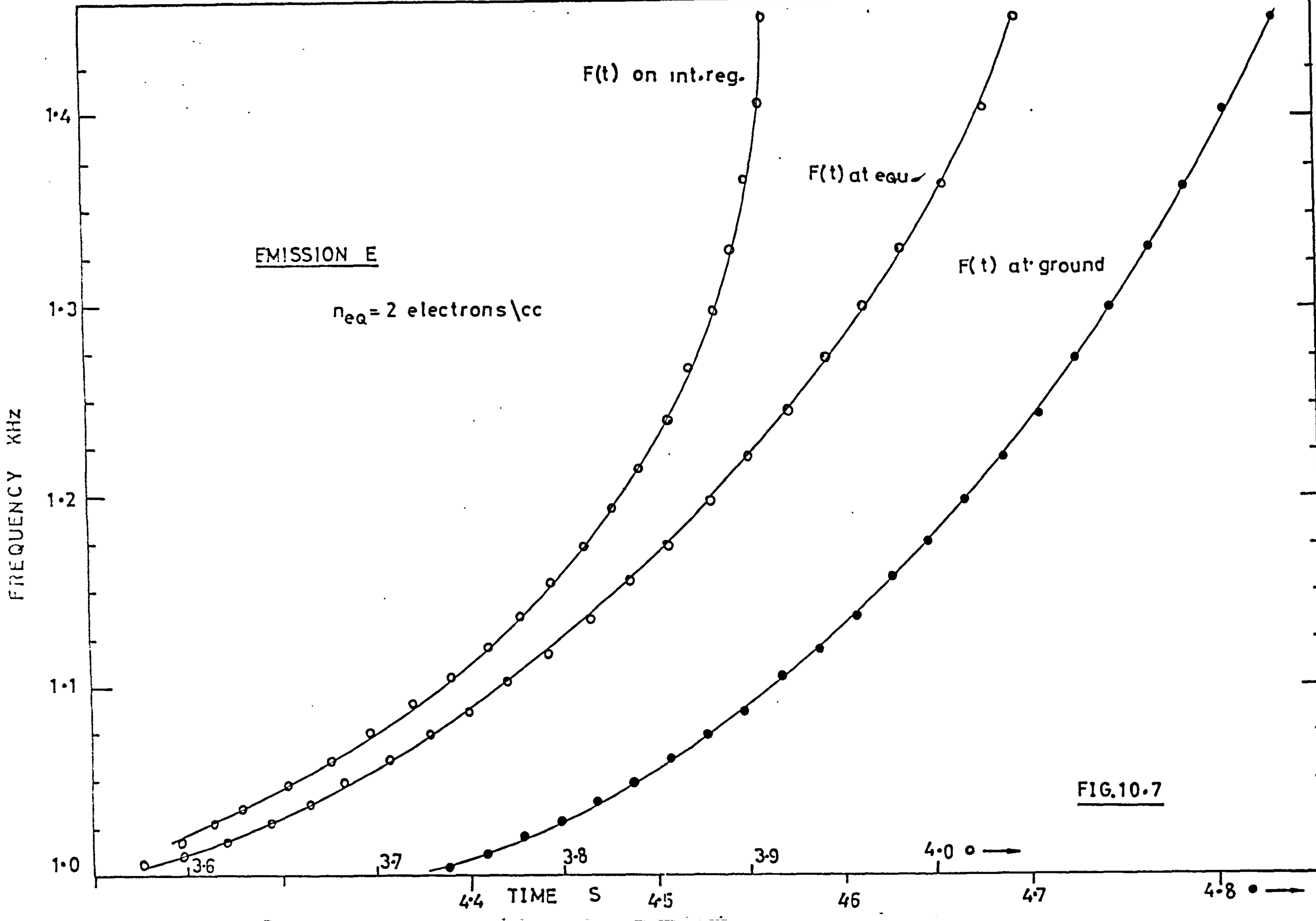
F(t) on int.reg.
F(t) at equ
F(t) at ground
EMISSION E
n_{eq}= 2 electrons\cc
FREQUENCY KHz
1·4
1·3
1·2
1·1
1·0
3·6
3·7
3·8
3·9
4·0
4·4
TIME S
4·5
4·6
4·7
4·8

FIG.10·7

passing through Andøya at L = 6.2 we see that a density of about 2 electrons/cc is given. Angerami points out that experimental evidence suggests that the ionisation along a field line in the region beyond the plasma-pause falls off with height at a much faster rate than the distribution in the plasmasphere. Also the slope of the ionisation distribution across field lines outside the plasma-pause is such that it can only be represented by a diffusive equilibrium model if unrealistic parameters for the ionic composition at 1000 km and electron temperature are assumed.

The low electron densities outside the plasma-pause mean that collisions have a comparatively small effect on the electron distribution in this region. Thus one might expect a good approximation to be obtained by considering the case where collisions are neglected. Such idealised situations have been studied by workers including Dowden 1960 and Eviatar et al 1964. Fig. 10.6a shows the comparison of the diffusive equilibrium model, the collisionless model due to Eviatar and an R^{-4} model for plasma density along a field line at L= 4. The R^{-4} model is an empirical one where

$$n_e = n_{eq} R^{-4}$$

The similarity between the collisionless model and the R^{-4} model is obvious and the simple expression was used in the calculations during the analysis of Andøya emissions.

10.3 The Analysis of High Latitude Discrete VLF Emissions

The results of the detailed analysis of the four emissions shown in Figs.10.3 & 10.4 are presented. Each emission is discussed in turn, the similarities or differences between emissions are dealt with thereafter.

Each emission was prepared for analysis in the standard manner which was described earlier and represented by between 20 and 30 frequency -time points.

Emission E frequency - time profile as received on the ground can be seen in Fig. 10.7 (curve (a)). When corrected for dispersion effects

suffered during propagation from the equator the profile becomes curve (b) showing that a 0.8 second delay had been introduced. The shape of the curve is modified due to the differential time delays at different frequencies. The curve shape near the nose frequency at about 1.2 KHz is unaltered but below that it is decreased and the emission is stretched out,whilst at frequencies greater than f_n the slope is increased and the profile is contracted.

The calculations described earlier are performed using the computer program P90T to yield the frequency time profile at the interaction region. A much smaller delay has to be removed in this case because the interaction region is between $9x10^5$ and $5x10^6$ m from the equator which is only a fraction of the path length from the equator to the observer. It is interesting to note that the rate of change of frequency tends to infinity at the end of the emission's lifetime and the interaction region velocity as shown in Fig.10.8 exceeds the parallel velocity of resonant electrons. The Helliwell criterion $-v_g < v_I < v_{11}$ is disobeyed only for the last two points on the emission profile. If the analysis is repeated with n_{eq} = 1.5 elelectrons/cc instead of 2 electrons/cc we see from Fig. 10.9 that the interaction region velocity lies within the acceptable limits. Reducing the electron density still further to 1 electron/10cc the interaction region velocity still fulfills the condition. If the electron density at the equator is increased however to a figure of 5 electrons/cc, we see from Fig. 10.11 that a physically impossible situation results. The interaction region velocity starts at a value which is $\frac{1}{2} \times v_{//}$ and after falling in the same manner as the previous $V_{//}$ curves it rises until half way through its lifetime it exceeds $V_{//}$ and continues until it exceeds the velocity of light. The velocity curve reappears from $-\infty$ and proceeds to decrease with negative time. This description of the interaction region velocity indicates that a value of n_{eq} = 5

EMISSION E

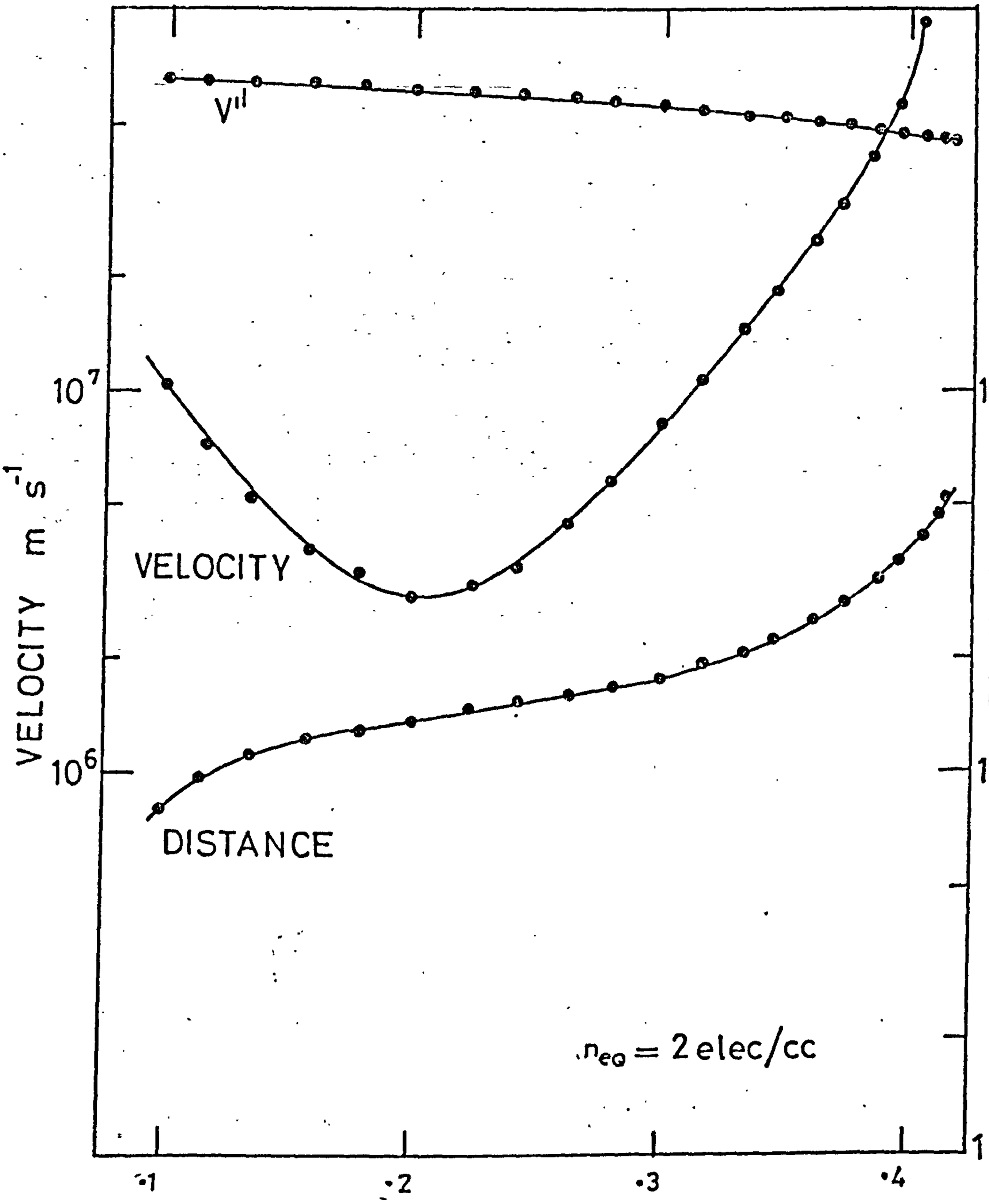

FIG. (10·8)

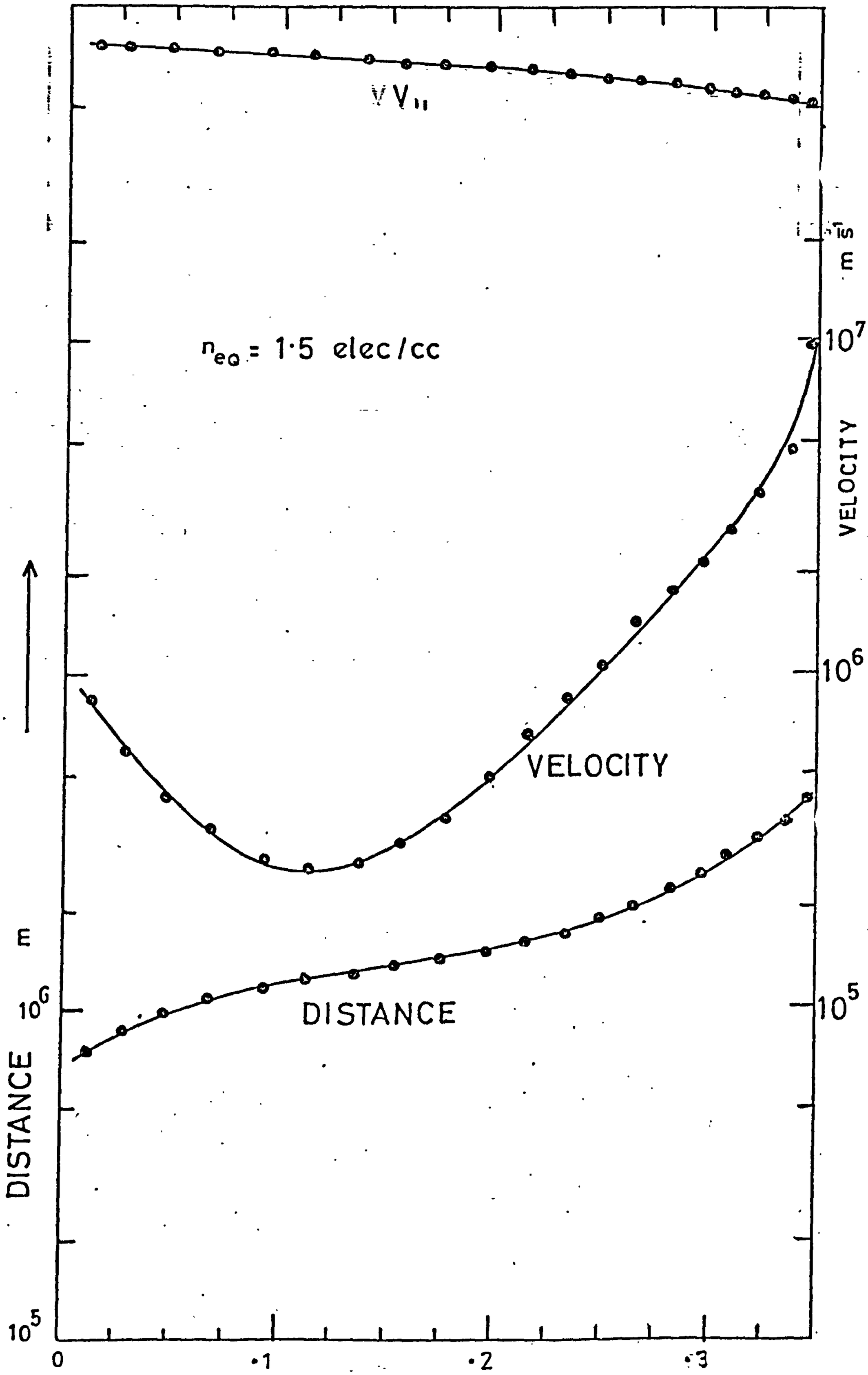
EMISSION 'E'
$V V_{11}$
n_{eo} = 1·5 elec/cc
E
VELOCITY
10^7
10^6
10^5
VELOCITY
DISTANCE
E
10^6
10^5
DISTANCE
0
·1
·2
·3
TIME s

FIG. (10.9)

Emission E

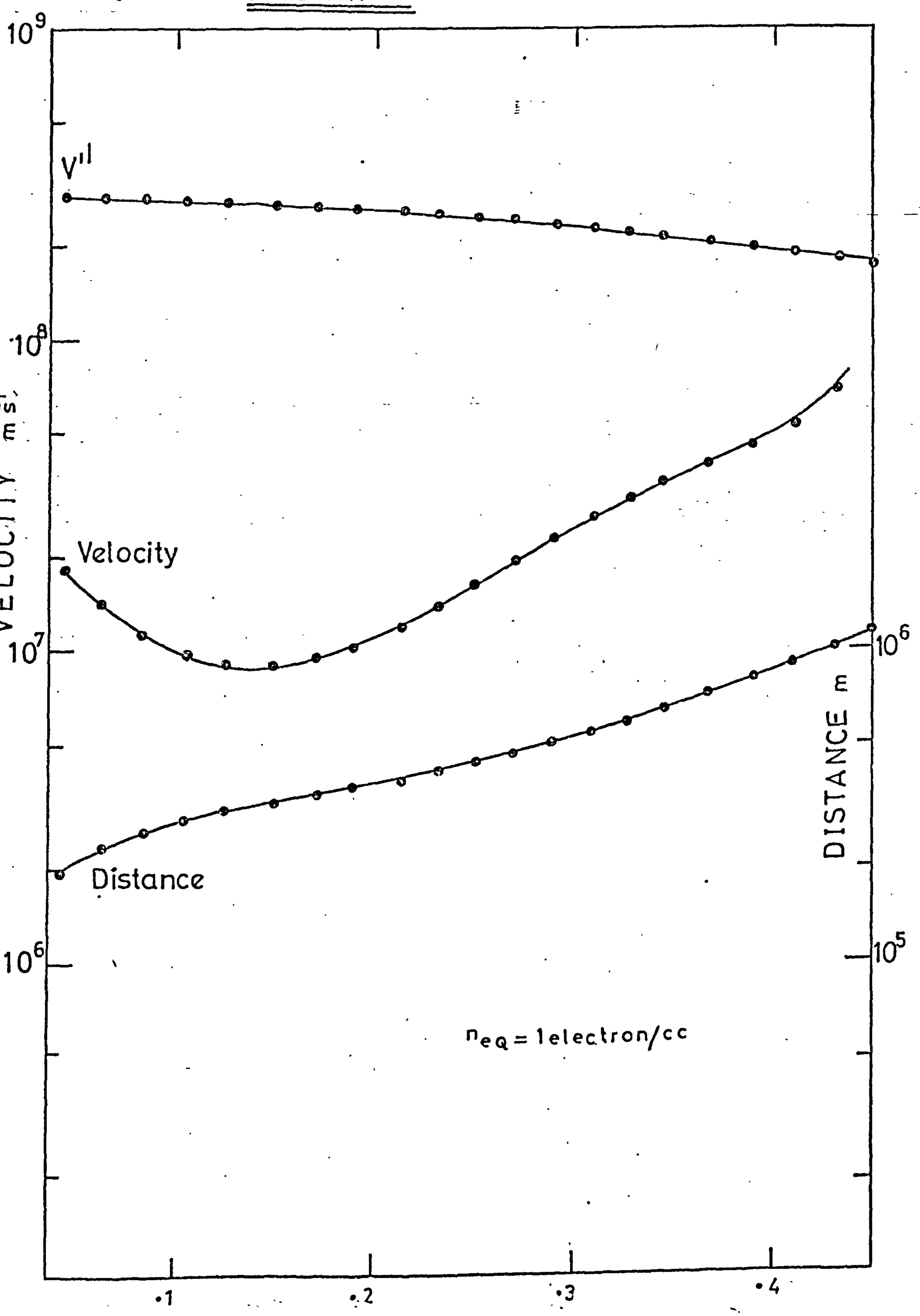

FIG. (10.10)

electrons/cc cannot have occurred during the generation of this emission. It is clear that values of n_{eq} between 1.5 and 2 electrons/cc represent an upper limit of equatorial electron density for this emission. To establish that the analysis program or method had not broken down at n_{eq} = 5 electrons/cc and produced the unrealistic interaction region movement, programs were written to recover the original received emission profile from data on the interaction region position and velocity. All the data resulting from the analysis of an emission using program P90T was written on punched cards which were used as the input data for the reconstitution program. This eliminates errors introduced by reading values from graphs or printouts. Due to the lack of space, details of this reconstitution program are not given but the result of its use on the data produced by the analysis of emission E with n_{eq}= 1.5 electrons/cc can be seen in Fig. 10.12. The extremely good agreement between the original and reconstituted profiles indicates the accuracy of the analysis program P90T. Very good agreement is also achieved when the completely unrealistic interaction region velocities obtained with n_{eq} = 5 electrons/cc are used in the reconstitution. This can be seen in Fig. 10.13. It is clear that the calculations do not break down for these high values of n_{eq} and that the unrealistic results do indicate an incorrect choice of parameters on which the analysis of emissions is based.

Fig. 10.14 shows the resonant energy of electrons as a function of time for equatorial electron densities of 1 and 1/10 electrons/cc. As in chapter 9, which dealt with medium latitude emissions, it can be seen that $E \propto 1/n_{eq}$. For the lower electron density resonant energies of 100 to 300 keV are required. Plots of resonant energy as functions of n_{eq} and $1/n_{eq}$ over the range $1/10 < n_{eq} < 5$ electrons/cc can be seen in Fig. 10.15. The graphs are similar to Fig. 9.25 for medium latitude emissions. The reciprocal relationship of energy with n_{eq} holds better for emission E than for the S.Uist emission.

In the discussion which follows,on the presentation of results from each emission, use will be made of the inverse relationship of E with n_{eq} along with information on the flux densities of electrons as a function of energy to show that a sensible lower limit may be placed on the equatorial electron density at L = 6.2 during the period in which the emissions were generated.

Emission A

The received emission profile can be seen in Fig. 10.16 together with the 0.2 second dispersion delay which has been removed to give the equatorial profile. Note that the dispersion delay with n_{eq} =1 electron/10cc is approximately ½ that incurred when n_{eq} = 2 electrons/cc. The emission was analysed using program P90T in the same way as emission E. The results,distance,velocity of the interaction region, the parallel velocity and energy of resonant electrons are given for a number of equatorial electron densities in Figs.10.17 to 10.21. The interaction region velocity falls within the permitted range for $n_{eq} < 5$ electrons/cc and a physically unrealistic situation with a split interaction region results at n_{eq} = 10 electrons/cc. Thus the results from this emission broadly confirm the limitation on n_{eq} imposed by the analysis of emission E.

Emission B

The received frequency-time profile is given in Fig.10.22 and the products of the analysis for values of n_{eq} = 1/10,1/2,5 and 10 electrons/cc are shown in Figs.10.23 to 10.28. The interaction region parameters obtained with an equatorial electron density of 1 electron/2cc were used as input data for the program which recalculates the observed emission profile.It can be seen from Fig.10.25 that the accuracy of the reconstituted profileis excellent.It is clear that the recovery of the original emission profile,from information regarding the motion of an interaction region such as that proposed by Helliwell,

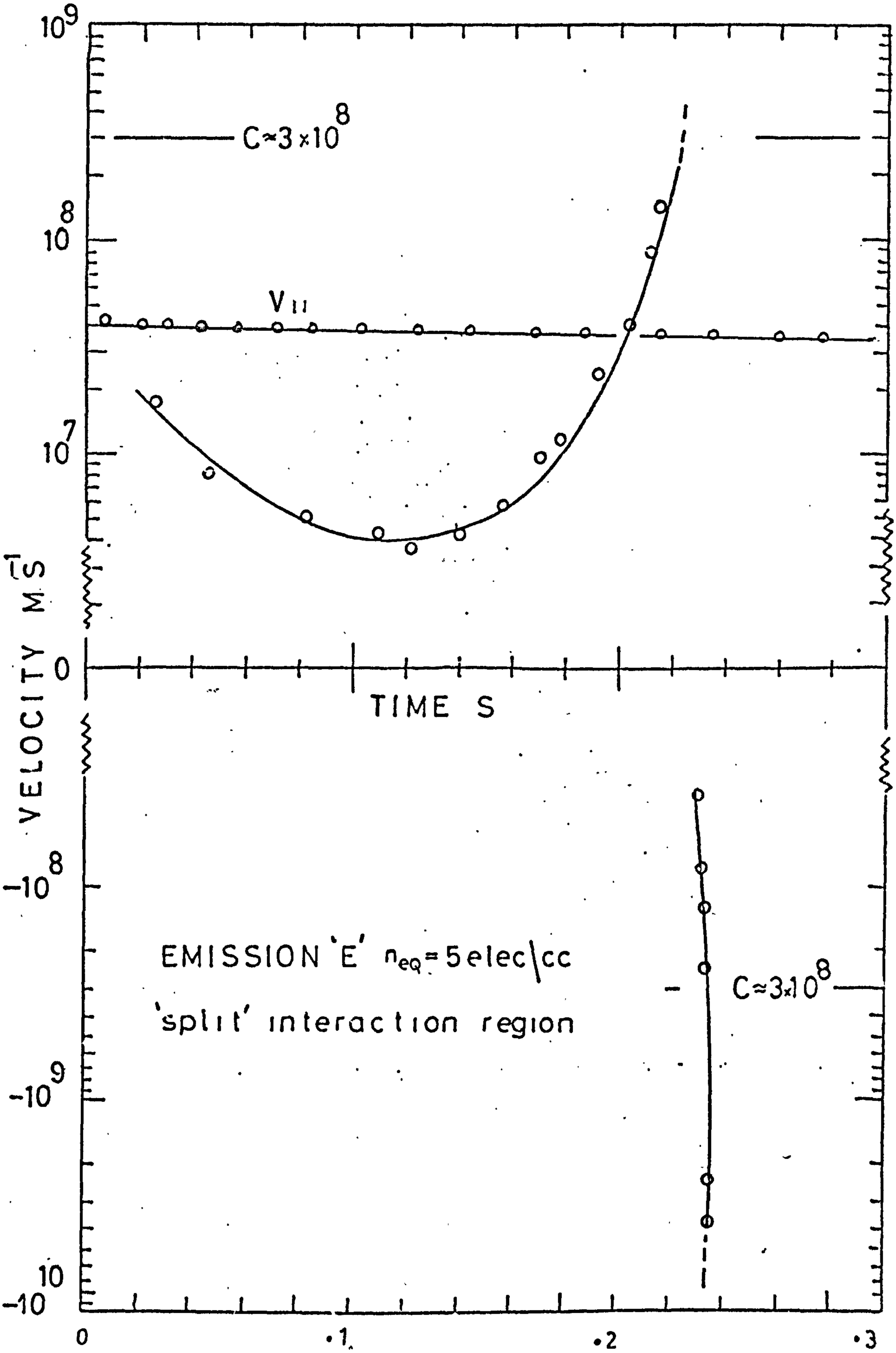
10^9
$C \approx 3 \times 10^8$
10^8
V_{11}
10^7
$\bar{M}S$
VELOCITY
0
TIME S
-10^8
EMISSION 'E' n_{eQ} = 5 elec\cc
'split' interaction region
$C \approx 3 \times 10^8$
-10^9
-10^{10}
0
·1
·2
·3

FIG(10.11)

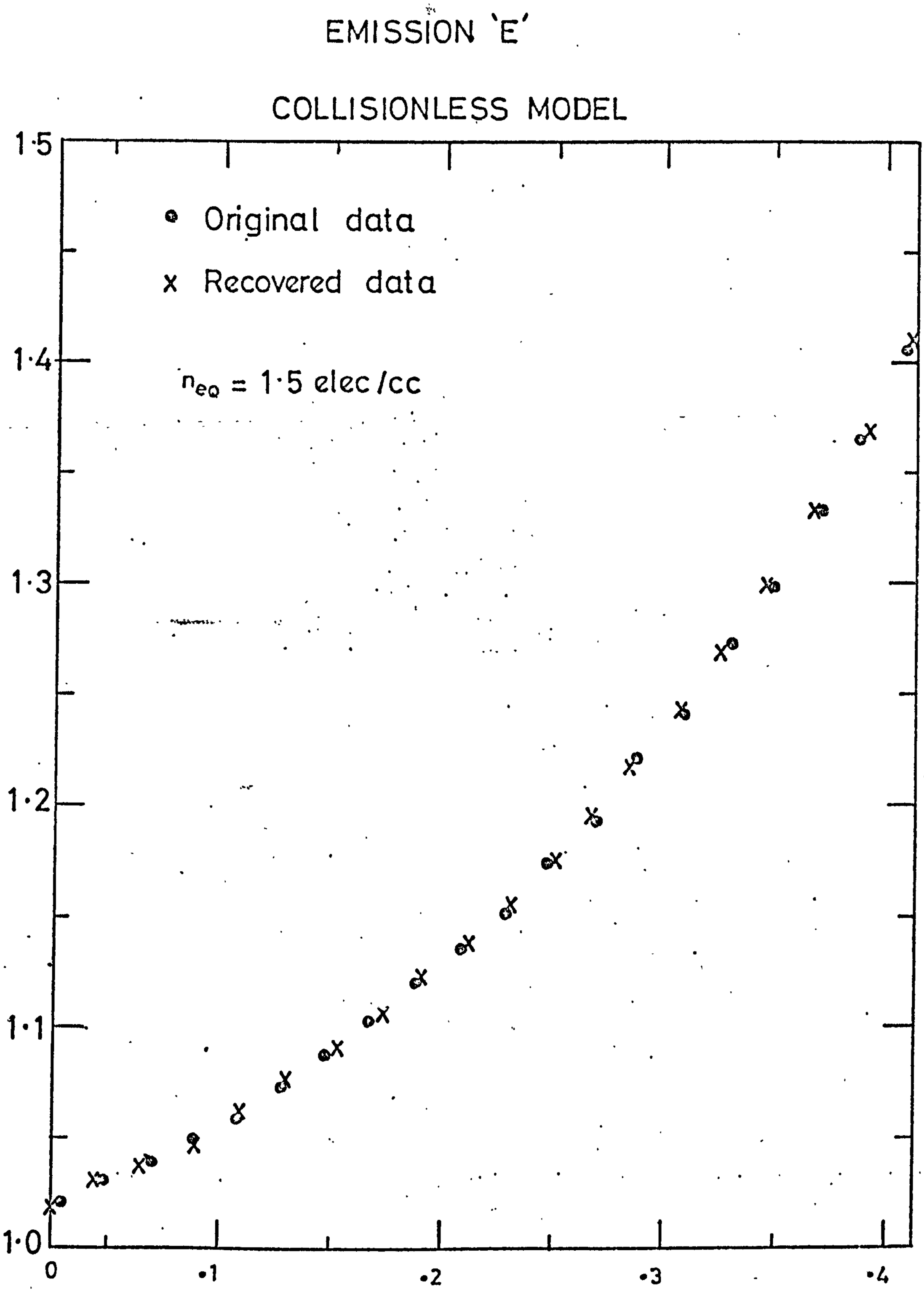
EMISSION 'E'
COLLISIONLESS MODEL
• Original data
x Recovered data
n_{eo} = 1·5 elec/cc
FREQUENCY (kHz)
1·5
1·4
1·3
1·2
1·1
1·0
0
·1
·2
·3
·4
TIME s

FIG. (10.12)

EMISSION OBSERVED AT ANDØYA (L=6·2)
at 1100 hr Z on 3 11 72
= 5elec\cc

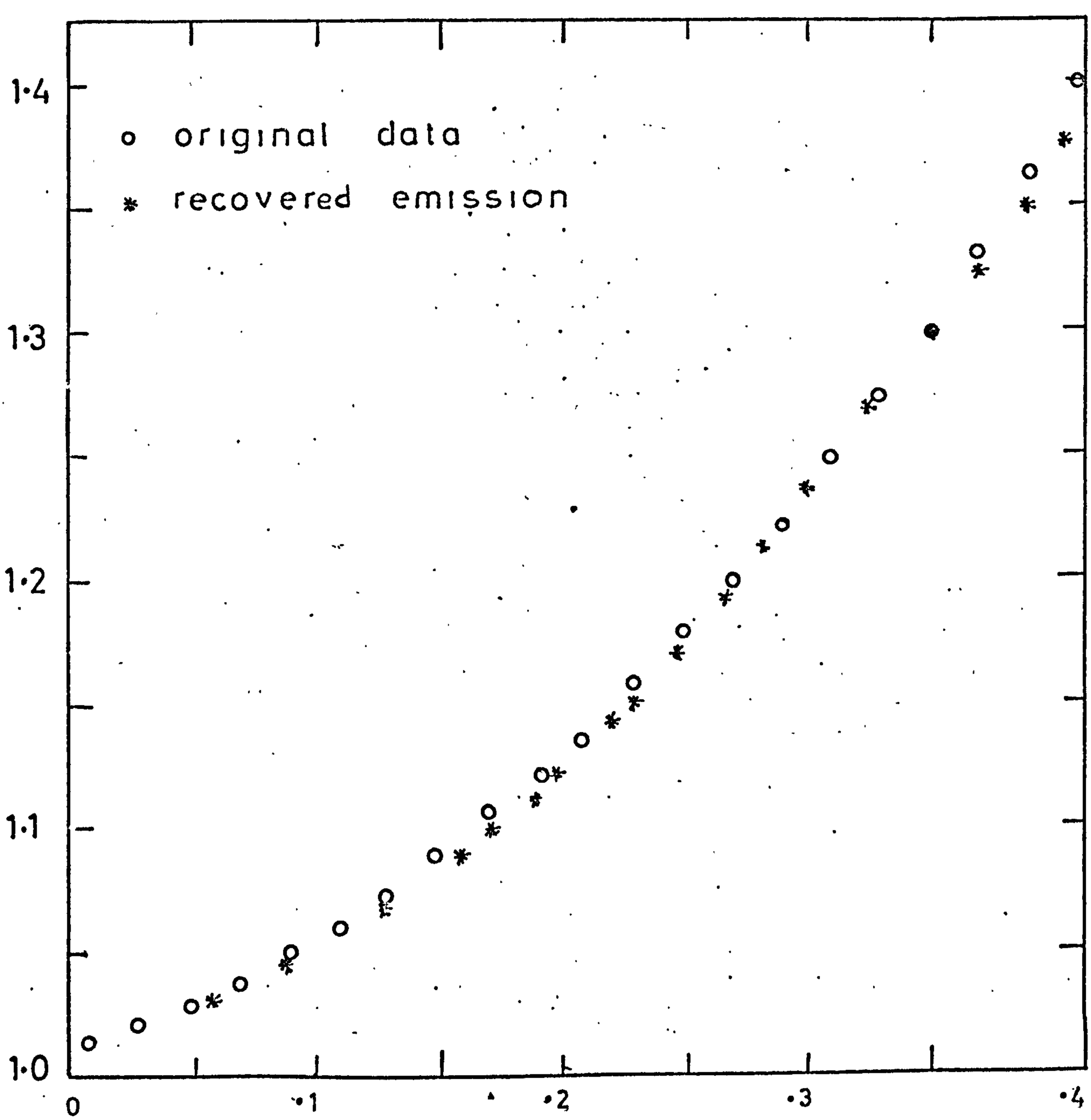

FIG (10.13)

EMISSION E

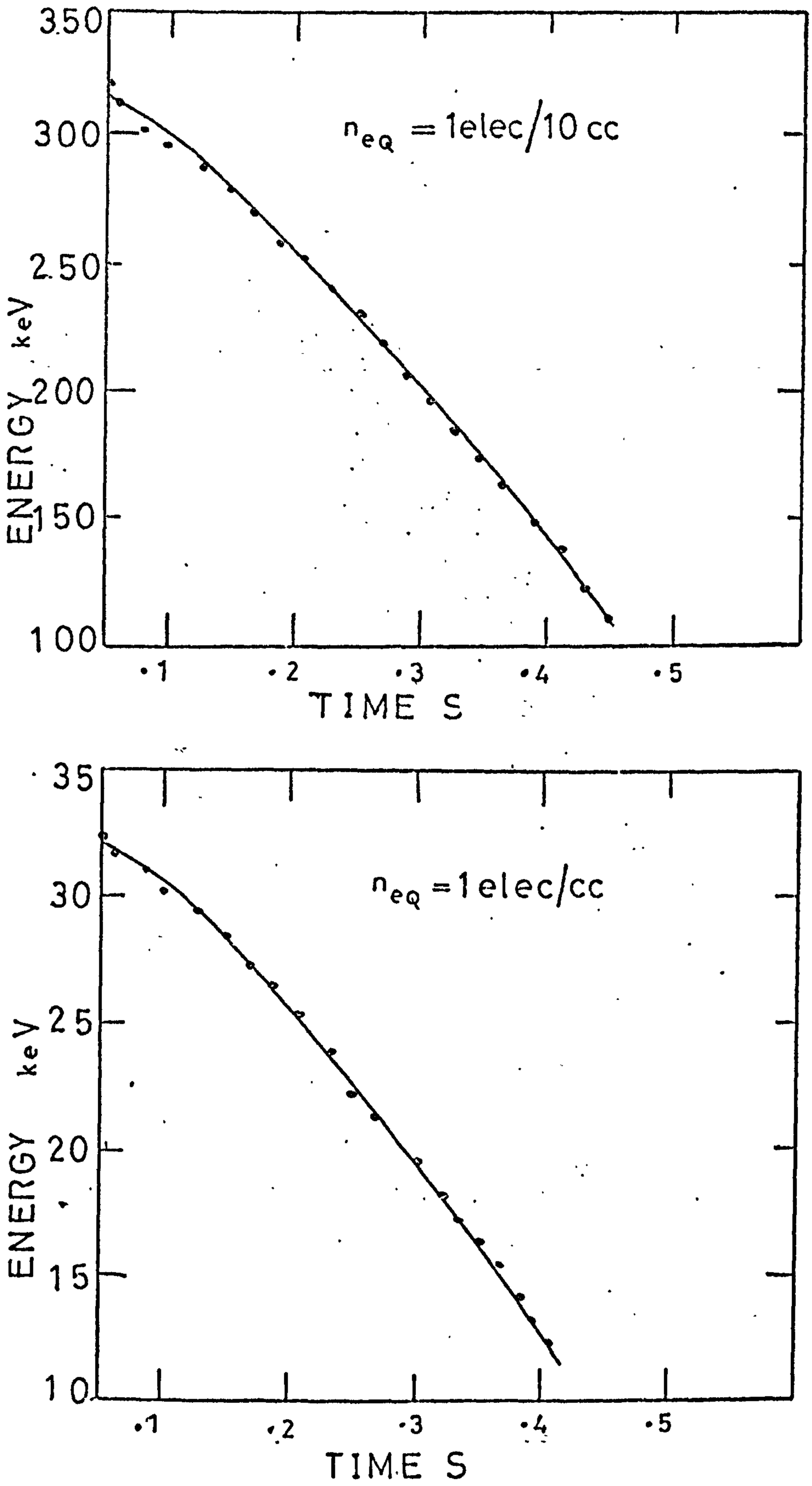

FIG(10.14)

EMISSION E

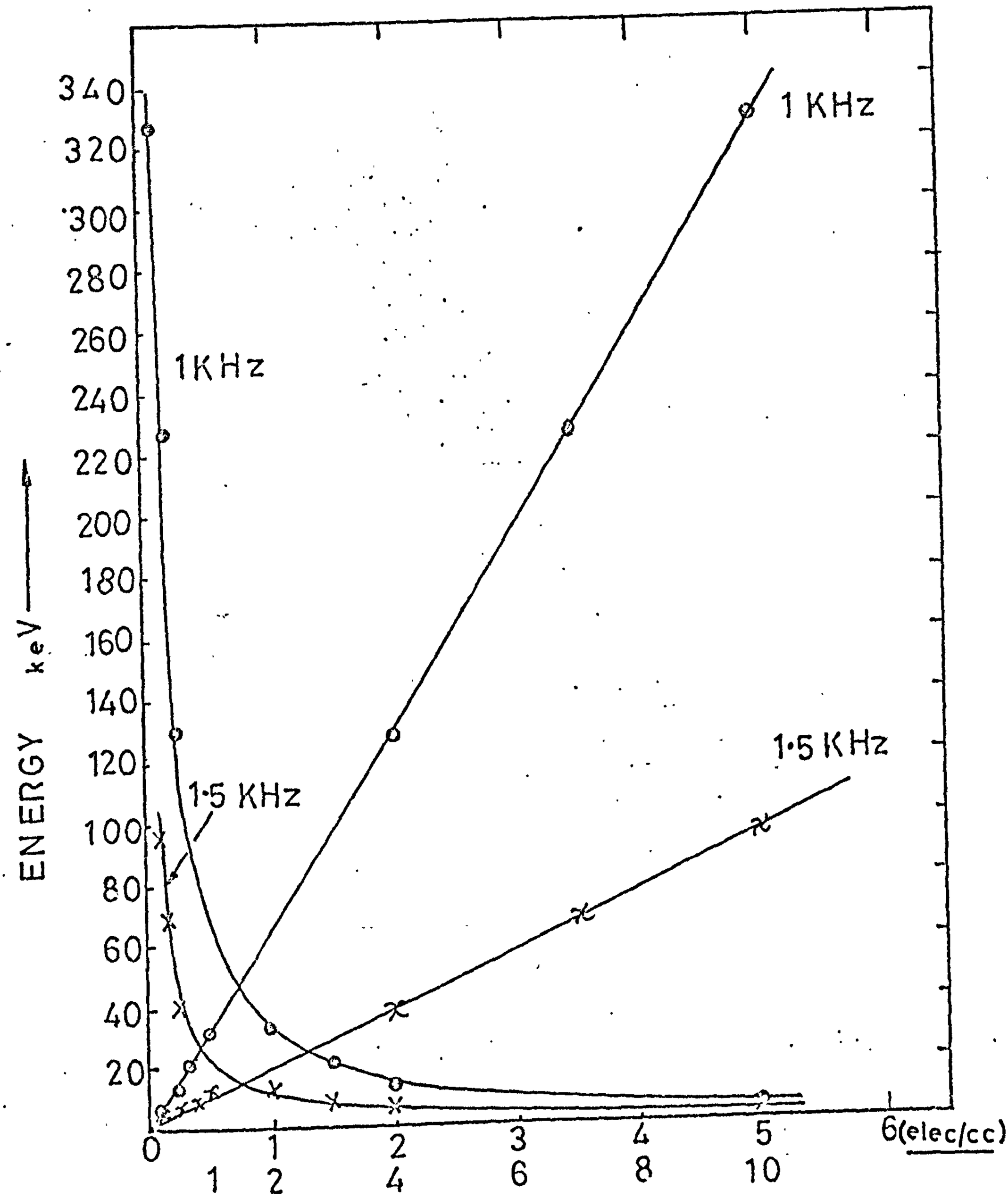

FIG.10.15

where a second order transverse resonance mechanism is operating, is a necessary but not sufficient condition to establish the validity of the proposed generation model. However, as we hope to show, this fact taken together with the constraints on interaction region motion and limits imposed upon the equatorial electron density by the analysis using this model would strongly suggest that V_{LF} discrete emissions are produced by a mechanism such as the one proposed.

Emission J

As for the other three emissions , the received frequency - time plot is given first, see Fig. 10.29. The half hop dispersion for an equatorial electron density of 1 electron/cc is also given in this figure. The distance of the interaction region from the equator, the interaction region velocity, the parallel velocity of resonant electrons and the electron resonant energy are all given as functions of true time for n_{eq} = 1/10, 1, 5 and 10 electrons/cc in Figs. 10.30 to 10.34. It can be seen that for this emission a physically unreal situation results with n_{eq} = 5 electrons/cc.

10.4 The Results of the Analysis of 4 High Latitude VLF Emissions

In this section reference is made to the graphical results of the analysis which were presented in 10.3 and the similarities and differences between the emissions are mentioned.

a) The received profile.

Whilst all the emissions are confined within a narrow range of frequencies (1.0 - 1.5 KHz) and last for between 0.3 - 0.6 s there are interesting differences in their frequency - time profiles which result in differing distance - time and velocity - time relations .

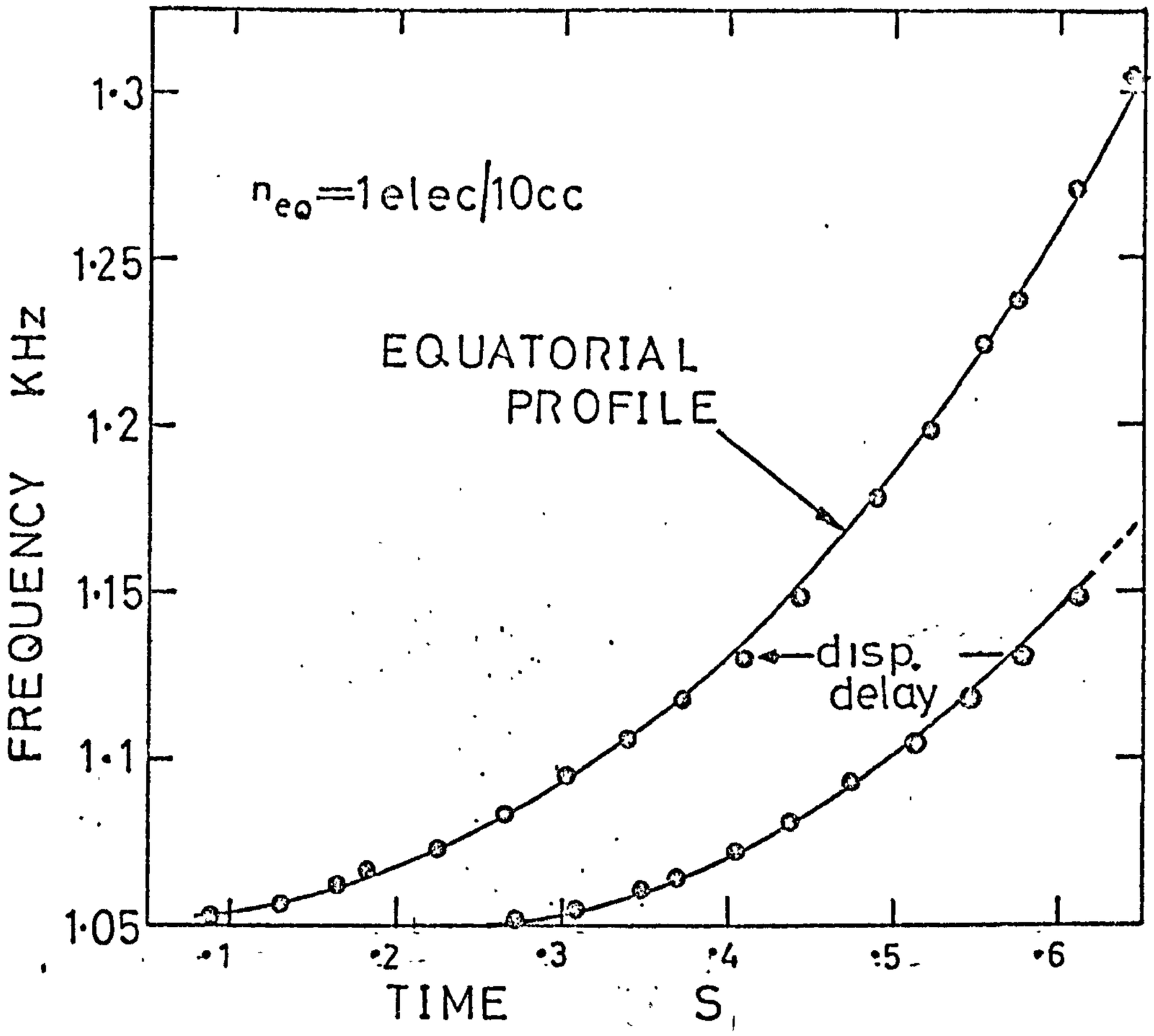
n_{eq}=1elec/10cc
EQUATORIAL PROFILE
disp.
delay
FREQUENCY KHz
1·3
1·25
1·2
1·15
1·1
1·05
·1
·2
·3
·4
·5
·6
TIME S

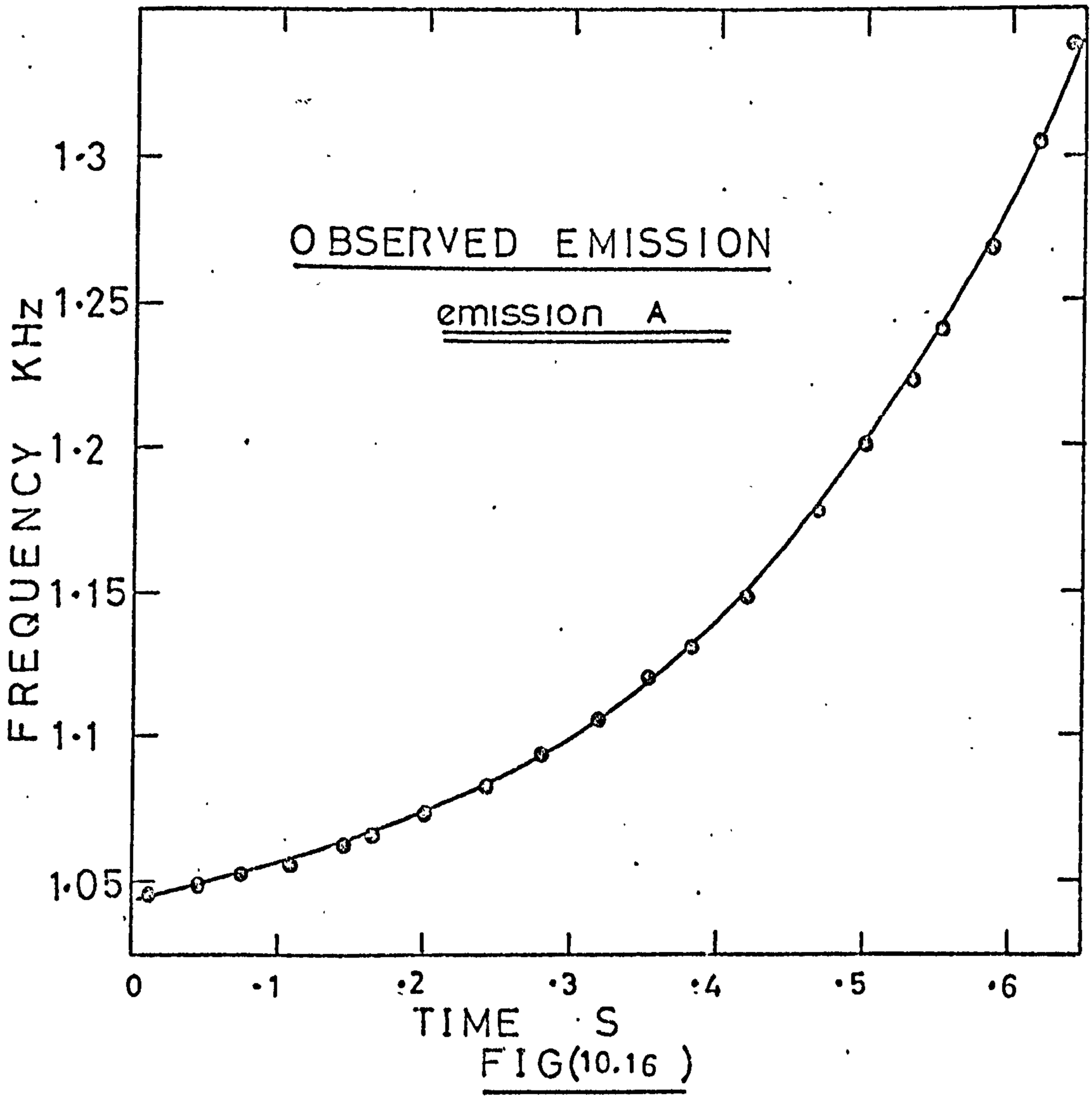
OBSERVED EMISSION
emission A
FREQUENCY KHz
1·3
1·25
1·2
1·15
1·1
1·05
0
·1
·2
·3
·4
·5
·6
TIME S

FIG(10.16)

EMISSION A

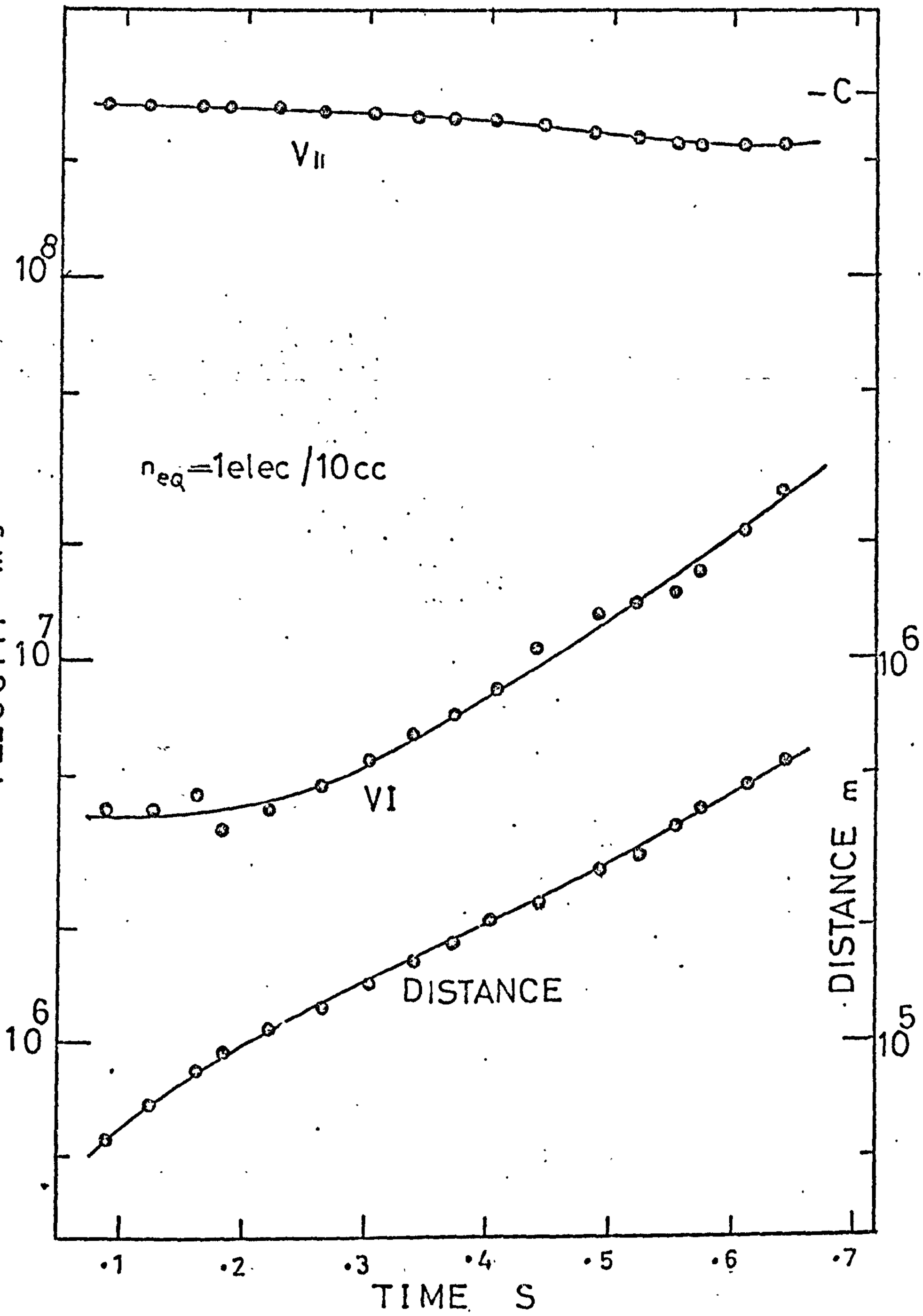

FIG(10.17)

EMISSION A

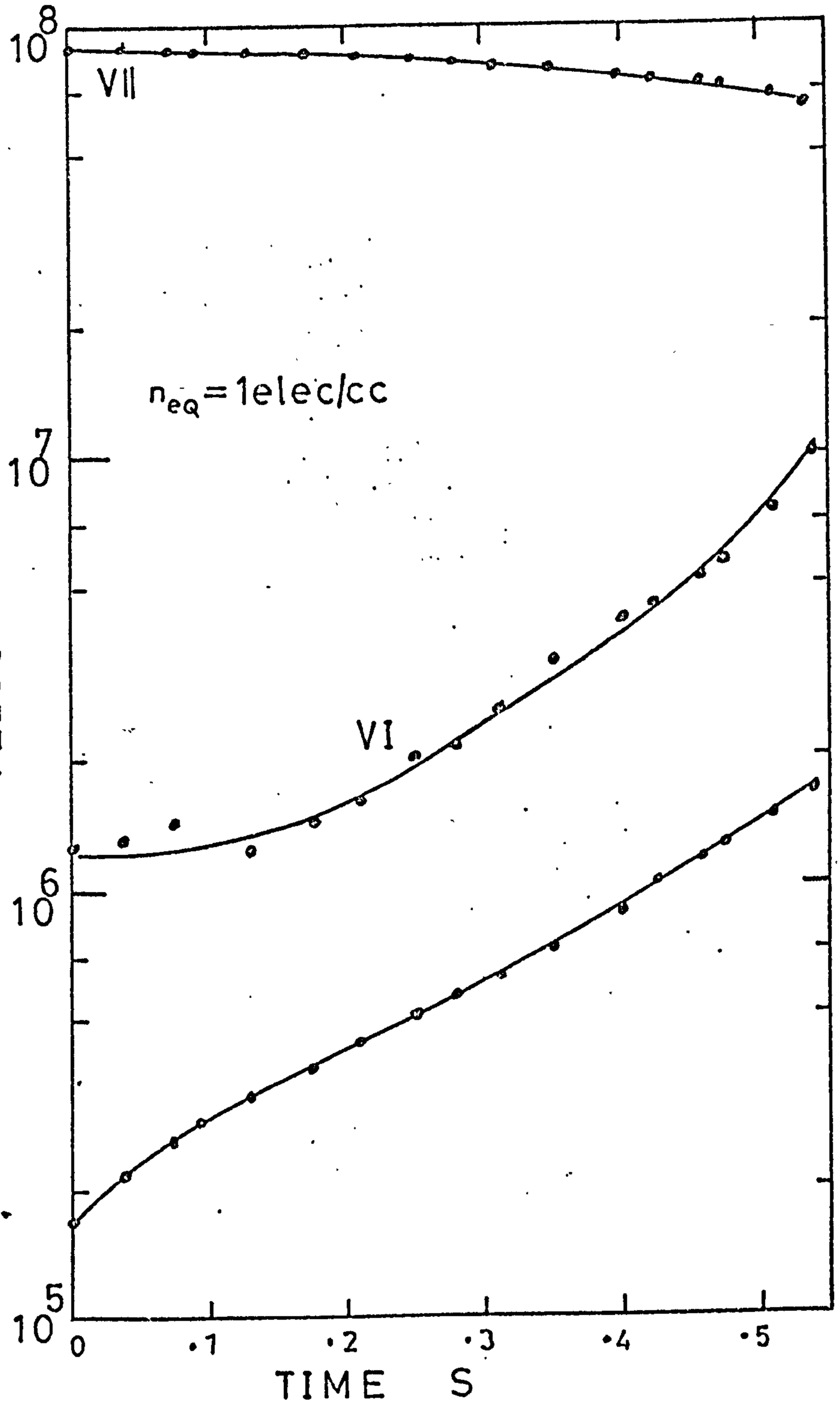

FIG.(10·18)

EMISSION A

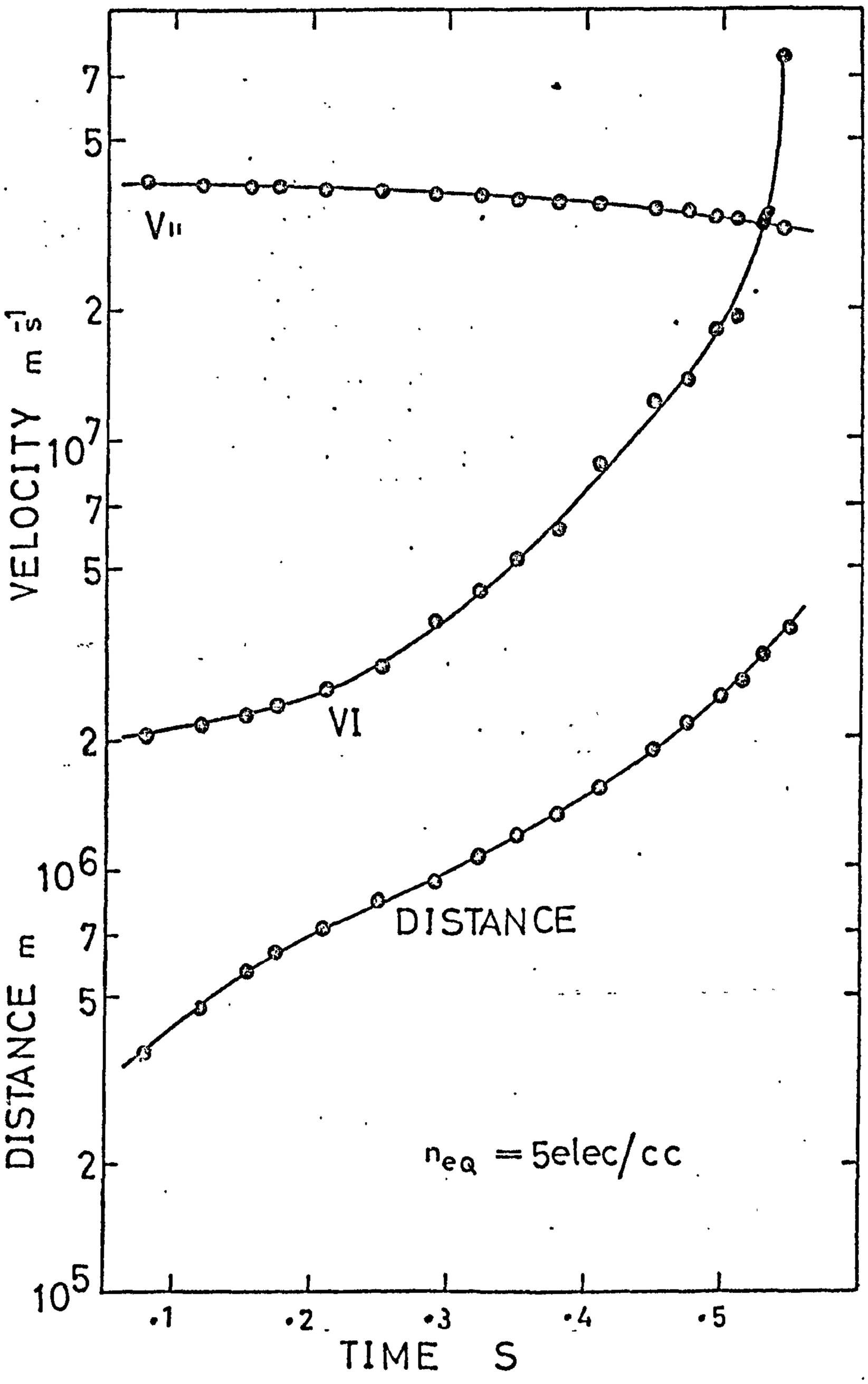

FIG.(10·19)

EMISSION A

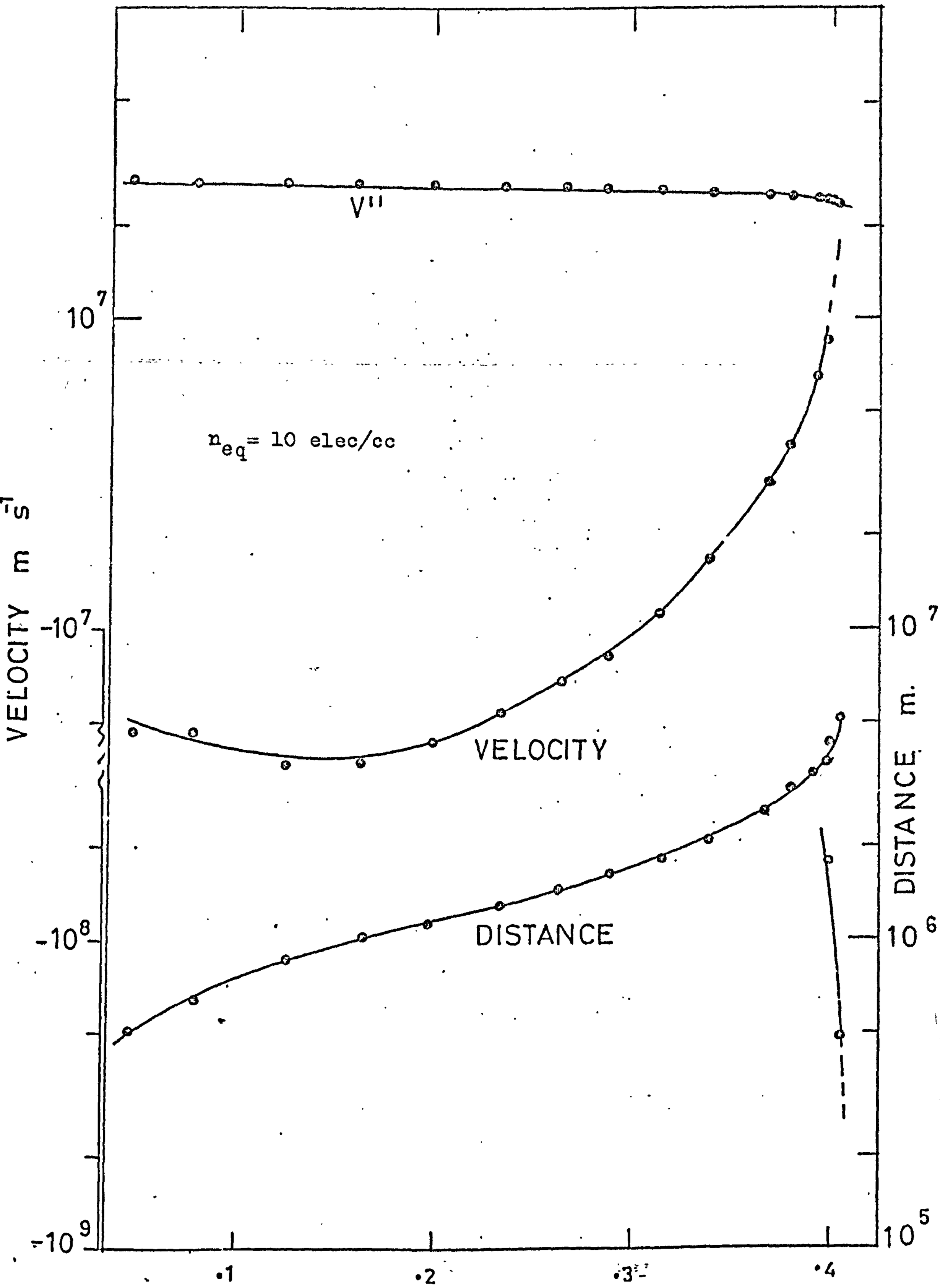

FIG (10·20)

EMISSION A

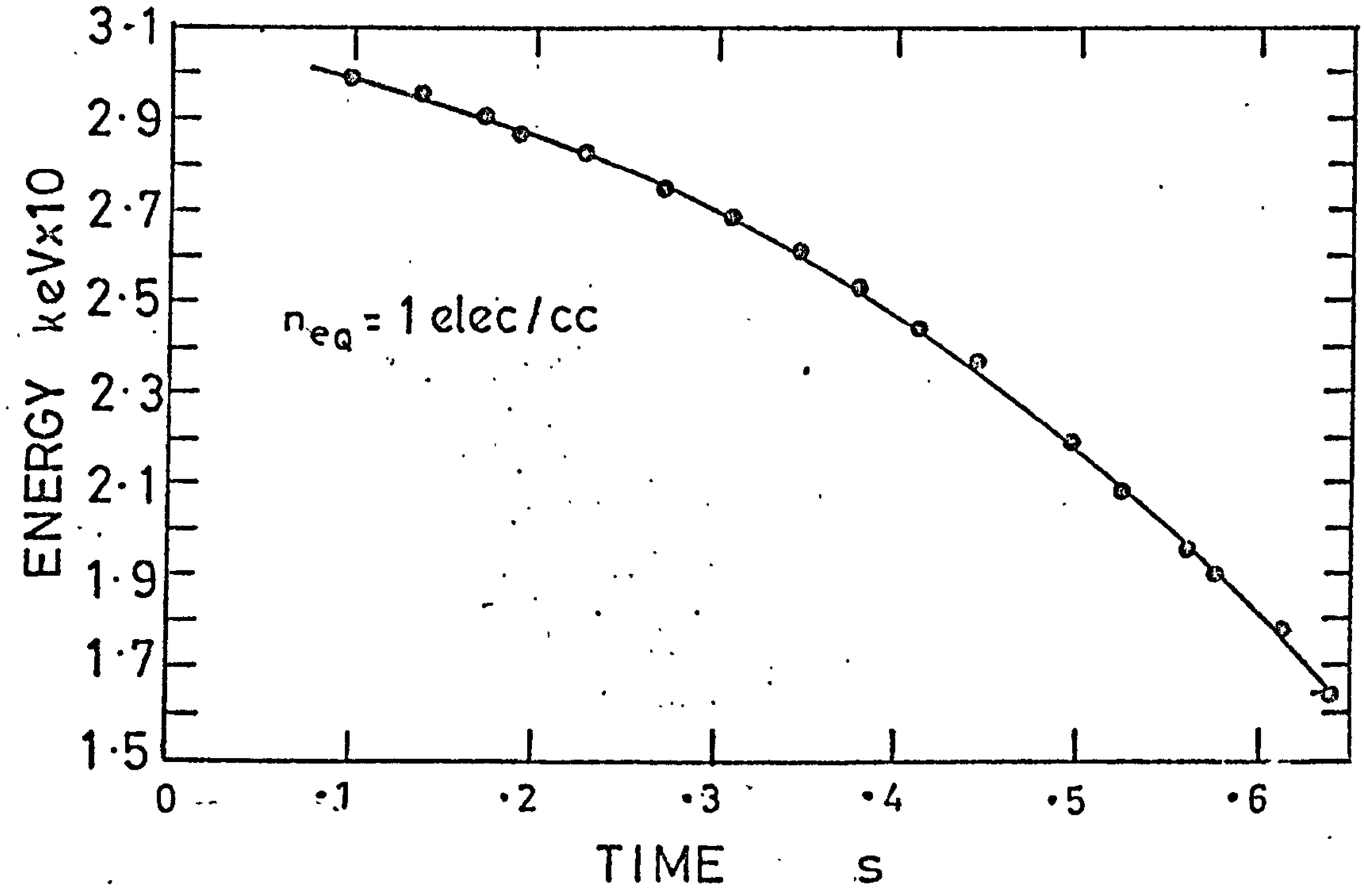

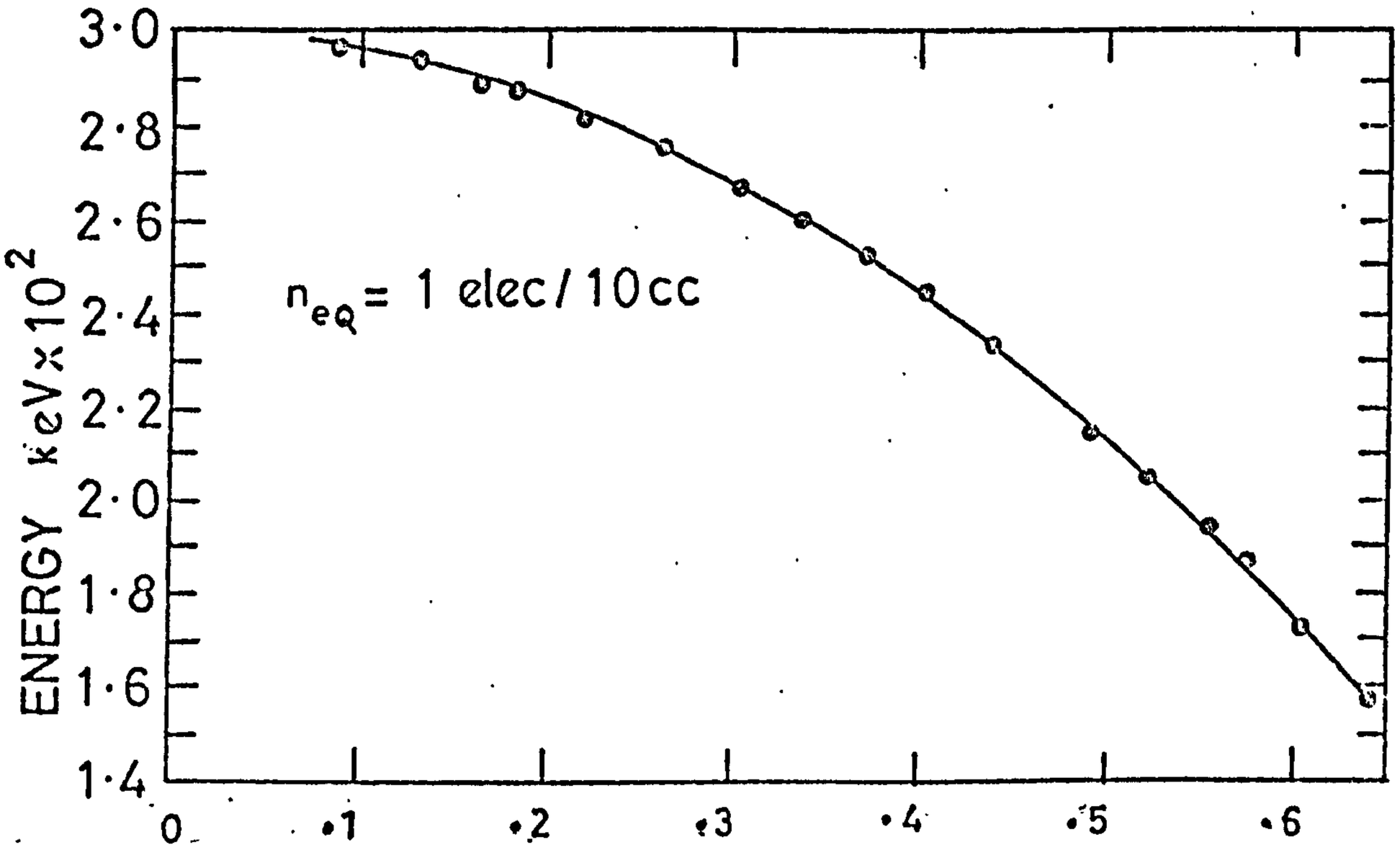

FIG. (10·21)

EMISSION B

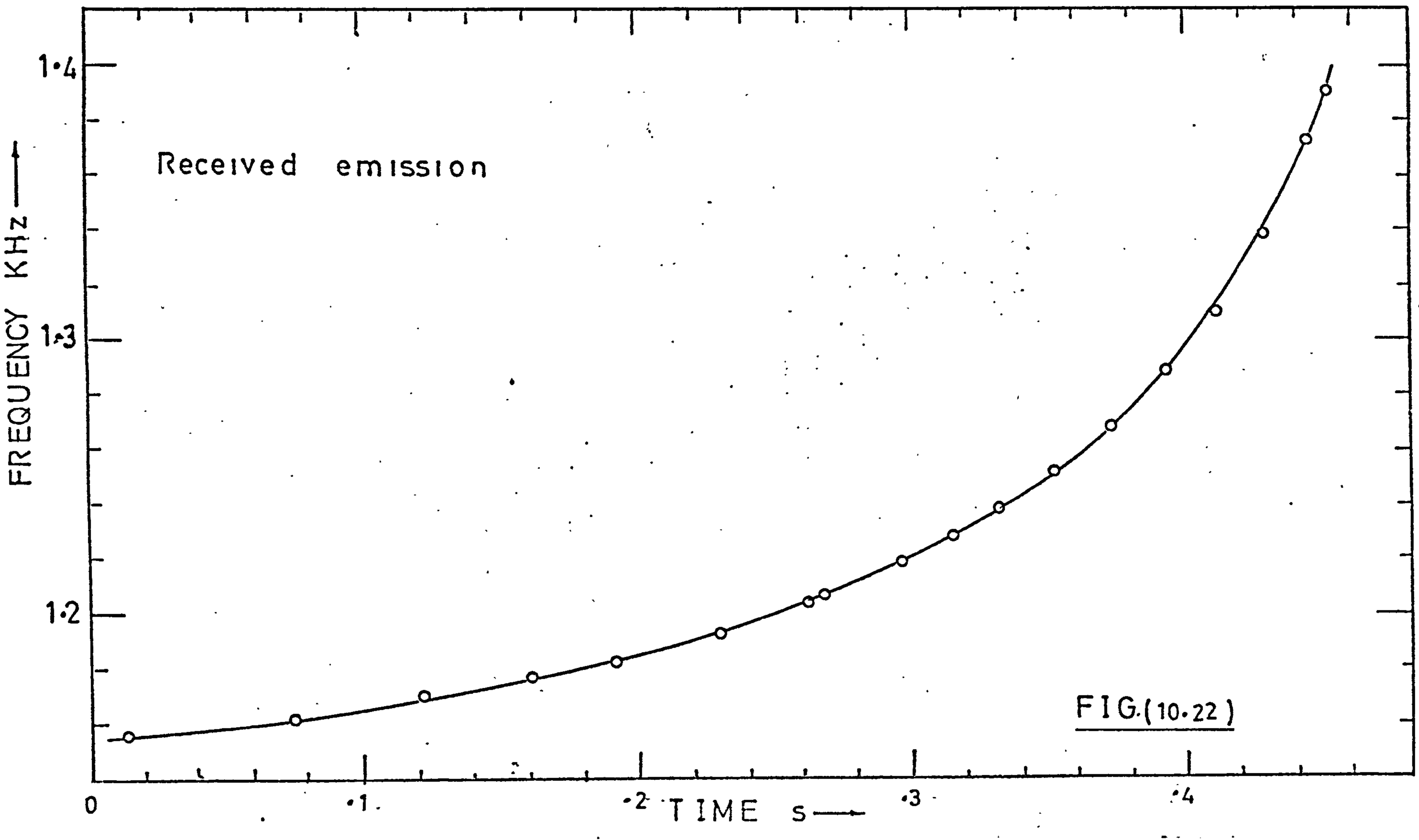

FIG.(10·22)

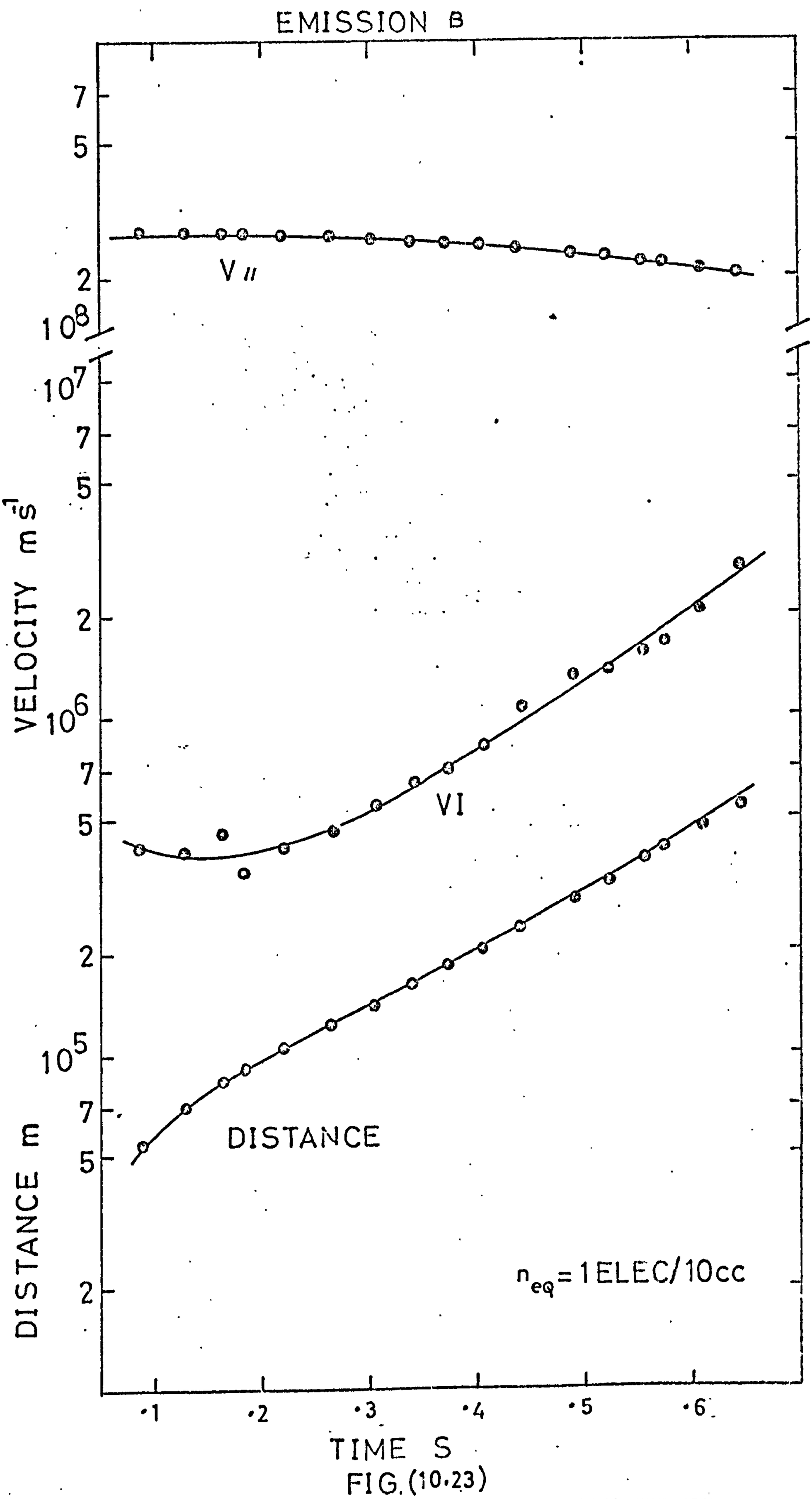
EMISSION B
VELOCITY m s⁻¹
DISTANCE
TIME S
VII
VI
n_{eq} = 1 ELEC/10cc
7
5
2
10^8
10^7
7
5
2
10^6
7
5
2
10^5
7
5
2
·1
·2
·3
·4
·5
·6

FIG.(10.23)

EMISSION B

n_{eQ} = 1 elec / 2 cc

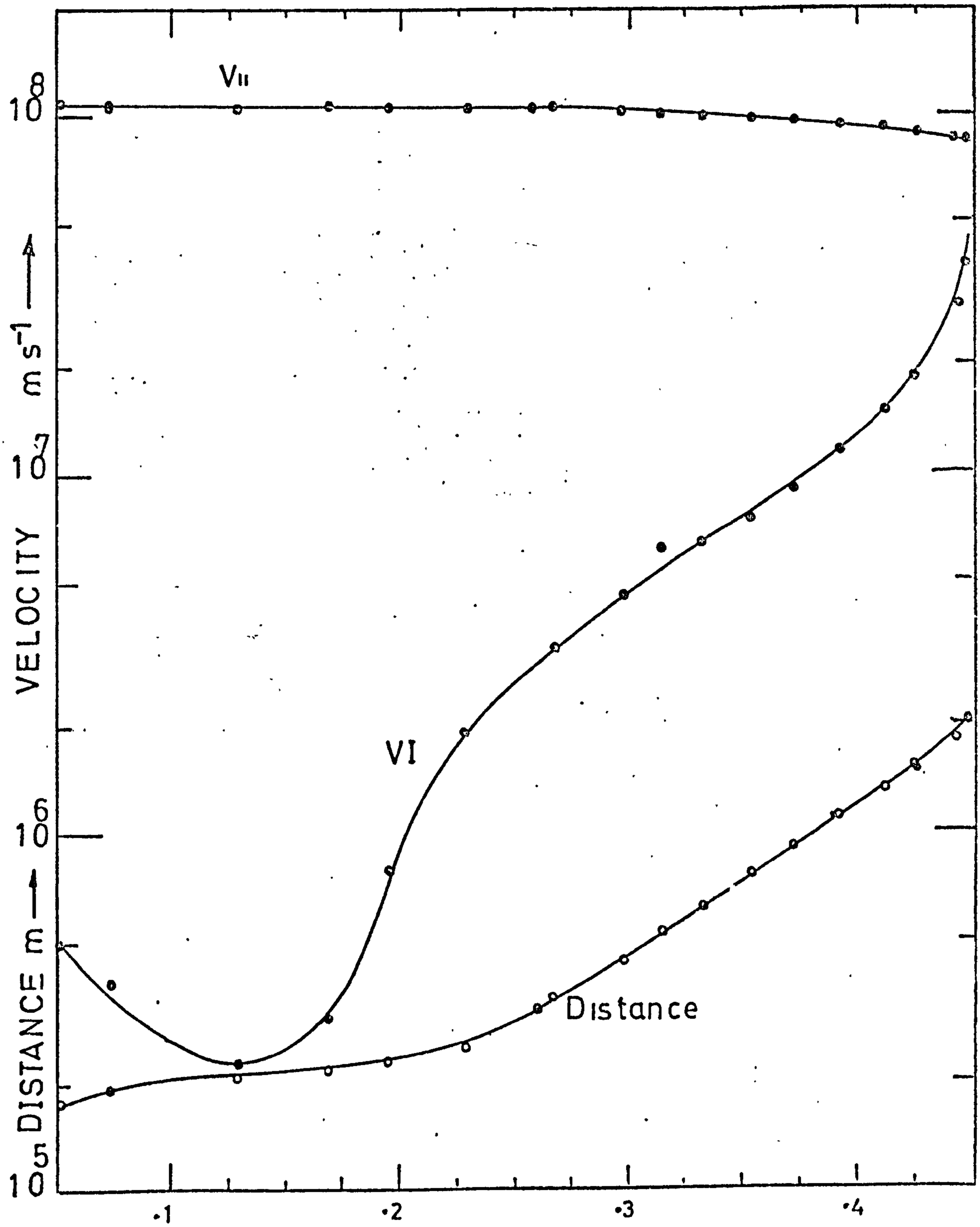

FIG (10·24)

$n_{eQ} = 1e1ec/2cc$

EMISSION B COLLISIONLESS MODEL

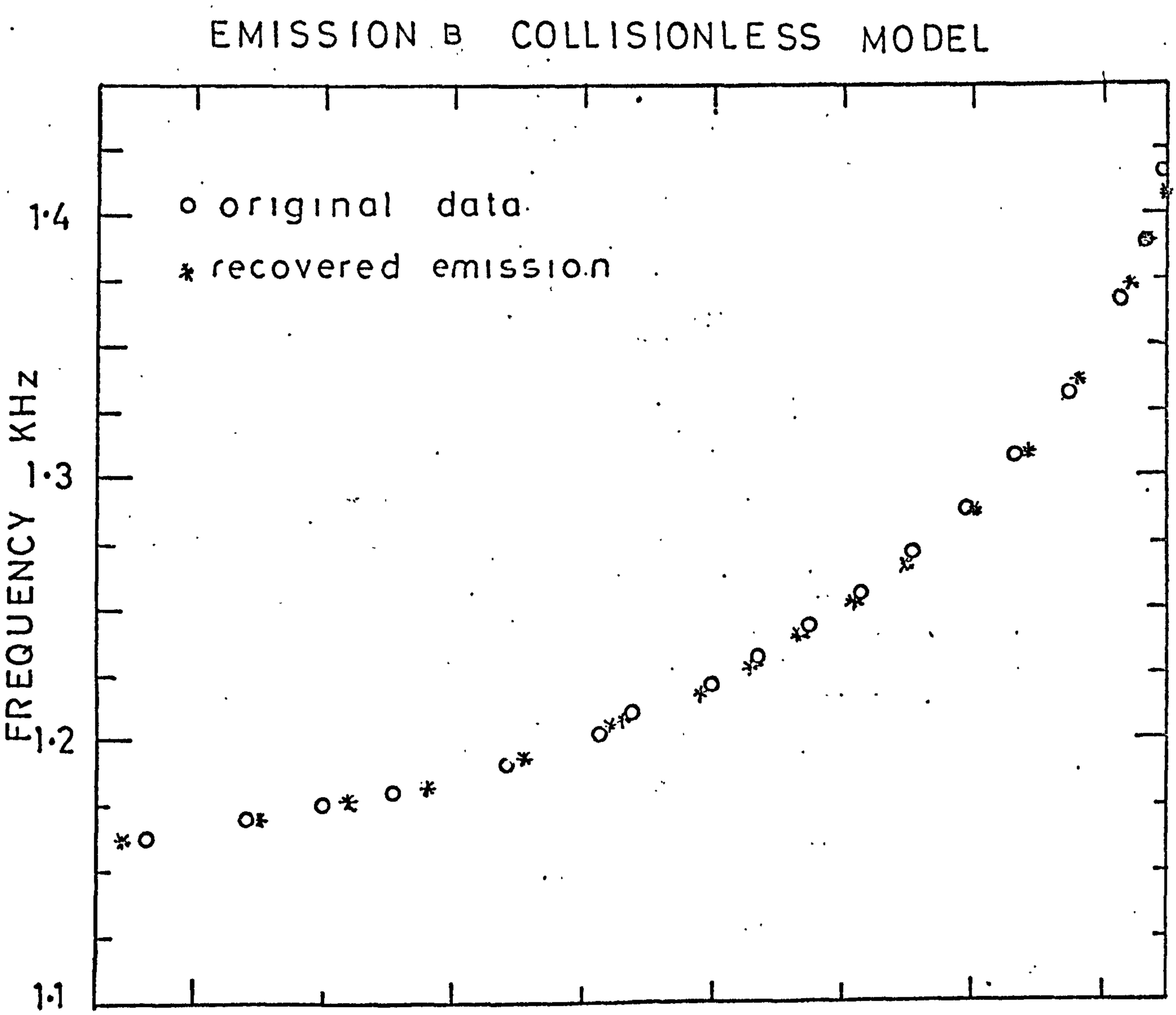

FIG(10.25)

EMISSION B

$n_{eQ} = 5 \text{ elec/cc}$

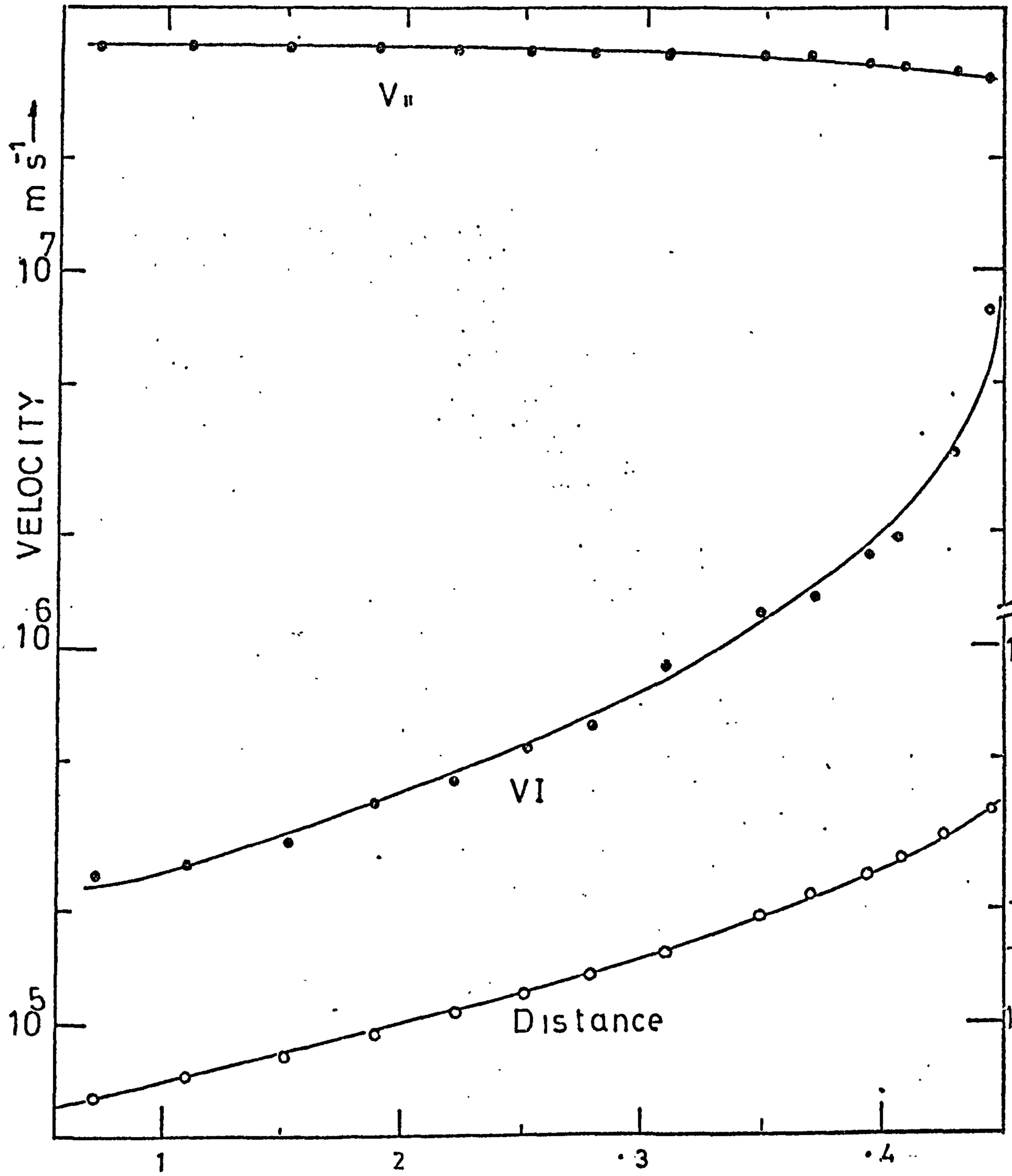

FIG (10·26)

EMISSION B

$n_{eo} = 10 \text{ elec/cc}$

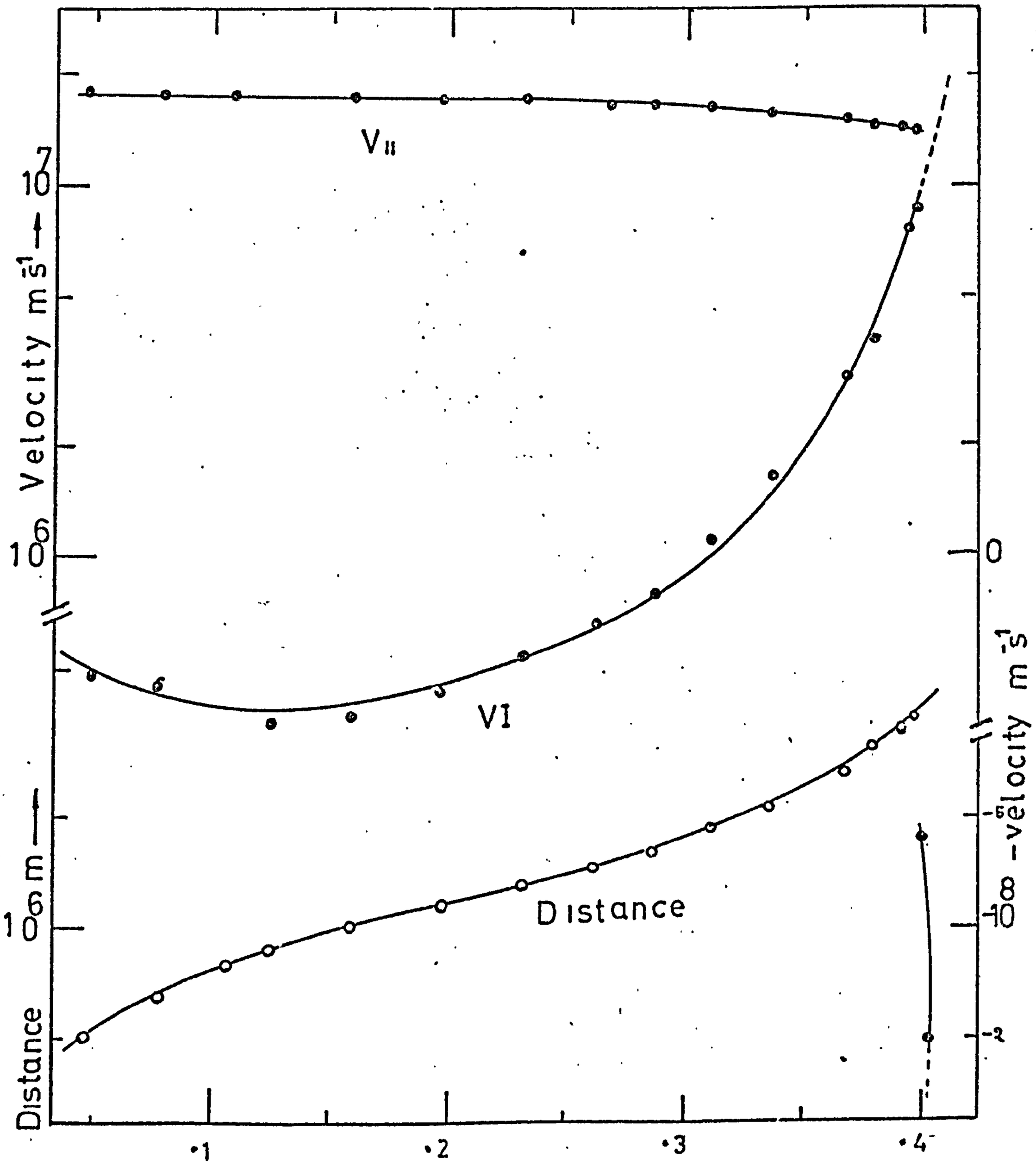

FIG(10·27)

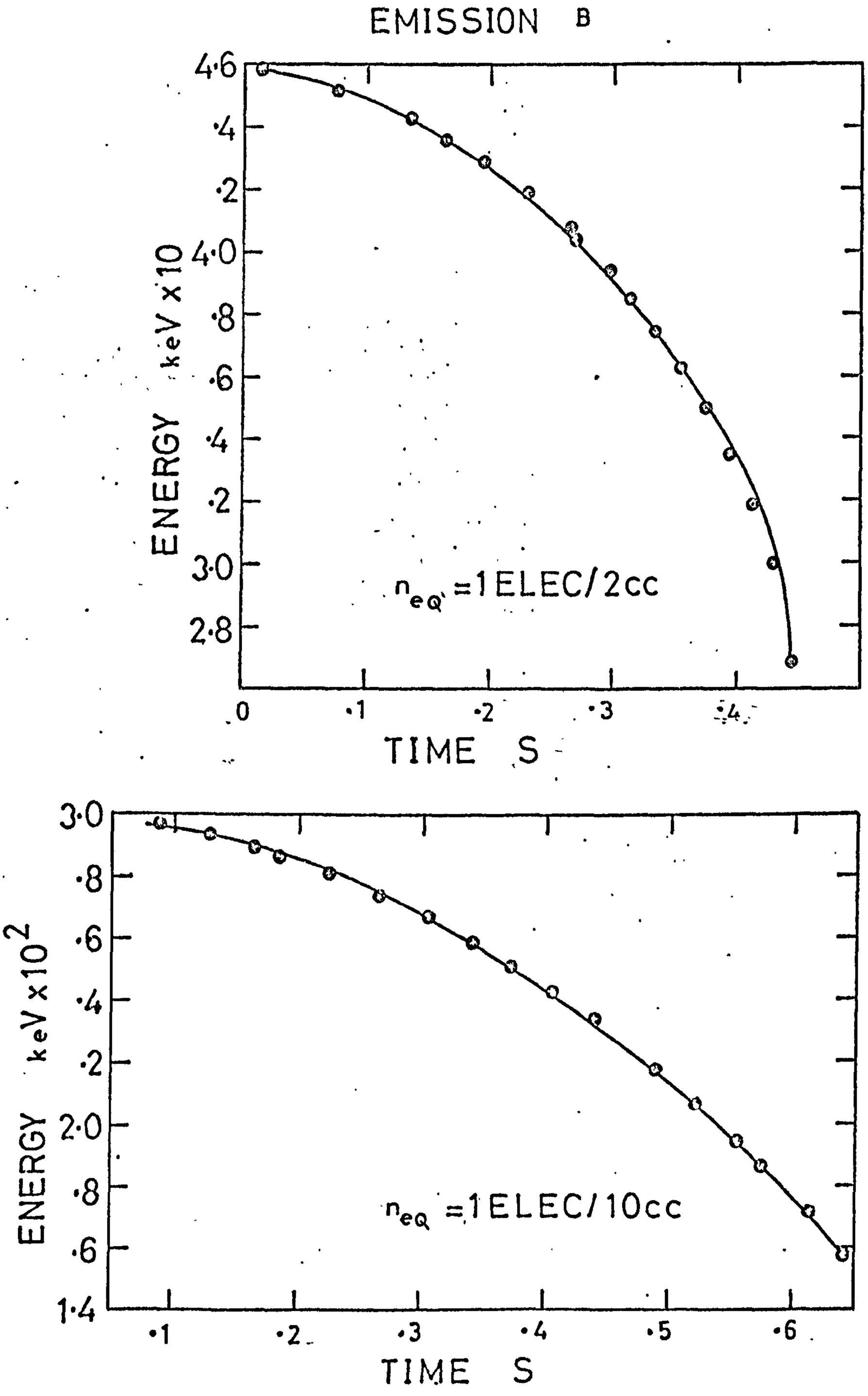
EMISSION B
ENERGY keV x10
4·6
·4
·2
4·0
·8
·6
·4
·2
3·0
2·8
0
·1
·2
·3
·4
n_{eQ} =1 ELEC/2cc
TIME S
ENERGY keV x10^2
3·0
·8
·6
·4
2·0
·8
·6
1·4
·1
·2
·3
·4
·5
·6
n_{eQ} =1 ELEC/10cc
TIME S

FIG(10·28)

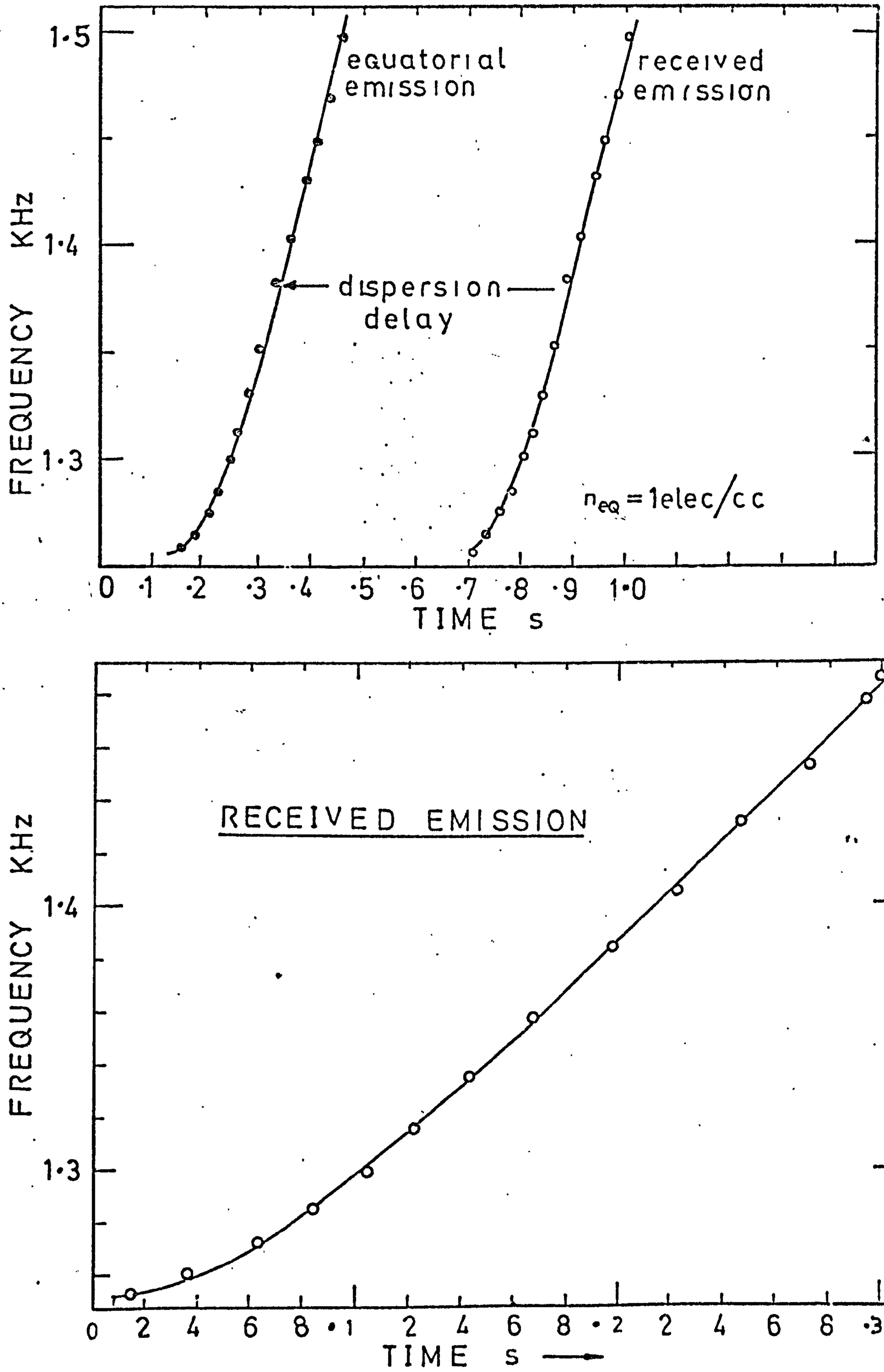
EMISSION J
1·5
1·4
1·3
FREQUENCY KHz
equatorial emission
received emission
dispersion delay
n_{eq} = 1elec/cc
0 ·1 ·2 ·3 ·4 ·5 ·6 ·7 ·8 ·9 1·0
TIME s
RECEIVED EMISSION
1·4
1·3
FREQUENCY KHz
0 2 4 6 8 ·1 2 4 6 8 ·2 2 4 6 6 ·3
TIME s

FIG (10.29)

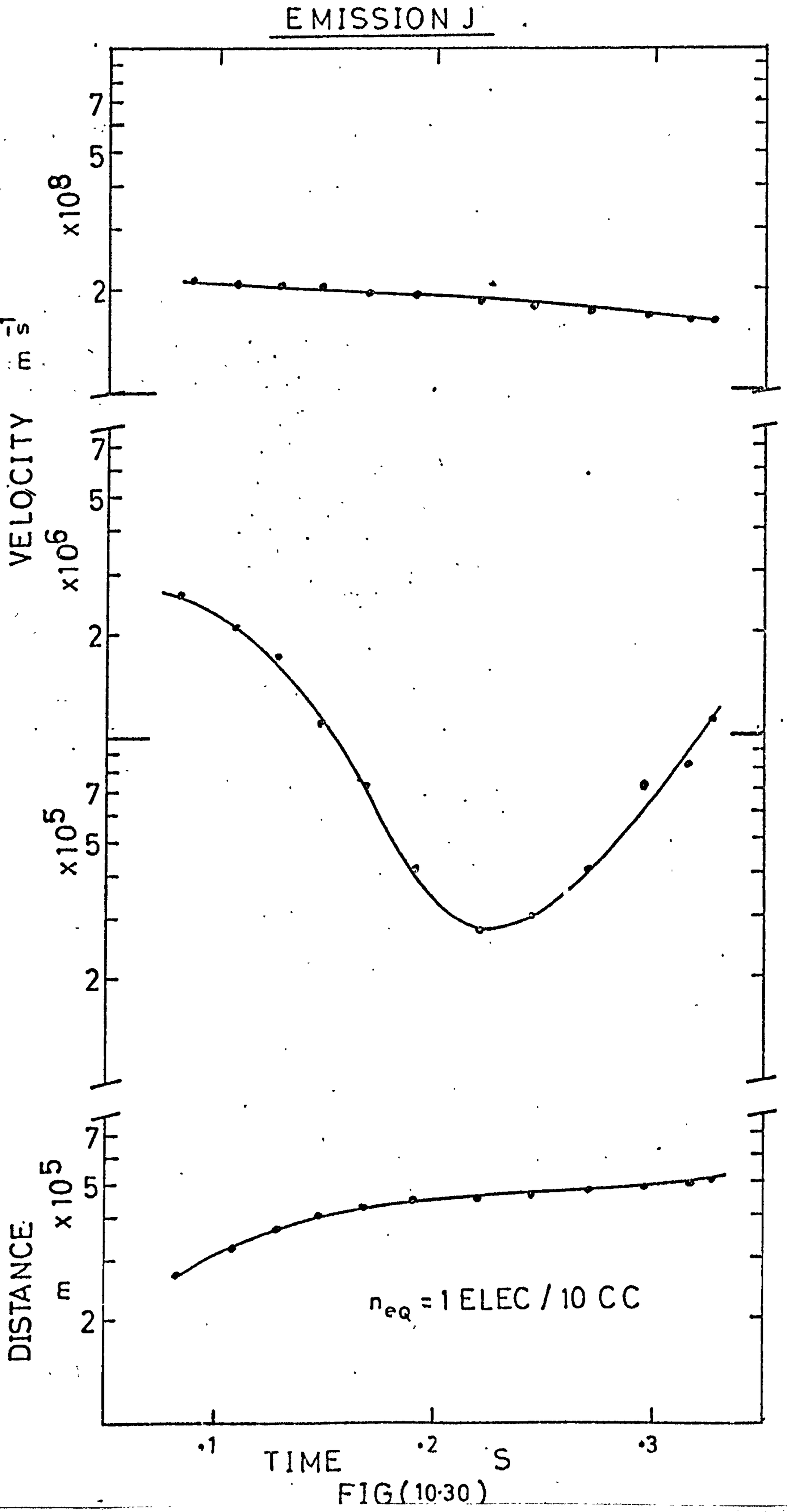
EMISSION J
EMISSION
7
5
2
x10^8
s^-1
VELOCITY
7
5
2
x10^6
7
5
2
x10^5
DISTANCE
m
7
5
2
x10^5
n_eQ = 1 ELEC / 10 CC
•1
•2
•3
TIME
S

FIG(10·30)

J 1 electron /cc

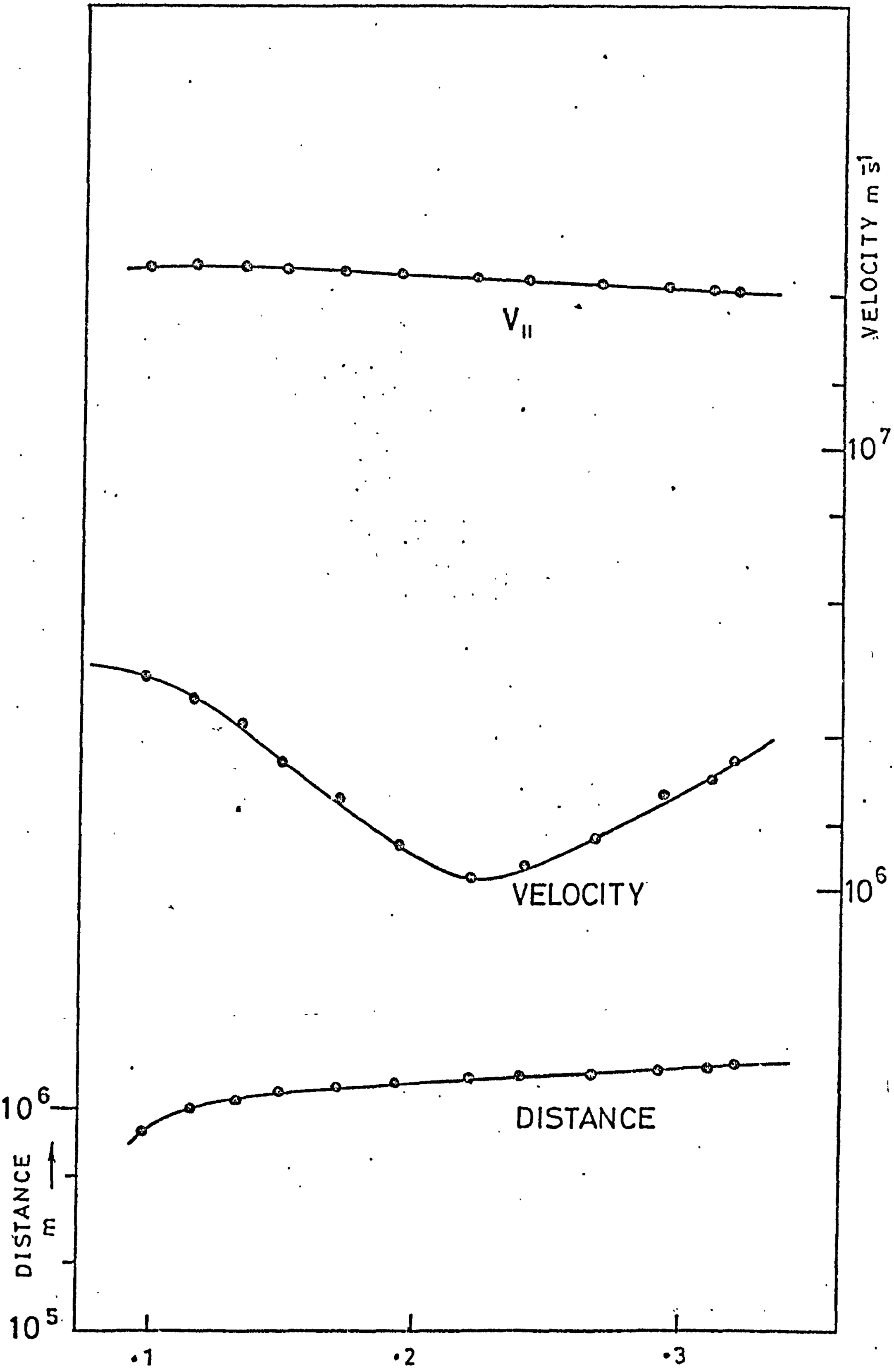

FIG(10.31)

EMISSION J

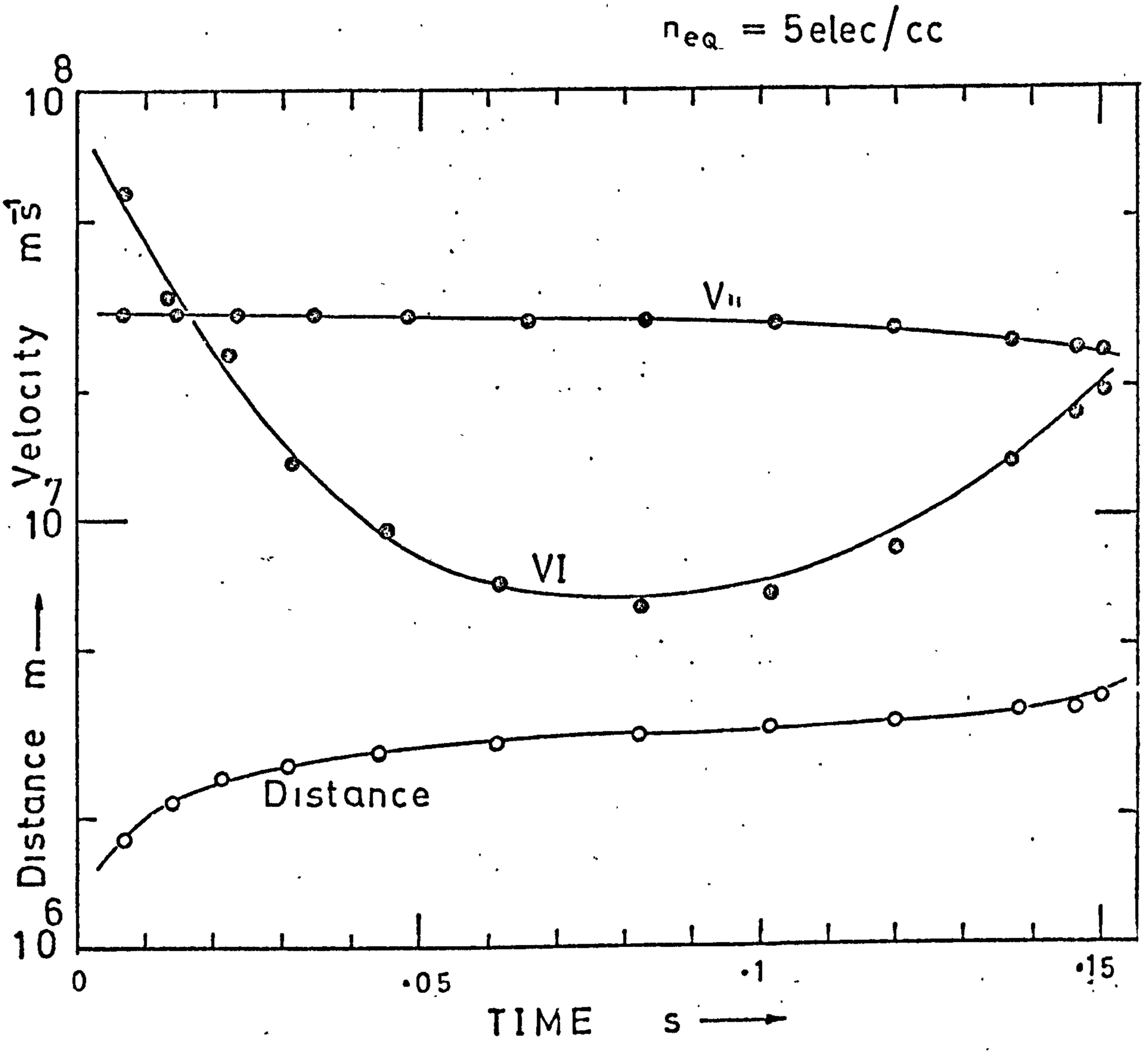

FIG.(10.32)

EMISSION J

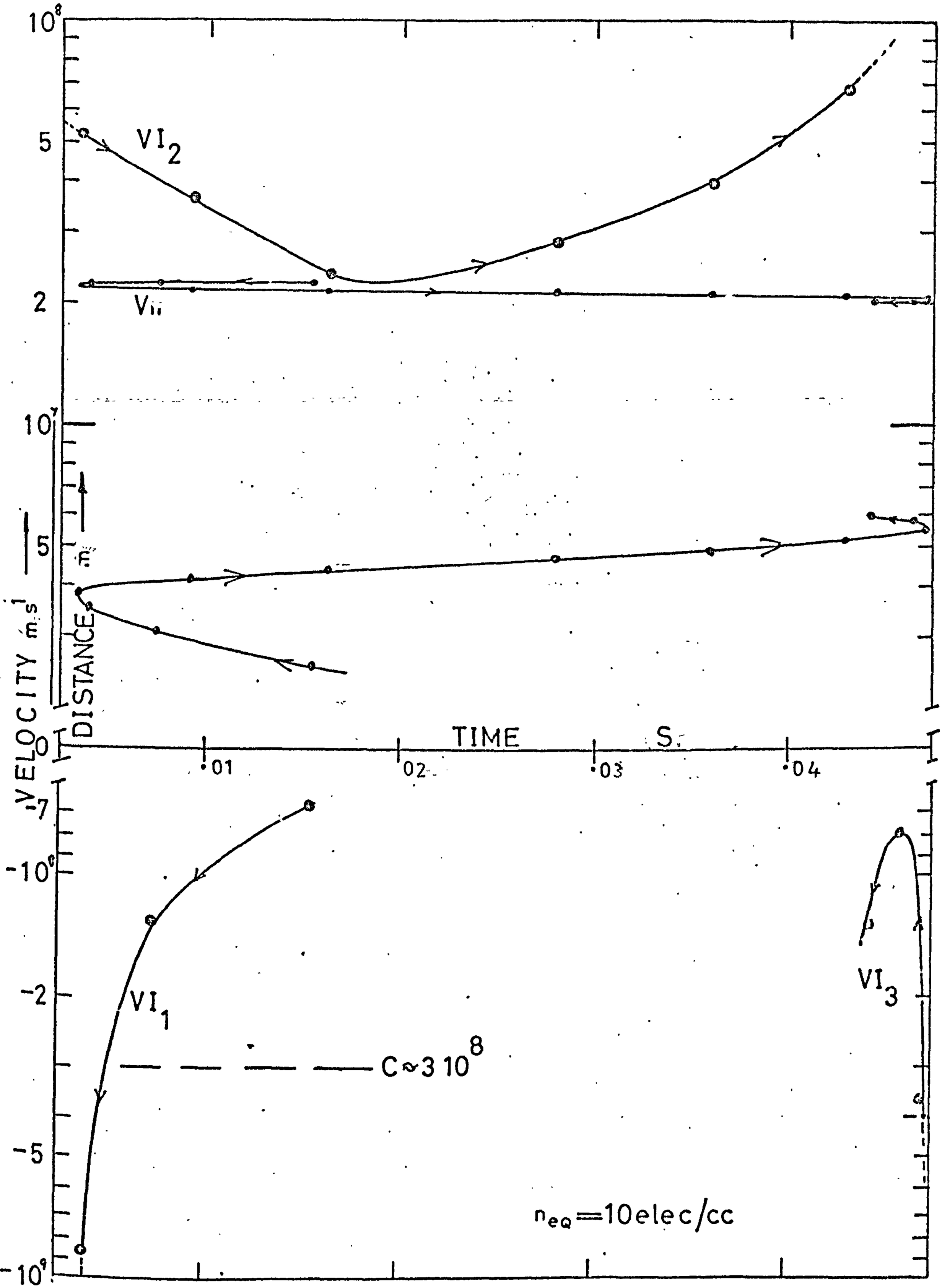

FIG (10·33)

EMISSION J

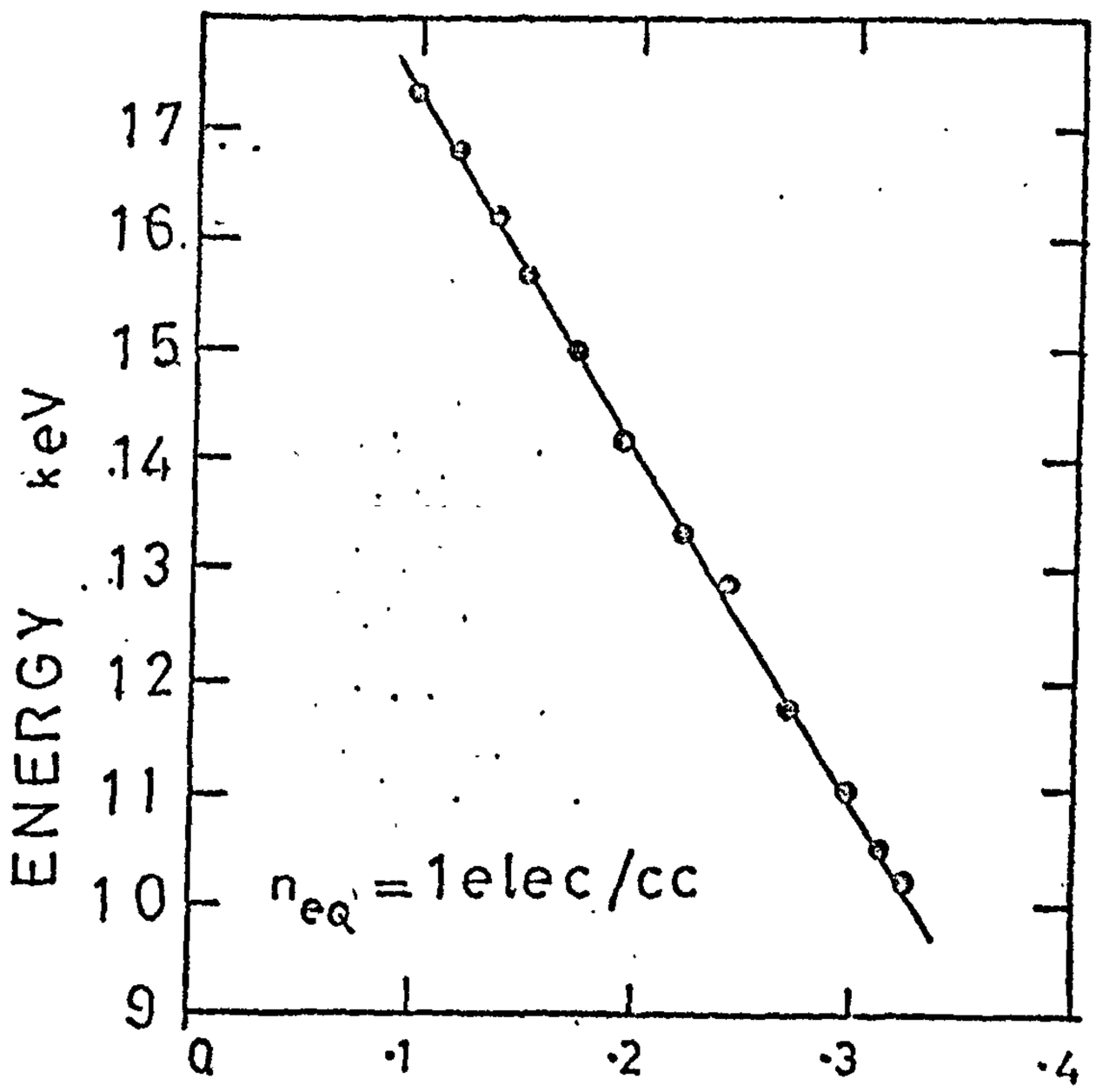

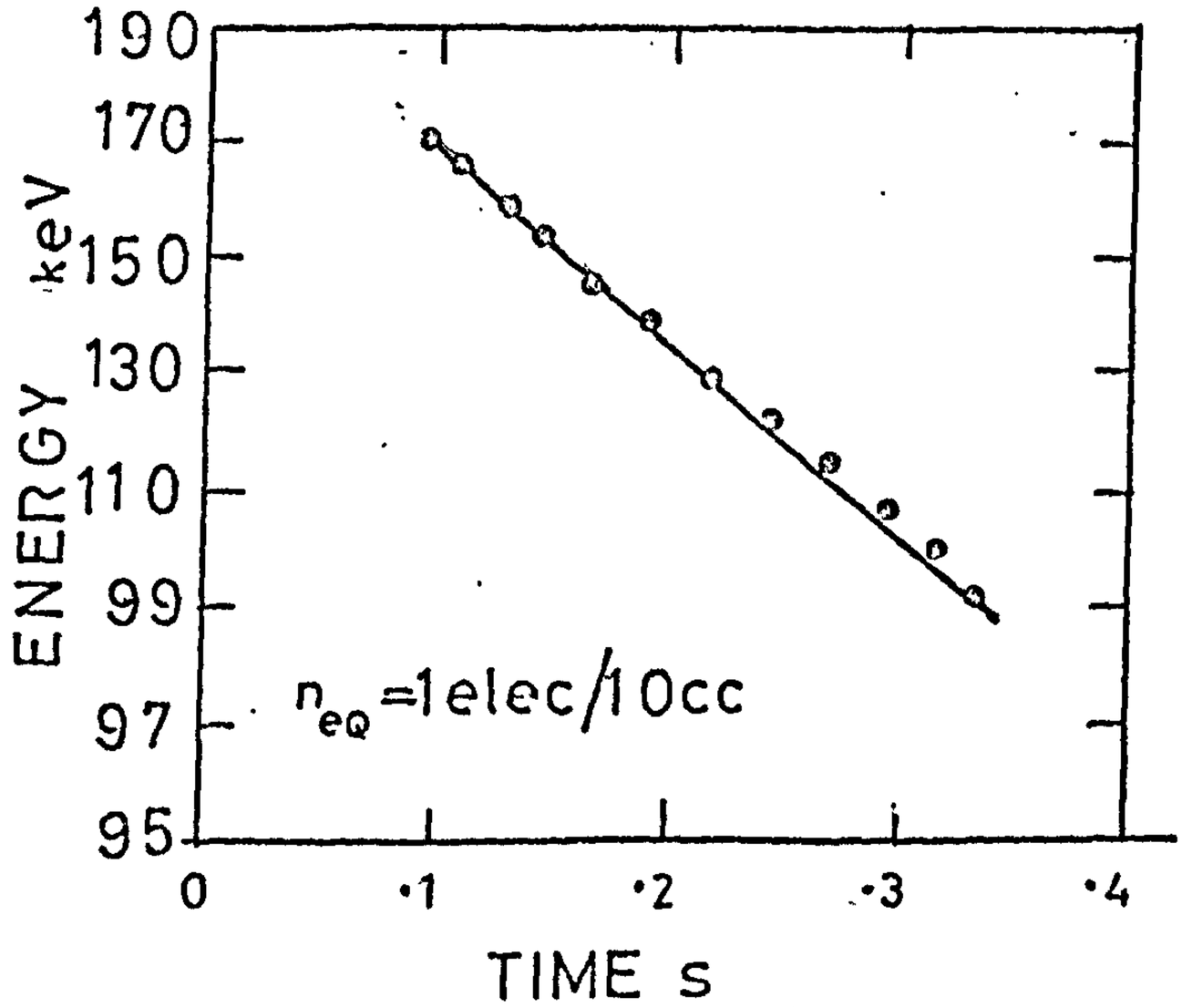

FIG(10·34)

Emission E starts at 1.0 KHz and has a continuously curved profile up to a maximum frequency of 1.45 KHz. Emission A has a 'hyperbolic' profile which starts and finishes as almost a straight line and has the greatest curvature half way through its life. Emission B covers the frequency range 1.15 KHz - 1.39 KHz by starting as almost a straight line and then rising rapidly in frequency. Emission J is about 0.3 seconds long (the shortest) and covers the frequency range 1.25 - 1.5 KHz. The profile is curved at the start of the emission but approaches a straight line which represents the greater part of the profile. A summary of frequency coverage for the four emissions is given in Fig. 10.35.

b) Interaction Region Distance - Time curves.

In all cases the interaction region moves smoothly away from the geomagnetic equator. No interaction region comes to rest or turns back on its self. This implies a steadily falling energetic electron energy spectrum over the energy range 10 keV to 40 keV which has little spacial or temporal variation associated with it.

c) Interaction Region Velocity -Time Curves.

The interaction region velocity for all four emissions is always +ve. For emissions A & B it increases with increasing true time while E & J show a minimum velocity about half way through the emission life time. In all cases the interaction region velocity obeys the necessary condition $-v_g < v_I < v_{11}$ for all values of true time if a realistic value of n_{eq} = 1 electron/cc is used in the analysis.

d) Resonant electron energies.

For all emissions the electron resonant energy falls with true time. The slope of the emission profile is +ve and increasing with time, therefore the interaction region is moving away from the equator and the local gyro-frequency and emission frequency are rising. The first

HIGH LATITUDE (L=6·196)

EMISSIONS

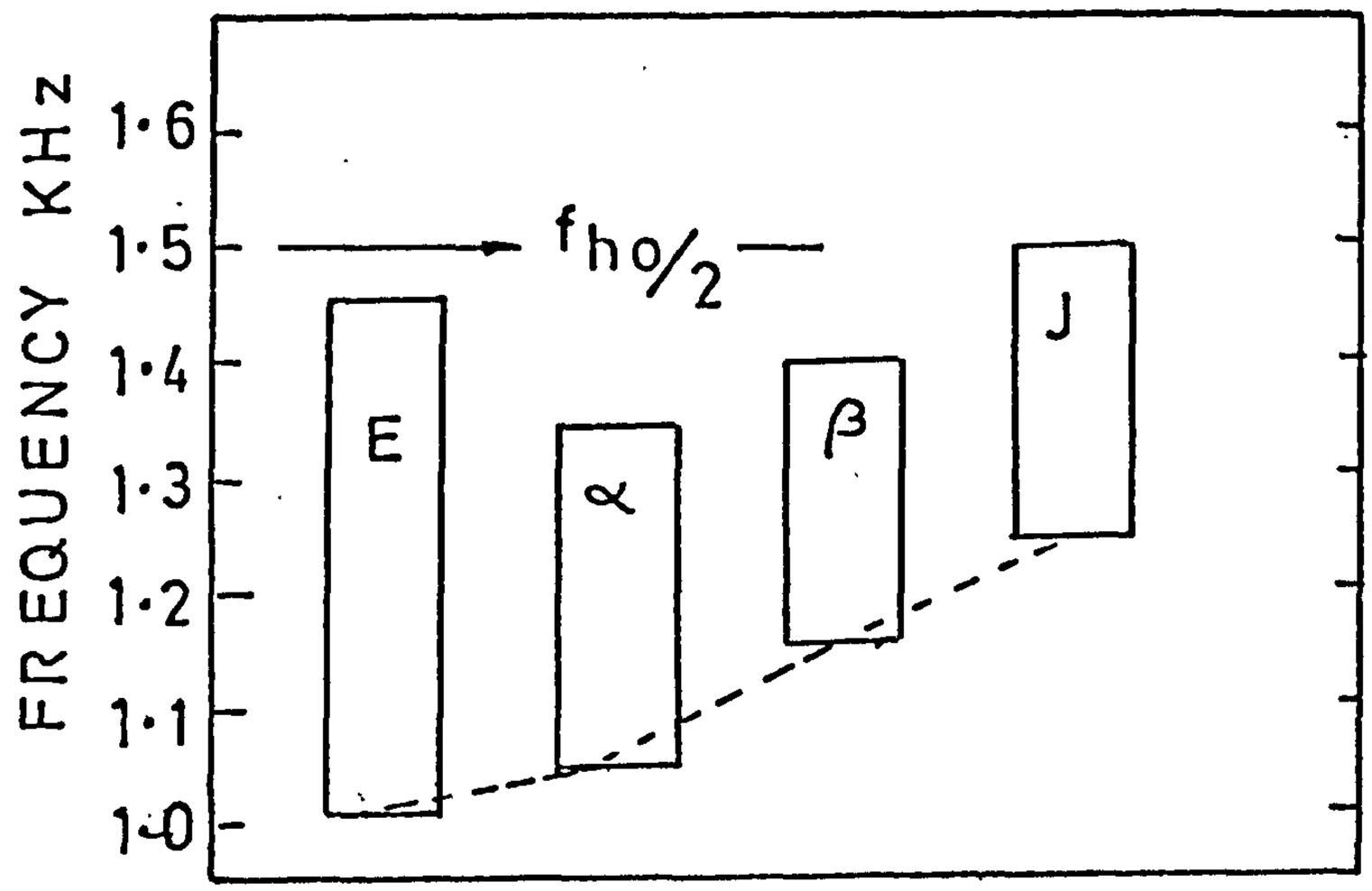

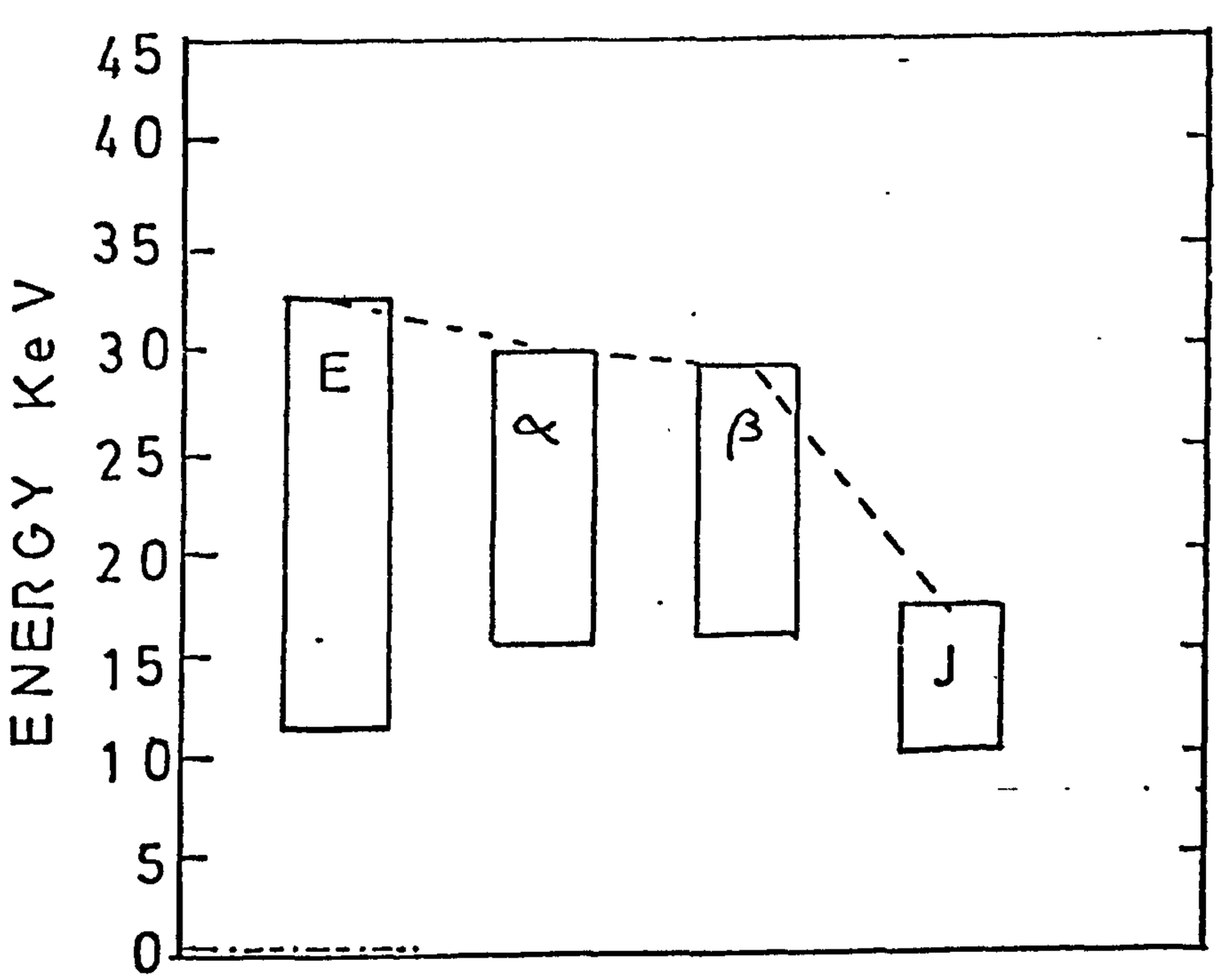

EMISSION

FIG(10.35)

resonance condition (equation 8.2,6) requires low resonant energies at high emitted frequencies and thus a falling resonant energy - true time curve results. For n_{eq} = 1 electron/cc the energy range required for the generation of the four emissions shown is 1-33 keV.See Fig. 10.35. It is clear from Fig.10.15 that the resonant energy E is proportional to $1/n_{eq}$ and it is therefore possible to attempt to place a lower limit on ambient plasma density. Gustafsson 1972 analysed the data from electron detectors aboard OGO-4 which was a polar orbiting satellite at a height of 400-900 km. The detectors centred on 0.7, 2.3, 7.3 and 24 keV provided information on the fluxes of precipitated particles over the invariant latitude range 64^{o} - 80^{o} during the magnetic local time period 22.30 to 08.00 hr. Fig. 10.36 (due to Gustafsson) shows that the precipitated electron flux is falling with increasing energy and magnetic local time.Unfortunately it is not possible to place an absolute value on the lower limit of the equatorial electron density as no direct data is available on the precipitated electron energies and fluxes during the chorus event at Andøya . However it is clear from the falling electron spectrum at these latitudes as given by Gustafsson,together with the inverse relationship of resonant energy with equatorial electron density shown in Fig. 10.15, that the available resonant electron flux falls with the value of n_{eq}. Therefore the likelihood of generating a strong discrete emission must fall with n_{eq}. Fig. 10.37 shows how the available electron flux decreases with energy and by using Fig. 10.15, with n_{eq}. The upper limit of 5 electrons/cc is shown to correspond to a particle flux of about 10^{7} cm^{-2} s^{-1} sr^{-1} keV^{-1}. The direct comparison of precipitated electrons and chorus emissions would yield a value for the equatorial electron density which could then be checked by direct measurement thereby

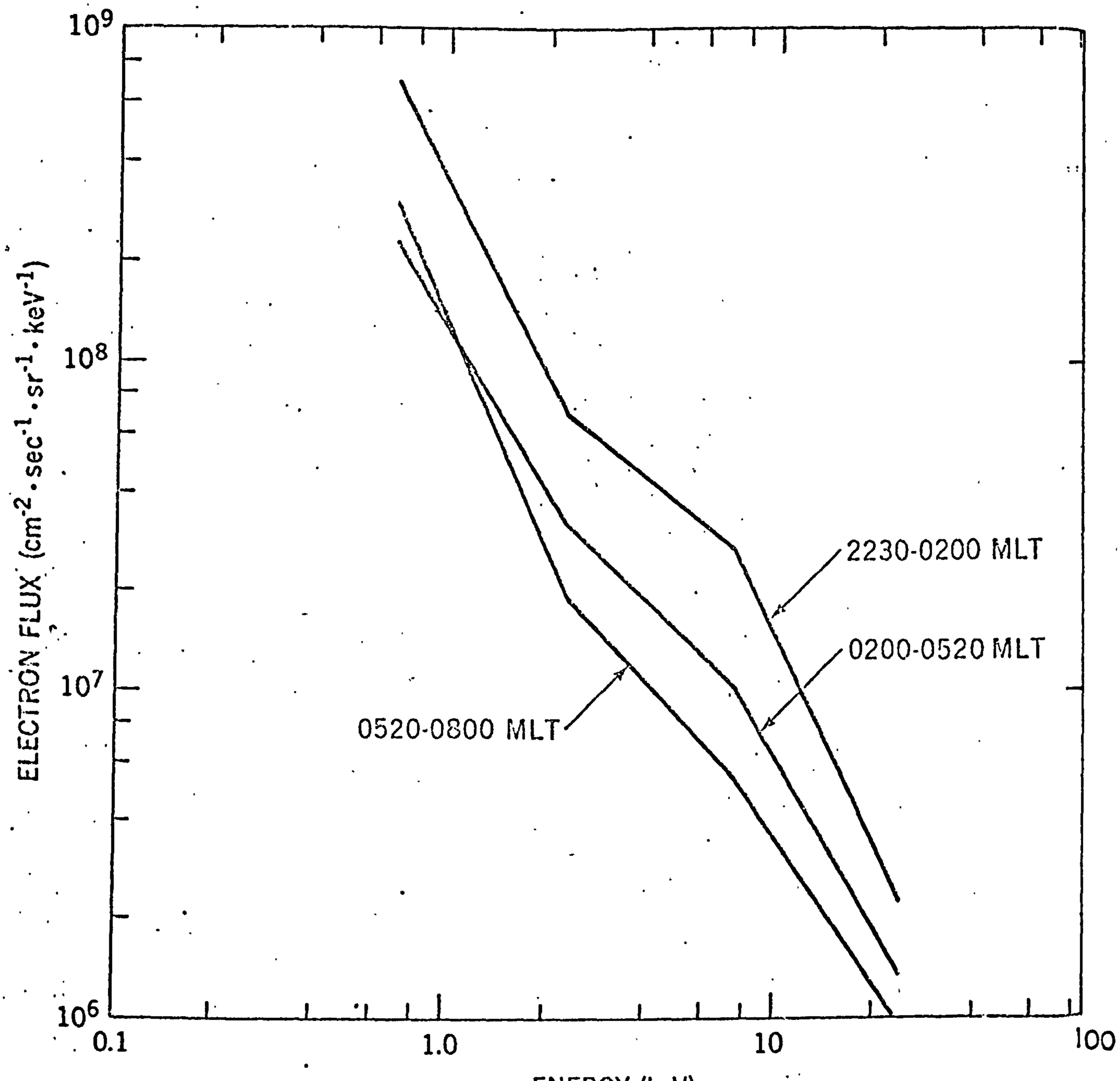
10^9
10^8
10^7
10^6
ELECTRON FLUX (cm^{-2}·sec^{-1}·sr^{-1}·keV^{-1})
2230-0200 MLT
0200-0520 MLT
0520-0800 MLT
0.1
1.0
10
100
ENERGY (keV)

FIG(10.36)

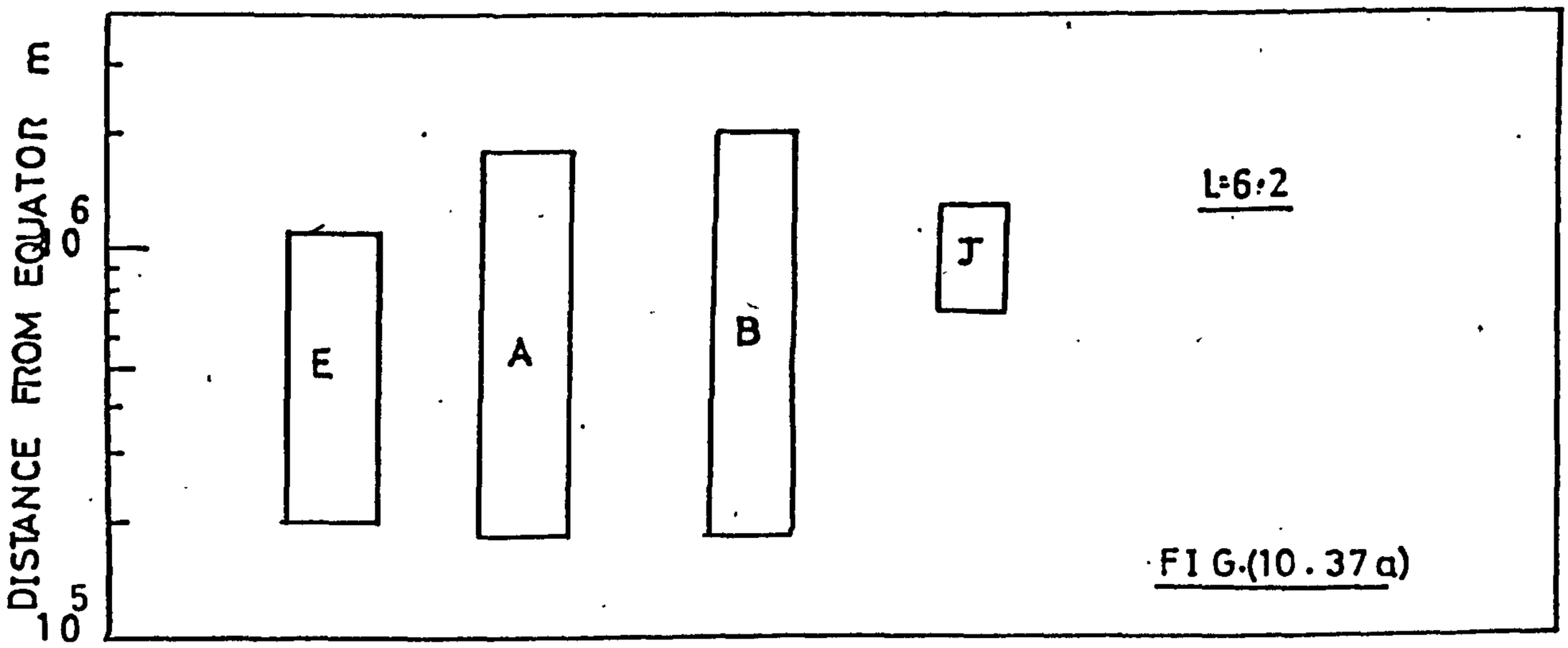

FIG.(10.37a)

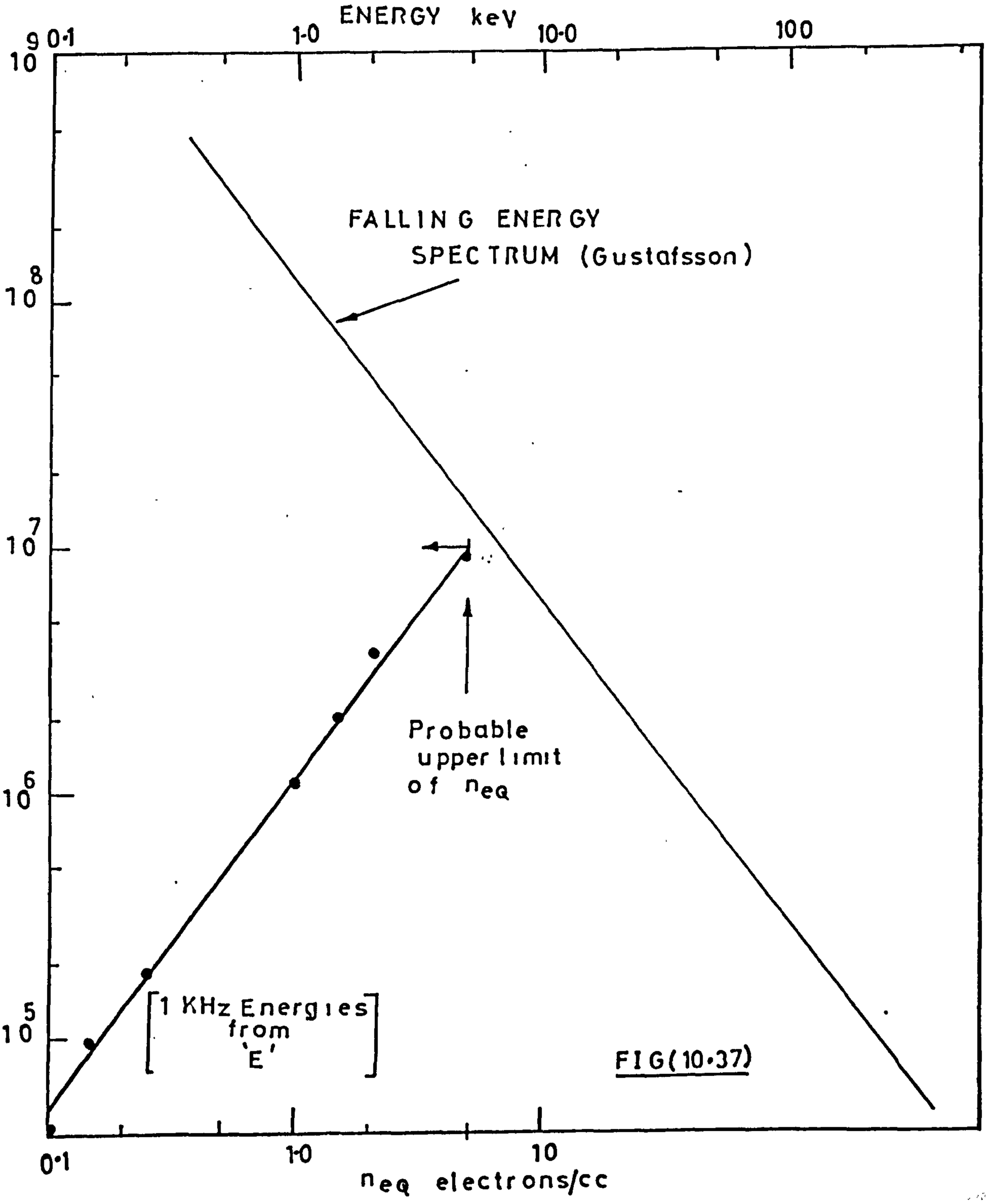

FIG(10·37)

supporting the proposition that such chorus elements are generated by wave-particle interactions as suggested by Helliwell.

10.4 Further aspects of High Latitude emission Analysis

Firstly we consider the effect on the predicted resonant electron energies of the assumed propagation path. Two emissions J & E were chosen and the calculated resonant energy as a function of true time was plotted in both cases assuming the following parameters; L = 6.196, f_{ho} = 3.0 KHz, n_{eq} = 1 electrons/cc and using a collisionless electron density model. See curve 1 in Figs. 10.38 & 39. The calculation of resonant energy as a function of true time was repeated for both emissions assuming a different propagation path corresponding to L = 6.969 where f_{ho} = 2.6 KHz. The equatorial electron density and the electron density model were not changed. The new results represented by curve 2 can be seen in Figs. 10.38 & 10.39.

For changes in L and f_{ho} of 12% & 10% respectively, we see that the estimate of resonant energy changes by approximately 100%. This 'error' is much greater than that introduced by inaccuracies in the estimate of absolute frequency, which is less than 1%, and that introduced by the inverse dependence of E on n_{eq}, where 100% change in n_{eq} produces a 100% change in E. Therefore the correct positioning of the propagation path is likely to be the determining factor in the absolute accuracy of the calculated energies.

In the case of the medium latitude emissions received at S.Uist during the firing of P47H, good correlation was obtained between single discrete emissions observed on the rocket and on the ground. This would indicate that the field line along which the emissions were propagating passed either through, or very close to, the ground station and the launching site.Thus an L Value of 3.4 can be used with

EMISSION J

n_{eo}=1elec/cc

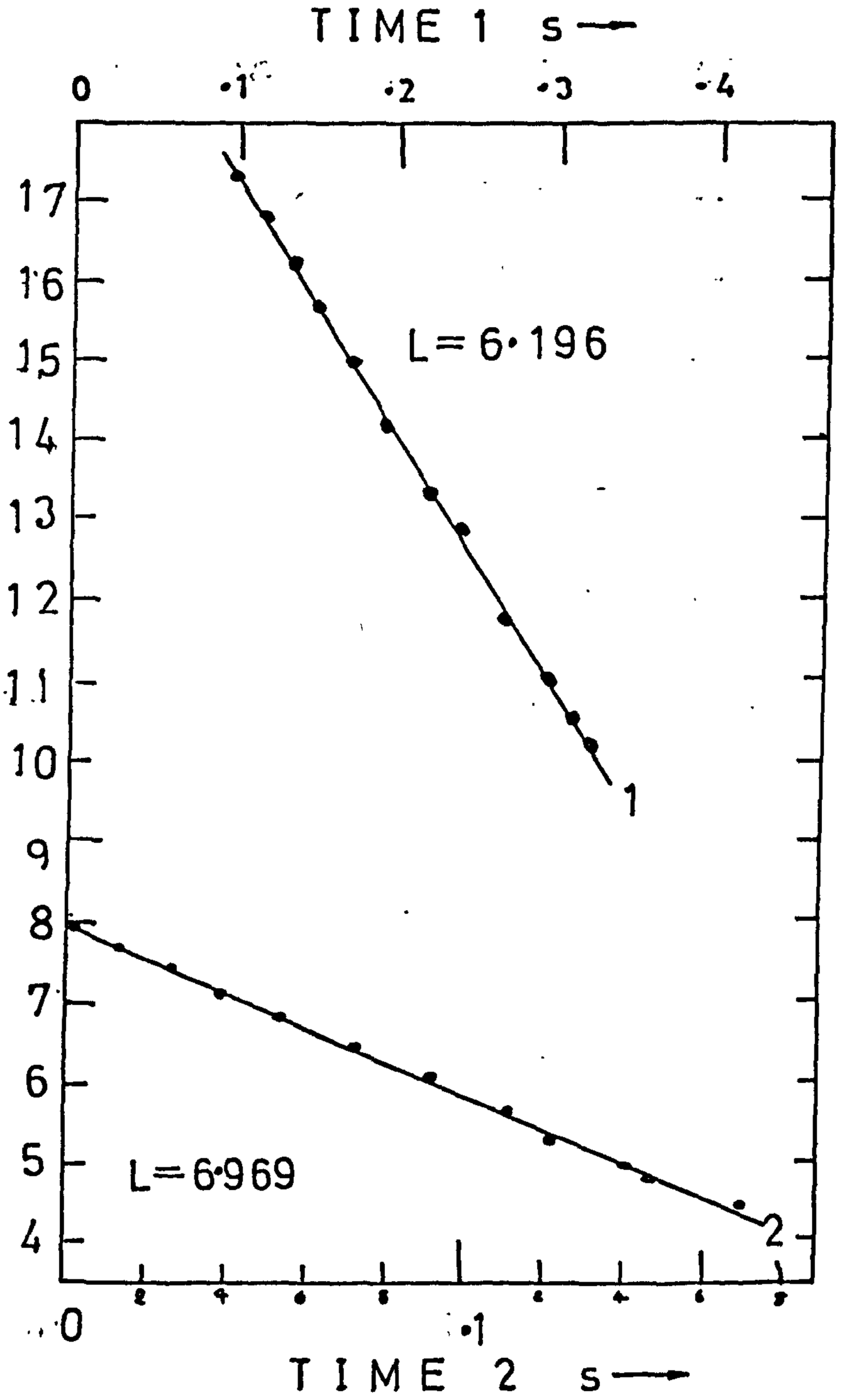

FIG.(10·38)

EMISSION E

$n_{eQ} = 1\ elec/cc$

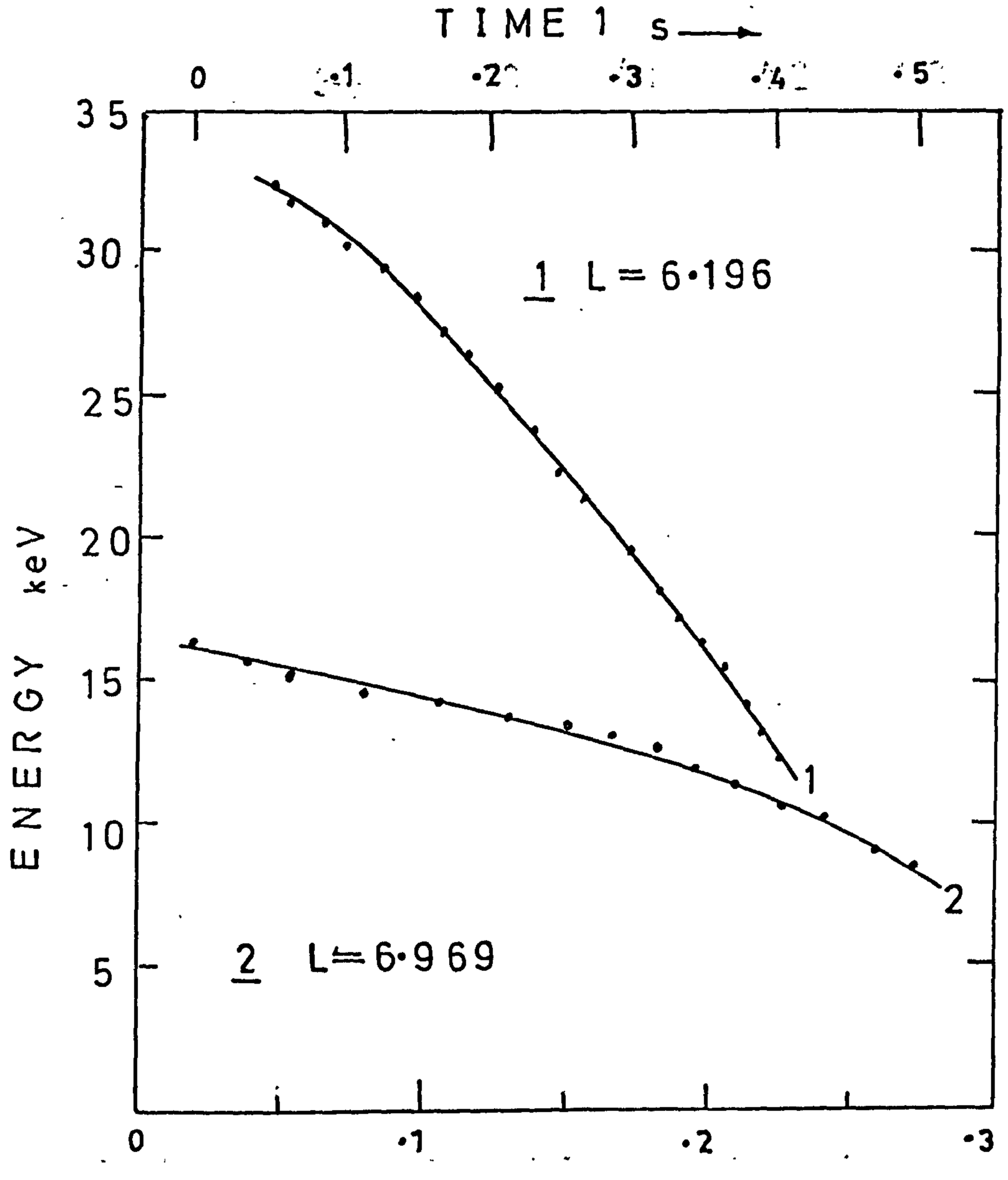

FIG.(10·39)

some measure of confidence.

Unfortunately the propagation path for the high latitude emissions had to be based on cut off frequency data and it is therefore not certain that an L value of 6.196 is appropriate.

It is of interest to examine the possible sources of weak whistler mode waves which are required for the interaction with the electron stream. There are three or possibly four sources of such waves.

a) Whistlers

It is well known that whistlers can trigger off emissions such as that shown in Fig. 1.11. There was however no evidence of whistlers received on the ground at Andøya during the reception of the polar chorus. Whistlers are received at high latitudes much less frequently than at medium latitudes due to the geographical location of centres of electrical storm activity. Although a further search of the recorded signals may reveal weak whistler activity, it is not considered to be the most likely source of triggering waves. It is unfortunate that at the time of the chorus event there was no satellite with VLF receiving equipment which was well positioned to provide information on weak signals above the ionosphere.

b) Man-made Transmissions.

Helliwell 1967 gives an example of the now well known phenomenon of triggering an emission by a long morse pulse from a powerful ground based VLF transmitter. This occurs mostly at medium latitudes where the equatorial gyro-frequency is of the order of 50 KHz and it is possible for resonance to take place at frequencies between 10KHz and 20 KHz which contains most of the high power VLF transmitted signals. At Andøya the emissions would be triggered by a man made signal at about 1 KHz. As there are few stations (which are mostly low power)

near this frequency. This source of input signals is not considered to be very likely.

c) A Plasma Instability.

In section 6.3 it was shown that using the simple expression of the first resonance condition, equation (6.3,6) and the triggering criterion produced by Kennel & Petschek (1966);

$A \gg \frac{\omega}{\omega_h - \omega}$ it was possible to derive an expression for the resonant energy parallel to the field line which electrons would require to sustain the instability. This is given in equation (6.3 7). On initial inspection it would seem possible to calculate A from knowledge of ω & ω_h substitute this value into (6.3 7) and compare the energy with that calculated by program P90T. It might then be possible to establish if the source of the weak input waves was a plasma instability.

Unfortunately this is not possible as the calculation of A from ω & ω_h and the substitution into (6.3 7)is merely a rearrangement of equation (6.3,5) which simply represents the first resonance condition. This condition, though not in the form of (6.3 5), is used to calculate the parallel valocity and hence the parallel energy of resonant electrons in the analysis program P90T. Thus given values of ω & ω_h the two energies must be the same and no useful information can be obtained. It would be most interesting to obtain data on the anistropy of the electrons present during the chorus event at Andøya in order to calculate the parallel resonanant energy such that the feasibility of a plasma instability being present at the time might be established.

d) Whistler mode Echo.

It is possible, having generated an emission from one of the sources described, that the partial reflection of the signal back towards the equator could provide weak whistler mode signals at the correct frequency such that other emissions may be formed. In the limited part of the data yet analysed from the whole event the marked periodicity which such echoing would establish was not in evidence. However a more careful and thorough investigation might prove interesting.

CHAPTER 11

CONCLUSIONS, COMMENTS AND SUGGESTIONS FOR FUTURE WORK

11.1 CORED LOOP ANTENNAS

For many years VLF radio receivers used large open loop aerials. This made them unsuitable for use either as a semi-mobile ground station, or on space vehicles where size and mass are important. In recent years due to the production of very high permeability special steel alloys and the realization of extremely low noise Field Effect Transistors, it became possible to construct small highly sensitive VLF antennas. Chapter 3, section 1 shows that it is possible to obtain the required sensitivity from such a small cored loop antenna. However it is not possible to derive the performance parameters by solving Maxwell's Equations and one is forced to adopt an empirical approach to optimising the antenna performance.

It was demonstrated that a simple equivalent circuit did not fully represent the antenna for all combinations of coil size and frequencies considered. Chapter 4 dealt with the production of a more representative equivalent circuit for the antenna and with the calculation of the noise output of such a circuit.

Throughout this work the equivalent circuits were modelled in complex algebra and written as computer programs. This enabled the amplitude and phase transfer functions to be calculated at any number of frequencies for various circuit parameters. The use of such programs made it possible to study in detail the noise introduced into the circuit by each element and consequently provided valuable information which was used in optimising the antenna sensitivity and frequency response.

11.1 (Contd) Such techniques were used during the period of this work to solve the problem of reducing the loop size of ground based VLF Goniometer receiver aerials by a factor of 20 or more without reducing the system sensitivity. A coupling transformer to connect the low impedance antenna to the very high input impedance FET preamplifier was designed using a suite of computer programs of the type described. The author was in collaboration with Dr. K. Bullough of the University of Sheffield and a report of this work will be published in the near future.

The engineering required to transform a laboratory prototype compact VLF receiver using cored antennas into a fully integrated Rocket Experiment was undertaken and the payload was successfully launched from ANDØYA in November 1973. The performance of the experiment was excellent throughout the flight and the data recovered is at present being analysed.

The design and production of a successful cored loop VLF rocket borne radio receiver was carried from first principles in less than two years and represents a significant step in the technology of VLF radio receivers on board space vehicles.

11.2 FUTURE USES AND THE DEVELOPMENT OF SMALL VLF ANTENNAS

There are two areas in which the performance of the antennas previously described may be improved.

1) The extension of the frequency range covered by the antenna.
2) The partial removal of the antenna resonance.

Increasing the coil inductance by winding a larger number of turns will extend the frequency range of the antenna from VLF/ELF (20 KHz to 300 Hz) to ULF (less than 300 Hz) and would enable the study of phenomena such as micropulsations and magnetosheath noise.

11.2 (Contd)

It is not possible to extend the frequency range above about 50 KHz using highly permeable MU Metal cores as the Hysteresis loss encountered at these frequencies drastically reduced the effective permeability of the material. However it is possible to obtain Ferrite cores which will work successfully up to a few MHz.

The presence of a distinct resonance peak which has a high Q (due to the minimisation of loss in the coil) restricts the dynamic range of the receiver when operating in wide band mode. It is desirable to fully utilise the rather limited dynamic range of telemetry systems (40 db) and consequently a linear frequency response over the band of interest is required. There are a number of ways this can be achieved. Logarithmic compression of the wide band signal ensures that the dynamic range of the telemetry is not exceeded but it prohibits the subsequent spectral analysis of the data. The intensity information at any frequency is lost and is not recoverable over the whole band by post telemetry antilogarithmic expansion. It is possible however to recover fully the frequency - time profile of the strongest emissions in the band which is being analysed.

The removal of the resonance peak by using an on board filter with the inverse transfer function of the antenna is the most straightforward approach. However the production of such a filter is not a simple matter and ensuring its frequency stability over a wide range of temperatures and mechanical loadings requires considerable thought.

A more practical approach is that adopted by Dr. Gendrin's group in France, Mayer 1969, where a second winding is introduced into the antenna coil. This winding,of only a few turns, carries the output signal from the preamplifier and forms a negative feedback network. The difficulty with this approach is the production of a phase compensation network which operates over the frequency range of the antenna to prevent the feedback from becoming positive.

11.2 (Contd)

The feedback method of reducing the antenna resonance would seem to be the best solution and should be the next step in the production of cored loop antennas.

The prospect for experimental work in VLF/ELF, ULF and magnetospheric physics in general in the next few years in Europe is very exciting with the advent of the I.M.S. in 1975. At the time of writing the author is working on the ESRO satellite GEOS which is to be launched into a geostationary orbit at 6.6 R_E in November 1975. This complicated fully integrated spacecraft carries an experiment produced by Dr. Gendrin's group which amongst other things measures magnetic fields in the VLF/ELF & ULF bands using small cored loop antennas of approximately the same size, mass and sensitivity as those described in this thesis.

The University of Sheffield is producing a Skylark payload based on SL1124 but with an additional 3 axis electric field experiment, the basis of which is being provided by the author in connection with the British Aircraft Corporation to be launched in conjunction with GEOS. Fig. 11.1 shows the receiver threshold claimed for the S300.5 magnetic sensors on GEOS compared with the sensitivity of the 25 cm rod antenna described in this work. The sensitivity of the electric field sensors on GEOS is given in Fig. 11.2 together with the threshold of the electric field experiment which is proposed for the new Sheffield Skylark Payload. The sensitivities and frequency coverage of the receivers on board GEOS mark a definite step forward in spacecraft born VLF receivers.

Many other groups throughout Europe have experiments on board GEOS or are launching rocket payloads or giving ground based support during what promises to be an exciting and progressive period in magnetospheric and Ionsopheric research over the next few years.

11.2 (cont'd) In the United States of America magnetospheric research continues at a great pace with the launching of a number of new earth orbiting and deep space probes. A new feature of such work is the investigations carried out into the Physics of the Jovian Magnetosphere by both fly - by and the proposed orbiting spacecraft together with measurements of the Decametric and decimetric radio emissions from the planet by ground based radio telescopes.

11.3 WAVE - PARTICLE INTERACTIONS; A SHORT REVIEW OF SIGNIFICANT STEPS IN THE WORK PRESENTED IN THIS THESIS

1) The Synthesis of emissions by Dowden's Cyclotron Theory

A computer model of the Backward Radiating Doppler Shifted Cyclotron Oscillation from Electrons which was proposed by Dowden was constructed. The calculations were performed entirely by a computer and no manual or graphical operations were involved. The examples of emissions analysed by Dowden were checked and the computer results were in good agreement. Emissions were synthesised for representative electron energies at the S.Uist, Halley Bay and Andøya VLF stations and shown to have spectral (frequency - time) characteristics similar to those observed. However, the unsatisfactory nature of the postulated 'electron bunch' leads one to discuss Helliwell's phenomenological theory of the generation of VLF emissions which makes use of the 'Second order Transverse Resonance Instability.

2) The analysis of VLF Emissions based on Helliwell's Theory

A computer model based on Helliwell's calculations was built using many of the software routines employed earlier in the Dowden model to give a fast non graphical method of analysing VLF triggered emissions. The model was tested using the Hook which was analysed by Helliwell using partially graphical techniques. The agreement between the results was very good ie. within 10% for all parameters.

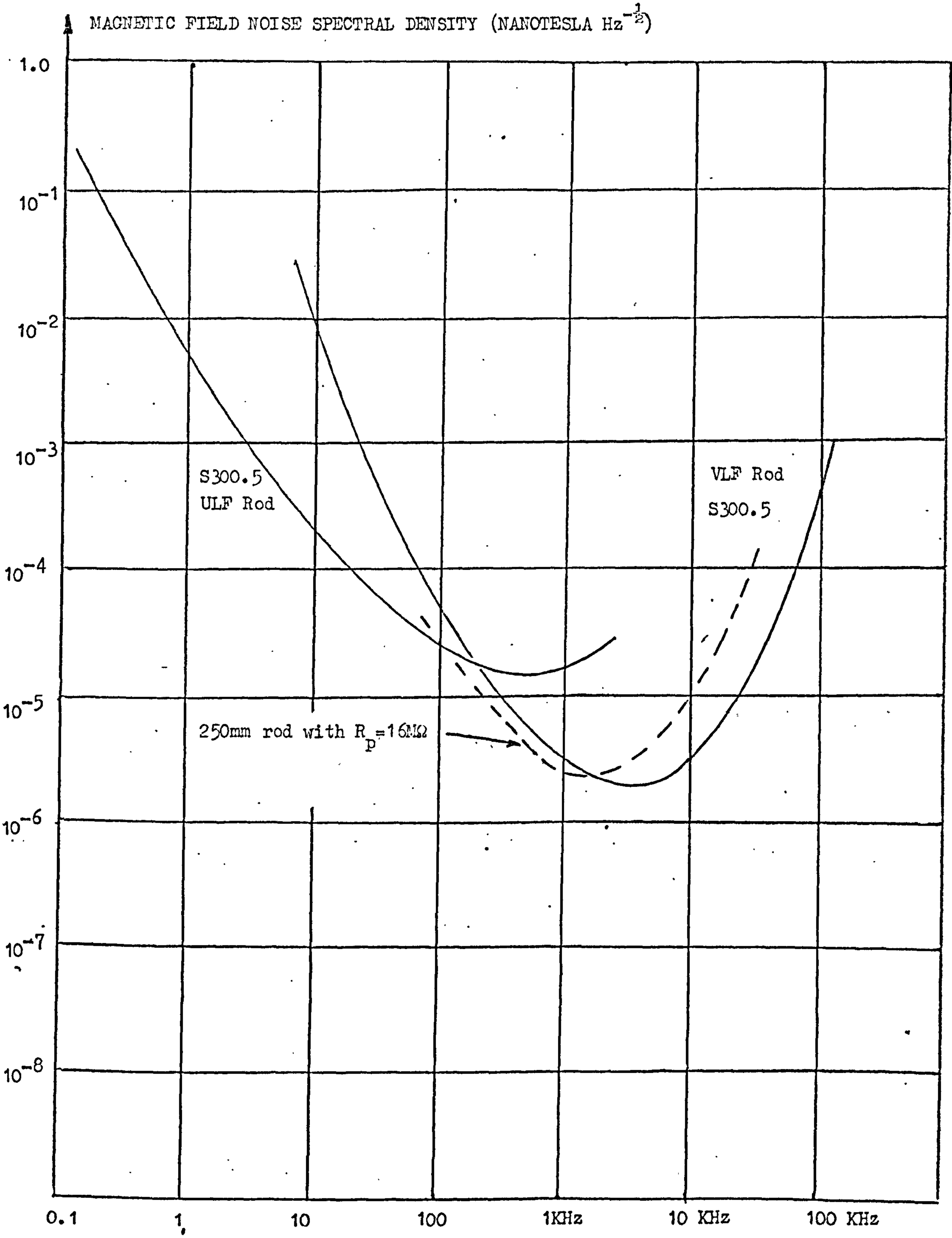
MAGNETIC FIELD NOISE SPECTRAL DENSITY (NANOTESLA Hz$^{-\frac{1}{2}}$)
1.0
10^{-1}
10^{-2}
10^{-3}
10^{-4}
10^{-5}
10^{-6}
10^{-7}
10^{-8}
S300.5
ULF Rod
VLF Rod
S300.5
250mm rod with R_p=16MΩ
0.1
1
10
100
1KHz
10 KHz
100 KHz
Frequency

Fig.(11.1)

ELECTRIC FIELD SPECTRAL DENSITY (VOLTS/m $Hz^{-\frac{1}{2}}$)

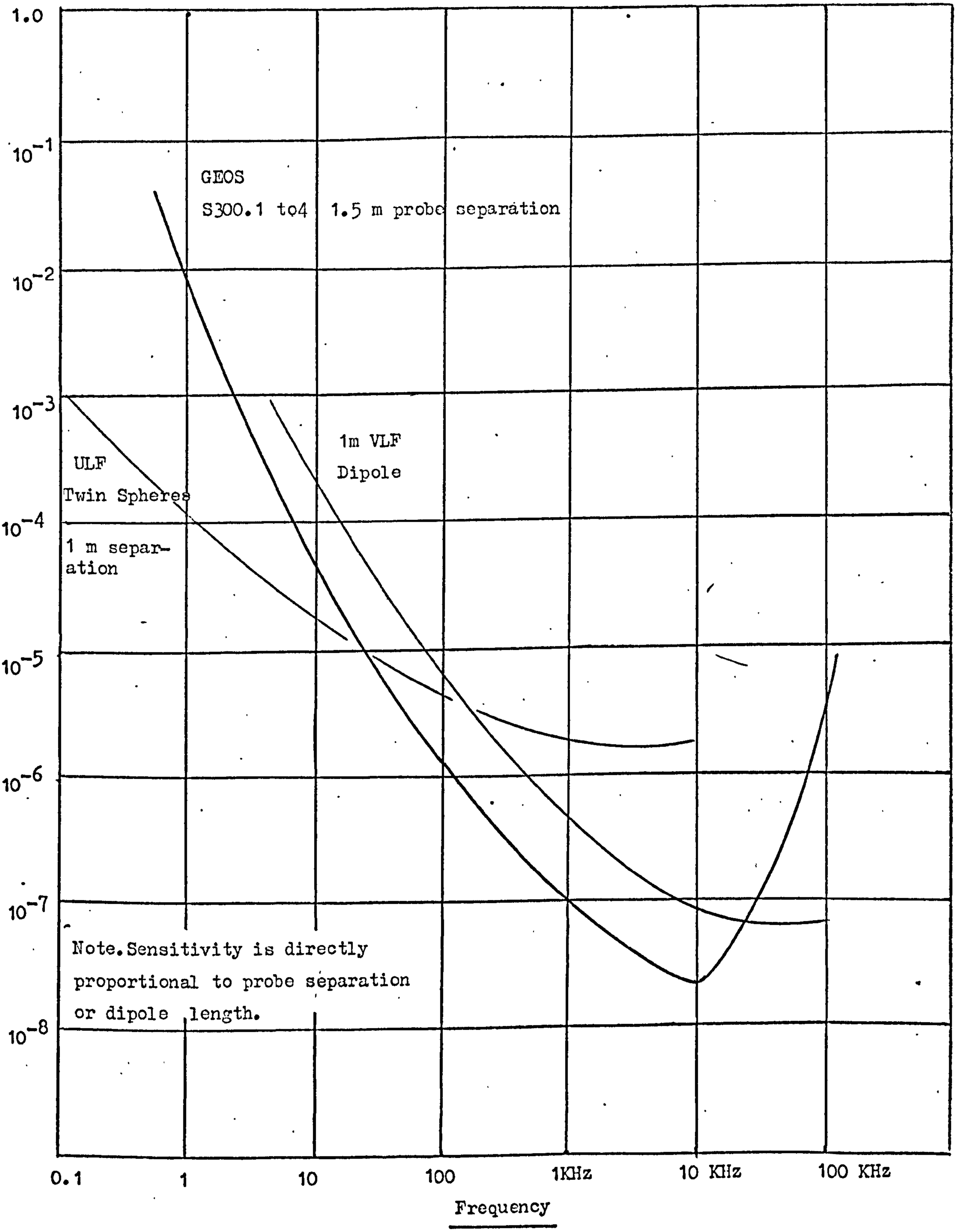

Fig.(11.2)

11.3 (Contd)

Unfortunately the assumption made by Helliwell in (Equation 8.2.9) concerning the value of the electron gyro-frequency f_h as a function distance, prevents the computer program for working outside the distance range $\pm$ 3 x 10^6m from the geomagnetic equator at L=4. This restriction was removed in Section 9.1 by showing that the basic equation 8.2.14 is 'well behaved' and can be solved numerically by a fast solution searching routine to give correct value of distance over the entire length of the field line being considered. This solution for S contains no approximations of the basic plasma equations called up in the solution of 8.2.14 and the accuracy of the value of S is determined entirely by the number of iterations allowed. This solution of Helliwell's basic equation is new and extremely useful not only for the analysis of VLF emissions but also for their synthesis where the emission can be followed from mirror point to mirror point.

A refinement of the computer model involved the exact differentiation of a fourth order polynomial which was fitted to the original data rather than a 'step by step' differentiation which can produce random errors in S. The differentiation gives values of df/dt at f which are used in the solution of equation 8.2.14 for values of S.

The model was then applied to data collected at S. Uist during the launch of a VLF rocket payload into Dawn Chorus, after being checked with Helliwell's Hook. A very slow riser recorded at high geomagnetic latitudes was successfully analysed using this computer model. This is possibly the first time Helliwell's Theory has been applied to High Latitude Emissions.

3) Helliwell's Theory in the Dowden Limit

Having computer models for both the Dowden and Helliwell theories of VLF emission generation enabled a quantatative check of Helliwell's statement that 'the Dowden criterion was a limiting case of the more general Helliwell model. 'Many millions of individual calculations had to be performed during the synthesis

11.3 (Contd)

of an emission using the Dowden model and the subsequent analysis of that emission using Helliwell's theory. It is noteworthy that the errors introduced during the digital computations were small enough to show up a discrepancy between the two models. This is the first time such a detailed study of the Helliwell theory in the Dowden limit has been made and it results in two statements.

First, the Helliwell model in the limit where $v_{//} = V_I$ is not exactly the situation described by Dowden 1962. This is because the basis of the Helliwell theory as shown in Fig. 8.4 where the interaction region has a finite size, becomes nonsense when taken to the Dowden limit.

Secondly, the two theories can be united and be described by a single equation (8.2.23) if the interaction region velocity is known, or may be approximated to during the analysis of the emission. Equation 8.2.23 reduces to the standard equation given by Helliwell 8.2.14 for $V_I << v_{//}$. This subtle extension of Heliwell's theory is new and may offer the prospect of better analysis of triggered emissions as it is more generally applicable.

4) The Analysis of Medium Latitude Emissions

Six representative 'Dawn Chorus' elements were chosen for analysis using the software which has been described. The emissions had been recorded at S. Uist in November 1970 during a magnetically disturbed period. (K_p 3+). All the emissions were analysable and gave sensible results in terms of the displacement of the interaction region from the geomagnetic equator, the interaction region velocities and the energies of resonant electrons. Of the many interesting points brought out in this section of the work, two are of particular interest.

a) Over a limited range of the equatorial electron density n_{eq}, there is a reciprocal relationship between n_{eq} and the energy of resonant electrons. This enables the value of n_{eq} to be fixed from measurements of precipitated electron energies and

11.3 (cont'd)

pitch angles and VLF discrete emissions which may be made by rocket probes or spacecraft. This is a new technique for measuring a difficult magnetospheric parameter.

b) There appears to be a linear rate of change of resonant energy of electrons as measured in the moving frame of the interaction region. This result was noticed for all the medium latitude emissions analysed although the degree of linearity was more marked in some cases than others. At the time of writing the author is not aware of any explanation of this result and so offers an opportunity for further study.

In all the cases analysed the interaction region obeyed the Helliwell criteria of $-v_g << V_I << V_{11}$ and thus the work lends support to the phenomenological theory of emission generation.

5) The Analysis of High Latitude Emissions

A more sophisticated model of Helliwell's theory was constructed which successively recalculates the emission profile as it travels away from the point of first observation. This larger computer program is capable of a much more accurate analysis of the observed emission and represents the final step in the construction of the computer model of wave particle interaction based on Helliwell's theory.

It was applied to four emissions recorded at Andøya in Norway during November 1972. The analysis of these emissions with a range of magnetospheric parameters showed that the major source of error in the results was due to the incorrect location of the field line along which the emission had travelled. The work comfirmed the reciprocal relationship between n_{eq} and E and with the aid of additional computer programs it was possible to show that an upper limit could be placed on n_{eq} with some accuracy. Also a probable lower limit could be derived from knowledge of the particle populations present in the vicinity of the generation region. The idea of using the analysis of discrete VLF emissions

with a fast computer program to provide data on the equatorial electron density is interesting and merits further consideration.

11.3 (Contd)

The interaction region velocities produced by the analysis of the high latitude emissions conforms to Helliwell's velocity criterion and again lends support to the idea that discrete emissions at High geomagnetic latitudes are generated by a process which has many of the elements put forward in Helliwell's phenomenological theory.

Considerable interest is being given to the study of high latitude magnetospheric phenomena with the launching of GEOS in the near future and it is hoped that the work on the analysis of high latitude triggered emissions presented here will be of use in this study.

11.4 SUGGESTED FURTHER EXPERIMENTAL WORK

1) The collection of more High Latitude discrete emissions for analysis with the sophisticated computer model. This would enable one to derive statistical relations of various kinds. For example a hystogram of the location and movement of the generation region or a distribution curve of resonant electron energies. The analysis of more data would of course give information on interaction region velocities and whether they obeyed the velocity criterion thus indicating the extent to which Helliwell's theory is applicable to a broad range of emission types under various conditions.

2) It would be most interesting to participate in joint experimental venture comprised of ground based VLF measurements with a spaced Goniometer array to provide information on duct exit points, a VLF and particle experiment on board a rocket to achieve heights of 200 km and a geostationary or synchronised fly-by of a suitable spacecraft carrying VLF receivers and particle detection equipment. With the data from a venture of this sort it would be possible to test many of the relations predicted from the computer model described.

3) The acquisition of whistler and discrete emission data together

11.4 (Contd) with particle energies and densities close to the equator during the time when the emissions were present would enable the one to check the validity of values of n_{eq} predicted from the analysis of the discrete emissions. It would also show whether the upper limits placed on n_{eq} by the analysis were realistic and the range of n_{eq} for which the limit was applicable.

There is great scope for experimental work in the field of magnetospheric physics and in the area concerned with wave-particle interactions. However it is probably more important at the moment to give much attention to the complicated mathematical problems which must be solved in order that we may move from a phenomenological theory of wave-particle interactions to a sound understanding of the physics of the generation mechanism or mechanisms.

11.5 COMPUTER MODELLING OF THE COMPLICATED INTERACTION PROCESS

The problems which arise in the production of computer models which can derive realistic emissions from purely theoretical considerations of an incident electromagnetic whistler mode wavefield and the properties of the ambient thermal plasma and a high energy particle population are very great. In this section a brief description of such work undertaken by Dr. Nunn at Kings College London will be given. It is clear that in such a short note it is impossible to do justice to Dr Nunn's work but it is hoped that the reader will gain some insight into the nature of the theoretical models used and the size and difficulties involved in the calculations which have to be performed. In the opinion of the author it is work of this nature combined with experimental data which will lead to a real understanding of the generation of VLF discrete emissions in the magnetosphere.

Nunn 1972 (private communication) refers to work produced earlier, Nunn 1971 to outline the basis on which the computer model is built Firstly it is assumed that the wave propogation vector k is everywhere parellel to the geomagnetic field B. This simplification implies that the

11.5
(Contd)

wavefield energy is confined within field aligned ducts and in making this assumption corrections for leakage and Landau Damping due to non parallel propagation have to be introduced into the model in an artificial manner.

Secondly the observed wave amplitudes of discrete emissions can only be explained if the particle motion is non linear. Thirdly the magneto-ionic medium is inhomogeneous due principally to the variation of geomagnetic field with position.

The problem as stated by Nunn, is to derive the resonant particle current with the aid of a suitable energetic electron spectrum and the equations of motion for the particles. The resonant current then modifies the electromagnetic wavefield as a function of position and time. The calculation of the time varying wavefield would involve following the trajectories of 2 million particles for about 2000 time steps. At the moment this is not practical with existing computer technology and some simplifying assumptions must be made.

It has been shown in Dysthe 1971 and Nunn 1971 that in an inhomogeneous medium cyclotron resonant electrons may became stably trapped undergoing a steady change in energy. For incident wavefields which can so stably trap particles for more than one trapping period, bunches of such particles completely dominate interaction with the wave. Under these conditions the electrons give rise to a small transverse current J_{res} which continuously modifies the wave field and causes the growth of an emission.

Nunn 1972 firstly derives the equations governing the time development of the wave field in the presence of a small non linear resonant particle current J_{res}.

Secondly he defines the equations of motion of resonant particles and shows that they can be stably trapped in an incident wavefield.

11.5 (Contd) The details of these calculations are both lengthy and complicated and are not presented here. However in order to understand some of the interesting results produced by this model it is necessary to define a few terms which appear in Figs.11.3 to 11.8.

a) R* is the dimensionless wave amplitude.
$R^* = R\, e^{i\phi}$

b) The quantity ϕ is the additional phase of the wave measured w.r.t. the phase of the initial wave field (possibly a morse pulse).

c) $J = (J_r + iJ_i)\, e^{i\phi}$
Where J_r is the component of the resonant particle current which is in phase with the wave electric field and J_i is the quadrature component.

Nunn 1972 states that the non linear currents J_r & J_i are complicated functions of the entire wave field R* and not simply of R* at one position or time. Further, while the in phase component of the particle resonant current merely increases or decreases the wave amplitude R, the out of phase component alters the phase of the wave ϕ. It is this current that gives rise to the sweeping frequency observed in triggered emissions.

In performing the calculations Nunn choses a time independent unperturbed energetic particle distribution $F_{(E)}$ to be of the form E^{-2}. He shows that the contribution to the resonant particle current J_{res} made by electrons with pitch angles $55^o < \alpha < 25^o$ is small and that the main contribution is made by electrons with pitch angles in the range $50^o > \alpha > 30^o$ which is in agreement with the calculations in Helliwell 1967.

Before giving some representative results it must be said that the computer model easily breaks down and that strict control must be kept over what Nunn calls 'exotic instabilities'. It was essential

Fig. 11.3

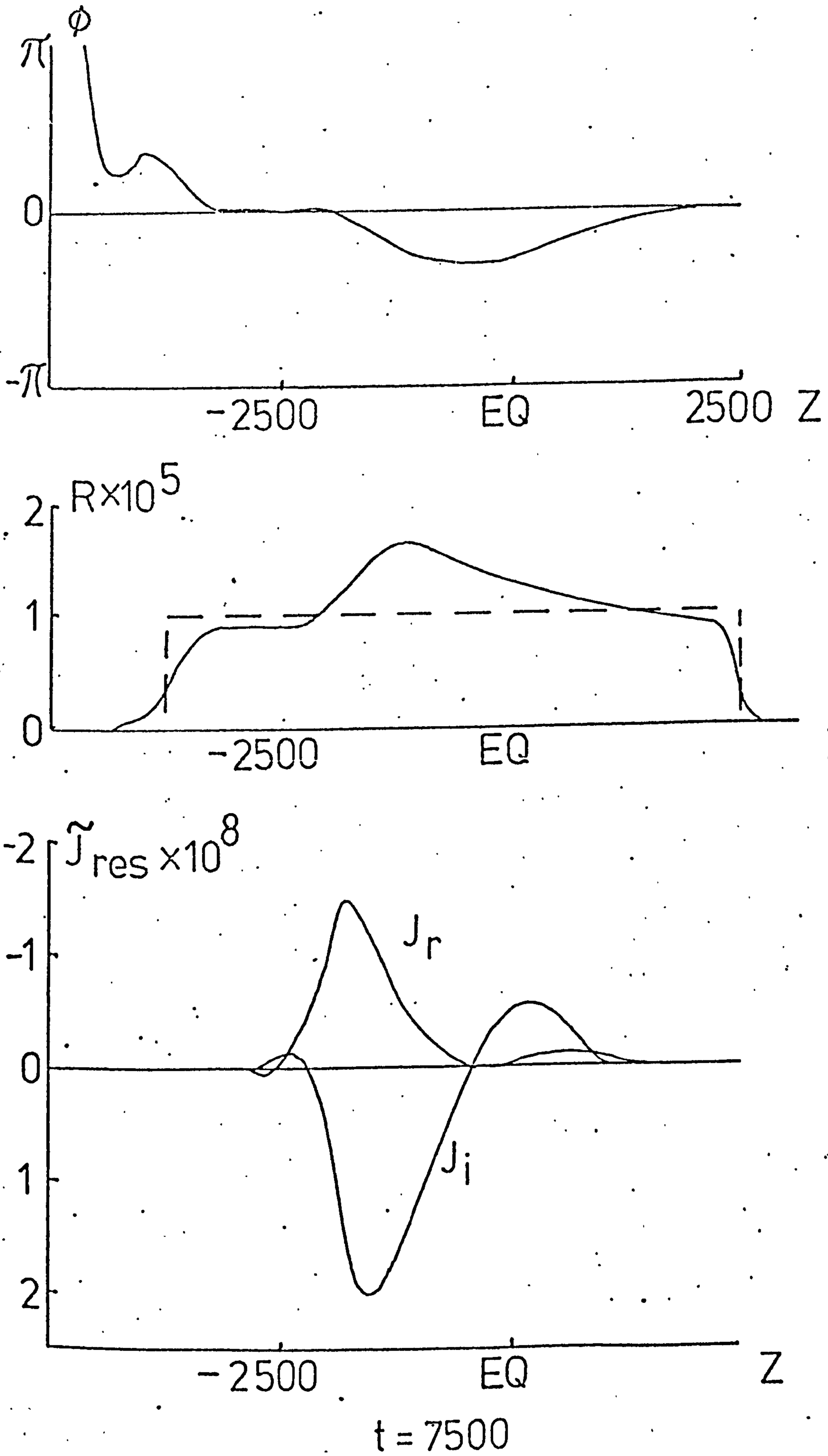
φ
π
0
-π
-2500
EQ
2500 Z
R×10^5
2
1
0
-2500
EQ
Z
J̃res ×10^8
-2
-1
0
1
2
Jr
Ji
-2500
EQ
Z
t = 7500

Fig. 11.4

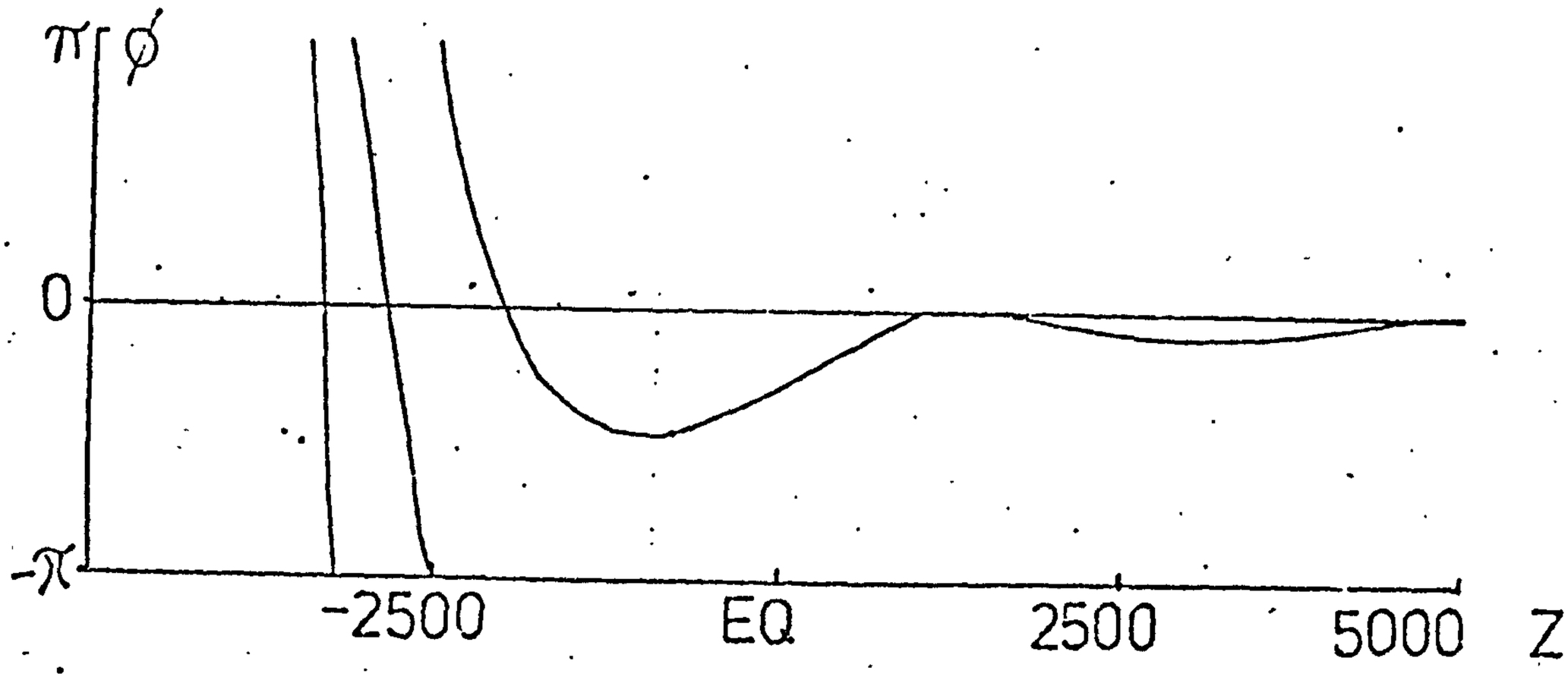

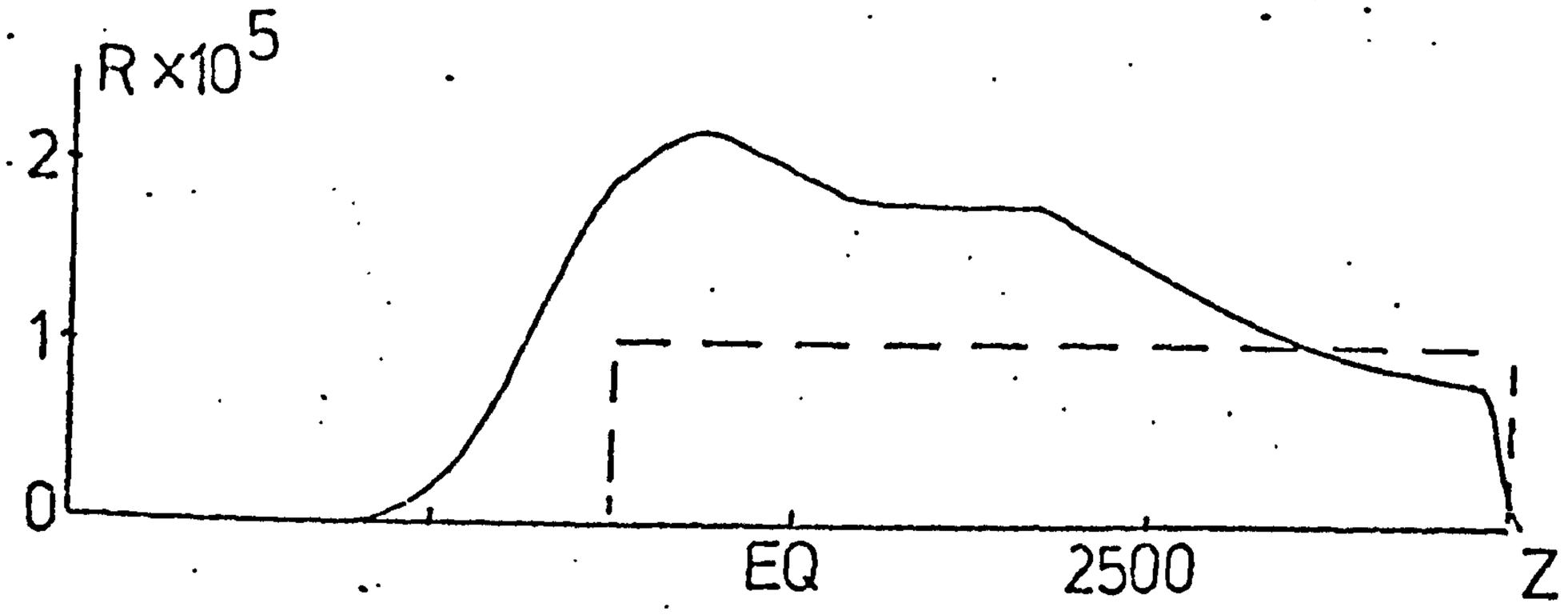

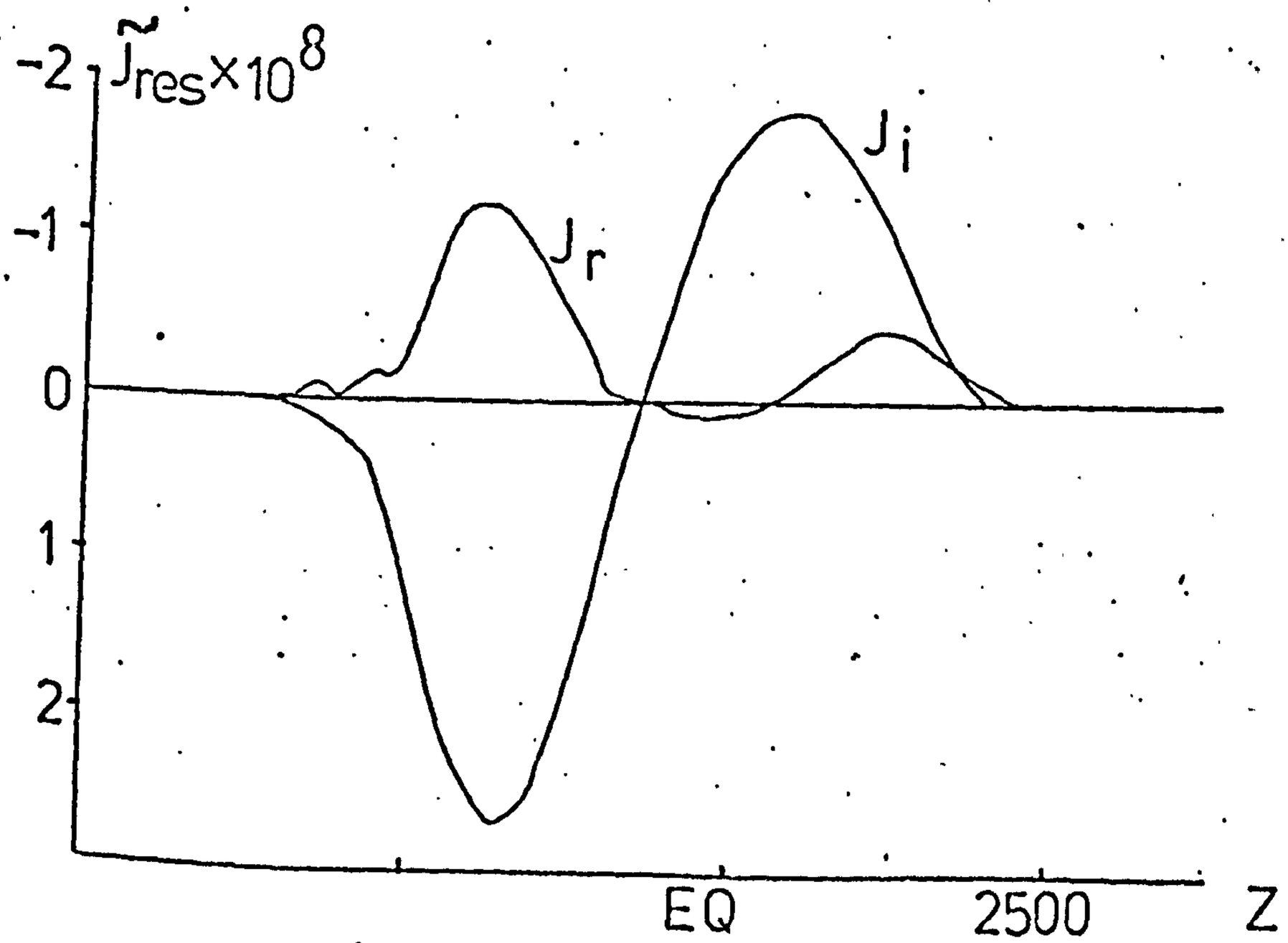

t = 10000

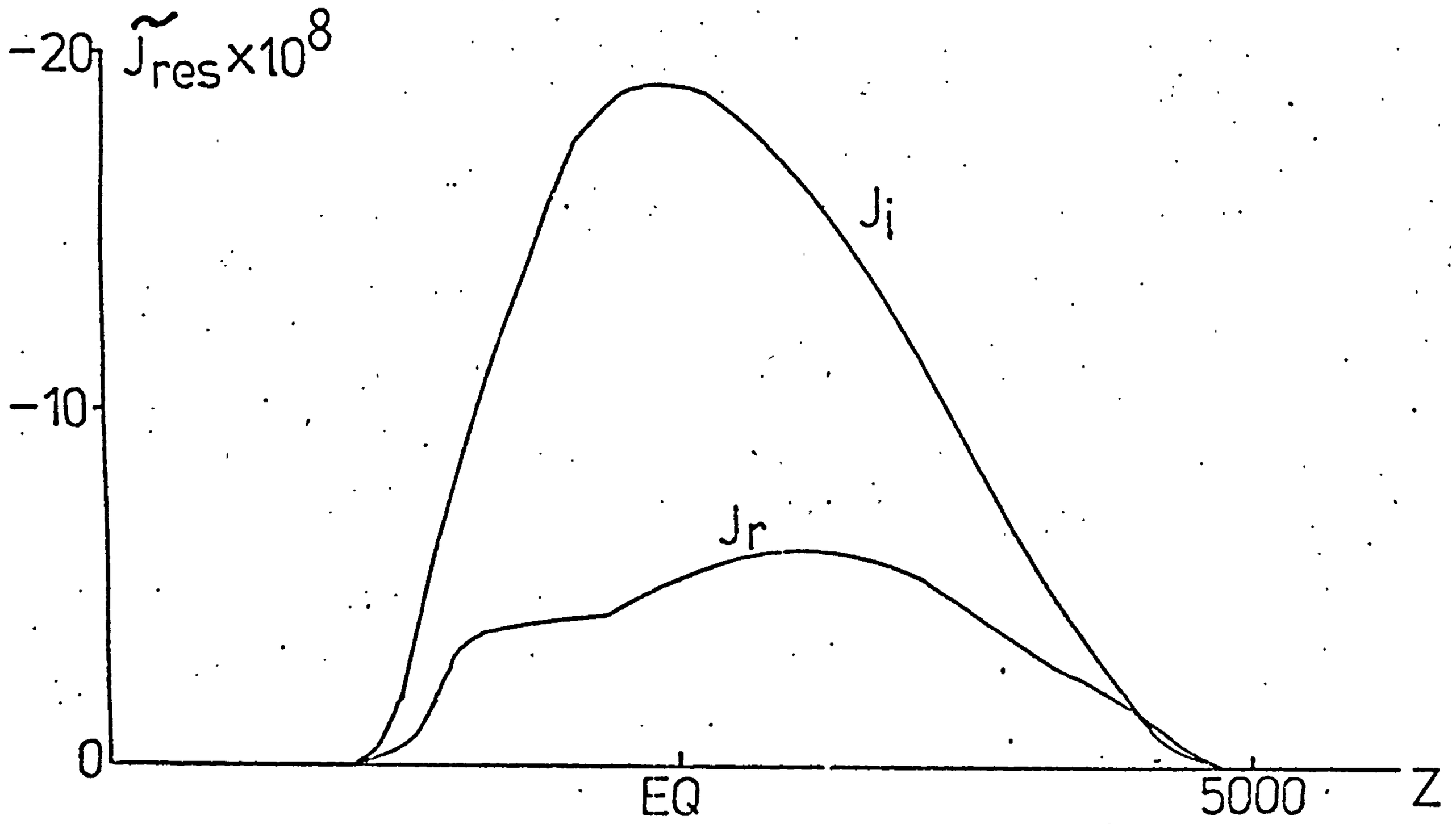

t = 15000

Fig.11.5

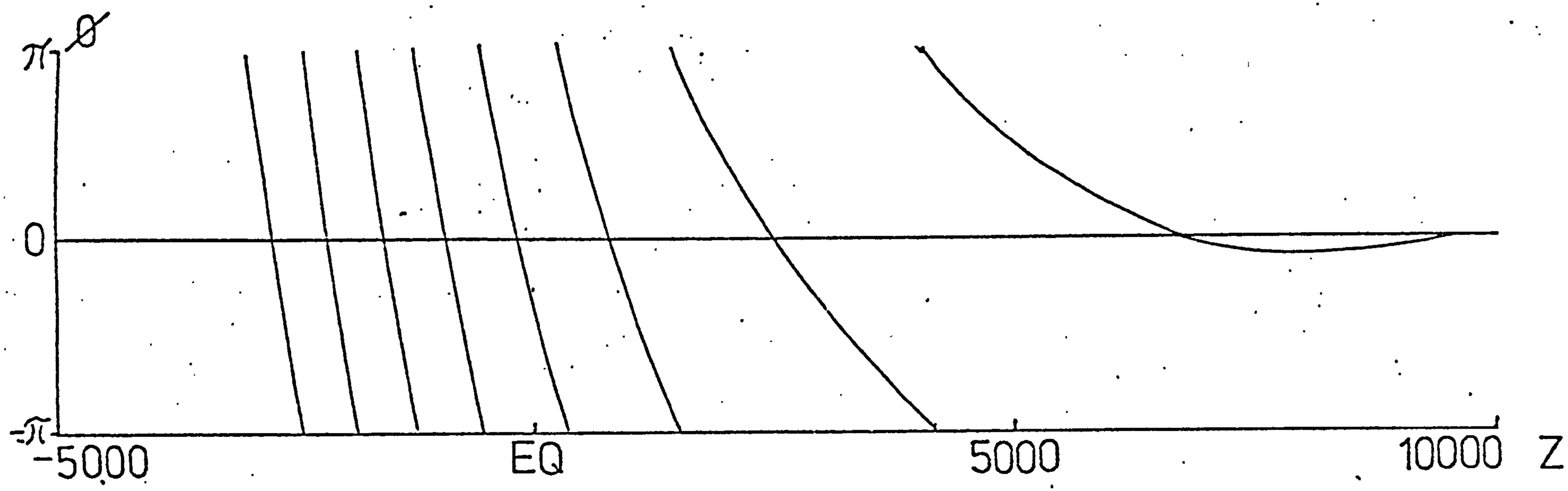

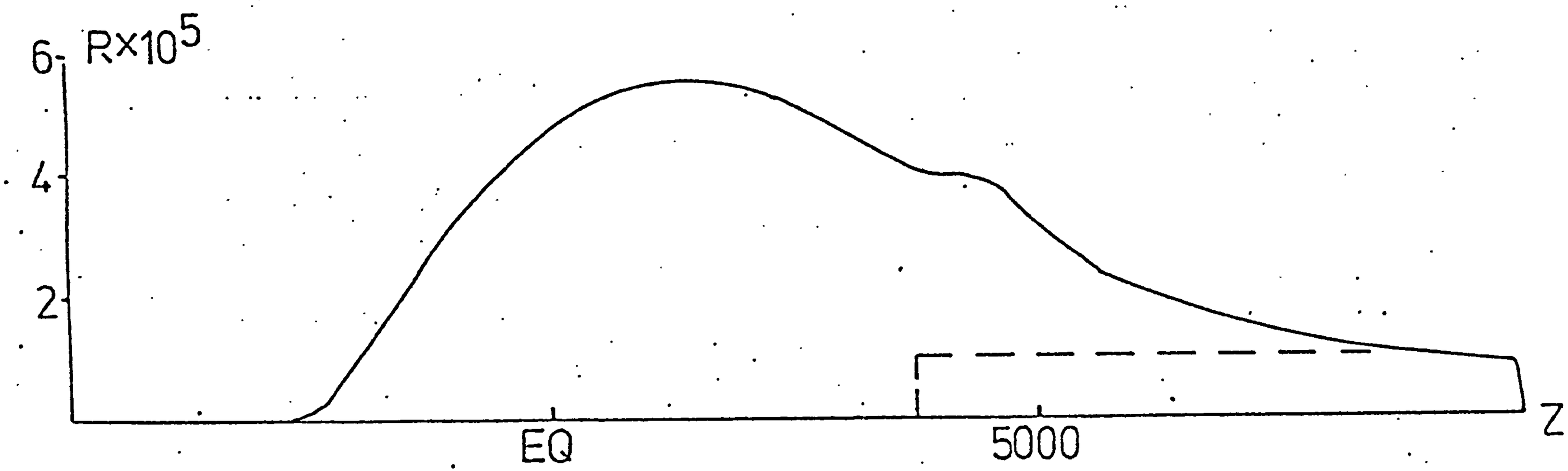

Fig. 11.6

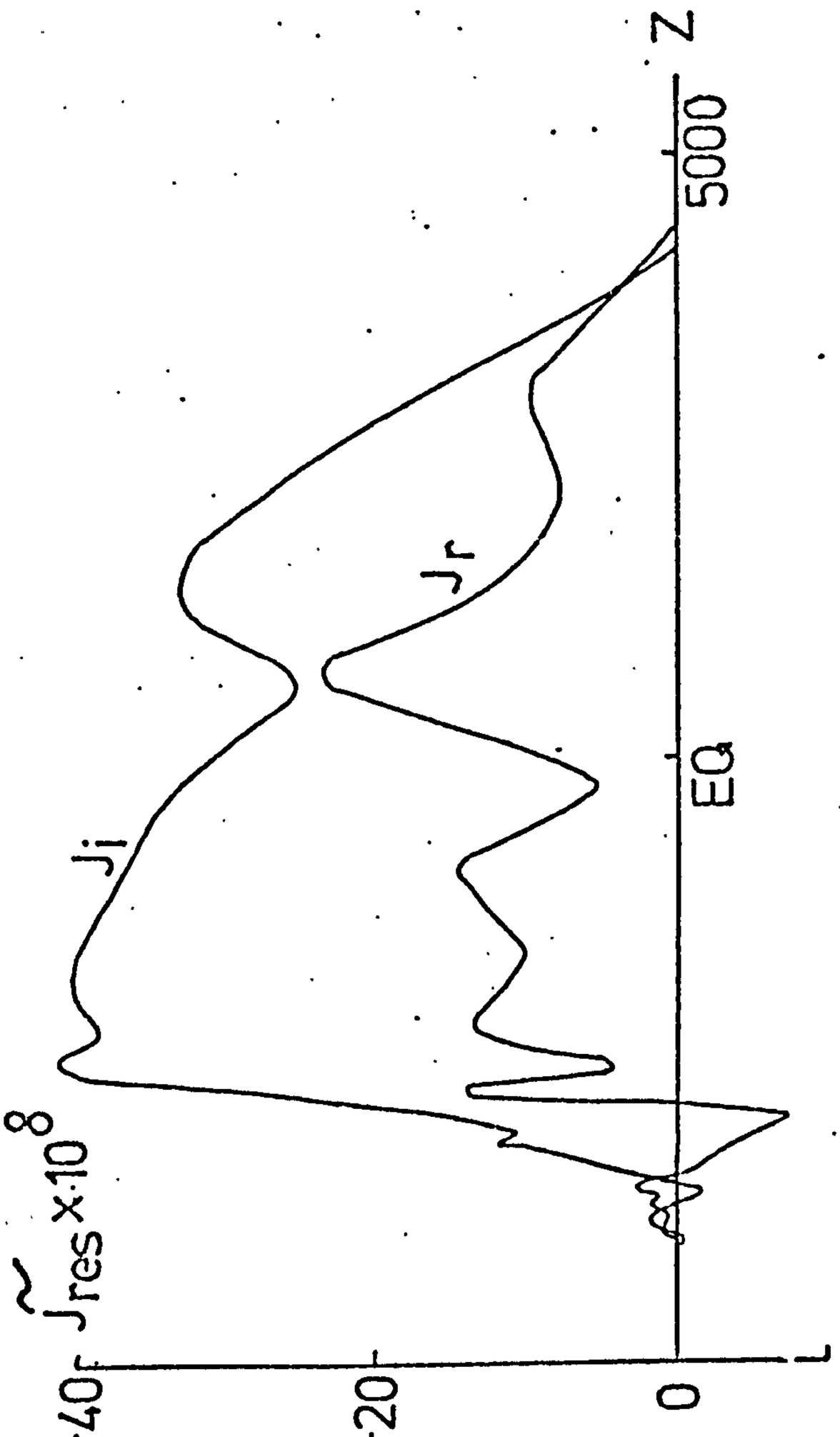

Fig.11.7

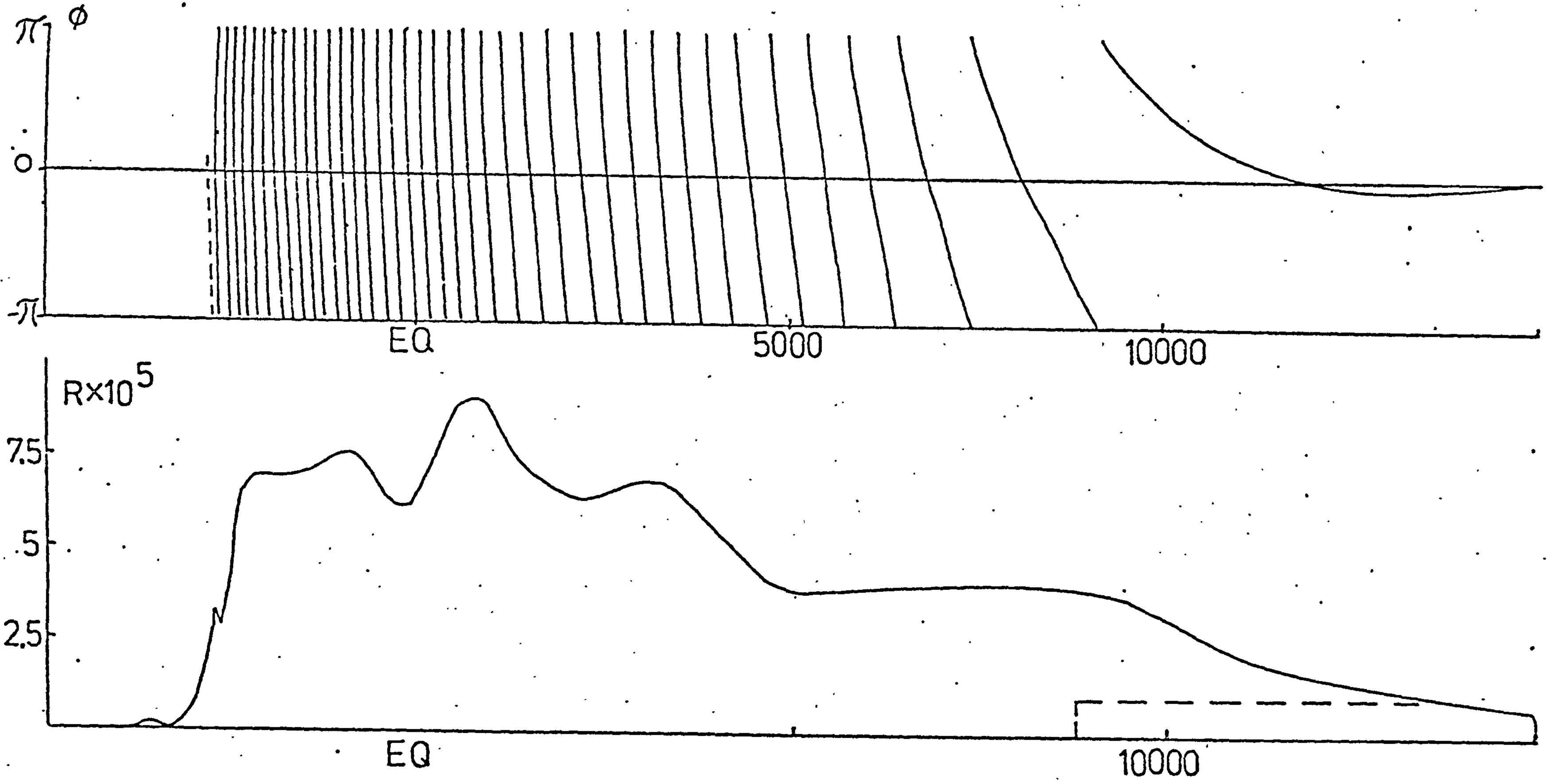

Fig.11.8

11.5 (Contd) to smooth the wavefield at every time step considered. The main instability is concerned with the growth of signal sidebands which, once excited, destroy the resonant current J_{res} as it is no longer dominated by a bunch of trapped particles and the model breaks down. 'Heavy numerical smoothing and the careful choice of triggering pulses' are two means whereby the instability can be controlled. It is not made very clear what impact this has on the results and whether more subtle techniques can be found to overcome this problem.

Nunn gives an example of a large amplitude riser which is triggered by a short morse pulse of about 60 ms duration. The original pulse is square and of normalised amplitude = 1. It is introduced from the left of the diagrams at time t = 0. Fig. 11.3 shows the wave-field intensity and resonant currents at t = 7500. In each case the ordinate is the distance along the field line from the geomagnetic equator in arbitrary units.

Note in Fig. 11.3 that as the trapped particles leave the morse pulse they become untrapped, both the inphase and out of phase currents tend to zero and the additional phase of the wave increases. In the second diagram Fig 11.4 we see the winding up of the phase continues and that a resonant particle now sees a steady acceleration of phase $\dot{\emptyset}$ to the left of the equator. By Figs. 11.5 & 11.6 at t =15000 a quasistatic generation region has established itself on the left of the equator. Nunn shows that as a result of the second differential of $\emptyset$ with z being constant the resonant particle current vector and the wave field vectors remain synchronised down to very small values of R. Nunn states that this condition which occurs at the low amplitude end of the generation region is Helliwell's linear generation condition. He emphasises that the Helliwell condition is applied at the point where the particles fall out of resonance and not at the centre of the generation region. Figs. 11.7 and 11.8 show the state of the generation region at t = 20000 where the wave frequency at the low power end (where Helliwell's linear theory applies) is several tens of Hz above the original frequency of the morse pulse.

11.5 (Contd) Nunn goes on to consider the application of the computer model to questions such as the length of morse pulse which is required at certain amplitudes before a triggered emission can be generated and the initial frequency offset between morse pulse and riser.

However the main point of describing this work is to show that although Helliwell's phenomenological theory can explain the generation of discrete emissions it remains a very simplified picture of what is a most complicated and fascinating phenomenon. Nunn indicates that the generation or interaction region grows along the field line and occupies many hundreds of km close to the geomagnetic equator. In the Helliwell picture the interaction region is seen to be smaller and to move over distances large compared to its length. It is clear that the full understanding of the physics of generating narrowband discrete VLF emissions is yet to be realised and that work on this interesting problem will continue apace.

APPENDIX 1

A1.1 CALCULATION OF SIGNAL & NOISE OUTPUT FROM EQUIVALENT CIRCUIT FIG. 3.5

Consider the equivalent circuit showing the noise generators in Fig. 3.5. The following is to derive the transfer functions T_p for the circuits shown in Fig. A1.1 where the noise generators have been separated. The transfer function for the signal source is identical to that derived for the E_{n1} noise source.

The series signal & noise sources.

From Fig. A1.1a and using Equation (3.5.1) we have;

$$V_{out} = E_{n1} \cdot \frac{\frac{R_p}{1 + j\omega CR_p}}{R_s + j\omega L + \frac{R_p}{1 + j\omega CR_p}}$$

$$= E_{n1} \cdot \frac{R_p}{(R_s + j\omega L)(1 + j\omega CR_p) + R_p}$$

$$= E_{n1} \cdot \frac{R_p((R_s+R_p - \omega^2 LCR_p)-j\omega(L+CR_pR_s))}{(R_s+R_p-\omega^2 LCR_p)^2+\omega^2(L+CR_pR_s)^2}$$

$$= E_{n1} \cdot \frac{(R_pR_s+R_p^2-\omega^2 LCR_p^2)-j\omega R_p(L+CR_pR_s)}{(R_s+R_p-\omega^2 LCR_p)^2 +\omega^2(L + CR_pR_s)^2}$$

Taking the real part (R) and the imaginary part (I) of the above equation we have;

A1.1.1
$$|V_{out}| = \sqrt{\frac{(4KTBR_s)((R_pR_s+R_p^2-\omega^2 LCR_p^2)^2+\omega^2 R_p^2(L+CR_pR_s)^2)}{(R_s+R_p-\omega^2 LCR_p)^2 +\omega (L+CR_pR_s)^2}}$$

Fig A1.1

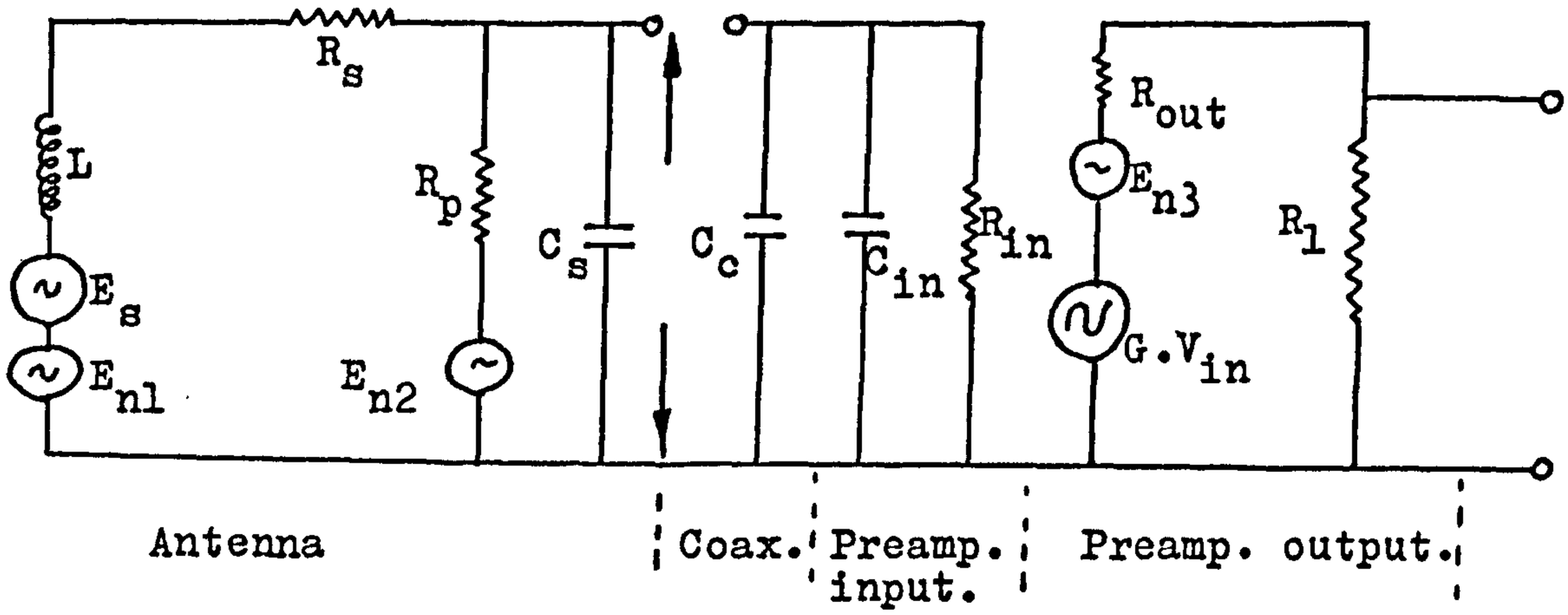

Fig.A(1.1a)

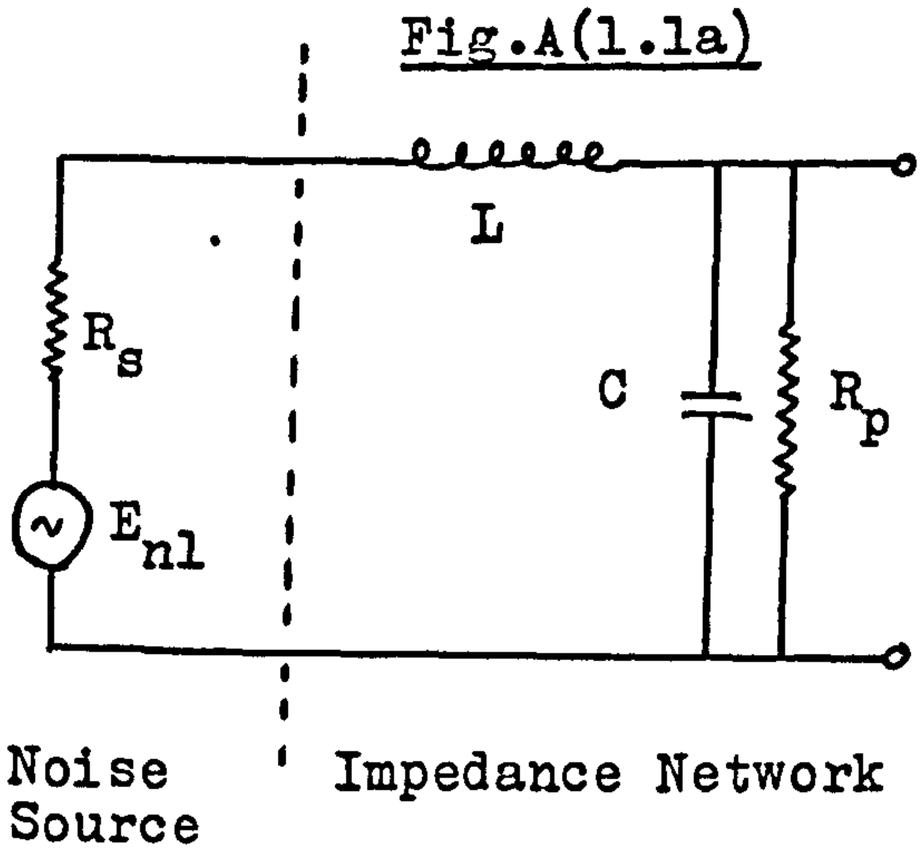

List of Knowns.

$R_p > R_s$

$C_s > C_c > C_{in}$, $(C_s + C_c + C_{in} = C)$

$R_{in} \approx 100\ M\Omega \gg R_p > R_s$

$E_{n2} > E_{n1} \gg E_{n3}$

$R_{in} = 100\ M\Omega$, $C_{in} = 14$ pf

$G = 60$ db .

Preamp frequency response:

$\pm$ 1db from 10Hz to 100 KHz.

Fig A(1.1b)

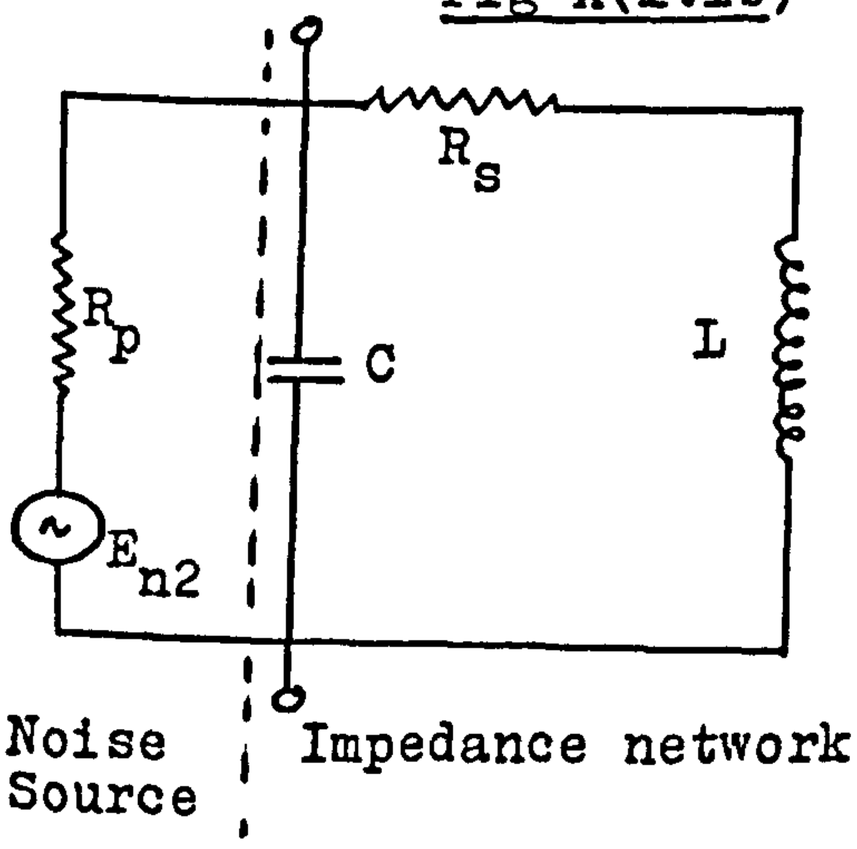

When $\omega = 0$ and $R_p = R_s$ then equation A(1.1,1) reduces to;

$$V_{out} = E_{n1} \cdot \frac{/ \ (R_p R_s + R_p^2)^2}{(R_s + R_p)^2} = E_{n1} \cdot \frac{R_p}{R_p + R_s}$$

$$V_{out} = R/2R$$

$$V_{out} = \tfrac{1}{2} E_{n1} \text{ , which is true.}$$

<u>The parallel noise source.</u>

From Fig A1.1b and using (3.5.1) we see that;

$$V_{out} = E_{n2} \cdot \frac{\left[\dfrac{R_s + j\omega L}{1 - \omega^2 LC + j\omega C R_s} \right]}{\left[R_p \dfrac{+ R_s + j\omega L}{1-\omega^2 LC + j\omega C R_s} \right]}$$

$$= E_{n2} \cdot \frac{(R_s + j\omega L) \cdot (R_p + R_s - \omega^2 LCR_p - j\omega(L + CR_p R_s))}{(R_p + R_S - \omega^2 LCR_p) + \omega^2 (L + CR_p R_s)^2}$$

Expanding the Numerator in two parts:

$$(1) = R_s R_p + R_s^2 - \omega^2 LCR_p R_s + j\omega L(R_p + R_s) - j\omega^3 L^2 CR_p$$

$$(2) = -j\omega R_s (L + CR_p R_s) + \omega^2 L(L + CR_p R_s)$$

Taking real and imaginary parts of the numerator we have:

$$(R)_{num.} = R_s R_p + R_s^2 + \omega^2 L^2$$

$$(I)_{num.} = j\omega(L(R_p + R_s) - \omega^2 L^2 CR_p - R_s(L + CR_p R_s))$$

$$\text{So } |V_{out}| = \frac{\sqrt{(4KTBR_p) \cdot ((R_s R_p + R_s^2 + \omega^2 L^2)^2 + \omega^2 (L(R_p + R_s) - \omega^2 L^2 CR_p - R_s (L + CR_p R_s))}}{(R_p + R_s - \omega^2 LCR_p)^2 + \omega^2 (L + CR_p R_s)^2}$$

which is equation A(1.1,2)

Again $\omega = 0$ and $R_p = R_s$ equation A(1.1,2) reduces to;

$$V_{out} = E_{n2} \cdot \frac{1}{2} \quad \text{as before.}$$

A1.2 SIGNAL & NOISE CALCULATIONS FOR 'NEW' EQUIVALENT CIRCUIT.

The circuit is shown in Fig A1.2 and we consider first the noise output from R_1.

Let the impedance of the parallel combination of C_1 & R_p = Za

$$\text{Then Za} = \frac{R_p}{1 + j\omega C_1 R_p}$$

Let the series combination of R_s and Za = Zb, then Zb is given by;

$$Zb = \frac{R_s(1+j\omega C_1 R_p) + R_p}{1 + j\omega C_1 R_p}$$

Let the impedance of the parallel combination of Zb and L be Zc

$$\text{where Zc} = \frac{j\omega L(R_p + R_s)\ 1 + j\omega C_1 R_p))}{R_p + R_s(1+j\omega C_1 R_p) + j\omega L(1+j\omega C_1 R_p}$$

If the impedance of the series combination of R_1 & C_s = Zd and

$$Zd = \frac{1+j\omega C_s R_1}{j\omega C_s}$$

$$\text{Then} \qquad V = V_{\cdot} \cdot \left[\frac{Zc}{Zc + Zd} \right]$$

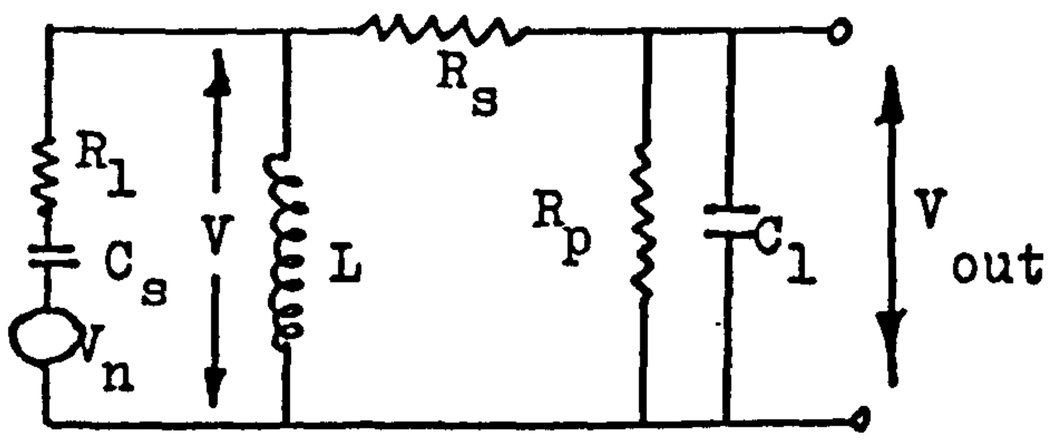

FigA1.2

Noise output from R_1

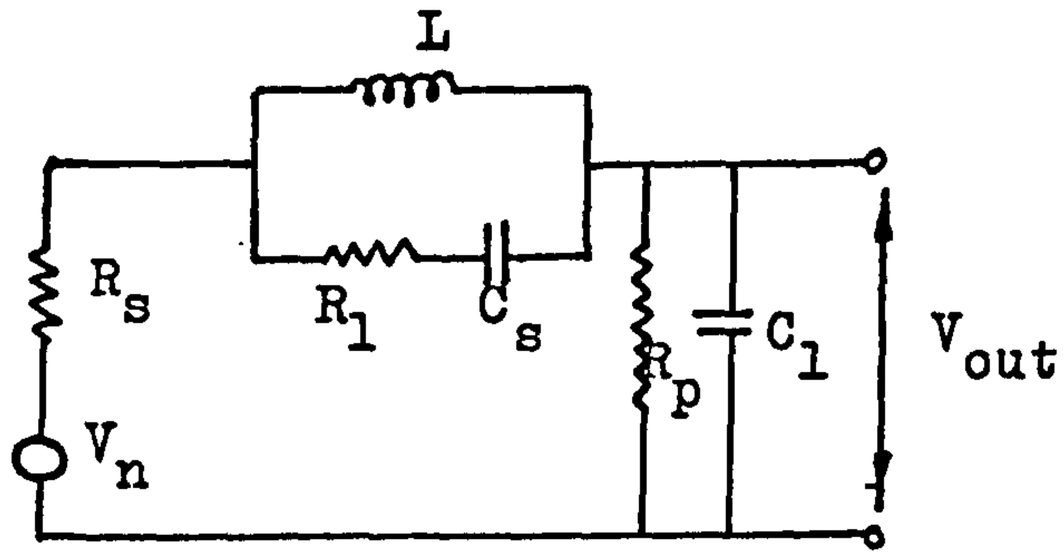

Fig A1.2a

Noise output from R_s

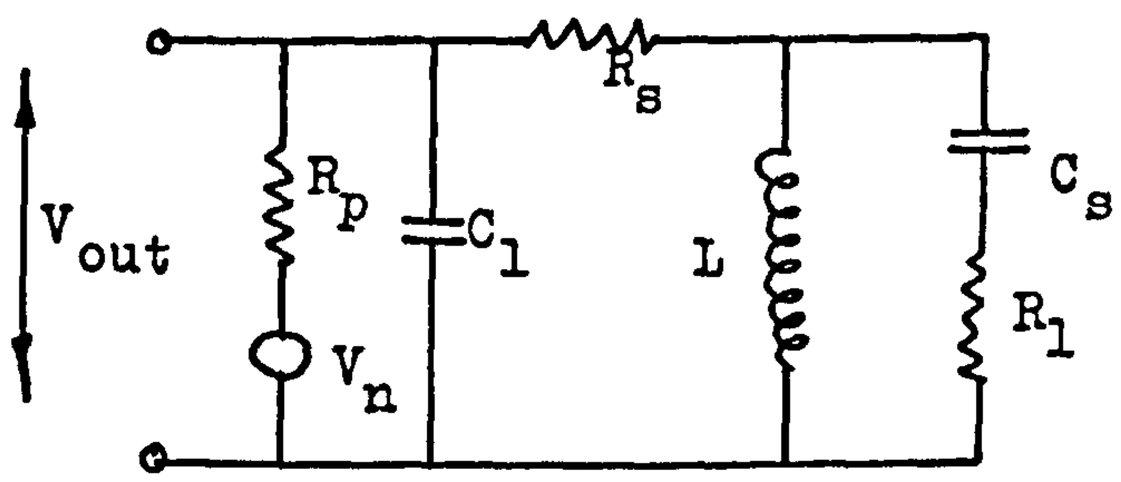

Fig A1.2b

Noise output from R_p

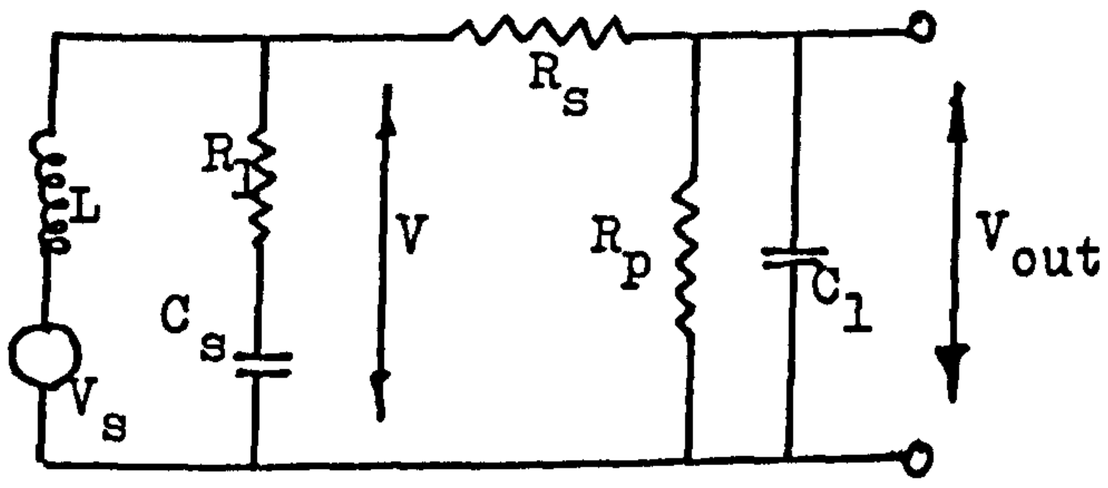

Fig A1.2c

Signal output.

Fig A1.2

Now let $A = 1+j\omega C_s R_1$

$B = 1+j\omega C_1 R_p$

& $C = R_p + R_s(1+j\omega C_1 R_p)$

Then it can be shown that ;

$$V = V_n \cdot \frac{\omega^2 L C_s C}{\omega^2 L C_s C - A(j\omega LB+C)}$$

It can also be shown that;

$$V_{out} = V \cdot \frac{R_p}{C}$$

and therefore that;

$$V_{out} = V_n \cdot \frac{\omega^2 LC_1 R_p}{\omega^2 LC_s C - A(j\omega LB+C)} \qquad (A1.2,1)$$

This equation is programmed into the computer using Fortran CMPLX function which means that it does not have to be reduced to determine V_{out} as previously.

We now deduce the noise output from R_s using the circuit shown in Fig. A1.2a.

Let the impedance of the network containing R_1, C_s & L = Za where

$$Za = \frac{j\omega L\ (1+j\omega C_s R_1)}{(1+j\omega C_s R_1) - \omega^2 LC_s}$$

Let the impedance of R_s & Za = Zb which is given by;

$$Zb = \frac{R_s A - \omega^2 LC_s R_s + j\omega LA}{A - \omega^2 LC_s}$$

Where $A = 1 + j\omega C_s R_1$

Let the impedance of the parallel combination of R_p & C_1 = Zc

where $Zc = \frac{R_p}{1 + j\omega C_1 R_p}$

So that the impedance seen by the noise source is Zd which is given by;

$$Zd = \frac{R_s AB - \omega^2 LC_s R_s B + j\omega LAB + R_p(A - \omega^2 LC_s)}{B(A - \omega^2 LC_s)}$$

where $B = 1 + j\omega C_1 R_p$

Now $V_{out} = V_n \cdot \frac{R_p/B}{Zd}$

and if $D = \omega^2 LC_s$ & $E = R_s + j\omega L$, then it can be shown that:

$$V_{out} = V_n \cdot \frac{R_p(A - D)}{ABE + R_p(A - D) - D} \qquad (A1.2,2)$$

This equation is also programmed, as are the following two for noise from R_p and signal output using the complex manipulation routine available in 1900 series FORTRAN

Noise from R_p.

Consider the circuit given in Fig A1.2b.

Let the impedance of the series R_1 & C_s = Za, then:

$$Za = A/\ j\omega C_s$$

The impedance of the R_1, C_s & L network is Zb

$$Zb = \frac{j\omega LA}{A-\omega^2 LC_s}$$

and when in series with R_s becomes;

$$Z_c = \frac{j\omega LA + R_s(A - \omega^2 LC_s)}{A - \omega^2 LC_s}$$

Then with Zc in parallel with C_1 the impedance becomes Zd where

$$Zd = \frac{j\omega LA + R_s(A-D)}{j\omega C_1 R_s(A-D) - (AS) + A - D}$$

where $S = \omega^2 LC_1$

Now $V_{out} = V_n . \frac{Zd}{Zd + R_p}$

which can be shown to give;

$$V_{out} = V_n . \frac{j\omega LA + R_s(A-D)}{R_p(A-D)(1+j\omega C_1 R_s) - AS.R_p} \qquad (A1.2,3)$$

The following is the calculation of the signal transfer function and it should be noted that it is not the same as that for R_s which it was in the simple equivalent circuit.

From Fig A1.2,4 we see that the impedance of R_p & C_1 in parallel can be given by ;

$$Za = \frac{R_p}{B}$$

and that for the series $R_1 C_s$ by;

$$Zb = \frac{A}{j\omega C_s}$$

The impedance seen by the inductor becomes Zc which is given by;

$$Zc = \frac{AC}{AB + j\omega C_1.C}$$

Now $$V = V_s \cdot \frac{Zc}{j\omega L + Zc}$$

amd $$V_{out} = V \cdot \frac{R_p}{C}$$

So $$V_{out} = V_s \cdot \left[\frac{R_p A}{j\omega L.AB - \omega^2 LC_s C + AC} \right] \quad (A1.2,4)$$

APPENDIX 2

A2.1 Equivalent Circuit Noise Calculations

PROGRAMS P90P, P90C and P90S calculate the noise and signal output from the antenna equivalent circuit for noise source R_p, R_s and the signal source respectively. The form of the programme is similar in each case and a general program will be given here.

PROGRAM P90X (X = P,C or S)

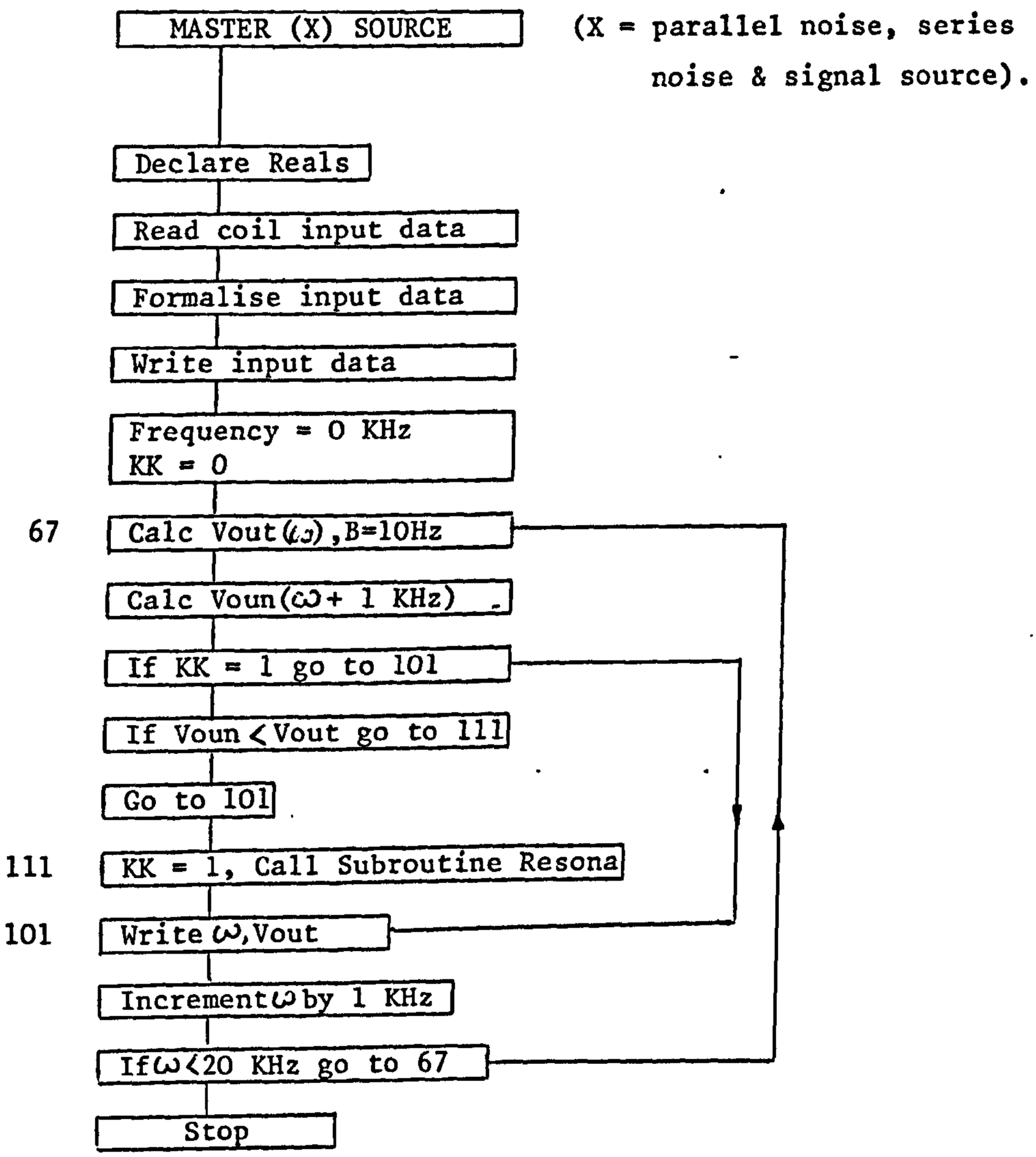

SUBROUTINE RESONA

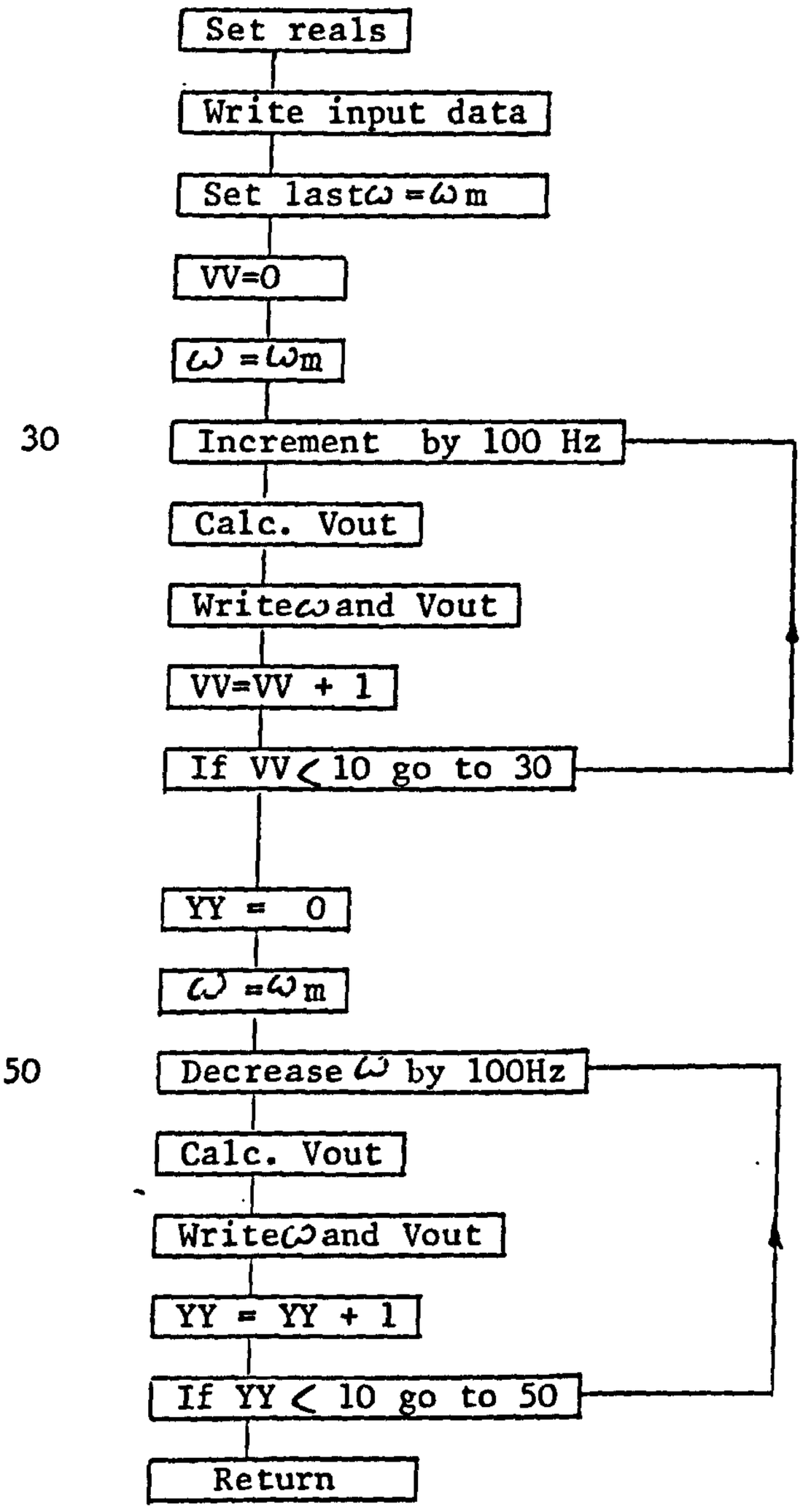

The program calculates the signal or noise output every 1KHz from 0Hz to 20 KHz and will after having discovered a resonance peak produce close spaced outputs every 100Hz from $F_{res} \pm$ 1KHz.
The three programs which constitute the suit enable the noise and minimum detectable signal characteristics to be produced.

A2.2 New Equivalent Circuit Signal & Noise Calculations

Programs P90C,N_1,N_2 & N_3 were written to calculate the signal output & the noise output from R_p, R_s and R_1 individually. Program P90S calculates all above mentioned quantities and then proceeds to calculate the minimum detectable signal which would be observed by the antenna. The structure of the first four programs are similar and an outline flow chart is given below.

PROGRAM P90X

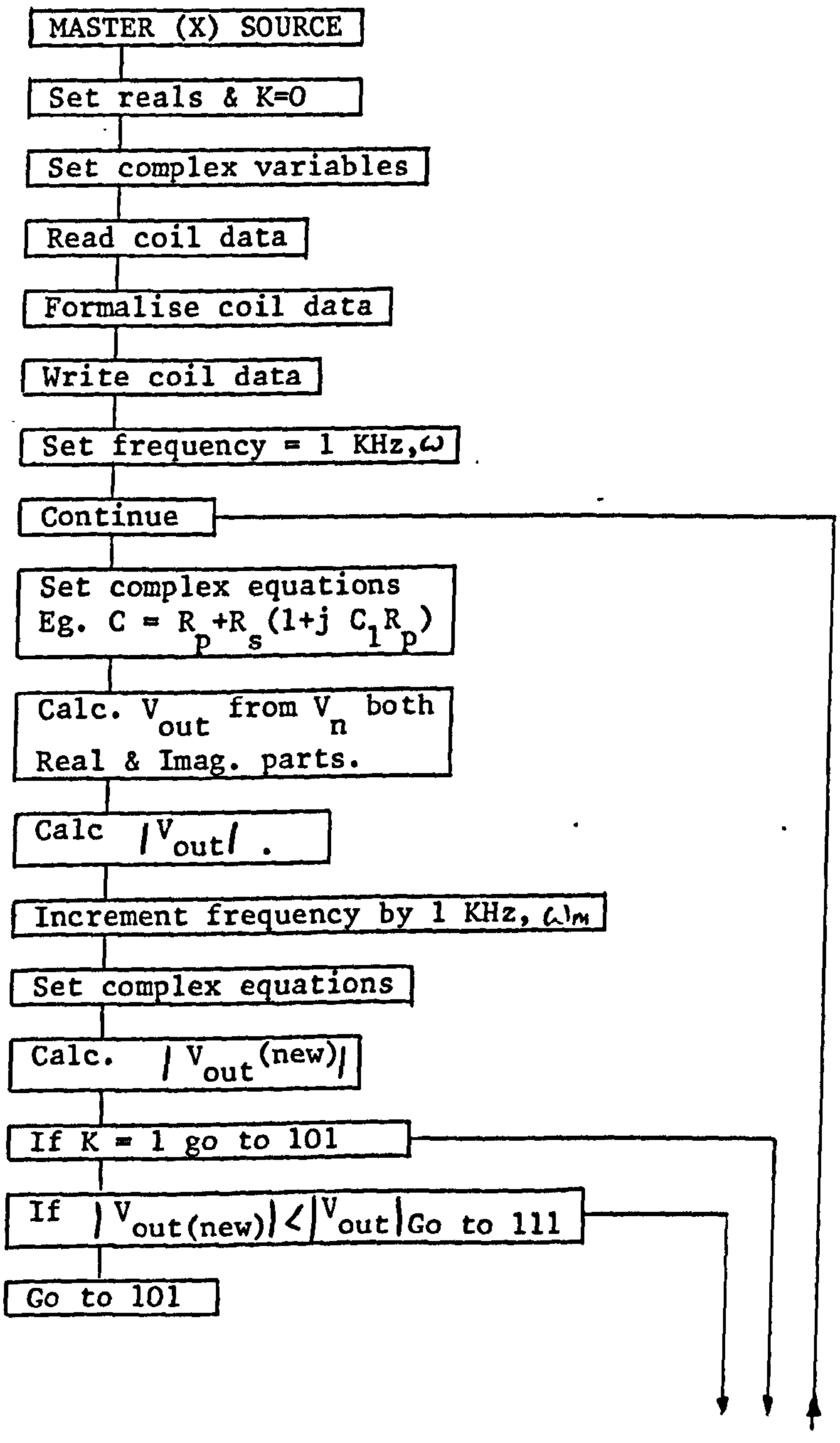

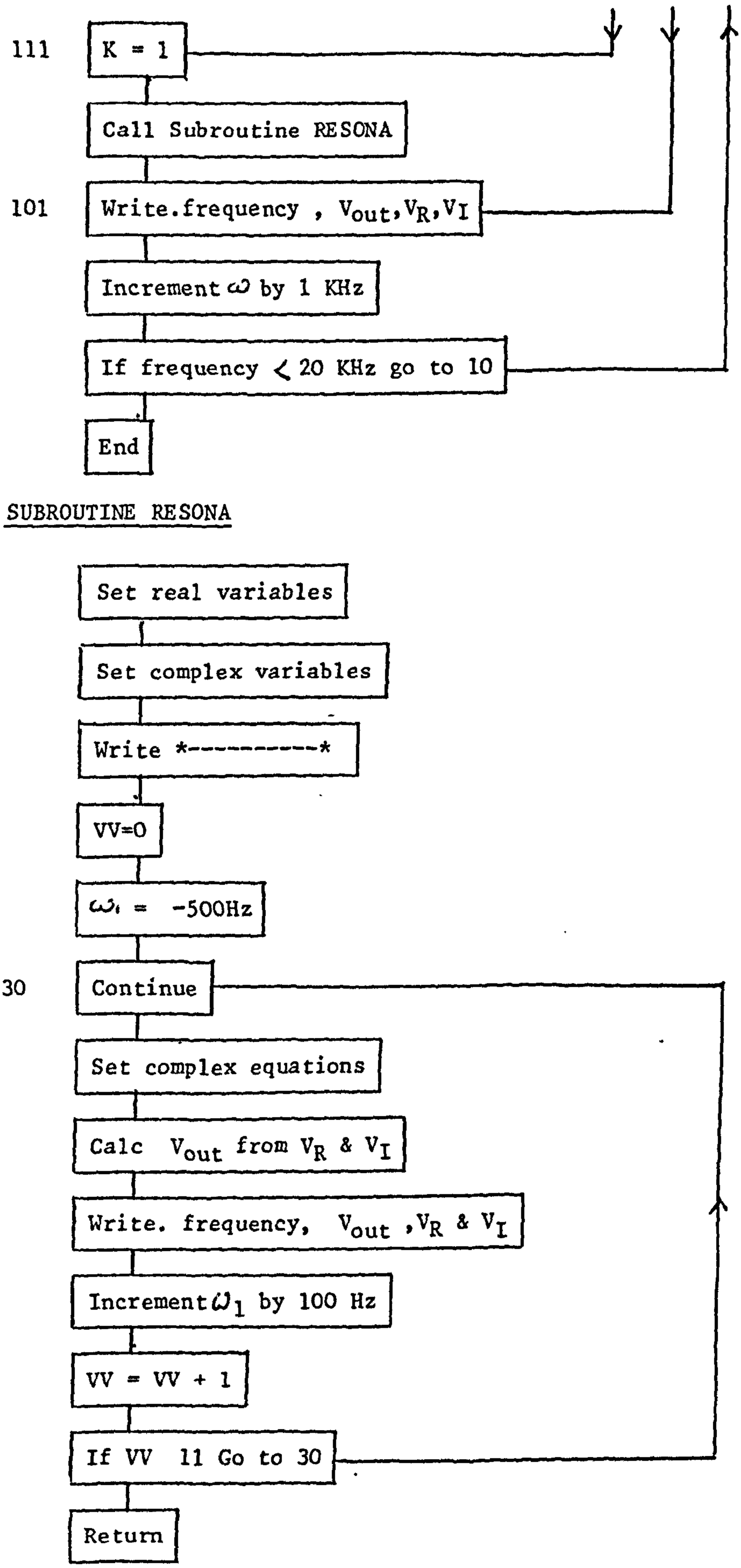

SUBROUTINE RESONA

Given below is a flow chart for program P90S which calculates each of the items required in order that the minimum detectable signal may be determined.

PROGRAM P90SMASH

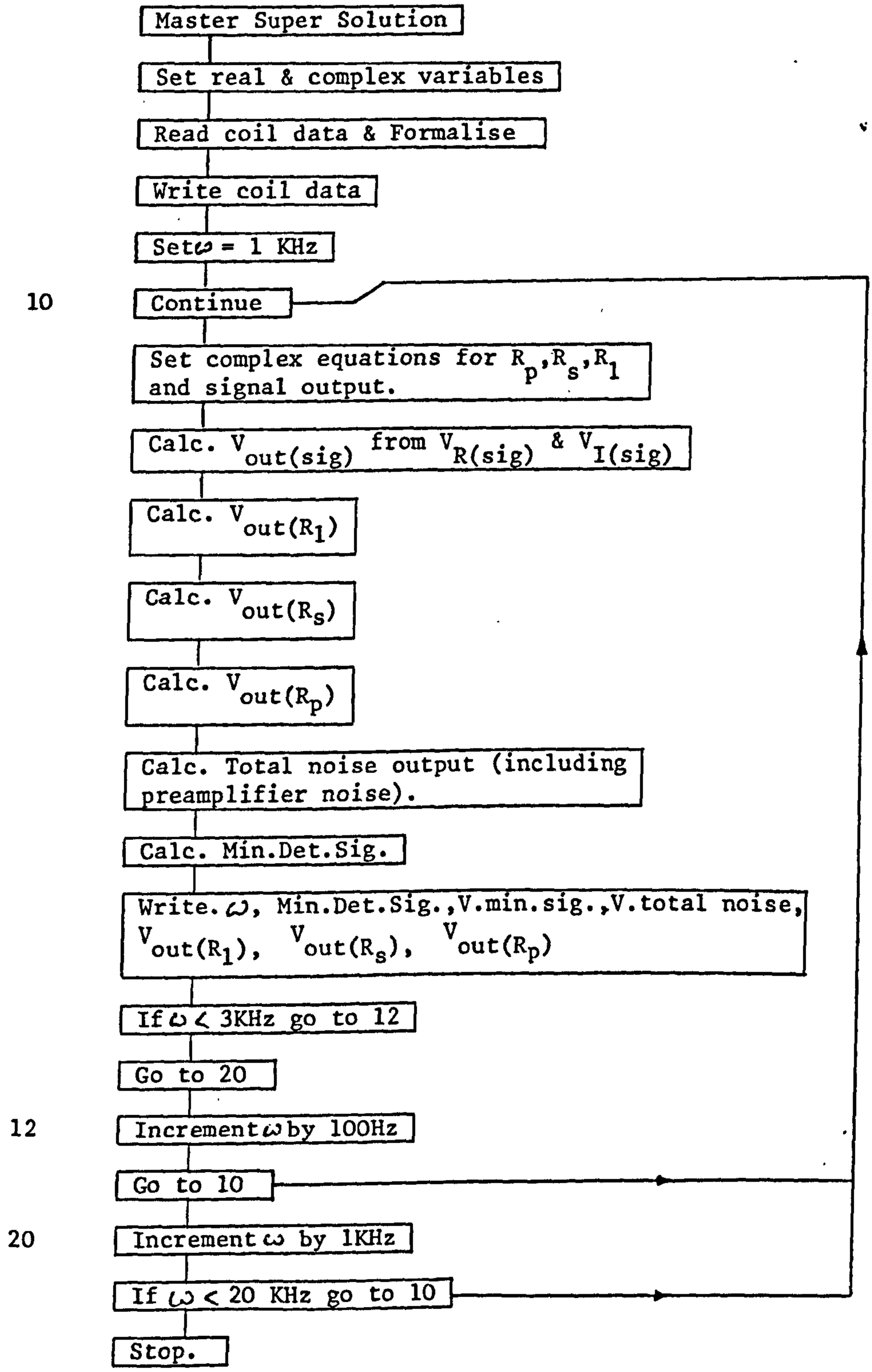

A2.2 SOME PROGRAMS USED IN THE CALCULATIONS BASED ON HELLIWELLS PHENOMELOGICAL THEORY

During the development of a suit of computer programs designed to perform calculations of emitted whistler mode signals based on the second reasonance condition applied to interacting electrons and RH circularly polarised waves, many programs and variations of programs are generated. It is clearly not possible to present all the logic and flow charts which are necessary for a good understanding of the development of the final suit of programs. The major points in the development are clearly stated in the text and therefore only certain additional explanations are given in the form of flow charts for the program.

These programs are a sample of the work done at each stage of the development.

(1) Program P(90 SUPERDOWDEN) An initial attempt at the solution of the problem.

(2) Programs P(90 CANT & TIRED) Showing how the 2nd reasonance condition equation may be solved with a golden section search.

(3) The distance calculation which uses the search and is a sub-routine which is called in all subsequent programs.

(4) Programs P(90 TIMESUP & ELEPH.) Samples of about 5 variations of the final program which tracks emissions back to their source.

Many programs such as the reconstitution programs have been omitted entirely. The complete set of final and development programs can be obtained from the UNIVERSITY OF SHEFFIELD together with program listings.

Program P90SUPERDOWDEN

A simplified logic flow chart is given which shows the organisation of the calculation of emissions which are generated by Dowden's Doppler shifted Cyclotron mechanism.

MASTER HARD DOWDEN

Dimention arrays, set reals, set constants.

100 Read start data (ϕ_o, ϕ_{start}, f_{ho}, f_{no}, & E)

Write input data.

Calculate TARC. from ϕ_o

Calculate TRAC from ϕ_{start}

Calculate f_{hstart}, and f_{nstart}.

Write ϕ_o, ϕ_{start}, TARC, TRAC, S, f_{hstart}, f_{nstart}.

Calculate v_{11} at ϕ_{start}.

Solve the Cubic for f_{start}.

Calculate v_g at ϕ_{start} (from f_{start})

Write v_{start}, v_{gstart}, and energy E

GO TO 654

30 Decrement ϕ by 2^o (Emission is in observers hemisphere.)

Calculate f_h, f_n, v_{11}.

Solve cubic for f

Calculate the distance S to ϕ

654 Set the no. of steps in the numerical integration according to distance S.

Calculate group delay for f from S to obs. (TIME)

Calculate the electron travel time from previous ϕ to new ϕ. (TSUM)

Accumulate total electron travel time delay (T2)

Calculate total time delay to date T3 = T2 + TIME

887 Write f,T3,T2,TIME,S,Ø

Plot f against T3

If (Ø 0) go to 70

Go to 30

C Calculate the form of the emission on the (S +ve) side of the equator

$Ø = Ø + 2^{o}$

If ($Ø$ 30^{o}) go to 99

Calculate f_h, f_n, v_n.

Solve cubic for f

Select numerical integration steps.

Calculate v_g for f at Ø (Ø for S + ve)

Calculate group delay from Ø to equator for f (TIMEP)

Calculate delay from equator to observer (TIMEE)

111 Continue

Set whistler delay time at frequency f = 2xTIMEE

Calculate TSUM for electron time delay on (S+ve side of equator)

Accumulate T2 (Total electron travel time delay

Calculate total delay to date T3=T2+TIMEP+TIMEE

Go to 887 (to print out results)&(Plot emission profile)

99 Plot whistler profile

Write whistler data, f & 2xTIMEE

999 STOP

P90 TIRED

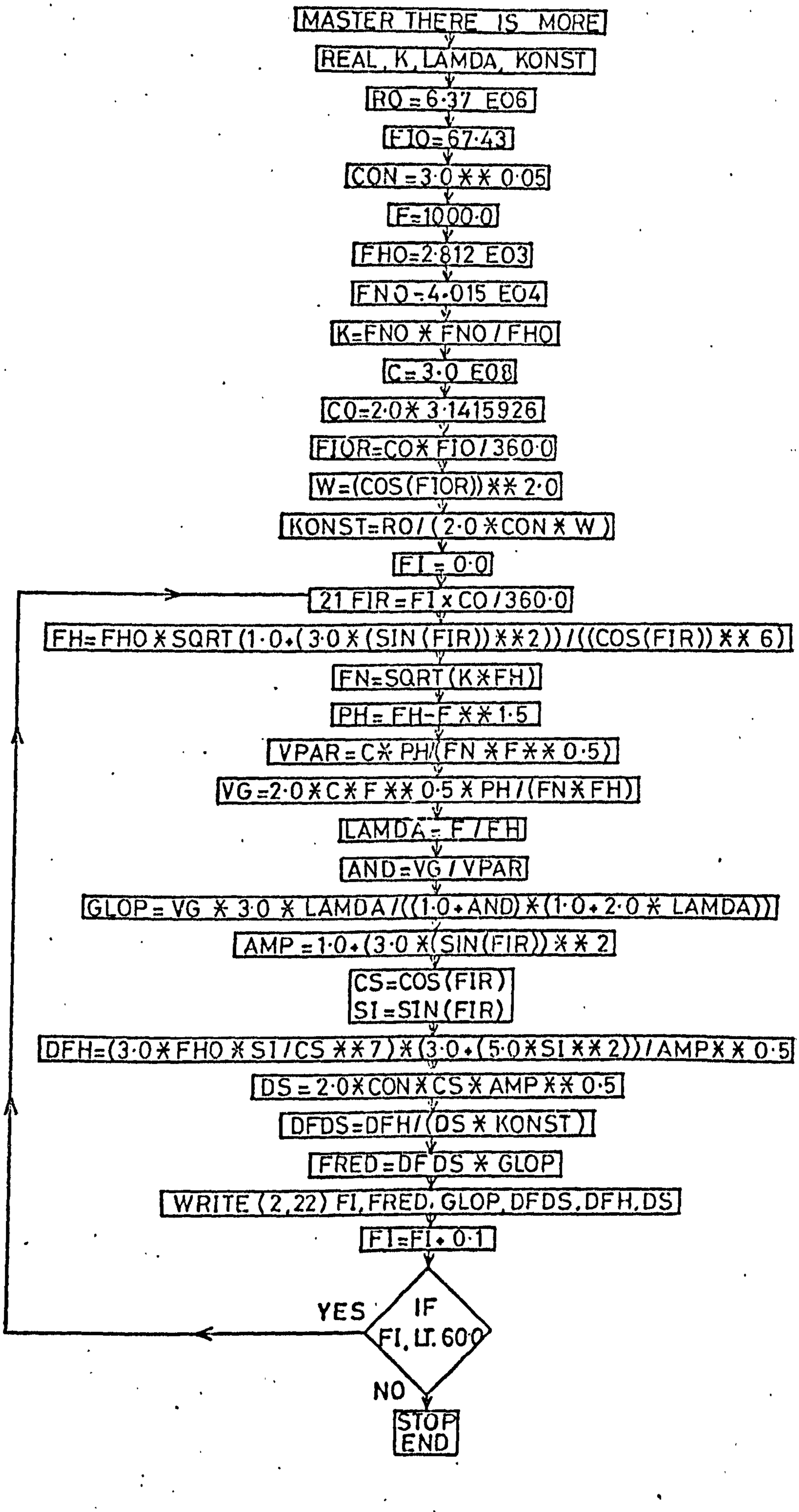
MASTER THERE IS MORE
REAL, K, LAMDA, KONST
RO = 6·37 E06
FIO = 67·43
CON = 3·0 ** 0·05
F = 1000·0
FHO = 2·812 E03
FNO = 4·015 E04
K = FNO * FNO / FHO
C = 3·0 E08
CO = 2·0 * 3·1415926
FIOR = CO * FIO / 360·0
W = (COS(FIOR)) ** 2·0
KONST = RO / (2·0 * CON * W)
FI = 0·0
21 FIR = FI x CO / 360·0
FH = FHO * SQRT (1·0 + (3·0 * (SIN (FIR)) ** 2)) / ((COS(FIR)) ** 6)
FN = SQRT (K * FH)
PH = FH - F ** 1·5
VPAR = C * PH / (FN * F ** 0·5)
VG = 2·0 * C * F ** 0·5 * PH / (FN * FH)
LAMDA = F / FH
AND = VG / VPAR
GLOP = VG * 3·0 * LAMDA / ((1·0 + AND) * (1·0 + 2·0 * LAMDA))
AMP = 1·0 + (3·0 * (SIN(FIR)) ** 2
CS = COS (FIR)
SI = SIN (FIR)
DFH = (3·0 * FHO * SI / CS ** 7) * (3·0 + (5·0 * SI ** 2)) / AMP ** 0·5
DS = 2·0 * CON * CS * AMP ** 0·5
DFDS = DFH / (DS * KONST)
FRED = DFDS * GLOP
WRITE (2,22) FI, FRED, GLOP, DFDS, DFH, DS
FI = FI + 0·1
YES
IF FI, LT. 600
NO
STOP
END

P90 CANT

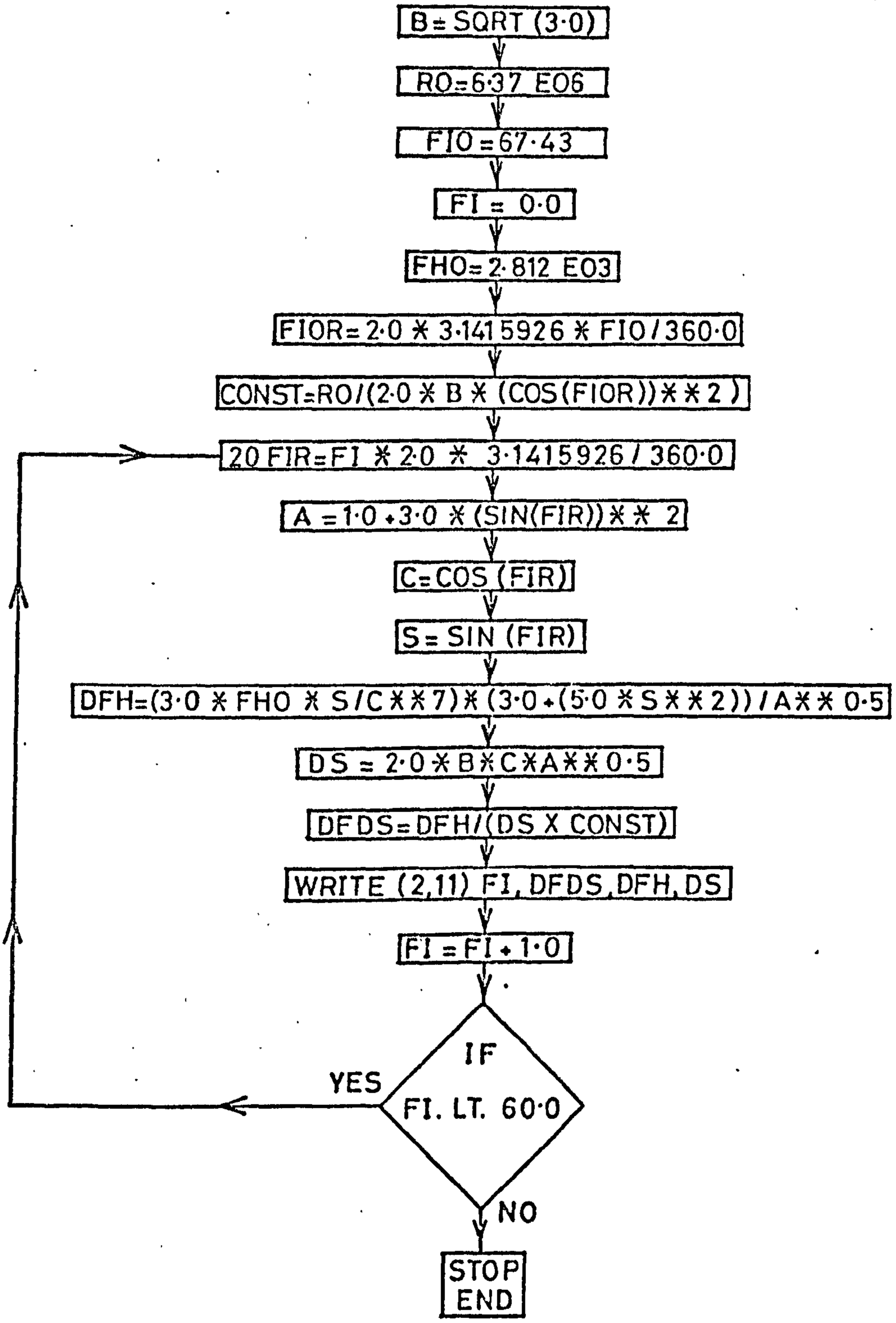
B = SQRT (3·0)
RO=6·37 E06
FIO = 67·43
FI = 0·0
FHO = 2·812 E03
FIOR = 2·0 * 3·1415926 * FIO / 360·0
CONST=RO/(2·0 * B * (COS(FIOR))**2)
20 FIR=FI * 2·0 * 3·1415926 / 360·0
A = 1·0 + 3·0 * (SIN(FIR))** 2
C=COS (FIR)
S = SIN (FIR)
DFH=(3·0 * FHO * S/C**7)*(3·0+(5·0 * S**2))/A** 0·5
DS = 2·0 * B * C * A** 0·5
DFDS=DFH/(DS X CONST)
WRITE (2,11) FI, DFDS, DFH, DS
FI = FI + 1·0
IF
FI. LT. 60·0
YES
NO
STOP
END

DISTANCE CALCULATION

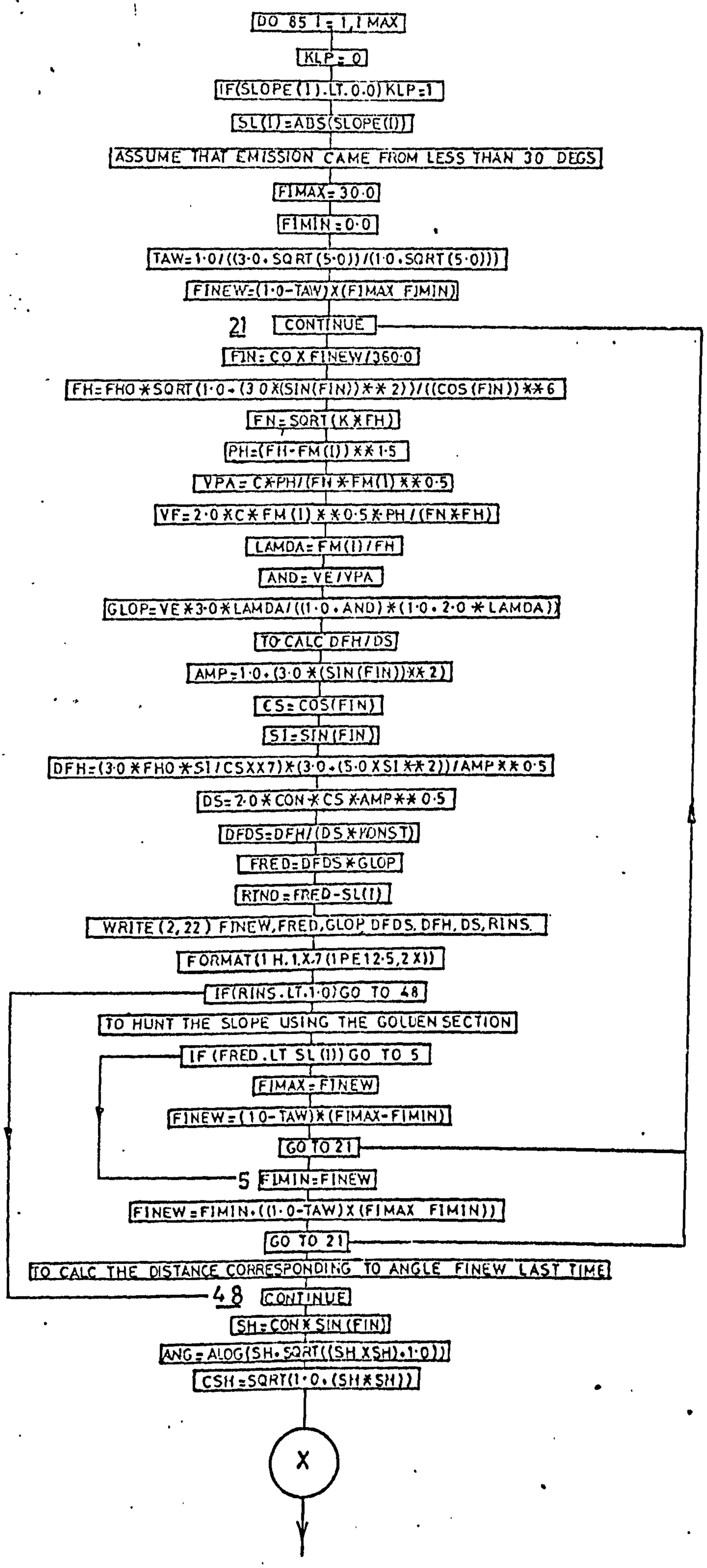

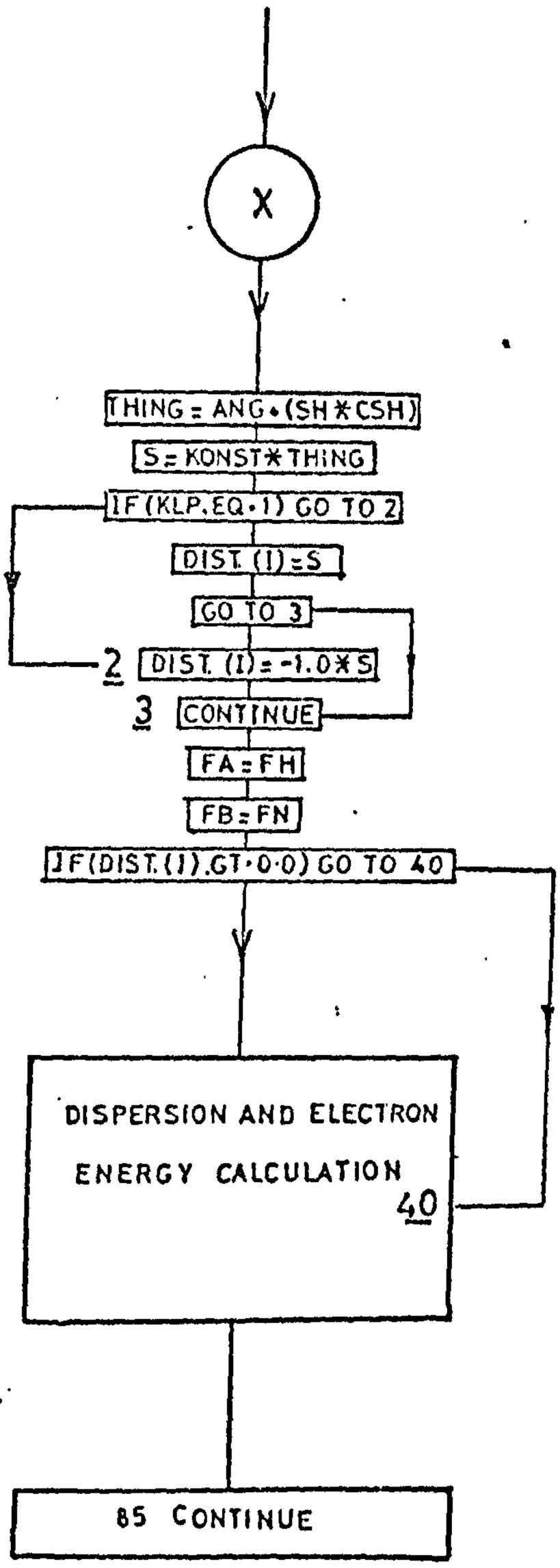
X
THING = ANG•(SH*CSH)
S = KONST*THING
IF (KLP.EQ.1) GO TO 2
DIST. (I) = S
GO TO 3
2
DIST. (I) = -1.0*S
3
CONTINUE
FA = FH
FB = FN
IF(DIST.(I).GT.0.0) GO TO 40
DISPERSION AND ELECTRON
ENERGY CALCULATION
40
85 CONTINUE

P9OELEPH.

START

READ IN DATA.
Time & frequency cordinates of points on the received emission profile.

CALCULATE EQUATORIAL EMISSION PROFILE.
Remove the effects of dispersion along the path from the observer to the equator.Perform a numerical integration Do for Imax points.

PLOT EQUATORIAL EMISSION PROFILE.
A 12" CALCOMP graph plotter is used to record the frequency time profile which would be observed at the top of the field line.

FIT POLYNOMIAL TO THE EQUATORIAL PROFILE.
A 4th order polynomial is fitted to the data points which represent the equatorial profile.The polynomial coefficients are determined.

PRODUCE POLY.FIT PROFILE.
Equatorial emission times are used to obtain poly.fit frequency values.These are stored in an arrayFM(I).The equatorial times & frequencies are stored in KORTIME(I) ,FR(I) repectivly.

THE SLOPES OF THE EMISSION ARE OBTAINED.
The expression for the 4th order polynomial is differentiated at points KORTIME(I) and FM(I) and the result is stored in SLOPE(I).

THE DISTANCE CALCULATION IS PERFORMED.
Given values of slope,frequency,L value & equatorial electron density the geomagnetic latitude of the interaction region is calculated. Then the distance from the top of the field line to the interaction region is calculated.
This section is nested in a DO loop labled DO 85 I=1,Imax.

ROUTE SWITCHING DESCISION.
Different dispersion correction calculations are performed next depending on the location of the interaction region in one or the other hemisphere.

1

1

CALCULATE DISPERSION CORRECTION IN
THE OBSERVERS HEMISPHERE.
A numerical integration is performed
along the field line from the equator
to the appropriate position.The
correction is applied.The new time
cordinate is CORTIM(I),the frequency
FM(I) is unchanged.
GO TO /////

CALCULATE DISPERSION CORRECTION IN
THE OTHER HEMISPHERE.
Again a numerical integral is arrived at
and used to give a corrected time cordinate.
Time stored in CORTIM(I) & frequency in FM(I).

/////

CALCULATE PARALLEL VELOCITY OF REASONANT
ELECTRONS. ALSO CALC. ENERGY OF ELECTRONS
A particular pitch angle is assumed in
calculating the energy of reasonant
electrons.Results stored in VPAR(I) &
EN(I).

85 CONTINUE.

WRITE OUT RESULTS.
Write poly.frequency,equatorial time,
slope, distance,true time,parallel
velocity and electron energy.

CALCULATE A SMOOTHED DISTANCE -TIME
CURVE.
A two point running mean smoothing
operation is performed.Results for
time & distance are stored in
TUMP(I) & CLUMP(I).

CALCULATE VELOCITY OF THE INTERACTION
REGION.
Difference differentiation is performed
on the smoothed distance -time curve.
Results in VI(I) & CORTIMM(I).

CALCULATE A SMOOTHED VELOCITY TIME CURVE.
A three point running mean smoothing
process is used.Results in VII(I) &
CORTIMM(I).

WRITE OUT RESULTS.
Write time for (VI),unsmoothed velocity,
true time,group velocity,parallel velocity
& smoothed interaction region velocity.

PLOT DISTANCE - TIME GRAPH.
Plot DIST(I) - KORTIM(I)
Plot smoothed distance - time graph.
CLUMP(I) - TUMP(I).

Note.

Programs P90OLWEN & P90 SONGBIRD are basically the same as P90ELEPH. The main departure from the scheme outlined above is in the production of a smoothed velocity - time curve. The two later programs use a polynimial fit to the velocity data and smoothed velocity output is taken from this polynomial.

A

START

READ IN DATA. Cords.Time,Freq, of points on the received emission profile.

CALCULATE EQUATORIAL EMISSION PROFILE.
Remove effects of dispersion along the path from the observer to the equator.
Perform numerical integration along the field line.Do for Imax points.

B

FIT POLYNOMIAL TO EQUATORIAL PROFILE.
A 4th order polynomial is fitted to the data points which represent the equatorial emission.The coefficients are determined.

PRODUCE POLY.FIT PROFILE.Equatorial emission times are used to obtain poly.fit frequency values.These are stored in the array JANE(I) The equatorial times in X(I) and the equatorial frequencies in FM(I).

C

THE SLOPES OF THE EMISSION ARE OBTAINED.
The expression for the 4th order polynomial is differentiated at points X(I),FM(I)and the results are stored in SLOPE(I).

D

SET PARAMETERS FOR DISTANCE CALCULATION.
The data point identifier is set to 2.
The initial range of ϕ is set to 10^{o}.
Certian arrays are transfered or set.

THE DISTANCE CALCULATION IS PERFORMED.
Given values of slope,frequency,L value & equatorial electron density the geomagnetic latitude of the interaction region is calculated.Then the distance from the top of the field line to the interaction region is calculated.
Becuase the equatorial slope is used the distance (S) will be a first guess, for the data point(I=2)at the start of the emission.

E

ROUTE SWITCHING IS PERFORMED.
If we are dealing with the first data point (I=2) parameters are set such that the dispersion delay encountered from the equator to S/2 can be calculated.If we are dealing with the better estimate of S having been round the loop.Then the dispersion delay must be calculated from the equator to S.

1

1

THE DISPERSION CALCULATION IS UNDERTAKEN.
A numerical integration is performed along the field line from the equator to the appropriate position and the dispersion delay is arrived at.New time cordinate isX(I) and the frequency cordinate is transfered to the array Y(I).

F

SLOPE & DISTANCE DIFFERENCE CALCULATION.
The diference between the first & second estimates of slope and distance associated with the first point on the emission profile is calculated.
If only the first estimate has been calculated GO TO B Use new data X(I),Y(I).
If both have been calculated write out the difference in estimates.

The position of the first point(I=2) has been established.Succesive polynomial fitting and dispersion corrections follow for all points up to and including IMAX.

G

SET POINT IDENTIFIER JK=2
66 Continue
JK=JK+1

FIT A 4th ORDER POLYNOMIAL.
Parameters are set.Polynomial coefficients are evaluated.

PRODUCE A POLY.FIT PROFILE.
Write FM(I) frequency.X(I) time.These values obtained from F. Write JANE(I) the poly.fit values of frequency.

CALCULATE DIFFERENTIAL OF POLYNOMIAL.
As before in C

SET PARAMETERS FOR USE WITH DISTANCE CALC.
FIMAX= 30^{o}, I=JK, certain arrays are transfered or set.

DISTANCE CALCULATION IS PERFORMED.
As before. Result S

H

CALCULATE PARALLEL VELOCITY & ENERGY.
The parallel velocity of reasonant electrons is calculated ,a pitch angle is assumed & the energy of reasonant electrons is obtained. Results in arrays VPAR(JK) &EN(JK).

DISPERSION CALCULATION.
The dispersion delay encountered along the field line from the equator to S.The new time cordinate is X(I) the frequency is unchanged Y(I).These provide the data for the next polynomial fit. This being an 'update' on the previous one.

2

I

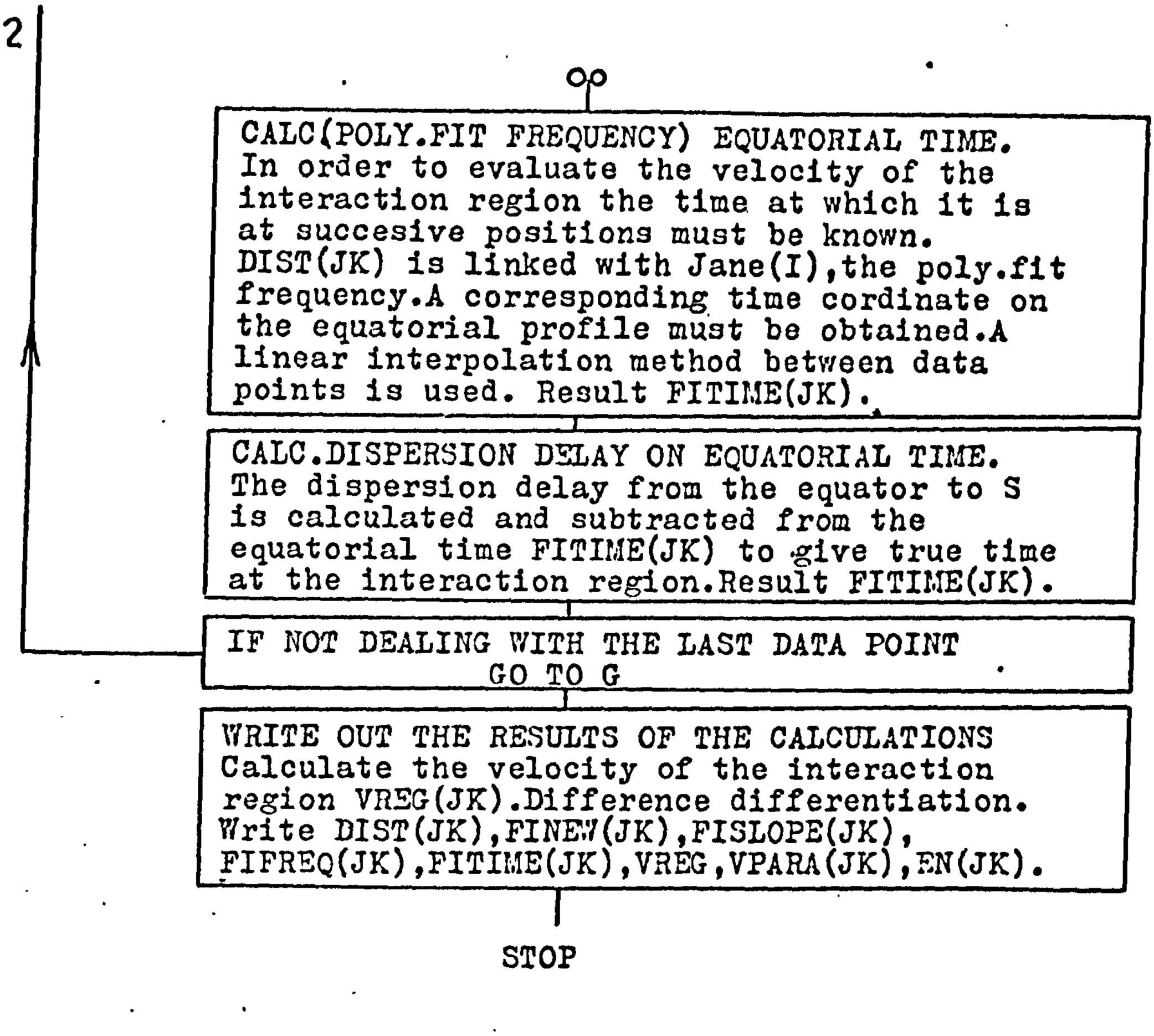

NOTE

The construction of this program is the same as that of P9OSADNESS at this general level. However differences exist as P9OT uses a COLLISIONLESS MODEL (aproximated to by R^{-4} variation of electron density with geocentric radius) & P9OS uses a GYROFREQUENCY MODEL.(which is aproximated to by an R^{-3} dependance).

APPENDIX 3

VERIFICATION OF THE PREAMPLIFIER NOISE FIGURE

Earlier in Chapter 3 a method was described for evaluating the effective input noise voltage of the high input impedance preamplifier. This method was based on the comparison of preamplifier noise and preamplifier noise plus the noise generated by a known resistor at room temperature. A figure of 1.13×10^{-8}V (for a 10 Hz Bandwidth) was derived. This appendix shows how this value may be derived from a different source thus lending support to the figure given.

Using the test method shown in Figure 3.10 the noise output from the antenna + Preamplifier and the preamplifier alone was measured, see Figure A3.1. The preamplifier noise is level over the frequency range 1 KHz to 20 KHz and is -34 db on the peak noise output at the antenna reasonance. From 5 KHz upwards the noise output tends to fall off at 6 db/octave until 10 KHz where it falls off at a slower rate possibly indicating an increasingly important contribution being made by the preamplifier noise.

Knowing the equivalent circuit and the location and output of the noise sources inthe antenna and preamplifier it is possible to calculate the noise output as a function of frequency for the system which was measured earlier. Consider Figure A3.2, here we have plotted the calculated noise output in Volts (for a 10 Hz Bandwidth) as a function of frequency. The dotted curve marked A_C refers to the calculated noise performance of the antenna and preamplifier assuming the preamplifier noise to be 1.13×10^{-8}V as measured earlier. If the Measured noise as in Figure A3.1 is scaled onto this plot assuming a preamplifier noise figure which is also 1.13×10^{-8}V we see that the curve A_M (the measured value) agrees well with the calculated response. As the calculated value of the noise output from the antenna at reasonance does not involve the assumed preamplifier noise figure the fact that the preamplifier noise at -34 db on the peak is within 1 db of the measured value must lend considerable support to this value.

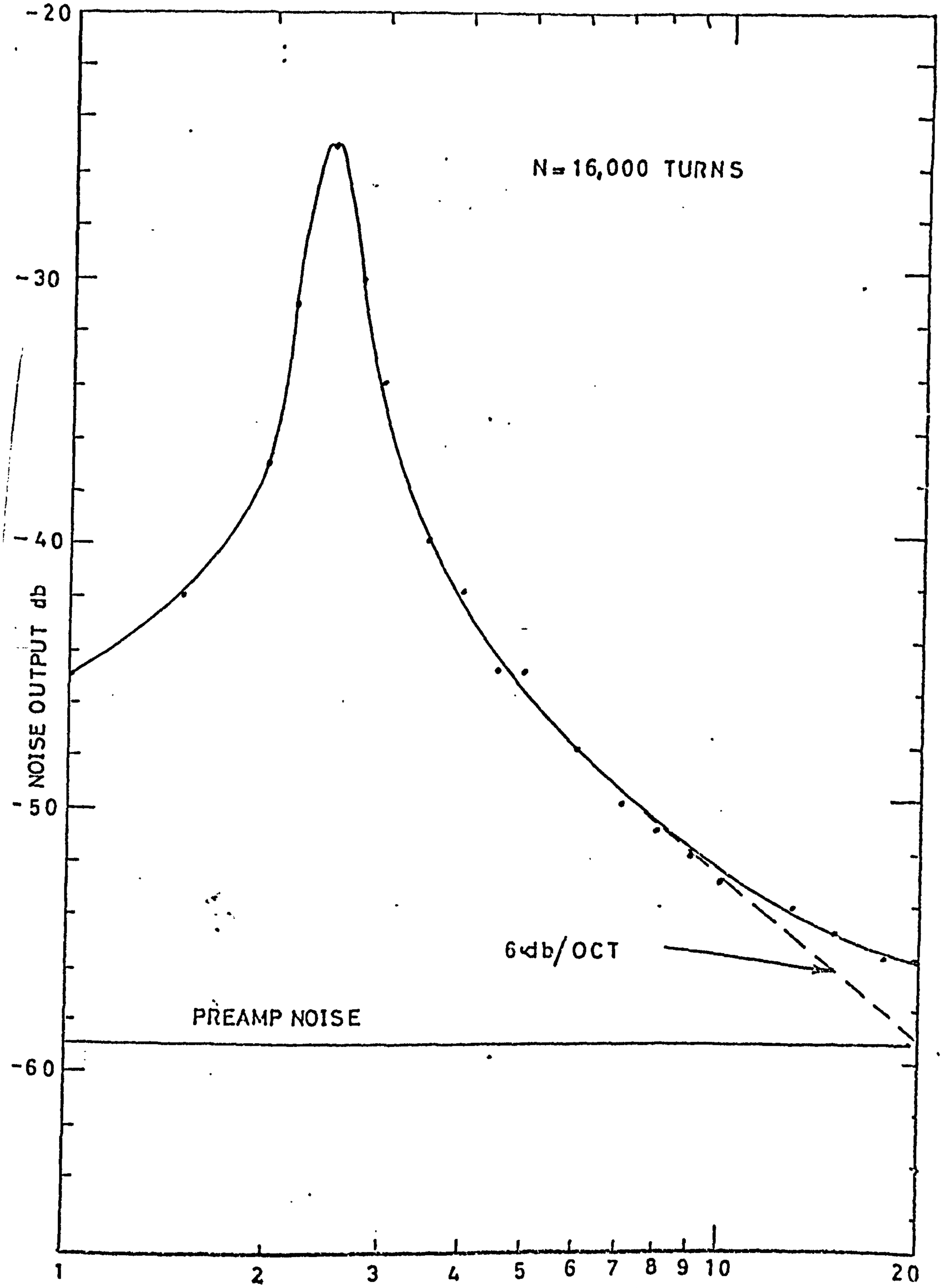
-20
-30
-40
-50
-60
NOISE OUTPUT db
N=16,000 TURNS
6db/OCT
PREAMP NOISE
1
2
3
4
5
6
7
8
9
10
20
FREQUENCY KHz

FIG(A3.1)

If the comparision of the calculated and measured noise outputs for the preamplifier and antenna are made using values for the preamplifier noise which are 6 db above and below the measured value, we see from Figure A3.2 that there is poor agreement in both cases.

In the light of this exercise it is thought that the measured preamplifier noise figure is accurate to about 1 db and is certainly good enough to be used in the calculations of system performance especially as the receiver is antenna noise limited and the preamplifier noise becomes significant only at 20 KHz which is the upper frequency limit of the study.

FIG (A3.2)

N = 16,000 TURNS

V NOISE OUTPUT (B=10 Hz)

10^{-7}

10^{-8}

C

A

C_M

C_C

A_M

A_C

B_C

B_M

B 2 3 4 5 6 7 8 9 10 FREQUENCY 20 KHz

REFERENCES

Aarons, J. et al 1960"Correlation of audio frequency electromagnetic radiation with auroral zone micropulsations". Nature 185 148-151.

Aarons, J. 1960 "Natural background noise as very low frequencies". The radio noise spectrum, ed.D.H. Menzel, Chap.8 pp111-122. Harvard Univ. Press.

Adachi, S & Mushiake,Y.1962 "On VLF emissions in the exosphere". Proc. IRE Trans. AP10(6),785-787.

Allcock,G.McK. 1957 "A study of audio frequency radio phenomenon known as 'dawn chorus'." Aust.J.Phys. 10 286-298.

Allcock,G.McK. & Mountjoy,J.C. 1970 "Dynamic spectral Characteristic of Chorus at Middle Latitude". J.G.R.Vol.75 No.13 pp 2503-2510.

Angerami,J.J. 1966"A study of the distribution of thermal electrons in the magnetosphere" Tech. Report No.3412-7 Stanford University.

Ashok[2], A wire antenna V.L.F. Receiver. Dept. of Physics Univ. of Southampton.

REFERENCES CONT.

Barkhausen,H Phys. Zeit.,20 401-403 1919.

Barrington,R.E. 1960 "The interaction of the whistler mode with the space charge modes of an electron stream". Proc.Symp.Phys.Processes Sun-Earth environ. DRTE Publ. 1025,pp223-230.

Barrington,R.E. & Belrose,J.S. 1963 "Preliminary results from Canada's Alouette Satellite."Nature,198(4881) p 651 - 656.

Beckingham,P. 1970 "A Rocket Borne Langmuir Probe with High Resolution". Ph.D. Thesis,Phys.Dept. Univ. of Sheffield.

Bell,T.F. & Buneman,O. 1964 "Plasma instability in the whistler mode caused by a gyrating electron stream". Phys.Rev. 133(5A), 25-26.

Bell,T.F.& Helliwell,R.A. 1960 "Travelling wave amplification in the ionosphere". in Proc.Symp. Phys. Processes Sun Earth Environ. DRTE Publ.1025,pp215-222.

Belrose,J.S. 1955 "Ferromagnetic loop Aerials". Wireless Engineer Feb. 1955.p 2-7.

Belrose,J.S.,Barrington,R.E. 1965 "V.L.F. noise bands observed by the Alouette 1 satellite". Rad.Sci. J. of Res. NBS/USNC-URSI, Vol. 69D p 69 - 76.

Benediktov,E.A. & Eydman,V.Ya. 1961 "On the incoherent radio emission of fast moving charged particles in the earth's magnetic field. "Radio-fizika 4(2) 253-258.

Beneteau,P.J.1962 "Designing low noise transistor circuits". Fairchild App. Rep. App-11/2.

Beneteau, P.J. & Blaser,L 1963 "Measurement of noise figures of transistors". Fairchild App.Rep. App.13/3.

Berthommier,C.Cory,H.,Gendrin,R., Sukhera,B.,Vigneron,J.1969 "A V.L.F. and particle rocket experiment at Kerguelen

Blaser,L. 1962 "The design of low noise, high input impedance amplifiers. "Fairchild App. Rep. App136/2.

Bleany & Bleany 1965. "Electricity and Magnetism" Edition 2 p45 & 140

Bozorth,R.M. & Chapin,D.M. 1942 "Demagnetising factors of rods". J. App. Phys. Vol. 13 p 320-326.

Brice,N.1962 "Discussion of a paper by R.L. Dowden, 'Doppler shifted cylclotron radiatio form electrons: A theory of VLF emissions from the exosphere". J.G.R. Vol 67, No.12 pp 4897-4899.

Brice,N.M.1963 "An explaination of triggered VLF emissions". J.G.R. 68, 4626-4628.

Brice,N.M.1964 "Fundamentals of VLF emission generation mechanisms. "J.G.R. 69,4515-4522.

Bullough,K & Sagredo,J.L.1973 "V.L.F. Observations at Halley Bay, Antarctica-1. The equipment and the measurement of signal bearing. "Plan. & Space Sci. 21 p899.

Bullough,K.Hughes,A.R.W.Kaiser T.R. 1969 "Satellite evidence for the generation of V.L.F. emissions at medium latitudes by the transverse reasonance instability".

Plan. & Space Sci. 17 p 363 - 374.

REFERENCES CONT.

Bullough,K 1971 "The principle zones of E.L.F./V.L.F. emission", Quart.J. Royal Ast. Soc. 12(2) p 173 - 174.

Bullough,K., Hughes,A.R.W. Hudson,T.,Hickinson,D.,Broomhead,P., Tomlinson,P. 1968 "The Sheffield University V.L.F. experiment on the satellite Ariel 3." J.Sci.Inst. (J. of Phys.E) Series 2 Vol 1 p 77 - 85.

Burton,E.T. & Boardman, E.M. "Audio frequency atmospherics" Proc. IRE 21 1476-1494 1933.

REFERENCES CONT.

Cantarano, S. & Pallottino, G.V. 1970 "A low noise fet amplifier for a spaceborne magnetometer". Electronic Engineering Sept. 1970.

Carpenter, D.L. 1963 "Whistler evidence of a 'knee' in the magnetospheric ionisation profile". J.Geophys. Res. 68 p1675.

Carpenter,D.L. 1966 "Whistler studies of the plasmapause in the magnetosphere; temporal variations of the position of the knee and some evidence on plasma motions near the knee". J.Geophys. Res. 71 p693.

Carpenter,D.L. 1967 "Relations between the dawn minimum in the equatorial radius of the plasmapause and D_{ST},K_p, and local K at Byrd station" J.Geophys. Res. 72 p2969.

Carpenter,D.L., Walter,F.,Barrington,R.E.,McEwen,D.J. 1968 "Alouette 1 & 2 observations of abrupt changes in whistler rate and V.L.F. noise variations at the plasmapause - a satellite ground study". J.Geophys. Res.73 (9) p 2929.

Carpenter,D.L. Dunckel, N & Walkup,J.F. 1964 "A new V.L.F. phenomenon: Whistlers trapped below the protonosphere". J.Geophys. Res. 69 No. 23 p5009 - 5017.

Cartwright, D.G. 1964 "Rocket observation of very low frequency radio noise at night". Plan & Space Sci. 12 p11-16.

REFERENCES CONT.

Cartwright,D.G. 1964a "Rocket observations of the intensity of very low frequency noise above the ionosphere", Pla. & Space Sci. 12 p 751-759.

Cawthraw, M.J. 1954 "Ferroxcube Aerial rods for Medium & Long wave reception". Mullard Tech. Comm. No.8 p181-185.

Chapell, C.R. et al 1970 "A study of the influence of magnetic activity on the location of the plasmapause". J.Geophys.Res. 75 p50.

Clemmow, P.C. 1962 "Wave amplification in a plasma stream in a medium of high refractive index". Proc.Phys. Soc. Lon. 80,1322-1332.

Crary,J.H. 1961 "The effect of the earth-ionosphere waveguide on whistlers" Tech. Rep. No.9 Stanford electronics labs. Stanford Univ. California.

Crouchely, J & Brice, N.M. 1960 "A study of chorus observed at Australian stations". Plan.Sp. Sci.2 238-245.

REFERENCES CONT.

Dinger, H.E. 1960 "A four year summary of whistler activity at Washington D.C." J.Geophys. Res. 65 571-575.

Dowden,R.L. 1962a "Wide band bursts of VLF radio noise (hiss) at Hobart". Aust. J. Phys.15(1),114-119.

Dowden,R.L. 1963a "Doppler shifted cylcotron generation of exospheric VLF noise (hiss)". Plan. Space Sci. 11(4), 361-369.

Dowden, R.L.1962 "Doppler shifted Cyclotron radiation from Electrons: A Theory of VLF Emissions from the Exosphere". J.G.R. Vol 67, No.5, 1745-1750.

Dowden, R.L.1963 "Very low frequency emissions from the exosphere". I.P.S. University of Tazmania.

Dowden, R.L.1971 "Electron energy spectrum and structure deduced from Analysis of VLF Discrete emissions by using the Helliwell Criterion". J.G.R. Vol.76 No.13 pp 3034-3045.

Dowden, R.L. & Allcock, G.McK. 1970 "Determination of the nose frequency of non nose whilsters". J.Att. Terr. Phys. Vol.33 pp 1125-1129.

Dowden, R.L. 1960 "Geomagnetic noise at 230 KHz." Nature 187 (4738) 677-678.

Dungey, J.W. 1963 "Reasonant effect of plasma waves on charged particles in a magnetic field". J.Fluid.Mech 15(1), 74-82.

Dysthe, K.B. 1971 Some studies of triggered whistler emissions. J.G.R. Vol.76 No.28 p 6915.

Egeland, A. 1959 "An investigation of the microstructure of the the perturbations in the geomagnetic field in the auroral zone." Inst. Thor. Astrophys. Blindern. Oslo. Report No. 6

Eidman, V.Ia 1958 "The radiation from an electron moving in a magnetoactive plasma." J.Exptl. Theoet.Phys. USSR. 34,131-138.

Ekersley, T.L. 1925 "Note on musical atmospheric disturbances" Phil. Mag. 49 p1250.

Ekersley, T.L.1926 "Electrical constitution of the upper atmosphere" Nature 117 p821.

Ekersley,T.L. 1928 "Nature 122 p768.

Ellis, G.R.A.1956 "On the propagation of whistling atmospherics" J.Atmos.Terrest. Phys. 8p338

Ellis,G.R.A.1960 "Directional observations of 5KHz radiation from the earths outer atmosphere."J.G.R.65(3),839-843.

Ellis,G.R.&Cartwright,C.A. 1959 "Directional observation of radio noise from outer atmosphere" Nature 184 p1307

ESRO[1] 1971 "The ESRO geostationary magnetospheric satellite" Proc. ESRO coll, Lyngby, Denmark.

Everden, W.A. 1954 "Ferrite Rod Aerials." Wireless World Sept.1954.

Eviator,A.,Lenchek,A.M.,&Singer,S.F. 1964"Distribution of density in an ion-exosphere of a non rotating planet." Phys. of Fluids, 7,p1775.

REFERENCES (CONT'D)

Frank,L.A.1970 J. Geophys. Res. 75 p 707

Frank,L.A. 1970a U. of Iowa 70-55, submitted to J.Geophys. Res.

Franklin, C.A., Nishizaki, T., Mather, W.E. 1967" A wide band receiver for Alouette II and Isis A. "Space Elec. Section Tech. Rep. No. 1, Defence res.Board. Otawa, Canada.

REFERENCES (CONT'D)

Gallet, R.M. 1959 "The V.L.F. emissions generated in the earths exosphere." Proc. IRE 47 211-231.

Gallet,R.M. & Helliwell, R.A. 1959 "Origin of VLF Emissions. " J.Res. Nat. Bureau of Standards, Vol 63D,No.1.

Gendrin, R.1960 "Generation des bruits tres basse frequence dans 1'exosphere par effet Cerenkov. "Compt.Rend. 251(10) 1122-1123

Gendrin,R. et al 1968 "A V.L.F. Particle rocket experiment at Kerguelen Islands; Part 1." Report Groupe de Recherches Ionospheriques, Paris.

Gershman,B.N. & Ugarov, V.A. 1961 "Propagation & generation of low frequency electromagnetic waves in the upper atmosphere." Sov. Phys.Usp. Eng. Trans. 3(5),743-764.

Ginzburg,V.L.1960 "Certain theoretical aspects of radiation due to superluminal motion in a medium." Soviet Phys. Usp. Engl. Trans. 3(5), 743-764.

Gringaux,K.I.et al 1960 "Results of observation of charged particles observed out to R=100, 00km with the aid of charded-particle traps on Soviet space rockets. "Astron.Zh.37 p716.

Gurnett,D.A. 1968 "Satellite observation s of V.L.F. emissions and their association with energetic charged particles." Earths particles and fields,ed. B.M. McCormac, p 337-349 Reinhold, New York.

Gustafsson,G. et al 1960 "Audio frequency electromagnetic radiation in the auroral zone." J.Geophys. Res.65 2749-2758.

REFERENCES (CONT'D)

Halcomb,S.W.&Sevin, L.J. 1963"Field effect transistors for low level circuits."Texas Inst. App. Report April 1963.

Haig 1970 "Numerical approximations to functions and data." Chapter 3 Atholone Press

Hansen,S.F. 1963 "A mechanism for the production of certain types of VLF emissions. "J.G.R.68, 5925-5935.

Helliwell,R.A. et al 1956 "Thenose whistler a new high latitude phenomenon." J.Geophys. Res.61 p139.

Helliwell, R.A. 1956 Stanford Univ. Radio Prop. Lab. Tech. Rep. Rpt. No. AFCRC-TR-56-189.

Helliwell,R.A. & Crystal,T.L. 1973 "A feedback model of Cyclotron interaction between whistler mode waves on energetic electrons in the magnetosphere."J.G.R. 78. No. 31 pp 7357-7371.

Helliwell,R.A.1965 "Whistler & Related Phenomena" Stanford Univ. Press Stanford, Calif. USA.

Helliwell,R.A. 1963 "Whistler-triggered periodic VLF Emissions." J.G.R. 68 5387, 5395.

Helliwell,R.A. & Brice, N.1964 "VLF emission periods and whistler mode group delays. "J.G.R. 69 4704-4708.

Helliwell,R.A., Katsufrakis, J., Trimpi, M., Brice, N. 1964 "Artificially stimulated VLF radiation from the ionosphere." J.G.R. 69 2391-2394.

Helliwell, R.A. 1956 "Low frequency propagation studies, 1. Whistlers and relation phenomenon. Final Rep. Univ. Stanford.

REFERENCES (CONT'D)

Helliwell, R.A. & Bell, T.F. 1960 "A new mechanism for accelerating electrons in the outer ionosphere. "J.G.R.65(6) pp1839-1842.

Helliwell,R.A. & Carpenter, D.L. 1961 "Whistlers-west IGY-IGC synoptic program. "SEL final report.Stanford University.

Helliwell,R.A. 1958 "Low frequency propagation studies, part 1: Whistlers & related phenomena) SEL Final report, Stanford University.

Helliwell.R.A. 1967 "A theory of discrete VLF emissions from the magnetosphere." J.Geophys. Res. 19 4773-4790.

Heikkila,W.J. & Winningham, J.D. 1971 J.Geophys. Res 76 p883.

Hess, W.N.[1] 1968 "The Radiation Belt and Magnetosphere" Blaisdell Pub. Co. Waltham, Mass. U.S.A.

Hones, E.W. 1970 in Particles & Fields in the Magnetosphere, D.Reidel Pub. Co. Dordrecht, Holland, p24

Hones,E.W., Asbridge, J.R., Bame, S.J. & Singer, S. 1971 J. Geophys.Res. 76 p63.

Hill, T.W., Dessler, A.J. 1971 submitted to J.Geophys. Res.

Hundhausen,A.J.1970 in Intercorrelated Satellite Observations Related to Solar Events. Reidel Pub. Co. Dordrecht, Holland, p.155.

REFERENCES (CONT'D)

Kendall,P.C 1970 "Space research: Particles & thier Fields, A brief Introduction for Mathematatitians. "Int.J.Math.Educ. Sci. Technol. Vol 1 245-264.

Kennel, C.F. & Petschek, H.E. 1966 "Limit on stably trapped particle fluxes." J.Geophys.Res. 71 (1) p1 - 28.

Kimura, I. 1961 "Amplification of VLF electromagnetic waves by a proton beam through the exosphere, an origin of the VLF emissions."Rep.Ion.Space. Res.Japan 15(2),171-191.

Knox,C.F.&Rycroft,M.J.1964 "Observations of background electromagnetic noise in East Greenland." Nature 201(4920),693-694

Kolomenskii,A.A.1956"Radiation emitted by an electron moving uniformly in a plasma in the presence of a magnetic field. "Sov.Dokl.Akad.Hayk,106,982.

Laaspere,T.,Johnson,W.C.,Semprebon,L.C. 1971 "Observations of auroral hiss,L.H.R. noise and other phenomena in the frequency range 20 Hz to 540 KHz on OGO 6."

Larmor, J. 1896 "On the theory of moving electrons and electric charges" Phil.Mag. 42. 201-204.

REFERENCES (CONT'D)

MacArthur, J.R. 1959 "Theory of the origins of VLF radio emissions from the earth's exosphere."Phys.Rev. Let.2(12) 491-492.

McKenzie,J.F. 1963 "Cerenkov radiation in a magnetoionic medium (with application to the generation of low frequency electromagnetic radiation inthe exosphere by the passage of charged corpuscular streams."Phil. Trans.Roy.Soc.Lon.A,255,585-606.

Meada,K. & Kimura, I. 1962 "Amplification of the VLF electromagnetic wave by a proton beam through the exosphere.". J.Phys.Soc. Japan, 17 Supp.A2 92-95.

Maeda,K & Kimura, I. 1963 "Origin & mechanism of VLF emissions." Space Res. 3, 310-323.

Marton, L. 1969 "Advances in Electronics & Electron Physics". Ed. Marton. Vol 27 Academic Press London.

Maxwell[4], J.C. 1881 "Atreatise on Electricity and Magnetism." Articles 437 and 438 Vol 2 2nd Ed. Clarendon Press Oxford.

Mayer,A 1969 "Etude, realisation et exploitation d'equipments scientifiques destines a la reception des ondes electromagnetiques naturelles de tres bass frequence et embarques a bord de trois fusees Dragon tirees a Kerguelen en mars et avril 1968. "Ph.D. thesis. La Faculte Des Sciences De Paris.

REFERENCES (CONT'D)

Mosoer.S.R.Gurnett, D.A. 1969 "V.L.F. measurements of the Poynting flux along the geomagnetic field with the Injun 5 satellite." J.Geophys. Res. 74(24) p5675-5687.

Mosier,S.R.Gurnett,D.A. 1971 "Theory of Inuun 5 V.L.F. Poynting flux measurements." J.Geophys.Res. 76(4) p 972-977.

Murcray,W.B. & Pope, J.H. 1960b" Radiation from protons of auroral energy in the vacinity of the earth." J.G.R.65(11), 3569-3574.

Murcray,W.B. & Pope, J.H. 1960a "Doppler shifted cyclotron frequency radiation from protons in the exosphere." Phys.Rev.Let.4(1),5-6.

Nunn,D 1971 "Theory of VLF Emissions" Plan & Sp. Sci. 19 pp11 1141-1167.

Nunn,D. 1972 A self consistent theory of triggered VLF emissions. Dept. of Matematics. Kings College London WC2.

REFERENCES (CONT'D)

Oliven,M.N., Venkatesen, D., & McCracken,K.G.1968"Microburst phenomena, 2 Aurroral Zone electrons." J.G.R. 73,pp2345-53.

Oliven,M.N. & Gurnett,D.A.1968 "Microburst phenomena,3 An association between microbursts and VLF Chorus."J.G.R.73,pp2355-62.

Ondoh,T. 1961 "On the origin of VLF noise in the earth's exosphere." J.Geomag. Geolec.12(2),77-83.

Ondoh,T. 1962 "A possibility of the generation of VLF emissions in the outer earths exosphere. "Plan.Space Sci. 9 69-70.

Ondoh,T. 1963 "A note on the VLF emissions in the outer exosphere." J.Geomag. Geoelec.14(3),175-176.

Orsak,L.E.,Rorden,L.H., Carpenter,G.B. & Ficklin,B.P. 1965 "V.L.F. propagation and noise in the ionosphere observed by sounding rockets." SRI Project Rpt 3749 Office of Res. Grants & Contracts NASA, Washington D.C.

Pierce,J.R. 1950 "Travelling wave tubes" D.Van Nostrand Co. N.Y. USA.

Pope,J.H. & Campbell,W.H."Observations of a unique V.L.F. emission." J.Geophys.Res. 65 2543-2544.

Preece, W.H., 1849 "Earth currents". Nature, 49 p-554.

Pulley,O.O. 1935 "A receiver discriminating between R.H. & L.H. circularly polarized wireless waves." Proc. Phys. Soc. 47 p 1098.

REFERENCES (CONT'D)

Russell,C.T.,Holzer,R.E. 1970 "A.C.magnetic fields." in Particles & fields in the Magnetosphere,ed. B.M.McCormac p 195-212. D. Reiddel,Dordrecht Holland.

Russell,C.T., Chappel,C.R.,Montgomery,M.D.,Neugebauer,M.& Scarf, F.L. 1971, submitted to J.Geophys.Res.

Russell,C.T.McPherron,R.L.,Coleman,P.J.Jnr. 1972 "Fluctuating magnetic fields in the magnetosphere,1 E.L.F. &V.L.F. fluctuations."Space Sci.Rev. 12 p 810-856.

Rycroft,M.J.1967 "A review of satellite observations of V.L.F. phenomena in the magnetosphere." inProc. IEE Conf. on M.F. L.F. & V.L.F. Rad. Prop., Conf.Publ. 36 p 267 - 294. Inst.Elec.London.

Rycroft,M.J.,Usher,R.A.,Adjepong,S.K.,Daniell,G.J.,Vavra,J., Bullough,K.,Gibbons,W.,&Kaiser,T.R. "Preliminary findings of a petrel rocket experiment to invertigate the V.L.F. emission 'chorus' inthe ionosphere." Space Res. XII Akademic-Verlag,Berlin.

Rycroft[3],M.J. The S.Uist V.L.F. station.Dept.of Physics Univ. of Southampton.

Rycroft,M.J. 1972 "V.L.F. Emissions int he magnetosphere." Radio Sci. 7 No.8,9 p 811-830.

Sagredo,J.L. 1971 "VLF goniometer observations at Halley Bay, Antarctica and the effect of the Ring-current on whistler propagation in the magnetosphere." Ph.D. Thesis Univ.Sheffield.U.K.

Sagredo,J.L. &Bullough,K.1973"V.L.F. Observations at Halley Bay Antarctica-11Magnetospheric structure deduced from whistler observations".Plan.&Sp. Sci.21 p 913 - 923.

Santirocco,R.A.1960 "Energy fluxes from the cyclotron radiation of the VLF radio emission."Proc.IRE 48/9) 1650.

Sevin,L.J. 1963 "Field effect transistors:Theory and Applications." Texas Inst.App. Report. April 1963.

Sevin,L.J. 1963a "Behavious of field effect transistor characteristics with temperature. Texas App. Rep. July 63.

Shawhan,S.D.&Gurnett,D.A. 1968 "Recent rocket measurements of A.C. electric & magnetic fields in the ionosphere. "Plasma Phys. Rep. 68-07 Royal Inst. of Tech. Stockholm.

Shawhan,S.D. 1969 "Use of multiple receivers to measure the wave characteristics of V.L.F. noise in space." Plasma Phys. Rep. Royal Ins. of Tech. No 68-19 Stockholm.

Shawhan,S.D. 1970 "The use of multiple receivers to measure the wave characteristics of very-low frequency noise in space."Space Sci. Rev. 10 p 689-736.

Shockly,W.1952 "A unipolar field effect transistor." Proc. IRE Vol 40 p 1365-1376.

REFERENCES (CONT'D)

Siliconix[5] 1968 "N-Channel silicon junction FET's." Data sheets Siliconix House,Saunders way,Swansea S.Wales.

Smith,R.L. 1960 "The use of nose whistlers in the study of the outer ionosphere." SEL Tech. Rep. 6 Stanford USA.

Smith,R.L. 1961 "Propagation characteristics of whistlers trapped in field aligned columns of enhanced ionisation."J.Geophys. Res. 66 p3699.

Smith,R.L. 1964 "An explanation of the subprotonspheric whistlers." J.Geophys. Res. 69 No 23 p5019-5021.

Sonograph Kay Elemetrics Co. Pine Brook N.J. USA.

Stiffel,E.L. 1958 "Kernel polyomials in linear algebra & thier numerical applications." App.Maths.Series No. 49 U.S. printing office.

Stix,T.H. 1963 "The theory of Plasma Waves." pp156-167 McGraw-Hill N.Y. USA.

Storey,L.R.O. 1953 "An investigation of whisteling atmospherics" Phil.Trans. Royal Soc A 246 113-141.

Stoner,E.C. 1945 "The demagnetising factors for ellipsoids." Ser.7,Vol.36 No263 p 803-820.

Super Mu-metal*1970 Telcon Mu-metal alloys Handbook. Telcon Metals ltd. Maor Royal, Crawley, Sussex.

Tolkein,††J.R.R. 1965 "Lord of the Rings." Allen & Unwin, London.

Ungstrup,E. 1959 "Observations of 'whistlers' and very low frequency phenomena at Godhavn, Greenland." Nature 184 806-807.

Ungstrup,E. 1971 "Rocket observations of V.L.F. hiss in Aurora." Plan. Space Sci. 19 1475-1495.

Van Der Ziel,A.1962 "Thermal noise in field effect transistors." Proc. IRE Aug.62.

Vavra,J. 1970 "A rocket-borne V.L.F. radio receiver." Internal report, Univ. of Southampton.

Vette,J.I. 1972 "Magnetospheric particle populations." NASA-Nat. Space Sci.Data Centre Greenbelt.

Vilar-Mestre,E.1966 "Etude et realisation d'un recepteur TBF destine a une experience sur fusee." M.Sc.Thesis,Paris.

Wait,J.R. 1953 "Receiving properties of a wire loop with a spheroidal core." Canadian J. of Tech., 31 p9-14.

Wait,J.R. 1953a "The receiving loop with a hollow prolate spheroidal core." Canadian J.of Tech.31, P132-137.

Watt,A.D. & Maxwell,E.L. 1957 "Characteristics of atmospheric noise from 1-100KHz." Proc.IRE 45 787-794.

Watts,J.M. 1957 "An observation of audio-frequency electromagnetic noise during a period of solar disturbance." J.Geophys. Res. 62 199-206.

Watts,J.M. 1959 "Direction finding on whistlers". J.Geophys.Res. 64 p 2029.